Recognition of Anionic Guests by Dipodal/Tripodal Receptors: Positional Isomeric and Electronic Effect

A Dissertation

Submitted in partial fulfillment for the degree of

Doctor of Philosophy

Utsab Manna

(Roll No. 146122028)

Thesis Supervisor: Prof. Gopal Das

Department of Chemistry

Indian Institute of Technology Guwahati

Assam -781039, India

Recognition of Anionic Guests by Dipodal/Tripodal Receptors: Positional Isomeric and Electronic Effect

A Dissertation

Submitted in partial fulfillment for the degree of

Doctor of Philosophy

Utsab Manna

(Roll No. 146122028)

Thesis Supervisor: Prof. Gopal Das

Department of Chemistry

Indian Institute of Technology Guwahati

Assam-781039, India

DEDICATED TO MY

PARENTS

INDIAN INSTITUTE OF TECHNOLOGY GUWAHATI

Department of Chemistry

STATEMENT

I do hereby declare that the matter embodied in this thesis is the result of investigations carried out by me in the Department of Chemistry, Indian Institute of Technology Guwahati, India, under the guidance of Dr. Gopal Das, Professor, Department of Chemistry, Indian Institute of Technology Guwahati, India. In keeping with the general practice of reporting scientific observations, due acknowledgements have been made wherever this work is based on the findings of other investigators.

December, 2018 **Utsab Manna**

IIT Guwahati

INDIAN INSTITUTE OF TECHNOLOGY GUWAHATI

Department of Chemistry

CERTIFICATE

This is to certify that **Mr. Utsab Manna** (Roll No. 146122028) has been working under my supervision since July, 2014 as a regular registered Ph. D. student. His thesis entitled **"Recognition of Anionic Guests by Dipodal/Tripodal Receptors: Positional Isomeric and Electronic Effect"** is an authentic record of the results obtained from the research work carried out under my supervision in the Department of Chemistry, Indian Institute of Technology Guwahati, Assam, India. I am forwarding his thesis to submit for the award of degree of Doctor of Philosophy, from this institute. I hereby certify that he has fulfilled all the requirements, according to the rules of this institute regarding the investigations embodied in his thesis and this work has not been submitted elsewhere for a degree.

Dr. Gopal Das
(Thesis Supervisor)
Professor
Department of Chemistry
IIT Guwahati
Assam - 781039, India

Acknowledgement

This opportunity to extend my gratitude should commence with my parents, whose love and inspiration has always been strength for me. Their eternal blessing and constant support has guided me this far and positively, this will take me far forward in future to achieve the success they dreamt of. I would also like to recognize my elder brother (dadavai) Abhisek Manna, who has been a source of encouragement and inspiration throughout my life. Besides, no words would suffice to express my feelings for beloved Mampi, my wife, whose love and care have so luxuriously continued to enrich my life. She has always been there to support and encourage me even in frustrating and difficult times of my life, for which I wish to submit my hearty thanks to her.

I wish to express my sincere gratitude towards my PhD supervisor Prof. Gopal Das, whose wide experience and personal guidance have given me freedom to think, plan and execute my ideas to develop the quality of work throughout the processes and especially for his unique style of leading the group that are reflected in happy faces of the group members. I would also like to be grateful to my doctoral committee members, Prof. Sandip Paul, Dr. Lal Mohan Kundu and Dr. Shyam P. Biswas for their advice and suggestions. I would also like to thank ex-Head Prof. B. K. Patel, present-Head Prof. T. Punniyamurthy, scientific officer Dr. Babulal Das and other staff members of the Department of Chemistry, IIT Guwahati for providing the necessary facilities.

I take this opportunity to thank my wonderful Lab seniors Sandeep Da, Arghya Da, Romen da, Najbul da, Abhijit da, Barun da, Soham Da, Nilotpal da as well the amazing Lab mates Rupinder, Biswajit, Santanu, Senjuti, Arnab, Asesh, Deepa, Megha, Debojit, Sourik, Sagnik for their co-operation in my research work, without which it would not been easy to complete the PhD thesis. It was great to work and spend times with these interesting human beings and I will always cherish the memories of their jokes, laughter and humor throughout my life. Most of these people have a positive approach towards life and I wish them success in every aspects of their life.

Finally, I would like to pay my sincere thanks of appreciation to my English teacher Suprovat sir for his motivation and inspiration for my academic career. Some friends without whom the list would be incomplete are, my childhood friends Sourav, Biplab, Prasanta, Rahul and Sovon, my school mates Debankar, Titas, Soma (presently my sister-in-law) and Soumya, my research batch mates Rajat, Mostakim, Bapan, Ayan and Nilu whose friendship had enrich my life and we often spend some good time whenever together. Still many names are missing whose contribution and help is worth mentioning.

Utsab

The contents of this thesis entitled **"Recognition of Anionic Guests by Dipodal/Tripodal Receptors: Positional Isomeric and Electronic Effect"** have been divided into six chapters based on the results of experimental work performed during the research period.

Chapter 1: Introduction

This chapter delivers a brief introduction on 'supramolecular anion-receptor chemistry' regarding the recognition of anions/hydrated anions or anionic associations within the preorganized cavity or self-assemblies of artificial receptors, isomeric with respect to either terminal substituents or starting materials. As anionic species with negative charges are omnipresent and their significance in chemical, environmental, biological, medical as well as industrial processes cannot be undervalued, hence the recognition of anions of different dimensionalities by acyclic synthetic hydrogen bonding scaffolds has materialized as one of the prominent and dynamic arena of research within the dominion of supramolecular chemistry. Numerous acyclic hosts, basically tripodal kinds of receptors have been synthesized for anionic guests over the last two decades with multi-arm hydrogen-bonding functionalities, because they have better tendencies to form molecular capsules with topological complementarities, rather than any rigid or less hydrogen bonding-functionalized dipodal receptor systems. Therefore we emphasize on the field of recent developments of rigid isomeric dipodal receptor systems basically for encapsulation or entrapment of anion/hydrated anions or anionic associations, besides few simple isomeric tripodal anion-receptor systems also in solid and solution state.

As anions have variety of shapes and sizes such as spherical, planar, tetrahedral, octahedral etc. compared to only spherical metal ions, the recognition of anions within the self-assemblies of rigid dipodal scaffolds are considered to be one of the challenging tasks to the supramolecular researchers. Furthermore, as anions are ubiquitous in nature playing various dynamic roles in biological systems for the maintenance of life, alongside having adverse effects on the environment in the form of anionic pollutants, therefore researchers are heavily involved in recognition of those anionic guest species within the potent macrocyclic or acyclic host molecules. Subsequently, inspired by the natural processes of effective and selective anion binding of proteins by precise noncovalent interactions, such as location of deep hydrophobic anion binding pocket between the two lobes of protein in SBP (sulfate binding protein) from S. typhimurium and in PBP (phosphate binding protein) from E. coli. etc., many acyclic artificial anion binding podands have extensively

been employed in past two decades, which can expand or contract their side arms in response to the various dimensions of incoming anionic guest species. The anion binding propensity of receptors varies with the appended peripheral functions (electron withdrawing and donating functionalization), since both the position and the nature of functional groups adjust the hydrogen bonding capability of particular receptor. Till last decade, the binding of anionic guests within the preorganized tripodal receptor systems or macrocyclic systems are extensively studied that are relatively understandable but the binding processes of acyclic rigid dipodal receptors containing positional or electronic aryl substituents with less preorganized cavities or less coopeativity remain more elusive in literature. Theoretical research by Hay *et al.* revealed that the position of electron withdrawing substituents on the terminal aryl moiety have significant consequences on the stability of anion complexes. Even the simplest tripodal urea and thiourea receptors derived from tren moiety with multi-armed hydrogen bonding functionality did not have any structural proof of anion-coordination abilities until the last decades may be because of highly electron-rich architectures and no electron-withdrawing terminal substituents. When two or more geometrically and functionally complementary receptor subunits are self-assemble to form a super molecule, then the structural features of the crystal void such as, shape, size, position or electronic properties, control the usefulness of that super-structure. These kinds of anion induced self-assemblies formed by hydrogen bond donation of receptors have exposed a number of motivating properties, e.g., anion recognition in water, encapsulation of anion-water clusters within dimeric/trimeric/tetrameric host assemblies, entrapment of cyclic fluoride-water tetramer, bare and hydrated asymmetric sulfate, sulfate-water-sulfate adduct, within linear dipodal receptors, fixation of aerial carbon dioxide (CO_2) as carbonate-water cluster even in dipodal receptor system, selective salt extraction from water, transmembrane anion transportation etc.

Chapter 2: Experimental methods and characterization

In this chapter, a detailed comprehensive report of the various reagents used in the synthesis of the receptors, their synthetic pathways, crystallization details, binding study and specifications of analytical instruments employed in the characterization of designed and synthesized free receptors and their various anion complexes with anions/hydrated-anions and anionic associations are represented thoroughly.

Chapter 3: *ortho*-Phenylenediamine based isomeric neutral scaffolds: Evidence of $[(Cl)_3$-DMSO] dual guest encapsulation and cyclic $[(F)_2(H_2O)_2]$ tetramer entrapment

(***Cryst. Growth Des.***, 2016, **16**, 7163; ***Dalton Trans.***, 2017, **46**, 11956)

The chapter describes the design and syntheses of two 3,4-halo-methylphenyl functionalized (**L_1** and **L_2**) and one 3,5-trifluoromethyl-phenyl functionalized (**L_3**) *ortho*-phenylenediamine based isomeric dipodal bis-urea receptors for recognition of anions/hydrated anions or anion-solvent guest association within the neutral host assemblies. The crystal structure analyses reveal that the chloro-methylphenyl disubstituted isomer **L_1**, with the aid of three symmetry-independent conformers in the unit cell encapsulate an unusual triangular $[(Cl)_3$-DMSO] guest assembly entirely sealed by three *n*-TBA^+ counteractions, whereas in presence of same chloride anion the bromo-methylphenyl disubstituted isomer **L_2** forms 2:2 noncooperative $[(\mathbf{L_2})(Cl^-)]_2$ complex. Furthermore, receptor **L_1** form noncapsular cation-sealed 2:2 host-guest assemblies with acetate and fully encapsulated 4:2 host-guest assemblies with double carbonate anions. In continuation with the diverse binding properties, receptor **L_2** form similar kinds of cation-sealed 2:1 pseudo-capsular host-guest assemblies with bigger tetrahedral sulfate and octahedral hexafluorosilicate anions. The X-ray analyses clearly explain that the diverse halide and acetate binding of 3-4-halo-methylphenyl substituted receptors are ascribed for the relative 3D orientations of the terminal aryl *meta*-substituents with respect to adjacent urea N−H moieties of particular receptor which played a vital role in the stabilization of the infrequent DMSO + host + salt co-crystals. In contrast, the X-ray analysis of larger SO_4^{2-} or SiF_6^{2-} encapsulated complexes show different binding modes from relatively smaller spherical and planar anions, which is attributed to the bigger size of those anions that overpowers the observation of aromatic *meta*-substituent driven anion binding.

On the other hand another newly synthesized 3,5-trifluoromethylphenyl *meta*-disubstituted bis-urea receptor (**L_3**) has been found to encapsulate cyclic fluoride-water $[(F^-)_2(H_2O)_2]$ tetramer inside the *n*-TBA cation sealed dimeric complementary cavity followed by the unusual $(Cl^-)_2$, $(Br^-)_2$, and $(I^-)_2$ anionic assemblies in 2:2 neutral host-guest fashion. Furthermore, the structural analyses also elucidate that receptor **L_3** form, divalent planar carbonate trapped complex *via* hydroxide ion induced fixation of atmospheric CO_2 at the air-solvent interface and divalent sulfate trapped complex *via* the hydrogen bonding-activated proton transfer from monovalent HSO_4^- anion, inside the highly hydrophobic

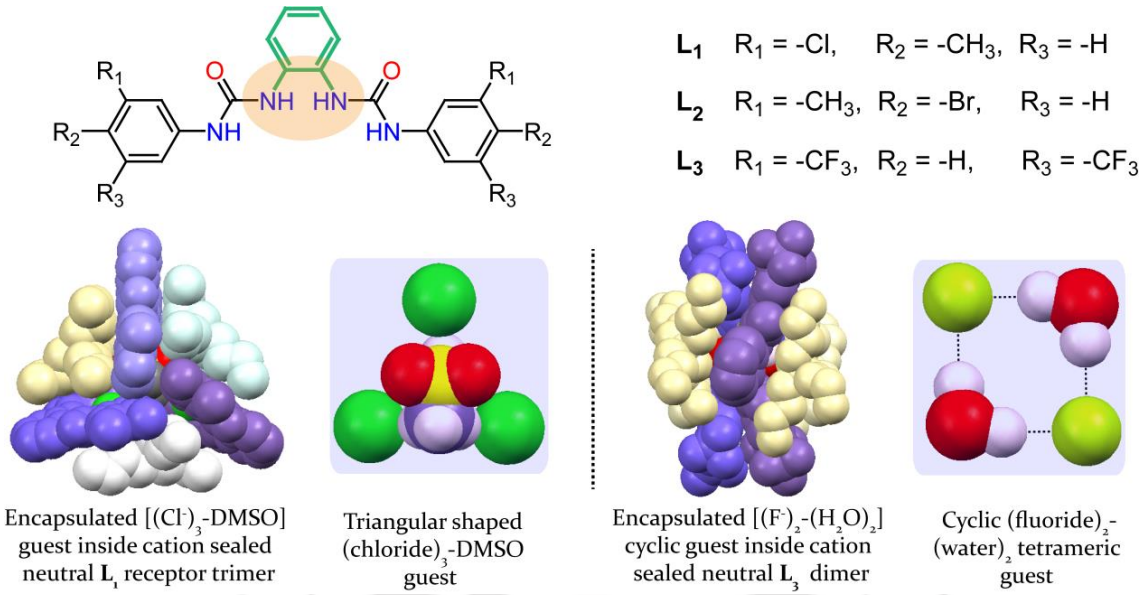

Fig 1. A comprehensive representation of molecular receptor structures and key finding of research work included in the chapter 3.

neutral cation sealed dimeric capsules of symmetry-independent host conformers, with the aid of full and reliable support from solution state studies.

Chapter 4: *meta*-Phenylenediamine based isomeric neutral scaffolds: Evidence of $[SO_4^{2-}\text{-}(H_2O)_3\text{-}SO_4^{2-}]$, aerial CO_2 fixed $[CO_3^{2-}\text{-}(H_2O)_2\text{-}CO_3^{2-}]$ and asymmetric sulfate recognition

(***Cryst. Growth Des.***, 2016, **16**, 2893; ***Dalton Trans.***, 2017, **46**, 10374; ***CrystEngComm***, 2017, **19**, 5622)

In this Chapter, *meta*-Phenylenediamine based terminal mono-aryl as well as di-aryl substituted five newly designed and synthesized bisurea receptors (**L_4-L_8**) have been extensively studied to investigate their comparative coordination properties with the anionic guests of variable shapes and sizes. First of all, the *meta*-nitrophenyl (**L_4**) and *para*-nitrophenyl (**L_5**) functionalized positional isomeric receptors have been found to entrap the cyclic fluoride-water $[(F^-)_2(H_2O)_2]$ tetrameric cluster within the tetrameric pillar-like assemblies of neutral receptor **L_4** and sulfate-water-sulfate $[SO_4^{2-}\text{-}(H_2O)_3\text{-}SO_4^{2-}]$ rugby-ball shaped adduct within the neutral self-assemblies of long straight trimeric pillar of receptor **L_5**. Additionally, receptor **L_4** has been authenticated structurally to entrap the divalent bare sulfate and monovalent acetate anion by similar non-cooperative interactions, while receptor **L_5** forms a host-guest assembly with the cation and solvent (DMSO) coordinated bromide anion. The X-ray analysis clearly unveils the semicircular

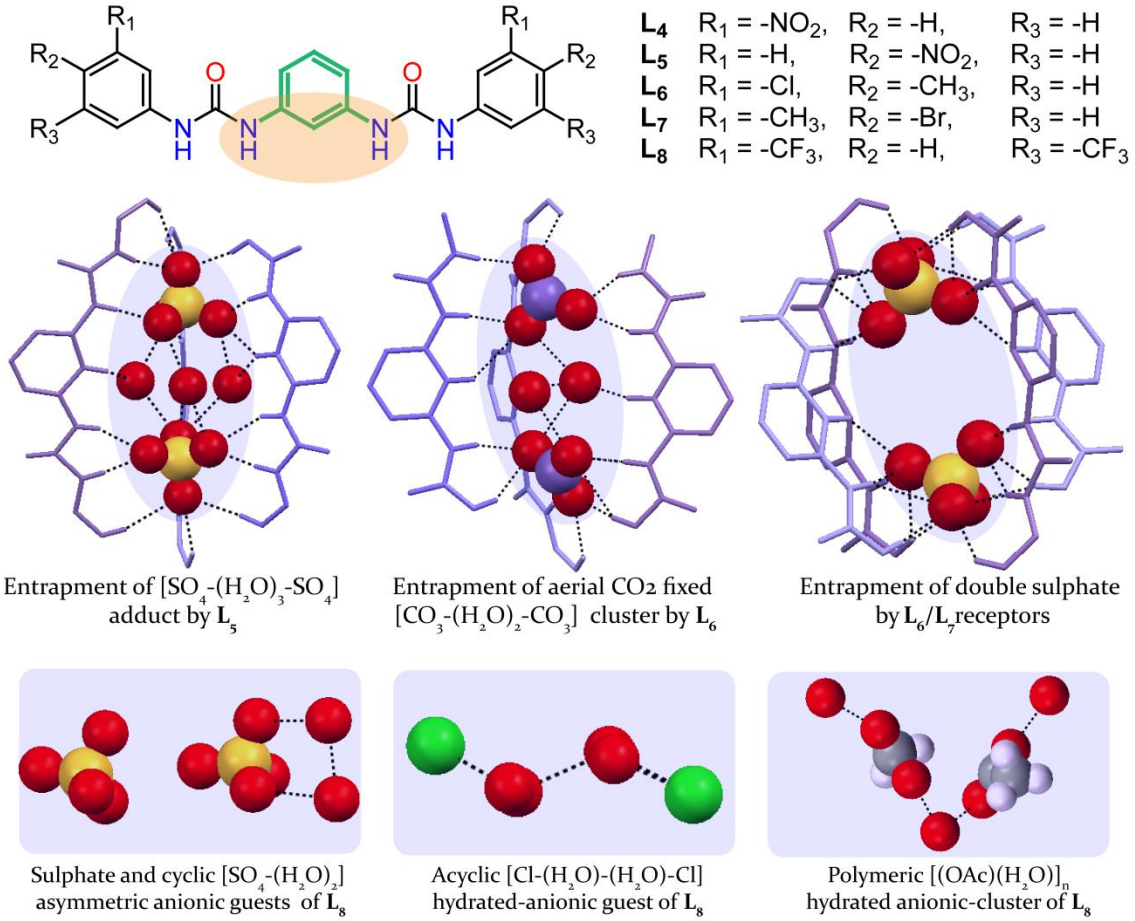

Fig 2. A comprehensive representation of molecular receptor structures and key finding of research work included in the chapter 4.

ligand architecture of $\mathbf{L_4}$ and linear ligand architecture of $\mathbf{L_5}$ in their corresponding host-guest assemblies that can be ascribed for the positional isomerism of *meta*-nitro and *para*-nitro functionality towards complex formation.

The another two halo-methylphenyl terminal aryl-disubstituted receptors $\mathbf{L_6}$ (chloro-methyl isomer) and $\mathbf{L_7}$ (bromo-methyl isomer), which are positional isomeric with respect to the receptors $\mathbf{L_1}$ and $\mathbf{L_2}$, have been found to capture an unprecedented $[CO_3^{2-}\text{-}(H_2O)_2\text{-}CO_3^{2-}]$ cluster within linear tetrameric long straight pillar-like barrel assemblies of receptor $\mathbf{L_6}$ entirely sealed by *n*-TBA cations and water-free naked sulfate-sulfate double anion by cooperative hydrogen-binding of urea groups inside the linear tetrameric neutral barrel of both receptors $\mathbf{L_6}$ and $\mathbf{L_7}$. Furthermore, receptor $\mathbf{L_6}$ self-assemble to form hexa-coordinated fluoride complex, tetra-coordinated bromide complex and receptor $\mathbf{L_7}$ self-assembles to form penta-coordinated fluoride complex in the solid state *via* semicircular receptor architectures and non-cooperative interactions of receptor urea moieties. Hence, it is clear that here the anion recognition is much more governed by the size and dimension of the anions rather than the terminal aromatic substituent effect.

The other bis-urea receptor **L_8** containing electron-withdrawing trifluoro-methylphenyl *meta*-disubstitution derived from similar *meta*-phenylelenediamine has also been recognized as a potential system for, unusual asymmetric entrapment of naked sulfate along with $R_3^3(5)$-type cyclic hydrated-sulfate anion, air-stable bicarbonate dimer capture by fluoride-induced atmospheric CO_2 fixation, entrapment of linear acetate-water polymeric assembly and also the trapping of chair-like $(chloride)_2$-$(water)_2$ hydrated-anionic assemblies. The noncooperative hydrogen-bonding interactions of urea –NH groups of semicircular receptor conformers in each complex irrespective of the dimensions of bound anions are heavily ascribed for the terminal aryl *meta*-difunctionalization driven steric assistance of ligand architecture.

Chapter 5: *para*-Phenylenediamine based isomeric neutral scaffolds: Evidence of cyclic $(HCO_3)_2$-dimer and $(H_2PO_4)_n$-polymer entrapment

(***Cryst. Growth Des.***, 2018, **18**, 6801; ***CrystEngComm***, 2018, DOI: 10.1039/C8CE01558A)

The highlight of this chapter is the entrapment of anions/hydrated anions or anionic associations within the neutral self-assemblies of seven newly designed and synthesized *para*-phenylediamine based terminal mono-aryl or di-aryl functionalized bis-urea

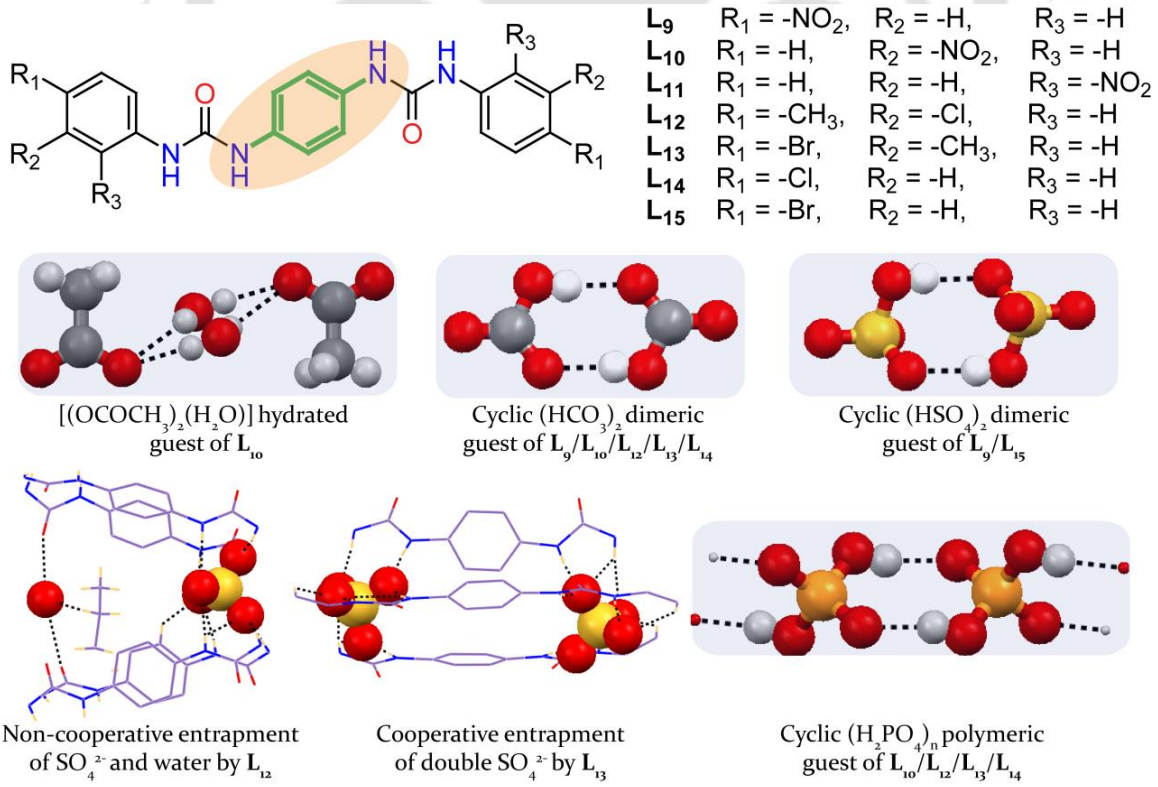

Fig 3. A comprehensive representation of molecular receptor structures and key finding of research work included in the chapter 5.

receptors **L_9-L_{15}**. Sets of three positional isomeric nitro-phenyl functionalized dipodal scaffolds (**L_9-L_{11}**) have been charged with anionic guests of different shapes and sizes, where *para*-nitro isomer (**L_9**) and *meta*-nitro-isomer (**L_{10}**) readily forms bicarbonate dimer $(HCO_3)_2$ entrapped non-cooperative self-assemblies in the solid state by either fluoride or hydroxide induced atmospheric CO_2 fixation. The acetate anions in bare and hydrated form are also trapped by hydrogen-bonding interactions with **L_9** and **L_{10}** respectively. Furthermore, receptor **L_9** entraps $(HSO_4)_2$-dimeric associations and receptor **L_{10}** has been found to self-assemble with divalent SO_4^{2-} and linear polymeric associations of $(H_2PO_4)_n$ by non-cooperative hydrogen-bonding interactions. In contrast the *ortho*-nitro isomer **L_{11}** has not been able to form any anion-receptor complexes, instead free **L_{11}** ligand structures from DMF or DMSO basic solvent medium are obtained in most of the cases, which happens due to the steric hindrance provided by the nitro group at the *ortho*-position and existence of strong intramolecular N-H···O interactions in free **L_{11}** structures.

On the other hand, two halo-methylphenyl terminal aryl-disubstituted receptors **L_{12}** (chloro-methyl isomer) and **L_{13}** (bromo-methyl isomer) (which are positional isomeric with respect to the receptors **L_1** and **L_2** or **L_6** and **L_7**) both readily form similar kinds of non-cooperative anion entrapped neutral host-guest complexes with homologous chloride or bromide anions and smaller planar acetate anions. Similarly, like receptors **L_9** and **L_{10}**, in presence of *n*-TBAF or *n*-$TBAH_2PO_4$ salts, both isomers **L_{12}** and **L_{13}** entrap dimeric associations of cyclic $(HCO_3)_2$ *via* aerial CO_2 fixation and polymeric associations of $(H_2PO_4)_n$ within non-cooperative host assemblies. In contrast, the chloro-methyl isomer **L_{12}** forms non-cooperative self-assemblies with divalent sulfate anion and water molecule; whereas the bromo-methyl receptor **L_{13}** forms divalent sulfate entrapped only cooperative barrel-shaped neutral assemblies.

Another two *para*-halophenyl substituted electronically isomeric linear bis-urea receptors **L_{14}** (*para*-chloro) and **L_{15}** (*para*-bromo) can readily form non-cooperative neutral complexes with chloride or bromide anions as well as with planar acetate anions just similar as receptors **L_{12}** and **L_{13}** in solid state. The *para*-chlorophenyl isomer **L_{14}** has been structurally authenticated to form cyclic $(HCO_3)_2$ anionic dimer by OH^- induced atmospheric CO_2 fixation and linear polymeric $(H_2PO_4)_n$ entrapped neutral self-assemblies, just like above described most of the *para*-phenylendiamine based receptors. Furthermore, in presence of *n*-$TBAHSO_4$ salts, receptor **L_{14}** show non-cooperative capture of divalent sulfate (SO_4^{2-}) anion, but receptor **L_{15}** forms cyclic $(HSO_4)_2$ anionic dimer trapped non-cooperative self-assemblies in solid state.

Hence it has clearly been witnessed from X-ray analysis of linear *para*-phenylendiamine based receptor-anion complexes that recognition of either halides or oxyanions become neither directed by anion sizes nor governed by any terminal aryl substituent effect.

Chapter 6: Tren-based positional and electronic isomeric receptors for encapsulation of anions/hydrated anions

(***CrystEngComm***, 2016, **18**, 5036; ***CrystEngComm***, 2018, **20**, 4406; ***New J. Chem.***, 2018, 42, 19164)

This chapter firstly describes the rationally designed and newly synthesized three N-bridged flexible isomeric polyammonium receptors (**L_{16}-L_{18}**) among which the *para*-nitrophenyl (**L_{16}**) and *para*-bromophenyl (**L_{17}**) functionalized tris-polyamine receptors

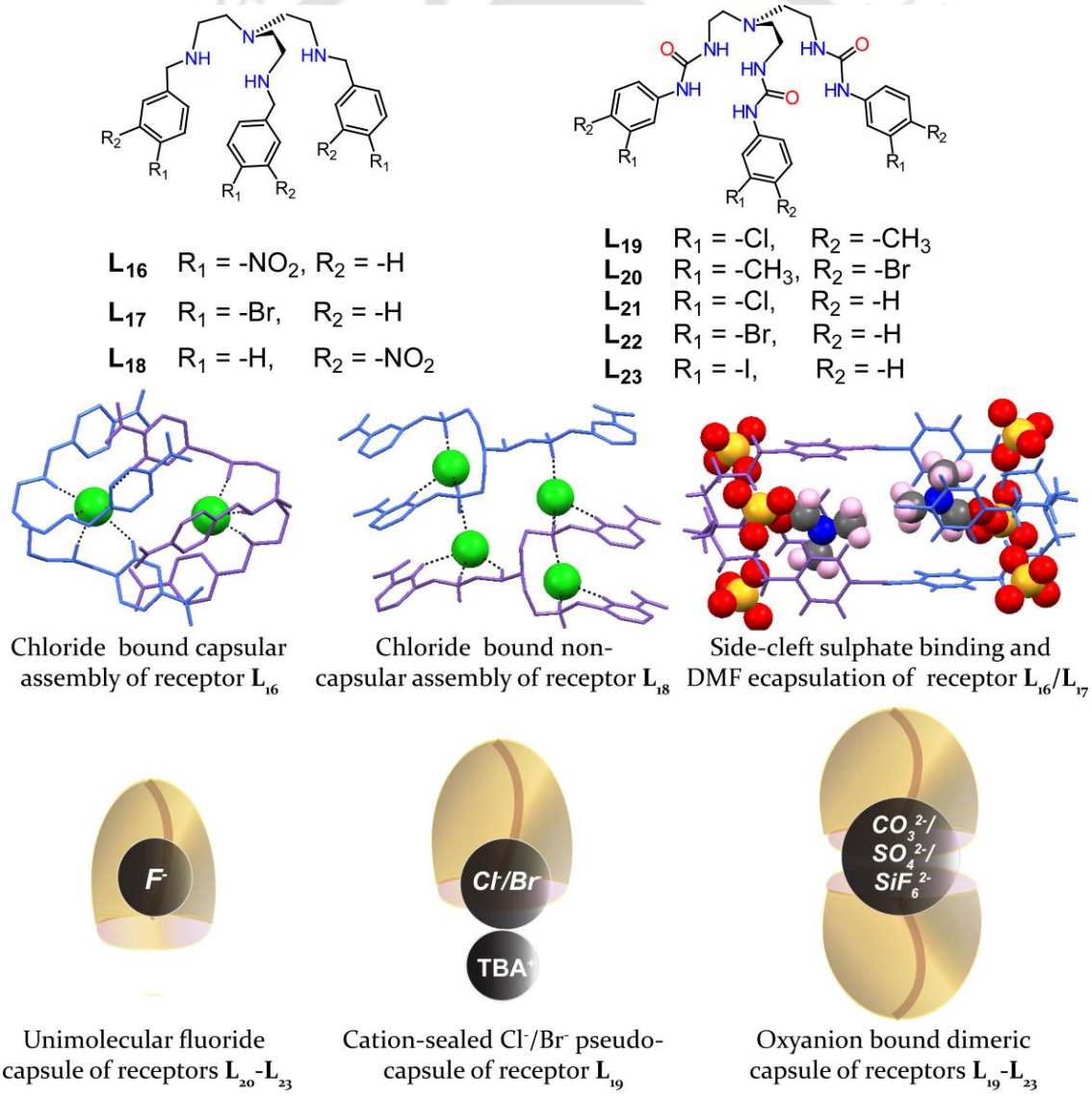

Fig 4. A comprehensive representation of molecular receptor structures and key finding of research work included in the chapter 6.

form protonated capsular assemblies with halide ions, whereas the *meta*-nitrophenyl functionalized tripodal polyamine receptor **L_{18}** (a positional isomer of receptor **L_{16}**) shows entrapment of chloride anion within the protonated non-capsular Y-shaped host-assemblies, which is the consequences of steric effect provided by the *meta*-nitro group towards the smaller tripodal receptor cavity. Furthermore, the presence of relatively smaller cavity in these polyamine based receptors hinders the binding of larger oxyanions such as divalent sulfate. As a result, the protonated tripodal scaffolds of receptors **L_{16}** and **L_{17}** both encapsulate small DMF solvent molecule inside the receptor cavity due to size mismatch with larger sulfate anion and these help in side-cleft binding of the larger sulfate outside the receptor cavities *via* construction of discrete sulfate-water clusters.

On the other hand, the two halo-methylphenyl terminal aryl-disubstituted tris-urea receptors **L_{19}** (chloro-methyl isomer) and **L_{20}** (bromo-methyl isomer) derived from flexible [tris(2-aminoethyl)-amine] skeleton, efficiently capture spherical chloride or bromide anions within the cation-sealed neutral unicapsular assemblies of **L_{19}** and encapsulate the smallest halide anion *via* formation of unimolecular polymeric host-guest assemblies of **L_{20}** and fluoride. The X-ray analyses also expose that the planar carbonate, tetrahedral sulfate and octahedral hexafluorosilicate divalent anions of varied dimensionalities are fully engulfed inside the dimeric capsular cages of either of the isomeric neutral receptors **L_{19}** or **L_{20}** in 2:1 host-guest fashion, irrespective of the size of counter-cations.

Another three *para*-halophenyl functionalized tren-based tripodal urea receptors **L_{21}** (*para*-chloro), **L_{22}** (*para*-bromo) and **L_{23}** (*para*-iodo) showcase a constant proof of fluoride encapsulation with 1:1 host-guest stoichiometry. Moreover, each isomer have been structurally authenticated to self-assemble into a 2:1 neutral dimeric molecular cage in the presence of either planar carbonate or larger tetrahedral sulfate anions irrespective of the size of counter-cations, just similar as in oxyanion complexes of receptors **L_{19}** or **L_{20}** . Hence, the X-ray analyses clearly unveils that the halide or oxyanion binding by tripodal tris-urea receptors doesn't heavily affected by the terminal aryl substituent effect, which is observed as one of the prominent effects in smaller cavity containing tripodal polyammine receptors.

Chapter 7: Phenyl and naphthyl substituted electron-rich tris-(thio)urea neutral receptors: Ice like cyclic $(H_2O)_6$ trapping within hexameric halide-receptor core

(***Cryst. Growth Des.***, 2018, **18**, 1818; ***Cryst. Growth Des.***, 2018, **18**, 3138; ***CrystEngComm***, 2018, **20**, 3741)

This chapter defines the development of two simple naphthyl and phenyl substituted modest tris-urea (**L_{24}** and **L_{25}**) receptors and their tris-thiourea analogues (**L_{26}** and **L_{27}**) derived from very common [tris(2-aminoethyl)-amine] skeleton for investigating their anion-coordination abilities inside the highly-electron-rich environment that were completely underexplored in solid state.

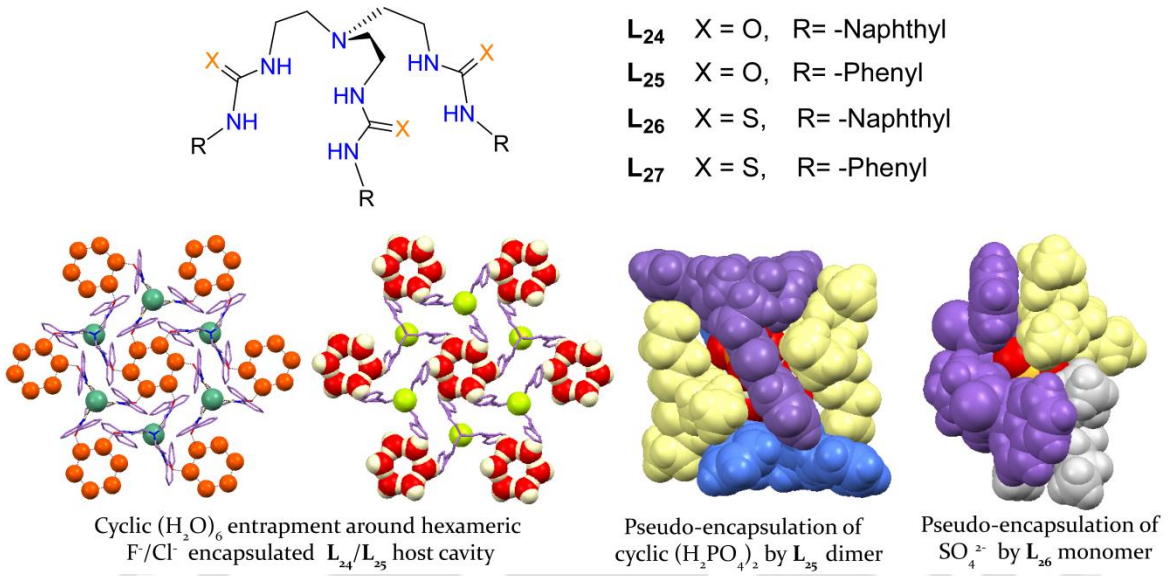

Fig 5. A comprehensive representation of molecular receptor structures and key finding of research work included in the chapter 7.

The single crystal X-ray analysis establishes the formation of unique hexameric receptor-anion-water neutral molecular self-assemblies, where the conformationally flexible C_{3v}-symmetric halide (F^-/Cl^-) encapsulated electron-rich naphthyl group containing N-bridged tripodal urea receptor **L_{24}** effectively entrap the chair-shaped ice-like neutral cyclic water hexamer within the hexameric cavity of receptor-halide bound host-guest association.

On the other hand, the naphthyl based electron-rich thio-urea analog **L_{26}** even in the absence of any π-acidic or electron-withdrawing aryl terminals effectively entraps spherical fluoride, relatively larger spherical chloride and bromide, planar nitrate, and tetrahedral divalent sulfate anions inside the relatively smaller inner tripodal cleft (compared to many previously reported tren-based thiourea receptors) *via* 1:1 host-guest complexation mode, regularly assisted by *n*-TBA/TEA counter-cations. The efficient binding of anions of varied dimensionality consistently observed from single crystal X-ray analyses are strongly corroborated, by the detailed solution state NMR binding studies as well as from the Hirshfeld surface analyses of neutral host-guest complexes.

Subsequently, the phenyl substituted simple tris-urea receptor **L_{25}** and its thio-urea analog **L_{27}**, despite their electron-rich tripodal cavities, are still capable of capturing chair-shaped cyclic water hexamer within the infrequent fluoride encapsulated hexameric **L_{25}** core (similar as receptor **L_{24}**) as well as encapsulating divalent carbonate anion inside the dimeric capsular cage of receptor **L_{27}** *via* hydroxide ion induced aerial CO_2 fixation. Moreover, structural analyses also elucidate the capturing of large dihydrogen phosphate $[(H_2PO_4^-)_2]$ dimeric association within the neutral dimeric pseudo-capsular assembly of receptor **L_{25}**, whereas the thiourea analogue **L_{27}** exhibits chloride and acetate bound 1:1 unimolecular capsular assembly and divalent sulfate bound dimeric cage *via* hydrogen-bonding activated proton transfer reaction from monovalent HSO_4^- anion.

Conclusion

In summary, this thesis provides some substantial outcomes in the domain of 'supramolecular anion recognition chemistry' where the anions/hydrated anions or anionic associations are captured by some series of isomeric dipodal or tripodal artificial acyclic receptors driven by positional or electronic effect of terminal aryl substituents or anion size or molecular host architectures in solid state, as also supported by solution state anion binding studies and Hirshfeld surface analyses of host-guest complexes. In general, the present findings from the experimental studies deliver the anionic guest induced capsular, pseudo-capsular, paddle-wheel shaped, linear barrel shaped or polymeric aggregated assembly formation *via* neutral host-guest associations. The results from this study have unveiled an interesting binding feature of anionic associations with an individual receptor or each set of isomeric receptors in the presence of a free or hydrated anion.

The *ortho*-phenylenediamine based receptor **L_1** has been shown to encapsulate the unique triangular $[(Cl)_3$-DMSO] dual guest association, while its isomeric receptor isomer **L_2** forms 2:2 noncooperative $[(\mathbf{L_2})(Cl^-)]_2$ complex. Another *ortho*-phenylene connected receptor **L_3** has been found to encapsulate cyclic $[(F^-)_2(H_2O)_2]$ tetramer as well as unusual $(Cl^-)_2$, $(Br^-)_2$ and $(I^-)_2$ anionic assemblies and divalent carbonate by hydroxide ion induced atmospheric CO_2 fixation. The cyclic $[(F^-)_2(H_2O)_2]$ tetramer, rugby-ball shaped $[SO_4^{2-}$-$(H_2O)_3$-$SO_4^{2-}]$ adduct, unprecedented $[CO_3^{2-}$-$(H_2O)_2$-$CO_3^{2}]$ cluster, double divalent sulfate anions as well as unusual asymmetric sulfate anions (naked and cyclic hydrated), linear $[(OCOCH_3)(H_2O)]_n$ polymeric assembly and acyclic $(Cl^-)_2$-$(H_2O)_2$ assemblies have been found to be captured within the neutral self-assemblies of isomeric *meta*-phenylenediamine based receptors **L_4-L_8**. Furthermore, the *para*-phenylenediamine

based linear isomeric receptors **L_9-L_{15}** have been found to entrap cyclic $(HCO_3^-)_2$ dimer by F^-/OH^- induced aerial CO_2 fixation and linear polymeric aggregation of $(H_2PO_4^-)_n$ in most of the cases within the non-cooperative receptor assemblies. On the other hand, the terminal aryl substituted multi-armed isomeric tripodal tris-amine (**L_{16}-L_{18}**)/ tris-urea (**L_{19}-L_{23}**) receptors demonstrated the cavity induced encapsulation of halide and oxyanions in either protonated or neutral host-guest assemblies. Moreover, the highly electron-rich isomeric tripodal tris-urea receptors **L_{24}-L_{25}** showed ice-like cyclic $(H_2O)_6$ inside unique hexameric receptor-anion neutral assemblies and among their thiourea analogues **L_{26}-L_{27}**, the receptor **L_{26}** form unimolecular pseudo-capsular assemblies with all anionic guests and the receptor **L_{27}** form dimeric receptor capsular cages with anions in either 2:2 or 2:1 host-guest fashions.

Chapter 1: Introduction

Chapter 2: Experimental Methods and Characterization

Chapter 1

Introduction

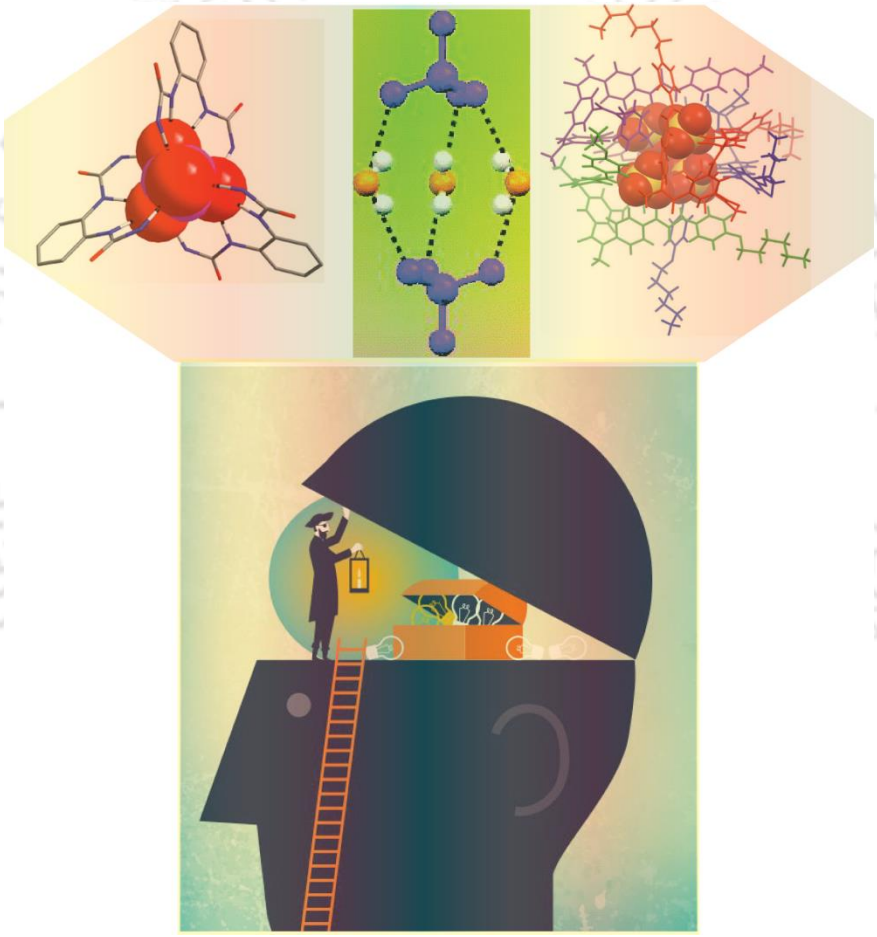

1.1 Supramolecular Chemistry: An Introduction to Host-Guest chemistry

One of the superior quotes and concepts as proposed on humanity by Sir Henry Maximilian Beerbohm (b. 1872, an English writer and caricaturist) is ‘’*In every human being one or the other of these two instincts is predominant: the active or positive instinct to offer hospitality, the negative or passive instinct to accept it. And either of these instincts is so significant of character that one might as well say that mankind is divisible into two great classes:* ***hosts and guests*** ‘’[1.1] The chemistry between host and guests known as supramolecular chemistry has been defined by one of its leading proponents, Jean-Marie Lehn, a Nobel laureate in the area in 1987, as the ‘chemistry of molecular assemblies and of the intermolecular bond’. More colloquially this may be articulated as ‘chemistry beyond the molecule’ and other definitions comprise phrases like ‘the chemistry of the non-covalent bond’ and ‘non-molecular chemistry’.

Basically the non-covalent interactions between a ‘host’ and a ‘guest’ molecule was made as definition of supramolecular chemistry, which exemplifies the relationship between molecular and supramolecular chemistry in terms of both structures as well as function.[1.1] While traditional chemistry emphases on the covalent bond and coordinative bond construction, supramolecular chemistry on the other hand, looks at the weaker and reversible noncovalent interactions among molecules such as hydrogen bonding, halogen bonding, ion-ion, ion-dipole interactions, cation/anion–π interactions, π–π interactions, Van-der Waals forces and hydrophobic effects.[1]

Assimilating these weaker interactions relative to strong covalent bonds and capitalize on them in new ways continues to define the essence of the field. The significant conceptions that have been explained by supramolecular host-guest chemistry include molecular self-assembly, molecular recognition, recognition of anions or anionic associations, mechanically-interlocked molecular architectures, dendrimers, foldamers and molecular electronic devices.[1] As it is accomplished today, supramolecular chemistry is one of the most lively, ever increasing and fast growing research areas of chemical endeavor and it deals with elusive interactions, and accordingly control over the processes involved can require great precision. In the context of some kind of non-covalent binding or complexation event between a ‘host’ and a ‘guest’ in supramolecular chemistry, commonly the host is referred to a large molecule or aggregate such as an enzyme or synthetic cyclic compound possessing a sizeable, central hole or cavity and the guest may be a simple inorganic anion, anion-water cluster or anionic associations, monatomic cation, an ion pair or a more sophisticated molecule such as a hormone, pheromone or neurotransmitter. Consecutively, a binding site is defined as a region of the host or guest molecule capable of sharing in a non-covalent interaction. According to another supramolecular chemistry Nobel laureate Donald Cram, ‘’ A host-guest relationship involves a complementary stereoelectronic arrangement of binding sites in host and guest’’. From the thermodynamic point

of view, the stability of a supramolecular host-guest complex can be enriched by operation of a macrocyclic effect or chelate effect. In comparison of cyclic hosts corands containing similar type of binding sites with acyclic host podands, it is evident that the macrocyclic effect makes cyclic hosts such as crown ethers up to a factor of 10^4 times more stable than closely related acyclic hosts. As a consequence, the guest binding inside the preorganized macrocyclic cavity is relatively straight forward to realize but the binding routes of acyclic receptors remain more elusive. Furthermore, a host molecule must contain appropriate binding sites having correct electronic character (polarity, hydrogen bond donor/acceptor ability, softness or hardness etc.) in order to bind the guest molecule *via* topological complementarity. Host preorganization, which is a case of alteration of conformational change upon guest binding, become a key concept that exemplifies a major enhancement in the overall free energy of guest complexation.[1.2]

1.2 Hydrogen bond:

A hydrogen bond is a connection between two molecules resulting from an electrostatic attraction between a proton in one molecule and an electronegative atom in the other or in particular, it may be regarded as a specific kind of dipole-dipole interaction in which a hydrogen atom attached to an electronegative atom or electron withdrawing group is attracted to a neighboring dipole on an contiguous molecule or functional group. The hydrogen bonding, commonly written D–H···A (where D is donor and A is acceptor), has been described as the 'master key interaction in supramolecular chemistry',[1.1] because of its relatively strong (4-120 kJ mol^{-1}) and highly directional nature. The formation of carboxylic acid dimer and base pairing in DNA (Scheme 1.1) are the typical examples of hydrogen bonding interactions. Subsequently, the hydrogen bonding is possibly the most important discriminating cohesive force in directing the self-assembly and crystallization processes of organic molecules.[1.3] The molecular Self-assembly is the process, where a defined arrangement is adopted *via* molecules by virtue of rotations about single bonds (intramolecular torsions) and intermolecular hydrogen bonding (Scheme 1.2, types of non-covalent interactions). Furthermore, the molecular self-assembly is highly precise, self-repairing and self-controlling since equilibrium-directed processes are implicated.[1.4]

Hydrogen bonds exist in a bewildering range of lengths, strengths as well as geometries and importantly a single, strong hydrogen bond per molecule can be sufficient to determine the solid-state structure and exert a marked impact in the solution as well as in the gas phases. The large numbers of weaker hydrogen bonds act in concerted way can display a substantial role in structure stabilization. Interestingly, the significant focus is also on the feeble hydrogen bonding interactions involving hydrogen atoms attached to carbon, besides electronegative atoms such as

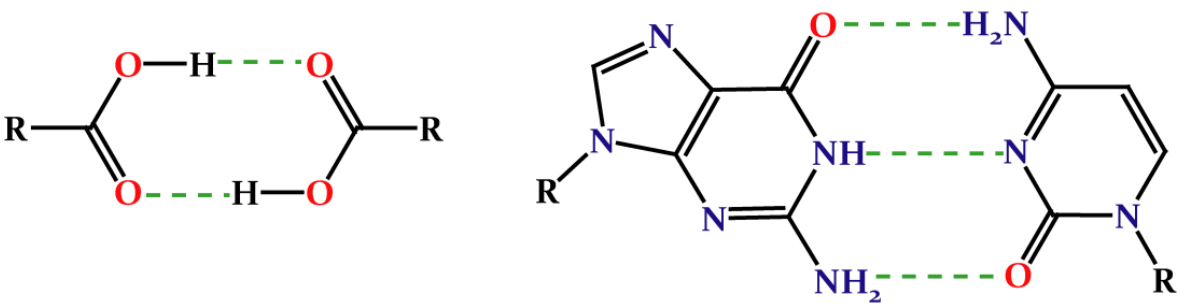

Scheme 1.1 A hydrogen bonded carboxylic acid dimer and base pairing in DNA (Guanine–Cytosine) by hydrogen bonding interactions.

nitrogen and oxygen (electronegativities: C 2.55, N 3.04, O 3.44 and H 2.20). The objective of the thesis is to reconnoiter the molecular self-assembly processes of some simple isomeric sets of acyclic rigid dipodal or flexible tripodal receptors in the course of investigating their coordination properties with anions/hydrated anions or anionic associations depending upon the electronic or positional isomeric effect of terminal aryl receptor substituents or guest dimensions.

1.3 Anion receptor chemistry

The binding of anionic guests with synthetic host (receptor) falls into the realm of 'supramolecular chemistry' in contrary to the simple transition-metal coordination.[1.5] Anion receptor chemistry has attracted ever-growing attention and has become one of the most extensively studied research fields in supramolecular chemistry because of the biological and environmental importance of anions as well as their potential applications in a wide range of areas such as sensors, catalysis, functional materials, transmembrane transport and so on.[1.6] As anions are ubiquitous in nature and roughly 70% of all enzymatic sites contain anions, playing essential structural roles in many proteins alongside they are critical for manipulation and storage of genetic information (DNA and RNA are polyanions). Furthermore, anions also take part in regulating osmotic pressure, maintaining cell volume, in the production of electrical signal and activating signal transduction pathways. Note that, the disruption of anion flux across the cell membranes is increasingly recognized as being the leading determining factor of many diseases. In fact, anion transport through cell phospholipid bilayers is known to be mediated by a variety of channels and anion transport proteins with at least 14 mitochondrial anion transport system have been pointed out so far. These include (among others) systems accountable for the trafficking of ADP, ATP, phosphate, citrate, maleate, fumarate, oxaloacetate, sulfate, glutamate and halide anions. In recent years, several X-ray crystal structures have been elucidated that authorizes the direct conception and visualization of enzyme–anionic substrate complexes, stabilized *via* multiple hydrogen-bonding interactions (Fig. 1.1).[1.7]

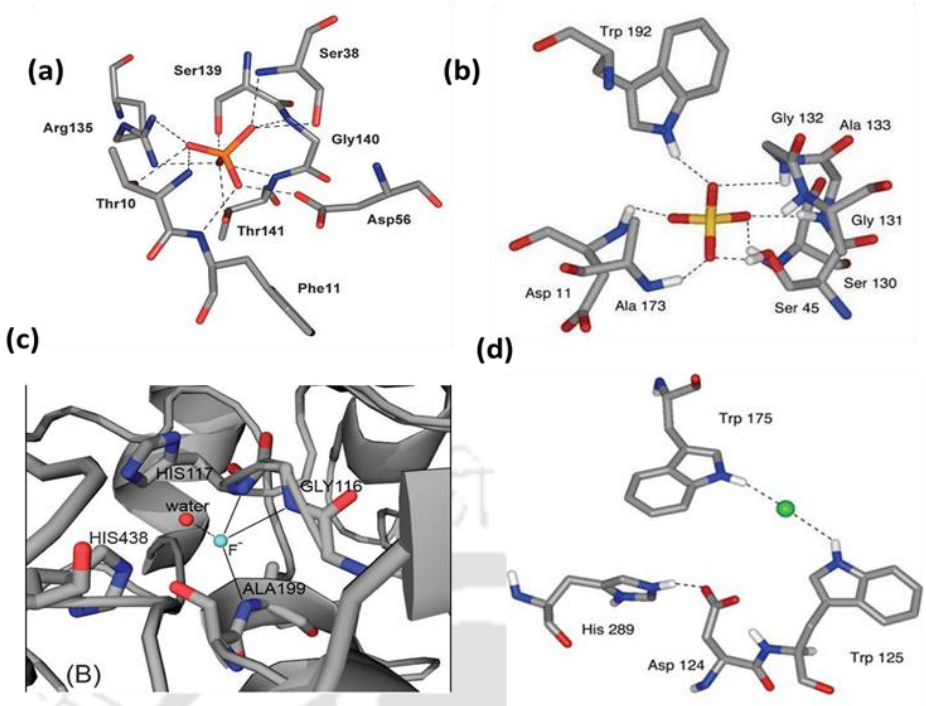

Fig. 1.1 Anion binding in biology depicting, (a) binding mode of phosphate anion in phosphate-binding protein, (b) binding mode of sulfate anion binding in sulfate-binding protein, where the sulfate is bound by seven hydrogen bonds from -NH and -OH bond donor group, (c) mono hydrated fluoride anion binding in human butyrylcholinesterase complex (PDB code = 2XMC) and (d) enzymatic active site of haloalkane dehalogenase the presence of a bound chloride anion.

The binding relationship between anionic guests and their hosts are mostly attributed to hydrogen-bonding and/or electrostatic interactions, with the former being the more influential in advancing selective binding through topological complementarity. Moyer and Bonnesen group has pointed out the important understandings of the factors influencing anion recognition in the traditional analytical sense, where simple physical properties such as size, charge, hydrophilicity and basicity tend to govern selective exchange of one anion over another.[1.8] Subsequently, the

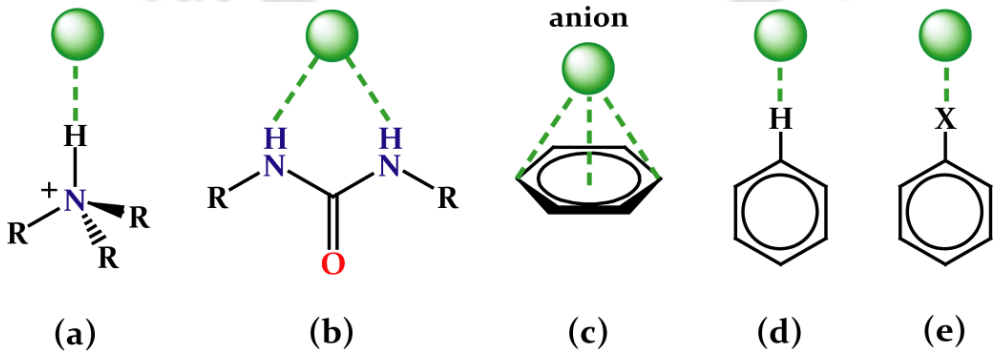

Scheme 1.2 Anion binding by different types of noncovalent interactions, (a) electrostatic N−H···A⁻ interaction by an ammonium cation, (b) complementary N−H···A⁻ interaction by an urea function, (c) anion–π interaction, (d) C−H···A⁻ weak interaction by an aryl function and (e) C−X···A⁻ halogen bonding by a halocarbon (X = F⁻, Cl⁻, Br⁻ and I⁻).

term *bias* for this type of phenomenon has been introduced by the group and they also deduce that truly selective anion receptors must encompass some elements of strategic design, including

appropriately situated hydrogen bond coordination sites. The introduction of multiple hydrogen bonding sites accompanied by the resulting topological considerations in anion receptors leads to the theory of double valence for anions also besides the transition-metal ions. Note that, for a anionic guest, the primary valence is the negative charge on the anion and the secondary valence is delivered by hydrogen bonds to the anion.[1.9] Bowman-James and co-workers has categorized the anion binding based on the coordination numbers which is helpful in defining the concepts of complementarity for a given anion and can assist to formulate the design strategies of optimal anion-binding host structures.[1.10] The most effectual approach to bind anions consist in taking advantage of their negative charge and therefore, the ammonium or quaternary ammonium receptors have been the basic receptor of choice since, they ensure an adequate electrostatic attraction reinforced by hydrogen bond contacts with the coordinated anions.[1.11] On the other hand, urea/thiourea, amide, pyrrole and indole functions have been the subject of demanding investigations for their performance in the building of neutral anion receptors *via* favourable hydrogen bonding interactions.[1.12] In particular, when an electron-withdrawing substituent is introduced into the host receptor, then the -NH protons are acidic enough and deprotonation can occur in some cases in the presence of a highly basic anion for e.g. fluoride, hydroxide and acetate.[1.13] The extensive structural modifications on the hydrogen bonding scaffold have been undertaken to increase the acidity of the -NH protons by introducing strong electron-withdrawing substituents(such as $-NO_2$ and $-CF_3$) *via* mediation of a π-system. The construction of a preorganized binding cleft or cavity using rigid (calixarene or polynorbornane) or flexible structural skeleton finally leads to the binding environment with size and shape complementary for a given anion. In recent times, Custelcean *et al.* has studied the structural role of anions in crystal engineering as anions play diverse roles in the formation of crystals.[1.14] The theoretical calculations on electrostatic anion–π interactions have also been complemented besides conventional N–H···A hydrogen bonding, by mounting experimental confirmations for their existence in the solid as well as in solution state.[1.15] But the examples of anion–π interactions in crystals remain extremely rare in experimental pathways because the C–H···A bonds tend to prevail in competition with anion–π interactions.[1.16] The weak σ interaction involving a small amount of charge transfer from the anion to an arene system become the another competitor, which is geometrically characterized by the anion being located above the periphery instead of the centre of the arene. Recently, the halogen bonding noncovalent interactions which are highly directional (∠D−X—A close to linear) in nature and behave like hydrogen bonds, has been demonstrated both experimentally and theoretically and this involved an electrophilic halogen atom (halocarbon) and a high electron density centre (such as anion).[1.17]

1.4 Anion coordination and anion directed self-assembly of acyclic receptors

Since the early days of anion coordination chemistry, the acyclic and macrocyclic tripodal scaffolds derived from tris(2-aminoethyl)amine bearing -NH functions have extensively been employed for anion binding and encryption featuring receptor cavities.[1.18] Although Nature demonstrate how proteins can selectively and proficiently bind anions by weak intermolecular forces, the development of novel and innovative artificial receptors containing rigid or flexible multi-armed scaffolds for the effective recognition of anions, basically in solid state still remains a challenging task, with hydrogen bonds being fundamental in determining binding selectivity *via* topological complementarity. In general, anions, hydrated-anions or hydrogen-bonded anionic associations as the guest have very high solvation energies that must be compensated by one, two or more host conformers for effective anion recognition and complexation. Among the design choices of receptor scaffolds, numerous tren-based or arene-based tripodal pre-organised flexible acyclic receptors containing either electron-withdrawing or electron-donating terminal aryl functionalization have been vastly reported from last two decades because of their potential ability to encapsulate the anions such as nitrate, phosphate and sulfate especially in solid state. On the other hand, less number of –NH functionalities containing less flexible and more challenging dipodal anion receptors with rigid aromatic isomeric diamine spacers are comparatively less in literature and have been the special case of interest in recent days because of their less preorganised cavity to encapsulate or entrapping an anion alongside lesser chance of forming cooperative anion complexes compared to tripodal receptors. Furthermore, the binding ability of multi-armed acyclic receptors vary with the attached terminal aryl functionality unit, since one or more functional groups systematically and consistently modify the hydrogen bonding capability towards the anions of different size and dimensions. Note that, urea and thiourea are among the most universally used fragments to design neutral receptors for the effective recognition of anions owing to their ability to act as hydrogen-bond donors.[1.19] The term recognition implies the association of host and guest through relatively strong reversible non-covalent interactions. Especially, urea and thiourea can establish two directional hydrogen-bonds with the Y-shaped carboxylate group or chelate a spherical anion and in this sense, the choice of the receptor should be directed towards the most acidic hydrogen-bond donors. Thus, after the seminal papers by Wilcox[1.20a] and Hamilton[1.20b] on urea-anion interactions, a variety of anion receptors have been reported containing one or more urea/thiourea fragments.[1.21] It should be noted that, among the bis-urea/thiourea receptors containing rigid aromatic diamine spacer, the *ortho*-phenylenediamine based bis-urea receptors obviously provide most converging binding sites towards incoming guests rather than *meta*-phenylenediamine based receptors and even least convergent *para*-phenylenediamine based linear receptors. As a consequence, the

more number of bis-urea/thiourea anion receptors have been reported till date in literature, derived from rigid aromatic 1,2-diamine compared to more divergent aromatic 1,3 or 1,4-diamine.

1.4.1 Rigid aromatic diamine centred (thio)urea based anion receptors:

Light, Gale and co-workers reported a tetra-urea neutral receptor **1** (Fig. 1.2a) derived from the reaction of benzene-1,2,4,5-tetramine and phenyl isocyanate in 1:4 equimolar ratio, which described cooperative entrapment of isophthalate dianions within the consecutive dimeric receptor assemblies in solid state.[1.22] The X-ray structure elucidates that the overall neutral complex encompasses tapes of encapsulated hydrogen-bonded isophthalate anions (Fig. 1.2b), that are arranged into parallel sheets interleaved with tetrabutylammonium layers and each of the two independent neutral molecules is disposed about a centre of inversion. Interestingly, it should be mentioned here that, the complete tetra-urea receptor architecture is the combination

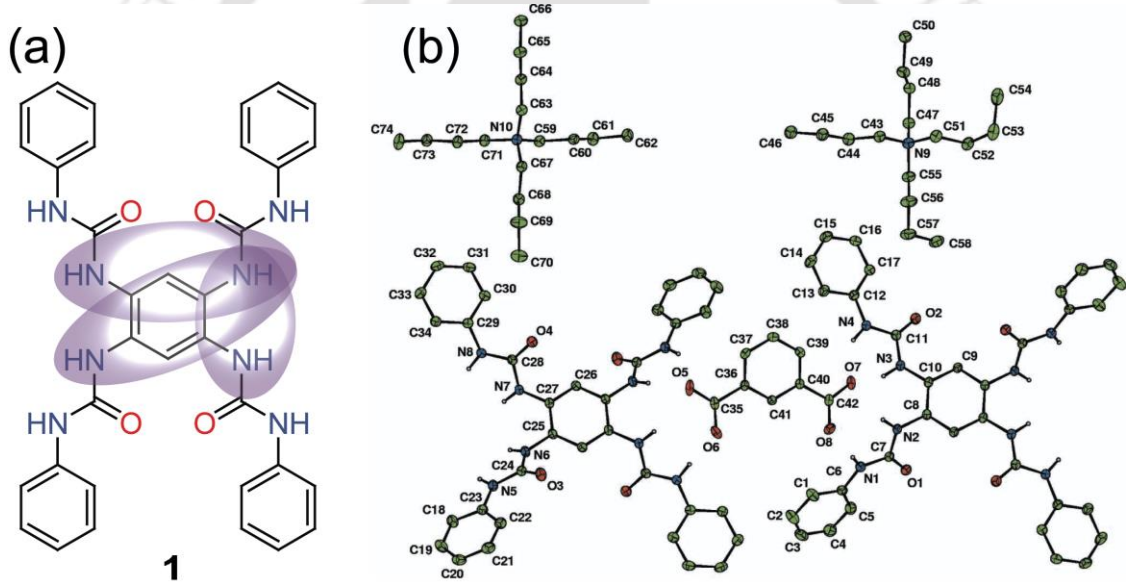

Fig. 1.2 (a) Molecular structure of receptor **1** containing *o*-, *m*- and *p*-phenylenediamine spacer and (b) the ORTEP plot (30% probability level) of isophthalate dianion binding of **1** through most convergent *o*-phenylenene connected bis-urea sides. Reproduced from ref. 1.22, with permission from the International Union of Crystallography.

of *ortho*-phenylenediamine, *meta*-phenylenediamine as well as *para*-phenylenediamine spacer, which is the special case of interest. More importantly, the binding of isopthalate anions occur through the *ortho*-phenylenediamine hydrogen-bond donor sites through cooperative host-guest complex formation, as expected from the most convergent bis-urea zones (Fig. 1.2b) compared to others. In recent past, Caltagirone and cooworkers has reported three fluorescent asymmetric bis-urea anion receptors as fluorometric chemosensors[1.23] derived from three rigid positional isomeric *ortho*-phenylenediamine (Fig. 1.3a), *meta*-phenylenediamine (Fig. 1.3b) and *para*-phenylenediamine (Fig. 1.3c). They studied the binding properties of asymmetric receptors

towards different anions (fluoride, acetate, hydrogencarbonate, dihydrogen phosphate, and hydrogen pyrophosphate $HPpi^{3-}$) with the aid of ^{1}H-NMR, UV-Vis and fluorescence spectroscopy followed by single crystal X-ray diffraction analysis of two complexes of a particular receptor and theoretical calculations.

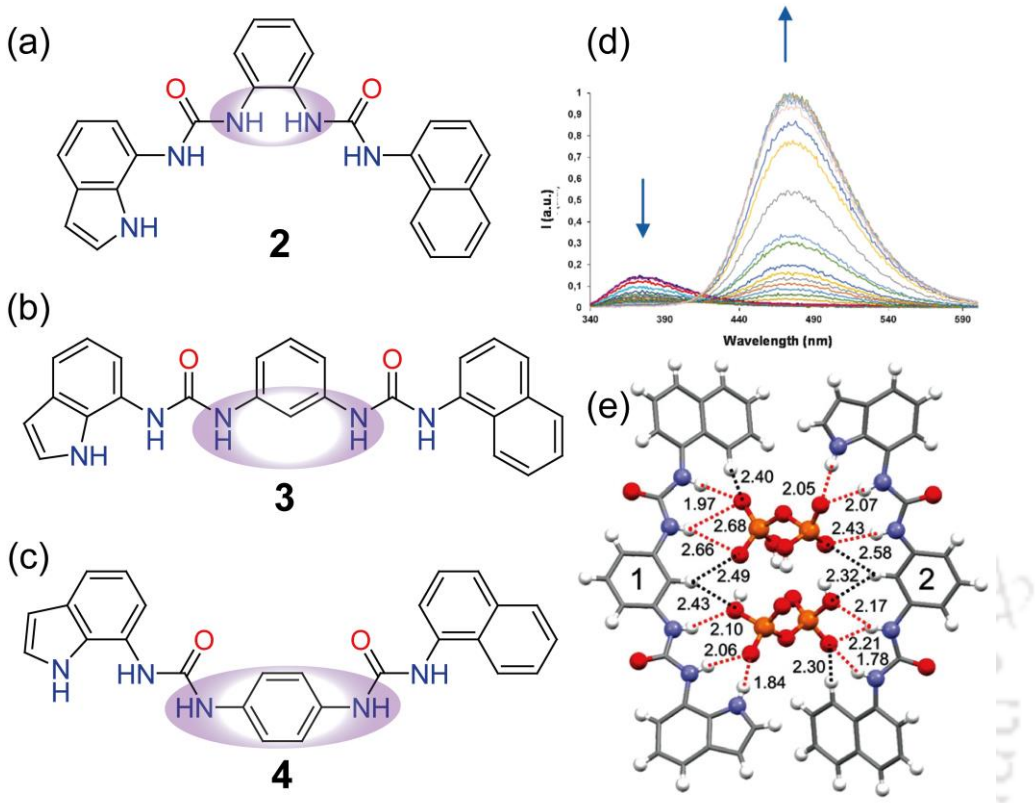

Fig. 1.3 Molecular structure of *o*-, *m*- and *p*-phenylenediamine based dipodal bis-urea hosts (a) **2**, (b) **3**, (c) **4** respectively; (d) changes in the fluorescence spectra of **2** upon addition of hydrogen pyrophosphate ($HPpi^{3-}$) anion in DMSO and (e) X-ray structure (partial) of the $HPpi^{3-}$ bound complex of **3** displaying intermolecular interactions in the receptor-anion complex. Reproduced from ref. 1.23, with permission from the Royal Society of Chemistry.

As expected from these isomeric bis-urea receptors, the most convergent *ortho*-phelynediamine based receptor showed a remarkable affinity for $HPpi^{3-}$ (DMSO-d_6/0.5% H_2O) which also acts as a fluorimetric chemosensor for this anion (Fig. 1.3d) and further when the *ortho*-isomer is included in cetyltrimethylammonium (CTAB) micelles, hydrogen pyrophosphate recognition can also be achieved in pure water. The ^{1}H-NMR titration experiments of each receptor with different anions displayed the change of the ^{1}H-NMR signals of all five NHs shows neat inflection point indicative for cooperative behavior of all NH protons towards anion binding in case of *ortho*- isomer, presumably due to better pre-organization with respect to *meta*- and *para*-isomer. Hence, these results are in agreement with the designed pre-organization degree of the three bis- urea receptors increasing in the order **2** > **3**> **4**. Subsequently, the report also described the crystallization of $H_2PO_4^-$ and $HPpi^{3-}$ (Fig. 1.3e) complexes of only *meta*-isomer **3**, despite many crystallization attempts from other isomers with anionic guests.

1.4.1a *ortho*-Phenylenediamine based (thio)urea anion receptors:

The design and study of rigid *ortho*-phenylenediamine based bisurea receptors for biologically relevant anions; especially Y-shaped oxyanions has become a very active research area in the field of supramolecular chemistry because these systems contain a convergent DDDD hydrogen bond donor array. Such receptors have proven to be excellent oxyanion receptors in solution and in the solid state.

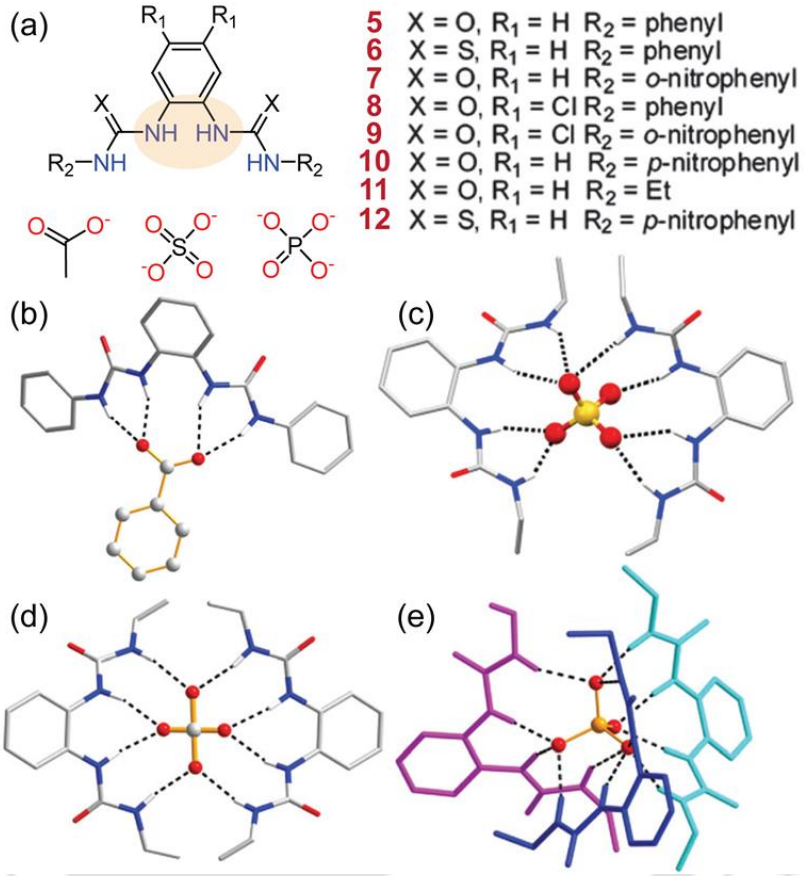

Fig. 1.4 (a) Representative structures of *o*-phenylenediamine based dipodal receptors **5**–**12,** binding monovalent AcO^-, divalent SO_4^{2-}, trivalent PO_4^{3-}; X-ray structure (partial) of the anion-receptor complexes (b) **5**.benzoate, (c) $(\mathbf{11})_2.SO_4^{2-}$, (d) $(\mathbf{11})_2.CO_3^{2-}$, and (e) $(\mathbf{11})_3.PO_4^{3-}$. Reproduced from ref. 1.24, with permission from the Royal Society of Chemistry.

Very recently, Wu and cooworkers have demonstrated recognition of anions by a class oligo-(thio)urea-based receptors, where a special emphasis has been given to *ortho*-phenylene-connected oligoureas in the course of application of anion binding and the self-assembly of important supramolecular architectures, including helicates, tetrahedral cages and so on.[1.24] Gale *et. al.*, Bowman-James *et. al.* and Wu *et. al.* have reported rigid *ortho*-phenylene connected similar kinds of bis-urea receptors **5-12** (Fig. 1.4a), which belong to the class of complementary tetradentate anion receptors. Gale and coworkers studied the anion binding properties of **5-10** (Fig. 1.4a), which revealed selective binding for Y-shaped carboxylate anions over other anions studied ($H_2PO_4^-$, HSO_4^-, Cl^-, Br^-).[1.25] The simple bis-urea receptor **5**, displayed excellent

selectivity for carboxylates in solution, with a crystal structure elucidation of the benzoate complex showing four hydrogen bonds between the receptor and anion through cooperative binding in the solid state.[1.25a] Whereas, by varying the functional groups in receptors **5**–**10**, the binding affinity of carboxylate anions have been modulated in solid as well as in solution state.[1.25b] However, the $H_2PO_4^-$ anion was also bound substantially, the binding of AcO^- was much stronger as determined in a DMSO solution. In recent years, the *ortho*-phenylene-connected bis-ureas **10**–**12** were also used in binding of divalent SO_4^{2-}, CO_3^{2-} anions as well as trivalent PO_4^{3-}anion. Bowman-James and coworkers reported the receptor **11** as a sulfate selective receptor in water-mixed DMSO-d_6 systems with the evidences of X-ray structures, where two of the ligands **11** form a bis-chelate around a single SO_4^{2-} ion in 2:1 host-guest fashion.[1.26] Subsequently, Wu and coworkers also studied the anion coordination behaviors of **10**–**12** towards higher coordinating CO_3^{2-}, SO_4^{2-}, and PO_4^{3-} oxyanions,[1.27] where the bis-urea ligands **10**–**11** and bis-thiourea ligand **12** readily formed the tris chelates $[PO_4(\mathbf{L})_3]^{3-}$ with trivalent PO_4^{3-} in the solid state, although the solution binding studies by ^{1}H NMR and UV-Vis spectroscopy revealed different binding properties of the ligands toward phosphate such as receptor **10** retains the 3:1 host-guest binding ratio, receptor **11** forms 1:1 complex and the more acidic thiourea receptor **12** undergoes deprotonation/decomposition in the presence of phosphate. Hence, as confirmed by the crystal structures of $(\mathbf{11})_2.SO_4^{2-}$, $(\mathbf{11})_2.CO_3^{2-}$ and $(\mathbf{11})_3.PO_4^{3-}$, the bisurea receptors presented a similar conformation as observed in the benzoate complex of **5** (Fig. 1.4b) with all urea NH donors directing to the cleft and donating four strong hydrogen bonds to the guest anion (Fig. 1.4c-e). Note that, as the hydrogen-bond accepting ability is stronger as the anion charge increases, hence the higher charged anions exposed a

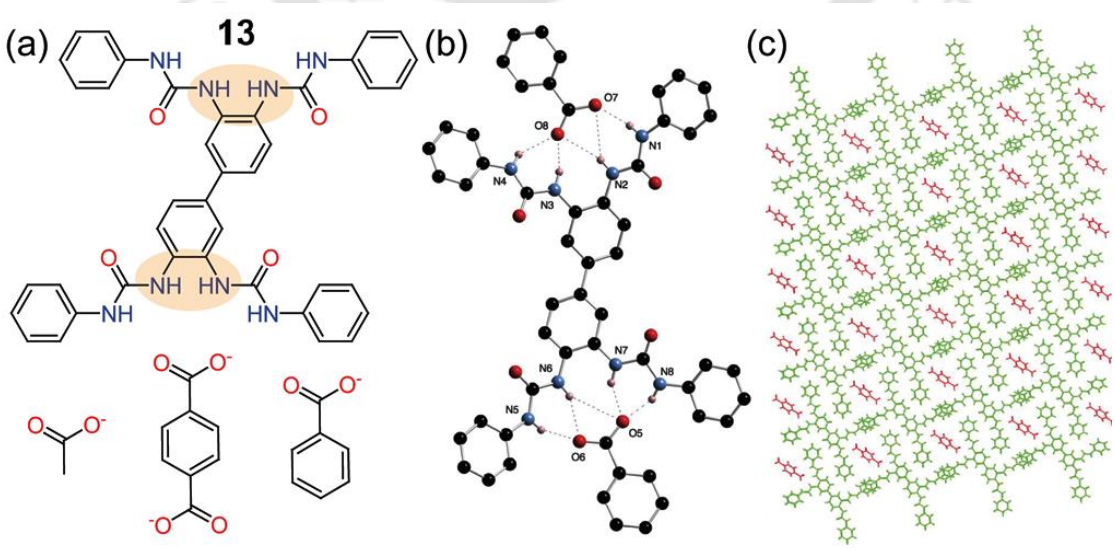

Fig. 1.5 (a) Molecular structure of receptor **13**, two 1,2-diamine spacer binding acetate, terephthalate, benzoate, (b) X-ray structure (partial) of complex **13.**$(benzoate)_2$ and (c) packing motif from *a* axis displaying sheet formation between **13** and terephphalate. Reproduced from ref. 1.28, with permission from the Royal Society of Chemistry.

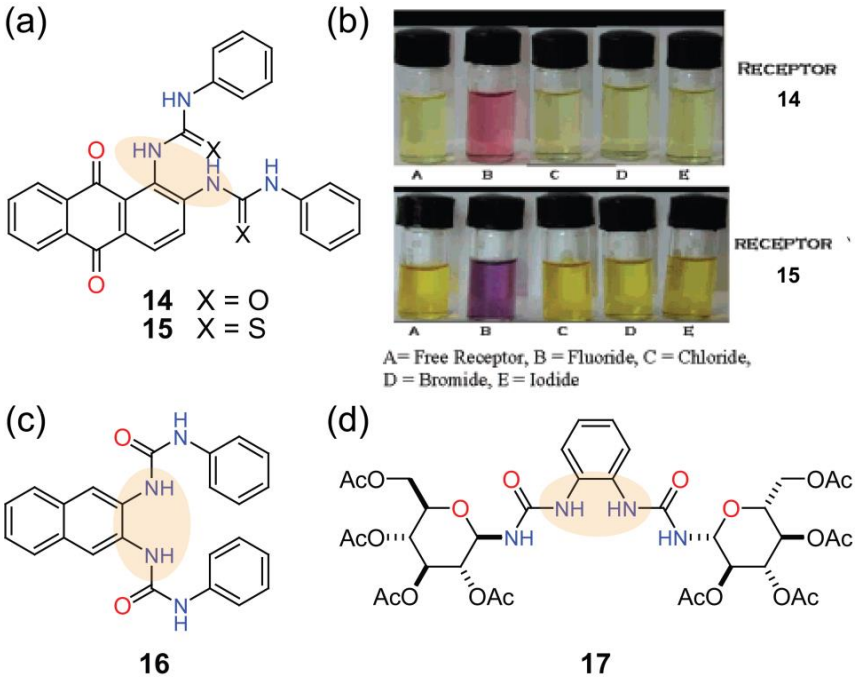

Fig. 1.6 (a) Representative structures of colorimetric fluoride sensors **14**-**15**, (b) color change in visible region of upon individual addition of halides in DMSO/CH_3CN of **14** and **15**, (adapted with permission from ref. 1.29 Copyright 2004 American Chemical Society) (c) molecular structure of fluorescent sensor **16** for halides and (d) Chiral bis-urea receptor **17** for chiral carboxylates derived from mandelic acid and three α-amino acids.

tendency to attract more than one receptor to saturate their coordination number. So, in the cases of divalent carbonate and planar sulfate, two bis-urea receptors were attracted affording the coordination number of eight, while in the case of trivalent phosphate, the three bis-urea receptors were involved affording coordination number of twelve. Gale and coworkers further explore the receptor architecture by providing more than one *ortho*-phenylenediamine motif, where the system containing two bis-urea clefts was synthesized by reaction of 3,3'-diaminobenzidine with phenyl isocyanate. The tetraurea functionalized biphenyl receptor **13** (Fig. 1.5a) was found to form neutral cooperative complex with acetate, benzoate (Fig. 1.5b) and terephthalate (Fig. 1.5c), where each carboxylate group was entrapped in the bis-urea hydrogen

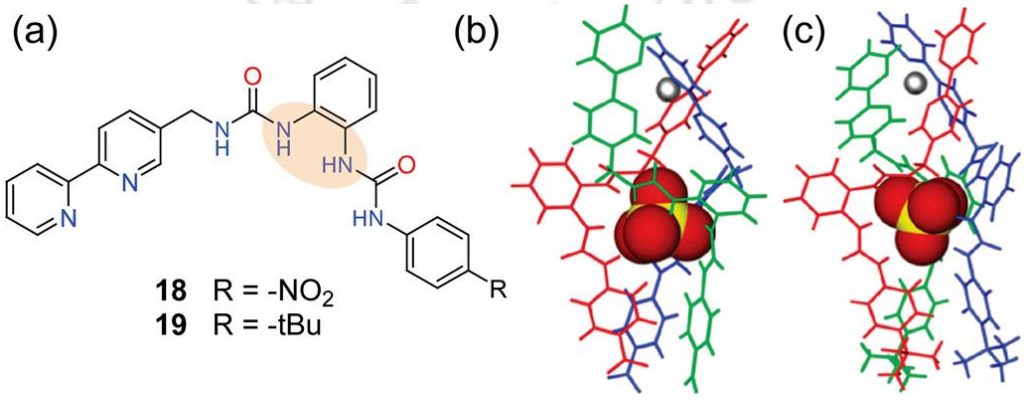

Fig. 1.7 (a) Representative structures of *o*-phenylenediamine based ion-pair receptors **18**–**19**; X-ray structures (partial) of ion pair-receptor complexes depicting (b) self-assembly of receptor **18** with $NiSO_4$ and (c) self-assembly of receptor **19** with $NiSO_4$. Reproduced from ref. 1.32, with permission from the Royal Society of Chemistry.

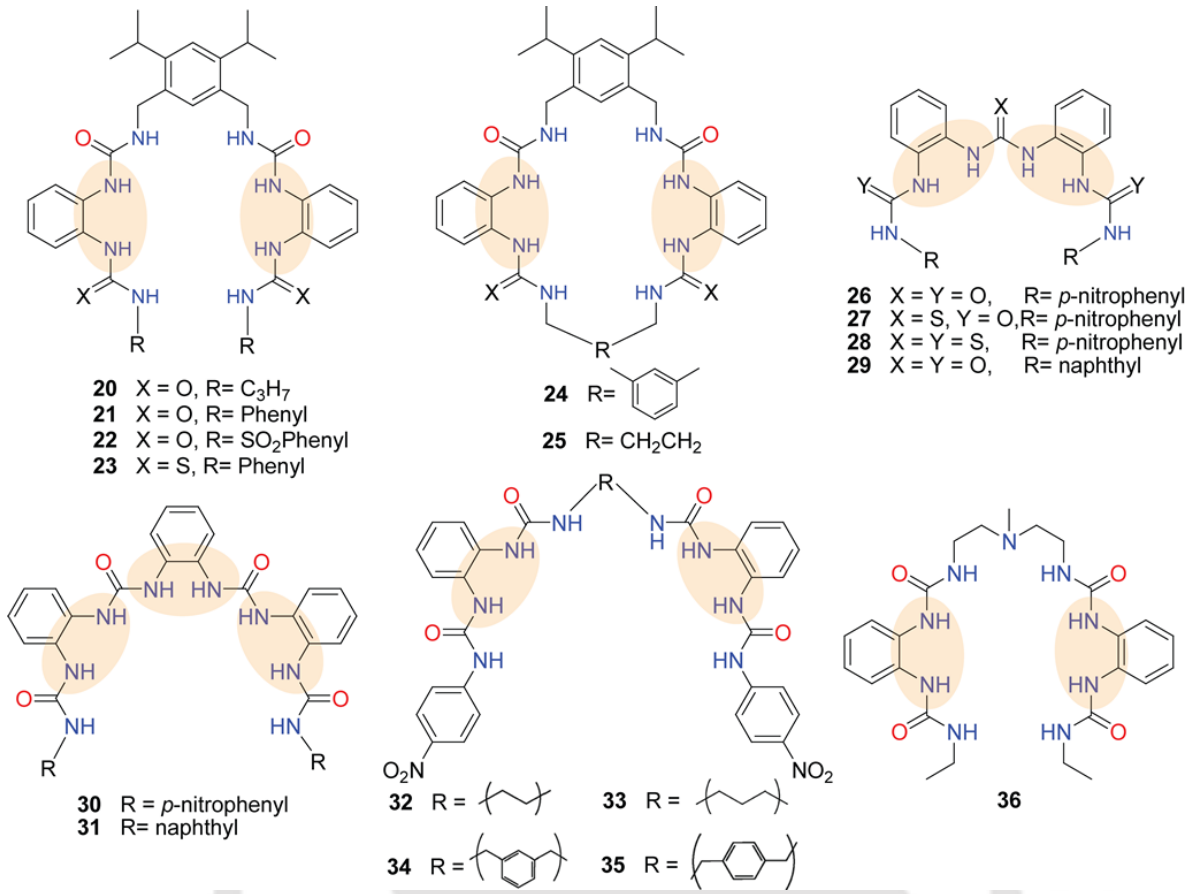

Scheme 1.3 (a) Representative molecular structures of tris-and tetrakis-urea anion-receptors **20**–**35** containing flexible or rigid spacers and using most convergent aromatic diamine (*o*-phenylenediamine) as linkers.

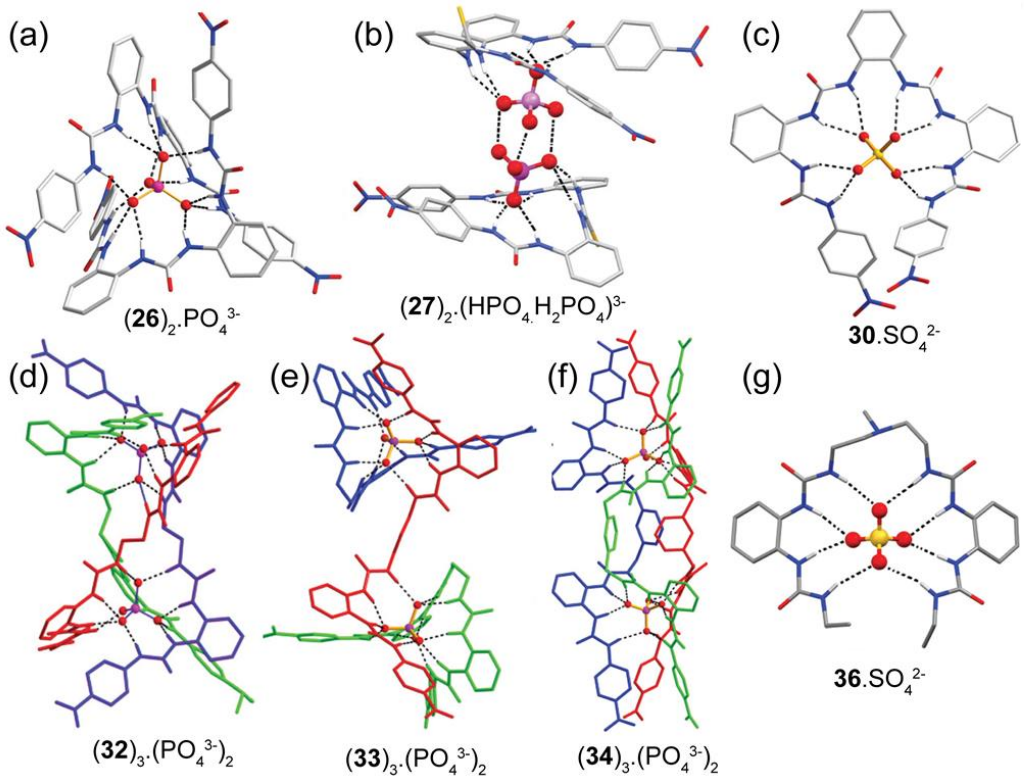

Fig. 1.8 X-ray structures (partial) of neutral host-guest complexes by some tris-and tetrakis-urea receptors as (a) $(\mathbf{26})_2.PO_4^{3-}$, (b) $(\mathbf{27})_2.(HPO_4.H_2PO_4)^{3-}$, (c) $\mathbf{30}.SO_4^{2-}$, (d) $(\mathbf{32})_3.(PO_4^{3-})_2$, (e) $(\mathbf{33})_3.(PO_4^{3-})_2$, (f) $(\mathbf{34})_3.(PO_4^{3-})_2$, and (g) $\mathbf{36}.SO_4^{2-}$. Reproduced from ref. 1.24, with permission from the Royal Society of Chemistry.

bond donor cleft of the neutral receptor molecules in solid state.[1.28] A. Das *et. al.*[1.29] and Tarr *et. al.*[1.30] reported novel colorimetric receptors (Fig. 1.6a,c) containing anthraquinone (**14**, **15**) or naphthyl (**16**) as chromogenic signaling subunits as well as based on *ortho*-phenylene connected bis urea/thiourea hydrogen-bond donor group, basically to investigate the selective fluoride ion sensing (Fig. 1.6b) compared to other halides in solution phase. The bisurea receptor **14** and its thio-urea analog **15** both have shown well-defined color change in the visible region of the spectrum was observed upon fluoride ion addition in DMSO/CH_3CN solution of individual receptors, but these receptors revealed no affinity towards other halides such as Cl^-, Br^- and I^- ions (Fig. 1.6b). However, the fluorescence experiments with *ortho*-phenylene connected naphthyl based bis-urea receptor **16** indicated quenching effects with all four halides, including F^- ion. Furthermore, Jurczak and coworkers reported chiral urea-type anion receptor **17** (Fig. 1.5d) synthesized from *ortho*-phenylenedimaine and 1-amino-1-deoxyglucose to investigate anion binding properties using chiral carboxylates derived from mandelic acid and three α-amino acids.[1.31] The ^{1}H-NMR solution state studies revealed that the association constants obtained in each complex formation of chiral guests by chiral receptors was lower than for pairs of studied chiral receptors and achiral guests. In 2012, Custelcean and coworkers established *ortho*-phenylene-(bis)urea based asymmetric heteroditopic ion-pair receptors **18** and **19** (Fig. 1.7a), which showed formation of $NiSO_4$ and $FeSO_4$ self-assembled [M$\mathbf{L}_3SO_4$] (M=Ni^{2+}, Fe^{2+}) type triple-stranded helicates and mesocates (Fig. 1.7b,c).[1.32] As mentioned earlier, using the preorganised hydrogen-bond donor platform of *ortho*-phenylenediamine connector, some oligourea-based (tris-urea, tetrakis-urea) anion receptors were also reported by Wu *et.al* in recent past and Reinhoudt *et. al* in 2000.[1.33] By tuning the length and rigidity of the spacer or linkers, these *ortho*-phenylene connected tris-urea or tetrakis-urea receptors have been found to trap oxyanions, especially the tetrahedral sulfate or phosphate in solid state (Fig. 1.8) *via* formation of neutral helicate, mesocate, mono-bridged or capsular assemblies. Reinhoudt and co-workers reported four acyclic and two macrocylic receptors **20**–**25** (Scheme 1.3) using four hydrogen bond donating two *ortho*-phenylene bis-urea moieties, which showed the better complex formation with $H_2PO_4^-$ over Cl^- in quantitative ^{1}H-NMR (DMSO-d_6) studies[1.33a], although there were no solid state evidence. However, the *ortho*-phenylene linker was utilized by Wu's group in the building of the tris-urea receptors **26**-**29** and tetrakis-urea receptors **30**-**35** (Scheme 1.3) which demonstrated very high affinities towards sulfate and phosphate anions (Fig. 1.8a-f) *via* formation of unimolecular or dimeric receptor capsule or constructions of helicate, mesocate, and mono-bridged anion-receptor motifs in solid state.[1.33b-e] But, the highly acidic tris-(thiourea) **28** underwent deprotonation and thus lost binding in the presence of most

of the basic anions.[1.33d] Furthermore, Bowman-James and coworkers also reported the sulfate selective (Fig. 1.8g) tetrakis-urea receptor **36**, which also incorporates aliphatic flexible linker and rigid (*o*-phenylene) connector (Scheme 1.3).[1.26]

1.4.1b *meta*-Phenylenediamine based (thio)urea anion receptors:

The design and synthesis of receptors derived from rigid 1,3-aromatic diamine or *meta*-phenylenediamine for binding studies of environmentally or biologically relevant anions become reflected as a less explored area in anion recognition chemistry compared to *ortho*-phenylenediamine connected receptors, which is probably the consequences of less preorganised or less cooperative hydrogen-bond donor sites of the former. K. Ghosh and co-workers reported

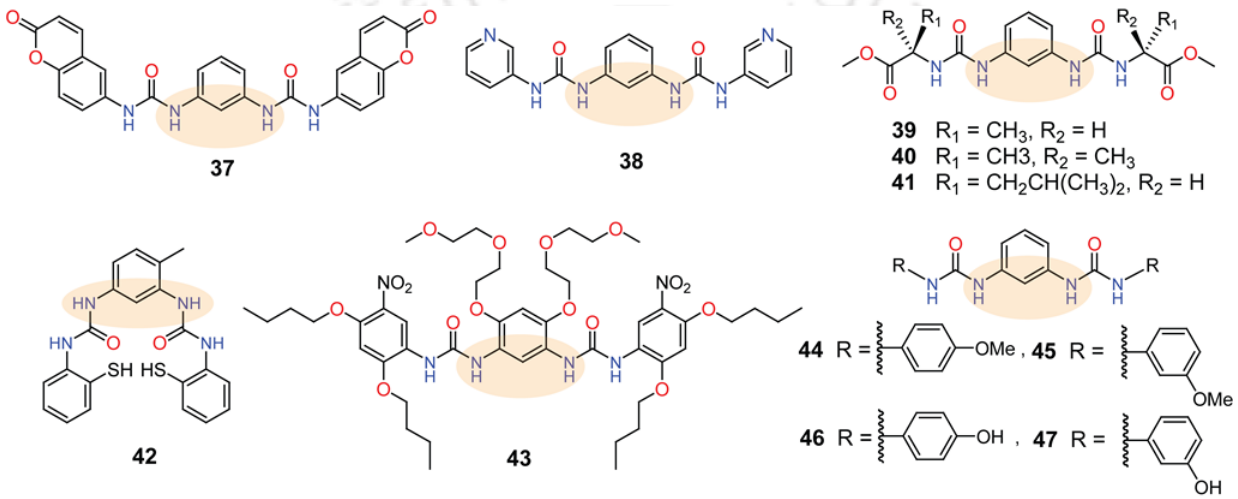

Scheme 1.4 Representative molecular structures of *m*-phenylenediamine based bis-urea anion-receptors **37**-**47**.

a *meta*-phenylenediamine based coumarin linked ditopic bis-urea receptor **37** (Scheme 1.4), which fluorometrically distinguished isomeric aromatic dicarboxylates in polar solvent DMSO as well as they also showed that ditopic receptor are more sensible towards dicarboxylates in organic solvent. The solution state ^{1}H-NMR analysis, UV-visible and fluorescence studies in the course of receptor-anion interaction reveal that the receptor is capable of distinguish isomeric aromatic dicarboxylates with moderate binding constant values.[1.34] In 2012, P. Dastidar's group reported a *meta*-phenylenediamine connected bis-pyridyl-bis-urea ion-pair receptor **38** (Scheme 1.4), which exhibited the formation of Cu^{II} coordination polymers capable of gelation as well as selective SO_4^{2-} separation. They demonstrated a series of four new coordination polymers by reacting ligand **38** and $CuSO_4$, $CuCl_2$, $CuBr_2$, and CuF_2 respectively from individual aqueous ethanolic DMF solution mixtures in 1:2 (metal : ligand) ratio and under these suitable conditions the systems produce metallogels.[1.35] The single crystal structures of the coordination polymers were used in structure-property correlation and *in situ* crystallization of one of the coordinated Cu^{II} polymer of receptor **38** has also been exploited for separating SO_4^{2-} anion from a complex

mixture of different oxyanions. V. Haridas and cooworkers synthesized amino acid-based three receptor molecules **39**–**41** containing bis-urea moiety connected with rigid *meta*-phenylenediamine spacer (Scheme 1.4) to inspect their anion binding affinities.[1.36] The binding of anions was studied by monitoring the ^{1}H NMR titrations of receptor **41** in chloroform upon sequential addition of tetrabutylammonium salts of anions, which describes the better binding efficiency of molecule **41** with phosphate and sulfate compared to other anions. Interestingly, all these receptors underwent proton transfer when treated with fluoride salts resulting in the formation of imidazolidinediones *via* cyclization and subsequently the crystal structure of one such diimidazolidinedione also displayed self-assembly formation through nonconventional hydrogen bonding interactions.[1.36] Kuwar and co-workers synthesized a *meta*-phenylenediamine and thiol based fluorescent bis-urea chemosensor **42** (Scheme 1.4) and note that despite the presence of anion binding bisurea moieties, the receptor showed excellent selectivity for Fe^{3+} ion with 'fluorescence off' mechanism in semi aqueous phase over other commonly coexistent interfering metal ions and the solution state binding studies were further supported by the detailed DFT calculations.[1.37] In 2016, Gong and coworkers reported another *meta*-phenylenediamine based bis-urea receptor **43** (Scheme 1.4) which exhibited as host for anions and its counter-cation with same affinity as observed in solution state. The ^{1}H NMR binding experiments with the aromatic oligourea receptor **43** were carried out by sequential addition of different tetraethylammonium anion salts to the individual ligand solutions in $CDCl_3$, resulting in the better binding affinity of the receptor toward $Et_4N^+Ac^-$ over other salts like $Et_4N^+Cl^-$ and $Et_4N^+I^-$ further demonstrated by 2D ROESY spectral analysis.[1.38] Very recently in 2018, Gunnlaugsson's group reported detailed solution-state anion recognition studies followed by few structural proofs of a series of electron-rich *meta*-phenylene based bis-urea receptors **44**–**47** (Scheme 1.4) and then analyzed the self-assembled host-guest structures. The ^{1}H NMR titration experiments (in DMSO-d_6) of receptors in solution state with a variety of *n*-TBA salts demonstrated the strong binding affinity towards $H_2PO_4^-$, AcO^- and BzO^- anions and comparatively weak binding towards Cl^-, HSO_4^- and SO_4^{2-} anions. Furthermore, the host-guest complexes of receptors **44** and **45** were characterized by X-ray crystallography to validate the anion-binding behavior, which results in the formation of mixed phosphate bound triple-stranded of receptor **45** and hydrated-acetate bound 1:2 host-guest complex of receptor **44** (Fig. 1.9a,b).[1.39]

1.4.1c *para*-Phenylenediamine based (thio)urea anion receptors:

The oligourea anion receptors based on most divergent binding site containing rigid *para*-phenylenediamine spacer have also been a rarely explored area compared to the *ortho*-

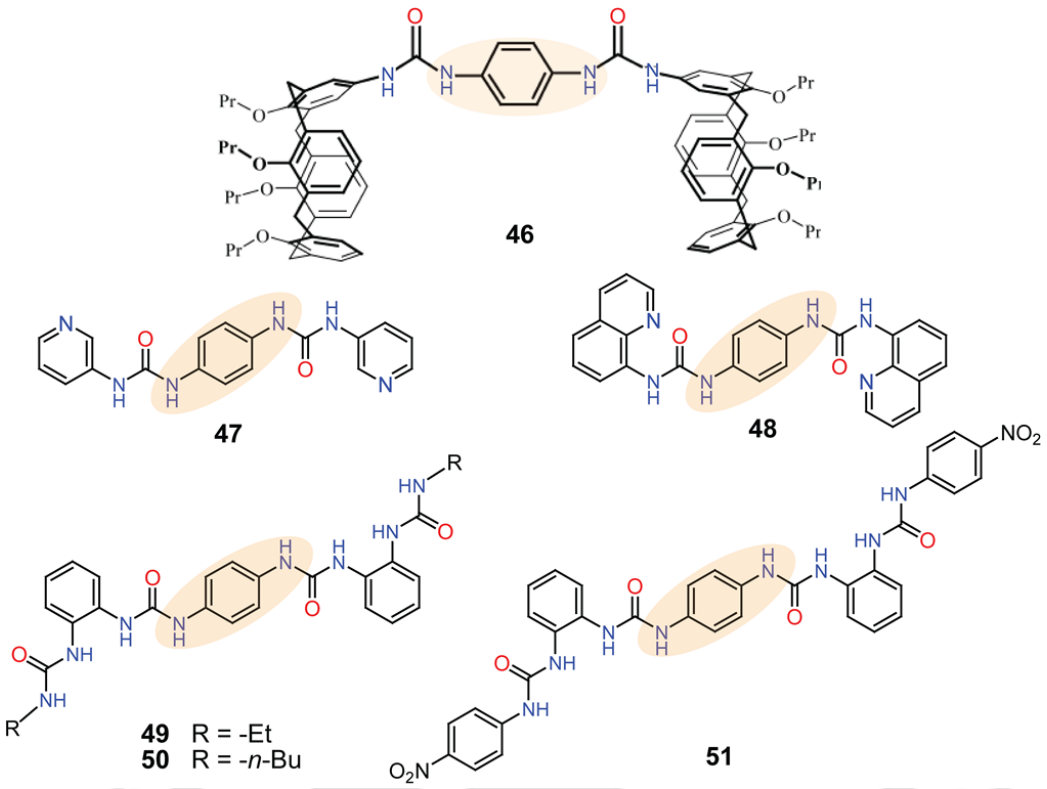

Scheme 1.5 Representative molecular structures of urea anion-receptors **46-51** based on *p*-phenylenediamine spacer.

phenylenediamine spacer, possibly because of the less preorganized as well as less cooperative linear host architectures. Lhotak, Sitbor and co-workers reported a bis-calix[4]arene derivative

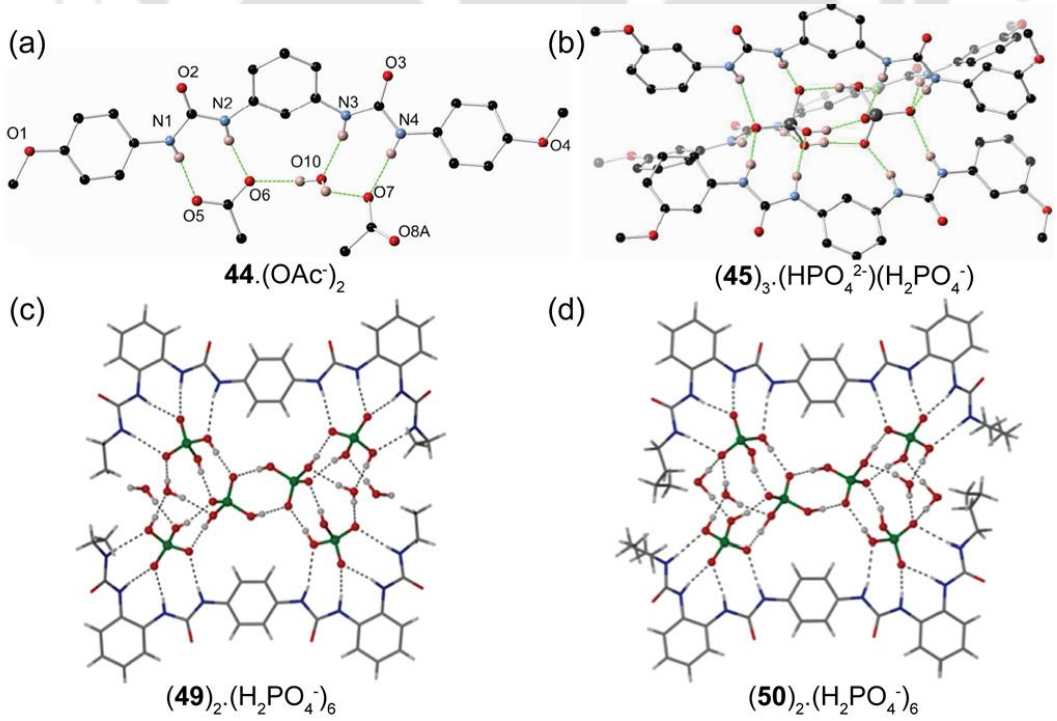

Fig. 1.9 X-ray structures (partial) of anion bound complexes of some *m*-phenylenediamine and *p*-phenylenediamine receptors displaying neutral host-guest self-assembly formation as (a) **44**.$(OAc^-)_2$, (b) $(\mathbf{45})_3.(HPO_4.H_2PO_4)^{3-}$ (adapted with permission from ref. 1.39 Copyright 2018 American Chemical Society), (c) $(\mathbf{49})_2.(H_2PO_4^-)_6$ and (d) $(\mathbf{50})_2.(H_2PO_4^-)_6$ (adapted with permission from ref. 1.43 Copyright 2013 American Chemical Society).

46 (Scheme 1.5) having two potential complexation sites for anions, where two calixarene units are connected *via* a rigid aromatic 1,4-aromatic diamine spacer. The anion binding studies of biscalixarene bis-urea receptor **46** were carried out by ^{1}H-NMR titration in $CDCl_3$/DMSO-d_6 mixture, with spherical halides (Cl^-, Br^-, I^-) and benzoate, which described the better complexation with chloride and benzoate anions.[1.40] According to the report, although the ligand was designed to complex two anions at both anion binding positions (urea units), but the Job plot measurement confirmed the exclusive 1:1 host-guest complexation and the possible explanation has been given as the repulsive interactions between two negatively charged sites in close proximity. P. Dastidar's group reported the formation of a Borromean weave shaped coordination polymer sustained by urea-sulfate hydrogen bonding interactions, when a pyridine substituted *para*-phenylenediamine based bis-urea receptor **47** (Scheme 1.5) is reacted with $ZnSO_4.7H_2O$. They have also demonstrated that the coordination polymer could be exploited to separate sulfate anion selectively from a complex mixture of oxyanions (sulfate, nitrate, perchlorate and triflate) *via in situ* crystallization of the corresponding coordination polymers.[1.41] Another *para*-phenylenediamine connected quinoline based bis-urea receptor **48** (Scheme 1.5) was designed and synthesized by Hossain *et. al.* to investigate its binding ability with different anionic guests such as halides, perchlorate, nitrate, dihydrogen phosphate and hydrogen sulfate by UV-Vis titration experiments in DMSO. The results from solution state binding studies demonstrated that the linear bis-urea ligand displayed high affinity and moderate selectivity towards hydrogen sulfate in 1:1 host-guest complexation mode over the other anions studied. The DFT studies suggested that an anion is bound within the dipodal receptor cleft *via* N–H···A and C–H···A interactions and subsequently the results from ^{1}H-NMR solution state studies also proposed that the binding aptitude is predominately governed by hydrogen bonding interactions and the basicity of anions.[1.42] Custelcean and coworkers established two tetrakis urea receptors **49** and **50** developed on a linear *para*-phenylenediamine spacer (Scheme 1.5), further connected with two convergent hydrogen bond donating *ortho*-penylene groups in two opposite sides of the linear *para*-phenylene moiety. They demonstrated the co-crystallization of both ligands in their neutral form with *n*-$TBAH_2PO_4$ salts resulted in the isolation of discrete $(H_2PO_4^-)_4$ and $(H_2PO_4^-)_6$ anionic associations stabilized in the crystalline state by multiple urea hydrogen bonding interactions (Fig. 1.9c,d).[1.43] Very recently, in 2018 Wu's group has reported another tetrakis urea receptor **51** (Scheme 1.5), developed by the similar combination of *para*-phenylene and *ortho*-phenylenediamine moieties as observed in the report of Custelcean *et. al.* Noticeably, Wu and coworkers demonstrated an anion-coordination-based A_4L_6 (A = anion, L = ligand) tetrahedral cage, was built by C_2-symmetric ligand and phosphate anion, which further

displayed reversible interconversion with A_2L_3 triple helicate *via* supramolecular transformation.[1.44]

1.4.2 Anion receptors based on flexible tripodal spacers:

Molecular self-assembly of acyclic tripodal podand receptors into well-defined architectures has a key feature to construct fascinating and complex structures from very simple building blocks, due to their high degree of convergence and when more than one subunits are geometrically and functionally complementary, they may self-assemble to produce a super molecule. In the course of rapid complexation/decomplexation kinetics, the more readily synthesized acyclic podands may undergo significant conformational changes in comparison with macrocyclic hosts upon the binding anionic guests. Along this line, the flexible tripodal receptors such as tren-based ligand system constitute a special class of acyclic ionophores, whose side arms upon functionalization with appropriate anion binding elements can efficiently employed to recognize one or more anionic guest species *via* topological complementarity with construction of self-assembling capsules in most of the cases (Scheme 1.7). These kinds of anion induced capsules and pseudocapsules of tripodal receptor scaffolds can create a distinct microenvironment to isolate an anionic guest from the bulk of solvent media by encapsulation and subsequently they have exposed a variety of exciting properties such as, encapsulation of hydrated anion clusters/adducts, fixation of atmospheric carbon dioxide as carbonate/bicarbonte, liquid-liquid extraction of anions from water, selective separation of anions by crystallization and transmembrane anion transportation.

1.4.2a Tripodal amine receptors with flexible Tren spacer:

The tripodal amine receptors derived from flexible Tris(2-aminoethyl)amine (tren) have been shown to coordinate with anionic guests of different dimensionality in their triprotonated form Bowman-James *et al.*[1.45a], Ghosh *et al.*[1.45b], Hossain *et al.*[1.45a,c] and our group[1.45d] reported tripodal polyamine receptors **52**–**55** (Scheme 1.6a) bearing terminal aryl functions as phenyl, pentafluorophenyl, thiopene and 4-chlorophenyl groups respectively to discuss the structural aspects of anion binding in their protonated forms. The X-ray structural elucidation each ligand in their triprotonated form reveal that the smaller tripodal cavity containing scaffolds always open up their three arms in either non-capsular or pseudo-capsular orientation to bind larger anionic guests such as bromide, iodide, nitrate, phosphate, hexafluorosilicate, *p*-toluenesulphonate etc through non-covalent interactions. The only exception were observed in case of smallest halide (fluoride anion) binding, where the pentafluorophenyl and 4-chlorophenyl substituted protonated tris-amine receptors **53** and **55** respectively, fully encapsulate the smallest spherical anion

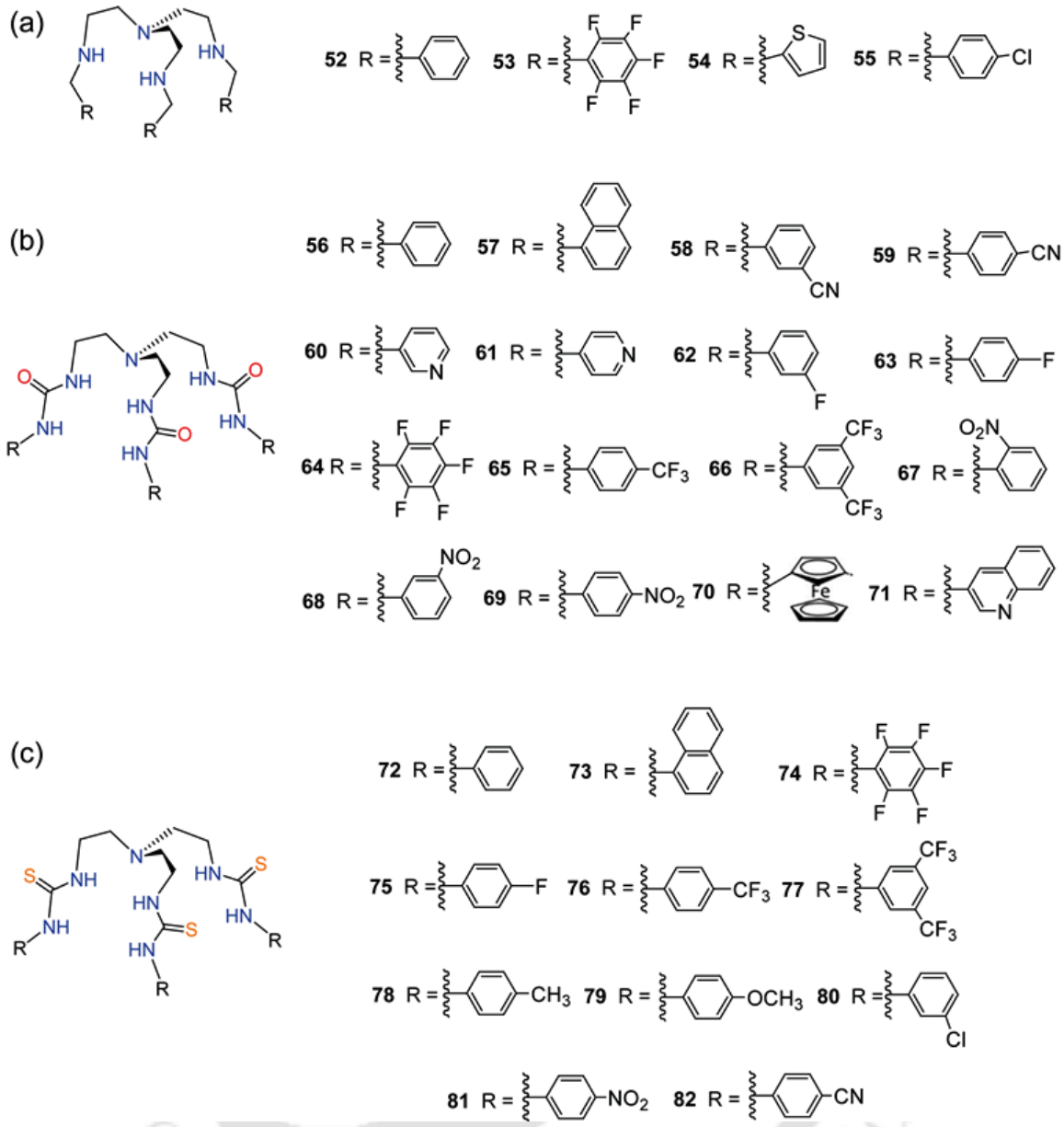

Scheme 1.6 (a) Representative molecular structures of flexible aliphatic Tris(2-aminoethyl)amine (tren) based (a) tris-amine, (b) tris-urea and (c) tris-thiourea anion-receptors.

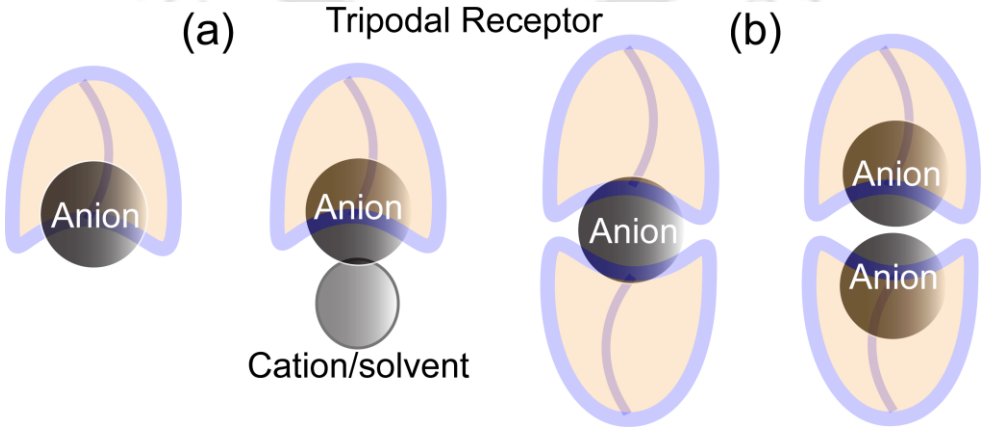

Scheme 1.7 Schematic diagrams of formation of (a) 1:1 receptor-anion and cation or solvent sealed capsular/pseudo-capsular monomeric assemblies and (b) 2:1 and 2:2 receptor-anion dimeric capsular/pseudo-capsular assemblies.

fluoride inside the tripodal capsular cavity by strong hydrogen-bonding interactions in 1:1 host-guest fashion.[1.45]

1.4.2b Tripodal (thio)-urea receptors with flexible Tren spacer:

As urea and thiourea functionalities can generate two directional hydrogen bonds with the anionic guests, a variety of tren-based acyclic receptors containing thio-(urea) subunits (Scheme 1.6b,c) have been developed and applied for anion recognition and sensing in solid and solution state over the last decades. However, the most of the anion complexation in solid state have been achieved, when the tripodal scaffold contain either electron-withdrawing π.-acidic or electron-donating substituents at the terminal aryl rings. Noticeably, it has also been observed from the survey of tripodal anion receptors that the (thio)-urea functionality is dominantly utilized over the other classes of hydrogen bond donors. In 1995, Morán *et al.* established the first tren-based simplest trisphenylurea receptor **56** and its thio-urea analog **72** (Scheme 1.6b,c) which showed tetrahedral oxyanion binding *via* 1:1 host-guest complexation mode based on only solution state ^{1}H-NMR experiments.[1.46a] Following on the similar concepts, Wu *et al.* reported the recognition of tetrahedral $H_2PO_4^-$ and HSO_4^- by complexation-prompted fluorescence enhancement[1.46b] of the tris-naphthylurea receptor **57** (Scheme 1.6b) and later the same group also reported the thio-urea analogue **73** (Scheme 1.6c) which exhibited considerable absorption spectral changes upon complexation with same anionic guests from DMF solutions in 1:1 host-guest fashion.[1.46c] Note that, no structural data were available for these simple phenyl and naphthyl substituted (thio)-urea receptors to support the host-guest complementarity and the shape recognition for the tetrahedral oxyanions. After these pioneering work on tren-based (thio)-urea anion-receptor chemistry by Moran's and S. Wu's group, a number of tripodal urea and thiourea receptors mostly with electron withdrawing aryl substituents have been developed for the recognition and separation of anionic guests like sulfate and phosphate. Most of these reports highlight the structural aspects of anion binding within the electron-deficient suitable tripodal (thio)-urea cleft, which were then associated to the observed selectivity in solution state. The 3-cyanophenyl functionalized tris-urea receptor **58** (Scheme 1.6b) reported by Custelcean's and Ghosh's group has been recognized as a versatile anion receptor accounting for, the selective sulpate separation *via* crystallization of Ag+ coordinated framework,[1.47a] the encapsulation of staggered conformer of divalent oxalate anion,[1.47b] and the uptake of aerial CO_2 as divalent CO_3^{2-} complex that further extracts sulfate, thiosulfate and chromate from water *via* anion exchange metathesis.[1.47c] Ghosh and coworkers further showed that the planar divalent oxalate anion conformer can be captured within the tripodal scaffold of the 3-fluorophenyl-functionalized tris-urea receptor **62** (Scheme 1.6b). Then the 3-pyridyl substituted tris-urea receptor **60** (Scheme 1.6b) self-assemble

into crystalline capsules upon complexation with Mg^{2+} salts of divalent oxyanions SO_4^{2-}, SeO_4^{2-}, CO_3^{2-}, SO_3^{2-} in aqueous methanol solutions, and the competitive crystallization experiments established the better anion selectivity of receptor towards sulfate over other anions, as reported by Custelcean *et al.*[1.48a] Structurally similar hydrated Mn^{2+}/Zn^{2+} bridged dimeric SO_4^{2-} capsules have also been developed by Wu and Janiak *et al.*[1.48b] Custelcean and coworkers has also demonstrated the sulfate separation from a highly competitive aqueous alkaline solution by selective crystallization of sodium-based coordination capsule $[Na_2SO_4(\mathbf{60})_2(H_2O)_4]$ and that provided a viable approach to sulfate separation for the first time from nuclear wastes.[1.48c] Another metal assisted anionic capsular assemblies was reported by Wu *et al.* where the tris(4-pyridylurea) receptor **61**(Scheme 1.6b) forms 2:2 dimeric capsules with chloride salts of alkali (Na/K) and alkaline earth metals (Mg/Ca), but the formation of 2:1 host-guest dimeric capsules were observed with carbonate salts of alkali metals (Na/K).[1.49] Ghosh and co-workers developed a pentafluorophenyl-substituted tris-urea receptor **64** (Scheme 1.6b), which has extensively been used as a versatile receptor for halide and oxyanions in solid state strongly supported from both ^1H NMR and isothermal calorimetry titration studies in solution phase.[1.50] The X-ray analyses clearly revealed that the monovalent F^-, OH^- and $H_2PO_4^-$ anions form 1:1 complexes, and divalent CO_3^{2-}, SO_4^{2-} and HPO_4^{2-} oxyanions formed 2:1 host-guest capsular complexes. P. A. Gale's group in 2011 demonstrated the transmembrane anion transport properties of a series of fluorinated tripodal tris-urea receptors **63-66** (Scheme 1.6b) and their thiourea analogues **74-77** (Scheme 1.6c) accompanied by the detailed solid and solution phase anion binding studies.[1.51] Based on the experimental results attained, they have proposed that increasing the degree of fluorination increases the lipophilicity of the tripodal receptors and this has shown to be the key contributing factor in the superior transport activity of the fluorinated compounds, with a maximum transport rate achieved with compound **66**. Furthermore, a set of three positional nitro-phenyl functionalized isomers of tris-urea receptor **67-69** (Scheme 1.6b) was extensively studied by our group, to investigate the recognition processes with various oxyanions such as sulfate, carbonate, mixed-phosphate, terephthalate etc.[52] The *para*-nitrophenyl substituted isomer **69** was previously established to form a large dimeric capsular complex with SO_4^{2-} *via* encapsulation of a rugby ball shaped ($SO_4^{2-}\cdot 3H_2O\cdot SO_4^{2-}$) adduct assembled by electrostatic nitro-nitro interactions.[1.52d] On the other hand, the anion complexation with *ortho*-nitro isomer **67** in the presence of different oxyanion salts was not fruitful probably because of the steric effect provided by the *ortho*-nitro groups, that hinders the facile inclusion and coordination of an anion due to electrostatic factor, as confirmed by 2D NOESY NMR analysis of the free receptor **67**.[1.52a] The ferrocene group substituted redox-active tris-urea scaffold **70** (Scheme 1.6b) has also been reported as an electrochemical sensor for SO_4^{2-} and $H_2PO_4^-$ anions, as demonstrated by

Wu and Yang *et al.*[1.53a] Moreover, another quinolone based tripodal tris-urea receptor **71** (Scheme 1.6b) has been employed by the same research group to control intermolecular SO_4^{2-} transfer between the receptors **70** and **71** driven by an electrochemical stimulus, which is noticed by the change of the fluorescence intensity before and after electrochemical oxidation of the ferrocene groups.[1.53b] The divalent tetrahedral oxyanion (sulfate, phosphate, carbonate) encapsulation in solid state *via* deprotonation of their monovalent state has also been observed from our group in the solid-state by employing the *para*-tolyl and *para*-methoxyphenyl-substituted thiourea receptors **78** and **79** (Scheme 1.6c).[1.54] The construction of 2:1 host-guest capsular complexes of a chlorophenyl substituted tris-thiourea receptor **80** (Scheme 1.6c) with sulfate and thiosulfate anion was also observed by our group.[1.55] We have further demonstrated a *para*-nitrophenyl substituted tris-thiourea hydrogen bonding scaffold **81** (Scheme 1.6c) that can selectively encapsulate a trivalent phosphate anion (PO_4^{3-}) inside the dimeric capsules assembled by aromatic π-stacking interactions between the receptor side-arms.[1.56] The anion binding aptitudes of a *para*-cyanophenyl-substituted thiourea **82** (Scheme 1.6c) was thoroughly explored by Ghosh and co-workers in combined solid and solution-phase. The solution-state ^{1}H NMR spectroscopy and ITC experiments showed relatively higher association constants with halides over oxyanions, which is different from its urea analogue **59** and in addition the receptor **82** form a 2:1 host-guest capsular complex with SO_4^{2-} anion as identical to the other thiourea receptors in solid state.[1.57]

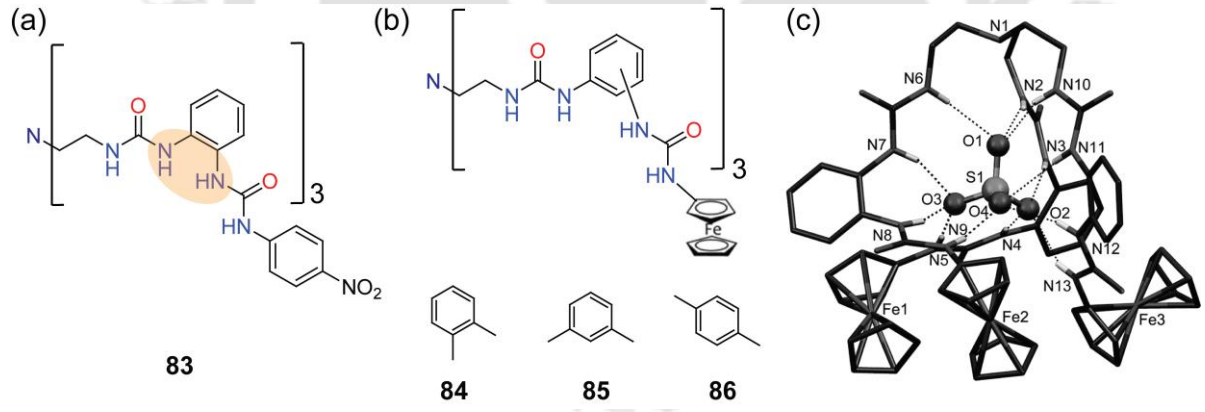

Fig. 1.10 (a) Molecular structure of *o*-phenyldiamine linked hexakis-urea receptor **83**, (b) representative structures of *o*-, *m*-, *p*-phenyldiamine linked hexakis-urea receptor **84**–**86** and (c) X-ray structures (partial) of **84**.SO_4^{2-} complex. Reproduced with permission from ref. 1.58 (b) Copyright Wiley-VCH Verlag GmbH & Co. KGaA.

Furthermore, it is interesting to note that the flexible aliphatic tren moiety have been used to make hexakis-urea anion receptor, when it is combined with rigid *ortho*-phenylenediamine *meta*-phenylenediamine and *para*-phenylenediamine groups, reported by Wu and co-workers. Firstly, they extended each of the three monourea arms of the tripodal receptor to an *ortho*-phenylene-bridged bisurea moiety to produce a hexakis-urea ligand **83** (Fig. 1.10a) that could completely encapsulate a sulfate ion through hydrogen bonding interactions and the receptor

also exhibited the almost-quantitative extraction of sulfate from the aqueous phase into the organic phase in a recyclable manner.[1.58a] Later they reported three ferrocenyl-functionalized tripodal hexakis-urea anion receptors with *ortho*- (**84**), *meta*- (**85**), and *para*-phenylene (**86**) bridges (Fig. 1.10b), which displayed strong binding affinities toward sulfate ions and particularly, the *meta*-phenylene bridged receptor **85** exhibited step-wise encapsulation of two divalent SO_4^{2-} ions in its "inner" and "outer" tripodal clefts, respectively owing to the trigonal bipyramidal host architecture, as observed from distinct NMR resonances and molecular modeling studies. But the *ortho*-phenylene bridged ligand **84** showed sulfate anion encapsulation (Fig. 1.10c) with excellent complementarity between the receptor and sulfate, as observed in the case of nitrophenyl analogue **83**.[1.58b]

1.5 Concluding remarks

As a whole, the acyclic receptors containing rigid or flexible scaffolds with suitably positioned binding sites can recognize anions/hydrated-anions or ion-pairs either in solid or in solution state or simultaneously in both phases, which also assist in the formation of molecular self-assembly process. In particular, the (thio)-urea functions can create two directional hydrogen bonds with anions. Hence the design of sophisticated three-dimensional architectures with two or more (thio)-urea functionalization have been utilized dominantly over the other functionalities, which can bind environmental and biologically relevant anions by cooperative or non-cooperative interactions. The rigid isomeric aromatic diamine based dipodal thio-(urea) receptors have shown their effective potential towards binding of anionic guests heavily depending upon the degree of convergence of hydrogen-bond donor groups as well as the electronic and positional isomeric effect of terminal aryl receptor substituents followed by the dimension of guest assemblage. The dipodal thio-(urea) receptors containing rigid *ortho*-phenylenediamine spacer have been used more predominantly in literature compared to its isomeric *meta*-phenylenediamine and *para*-phenylenediamine spacer with mono-substituted terminal aryl groups in most of the cases. The convergent anion binding sites with more preorganized and cooperative architectures of rigid *ortho*-phenylene connection have also been utilized to produce several tetrakis-urea and hrexakis-urea anion receptors. On the other hand, the tris(2-aminoethyl)amine based tripodal receptors mostly with π-acidic or electron-withdrawing terminals in anion receptor chemistry have exposed their high potential towards anion assisted capsule and pseudo-capsule formation from the last two decades. It was also found that the position of the attached substituents in aryl terminals play a significant role towards the formation of different microenvironment for anion encapsulation and hence the architecture of the resulting complex. Furthermore, it should also be noted that after the seminal

work on tren-based simplest (thio)-urea anion receptors in only solution state by Moran and Wu's group, the solid state anion complexation of those highly electron-rich tripodal scaffolds was underexplored till the last year. Thus, the recognition of anions, hydrated-anions, anionic associations in molecular receptor barrel or capsules *via* self-assembly processes is an ever-interesting research field which can expand substantially and bring immense advances in specialized applications such as: (a) removal and extraction of toxic anions and salts from water water, (b) utilizing the binding and selectivity of the molecular capsules towards anionic species for the drug delivery, and (c) membrane transport, (d) solubilize insoluble anion/salts, (e) utilizing the molecular capsules as molecular reactors by stabilizing the anionic reactive intermediates inside the nanocavity etc.

References

1.1 J. W. Steed and J. L. Atwood, *Supramolecular chemistry*, John Wiley and Sons, Ltd; pp 1-6 1997.

1.2 D. J. Cram, *Angew. Chem., Int. Ed.*, 1986, **25**, 1039.

1.3 T. Steiner,. *Angew. Chem., Int. Ed*., 2002, **41**, 48.

1.4 (*a*) D. S. Lawrence, T. Jiang and M. Levett, *Chem. Rev*., 1995, **95**, 2229; (*b*) L. M. Greig and D. Philp, *Chem. Soc. Rev*., 2001, **30**, 287.

1.5 A. Bianchi, K. Bowman-James and E. Garcia-Espana, *Supramolecular Chemistry of Anions*, Wiley-VCH, New York, 1997.

1.6 N. Busschaert, C. Caltagirone, W. Van Rossom and P. A. Gale, *Chem. Rev*., 2015, **115**, 8038.

1.7 J. L. Sessler, P. A. Gale and W. S. Cho, *Anion Receptor Chemistry*, The Royal Society of Chemistry, Cambridge, UK, 2006.

1.8 B. A. Moyer and P. V. Bonnesen, *Physical factors in anion separations, In Supramolecular Chemistry of Anions*; Wiley-VCH: New York, 1997; chapter 1.

1.9 D. J. Mercer and S. J. Loeb, *Chem. Soc. Rev*., 2010, **39**, 3612.

1.10 K. Bowman-James, *Acc. Chem. Res*., 2005, **38**, 671.

1.11 (*a*) H.-J. Schneider and A. K. Yatsimirsky, *Chem. Soc. Rev*., 2008, **37**, 263; (*b*) E. Garcia-Espana, P. Diaz, J. M. Llinares and A. Bianchi, *Coord. Chem. Rev*., 2006, **250**, 2952; (*c*) S. O. Kang, M. A. Hossain and K. Bowman-James, *Coord. Chem. Rev*., 2006, **250**, 3038.

1.12 (*a*) P. A. Gale, *Chem. Commun*., 2008, 4525; (*b*) C. Caltagirone and P. A. Gale, *Chem. Soc. Rev*., 2009, **38**, 520; (*c*) P. A. Gale, *Acc. Chem. Res*., 2006**, 39**, 465; (d) A-F. Li, J-H. Wang, F. Wang and Y-B. Jiang, *Chem. Soc. Rev.*, 2010, **39**, 3729.

1.13 (*a*) T. Gunnlaugsson, P. E. Kruger, P. Jensen, F. M. Pfeffer and G. M. Hussey, *Tetrahedron Lett*., 2003, **44**, 8909; (*b*) S. Camiolo, P. A. Gale, M. B. Hursthouse and M. E. Light, *Org. Biomol. Chem*., 2003, **1**, 741; (*c*) V. Amendola, D. Esteban-Gomez, L. Fabbrizzi and M. Licchelli, *Acc. Chem. Res*., 2006, **39**, 343.

1.14 R. Custelcean, *Chem. Soc. Rev.*, 2010, **39**, 3675.

1.15 (*a*) B. L. Schottel, H. T. Chifotides and K. R. Dunbar, *Chem. Soc. Rev*., 2008, **37**, 68; (*b*) H. T. Chifotides, B. L. Schottel and K. R. Dunbar, *Angew. Chem., Int. Ed.*, 2010, **49**, 7202.

1.16 (*a*) B. P. Hay and V. S. Bryantsev, *Chem. Commun*., 2008, 2417; (*b*) B. P. Hay and R. Custelcean, *Cryst. Growth Des*., 2009, **9**, 2539.

1.17 G. Cavallo, P. Metrangolo, T. Pilati, G. Resnati, M. Sansoteraa and G. Terraneo, *Chem. Soc. Rev.*, 2010, **39**, 3772.

1.18 (a) P. Ballester, *Chem. Soc. Rev.*, 2010, **39**, 3810; (b) M. Arunachalam and P. Ghosh, *Chem. Commun*., 2011, **47**, 8477; (c) S. K. Dey, A. Basu, R. Chutia and G. Das *RSC Adv.*, 2016, **6**, 26568.

1.19 (a) P. D. Beer and P. A. Gale, *Angew. Chem., Int. Ed.*, 2001, **40**, 486; (b) F. P. Schmidtchen and M. Berger, *Chem. Rev.*, 1997, **97**, 1609; (c) D. E. Gomez, L. Fabbrizzi, M. Licchelli and E. Monzani *Org . Biomol. Chem.* 2005, **3**, 1495.

1.20 (a) P. J. Smith, M. V. Reddington and C. S. Wilcox, *Tetrahedron Lett.*, 1992, **33**, 6085; (b) E. Fan, S. A. van Arman, S. Kincaid and A. D. Hamilton, *J. Am. Chem. Soc.*, 1993, **115**, 369.

1.21 (a) J. Scheerder, J. F. J. Engbersen, A. Casnati, R. Ungaro and D. N. Reinhoudt, *J. Org. Chem.*, 1995, **60**, 6448; (b) M. P. Hughes and B. D. Smith, *J. Org. Chem.*, 1997, **62**, 4492; (c) R. J. Fitzmaurice, G. M. Kyne, D. Douheret and J. D. Kilburn, *J. Chem. Soc., Perkin Trans. 1*, 2002, 841; (d) A. J. Evans, S. E. Matthews, A. R. Cowley and P. D. Beer, *Dalton Trans.*, 2003, 4644; (e) H. Miyaji, S. R. Collinson, I. Prokes and J. H. R. Tucker, *Chem. Commun.*, 2003, 64; (f) T. Gunnlaugsson, A. P. Davis, G. M. Hussey, J. Tierney and M. Glynn, *Org. Biomol. Chem.*, 2004, **2**, 1856. (g) M. Boiocchi, L. D. Boca, D. E. Gomez, L. Fabbrizzi, M. Licchelli and E. Monzani *J. Am. Chem. Soc.* 2004, **126**, 16507; (h) E. M. Boyle, T. McCabe and T.Gunnlaugsson *Supramol. Chem.* 2010, **22**, 586; (i) I. L. Kirby, M.Brightwell, M. B. Pitak, C. Wilson, S. J. Coles and P. A. Gale *Phys.Chem.Chem.Phys.*, 2014, **16**, 10943.

1.22 M. E. Light, P. A. Gale and S. J. Brooks *Acta Cryst.* 2006. **E62**, 1905.

1.23 A. Casula, C. Bazzicalupi, A. Bettoschi, E. Cadoni, S. J. Coles, P. N. Horton, F. Isaia, V. Lippolis, L. K. Mapp, G. M. Marini, R. Montis, M. A. Scorciapino and C. Caltagirone *Dalton Trans.*, 2016, **45**, 3078.

1.24 C. Jia, W. Zuo, D. Zhang, X.-J. Yang and B. Wu *Chem. Commun.*, 2016, **52**, 9614.

1.25 (a) S. J. Brooks, P. A. Gale and M. E. Light, *Chem. Commun*., 2005, 4696; (b) S. J. Brooks, P. R. Edwards, P. A. Gale and M. E. Light, *New J. Chem*., 2006, **30**, 65.

1.26 C. Jia, Q.-Q. Wang, R. A. Begum, V. W. Day and K. Bowman-James, *Org. Biomol. Chem.*, 2015, **13**, 6953.

1.27 R. Li, Y. Zhao, S. Li, P. Yang, X. Huang, X.-J. Yang and B. Wu, *Inorg. Chem.*, 2013, **52**, 5851.

1.28 S. J. Brooks, P. A. Gale and M. E. Light *CrystEngComm*, 2005, **7**, 586.

1.29 D. A. Jose, D. K. Kumar, B. Ganguly, and A. Das *Org. Lett.*, 2004, **6**, 3445.

1.30 G. Xu and M. A. Tarr *Chem. Commun*, 2004, 1050.

1.31 P. Hamankiewicz, J. M. Granda, J. Jurczak Tetrahedron Lett. 2013, **54**, 5608.

1.32 R. Custelcean, P. V. Bonnesen, B. D. Roach and N. C. Duncan, *Chem. Commun*, 2012, **48**, 7438.

1.33 (a) B. H. M. Snellink-Ruel, M. M. G. Antonisse, J. F. J. Engbersen, P. Timmerman and D. N. Reinhoudt *Eur. J. Org. Chem.* **2000**, 165; (b) C. Jia, B. Wu, S. Li, X. Huang and X.-J. Yang *Org. Lett.*, 2010, **12**, 5612; (c) S. Li, C. Jia, B. Wu, Q. Luo, X. Huang, Z. Yang, Q-S. Li and X.-J. Yang *Angew. Chem. Int. Ed.* 2011, 50, 5721; (d) Y. Zhang, R. Zhang, Y. Zhao, L. Ji, C. Jia and B. Wu*New J. Chem.*, 2013, **37**, 2266; (e) B. Wu, S. Li, Y. Lei, H. Hu, N. S. Amadeu, C. Janiak, J. S. Mathieson, D-L. Long, L. Cronin, and X.-J. Yang *Chem. Eur. J.* 2015, **21**, 2588.

1.34 K. Ghosh, S. Adhikari, R. Fröhlich, I. D. Petsalakis, G. Theodorakopoulos *J. Mol. Struct.* 2011, **1004**, 193.

1.35 M. Paul, N. N. Adarsh and P. Dastidar *Cryst. Growth Des.* 2012, **12**, 4135.

1.36 V. Haridas, S. Sadanandan, G. Hundal, C. H. Suresh *Tetrahedron Lett.* 2012, **53**, 5523.

1.37 U. Fegade, A. Singh, G. K. Chaitanya, N. Singh, S. Attarde and A. Kuwar *Spectrochim. Acta Part A: Molecular and Biomolecular Spectroscopy* 2014, **121**, 569.

1.38 A. L. Connor, T. Hu, C. S. F. Detchou, R. Liu, S. V. S. R. K. Pulavarti, T. Szyperski, Z. Lu and B. Gong *Chem. Commun.*, 2016, **52**, 9905.

1.39 D. M. Gillen, C. S Hawes, and T. Gunnlaugsson *J. Org. Chem.*, 2018, **83**, 10398.

1.40 V. Stastny, P. Lhotak, V. Michlova I. Stibor and J. Sykora *Tetrahedron* 2002, **58**, 7207.

1.41 N. N. Adarsh and P. Dastidar *Cryst. Growth Des.* 2010, **10**, 483.

1.42 T. H. Russ, A. Pramanik, M. E. Khansari, B. M. Wong and M. A. Hossain *Nat Prod Commun.* 2012, **7**, 301.

1.43 A. Rajbanshi, S. Wan, and R. Custelcean *Cryst. Growth Des.* 2013, **13**, 2233.

1.44 X. Bai, C. Jia, Y. Zhao, D. Yang, S-C. Wang, A. Li, Y-T. Chan, Y-Y. Wang, X-J. Yang and B. Wu *Angew. Chem. Int. Ed.* 2018, **57**, 1851.

1.45 (a) M. A. Hossain, J. A. Liljegren, D. Powell and K. Bowman-James, *Inorg. Chem*., 2004, **43**, 3751; (b) P. Bose, I. Ravikumar, and P. Ghosh, *Inorg. Chem*., 2011, **50**, 10693; (c) M. Isiklan, M. A. Saeed, A. Pramanik, B. M. Wong, F. R. Fronczek, and M. A. Hossain, *Cryst. Growth Des*., 2011, **11**, 959; (d) M. N. Hoque, U. Manna and G. Das *Supramol. Chem.* 2016, **28**, 284.

1.46 (a) C. Raposo, M. Almaraz, M. Martin, V. Weinrich, M. L. Mussons, V. Alcazar, M. C. Caballero and J. R. Morán, *Chem. Lett*., 1995, **37**, 2795; (b) H. Xie, S. Yi, X. Yang and S. Wu, *New. J. Chem.* 1999, **23**, 1105; (c) H. Xie, S. Yi and S. Wu, *J. Chem. Soc. Perkin Trans. 2* 1999, 2751.

1.47 (a) R. Custelcean, B. A. Moyer and B. P. Hay, *Chem. Commun*., 2005, 5971; (b) P. Bose, R. Dutta and P. Ghosh, *Org. Biomol. Chem*., 2013, **11**, 4581; (c) R. Dutta, S. Chakraborty, P. Bose and P. Ghosh, *Eur. J. Inorg. Chem.*, 2014, **25**, 4134.

1.48 R. Custelcean, P. Remy, P. V. Bonnesen, D. Jiang and B. A. Moyer, *Angew. Chem. Int. Ed*., 2008, **47**, 1866; (b) B. Wu, J. Liang, J. Yang, C. Jia, X.-J. Yang, H. Zhang, N. Tang and C. Janiak, *Chem. Commun*., 2008, 1762; (c) A. Rajbanshi, B. A. Moyer and R. Custelcean, *Cryst. Growth Des*., 2011, **11**, 2702.

1.49 R. Zhang, Y. Zhao, J. Wang, L. Ji, X.–J. Yang and B. Wu, *Cryst. Growth Des*., 2014, **14**, 544.

1.50 (a) B. Akhuli, I. Ravikumar and P. Ghosh, *Chem. Sci*., 2012, **3**, 1522; (b) I. Ravikumar, P. S. Lakshminarayanan, M. Arunachalam, E. Suresh and P. Ghosh, *Dalton Trans*., 2009, 4160; (c) P. S. Lakshminarayanan, I. Ravikumar, E. Suresh and P. Ghosh, *Chem. Commun*. 2007, 5214; (d) R. Dutta, P. Bose and P. Ghosh, *Dalton Trans*., 2013, **42**, 11371; (e) I. Ravikumar and P. Ghosh, *Chem. Commun*. 2010, **46**, 1082.

1.51 N. Busschaert, M. Wenzel, M. E. Light, P. Iglesias-Hernandez, R. Perez-Tomas and P. A. Gale, *J. Am. Chem. Soc*., 2011, **133**, 14136.

1.52 (a) R. Chutia, S. K. Dey and G. Das, *Cryst. Growth Des*., 2013, **13**, 883; (b) S. K. Dey, R. Chutia and G. Das, *Inorg. Chem*., 2012, **51**, 1727; (c) R. Chutia, S. K. Dey and G. Das, *Cryst. Growth Des*., 2015, **15**, 4993; (d) D. A. Jose, D. K. Kumar, B. Ganguly and A. Das, *Inorg. Chem*., 2007, **46**, 5817.

1.53 (a) M. Li, B. Wu, C. Jia, X. Huang, Q. Zhao, S. Shao and X.–J. Yang, *Chem. Eur., J*., 2011, **17**, 2272; (b) M. Li, Y. Hao, B. Wu, C. Jia, X. Huang, X.–J. Yang, *Org. Biomol. Chem*., 2011, **9**, 5637.

1.54 A. Gogoi and G. Das, *Supramolecular Chem*., 2013, **25**, 819.

1.55 A. Basu and G. Das, *Dalton Trans*., 2012, **41**, 10792.

1.56 (a) S. K. Dey and G. Das, *Dalton Trans*., 2011, **40**, 12048; (b) S. K. Dey and G. Das, *Dalton Trans*., 2012, **41**, 8960.

1.57 P. Bose, R. Dutta, S. Santra, B. Chowdhury and P. Ghosh, *Eur. J. Inorg. Chem*., 2012, **35**, 5791.

1.58 (a) C. Jia, B. Wu, S. Li, X. Huang, Q. Zhao, Q.-S. Li, X.-J. Yang, *Angew. Chem. Int. Ed.* 2011, **50**, 486; (b) X. Huang, B. Wu, C. Jia, B. P. Hay, M. Li and X.-J. Yang *Chem. Eur. J.* 2013, **19**, 9034.

Chapter 2

Experimental Methods

&

Characterization

In this chapter, a detailed report of the various reagents used in the synthesis of acyclic dipodal (**L_1-L_{15}**) and tripodal receptors (**L_{16}-L_{27}**) (Scheme 2.1), their synthetic procedures, crystallization details and specifications of instruments/equipment employed in the characterization of synthesized receptors and their various complexes with anions/hydrated-anions are presented.

2.1 Materials

All reagents and solvents were obtained from commercial sources and used as received without further purification. *ortho*-Phenylenediamine, *meta*-Phenylenediamine, *para*-Phenylenediamine, Tris(2-aminoethyl)amine (tren), 2-Nitrophenylisocyanate, 3-Nitrophenylisocyanate, 4-Nitrophenylisocyanate, 3-Chloro-4-methylphenyl isocyanate, 4-Bromo-3-methylphenyl isocyanate, 3,5-Bis(trifluoromethyl)phenyl isocyanate, 4-Chlorophenyl isocyanate, 4-Bromophenyl isocyanate, 4-Iodophenyl isocyanate, 1-naphthyl isocyanate, 1-naphthyl isothiocyanate, phenyl isocyanate, phenyl isothiocyanate, 4-Nitrobenzaldehyde, 3-Nitrobenzaldehyde and 4-Bromobenzaldehyde were purchased from Sigma-Aldrich (U.S.A). All quaternary ammonium salts were purchased from Sigma-Aldrich (U.S.A) whereas, inorganic salts such as HF, HCl, HBr, HI, HNO_3, H_2SO_4 were obtained either from Merck or LOBA chemicals (India). All sodium, potassium salts and deuterated solvent such as DMSO-d_6, $CDCl_3$ were purchased from Merck chemicals (India) and used as received. Solvents for synthesis and crystallization experiments were purchased either from Merck, India, and dried using standard techniques, wherever mentioned in the synthetic procedures.

2.2 Experimental methods

^{1}H NMR and 2D NOESY NMR spectra were recorded on a Varian FT-600 MHz and FT-400 MHz instrument, chemical shifts were recorded in parts per million (ppm) on the scale using tetramethylsilane (TMS) or residual solvent peak as a reference. ^{13}C spectra were obtained at 150 MHz and FT-100 MHz at 298 K. FT-IR spectra were recorded on a Perkin-Elmer-Spectrum One FT-IR spectrometer with KBr disks in the range 4000-450 cm^{-1}. Powder X-ray diffraction patterns of dried crystalline powder were recorded using a Bruker-D8 Advance X-ray diffractometer with Cu-$K\alpha$ radiation at λ = 0.15418 nm. Thermal analysis (TGA) of dried samples was performed using an SDTA 851-E TGA thermal analyser (*Mettler Toledo*) with a heating rate of 5-10^{o}C/min in a N_2 atmosphere. The electrospray ionization mass spectrometry (ESI-MS) spectra of free receptors were recorded in methanol. The FT-IR spectra of the air-dried samples were recorded on a PerkinElmer FT-IR spectrometer with KBr disks in the range 4000-450 cm^{-1}.The absorption spectra were recorded on a Perkin-Elmer Lambda-25/35 UV-Visible spectrophotometer with a quartz cuvette. Association constants of anions with receptors were obtained by ^{1}H NMR titrations of the receptor with tetraethyl ammonium (TEA) or

tetrabutyl ammonium (TBA) anion salts in DMSO-d_6 at 298 K. The initial concentration of the receptor solution was 10 mM. Aliquots of anions were added from the stock solutions up to 1:10 host-guest stoichiometry. The residual solvent peak in DMSO-d_6 (2.50 ppm) was used as an internal reference, and each titration was performed with at least 10-15 measurements. For some receptors WinEQNMR2 software was used to calculate the binding constants (K) values[2.1a] and for few receptors following equation was used to determine the association constant (K) values. $\Delta\delta = \{([A]_0 + [\mathbf{L}]_0 + 1/K) +/-(([A]_0 + [\mathbf{L}]_0 + 1/K)^2 - 4[\mathbf{L}]_0[A]_0)^{1/2}\} \Delta\delta_{max}/2[\mathbf{L}]$, [2.1b] where, **L** = receptor and A = anion. An error limit in log K was less than 15%.

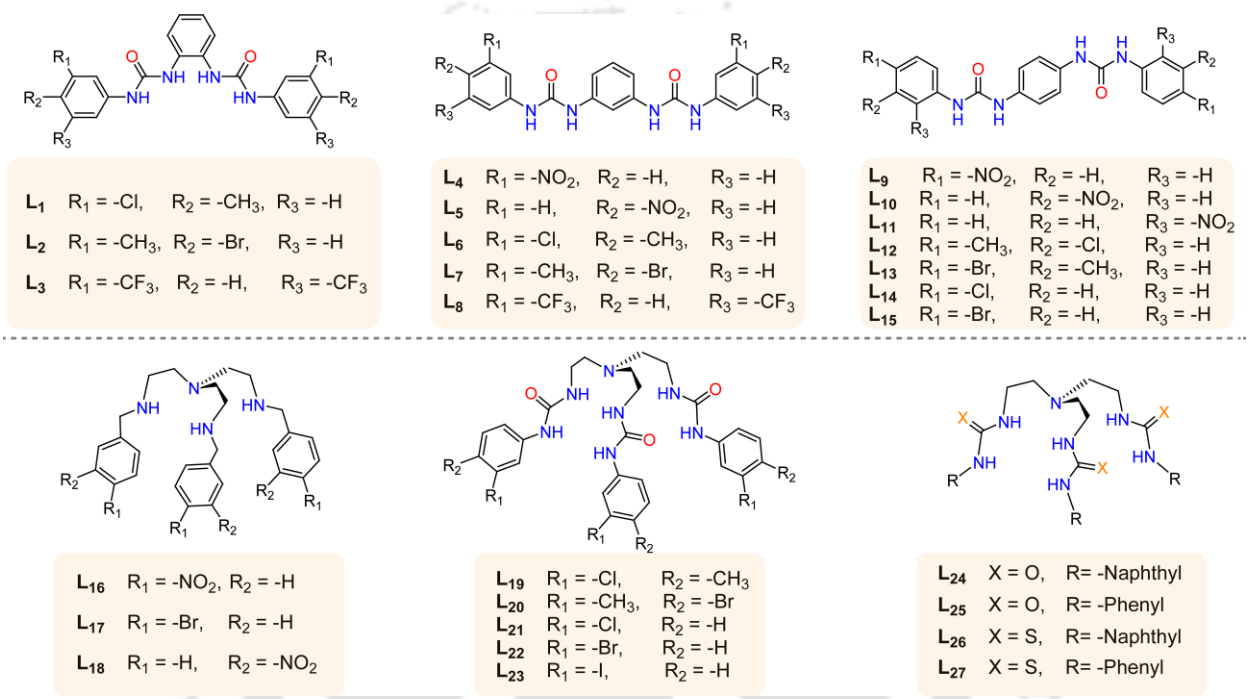

Scheme 2.1 Comprehensive representation of molecular structures of the receptors $\mathbf{L_1}$-$\mathbf{L_{27}}$ included in the thesis.

2.3 Single crystal X-ray crystallography

In each case, a crystal of suitable size was selected from the mother liquor and immersed in silicone oil, and it was mounted on the tip of a glass fiber and cemented using epoxy resin. The intensity data were collected using a Bruker SMART APEX-II CCD diffractometer, equipped with a fine focus 1.75 kW sealed tube Mo-K_α radiation (λ = 0.71073 Å) at 298(3) K, with increasing ω (width of 0.3^o per frame) at a scan speed of 5 s/ frame. Subsequently, the X-ray crystallographic intensity data were also collected using a Supernova, single source at offset, Eos diffractometer using Mo-Kα radiation (λ = 0.71073 Å) equipped with a CCD area detector, and the corresponding data refinement and cell reduction were carried out by CrysAlisPro.[2.2] The SMART software was used for data acquisition. Data integration and reduction were undertaken with SAINT and XPREP software.[2.3] Multi-scan empirical absorption corrections were applied to the data using the program SADABS.[2.4]

All the crystal structures were solved by direct methods using SHELXTL-2014[2.5] and were refined on F^2 by the full-matrix least-squares technique using the SHELXL-2014 program package. All non-hydrogen atoms were refined anisotropically and hydrogen atoms attached to all carbon atoms were geometrically fixed and the positional and temperature factors are refined isotropically. Hydrogen atoms attached with the amine/urea/thiourea nitrogen atoms were located from electron Fourier map and refined isotropically. Usually, temperature factors of hydrogen atoms attached to carbon atoms are refined by restraints -1.2 or -1.5 U_{iso} (C), although the isotropic free refinement is also acceptable. Structural illustrations have been drawn with ORTEP-3 for Windows[2.6] and graphics were generated using MERCURY 2.3[2.7] for Windows. PLATON/SQUEEZE[2.8] was used to refine the host framework in some host-guest complexes excluding the disordered counter-cation or solvent molecules. All the crystallographic data have been deposited in the CCDC. Crystallographic parameters for data collection and crystallographic refinement details of the receptors and their anion complexes are summarized in the respective chapters.

2.4 Synthesis and characterization of receptors L_1-L_{27}

2.4.1 *ortho*-Phenylenediamine based receptors L_1-L_3

The halo-methylphenyl (**L_1**, **L_2**) and bis-(trifluoromethyl)-phenyl (**L_3**) terminal aryl di-substituted bis-urea receptors have been synthesized in quantitative yield by the individual reaction of *o*-Phenylenediamine (0.324 g, 3.0 mmol) with 3-Chloro-4-methylphenyl isocyanate (958 µL, 7.0 mmol), 4-Bromo-3-methylphenyl isocyanate (984 µL, 7.0 mmol) and 3,5-Bis(trifluoromethyl)phenyl isocyanate (1210 µL, 7.0 mmol) in dry acetonitrile medium separately. The individual reaction mixtures of amine and corresponding isocyanate were taken in three separate 50 mL round bottomed flasks, vigorously stirred for overnight at room temperature. Then, the off-white solid precipitate obtained in each case, were filtered off and washed several times with acetonitrile, THF to remove unreacted reagents and then dried in a vacuum to yield receptors **L_1**, **L_2** and **L_3** from respective flasks. The precipitate thus collected of ligands **L_1**-**L_3** was dried in air and characterized by NMR, FT-IR, ESI-MS and single crystal X-ray diffraction analyses. Yield: ~82%, ~88% and ~75% based on respective **L_1**, **L_2** and **L_3**.

L_1: ^{1}H NMR (600 MHz, DMSO-d_6) δ (ppm): 2.748 (s, 6H, Ar-CH_3), 7.339-7.355 (m, 2H, Ar-H), 7.426-7.439 (d, 2H, ~7.8 Hz, Ar-H), 7.471-7.485 (d, 2H, ~8.4 Hz, Ar-H), 7.815-7.831 (m, 2H, Ar-H), 7.975 (s, 2H, Ar-H), 8.327 (s, 2H, NH_a), 9.426 (s, 2H, NH_b). ^{13}C NMR (150 MHz, DMSOd_6) δ (ppm): 18.82, 112.90, 116.87, 118.12, 124.21, 128.17, 131.17, 131.22, 133.13, 139.03 and 153.12. FT-IR spectra (KBr pellet): 3328 cm^{-1} *vs*(N-H), 3145 cm^{-1} *vs*(C-H), 2864 cm^{-1} *vs*(C-H), 1670 cm^{-1} *vs*(C=O), 665 cm^{-1} *vs*(C-Cl). ESI-MS: m/z 444.1072 [**L_1**+H].

L_2: ^{1}H NMR (400 MHz, DMSO-d_6) δ (ppm): 2.699 (s, 6H, Ar-CH_3), 7.279-7.303 (m, 2H, Ar-H), 7.446-

7.468 (d, 2H, ~8.8 Hz, Ar-H), 7.635-7.657 (d, 2H, ~8.8 Hz, Ar-H), 7.665 (s, 2H, Ar-H), 7.762-7.786 (m, 2H, Ar-H), 8.280 (s, 2H, NH_a), 9.342 (s, 2H, NH_b). ^{13}C NMR (100 MHz, DMSO-d_6) δ (ppm): 22.72, 115.84, 117.69, 120.49, 124.23, 127.27, 131.24, 132.25, 137.43, 139.45, 153.13. IR spectra (KBr pellet): 3326 cm^{-1} *vs*(N-H), 3138 cm^{-1} *vs*(C-H), 2862 cm^{-1} *vs*(C-H), 1665 cm^{-1} *vs*(C=O), 580 cm^{-1} *vs*(C-Br). ESI-MS: m/z 533.0139 [**L_2**+H].

L_3: ^{1}H NMR (600 MHz, DMSO-d_6) δ (ppm): 7.165-7.193 (m, 2H, Ar-H), 7.572-7.599 (m, 2H, Ar-H), 7.620 (s, 4H, Ar-H), 8.119 (s, 2H, Ar-H), 8.319 (s, 2H, NHa), 9.811 (s, 2H, NHb). ^{13}C NMR (150 MHz, DMSO-d_6) δ (ppm): 113.13, 117.89, 122.40, 124.21, 124.91, 124.98, 130.59, 130.80, 141.93 and 153.15. IR spectra (KBr pellet): 3327 cm^{-1} *vs*(N-H), 3138 cm^{-1} *vs*(C-H), 1670 cm^{-1} *vs*(C=O), 1257 cm^{-1} *vs*(C-F). ESI-MS: m/z 619.0944 [**L_3** + H].

2.4.2 *meta*-Phenylenediamine based receptors L_4-L_8

The nitro-phenyl (**L_4**, **L_5**), halo-methylphenyl (**L_6**, **L_7**) and bis-(trifluoromethyl)-phenyl (**L_8**) terminal aryl mono- and di-substituted *m*-Phenylenediamine based bis-urea receptors were synthesized in the same way as **L_1-L_3** only replacing the starting materials such as, reacting *m*-Phenylenediamine (0.324 g, 3.0 mmol) with 3-Nitrophenyl isocyanate (1.148 g, 7.0 mmol), 4-Nitrophenyl isocyanate (1.148 g, 7.0 mmol), 3-Chloro-4-methylphenyl isocyanate (958 µL, 7.0 mmol), 4-Bromo-3-methylphenyl isocyanate (984 µL, 7.0 mmol) and 3,5-Bis(trifluoromethyl)phenyl isocyanate (1210 µL, 7.0 mmol) to produce **L_4**, **L_5**, **L_6**, **L_7** and **L_8** respectively. Yield: ~80%, ~85%, 82%, ~85% and ~80% of respective ligands **L_4-L_8**.

L_4: ^{1}H NMR (600 MHz, DMSO-d_6) δ (ppm): 7.781 (s, 1H, Ar-H), 7.104-7.118 (d, 2H, Ar-H), 7.212 (t, 1H, Ar-H), 7.692-7.705 (d, 2H, Ar-H), 7.569 (t, 2H, Ar-H), 7.820-7.833 (d, 2H, Ar-H), 8.595 (s, 2H, Ar-H), 8.915 (s, 2H, NH_a), 9.133 (s, 2H, NH_b). ^{13}C-NMR (150 MHz, DMSO-d_6) δ (ppm): 108.57, 112.10, 112.45, 116.28, 124.31, 129.17, 130.07, 139.72, 141.02, 148.15 and 152.34. FT-IR spectra (KBr pellet): 3454 cm^{-1} *vs*(N-H), 3112 cm^{-1} *vs*(C-H), 1690 cm^{-1} *vs*(C=O), 1596 cm^{-1} *vs*(C=C),1522 cm^{-1} *vs*(NO_2-asym), 1356 cm^{-1} *vs*(NO_2-sym), 1214 cm^{-1} *vs*(C-N).

L_5: ^{1}H NMR (600 MHz, DMSO-d_6) δ (ppm): 7.764 (s, 1H, Ar-H), 7.115-7.128 (d, 2H, Ar-H), 7.229 (t, 1H, Ar-H), 7.687-7.705 (d, 4H, Ar-H), 8.189-8.204 (d, 4H, Ar-H), 8.988 (s, 2H, NH_a), 9.363 (s, 2H, NH_b). ^{13}C NMR (150 MHz, DMSO-d_6) δ (ppm): 108.63, 112.71, 117.46, 125.15, 129.27, 139.53, 141.01, 146.33 and 151.85. FT-IR spectra (KBr pellet): 3450 cm^{-1} *vs*(N-H), 3150 cm^{-1} *vs*(C-H), 1698 cm^{-1} *vs*(C=O), 1592 cm^{-1} *vs*(C=C),1527 cm^{-1} *vs*(NO_2-asym), 1351 cm^{-1} *vs*(NO_2-sym), 1216 cm^{-1} *vs*(C-N).

L_6: ^{1}H NMR (600 MHz, DMSO-d_6) δ (ppm): 2.257 (s, 6H, Ar-CH_3), 7.053-7.067 (d, 2H, ~8.4 Hz, Ar-H), 7.155-7.185 (m, 3H, Ar-H), 7.225-7.239 (d, 2H, ~8.4 Hz, Ar-H), 7.686 (s, 2H, Ar-H), 7.703 (s, 1H, Ar-H), 8.683 (s, 2H, NH_a), 8.739 (s, 2H, NH_b). ^{13}C NMR (150 MHz, DMSO-d_6) δ (ppm): 18.125, 108.111, 111.974, 116.926, 118.091, 128.219, 129.108, 131.177, 133.132, 138.889, 139.974 and 152.349. FT-IR spectra (KBr pellet): 3292 cm^{-1} *vs*(N-H), 3126 cm^{-1} *vs*(C-H), 2844 cm^{-1} *vs*(C-H), 1634 cm^{-1} *vs*(C=O), 659 cm^{-1} *vs*(C-Cl). ESI-MS: m/z 444.0992 [**L_6**+H].

L_7: ^{1}H NMR (600 MHz, DMSO-d_6) δ (ppm): 2.313 (s, 6H, Ar-CH_3), 7.048-7.060 (d, 2H, ~7.2 Hz, Ar-

H), 7.152-7.179 (t, 1H, ~7.8 Hz, Ar-H), 7.216-7.256 (m, 4H, Ar-H), 7.439 (s, 2H, Ar-H), 7.455 (s, 1H, Ar-H), 8.654 (s, 2H, NH_a), 8.736 (s, 2H, NH_b). ^{13}C NMR (150 MHz, DMSO-d_6) δ (ppm): 22.707, 111.930, 115.852, 117.664, 120.489, 129.108, 129.165, 132.235, 137.455, 139.291, 140.025 and 152.338. FT-IR spectra (KBr pellet): 3293 cm^{-1} *vs*(N-H), 3127 cm^{-1} *vs*(C-H), 2843 cm^{-1} *vs*(C-H), 1639 cm^{-1} *vs*(C=O), 576 cm^{-1} *vs*(C-Br). ESI-MS: m/z 533.0145 [$\mathbf{L_7}$+H].

L_8: ^1H NMR (600 MHz, DMSO-d_6) δ (ppm): 7.123-7.137 (d, 2H, ~8.4 Hz, Ar-H), 7.203-7.230 (t, 1H, ~7.8 Hz, Ar-H), 7.636 (s, 2H, Ar-H), 7.792 (s, 1H, Ar-H), 8.139 (s, 4H, Ar-H), 9.084 (s, 2H, NH_a), 9.297 (s, 2H, NH_b). FT-IR spectra (KBr pellet): 3199 cm-1 *vs*(N-H), 3289 cm^{-1} *vs*(C-H), 3096 cm^{-1} *vs*(C-H), 1641 cm^{-1} *vs*(C=O), 1258 cm^{-1} *vs*(C-F). ESI-MS: m/z 619.0961 [$\mathbf{L_8}$+H].

2.4.3 *para*-Phenylenediamine based receptors L_9-L_{15}

The nitro-phenyl (**L_9**, **L_{10}**, **L_{11}**), halo-methylphenyl (**L_{12}**, **L_{13}**) and *para*-halophenyl (**L_{14}**, **L_{15}**) terminal aryl mono- and di-substituted *p*-Phenylenediamine based bis-urea receptors were synthesized in the same way as **L_1-L_8** only replacing the starting materials such as, reacting *p*-Phenylenediamine (0.324 g, 3.0 mmol) with 4-Nitrophenyl isocyanate (1.148 g, 7.0 mmol), 3-Nitrophenyl isocyanate (1.148 g, 7.0 mmol), 2-Nitrophenyl isocyanate (1.148 g, 7.0 mmol), 3-Chloro-4-methylphenyl isocyanate (958 µL, 7.0 mmol), 4-Bromo-3-methylphenyl isocyanate (984 µL, 7.0 mmol), 4-Chlorophenyl isocyanate (1.074 g, 7.0 mmol) and 4-Bromophenyl isocyanate (1.386, 7.0 mmol) to produce **L_9**, **L_{10}**, **L_{11}**, **L_{12}**, **L_{13}**, **L_{14}** and **L_{15}** respectively. Yield: ~80%, ~75%, ~75%, ~85%, 80%, ~90% and ~85% of respective ligands **L_9-L_{15}**.

L_9: ^1H NMR (600 MHz, DMSO-d_6) δ (ppm): 7.418 (s, 4H, Ar-H), 7.677-7.692 (d, 4H, ~9.0 Hz, Ar-H), 8.180-8.196 (d, 4H, ~9.6 Hz, Ar-H), 8.846 (s, 2H, NH_a), 9.404 (s, 2H, NH_b). IR spectra (KBr pellet): 3358 cm^{-1} *vs*(N-H), 3278 cm^{-1} *vs*(C-H), 1660 cm^{-1} *vs*(C=O), 1571 cm^{-1} *vs*(C=C), 1506 cm^{-1} *vs*(NO_2-*asym*), 1332 cm^{-1} *vs*(NO_2-*sym*),1223 cm^{-1} *vs*(C-N). ESI-MS: m/z 437.1718 [$\mathbf{L_9}$+H].

L_{10}: ^1H NMR (600 MHz, DMSO-d_6) δ (ppm): 7.409 (s, 4H, Ar-H), 7.546-7.574 (t, 2H, ~8.4 Hz, Ar-H), 7.695-7.711 (d, 2H, ~9.6 Hz, Ar-H), 7.808-7.822 (d, 2H, ~8.4 Hz, Ar-H), 8.571 (s, 2H, Ar-H), 8.749 (s, 2H, NH_a), 9.173 (s, 2H, NH_b). IR spectra (KBr pellet): 3370 cm^{-1} *vs*(N-H), 3318 cm^{-1} *vs*(C-H), 1666 cm^{-1} *vs*(C=O), 1560 cm^{-1} *vs*(C=C), 1520 cm^{-1} *vs*(NO_2-*asym*), 1345 cm^{-1} *vs*(NO_2-*sym*), 1219 cm^{-1} *vs*(C-N). ESI-MS: m/z 437.1233 [$\mathbf{L_{10}}$+H].

L_{11}: ^1H NMR (600 MHz, DMSO-d_6) δ (ppm): 7.178-7.206 (t, 2H, ~8.4 Hz, Ar-H), 7.443 (s, 4H, Ar-H), 7.682-7.711 (t, 2H, ~8.4 Hz, Ar-H), 8.086-8.102 (d, 2H, ~9.6 Hz, Ar-H), 8.305-8.320 (d, 2H, ~9.0 Hz, Ar-H), 9.581 (s, 2H, NH_a), 9.784 (s, 2H, NH_b). IR spectra (KBr pellet): 3352 cm^{-1} *vs*(N-H), 3278 cm^{-1} *vs*(C-H), 1656 cm^{-1} *vs*(C=O), 1570 cm^{-1} *vs*(C=C), 1509 cm^{-1} *vs*(NO_2-*asym*), 1338 cm^{-1} *vs*(NO_2-*sym*), 1224 cm^{-1} *vs*(C-N). ESI-MS: m/z 437.1240 [$\mathbf{L_{11}}$+H].

L_{12}: ^1H NMR (600 MHz, DMSO-d_6) δ (ppm): 2.252 (s, 6H, Ar-CH_3), 7.161-7.175 (d, 2H, ~8.4 Hz, Ar-H), 7.221-7.234 (d, 2H, ~7.8 Hz, Ar-H), 7.349 (s, 4H, Ar-H), 7.690 (s, 2H, Ar-H), 8.576 (s, 2H, NH_a), 8.702 (s, 2H, NH_b). IR spectra (KBr pellet): 3292 cm^{-1} *vs*(N-H), 3069 cm^{-1} *vs*(C-H), 2918 cm^{-1} *vs*(C-H),

1634 cm^{-1} *vs*(C=O), 637 cm^{-1} *vs*(C-Cl).

L_{13}: ^{1}H NMR (600 MHz, DMSO-d_6) δ (ppm): 2.304 (s, 6H, Ar-CH_3), 7.231-7.245 (d, 2H, ~8.4 Hz, Ar-H), 7.349 (s, 4H, Ar-H), 7.430-7.440 (d, 2H, ~6.0 Hz, Ar-H), 7.445 (s, 2H, Ar-H), 8.570 (s, 2H, NH_a), 8.672 (s, 2H, NH_b). IR spectra (KBr pellet): 3299 cm^{-1} *vs*(N-H), 3069 cm^{-1} *vs*(C-H), 2925 cm^{-1} *vs*(C-H), 1640 cm^{-1} *vs*(C=O), 526 cm^{-1} *vs*(C-Br).

L_{14}: ^{1}H NMR (600 MHz, DMSO-d_6) δ (ppm): 7.307-7.322 (d, 4H, ~9.0 Hz, Ar-H), 7.352 (s, 4H, Ar-H), 7.464-7.479 (d, 4H, ~9.0 Hz, Ar-H), 8.580 (s, 2H, NH_a), 8.756 (s, 2H, NH_b). IR spectra (KBr pellet): 3292 cm^{-1} *vs*(N-H), 3076 cm^{-1} *vs*(C-H), 1634 cm^{-1} *vs*(C=O), 644 cm^{-1} *vs*(C-Cl). ESI-MS: m/z 415.0761 [L_{14}+H].

L_{15}: ^{1}H NMR (600 MHz, DMSO-d_6) δ (ppm): 7.351 (s, 4H, Ar-H), 7.412-7.427 (d, 4H, ~9.0 Hz, Ar-H), 7.432-7.448 (d, 4H, ~9.6 Hz, Ar-H), 8.586 (s, 2H, NH_a), 8.762 (s, 2H, NH_b). IR spectra (KBr pellet): 3299 cm^{-1} *vs*(N-H), 3076 cm^{-1} *vs*(C-H), 1640 cm^{-1} *vs*(C=O), 607 cm^{-1} *vs*(C-Br). ESI-MS: m/z 505.2766 [L_{15}+H].

2.4.4 Tris(2-aminoethyl)amine (tren) based electron-deficient receptors L_{16}-L_{23}

The nitro- or bromophenyl (**L_{16}**, **L_{17}**, **L_{18}**) substituted tris-amine receptors were synthesized by the individual reaction of Tris(2-aminoethyl)amine (599 μL, 4.0 mmol) with 4-Nitrobenzaldehyde (1.964 g, 13.0 mmol), 4-Bromobenzaldehyde (2.405 g, 13.0 mmol) and 3-Nitrobenzaldehyde (1.964 g, 13.0 mmol) in methanol medium followed by $NaBH_4$ reduction to produce **L_{16}**, **L_{17}** and **L_{18}** respectively. On the other hand, the halo-methylphenyl (**L_{19}**, **L_{20}**) and *para*-halophenyl (**L_{21}**, **L_{22}**, **L_{23}**) terminal aryl mono- or di-substituted tris-urea receptors were synthesized in quantitative yield by the individual reaction of Tris(2-aminoethyl)amine (599 μL, 4.0 mmol) with 3-Chloro-4-methylphenyl isocyanate (1.780 mL, 13.0 mmol), 4-Bromo-3-methylphenyl isocyanate (1.830 mL, 13.0 mmol), 4-Chlorophenyl isocyanate (1.996 g, 13.0 mmol), 4-Bromophenyl isocyanate (2.574 g, 13.0 mmol) and 4-Iodophenyl isocyanate (3.185 g, 13.0 mmol) in dry acetonitrile medium to produce **L_{19}**, **L_{20}**, **L_{21}**, **L_{22}** and **L_{23}** respectively. The individual reaction mixtures of Tren and corresponding aldehyde or isocyanate were taken in separate 50 mL round bottomed flasks, vigorously stirred for overnight at room temperature. The water-chloroform work-up of reduced solid **L_{16}**, **L_{17}** and **L_{18}** schiff basees gave reddish yellow solid, pale yellow liquid and yellowish oily liquid respectively of receptors **L_{16}**, **L_{17}** and **L_{18}** as desired products. On the other hand, the off-white solid precipitate obtained in each case of tris-urea receptors **L_{19}-L_{23}** were filtered off and washed several times with acetonitrile, THF to remove unreacted reagents and then dried in a vacuum to yield receptors **L_{19}**, **L_{20}**, **L_{21}**, **L_{22}** and **L_{23}** respectively from respective flasks. The desired products of tris-amine and tris-urea receptors **L_{16}-L_{23}** were dried in air and characterized by NMR, FT-IR, ESI-MS and single crystal X-ray diffraction analyses. Yield: ~80%, ~85%, ~85%, ~90%, ~85%, ~80%, ~85%

and ~85% based on respective ligands **L_{16}**, **L_{17}**, **L_{18}**, **L_{19}**, **L_{20}**, **L_{21}**, **L_{22}** and **L_{23}**.

L_{16}: ^{1}H-NMR (600 MHz, $CDCl_3$) δ (ppm): 3.00 (t, 6H, ~5.4 Hz, -NCH_2CH_2), 3.48 (s, 3H, -NH), 3.77 (t, 6H, ~5.8 Hz, -NCH_2), 3.83 (s, 6H, -CH_2), 7.78-7.79 (d, 6H, ~7.8 Hz, Ar-H), 8.21-8.23 (d, ~7.4 Hz, 6H, Ar-H).^{13}C-NMR (150 MHz, $CDCl_3$) δ (ppm): 47.46, 53.30, 54.32, 123.72, 128.61, 147.40 and 148.13. FT-IR spectra (KBr pellet): 3324 cm^{-1} *vs*(N-H), 3112 cm^{-1} *vs*(C-H), 2952 cm^{-1} *vs*(C-H), 1536 cm^{-1} *vs*(C=C), 1496 cm^{-1} *vs*(NO_2-asym), 1366 cm^{-1} *vs*(NO_2-sym), 1227 cm^{-1} *vs*(C-N). ESI-MS: m/z 552.2557 [**L_{16}**+H].

L_{17}: ^{1}H-NMR (600 MHz, $CDCl_3$) δ (ppm): 2.60 (t, 6H, ~5.4 Hz, -NCH_2CH_2), 3.28 (s, 3H, -NH), 3.53 (t, 6H, ~5.8 Hz, -NCH_2), 3.81 (s, 6H, -CH_2), 7.48-7.49 (d, 6H, ~6.8 Hz, Ar-H), 7.81-7.82 (d, 6H, ~7.4 Hz, Ar-H). ^{13}C-NMR (150 MHz, $CDCl_3$) δ (ppm): 47.45, 53.30, 54.33, 122.40, 127.72, 133.62 and 138.18. FT-IR spectra (KBr pellet): 3312 cm^{-1} *vs*(N-H), 3140 cm^{-1} *vs*(C-H), 2862 cm^{-1} *vs*(C-H), 1510 cm^{-1} *vs*(C=C). ESI-MS: m/z 654.0294 [**L_{17}**+H].

L_{18}: ^{1}H-NMR (600 MHz, $CDCl_3$) δ (ppm): 3.09 (t, 6H, ~6.0 Hz, -NCH_2CH_2), 3.46 (s, 3H, -NH), 3.76 (t, 6H, ~6.4 Hz, -NCH_2,), 3.90 (s, 6H, -CH_2), 7.50 (t, 3H, ~5.8 Hz, Ar-H), 7.99-8.00 (d, 3H, ~7.6 Hz, Ar-H), 8.20-8.21 (d, 3H, ~7.8 Hz, Ar-H), 8.31 (s, Ar-H, 3H). ^{13}C-NMR (150 MHz, $CDCl_3$) δ (ppm): 51.55, 55.44, 60.27, 122.94, 125.40, 129.74, 133.37, 138.18 and 148.60. FT-IR spectra (KBr pellet): 3390 cm^{-1} *vs*(N-H), 3123 cm^{-1} *vs*(C-H), 2988 cm^{-1} *vs*(C-H), 1562 cm^{-1} *vs*(C=C),1497 cm^{-1} *vs*(NO_2-asym), 1339 cm^{-1} *vs*(NO_2-sym), 1274 cm^{-1} *vs*(C-N). ESI-MS: m/z 552.2614 [**L_{18}** + H].

L_{19}: ^{1}H NMR (DMSO-d_6, 600 MHz) δ (ppm); 2.214 (s, 9H, Ar-CH_3), 2.568-2.590 (t, ~6.6 Hz, 6H, -NCH_2), 3.152-3.184 (q, ~6.6 Hz, 6H, -NCH_2CH_2), 6.165-6.183 (t, ~5.4 Hz, 3H, -NH_a), 7.068-7.081 (d, 3H, ~7.8 Hz, Ar-H), 7.128-7.142 (d, 3H, ~8.4 Hz, Ar-H), 7.606 (s, 3H, Ar-H), 8.592 (s, 3H, -NH_b). FT-IR spectra (KBr pellet): 1654 cm^{-1} *vs*(C=O), 2828 cm^{-1} *vs*(C-H), 2929 cm^{-1} *vs*(C-H), 3321 cm^{-1} *vs*(N-H). ESI-MS: m/z 648.2057.

L_{20}: ^{1}H NMR (DMSO-d_6, 600 MHz) δ (ppm); 2.235 (s, 9H, Ar-CH_3), 2.565-2.587 (t, ~6.6 Hz, 6H, -NCH_2), 3.150-3.182 (q, ~6.6 Hz, 6H, -NCH_2CH_2), 6.186-6.204 (t, ~5.4 Hz, 3H, -NH_a), 7.162-7.177 (d, 3H, ~9.0 Hz, Ar-H), 7.320 (s, 3H, Ar-H), 7.340-7.354 (d, 3H, ~8.4 Hz, Ar-H), 8.569 (s, 3H, -NH_b). FT-IR spectra (KBr pellet):1655 *vs*(C=O), 2822 cm^{-1} *vs*(C-H), 2923 cm^{-1} *vs*(C-H), 3314 cm^{-1} *vs*(N-H). ESI-MS: m/z 782.0500.

L_{21}: ^{1}H NMR (DMSO-d_6, 600 MHz) δ (ppm); 2.572-2.595 (t, ~7.2 Hz, 6H, -NCH_2), 3.159-3.190 (q, ~6.6 Hz, 6H, -NCH_2CH_2), 6.619-6.187 (t, ~5.4 Hz, 3H, -NH_a), 7.222-7.237 (d, 6H, ~9.0 Hz, Ar-H), 7.383-7.398 (d, 6H, ~9.0 Hz, Ar-H), 8.659 (s, 3H, -NH_b). ^{13}C NMR (150 MHz, DMSO-d_6): δ (ppm) 37.509, 53.781, 119.148, 124.422, 128.400, 139.463 and 155.100. ESI-MS: m/z 606.1572 [**L_{21}**+H].

L_{22}: ^{1}H NMR (DMSO-d_6, 600 MHz) δ (ppm); 2.566-2.587 (t, ~6.6 Hz, 6H, -NCH_2), 3.152-3.183 (q, ~6.0 Hz, 6H, -NCH_2CH_2), 6.176-6.194 (t, ~5.4 Hz, 3H, -NH_a), 7.325-7.340 (d, 6H, ~9.0 Hz, Ar-H), 7.345-7.361 (d, 6H, ~9.6 Hz, Ar-H), 8.666 (s, 3H, -NH_b). ^{13}C NMR (150 MHz, DMSO-d_6): δ (ppm) 37.547, 53.794, 112.234, 119.662, 131.347, 139.905 and 155.139. ESI-MS: m/z 740.0073 [**L_{22}**+H)].

L_{23}: ^{1}H NMR (DMSO-d_6, 600 MHz) δ (ppm): 2.568-2.590 (t, ~6.6 Hz, 6H, -NCH_2), 3.155-3.187 (q,

~6.6 Hz, 6H, -NCH_2CH_2), 6.175-6.193 (t, ~5.4 Hz, 3H, -NH_a), 7.330-7.345 (d, 6H, ~9.0 Hz, Ar-H), 7.348-7.363 (d, 6H, ~9.6 Hz, Ar-H), 8.668 (s, 3H, -NH_b). ^{13}C NMR (150 MHz, DMSO-d_6): δ (ppm) 37.502, 53.758, 112.264, 119.596, 131.306, 139.897 and 155.081. ESI-MS: m/z 881.9675 [$\mathbf{L_{23}}$+H].

2.4.5 Tris(2-aminoethyl)amine (tren) based electron-rich receptors L_{24}-L_{27}

Highly electron-rich naphthyl (**L_{24}**, **L_{26}**) and phenyl (**L_{25}**, **L_{27}**) group substituted and no terminal aryl electron-withdrawing or π-acidic functionalization containing tris-(thio)-urea receptors have been synthesized in quantitative yield by the individual reaction of Tris(2-aminoethyl)amine (599 µL, 4.0 mmol) with 1-naphthyl isocyanate (1868 µL, 13.0 mmol), phenyl isocyanate (1412 µL, 13.0 mmol), 1-naphthyl isothiocyanate (2.408 g, 13.0 mmol) and phenyl isothiocyanate (1556 µL, 13.0 mmol) in dry acetonitrile medium separately. The individual reaction mixtures of amine and corresponding isocyanates/isothiocyanates were taken in four separate 50 mL round bottomed flasks, vigorously stirred for overnight at room temperature. Then, the off-white solid precipitate obtained in each case, were filtered off and washed several times with acetonitrile, THF to remove unreacted reagents and then dried in a vacuum to yield receptors **L_{24}**, **L_{25}**, **L_{26}** and **L_{27}** from respective flasks. The precipitate thus collected of ligands **L_{24}**-**L_{27}** were dried in air and characterized by NMR, FT-IR, ESI-MS and single crystal X-ray diffraction analyses. Yield: ~84%, ~80%, ~85% and ~65% based on respective **L_{24}**, **L_{25}**, **L_{26}** and **L_{27}**.

L_{24}: ^{1}H NMR (600 MHz, DMSO-d_6) δ(ppm): 2.701-2.723 (t, 6H, ~6.6 Hz, -NCH_2), 3.305-3.336 (q, 6H, ~6.6 Hz, -NCH_2CH_2), 6.682-6.700 (t, 3H, ~5.4 Hz, -NH_a), 7.334-7.360 (t, 3H, ~7.8 Hz, Ar-H), 7.421-7.445 (t, 3H, ~7.2 Hz, Ar-H), 7.455-7.479 (t, 3H, ~7.2 Hz, Ar-H), 7.514-7.528 (d, 3H, ~8.4 Hz, Ar-H), 7.849-7.862 (d, 3H, ~7.8 Hz, Ar-H), 7.948-7.961 (t, 2H, ~7.8 Hz, Ar-H), 8.060-8.074 (d, 2H, ~8.4 Hz, Ar-H), 8.610 (s, 3H, -NH_b); ^{13}C NMR (150 MHz, DMSO-d_6) δ (ppm): 37.850, 54.335, 110.046, 116.393, 121.491, 122.206, 125.530, 125.694, 125.830, 128.266, 133.701, 135.073, 155.905; FT-IR spectra (KBr pellet): 1631 cm^{-1} *vs*(C=O), 2931 cm^{-1} *vs*(C-H), 3048 cm^{-1} *vs*(C-H), 3304 cm^{-1} *vs*(N-H); ESI-MS: m/z 654.3061 [$\mathbf{L_{24}}$+H].

L_{25}: ^{1}H NMR (600 MHz, DMSO-d_6) δ (ppm): 2.572-2.594 (t, 6H, ~6.6 Hz, -NCH_2), 3.164-3.195 (q, 6H, ~6.6 Hz, -NCH_2CH_2), 6.163-6.181 (t, 3H, ~5.4 Hz, -NH_a), 6.863-6.886 (t, 3H, ~6.6 Hz, Ar-H), 7.179-7.205 (t, 6H, ~7.8 Hz, Ar-H), 7.359-7.373 (d, 6H, ~8.4 Hz, Ar-H), 8.526 (s, 3H, -NH_b). FT-IR (KBr pellet): 1647 cm^{-1} *vs*(C=O), 2823 cm^{-1} *vs*(C-H), 3038 cm^{-1} *vs*(C-H), 3305 cm^{-1} *vs*(N-H). ESI-MS: m/z 504.2758 [$\mathbf{L_{25}}$ + H].

L_{26}: ^{1}H NMR (600 MHz, DMSO-d_6) δ (ppm): 2.56 (bs, 6H, -NCH_2), 3.42 (bs, 6H, -NCH_2CH_2), 7.35 (bs, 3H, -NH_a), 7.44-7.45 (d, 3H, ~6.6 Hz, Ar-H), 7.49-7.55 (m, 9H, Ar-H), 7.84-7.87 (m, 6H, Ar-H), 7.94-7.95 (d, 3H, ~5.4 Hz, Ar-H), 9.67 (s, 3H, -NH_b); ^{13}C NMR (150 MHz, DMSO-d_6) δ (ppm): 42.8, 52.8, 123.5, 125.9, 126.4, 126.9, 127.0, 127.5, 128.8, 130.5, 134.7, 134.9 and 182.3. FT-IR (KBr pellet): 780 cm^{-1} *vs*(C=S, asym), 1527 cm^{-1} *vs*(C=S, sym), 2937 cm^{-1} *vs*(C-H), 3051 cm^{-1} *vs*(C-H), 3366 cm^{-1} *vs*(N-H). ESI-MS: m/z 702.2684 [$\mathbf{L_{26}}$+H].

L_{27}: ^{1}H NMR (600 MHz, DMSO-d_6) δ (ppm): 2.705-2.723 (t, 6H, ~5.4 Hz, -NCH_2), 3.577-3.610 (q, 6H, ~6.6 Hz, -NCH_2CH_2), 7.088-7.112 (t, 3H, ~7.2 Hz, Ar-H), 7.300-7.326 (t, 6H, ~7.8 Hz, Ar-H), 7.369-7.382 (d, 6H, ~7.8 Hz, Ar-H), 7.626 (s, 3H, -NH_a), 9.611 (s, 3H, -NH_b). FT-IR (KBr pellet): 1535 cm^{-1} *vs*(C=S), 2938 cm^{-1} *vs*(C-H), 3181 cm^{-1} *vs*(C-H), 3279 cm^{-1} *vs*(N-H). ESI-MS: m/z 552.3274 [**L_{27}**+H].

2.5 Synthesis and characterization of anion complexes of the receptors L_1-L_{27}

2.5.1 Complexes of *ortho*-Phenylenediamine based receptors L_1-L_3

The neutral complexes of individual *ortho*-Phenylenediamine based receptors **L_1-L_3** with anions, hydrated-anions or solvated anions were attained as suitable crystals for X-ray diffraction analysis upon slow evaporation of the 5 mL basic DMF or DMSO or mixed solution of individual receptors **L_1** (100 mg, 0.225 mmol)/**L_2** (100 mg, 0.187 mmol)/**L_3**(100 mg, 0.161 mmol) and excess tetrabutylammonium/tetraethylammonium salts (10 eqv.) of respective anions. Most of the cases colorless crystals of the hydrated or non-hydrated complexes were obtained at room temperature within one week to one month and they were collected by pressing between filter paper before characterization by different techniques. Note that, the aerial CO_2 fixed carbonate complex **3e** was achieved from the reaction of ligand **L_3** and *n*-TBAOH salt.

Chloride Complex [(*n*-TBA)$_3${(L_1)$_3$(Cl)$_3$(DMSO)}] (1a).

^{1}H NMR (600 MHz, DMSO-d_6) δ (ppm): 1.160-1.185 (t, 12H, ~7.2 Hz, $TBACH_3$), 1.515-1.576 (m, 8H, $TBACH_2$), 1.777-1.829 (m, 8H, $TBACH_2$), 2.787 (s, 6H, Ar-CH_3), 3.385-3.413 (t, 8H, ~9.0 Hz, N^+-$TBACH_2$), 7.298-7.326 (m, 2H, Ar-H), 7.441-7.457 (d, 2H, ~9.6 Hz, Ar-H), 7.471-7.484 (d, 2H, ~ 7.8 Hz, Ar-H), 7.874-7.901 (m, 2H, Ar-H), 7.947 (s, 2H, Ar-H), 8.655 (s, 2H, NH_a), 9.812 (s, 2H, NH_b); ^{13}C NMR (150 MHz, DMSO-d_6) δ (ppm): 14.14, 19.46, 19.86, 23.71, 58.17, 117.35, 118.56, 124.09, 124.40, 128.64, 131.47, 131.81, 133.74, 139.83 and 153.71. FT-IR spectra (KBr pellet): 3386 cm^{-1} *vs*(N-H), 3148 cm^{-1} *vs*(C-H), 2868 cm^{-1} *vs*(C-H), 1674 cm^{-1} *vs*(C=O), 668 cm^{-1} *vs*(C-Cl). Yield 66% based on **L_1**.

Acetate Complex [(*n*-TBA){(L_1)(CH_3COO)}] (1b).

^{1}H NMR (600 MHz, DMSO-d6) δ (ppm): 1.158-1.183 (t, 12H, ~7.8 Hz, $TBACH_3$), 1.511-1.572 (m, 8H, $TBACH_2$), 1.768-1.820 (m, 8H, $TBACH_2$), 2.103 (s, 3H, Acetate-CH_3), 2.752 (s, 6H, Ar-CH_3), 3.371-3.399 (t, 8H, ~ 8.4 Hz, N^+-$TBACH_2$), 7.221-7.248 (m, 2H, Ar-H), 7.451-7.465 (d, 2H, ~8.4 Hz, Ar-H), 7.503-7.518 (d, 2H, ~9.0 Hz, Ar-H), 8.002-8.028 (m, 2H, Ar-H), 8.001 (s, 2H, Ar-H), 9.796 (s, 2H, NH_a), 10.832 (s, 2H, NH_b); ^{13}C NMR (150 MHz, DMSO-d6) δ (ppm): 14.12, 19.45, 19.85 , 23.70, 25.96, 58., 117.34, 118.50, 123.03, 123.31, 128.12, 130.86, 131.70, 133.67, 140.50, 153.93, 176.71. FT-IR spectra (KBr pellet): 3388 cm^{-1} *vs*(N-H), 3146 cm^{-1} *vs*(C-H), 2866 cm^{-1} *vs*(C-H), 1671 cm^{-1} *vs*(C=O), 664 cm^{-1} *vs*(C-Cl). Yield 80% based on **L_1**.

Carbonate complex [($TEA)_2${(L_1)$_2$(CO_3)}] (1c).

^{1}H NMR (600 MHz, DMSO-d_6) δ (ppm): 1.396-1.421 (t, 24H, ~7.2 Hz, $TBACH_3$), 2.799 (s, 6H, Ar-CH_3), 3.431-3.467 (t, 16H, ~7.2 Hz, N^+-$TBACH_2$), 7.305-7.333 (m, 2H, Ar-H), 7.444-7.458 (d, 2H, ~8.4 Hz, Ar-H), 7.476-7.489 (d, 2H, ~7.8 Hz, Ar-H), 7.903-7.931 (m, 2H, Ar-H), 7.983 (s, 2H, Ar-H), 8.832

(s, 2H, NHa), 9.822 (s, 2H, NHb). ^{13}C NMR (150 MHz, DMSO-d_6) δ (ppm): 7.71, 19.45, 52.05, 117.50, 118.73, 124.18, 124.33, 128.59, 131.50, 131.74, 133.72, 139.93, 153.79 and 173.78. FT-IR spectra (KBr pellet): 3381 cm^{-1} *vs*(N-H), 3152 cm^{-1} *vs*(C-H), 2864 cm^{-1} *vs*(C-H), 1668 cm^{-1} *vs*(C=O), 662 cm^{-1} *vs*(C-Cl). Yield 75% based on **L_1**.

Chloride Complex [(*n*-TBA){(L_2) (Cl)}] (2a).

^{1}H NMR (400 MHz, DMSO-d_6) δ (ppm): 1.115-1.151 (t, 12H, ~7.2 Hz, $TBACH_3$), 1.460-1.551 (m, 8H, $TBACH_2$), 1.722-1.801 (m, 8H, $TBACH_2$), 2.701 (s, 6H, Ar-CH_3), 3.338-3.378 (t, 8H, ~8.0 Hz, N^+-$TBACH_2$), 7.254-7.291 (m, 2H, Ar-H), 7.456-7.472 (d, 2H, ~6.4 Hz, Ar-H), 7.634-7.656 (d, 2H, ~ 8.8 Hz, Ar-H), 7.668 (s, 2H, Ar-H), 7.786-7.824 (m, 2H, Ar-H), 8.390 (s, 2H, NH_a), 9.466 (s, 2H, NH_b). ^{13}C NMR (100 MHz, DMSO-d_6) δ (ppm): 14.15, 19.86, 23.31, 23.71, 58.17, 116.29, 118.21, 121.00, 124.32, 124.54, 131.41, 132.83, 137.99, 140.15 and 153.69. IR spectra (KBr pellet): 3379 cm^{-1} *vs*(N-H), 3142 cm^{-1} *vs*(C-H), 2864 cm^{-1} *vs*(C-H), 1668 cm^{-1} *vs*(C=O), 586 cm^{-1} *vs*(C-Br). Yield 70% based on **L_2**.

Sulfate Complex [(*n*-TBA)$_2${(L_2)$_2$(SO_4)}] (2b).

^{1}H NMR (400 MHz, DMSO-d_6) δ (ppm): 1.291-1.328 (t, 24H, ~7.6 Hz, $TBACH_3$), 1.636-1.727 (m, 16H, $TBACH_2$), 1.895-1.989 (m, 16H, $TBACH_2$), 2.899 (s, 6H, Ar-CH_3), 3.509- 3.551 (t, 8H, ~8.4 Hz, N+-$TBACH_2$), 7.389-7.428 (m, 2H, Ar-H), 7.596-7.618 (d, 2H, ~ 8.8 Hz, Ar-H), 7.715-7.737 (d, 2H, ~8.8 Hz, Ar-H), 7.836 (s, 2H, Ar-H), 8.241-8.282 (m, 2H, Ar-H), 9.764 (s, 2H, NH_a), 10.441 (s, 2H, NH_b). ^{13}C NMR (100 MHz, DMSO-d_6) δ (ppm): 14.12, 19.84, 23.05, 23.69, 58.15, 115.85, 118.25, 121.06, 123.35, 123.48, 130.59, 132.36, 137.53, 140.72 and 153.49. IR spectra (KBr pellet): 3385 cm^{-1} *vs*(N-H), 3143 cm^{-1} *vs*(C-H), 2863 cm^{-1} *vs*(C-H), 1664 cm^{-1} *vs*(C=O), 588 cm^{-1} *vs*(C-Br). Yield 65% based on **L_2**.

Hexafluorosilicate Complex [(*n*-TBA)$_2${(L_2)$_2$(SiF_6)}] (2c).

^{1}H NMR (400 MHz, DMSO-d_6) δ (ppm): 1.123-1.160 (t, 24H, ~7.2 Hz, $TBACH_3$), 1.467-1.556 (m, 16H, $TBACH_2$), 1.729-1.819 (m, 16H, $TBACH_2$), 2.714 (s, 6H, Ar-CH_3), 3.345-3.387 (t, 16H, ~8.8 Hz, N^+-$TBACH_2$), 7.255-7.298 (m, 2H, Ar-H), 7.478-7.500 (d, 2H, ~8.8 Hz, Ar-H), 7.626-7.648 (d, 2H, ~8.8 Hz, Ar-H), 7.690 (s, 2H, Ar-H), 7.828-8.870 (m, 2H, Ar-H), 8.469 (s, 2H, NHa), 9.426 (s, 2H, NHb). ^{13}C NMR (100 MHz, DMSO-d_6) δ (ppm): 13.96 (×8C, TBACH3), 19.68, 23.12, 23.49, 58.12, 116.05, 118.07, 120.85, 124.15, 124.21, 131.28, 132.53, 137.67, 140.02, 153.42. IR spectra (KBr pellet): 3387 cm^{-1} *vs*(N-H), 3146 cm^{-1} *vs*(C-H), 2868 cm^{-1} *vs*(C-H), 1670 cm^{-1} *vs*(C=O), 586 cm^{-1} *vs*(C-Br). Yield 70% based on **L_2**.

Fluoride-water complex [(*n*-TBA){(L_3)(F)(H_2O)}] (3a).

^{1}H NMR (600 MHz, DMSO-d_6) δ (ppm): 0.914-0.939 (t, 12H, ~7.8 Hz, $TBACH_3$), 1.269-1.330 (m, 8H, $TBACH_2$), 1.529-1.581 (m, 8H, $TBACH_2$), 3.136-3.165 (t, 8H, ~8.4 Hz, N^+-$TBACH_2$), 7.156-7.184 (m, 2H, Ar-H), 7.599-7.627 (m, 2H, Ar-H), 7.596 (s, 4H, Ar-H), 8.114 (s, 2H, Ar-H), 10.685 (s, 2H, NH_a), 11.788 (s, 2H, NH_b). IR spectra (KBr pellet): 3476 cm^{-1} *vs*(O-H), 3368 cm-1 *vs*(N-H) 3028 cm^{-1} *vs*(C-H), 2863 cm^{-1} *vs*(C-H), 1674 cm^{-1} *vs*(C=O), 1268 cm^{-1} *vs*(C-F). Yield 65% based on **L_3**.

Chloride complexes [(*n*-TBA){(L_3)(Cl)}] (3b^1) and [(TEA){(L_3)(Cl)}] (3b^2).

3b^1: ^{1}H NMR (600 MHz, DMSO-d_6) δ (ppm): 0.914-0.938 (t, 12H, ~7.2 Hz, $TBACH_3$), 1.270-1.331 (m,

8H, $TBACH_2$), 1.533-1.586 (m, 8H, $TBACH_2$), 3.144-3.172 (t, 8H, ~8.4 Hz, N^+-$TBACH_2$), 7.154-7.183 (m, 2H, Ar-H), 7.596-7.625 (m, 2H, Ar-H), 7.623 (s, 4H, Ar-H), 8.128 (s, 2H, Ar-H), 8.636 (s, 2H, NH_a), 10.246 (s, 2H, NH_b). IR spectra (KBr pellet): 3354 cm^{-1} *vs*(C-H) 3024 cm^{-1} *vs*(C-H), 2850 cm^{-1} *vs*(C-H), 1668 cm^{-1} *vs*(C=O), 1256 cm^{-1} *vs*(C-F). Yield: 65% based on **L_3**.

3b[2]: 1H NMR (600 MHz, DMSO-d6) δ (ppm): 1.141-1.165 (t, 12H, ~7.2 Hz, TEA-CH_3), 3.181-3.217 (q, 8H, ~7.2 Hz, N^+-TEA-CH_2), 7.135-7.162 (m, 2H, Ar-H), 7.614-7.644 (m, 2H, Ar-H), 7.615 (s, 4H, Ar-H), 8.112 (s, 2H, Ar-H), 8.355 (s, 2H, NH_a), 10.218 (s, 2H, NH_b). Yield: 70% based on **L_3**.

Bromide complex [(*n*-TBA){(L_3)(Br)}] (3c).

^{1}H NMR (600 MHz, DMSO-d_6) δ (ppm): 0.917-0.942 (t, 12H, ~7.8 Hz, $TBACH_3$), 1.273-1.334 (m, 8H, $TBACH_2$), 1.538-1.589 (m, 8H, $TBACH_2$), 3.148-3.176 (t, 8H, ~8.4 Hz, N^+-$TBACH_2$), 7.154-7.182 (m, 2H, Ar-H), 7.585-7.613 (m, 2H, Ar-H), 7.613 (s, 4H, Ar-H), 8.121 (s, 2H, Ar-H), 8.121 (s, 2H, NH_a), 9.920 (s, 2H, NH_b). IR spectra (KBr pellet): 3350 cm^{-1} *vs*(N-H) 3031 cm^{-1} *vs*(C-H), 2853 cm^{-1} *vs*(C-H), 1670 cm^{-1} *vs*(C=O), 1244 cm^{-1} *vs*(C-F). Yield 70% based on **L_3**.

Iodide complex [(*n*-TBA){(L_3)(I)}] (3d).

^{1}H NMR (600 MHz, DMSO-d_6) δ (ppm): 0.918-0.942 (t, 12H, ~7.8 Hz, $TBACH_3$), 1.275-1.336 (m, 8H, $TBACH_2$), 1.542-1.594 (m, 8H, $TBACH_2$), 3.158-3.186 (t, 8H, ~8.4 Hz, N^+-$TBACH_2$), 7.149-7.177 (m, 2H, Ar-H), 7.593 (s, 4H, Ar-H), 7.595-7.622 (m, 2H, Ar-H), 8.111 (s, 2H, Ar-H), 8.427 (s, 2H, NH_a), 9.911 (s, 2H, NH_b). IR spectra (KBr pellet): 3338 cm^{-1} *vs*(N-H) 3034 cm^{-1} *vs*(C-H), 2858 cm^{-1} *vs*(C-H), 1677 cm^{-1} *vs*(C=O), 1237 cm^{-1} *vs*(C-F). Yield 80% based on **L_3**.

Carbonate complex [(*n*-TBA)$_2${(L_3)$_2$(CO_3)}] (3e).

^{1}H NMR (600 MHz, DMSO-d_6) δ (ppm): 0.912-0.937 (t, 24H, ~7.2 Hz, $TBACH_3$), 1.267-1.328 (m, 16H, $TBACH_2$), 1.527-1.580 (m, 16H, $TBACH_2$), 3.135-3.163 (t, 16H, ~8.4 Hz, N^+-$TBACH_2$), 7.158-7.187 (m, 2H, Ar-H), 7.602-7.629 (m, 2H, Ar-H), 7.599 (s, 4H, Ar-H), 8.121 (s, 2H, Ar-H), 10.558 (s, 2H, NH_a), 11.699 (s, 2H, NH_b). ^{13}C NMR (150 MHz, DMSO-d_6) δ (ppm): 13.31, 19.11, 23.02, 57.58, 113.32, 117.79, 122.35, 124.22, 124.89, 124.94, 130.61, 130.89, 141.90, 155.45 and 171.56. IR spectra (KBr pellet): 3382 cm^{-1} *vs*(N-H), 3044 cm^{-1} *vs*(C H) 2862 cm^{-1} *vs*(C-H), 1665 cm^{-1} *vs*(C=O), 1245 cm^{-1} *vs*(C-F). Yield 65% based on **L_3**.

Sulfate complex [(*n*-TBA)$_2${(L_3)$_2$(SO_4)}] (3f).

^{1}H NMR (600 MHz, DMSO-d_6) δ (ppm): 0.912-0.936 (t, 24H, ~7.2 Hz, $TBACH_3$), 1.267-1.329 (m, 16H, $TBACH_2$), 1.530-1.583 (m, 16H, $TBACH_2$), 3.141-3.169 (t, 16H, ~8.4 Hz, N^+-$TBACH_2$),7.041-7.069 (m, 2H, Ar-H), 7.426 (s, 4H, Ar-H), 7.816-7.844 (m, 2H, Ar-H), 8.119 (s, 2H, Ar-H), 9.651 (s, 2H, NH_a), 10.945 (s, 2H, NH_b). IR spectra (KBr pellet): 3387 cm^{-1} *vs*(N-H), 3052 cm^{-1} *vs*(C-H), 2857 cm^{-1} *vs*(C-H), 1678 cm^{-1} *vs*(C=O), 1238 cm^{-1} *vs*(C-F). Yield 70% based on **L_3**.

2.5.2 Complexes of *meta*-Phenylenediamine based receptors L_4-L_8

The neutral host-guest complexes of individual *meta*-Phenylenediamine based receptors **L_4-L_8** with anions, hydrated-anions or solvated anions were attained as suitable crystals for X-ray diffraction analysis upon slow evaporation of the 5 mL basic DMF or DMSO or mixed solution

of individual receptors **L_4** (100 mg, 0.238 mmol)/**L_5** (100 mg, 0.238 mmol)/**L_6** (100 mg, 0.225 mmol)/**L_7** (100 mg, 0.187 mmol)/**L_8** (100 mg, 0.161 mmol) and excess tetrabutylammonium/tetraethylammonium salts (10 eqv.) of respective anions. Most of the cases pale yellow or colorless crystals of the hydrated or non-hydrated complexes were obtained at room temperature within one week to one month and they were collected by pressing between filter paper before characterization by different techniques. Note that, the aerial CO_2 fixed hydrated-carbonate complex **6a** of ligand **L_6** and bicarbonate-dimer complex **8b** of ligand **L_8** were achieved from the reaction of respective ligand and *n*-TBAOH or *n*-TBAF salts.

Fluoride-water complex [(*n*-TBA){(L_4)(F)(H_2O)}](4a).

^{1}H NMR (600 MHz, DMSO-d_6) δ (ppm): 0.913 (t, 12H, TBACH_3), 1.270-1.307 (m, 8H, TBACH_2), 1.532-1.568 (m, 8H, TBACH_2), 3.141 (t, 8H, TBACH_2), 7.108 (t, 1H, Ar-H), 7.224-7.236 (d, 2H, Ar-H), 7.520 (s, 1H, Ar-H), 7.437 (t, 2H, Ar-H), 7.679-7.692 (d, 2H, Ar-H), 7.706-7.720 (d, 2H, Ar-H), 8.587 (s, 2H, Ar-H), 10.761 (s, 2H,NH_a), 10.833 (s, 2H,NH_b). ^{13}C NMR (150 MHz, DMSO-d_6) δ (ppm): 13.45, 19.17, 23.02, 57.48, 108.12, 111.70, 111.80, 115.28, 124.04, 128.87, 129.73, 140.37, 142.34, 148.12 and 153.37. IR spectra (KBr pellet): 3450 cm^{-1} *vs*(N-H), 3150 cm^{-1} *vs*(aromatic C-H), 1698 cm^{-1} *vs*(C=O), 1592 cm^{-1} *vs*(C=C),1527 cm^{-1} *vs*(NO_2-asym), 1351 cm^{-1} *vs*(NO_2-sym), 1216 cm^{-1} *vs*(C-N). Yield: 70% based on **L_4**.

Sulfate complex [2(*n*-TBA){(L_4)$_2$(SO_4)$_2$}] (4b).

^{1}H NMR (600 MHz, DMSO-d_6) δ (ppm): 0.909 (t, 12H, TBACH_3), 1.267-1.304 (m, 8H, TBACH_2), 1.515-1.554 (m, 8H, TBACH_2), 3.139 (t, 8H, TBACH_2), 7.043 (t, 1H, Ar-H), 7.386-7.399 (d, 2H, Ar-H), 7.451 (s, 1H, Ar-H), 7.323 (t, 2H, Ar-H), 7.654-7.667 (d, 2H, Ar-H), 7.767-7.782 (d, 2H, Ar-H), 8.607 (s, 2H, Ar-H), 10.018 (s, 2H, NH_a), 10.461 (s, 2H, NH_b). ^{13}C NMR (150 MHz, DMSO-d_6) δ (ppm): 13.45, 19.18, 23.03, 57.50, 108.42, 111.88, 111.96, 115.37, 124.39, 128.47, 129.30, 140.30, 141.96, 147.90 and 152.79. FT-IR spectra (KBr pellet): 3478 cm^{-1} *vs*(N-H), 3116 cm^{-1} *vs*(C-H), 1720 cm^{-1} *vs*(C=O), 1594 cm^{-1} *vs*(C=C), 1524 cm^{-1} *vs*(NO_2-asym), 1352 cm^{-1} *vs*(NO_2-sym), 1221 cm^{-1} *vs*(C-N), 1178 cm^{-1} *vs*(S-O). Yield 80% based on **L_4**.

Acetate complex [(*n*-TBA){(L_4)(CH_3COO)}] (4c).

^{1}H NMR (600 MHz, DMSO-d_6) δ (ppm): 0.921 (t, 12H, TBACH_3), 1.263-1.312 (m, 8H, TBACH_2), 1.523-1.574 (m, 8H, TBACH_2), 3.143 (t, 8H, TBACH_2), 1.808 (s, 3H, acetate-CH_3), 7.132 (t, 1H, Ar-H), 7.203-7.217 (d, 2H, Ar-H), 7.720 (s, 1H, Ar-H), 7.526 (t, 2H, Ar-H), 7.756-7.769 (d, 2H, Ar-H), 7.790-7.803 (d, 2H, Ar-H), 8.664 (s, 2H, Ar-H), 10.266 (s, 2H, NH_a), 10.656 (s, 2H, NH_b). ^{13}C-NMR (150 MHz, DMSO-d_6) δ (ppm): 13.45, 19.18, 23.03, 57.51, 24.91, 108.62, 111.80, 112.13, 115.49, 124.12, 128.64, 129.77, 140.41, 142.15, 148.13, 153.05 and 176.30. FT-IR spectra (KBr pellet): 3446 cm^{-1} *vs*(N-H), 3098 cm^{-1} *vs*(C-H), 1680 cm^{-1} *vs*(C=O), 1584 cm^{-1} *vs*(C=C),1525 cm^{-1} *vs*(NO_2-asym), 1359 cm^{-1} *vs*(NO_2-sym), 1209 cm^{-1} *vs*(C-N), 1274 cm^{-1} *vs*(C-O acetate). Yield 80% based on **L_4**.

Sulfate-water complex [(*n*-TBA)$_4${(L_5)$_3$(SO_4)$_2$(H_2O)$_3$}] (5a).

^{1}H NMR (600 MHz, DMSO-d_6) δ (ppm): 0.920 (t, 12H, TBACH_3), 1.276-1.313 (m, 8H, TBACH_2),

1.539-1.575 (m, 8H, $TBACH_2$), 3.148 (t, 8H, $TBACH_2$), 7.469 (s, 1H, Ar-H), 7.349-7.362 (d, 2H, Ar-H), 7.061 (t, 1H, Ar-H), 7.751-7.766 (d, 4H, Ar-H), 8.011-8.025 (d, 4H, Ar-H), 10.128 (s, 2H, NH_a), 10.724 (s, 2H, NH_b). ^{13}C NMR (150 MHz, DMSO-d_6) δ (ppm): 13.47, 19.19, 23.04, 57.49, 108.65, 112.65, 117.40, 125.16, 129.25, 139.52, 140.98, 146.34 and 151.84. FT-IR spectra (KBr pellet): broad band at 3424 cm-1 *vs*(O-H), 3448 cm^{-1} *vs*(N-H), 3094 cm^{-1} *vs*(aromatic C-H), 1698 cm^{-1} *vs*(C=O), 1584 cm^{-1} *vs*(C=C), 1532 cm^{-1} *vs*(NO_2-asym), 1366 cm^{-1} *vs*(NO_2-sym), 1212 cm^{-1} *vs*(C-N), 1196 cm^{-1} *vs*(S-O). Yield 68% based on **L_5**.

Bromide complex [(*n*-TBA){(L_5)(Br)(DMSO)}] (5b).

^1H NMR (600 MHz, DMSO-d_6) δ (ppm): 0.929 (t, 12H, $TBACH_3$), 1.285-1.321 (m, 8H, $TBACH_2$), 1.549-1.582 (m, 8H, $TBACH_2$), 3.158 (t, 8H, $TBACH_2$), 7.747 (s, 1H, Ar-H), 7.127-7.141 (d, 2H, Ar-H), 7.228 (t, 1H, Ar-H), 7.692-7.706 (d, 4H, Ar-H), 8.190-8.204 (d, 4H, Ar-H), 9.060 (s, 2H, NH_a), 9.457 (s, 2H, NH_b). ^{13}C NMR (150 MHz, DMSO-d_6) δ (ppm): 13.47, 19.19, 23.04, 57.49, 108.65, 112.65, 117.40, 125.16, 129.25, 139.52, 140.98, 146.34 and 151.84. FT-IR spectra (KBr pellet): 3452 cm-1 *vs*(N-H), 3094 cm-1 *vs*(aromatic C-H), 1690 cm^{-1} *vs*(C=O), 1578 cm^{-1} *vs*(C=C), 1523 cm^{-1} *vs*(NO_2-asym), 1362 cm^{-1} *vs*(NO_2-sym), 1215 cm^{-1} *vs*(C-N). Yield 70% based on **L_5**.

Carbonate-water complex [(*n*-TBA)$_4${(L_6)$_4$(CO_3)$_2$(H_2O)$_2$}] (6a).

^1H NMR (400 MHz, DMSO-d_6) δ (ppm): 0.862-0.898 (t, 12H, ~7.2 Hz, $TBACH_3$), 1.116-1.305 (m, 8H, $TBACH_2$), 1.456-1.547 (m, 8H, $TBACH_2$), 2.188 (s, 6H, Ar-CH_3), 3.091-3.129 (t, 8H, ~7.6 Hz, N^+-$TBACH_2$), 7.054-7.075 (d, 2H, ~8.4 Hz, Ar-H), 7.158-7.196 (m, 3H, Ar-H), 7.227-7.247 (d, 2H, ~8.0 Hz, Ar-H), 7.688 (s, 2H, Ar-H), 7.866 (s, 1H, Ar-H), 9.361 (s, 2H, NH_a), 9.488 (s, 2H, NH_b). ^{13}C NMR (100 MHz, DMSO d_6) δ (ppm): 13.368, 18.822, 19.200, 23.055, 57.356, 109.228, 111.483, 116.938, 117.903, 126.663, 130.676, 132.831, 133.028, 140.569, 140.945, 153.421 and 171.503. FT-IR spectra (KBr pellet): 3418 cm^{-1} *vs*(O-H), 3346 cm^{-1} *vs*(N-H), 3138 cm^{-1} *vs*(C-H), 2862 cm^{-1} *vs*(C-H), 1682 cm^{-1} *vs*(C=O), 675 cm^{-1} *vs*(C-Cl). Yield 88% based on **L_6**.

Sulfate complex [(*n*-TBA)$_2${(L_6)$_2$(SO_4)}] (6b).

^1H NMR (400 MHz, DMSO-d_6) δ (ppm): 0.895-0.931 (t, 12H, ~7.2 Hz, $TBACH_3$), 1.243-1.331 (m, 8H, $TBACH_2$), 1.502-1.579 (m, 8H, $TBACH_2$), 2.225 (s, 6H, Ar-CH_3), 3.121-3.163 (t, 8H,~8.4 Hz, N^+-$TBACH_2$), 6.987-7.028 (t, 1H, ~8.0 Hz, Ar-H), 7.092-7.113 (d, 2H, ~8.4 Hz, Ar-H), 7.230-7.252 (d, 2H, ~8.8 Hz, Ar-H), 7.287-7.308 (d, 2H, ~8.4 Hz, Ar-H), 7.552 (s, 2H, Ar-H), 7.761 (s, 1H, Ar-H), 9.815 (s, 2H, NH_a), 9.894 (s, 2H, NH_b). FT-IR spectra (KBr pellet): 3338 cm^{-1} *vs*(N-H), 3138 cm^{-1} *vs*(C-H), 2854 cm^{-1} *vs*(C-H), 1674 cm^{-1} *vs*(C=O), 1192 cm^{-1} *vs*(S-O), 666 cm^{-1} *vs*(C-Cl). Yield 65% based on **L_6**.

Fluoride complex [(*n*-TBA){(L_6)(F)}] (6c).

^1H NMR (600 MHz, DMSO-d_6) δ (ppm): 0.917-0.941 (t, 12H, ~7.2 Hz, $TBACH_3$), 1.270-1.331 (m, 8H, $TBACH_2$), 1.530-1.582 (m, 8H, $TBACH_2$), 2.250 (s, 6H, Ar-CH_3), 3.138-3.165 (t, 8H, ~8.4 Hz, N+-$TBACH_2$), 7.062-7.075 (d, 2H, ~7.8 Hz, Ar-H), 7.131-7.182 (m, 3H, Ar-H), 7.210-7.223 (d, 2H, ~7.8 Hz, Ar-H), 7.649 (s, 2H, Ar-H), 7.701 (s, 1H, Ar-H), 9.230 (s, 2H, NH_a), 9.305 (s, 2H, NH_b). FT-IR spectra (KBr pellet): 3326 cm^{-1} *vs*(N-H), 3138 cm^{-1} *vs*(C-H), 2846 cm^{-1} *vs*(C-H), 1662 cm^{-1} *vs*(C=O),

661 cm^{-1} *vs*(C-Cl). Yield 70% based on **L_6**.

Bromide complex [(*n*-TBA)$_2${(L_6)$_2$(Br_2)$_2$}] (6d).

^{1}H NMR (400 MHz, DMSO-d_6) δ (ppm): 0.909-0.945 (t, 12H, ~7.2 Hz, $TBACH_3$), 1.255-1.345 (m, 8H, $TBACH_2$), 1.517-1.597 (m, 8H, $TBACH_2$), 2.255 (s, 6H, Ar-CH_3), 3.137-3.178 (t, 8H, ~8.4 Hz, N+-$TBACH_2$), 7.060-7.080 (d, 2H, ~8.0 Hz, Ar-H), 7.143-7.192 (m, 3H, Ar-H), 7.227-7.248 (d, 2H, ~8.4 Hz, Ar-H), 7.653 (s, 2H, Ar-H), 7.702 (s, 1H, Ar-H), 8.832 (s, 2H, NHa), 8.847 (s, 2H, NHb). FT-IR spectra (KBr pellet): 3329 cm^{-1} *vs*(N-H), 3122 cm^{-1} *vs*(C-H), 2857 cm^{-1} *vs*(C-H), 1652 cm^{-1} *vs*(C=O), 654 cm^{-1} *vs*(C-Cl). Yield 66% based on **L_6**.

Sulfate complex [(*n*-TBA)$_2${(L_7)$_2$(SO_4)}] (7a).

^{1}H NMR (600 MHz, DMSO-d_6) δ (ppm): 0.919-0.943 (t, 12H, ~7.2 Hz, $TBACH_3$), 1.273-1.333 (m, 8H, $TBACH_2$), 1.533-1.585 (m, 8H, $TBACH_2$), 2.298 (s, 6H, Ar-CH3), 3.140-3.168 (t, 8H, ~8.4 Hz, N^+-$TBACH_2$), 7.059-7.071 (d, 2H, ~7.2 Hz, Ar-H), 7.132-7.156 (t, 1H, ~7.2 Hz, Ar-H), 7.218-7.260 (m, 4H, Ar-H), 7.460 (s, 2H, Ar-H), 7.692 (s, 1H, Ar-H), 9.682 (s, 2H, NH_a), 9.821 (s, 2H, NH_b). FT-IR spectra (KBr pellet): 3342 cm^{-1} *vs*(N-H), 3133 cm^{-1} *vs*(C-H), 2843 cm^{-1} *vs*(C-H), 1650 cm^{-1} *vs*(C=O), 1188 cm^{-1} *vs*(S-O), 582 cm^{-1} *vs*(C-Br). Yield 80% based on **L_7**.

Fluoride complex [(*n*-TBA){(L_7)(F)}] (7b).

^{1}H NMR (400 MHz, DMSO-d_6) δ (ppm): 0.909-0.946 (t, 12H, ~7.6 Hz, $TBACH_3$), 1.269-1.328 (m, 8H, $TBACH_2$), 1.528-1.581 (m, 8H, TBA- CH_2), 2.287 (s, 6H, Ar-CH_3), 3.127-3.168 (t, 8H, ~8.0 Hz, N+-$TBACH_2$), 7.051-7.073 (d, 2H, ~8.8 Hz, Ar-H), 7.125-7.167 (t, 1H, ~8.8 Hz, Ar-H), 7.218-7.270 (m, 4H, Ar-H), 7.443 (s, 2H, Ar-H), 7.679 (s, 1H, Ar-H), 9.022 (bs, 2H, NH_a), 9.057 (bs, 2H, NH_b). FT-IR spectra (KBr pellet): 3327 cm^{-1} *vs*(N-H), 3126 cm^{-1} *vs*(C-H), 2849 cm^{-1} *vs*(C-H), 1665 cm^{-1} *vs*(C=O), 578 cm^{-1} *vs*(C-Br). Yield 75% based on **L_7**.

Sulfate-water complex [(*n*-TBA)$_4${(L_8)$_3$(SO_4)$_2$(H_2O)$_2$}] (8a).

^{1}H NMR (600 MHz, DMSO-d_6) δ (ppm): 0.892-0.916 (t, 12H, ~7.2 Hz, $TBACH_3$), 1.251-1.311 (m, 8H, $TBACH_2$), 1.514-1.566 (m, 8H, $TBACH_2$), 3.128-3.156 (t, 8H, ~8.4 Hz, N^+-TBA- CH_2), 6.890-6.917 (t, 1H, ~8.4 Hz, Ar-H), 7.267-7.278 (d, 2H, ~6.6 Hz, Ar-H), 7.341 (s, 2H, Ar-H), 7.816 (s, 1H, Ar-H), 8.129 (s, 4H, Ar-H), 10.320 (s, 2H, NH_a), 11.212 (s, 2H, NH_b). FT-IR spectra (KBr pellet): 3425 cm^{-1} *vs*(O-H), 3302 cm^{-1} *vs*(N-H), 3218 cm^{-1} *vs*(C-H), 2853 cm^{-1} *vs*(C-H), 1678 cm^{-1} *vs*(C=O), 1273 cm^{-1} *vs*(C-F), 1198 cm^{-1} *vs*(S-O). Yield 75% based on **L_8**.

Bicarbonate complex [(*n*-TBA)$_2${(L_8)(HCO_3)$_2$}] (8b).

^{1}H NMR (600 MHz, DMSO-d_6) δ (ppm): 0.906-0.930 (t, 12H, ~7.2 Hz, $TBACH_3$), 1.261-1.323 (m, 8H, $TBACH_2$), 1.523-1.575 (m, 8H, $TBACH_2$), 3.134-3.162 (t, 8H, ~7.8 Hz, N^+- $TBACH_2$), 6.923-7.107 (m, 3H, Ar-H), 7.477 (s, 2H, Ar-H), 7.865 (s, 1H, Ar-H), 8.254 (s, 4H, Ar-H), 11.221 (s, 2H, NH_a), 12.105 (s, 2H, NH_b). FT-IR spectra (KBr pellet): 3258 cm^{-1} *vs*(N-H), 3039 cm^{-1} *vs*(C-H), 2876 cm^{-1} *vs*(C-H), 1676 cm^{-1} *vs*(C=O), 1257 cm^{-1} *vs*(C-F). Yield 70% based on **L_8**.

Acetate-water complex [(*n*-TBA){(L_8)($OCOCH_3$)(H_2O)}] (8c).

^{1}H NMR (600 MHz, DMSO-d_6) δ (ppm): 0.896-0.921 (t, 12H, ~7.8 Hz, $TBACH_3$), 1.251-1.312 (m, 8H,

$TBACH_2$), 1.512-1.564 (m, 8H, $TBACH_2$), 1.752 (s, 3H, Acetate-CH_3), 3.122-3.150 (t, 8H, ~8.4 Hz, N+-$TBACH_2$), 7.028-7.098 (m, 3H, Ar-H), 7.475 (s, 2H, Ar-H), 8.068 (s, 1H, Ar-H), 8.321 (s, 4H, Ar-H), 12.077 (s, 2H, NH_a), 13.110 (s, 2H, NH_b). FT-IR spectra (KBr pellet): 3451 cm-1 *vs*(O-H), 3345 cm^{-1} *vs*(N-H), 3038 cm^{-1} *vs*(C-H), 2836 cm^{-1} *vs*(C-H), 1658 cm^{-1} *vs*(C=O), 1265 cm^{-1} *vs*(C-F). Yield 65% based on **L_8**.

Chloride-water complex [(*n*-TBA){(L_8)(Cl)(H_2O)}] (8d).

^{1}H NMR (600 MHz, DMSO-d_6) δ (ppm): 0.908-0.945 (t, 12H, ~7.2 Hz, $TBACH_3$), 1.254-1.347 (m, 8H, $TBACH_2$), 1.515-1.596 (m, 8H, $TBACH_2$), 3.137-3.179 (t, 8H, ~7.8 Hz, N+-$TBACH_2$), 7.121-7.135 (d, 2H, ~8.4 Hz, Ar-H), 7.205-7.232 (t, 1H, ~7.8 Hz, Ar-H), 7.648 (s, 2H, Ar-H), 7.788 (s, 1H, Ar-H), 8.140 (s, 4H, Ar-H), 9.097 (s, 2H, NH_a), 9.313 (s, 2H, NH_b). FT-IR spectra (KBr pellet): 3373 cm^{-1} *vs*(N-H), 3289 cm^{-1} *vs*(C-H), 3108 cm^{-1} *vs*(C-H), 1667 cm^{-1} *vs*(C=O), 1261 cm^{-1} *vs*(C-F). Yield 70% based on **L_8**.

2.5.3 Complexes of *para*-Phenylenediamine based receptors L_9-L_{15}

The neutral host-guest complexes of individual *para*-Phenylenediamine based receptors **L_9-L_{15}** with anions, hydrated-anions or anionic associations were attained as suitable crystals for X-ray diffraction analysis upon slow evaporation of the 5 mL basic DMF or DMSO or mixed solution of individual receptors **L_9** (100 mg, 0.238 mmol)/**L_{10}** (100 mg, 0.238 mmol)/**L_{12}** (100 mg, 0.225 mmol)/**L_{13}** (100 mg, 0.187 mmol)/**L_{14}** (100 mg, 0.242 mmol)/ **L_{15}** (100 mg, 0.198 mmol) and excess tetrabutylammonium/tetraethylammonium salts (10 eqv.) of respective anions. Most of the cases pale yellow or colorless crystals of the non-hydrated complexes were obtained at room temperature within one week to one month and they were collected by pressing between filter paper before characterization by different techniques. Note that, anion complexation with bis-urea isomer **L_{11}** was not fruit full due to steric hindrance of *ortho*-nitro substituents. The aerial CO_2 fixed bicarbonate-dimer complexes **9a, 10a, 10b, 12b, 13c** and **14b** were achieved from the reaction of respective ligands and *n*-TBAOH or *n*-TBAF salts.

Bicarbonate complexes [(*n*-TBA)$_2${(L_9)(HCO_3)$_2$}] (9a), [(*n*-TBA)$_2${(L_{10})(HCO_3)$_2$}(DMF)] (10a) and [(n-TBA)$_2${(L_{10})(HCO_3)$_2$}] (10b).

9a: ^{1}H NMR (600 MHz, DMSO-d_6) δ (ppm): 0.911-0.935 (t, 12H, ~7.2 Hz, $TBACH_3$), 1.265-1.326 (m, 8H, $TBACH_2$), 1.525-1.577 (m, 8H, $TBACH_2$), 3.134-3.162 (t, 8H, ~8.4 Hz, N+-$TBACH_2$), 7.443 (s, 4H, Ar-H), 7.741-7.756 (d, 4H, ~9.0 Hz, Ar-H), 8.124-8.139 (d, 4H, ~9.0 Hz, Ar-H), 10.021 (bs, 2H, NH_a), 10.636 (bs, 2H, NH_b). FT-IR spectra (KBr pellet): 3475 cm^{-1} *vs*(O-H), 3364 cm^{-1} *vs*(N-H), 2958 cm^{-1} *vs*(C-H), 1710 cm^{-1} *vs*(C=O), 1582 cm^{-1} *vs*(C=C), 1502 cm^{-1} *vs*(NO_2-asym), 1338 cm^{-1} *vs*(NO_2-sym), 1212 cm^{-1} *vs*(C-N), 848 cm^{-1} *vs*(HCO3-).Yield 65% based on **L_9**.

10a: ^{1}H NMR (600 MHz, DMSO-d_6) δ (ppm): 0.907-0.931 (t, 12H, ~7.2 Hz, $TBACH_3$), 1.261-1.323 (m, 8H, $TBACH_2$), 1.521-1.574 (m, 8H, $TBACH_2$), 3.132-3.160 (t, 8H, ~8.4 Hz, N+-$TBACH_2$), 7.426-7.65 (m, 6H, Ar-H), 7.684-7.697 (d, 2H, ~7.8 Hz, Ar-H), 7.862-7.876 (d, 2H, ~8.4 Hz, Ar-H), 8.653 (s, 2H, Ar-H), 11.354 (bs, 2H, NH_a), 12.061 (bs, 2H, NH_b). FT-IR spectra (KBr pellet): 3448 cm-1 *vs*(O-H),

3352 cm-1 *vs*(N-H), 2964 cm^{-1} *vs*(C-H), 1706 cm^{-1} *vs*(C=O), 1565 cm^{-1} *vs*(C=C), 1509 cm-*vs*(NO_2-asym), 1352 cm^{-1} *vs*(NO_2-sym), 1224 cm^{-1} *vs*(C-N), 844 cm-1 *vs*(HCO_3^-).Yield 60% based on **L_{10}**.

10b: ^{1}H NMR (600 MHz, DMSO-d_6) δ (ppm): 0.914-0.939 (t, 12H, ~7.2 Hz, $TBACH_3$), 1.268-1.329 (m, 8H, $TBACH_2$), 1.528-1.581 (m, 8H, $TBACH_2$), 3.137-3.165 (t, 8H, ~8.4 Hz, N^+-$TBACH_2$), 7.416 (s, 4H, Ar-H), 7.519-7.547 (t, 2H, ~8.4 Hz, Ar-H), 7.746-7.759 (d, 2H, ~7.8 Hz, Ar-H), 7.778-7.791 (d, 2H, ~7.8 Hz, Ar-H), 8.587 (s, 2H, Ar-H), 9.473 (bs, 2H, NH_a), 9.929 (bs, 2H, NH_b). IR spectra (KBr pellet): 3465 cm^{-1} *vs*(O-H), 3370 cm^{-1} *vs*(N-H), 2958 cm^{-1} *vs*(C-H), 1559 cm^{-1} *vs*(C=C), 1704 cm^{-1} *vs*(C=O), 1508 cm^{-1} *vs*(NO_2-asym), 1336 cm^{-1} *vs*(NO_2-sym), 1217 cm^{-1} *vs*(C-N), 846 cm^{-1} *vs*(HCO_3^-).Yield 70% based on **L_{10}**.

Acetate complex [(*n*-TBA)$_2${(L_9)($OCOCH_3$)$_2$}] (9b) and acetate-water complex [(n-TBA)$_2${(L_{10})($OCOCH_3$)$_2$(H_2O)$_2$}] (10c)

9b: ^{1}H NMR (600 MHz, DMSO-d_6) δ (ppm): 0.914-0.938 (t, 12H, ~7.2 Hz, $TBACH_3$), 1.267-1.328 (m, 8H, $TBACH_2$), 1.526-1.579 (m, 8H, $TBACH_2$), 1.773 (s, 3H, acetate-CH_3), 3.135- 3.163 (t, 8H, ~8.4 Hz, N^+-$TBACH_2$), 7.470 (s, 4H, Ar-H), 7.832- 7.848 (d, 4H, ~ 9.6 Hz, Ar-H), 8.119-8.134 (d, 4H, ~9.0Hz, Ar-H), 12.030 (s, 2H, NH_a), 12.834 (s, 2H, NH_b). FT-IR spectra (KBr pellet): 3423 cm^{-1} *vs*(N-H), 2964 cm^{-1} *vs*(C-H), 1706 cm^{-1} *vs*(C=O), 1576 cm^{-1} *vs*(C=C), 1501 cm^{-1} *vs*(NO_2-asym), 1305 cm^{-1} *vs* (NO_2-sym), 1219 cm^{-1} *vs*(C-N), 853 cm^{-1} *vs*(-COO), 642 cm^{-1} *vs*(-COO deformation). Yield 65% based on **L_9**.

10c: ^{1}H NMR (600 MHz, DMSO-d6) δ (ppm): 0.912-0.937 (t, 12H, ~7.2 Hz, $TBACH_3$), 1.265-1.327 (m, 8H, $TBACH_2$), 1.525-1.578 (m, 8H, $TBACH_2$), 1.777 (s, 3H, acetate-CH_3), 3.134- 3.162 (t, 8H, ~ 8.4 Hz, N^+-$TBACH_2$), 7.445 (s, 4H, Ar-H), 7.474- 7.501 (t, 2H, ~8.4 Hz, Ar-H), 7.702-7.715 (d, 2H, ~7.8 Hz, Ar-H), 7.860-7.874 (d, 2H, ~8.4 Hz, Ar-H), 8.683 (s, 2H, Ar-H), 11.534 (s, 2H, NH_a), 12.205 (s, 2H, NH_b). FT-IR spectra (KBr pellet): 3465 cm^{-1} *vs*(O-H), 3377 cm^{-1} *vs*(N-H), 2966 cm^{-1} *vs*(C-H), 1702 cm^{-1} *vs*(C=O), 1535 cm^{-1} *vs*(C=C), 1508 cm^{-1} *vs*(NO_2-asym), 1320 cm^{-1} *vs*(NO_2-sym), 1224 cm^{-1} *vs*(C-N), 885 cm^{-1} *vs*(-COO), 643 cm^{-1} *vs*(-COO deformation). Yield 75% based on **L_{10}**.

Bisulfate complex [(*n*-TBA)$_2${(L_9)(HSO_4)$_2$}] (9c), Sulfate complex [(*n*-TBA)$_4${(L_{10})$_3$(SO_4)$_2$}] (10d)

9c: ^{1}H NMR (600 MHz, DMSO-d_6) δ (ppm): 0.918-0.942 (t, 12H, ~7.2 Hz, $TBACH_3$), 1.271-1.332 (m, 8H, $TBACH_2$), 1.532-1.585 (m, 8H, $TBACH_2$), 3.142-3.170 (t, 8H, ~8.4 Hz, N^+-$TBACH_2$), 7.419 (s, 4H, Ar-H), 7.692-7.707 (d, 4H, ~9.0 Hz, Ar-H), 8.175-8.191 (d, 4H, ~9.6 Hz, Ar-H), 8.979 (s, 2H, NHa), 9.551 (s, 2H, NH_b). FT-IR spectra (KBr pellet): 3435 cm^{-1} *vs*(O-H), 3331 cm^{-1} *vs*(N-H), 2960 cm^{-1} *vs*(C-H), 1712 cm^{-1} *vs*(C=O), 1562 cm^{-1} *vs*(C=C), 1502 cm^{-1} *vs*(NO_2-asym), 1326 cm^{-1} *vs*(NO_2-sym), 1205 cm^{-1} *vs*(C-N), 1108 cm^{-1} *vs*(-HSO_4^-).Yield 70% based on **L_9**.

10d: ^{1}H NMR (600 MHz, DMSO-d_6) δ (ppm): 0.895-0.920 (t, 24H, ~7.8 Hz, $TBACH_3$), 1.251-1.313 (m, 16H, $TBACH_2$), 1.511-1.563 (m, 16H, $TBACH_2$), 3.118-3.146 (t, 16H, ~8.4 Hz, N^+-$TBACH_2$), 7.365 (s, 4H, Ar-H), 7.433-7.460 (t, 2H, ~8.4 Hz, Ar-H), 7.692-7.705 (d, 2H, ~7.8 Hz, Ar-H), 7.812-7.827 (d, 2H, ~9.0 Hz, Ar-H), 8.602 (s, 2H, Ar-H), 9.830 (s, 2H, NH_a), 10.648 (s, 2H, NH_b). FT-IR spectra (KBr

pellet): 3326 cm^{-1} *vs*(N-H), 2962 cm^{-1} *vs*(C-H), 1702 cm^{-1} *vs*(C=O), 1558 cm^{-1} *vs*(C=C), 1512 cm^{-1} *vs*(NO_2-asym), 1306 cm^{-1} *vs*(NO_2-sym),), 1205 cm^{-1} *vs*(C-N), 1112 cm^{-1} *vs*(-SO_4^{2-}).Yield 60% based on **L_{10}**.

Biphosphate Complex [(*n*-TBA)$_2${(L_{10})(H_2PO_4)$_2$}] (10e).

10e: 1H NMR (600 MHz, DMSO-d_6) δ (ppm): 0.916-0.940 (t, 12H, ~7.2 Hz, $TBACH_3$), 1.270-1.330 (m, 8H, $TBACH_2$), 1.531-1.584 (m, 8H, $TBACH_2$), 3.141-3.168 (t, 8H, ~8.4 Hz, N^+-$TBACH_2$), 7.456-7.484 (t, 2H, ~8.4 Hz, Ar-H), 7.500 (s, 4H, Ar-H), 7.705-7.718 (d, 2H, ~ 7.8 Hz, Ar-H), 7.985-7.999 (d, 2H, ~8.4 Hz, Ar-H), 8.720 (s, 2H, Ar-H), 10.777 (s, 2H, NH_a), 11.431 (s, 2H, NH_b). FT-IR spectra (KBr pellet): 3437 cm^{-1} *vs*(O-H), 3318 cm^{-1} *vs*(N-H), 2966 cm^{-1} *vs*(C-H), 1705 cm^{-1} *vs*(C=O), 1582 cm^{-1} *vs*(C=C), 1516 cm^{-1} *vs*(NO_2-asym), 1311 cm^{-1} *vs*(NO_2-sym),), 1200 cm^{-1} *vs*(C-N), 1099 cm^{-1} *vs*(-$H_2PO_4^-$).Yield 65% based on **L_{10}**.

Bromide complex [(*n*-TBA)$_2${(L_{12})($Br)_2$}] (12a), chloride complex [(*n*-TBA){(L_{13})(Cl)}] (13a) and bromide complex [(*n*-TBA)$_2${(L_{13})($Br)_2$}] (13b).

12a: ^{1}H NMR (600 MHz, DMSO-d_6) δ (ppm): 0.919-0.943 (t, 12H, ~7.2 Hz, $TBACH_3$), 1.272-1.333 (m, 8H, $TBACH_2$), 1.534-1.586 (m, 8H, $TBACH_2$), 2.252 (s, 6H, Ar-CH_3), 3.145-3.173 (t, 8H, ~8.4 Hz, N^+-$TBACH_2$), 7.164-7.178 (d, 2H, ~8.4 Hz, Ar-H), 7.221-7.233 (d, 2H, ~7.2 Hz, Ar-H), 7.351 (s, 4H, Ar-H), 7.691 (s, 2H, Ar-H), 8.636 (s, 2H, NH_a), 8.773 (s, 2H, NH_b). FT-IR spectra (KBr pellet): 3240 cm^{-1} *vs*(N-H), 3056 cm^{-1} *vs*(C-H), 2958 cm^{-1} *vs*(C-H), 1693 cm^{-1} *vs*(C=O), 683 cm^{-1} *vs*(C-Cl). Yield 75% based on **L_{12}**.

13a: ^{1}H NMR (600 MHz, DMSO-d_6) δ (ppm): 0.918-0.943 (t, 12H, ~7.2 Hz, $TBACH_3$), 1.271-1.333 (m, 8H, $TBACH_2$), 1.532-1.585 (m, 8H, $TBACH_2$), 2.302 (s, 6H, Ar-CH_3), 3.142-3.171 (t, 8H, ~8.4 Hz, N^+-$TBACH_2$), 7.237-7.251 (d, 2H, ~8.4 Hz, Ar-H), 7.346 (s, 4H, Ar-H), 7.426-7.441 (d, 2H, ~9.0 Hz, Ar-H), 7.446 (s, 2H, Ar-H), 8.794 (s, 2H, NH_a), 8.916 (s, 2H, NH_b). FT-IR spectra (KBr pellet): 3266 cm^{-1} *vs*(N-H), 3082 cm^{-1} *vs*(C-H), 2958 cm^{-1} *vs*(C-H), 1706 cm^{-1} *vs*(C=O), 565 cm^{-1} *vs*(C-Br). Yield 70% based on **L_{13}**.

13b: ^{1}H NMR (600 MHz, DMSO-d_6) δ (ppm): 0.917-0.942 (t, 12H, ~7.8 Hz, $TBACH_3$), 1.272-1.333 (m, 8H, $TBACH_2$), 1.534-1.587 (m, 8H, $TBACH_2$), 2.302 (s, 6H, Ar-CH_3), 3.147-3.175 (t, 8H, ~ 8.4 Hz, N^+-$TBACH_2$), 7.238-7.253 (d, 2H, ~9.0 Hz, Ar-H), 7.351 (s, 4H, Ar-H), 7.428-7.443 (d, 2H, ~9.0 Hz, Ar-H), 7.449 (s, 2H, Ar-H), 8.701 (s, 2H, NH_a), 8.810 (s, 2H, NH_b). FT-IR spectra (KBr pellet): 3233 cm^{-1} *vs*(N-H), 3056 cm^{-1} *vs*(C-H), 2951 cm^{-1} *vs*(C-H), 1693 cm^{-1} *vs*(C=O), 558 cm^{-1} *vs*(C-Br). Yield 75% based on **L_{13}**.

Acetate complex [(*n*-TBA)$_2${(L_{13})($OCOCH_3$)$_2$}] (13d).

13d: ^{1}H NMR (600 MHz, DMSO-d_6) δ (ppm): 0.915-0.940 (t, 12H, ~7.8 Hz, $TBACH_3$), 1.268-1.329 (m, 8H, $TBACH_2$), 1.527-1.579 (m, 8H, $TBACH_2$), 1.170 (s, 3H, Acetate-CH_3), 2.291 (s, 6H, Ar-CH_3), 3.135-3.163 (t, 8H, ~ 8.4 Hz, N^+-$TBACH_2$), 7.288-7.302 (d, 2H, ~8.4 Hz, Ar-H), 7.375 (s, 4H, Ar-H), 7.388-7.402 (d, 2H, ~8.4 Hz, Ar-H), 7.525 (s, 2H, Ar-H), 9.893 (s, 2H, NH_a), 10.027 (s, 2H, NH_b). FT-IR spectra (KBr pellet): 3430 cm^{-1} *vs*(O-H), 3299 cm^{-1} *vs*(N-H), 3062 cm^{-1} *vs*(C-H), 2964 cm^{-1} *vs*(C-H),

1634 cm^{-1} *vs*(C=O), 526 cm^{-1} *vs*(C-Br). Yield 70% based on **L_{13}**.

Bicarbonate complexes [(*n*-TBA)$_2${(L_{12})(HCO_3)$_2$}] (12b) and [(*n*-TBA)$_2${(L_{13})(HCO_3)$_2$}] (13c).

12b: ^{1}H NMR (600 MHz, DMSO-d_6) δ (ppm): 0.913-0.938 (t, 12H, ~7.8 Hz, $TBACH_3$), 1.266-1.328 (m, 8H, $TBACH_2$), 1.526-1.579 (m, 8H, $TBACH_2$), 2.231 (s, 6H, Ar-CH_3), 3.136-3.164 (t, 8H, ~ 8.4 Hz, N^+-$TBACH_2$), 7.142-7.156 (d, 2H, ~8.4 Hz, Ar-H), 7.347-7.361 (d, 2H, ~8.4 Hz, Ar-H), 7.377 (s, 4H, Ar-H), 7.738 (s, 2H, Ar-H), 10.817 (s, 2H, NH_a), 11.134 (s, 2H, NH_b). IR spectra (KBr pellet): 3423 cm^{-1} *vs*(O-H), 3240 cm^{-1} *vs*(N-H), 3056 cm^{-1} *vs*(C-H), 2951 cm^{-1} *vs*(C-H), 1693 cm^{-1} *vs*(C=O), 683 cm^{-1} *vs*(C-Cl). Yield 70% based on **L_{12}**.

13c: ^{1}H NMR (600 MHz, DMSO-d_6) δ (ppm): 0.916-0.940 (t, 12H, ~7.2 Hz, $TBACH_3$), 1.269-1.329 (m, 8H, $TBACH_2$), 1.526-1.581 (m, 8H, $TBACH_2$), 2.276 (s, 6H, Ar-CH_3), 3.138-3.166 (t, 8H, ~ 8.4 Hz, N^+-$TBACH_2$), 7.340-7.365 (m, 4H, Ar-H), 7.382 (s, 4H, Ar-H), 7.543 (s, 2H, Ar-H), 10.539 (s, 2H, NH_a), 10.733 (s, 2H, NH_b). 12.061 (bs, 2H, NH_b). FT-IR spectra (KBr pellet): 3430 cm^{-1} *vs*(O-H), 3240 cm^{-1} *vs*(N-H), 3056 cm^{-1} *vs*(C-H), 2964 cm^{-1} *vs*(C-H), 1699 cm^{-1} *vs*(C=O), 520 cm^{-1} *vs*(C-Br). Yield 65% based on **L_{13}**.

Sulfate complexes [(*n*-TBA)$_2${(L_{12})$_2$(SO_4)$_($H$_2$O)}] (12c) and [(*n*-TBA)$_4${(L_{13})$_3$(SO_4)$_2$}] (13e)

12c: ^{1}H NMR (600 MHz, DMSO-d_6) δ (ppm): 0.900-0.924 (t, 24H, ~7.2 Hz, $TBACH_3$), 1.253-1.315 (m, 16H, $TBACH_2$), 1.510-1.562 (m, 16H, $TBACH_2$), 2.237 (s, 6H, Ar-CH_3), 3.118-3.146 (t, 16H, ~ 8.4 Hz, N^+-$TBACH_2$), 7.150-7.164 (d, 2H, ~8.4 Hz, Ar-H), 7.317-7.330 (d, 2H, ~7.8 Hz, Ar-H), 7.372 (s, 4H, Ar-H), 7.730 (s, 2H, Ar-H), 9.615 (bs, 2H, NH_a), 10.034 (bs, 2H, NH_b). FT-IR spectra (KBr pellet): 3449 cm^{-1} *vs*(O-H), 3259 cm^{-1} *vs*(N-H), 3062 cm^{-1} *vs*(C-H), 2964 cm^{-1} *vs*(C-H), 1693 cm^{-1} *vs*(C=O), 617 cm^{-1} *vs*(C-Cl). Yield 65% based on **L_{12}**.

13e: ^{1}H NMR (600 MHz, DMSO-d_6) δ (ppm): 0.895-0.920 (t, 24H, ~7.8 Hz, $TBACH_3$), 1.249-1.310 (m, 16H, $TBACH_2$), 1.504-1.566 (m, 16H, $TBACH_2$), 2.259 (s, 6H, Ar-CH_3), 3.112-3.140 (t, 16H, ~ 8.4 Hz, N^+-$TBACH_2$), 7.320-7.334 (d, 2H, ~8.4 Hz, Ar-H), 7.347-7.362 (d, 2H, ~9.0 Hz, Ar-H), 7.373 (s, 4H, Ar-H), 7.532 (s, 2H, Ar-H), 9.710 (s, 2H, NH_a), 10.045 (s, 2H, NH_b). FT-IR spectra (KBr pellet): 3436 cm^{-1} *vs*(O-H), 3299 cm^{-1} *vs*(N-H), 3062 cm^{-1} *vs*(C-H), 2951 cm^{-1} *vs*(C-H), 1699 cm^{-1} *vs*(C=O), 520 cm^{-1} *vs*(C-Br). Yield 75% based on **L_{13}**.

Biphosphate complexes [(*n*-TBA)$_2${(L_{12})(H_2PO_4)$_2$}(DMSO)] (12d) and [(*n*-TBA)$_2${(L_{13})(H_2PO_4)$_2$}] (13f):

12d: ^{1}H NMR (600 MHz, DMSO-d_6) δ (ppm): 0.914-0.938 (t, 12H, ~7.2 Hz, $TBACH_3$), 1.268-1.329 (m, 8H, $TBACH_2$), 1.528-1.580 (m, 8H, $TBACH_2$), 2.232 (s, 6H, Ar-CH_3), 3.138-3.166 (t, 8H, ~ 8.4 Hz, N^+-$TBACH_2$), 7.135-7.149 (d, 2H, ~8.4 Hz, Ar-H), 7.412-7.429 (m, 6H, Ar-H), 7.796 (s, 2H, Ar-H), 10.212 (s, 2H, NH_a), 10.511 (s, 2H, NH_b). FT-IR spectra (KBr pellet): 3430 cm^{-1} *vs*(O-H), 3240 cm^{-1} *vs*(N-H), 3056 cm^{-1} *vs*(C-H), 2958 cm^{-1} *vs*(C-H), 1693 cm^{-1} *vs*(C=O), 637 cm^{-1} *vs*(C-Cl). Yield 75% based on **L_{12}**.

13f: ^{1}H NMR (600 MHz, DMSO-d_6) δ (ppm): 0.917-0.941 (t, 12H, ~7.2 Hz, $TBACH_3$), 1.270-1.332 (m, 8H, $TBACH_2$), 1.530-1.583 (m, 8H, $TBACH_2$), 2.275 (s, 6H, Ar-CH_3), 3.140-3.168 (t, 8H, ~ 8.4 Hz, N^+-

$TBACH_2$), 7.347-7.361 (d, 2H, ~8.4 Hz, Ar-H), 7.399-7.413 (d, 2H, ~8.4 Hz, Ar-H), 7.425 (s, 4H, Ar-H), 7.608 (s, 2H, Ar-H), 10.099 (s, 2H, NH_a), 10.321 (s, 2H, NH_b). FT-IR spectra (KBr pellet): 3423 cm^{-1} *vs*(O-H), 3240 cm^{-1} *vs*(N-H), 3056 cm^{-1} *vs*(C-H), 2958 cm^{-1} *vs*(C-H), 1686 cm^{-1} *vs*(C=O), 552 cm^{-1} *vs*(C-Br). Yield 60% based on **L_{13}**.

Bromide complex [(*n*-TBA)$_2${(L_{14})($Br)_2$}] (14a), chloride complex [(*n*-TBA)$_2${(L_{15})($Cl)_2$}] (15a) and bromide complex [(*n*-TBA)$_2${(L_{15})($Br)_2$}] (15b).

14a: ^{1}H NMR (600 MHz, DMSO-d_6) δ (ppm): 0.918-0.943 (t, 12H, ~7.2 Hz, $TBACH_3$), 1.272-1.333 (m, 8H, $TBACH_2$), 1.534-1.586 (m, 8H, $TBACH_2$), 3.144-3.172 (t, 8H, ~8.4 Hz, N^+-$TBACH_2$), 7.306-7.320 (d, 4H, ~8.4 Hz, Ar-H), 7.353 (s, 4H, Ar-H), 7.467-7.481 (d, 4H, ~8.4 Hz, Ar-H), 8.635 (s, 2H, NH_a), 8.819 (s, 2H, NH_b). FT-IR spectra (KBr pellet): 3240 cm^{-1} *vs*(N-H), 3051 cm^{-1} *vs*(C-H), 1693 cm^{-1} *vs*(C=O), 657 cm^{-1} *vs*(C-Cl). Yield 80% based on **L_{14}**.

15a: ^{1}H NMR (600 MHz, DMSO-d_6) δ (ppm): 0.918-0.942 (t, 12H, ~7.2 Hz, $TBACH_3$), 1.271-1.332 (m, 8H, $TBACH_2$), 1.532-1.584 (m, 8H, $TBACH_2$), 3.143-3.171 (t, 8H, ~8.4 Hz, N^+-$TBACH_2$), 7.347 (s, 4H, Ar-H), 7.240-7.256 (bs, 8H, Ar-H), 8.902 (bs, 2H, NH_a), 9.127 (bs, 2H, NH_b). FT-IR spectra (KBr pellet): 3246 cm^{-1} *vs*(N-H), 3050 cm^{-1} *vs*(C-H), 1699 cm^{-1} *vs*(C=O), 513 cm^{-1} *vs*(C-Br). Yield 65% based on **L_{15}**.

15b: ^{1}H NMR (600 MHz, DMSO-d_6) δ (ppm): 0.919-0.944 (t, 12H, ~7.2 Hz, $TBACH_3$), 1.272-1.333 (m, 8H, $TBACH_2$), 1.534-1.586 (m, 8H, $TBACH_2$), 3.145-3.173 (t, 8H, ~8.4 Hz, N^+-$TBACH_2$), 7.352 (s, 4H, Ar-H), 7.414-7.430 (d, 4H, ~9.6 Hz, Ar-H), 7.431-7.447 (d, 4H, ~9.6 Hz, Ar-H), 8.641 (s, 2H, NH_a), 8.824 (s, 2H, NH_b). FT-IR spectra (KBr pellet): 3240 cm^{-1} *vs*(N-H), 3056 cm^{-1} *vs*(C-H), 1693 cm^{-1} *vs*(C=O), 510 cm^{-1} *vs*(C-Br). Yield 70% based on **L_{15}**.

Acetate complexes [(*n*-TBA)$_2${(L_{14})($OCOCH_3)_2$}] (14c) and[(*n*-TBA)$_2${(L_{15})($OCOCH_3)_2$}] (15c).

14c: ^{1}H NMR (600 MHz, DMSO-d_6) δ (ppm): 0.909-0.933 (t, 12H, ~7.2 Hz, $TBACH_3$), 1.262-1.323 (m, 8H, $TBACH_2$), 1.519-1.572 (m, 8H, $TBACH_2$), 1.767 (s, 3H, Acetate-CH_3), 3.127-3.155 (t, 8H, ~8.4 Hz, N^+-$TBACH_2$), 7.245-7.260 (d, 4H, ~9.0 Hz, Ar-H), 7.387 (s, 4H, Ar-H), 7.565-7.580 (d, 4H, ~9.0 Hz, Ar-H), 10.498 (s, 2H, NH_a), 10.768 (s, 2H, NH_b). FT-IR spectra (KBr pellet): 3416 cm^{-1} *vs*(O-H), 3299 cm^{-1} *vs*(N-H), 3056 cm^{-1} *vs*(C-H), 1699 cm^{-1} *vs*(C=O), 646 cm^{-1} *vs*(C-Cl). Yield 70% based on **L_{14}**.

15c: ^{1}H NMR (600 MHz, DMSO-d_6) δ (ppm): 0.912-0.937 (t, 12H, ~7.2 Hz, $TBACH_3$), 1.265-1.326 (m, 8H, $TBACH_2$), 1.523-1.576 (m, 8H, $TBACH_2$), 1.738 (s, 3H, Acetate-CH_3), 3.132-3.160 (t, 8H, ~8.4 Hz, N^+-$TBACH_2$), 7.346-7.360 (d, 4H, ~8.4 Hz, Ar-H), 7.393 (s, 4H, Ar-H), 7.556-7.571 (d, 4H, ~9.0 Hz, Ar-H), 11.166 (s, 2H, NH_a), 11.481 (s, 2H, NH_b). FT-IR spectra (KBr pellet): 3416 cm^{-1} *vs*(O-H), 3300 cm^{-1} *vs*(N-H), 3050 cm^{-1} *vs*(C-H), 1693 cm^{-1} *vs*(C=O), 513 cm^{-1} *vs*(C-Br). Yield 65% based on **L_{15}**.

Bicarbonate complex [(*n*-TBA)$_2${(L_{14})($HCO_3)_2$}] (14b).

14b: ^{1}H NMR (600 MHz, DMSO-d_6) δ (ppm): 0.914-0.938 (t, 12H, ~7.2 Hz, $TBACH_3$), 1.267-1.328 (m, 8H, $TBACH_2$), 1.527-1.579 (m, 8H, $TBACH_2$), 3.136-3.164 (t, 8H, ~8.4 Hz, N^+-$TBACH_2$), 7.247-7.262 (d, 4H, ~9.0 Hz, Ar-H), 7.394 (s, 4H, Ar-H), 7.574-7.589 (d, 4H, ~9.0 Hz, Ar-H), 10.488 (s, 2H, NH_a),

10.756 (s, 2H, NH_b). FT-IR spectra (KBr pellet): 3416 cm^{-1} *vs*(O-H), 3240 cm^{-1} *vs*(N-H), 3056 cm^{-1} *vs*(C-H), 1693 cm^{-1} *vs*(C=O), 657 cm^{-1} *vs*(C-Cl). Yield 70% based on **L_{14}**.

Sulfate complex [(*n*-TBA)$_2${(L_{14})$_2$(SO_4)}] (14d), bisulfate complex [(*n*-TBA)$_2${(L_{15})(HSO_4)$_2$}(DMF)] (15d).

14d: ^{1}H NMR (600 MHz, DMSO-d_6) δ (ppm): 0.919-0.943 (t, 24H, ~7.2 Hz, $TBACH_3$), 1.272-1.333 (m, 16H, $TBACH_2$), 1.532-1.585 (m, 16H, $TBACH_2$), 3.142-3.170 (t, 16H, ~8.4 Hz, N^+-$TBACH_2$), 7.303-7.318 (d, 4H, ~9.0 Hz, Ar-H), 7.353 (s, 4H, Ar-H), 7.469-7.484 (d, 4H, ~9.0 Hz, Ar-H), 9.618 (s, 2H, NH_a), 10.024 (s, 2H, NH_b). FT-IR spectra (KBr pellet): 3416 cm^{-1} *vs*(O-H), 3240 cm^{-1} *vs*(N-H), 3056 cm^{-1} *vs*(C-H), 1699 cm^{-1} *vs*(C=O), 657 cm^{-1} *vs*(C-Cl). Yield 65% based on **L_{14}**.

15d: ^{1}H NMR (600 MHz, DMSO-d_6) δ (ppm): 0.906-0.930 (t, 12H, ~7.2 Hz, $TBACH_3$), 1.260-1.321 (m, 8H, $TBACH_2$), 1.521-1.569 (m, 8H, $TBACH_2$), 3.128-3.156 (t, 8H, ~8.4 Hz, N^+-$TBACH_2$), 7.363-7.378 (d, 4H, ~9.0 Hz, Ar-H), 7.396 (s, 4H, Ar-H), 7.516-7.531 (d, 4H, ~9.0 Hz, Ar-H), 8.626 (s, 2H, NH_a), 8.806 (s, 2H, NH_b). FT-IR spectra (KBr pellet): 3426 cm^{-1} *vs*(O-H), 3246 cm^{-1} *vs*(N-H), 3056 cm^{-1} *vs*(C-H), 1699 cm^{-1} *vs*(C=O), 520 cm^{-1} *vs*(C-Br). Yield 65% based on **L_{15}**.

Biphosphate complex [(*n*-TBA)$_2${(L_{14})(H_2PO_4)$_2$}] (14e).

1e: ^{1}H NMR (600 MHz, DMSO-d_6) δ (ppm): 0.915-0.940 (t, 12H, ~7.2 Hz, $TBACH_3$), 1.269-1.330 (m, 8H, $TBACH_2$), 1.529-1.581 (m, 8H, $TBACH_2$), 3.139-3.167 (t, 8H, ~8.4 Hz, N^+-$TBACH_2$), 7.228-7.243 (d, 4H, ~9.0 Hz, Ar-H), 7.421 (s, 4H, Ar-H), 7.618-7.633 (d, 4H, ~9.0 Hz, Ar-H), 10.116 (s, 2H, NH_a), 10.435 (s, 2H, NH_b). FT-IR spectra (KBr pellet): 3428 cm^{-1} *vs*(O-H), 3240 cm^{-1} *vs*(N-H), 3058 cm^{-1} *vs*(C-H), 1699 cm^{-1} *vs*(C=O), 656 cm^{-1} *vs*(C-Cl). Yield 70% based on **L_{14}**.

2.5.4 Complexes of tris(2-aminoethyl)-amine based receptors L_{16}-L_{23}

The protonated host-guest salt complexes of tris(2-aminoethyl)-amine based tris-amine receptors **L_{16}-L_{18}** with anions/hydrated-anions were attained from the individual 5 mL DMF or DMSO solutions ligands **L_{16}** (100 mg, 0.182 mmol)/**L_{17}** (100 mg, 0.154 mmol)/**L_{18}** (100 mg, 0.182 mmol) and inorganic acids such as HF, HCl, H_2SO_4 etc. On the other hand, the neutral host-guest complexes of tris(2-aminoethyl)-amine based tris-urea receptors **L_{19}-L_{23}** with halides and oxyanions were attained as suitable crystals for X-ray diffraction analysis upon slow evaporation of the 5 mL basic DMF or DMSO or mixed solution of individual receptors **L_{19}** (100 mg, 0.154 mmol)/**L_{20}** (100 mg, 0.128 mmol)/**L_{21}** (100 mg, 0.165 mmol)/**L_{22}** (100 mg, 0.135 mmol)/**L_{23}** (100 mg, 0.114 mmol) and excess tetrabutylammonium/tetraethylammonium salts (10 eqv.) of respective halides or oxyanions. Most of the cases colorless crystals of capsular, pseudo-capsular complexes were obtained at room temperature within one week to one month and they were collected by pressing between filter paper before characterization by different techniques.

Chloride complex [($L_{16}H_3Cl_3$)$_2$] (16a).

^{1}H-NMR (600 MHz, DMSO-d_6) δ (ppm): 3.10 (t, 6H, -NCH_2CH_2, ~5.6 Hz), 3.54 (s, 3H, NH), 3.75 (t, 6H, -NCH_2, ~6.2 Hz), 3.98 (s, 6H,-CH_2), 7.86-7.87 (d, 6H, Ar-H, ~8.0 Hz), 8.23-8.24 (d, 6H, Ar-H,

~7.2 Hz). ^{13}C NMR (150 MHz, DMSO-d_6) δ (ppm): 47.69, 52.81, 54.70, 125.29, 130.26, 145.48 and 149.64. Yield 70% based on **L_{16}**.

Fluoride complex [$(L_{17}H_3F_3)$] (17a).

^{1}H-NMR (600 MHz, DMSO-d6) δ (ppm): 3.20 (t, 6H, ~5.8 Hz), 3.52 (s, 3H), 3.73 (t, 6H, ~6.4 Hz), 3.90 (s, 6 H), 7.50-7.52 (d, 6H, ~10.8 Hz), 7.97-7.98 (d, 6H, ~8.4 Hz). ^{13}C NMR (150 MHz, DMSO-d_6) δ (ppm): 45.60, 51.3, 52.81, 120.46, 126.71, 134.23 and 139.35. Yield 80% based on **L_{17}**.

Sulfate complexes [$\{(L_{16}H_3)_2(SO_4)_3(H_2O)_8\}(DMF)_3$] (16b) and sulfate complex [$\{(L_{17}H_3)_2(SO_4)_3(H_2O)_8\}(DMF)_4$] (17b).

16b:^{1}H-NMR (600 MHz, DMSO-d_6) δ (ppm): 3.15 (t, 6H, ~6.2 Hz), 3.53 (s, 3H), 3.78 (t, 6H, ~5.8 Hz), 3.89 (s, 6H), 7.42-7.44 (d, 6H, ~10.2 Hz), 8.15-817 (d, 6H, ~9.8 Hz). ^{13}C NMR (150 MHz, DMSO-d_6) δ (ppm): 48.14, 52.29, 54.86, 122.72, 129.30, 147.73 and 149.31. Yield 80% based on **L_{16}**.

17b: 1H-NMR (600 MHz, DMSO-d_6) δ (ppm): 3.22 (t, 6H, ~5.4 Hz), 3.52 (s, 3H), 3.74 (t, 6H, ~6.0 Hz), 3.99 (s, 6H), 7.53-7.54 (d, 6H, ~7.8 Hz), 8.12-8.13 (d, 6H, ~7.0 Hz). 13C NMR (150 MHz, DMSO-d_6) δ (ppm): 45.60, 52.01, 53.75, 122.72, 129.46, 134.40 and 140.79. Yield 65% based on **L_{17}**.

Chloride complex [$(L_{18}H_3Cl_3)$] (18a).

^{1}H-NMR (600 MHz, DMSO-d_6) δ (ppm): 3.09 (t, 6H, ~6.2 Hz), 3.48 (s, 3H), 3.75(t, 6H, ~5.8 Hz), 3.90 (s, 6H), 7.50 (t, 3H, ~6.4 Hz), 7.99-8.00 (d, 3H, ~7.8 Hz), 8.20-8.21 (d, 3H, ~8.4 Hz), 8.31 (s, 3H). ^{13}C NMR (150 MHz, DMSO-d_6) δ (ppm): 44.0, 49.01, 49.54, 123.77, 125.30, 130.02, 133.72, 137.28 and 147.78. Yield 70% based on **L_{18}**.

Chloride complex [(*n*-TBA){(L_{19})(Cl)}] (19a), bromide complex [(*n*-TBA){(L_{19})(Br)}] (19b) and fluoride complex [(*n*-TBA){(L_{20})(F)}] (20a).

19a: 1H NMR (DMSO-d_6, 600 MHz): δ (ppm) 0.916-0.940 (t, ~7.2 Hz, 12H, $TBACH_3$), 1.271-1.332 (m, 8H, $TBACH_2$), 1.531-1.584 (m, 8H, $TBACH_2$), 2.203 (s, 9H, Ar-CH_3), 2.469-2.488 (t, 6H, ~6.0 Hz, -NCH_2), 3.139-3.198 (m, 14H, TBA-N^+-CH_2 & -NCH_2CH_2), 6.529-6.547 (t, ~5.4 Hz, 3H, -NH_a), 7.103-7.117 (d, ~8.4 Hz, 3H, Ar-H), 7.135-7.149 (d, ~8.4 Hz, 3H, Ar-H), 7.601 (s, 3H, Ar-H), 9.150 (s, 3H, -NH_b); FT-IR spectra (KBr pellet): 1691 cm^{-1} *vs*(C=O), 2961 cm^{-1} *vs*(C-H), 3245 cm^{-1} *vs*(C-H), 3352 cm^{-1} *vs*(N-H). Yield 75% based on **L_{19}**.

19b: ^{1}H NMR (DMSO-d_6, 600 MHz): δ (ppm) 0.920-0.945 (t, ~7.2 Hz, 12H, $TBACH_3$), 1.276-1.337 (m, 8H, $TBACH_2$), 1.538-1.589 (m, 8H, $TBACH_2$), 2.211 (s, 9H, Ar-CH_3), 2.542-2.563 (t, 6H, ~6.0 Hz, -NCH_2), 3.146-3.189 (m, 14H, TBA-N^+-CH_2 & -NCH_2CH_2), 6.253-6.262 (t, ~5.4 Hz, 3H, -NH_a), 7.099-7.113 (d, ~8.4 Hz, 3H, Ar-H), 7.125-7.139 (d, ~8.4 Hz, 3H, Ar-H), 7.611 (s, 3H, Ar-H), 8.728 (s, 3H, -NH_b); FT-IR spectra (KBr pellet): 1692 cm^{-1} *vs*(C=O), 2961 cm^{-1} *vs*(C-H), 3255 cm^{-1} *vs*(C-H), 3345 cm^{-1} *vs*(N-H). Yield 70% based on **L_{19}**.

20a: 1H NMR (DMSO-d6, 600 MHz): δ (ppm) 0.918-0.942 (t, ~7.2 Hz, 12H, $TBACH_3$), 1.273-1.334 (m, 8H, $TBACH_2$), 1.532-1.585 (m, 8H, $TBACH_2$), 2.168 (s, 9H, Ar-CH_3), 2.451-2.469 (t, 6H, ~5.4 Hz, -NCH_2), 3.139-3.192 (m, 14H, TBA-N^+-CH_2 & -NCH_2CH_2), 7.210-6.227 (t, ~4.8 Hz, 3H, -NH_a), 7.259 (s, 3H, Ar-H), 7.316-7.331 (d, ~9.0 Hz, 3H, Ar-H), 7.347-7.361 (d, ~8.4 Hz, 3H, Ar-H), 10.579 (s, 3H, -

NH_b); FT-IR spectra (KBr pellet): 1698 cm^{-1} *vs*(C=O), 2954 cm^{-1} *vs*(C-H), 3345 cm^{-1} *vs*(C-H), 3453 cm^{-1} *vs*(N-H). Yield 75% based on **L_{20}**.

Carbonate complex [$(TEA)_2\{(L_{19})_2(CO_3)\}$] (19c).

^{1}H NMR (DMSO-d6, 600 MHz): δ (ppm) 1.136-1.160 (t, ~7.2 Hz, 24H, TEA-CH_3), 2.101 (s, 9H, Ar-CH_3), 2.423-2.439 (t, ~4.8 Hz, 6H, -NCH_2), 3.068-3.091 (q, ~4.8 Hz, 6H, -NCH_2CH_2), 3.172-3.208 (q, ~7.2 Hz, 16H, TEA-N^+-CH_2), 6.781-7.791 (d, ~6.0 Hz, 3H, Ar-H), 7.128-7.137 (d, ~5.4 Hz, 3H, Ar-H), 7.585 (s, 3H, Ar-H), 7.991 (bs, 3H, -NHa), 10.133 (s, 3H, -NH_b); FT-IR spectra (KBr pellet): 1690 *vs*(C=O), 2948 cm^{-1} *vs*(C-H), 3295 cm^{-1} *vs*(C-H), 3470 cm^{-1} *vs*(N-H). Yield 70% based on **L_{19}**.

Sulfate complexes [$(n\text{-}TBA)_2\{(L_{19})_2(SO_4)\}$] (19d) and [$(n\text{-}TBA)_2\{(L_{20})_2(SO_4)\}$] (20b).

19d: ^{1}H NMR (DMSO-d_6, 600 MHz): δ (ppm) 0.914-0.939 (t, ~7.2 Hz, 24H, TBACH_3), 1.270-1.331 (m, 16H, TBACH_2), 1.530-1.583 (m, 16H, TBACH_2), 2.145 (s, 9H, Ar-CH_3), 2.363-2.378 (t, 6H, ~4.8 Hz, -NCH_2), 3.034-3.059 (q, ~5.4 Hz, 6H, -NCH_2CH_2), 3.139-3.167 (t, ~8.4 Hz, 16H, n-TBAN+- CH2), 6.898-6.912 (d, ~8.4 Hz, 3H, Ar-H), 7.255-7.269 (d, ~8.4 Hz, 3H, Ar-H), 7.683 (s, 3H, Ar-H), 7.713 (s, 3H, -NH_a), 9.632 (s, 3H, -NH_b); FT-IR spectra (KBr pellet): 1686 cm^{-1} *vs*(C=O), 2967 cm^{-1} *vs*(C-H), 3299 cm^{-1} *vs*(C-H), 3378 cm^{-1} *vs*(N-H). Yield 70% based on **L_{19}**.

20b: ^{1}H NMR (DMSO-d_6, 600 MHz): δ (ppm) 0.918-0.942 (t, ~7.2 Hz, 24H, TBACH_3), 1.272-1.334 (m, 16H, TBACH_2), 1.534-1.586 (m, 16H, TBACH_2), 1.949 (s, 9H, Ar-CH_3), 2.427 (bs, 6H, -NCH_2), 3.044 (bs, 6H, -NCH_2CH_2), 3.141- 3.169 (t, ~8.4 Hz, 16H, n-TBA-N^+-CH_2), 7.071-7.086 (d, ~9.0 Hz, 3H, Ar-H), 7.211 (s, 3H, Ar-H), 7.340 (bs, 3H, -NH_a), 7.353-7.368 (d, ~9.0 Hz, 3H, Ar-H), 9.205 (s, 3H, -NH_b); FT-IR spectra (KBr pellet): 1691 cm^{-1} *vs*(C=O), 2954 cm^{-1} *vs*(C-H), 3302 cm^{-1} *vs*(C-H), 3472 cm^{-1} *vs*(N-H). Yield 65% based on **L_{20}**.

Hexafluorosilicate complex [$(TEA)_2\{(L_{20})_2(SiF_6)\}$] (20c).

^{1}H NMR (DMSO-d_6,, 600 MHz): δ (ppm) 1.142-1.166 (t, ~7.2 Hz, 24H, TEA-CH_3), 2.181 (s, 9H, Ar-CH3), 2.458-2.475 (t, ~5.4 Hz, 6H, -NCH_2), 3.119 (bs, 6H, -NCH_2CH_2), 3.178- 3.214 (q, ~7.2 Hz, 16H, TEA-N^+-CH_2), 6.591 (bs, 3H, Ar-H), 7.203-7.372 (bs, 6H, Ar-H), 8.688 (bs, 3H, -NH_a), 10. 572 (bs, 3H, -NH_b); FT-IR spectra (KBr pellet): 1686 cm^{-1} *vs*(C=O), 2961 cm^{-1} *vs*(C-H), 3386 cm^{-1} *vs*(C-H), 3491 cm^{-1} *vs*(N-H). Yield 75% based on **L_{20}**.

Fluoride complexes [$(n\text{-}TBA)\{(L_{21})(F)\}$] (21a), [$(TBA)\{(L_{22})(F)\}$] (22a) and [$(n\text{-}TBA)\{(L_{23})(F)\}$] (23a):

21a: ^{1}H NMR (DMSO-d_6, 600 MHz): δ (ppm) 0.917-0.941 (t, ~7.2 Hz, 12H, TBACH_3), 1.272-1.333 (m, 8H, TBACH_2), 1.531-1.584 (m, 8H, TBACH_2), 2.451-2.468 (t, 6H, ~5.4 Hz, -NCH_2), 3.137-3.191 (m, 14H, TBA-N^+-CH_2 & -NCH_2CH_2), 7.168 (bs, 3H, -NH_a), 7.183-7.198 (d, ~9.0 Hz, 6H, Ar-H), 7.422-7.437 (d, ~9.0 Hz, 6H, Ar-H), 10.605 (s, 3H, -NH_b); FT-IR spectra (KBr pellet): 1690 cm^{-1} *vs*(C=O), 2961 cm^{-1} *vs*(C-H), 3329 cm^{-1} *vs*(C-H), 3445 cm^{-1} *vs*(N-H). Yield 65% based on **L_{21}**.

22a: ^{1}H NMR (DMSO-d_6, 600 MHz): δ (ppm) 0.917-0.942 (t, ~7.2 Hz, 12H, TBACH_3), 1.272-1.333 (m, 8H, TBACH_2), 1.531-1.584 (m, 8H, TBACH_2), 2.451-2.469 (t, 6H, ~6.0 Hz, -NCH_2), 3.137-3.192 (m, 14H, TBA-N^+-CH_2 & -NCH_2CH_2), 7.179 (bs, 3H, -NH_a), 7.305-7.320 (d, ~9.0 Hz, 6H, Ar-H), 7.375-

7.389 (d, ~8.4 Hz, 6H, Ar-H), 10.627 (s, 3H, -NH_b); FT-IR spectra (KBr pellet): 1685 *vs*(C=O), 2961 cm^{-1} *vs*(C-H), 3327 cm^{-1} *vs*(C-H), 3469 cm^{-1} *vs*(N-H). Yield 70% based on **L_{22}**.

23a: ^{1}H NMR (DMSO-d_6, 600 MHz): δ (ppm) 0.917-0.941 (t, ~7.2 Hz, 12H, $TBACH_3$), 1.271-1.333 (m, 8H, $TBACH_2$), 1.530-1.582 (m, 8H, $TBACH_2$), 2.444-2.462 (t, 6H, ~5.4 Hz, -NCH_2), 3.137-3.190 (m, 14H, TBA-N^+-CH_2 & -NCH_2CH_2), 7.175 (bs, 3H, -NH_a), 7.244-7.259 (d, ~9.0 Hz, 6H, Ar-H), 7.451-7.466 (d, ~9.0 Hz, 6H, Ar-H), 10.657 (s, 3H, -NH_b); FT-IR spectra (KBr pellet): 1683 *vs*(C=O), 2961 cm^{-1} *vs*(C-H), 3327 cm^{-1} *vs*(C-H), 3449 cm^{-1} *vs*(N-H). Yield 65% based on **L_{23}**.

Carbonate complexes [$(TEA)_2${$(L_{22})_2(CO_3)$}] (22b) and [$(TEA)_2${$(L_{23})_2(CO_3)(H_2O)_2$}] (23b):

^{1}H NMR (DMSO-d_6, 600 MHz): δ (ppm) 1.135-1.159 (t, ~7.2 Hz, 24H, TEA-CH_3), 2.394-2.410 (t, 6H, ~4.8 Hz, -NCH_2), 3.016-3.042 (q, 6H, ~4.8 Hz, -NCH_2CH_2), 3.171-3.207 (q, 16H, ~7.2 Hz, TEA-N^+-CH_2), 6.696-7.009 (d, ~7.8 Hz, 6H, Ar-H), 7.391-7.406 (d, ~9.0 Hz, 6H, Ar-H), 7.958 (bs, 3H, -NH_a), 10.133 (s, 3H, -NH_b); FT-IR spectra (KBr pellet): 1689 *vs*(C=O), 2966 cm^{-1} *vs*(C-H), 3297 cm^{-1} *vs*(C-H), 3494 cm^{-1} *vs*(N-H). Yield: 60% based on **L_{22}** of **22b**.

Sulfate complexes [$(n$-TBA$)_2${$(L_{21})_2(SO_4)(H_2O)$}] (21b) and [$(n$-TBA$)_2${$(L_{23})_2(SO_4)$}] (23c):

21b: ^{1}H NMR (DMSO-d_6, 600 MHz): δ (ppm) 0.917-0.941 (t, ~7.2 Hz, 24H, $TBACH_3$), 1.272-1.333 (m, 16H, $TBACH_2$), 1.533-1.585 (m, 16H, $TBACH_2$), 2.401-2.418 (t, 6H, ~5.4 Hz, -NCH_2), 3.050-3.077 (q, 6H, ~5.4 Hz, -NCH_2CH_2), 3.140-3.169 (t, 16H, ~9.0 Hz, TBA-N^+-CH_2), 7.006-7.021 (d, ~9.0 Hz, 6H, Ar-H), 7.236 (bs, 3H, -NH_a), 7.478-7.493 (d, ~9.0 Hz, 6H, Ar-H), 9.333 (s, 3H, -NH_b); FT-IR spectra (KBr pellet): 1683 *vs*(C=O), 2981 cm^{-1} *vs*(C-H), 3303 cm^{-1} *vs*(C-H), 3463 cm^{-1} *vs*(N-H), 3524 cm^{-1} *vs*(O-H). Yield: 65% based on **L_{21}**.

23c: ^{1}H NMR (DMSO-d_6, 600 MHz): δ (ppm) 0.918-0.942 (t, ~7.2 Hz, 24H, $TBACH_3$), 1.273-1.334 (m, 16H, $TBACH_2$), 1.533-1.586 (m, 16H, $TBACH_2$), 2.384-2.400 (t, 6H, ~4.8 Hz, -NCH_2), 3.029-3.055 (q, 6H, ~5.4 Hz, -NCH_2CH_2), 3.140-3.168 (t, 16H, ~8.4 Hz, TBA-N^+-CH_2), 7.240 (bs, 3H, -NH_a), 7.284-7.299 (d, ~9.0 Hz, 6H, Ar-H), 7.308-7.324 (d, ~8.4 Hz, 6H, Ar-H), 9.328 (s, 3H, -NH_b); FT-IR spectra (KBr pellet): 1677 *vs*(C=O), 2955 cm^{-1} *vs*(C-H), 3303 cm^{-1} *vs*(C-H), 3457 cm^{-1} *vs*(N-H). Yield: 65% based on **L_{23}**.

2.5.5 Complexes of tris(2-aminoethyl)-amine based receptors L_{24}-L_{27}

The neutral host-guest complexes of tris(2-aminoethyl)-amine based tris-(thio)-urea receptors **L_{24}-L_{27}** with anions, hydrated-anions or water assisted anionic guests were attained as suitable crystals for X-ray diffraction analysis upon slow evaporation of the 5 mL basic DMF or DMSO or mixed solvents of individual receptors **L_{24}** (100 mg, 0.155 mmol)/**L_{25}** (100 mg, 0.198 mmol)/**L_{26}** (100 mg, 0.142 mmol)/**L_{27}** (100 mg, 0.181 mmol) and excess tetrabutylammonium/tetraethylammonium salts (10 eqv.) of respective halides or oxyanions.

Most of the cases colorless crystals of capsular/pseudo-capsular complexes were obtained at room temperature within one week to one month and they were collected by pressing between filter paper before characterization by different techniques. Note that, the aerial CO_2 fixed

carbonate complex **27c** of tris-thiourea ligand $\mathbf{L_{27}}$ were achieved from the reaction of respective ligand and *n*-TBAOH salts.

Fluoride-water complex [(*n*-TBA){($\mathbf{L_{24}}$)(F)($\mathbf{H_2O}$)$_3$}] (24a) and chloride-water complex [(*n*-TBA){($\mathbf{L_{24}}$)(Cl)($\mathbf{H_2O}$)$_3$}] (24b)

24a: ^{1}H NMR (600 MHz, DMSO-d_6) δ(ppm): 0.892-0.916 (t, 12H, ~7.2 Hz, $TBACH_3$), 1.256-1.304 (m, 8H, $TBACH_2$), 1.499-1.551 (m, 8H, $TBACH_2$), 2.547-2.562 (t, 6H, ~4.8 Hz, $-NCH_2$), 3.105-3.133 (t, 8H, ~8.4 Hz, $TBACH_2$), 3.329-3.351 (q, 6H, ~4.8 Hz, $-NCH_2CH_2$), 5.591-6.016 (t, 3H, ~7.8 Hz, Ar-H), 6.992-7.017 (t, 3H, ~7.8 Hz, Ar-H), 7.320-7.346 (t, 3H, ~7.8 Hz, Ar-H), 7.404-7.417 (d, 3H, ~7.8 Hz, Ar-H), 7.685-7.699 (d, 3H, ~8.4 Hz, Ar-H), 8.177-8.189 (d, 3H, ~7.2 Hz, Ar-H), 8.294-8.333 (d, 3H, ~23.4 Hz, $-NH_a$), 8.530-8.544 (d, 3H, ~8.4 Hz, Ar-H), 10.508-10.558 (d, 3H, ~50.0 Hz, $-NH_b$); ^{13}C NMR (150 MHz, DMSO-d_6) δ (ppm): 13.471, 19.150, 22.99, 35.557, 51.679, 57.444, 109.641, 114.424, 120.706, 121.167, 124.641, 125.052, 125.810, 127.877, 133.536, 136.039, 155.879. FT-IR spectra (KBr pellet): 1680 (C=O), 2959 cm^{-1} (C-H), 3058 cm^{-1} (C-H), 3285 cm^{-1} (O-H), 3435 cm^{-1} (N-H). Yield: 64% based on $\mathbf{L_{24}}$.

24b: ^{1}H NMR (600 MHz, DMSO-d_6) δ(ppm): 0.909-0.933 (t, 12H, ~7.2 Hz, $TBACH_3$), 1.259-1.320 (m, 8H, $TBACH_2$), 1.516-1.567 (m, 8H, $TBACH_2$), 2.601-2.619 (t, 6H, ~5.4 Hz, $-NCH_2$), 3.124-3.151 (t, 8H, ~8.4 Hz, $TBACH_2$), 3.331-3.359 (q, 6H, ~5.4 Hz, $-NCH_2CH_2$), 7.134-7.160 (t, 3H, ~7.8 Hz, Ar-H), 7.324-7.394 (m, 9H, 6Ar-H, $3NH_a$), 7.508-7.522 (d, 3H, ~8.4 Hz, Ar-H), 7.822-7.835 (d, 3H, ~7.8 Hz, Ar-H), 7.975-7.987 (d, 3H, ~7.2 Hz, Ar-H), 8.363-8.378 (d, 3H, ~9.0 Hz, Ar-H), 8.965 (s, 3H, -NHb); ^{13}C NMR (150 MHz, DMSO-d_6) δ (ppm): 13.471, 19.182, 23.023, 36.810, 53.395, 57.480, 116.639, 121.887, 121.966, 125.127, 125.526, 125.623, 125.768, 128.142, 133.688, 135.210, 155.649; FT-IR spectra (KBr pellet): 1674 (C = O), 2962 cm^{-1} (C-H), 3051 cm^{-1} (C-H), 3313 cm^{-1} (O-H), 3450 cm^{-1} (N-H). Yield: 72% based on $\mathbf{L_{24}}$.

Fluoride-water complex [(*n*-TBA){($\mathbf{L_{25}}$)(F)($\mathbf{H_2O}$)$_3$}] (25a).

^{1}H NMR (600 MHz, DMSO-d_6) δ (ppm): 0.916-0.941 (t, 12H, ~7.8 Hz, $TBACH_3$), 1.271-1.332 (m, 8H, $TBACH_2$), 1.529-1.582 (m, 8H, $TBACH_2$), 2.457-2.475 (t, 6H, ~5.4 Hz, $-NCH_2$), 3.135-3.163 (t, 8H, ~8.4 Hz, $TBACH_2$), 3.176-3.201 (q, 6H, ~7.2 Hz, $-NCH_2CH_2$), 6.781-6.805 (t, 3H, ~7.2 Hz, Ar-H), 7.122-7.148 (t, 6H, ~7.8 Hz, Ar-H), 7.298-7.315 (t, 3H, ~5.4 Hz, $-NH_a$), 7.415-7.421 (d, 6H, ~7.2 Hz, Ar-H), 10.536 (s, 3H, $-NH_b$). FT-IR spectra (KBr pellet): 1687 cm-1 *vs*(C=O), 2885 cm^{-1} *vs*(C-H), 2969 cm^{-1} *vs*(C-H), 3333 cm^{-1} *vs*(O-H), 3426 cm^{-1} *vs*(N-H). Yield: 70% based on $\mathbf{L_{25}}$.

Biphosphate complex [(*n*-TBA){($\mathbf{L_{25}}$)($\mathbf{H_2PO_4}$)}] (25b).

^{1}H NMR (600 MHz, DMSO-d_6) δ (ppm): 0.920- 0.994 (t, 12H, ~7.2 Hz, $TBACH_3$), 1.275-1.336 (m, 8H, $TBACH_2$), 1.535-1.588 (m, 8H, $TBACH_2$), 2.388-2.404 (t, 6H, ~4.8 Hz, $-NCH_2$), 3.023-3.052 (q, 6H, ~6.0 Hz, $-NCH_2CH_2$), 3.142-3.170 (t, 8H, ~8.4 Hz, $TBACH_2$), 6.779-6.803 (t, 3H, ~7.2 Hz, Ar-H), 7.093-7.119 (t, 6H, ~7.8 Hz, Ar-H), 7.396 (s, 3H, $-NH_a$), 7.521-7.534 (d, 6H, ~7.8 Hz, Ar-H), 9.693 (s, 3H, $-NH_b$). FT-IR spectra (KBr pellet): 1378 cm-1 *vs* (P=O), 1674 cm^{-1} *vs*(C=O), 2959 cm^{-1} *vs*(C-H), 3285 cm^{-1} *vs*(C-H), 3353 cm^{-1} *vs*(N-H). Yield: 65% based on $\mathbf{L_{25}}$.

Fluoride complexes [(*n*-TBA){(L_{26})(F)}] (26a^1) and [(TEA){(L_{26})(F)}] (26a^2).

^{1}H NMR (600 MHz, DMSO-d_6) δ (ppm): 1.13-1.16 (t, 12H, ~7.2 Hz, TEA-CH_3), 2.79-2.81 (t, 6H, ~5.4 Hz, -NCH_2), 3.17-3.20 (q, 8H, ~7.2 Hz, TEA-CH_2), 3.78- 3.80 (t, 6H, ~5.4 Hz, -NCH_2CH_2), 6.11-6.13 (t, 3H, ~7.2 Hz, Ar-H), 6.99-7.02 (t, 3H, ~7.8 Hz, Ar-H), 7.38-7.41 (t, 3H, ~7.8 Hz, Ar-H), 7.62-7.64 (d, 3H, ~7.8 Hz, Ar-H), 7.68-7.69 (d, 3H, ~8.4 Hz, Ar-H), 7.73-7.75 (d, 3H, ~8.4 Hz, Ar-H), 7.81-7.82 (d, 3H, ~7.2 Hz, Ar-H), 9.36-9.39 (d, 3H, -NH_a), 11.33-11.39 (d, 3H, -NH_b); FT-IR spectra (KBr): 783 cm^{-1} *vs*(C=S, asym), 1547 cm^{-1} *vs*(C=S, sym), 2992 cm^{-1} *vs*(C-H), 3266 cm^{-1} *vs*(C-H), 3419 cm^{-1} *vs*(N-H). Yield: 85% based on L_{26} of **26a^2**.

Chloride complexes [(*n*-TBA){(L_{26})(Cl)}] (26b^1) and [(TEA){(L_{26})(Cl)(H_2O)}] (26b^2).

^{1}H NMR (600 MHz, DMSO-d_6) δ (ppm): 0.92-0.95 (t, 12H, ~7.8 Hz, TBACH_3), 1.27-1.34 (m, 8H, TBACH_2), 1.54-1.59 (m, 8H, TBACH_2), 2.64 (bs, 6H, -NCH_2), 3.14- 3.17 (t, 8H, ~8.4 Hz, TBACH_2), 3.54-3.57 (q, 6H, ~6.6 Hz, -NCH_2CH_2), 7.41-7.43 (t, 3H, ~6.6 Hz, Ar-H), 7.47-7.50 (m, 9H, Ar-H), 7.81-7.82 (t, 3H, ~4.8 Hz, Ar-H), 7.84 (bs, 3H, -NH_a), 7.89-7.90 (d, 3H, ~8.4 Hz, Ar-H), 7.92-7.93 (d, 3H, ~8.4 Hz, Ar-H), 9.91 (s, 3H, -NH_b); FT-IR spectra (KBr): 786 cm^{-1} *vs*(C=S, asym), 1540 *vs*(C=S, sym), 3031 cm^{-1} *vs*(C-H), 3239 cm^{-1} *vs*(C-H), 3467 cm^{-1} *vs*(N-H). Yield: 65% based on L_{26} of **26b^1**.

Bromide complexes [(*n*-TBA){(L_{26})(Br)}] (26c^1) and [(TEA){(L_{26})(Br)(H_2O)}] (26c^2).

^{1}H NMR (600 MHz, DMSO-d_6) δ (ppm) of 3b: 1.14-1.17 (t, 12H, ~7.2 Hz, TEA-CH_3), 2.56 (bs, 6H, -NCH_2), 3.18-3.22 (q, 8H, ~7.2 Hz, TEA-CH_2), 3.42 (bs, 6H, -NCH_2CH_2), 7.37 (bs, 3H, -NH_a), 7.44-7.45 (d, 3H, ~8.4 Hz, - Ar-H), 7.49-7.50 (d, 3H, ~7.8 Hz, Ar-H), 7.51-7.54 (m, 6H, Ar-H), 7.84-7.85 (d, 3H, ~7.8 Hz, Ar-H), 7.86-7.87 (d, 3H, ~ 6.6 Hz, Ar-H), 7.94-7.96 (t, 3H, ~5.4 Hz, Ar-H), 9.68 (s, 3H, -NH_b); FT-IR spectra (KBr): 777 cm^{-1} *vs*(C = S, asym), 1530 *vs*(C = S, sym), 2962 cm^{-1} *vs*(C-H), 3285 cm^{-1} *vs*(C-H), 3457 cm^{-1} *vs*(N-H). Yield: 75% based on L_{26} of **26c^2**.

Nitrate complex [(TEA){(L_{26})(NO_3)}] (26d).

^{1}H NMR (600 MHz, DMSO-d_6) δ (ppm): 1.14-1.17 (t, 12H, ~7.2 Hz, TEA-CH_3), 2.56 (bs, 6H, -NCH_2), 3.18-3.21 (q, 8H, ~7.2 Hz, TEA-CH_2), 3.41 (bs, 6H, -NCH_2CH_2), 7.35 (bs, 3H, -NH_a), 7.44-7.45 (d, 3H, ~7.2 Hz, Ar-H), 7.49-7.50 (d, 3H, ~7.8 Hz, Ar-H), 7.51-7.54 (m, 6H, Ar-H), 7.84-7.87 (m, 6H, Ar-H), 7.94- 7.96 (t, 3H, ~4.8 Hz, Ar-H), 9.67 (s, 3H, -NH_b); FT-IR spectra (KBr): 783 cm^{-1} *vs*(C=S, asym), 1395 cm^{-1} *vs*(N-O), 1540 cm^{-1} *vs*(C=S, sym), 3051 cm^{-1} *vs*(C-H), 3310 cm^{-1} *vs*(C-H), 3467 cm^{-1} *vs*(N-H). Yield: 65% based on L_{26}.

Sulfate complex [(TBA)$_2$){(L_{26})(SO_4)}] (26e).

^{1}H NMR (600 MHz, DMSO-d_6) δ (ppm): 0.92-0.94 (t, 12H, ~7.8 Hz, TBACH_3), 1.27-1.33 (m, 8H, TBACH_2), 1.53-1.58 (m, 8H, TBACH_2), 2.64 (bs, 6H, -NCH_2), 3.13-3.17 (t, 8H, ~8.4 Hz, TBACH_2),3.68-3.70 (q, 6H, ~4.8 Hz, -NCH_2CH_2), 7.30-7.33 (t, 3H, ~7.8 Hz, Ar-H), 7.38-7.40 (d, 3H, ~7.2 Hz, Ar-H), 7.41-7.44 (m, 6H, Ar-H), 7.73-7.74 (d, 3H, ~ 8.4 Hz, Ar-H), 7.86-7.87 (d, 3H, ~8.4 Hz, Ar-H), 8.06-8.07 (d, 3H, ~8.4 Hz, Ar-H), 10.37-10.39 (t, 3H, ~6.0 Hz, -NH_a), 11.24 (s, 3H, -NH_b); FT-IR spectra (KBr): 777 cm^{-1} *vs*(C=S, asym), 1118 cm^{-1} *vs*(S-O), 1547 cm^{-1} *vs*(C=S, sym), 2959 cm^{-1} *vs*(C-H), 3233 cm^{-1} *vs*(C-H), 3426 cm^{-1} *vs*(N-H). Yield: 80% based on L_{26}.

Chloride complex [(*n*-TBA){(L_{27})(Cl)}] (27a)

^{1}H NMR (600 MHz, DMSO-d_6) δ (ppm): 0.0.918-0.942 (t, 12H, ~7.2 Hz, $TBACH_3$), 1.272-1.334 (m, 8H, $TBACH_2$), 1.533-1.585 (m, 8H, $TBACH_2$), 2.670-2.690 (t, 6H, ~6.0 Hz, $-NCH_2$), 3.140-3.168 (t, 8H, ~8.4 Hz, $TBACH_2$), 3.616-3.645 (q, 6H, ~6.0 Hz, $-NCH_2CH_2$), 7.038-7.063 (t, 3H, ~7.8 Hz, Ar-H), 7.243-7.270 (t, 6H, ~8.4 Hz, Ar-H), 7.513- 7.526 (d, 6H, ~7.8 Hz, Ar-H), 8.067 (s, 3H, $-NH_a$), 10.149 (s, 3H, $-NH_b$). FT-IR spectra (KBr pellet): 1547 cm^{-1} *vs*(C=S), 2952 cm^{-1} *vs*(C-H), 3064 cm^{-1} *vs*(C-H), 3299 cm^{-1} *vs*(N-H). Yield: 75% based on **L_{27}**.

Acetate encapsulated complex [(*n*-TBA){(L_{27})($OCOCH_3$)}] (27b).

^{1}H NMR (600 MHz, DMSO-d_6) δ (ppm): 0.0.917-0.941 (t, 12H, ~7.2 Hz, $TBACH_3$), 1.269-1.330 (m, 8H, $TBACH_2$), 1.528-1.581 (m, 8H, TBA- CH_2), 1.174 (S, 6H, acetate-CH3), 2.638-2.656 (t, 6H, ~5.4 Hz, $-NCH_2$), 3.136-3.164 (t, 8H, ~8.4 Hz, $TBACH_2$), 3.558- 3.581 (q, 6H, ~4.8 Hz, $-NCH_2CH_2$), 7.003-7.028 (t, 3H, ~7.8 Hz, Ar-H), 7.220-7.246 (t, 6H, ~7.8 Hz, Ar-H), 7.524-7.537 (d, 6H, ~7.8 Hz, Ar-H), 8.650 (s, 3H, $-NH_a$), 10.882 (s, 3H, $-NH_b$). FT-IR spectra (KBr pellet): 1539 cm^{-1} *vs*(C=S), 2951 cm^{-1} *vs*(C-H), 3045 cm^{-1} *vs*(C-H), 3310 cm^{-1} *vs*(N-H). Yield: 80% based on **L_{27}**.

Carbonate encapsulated complex [(*n*-TBA)$_2${(L_{27})$_2$(CO_3)}] (27c)

^{1}H NMR (600 MHz, DMSO-d_6) δ (ppm): 0.920-0.944 (t, 24H, ~7.2 Hz, $TBACH_3$), 1.275-1.336 (m, 16H, $TBACH_2$), 1.535-1.587 (m, 16H, $TBACH_2$), 2.530-2.546 (m, 6H, $-NCH_2$), 3.141-3.169 (t, 16H, ~8.4 Hz, $TBACH_2$), 3.340-3.389 (m, 6H, $-NCH_2CH_2$), 6.963-6.987 (t, 3H, ~7.2 Hz, Ar-H), 7.149-7.175 (t, 6H, ~7.8 Hz, Ar-H), 7.475-7.486 (d, 6H, ~6.6 Hz, Ar-H), 8.762 (bs, 3H, $-NH_a$), 10.571 (bs, 3H, $-NH_b$). FT-IR spectra (KBr pellet): 1540 cm^{-1} *vs*(C=S), 2959 cm^{-1} *vs*(C-H), 3045 cm^{-1} *vs*(C-H), 3281 cm^{-1} *vs*(N-H). Yield: 70% based on **L_{27}**.

Sulfate complex [(*n*-TBA)$_2${(L_{27})$_2$(SO_4)}] (27d).

^{1}H NMR (600 MHz, DMSO-d_6) δ (ppm): 0.915-0.939 (t, 24H, ~7.2 Hz, $TBACH_3$), 1.269-1.330 (m, 16H, $TBACH_2$), 1.527-1.580 (m, 16H, $TBACH_2$), 2.557-2.573 (t, 6H, ~4.8 Hz, $-NCH_2$), 3.135-3.163 (t, 16H, ~8.4 Hz, $TBACH_2$), 3.465-3.488 (q, 6H, ~4.8 Hz, $-NCH_2CH_2$), 6.982-7.006 (t, 3H, ~7.2 Hz, Ar-H), 7.189-7.215 (t, 6H, ~7.8 Hz, Ar-H), 7.585-7.596 (d, 6H, ~6.6 Hz, Ar-H), 9.108 (s, 3H, $-NH_a$), 10.650 (s, 3H, $-NH_b$). FT-IR spectra (KBr pellet): 1544 cm^{-1} *vs*(C=S), 2963 cm^{-1} *vs*(C-H), 3051 cm^{-1} *vs* (C-H), 3283 cm^{-1} *vs*(N-H). Yield: 85% based on **L_{27}**.

References

2.1 (a) M. J. Hynes, EQNMR: A computer program for the calculation of stability constants from nuclear magnetic resonance chemical shift data, *J. Chem. Soc., Dalton Trans.*, 1993, 311; (b) H. J. Schneider, R. Kramer, S. Simova and U. Schneider *J. Am. Chem. Soc.*,1988, 110, 6442.

2.2 CrysAlisPro, version 1171.33.34d, Oxford Diffraction Ltd. [release 27-02-2009 CrysAlis 171. NET]

2.3 *SMART, SAINT and XPREP*; *Siemens Analytical X-ray Instruments Inc*.: Madison, WI, 1995.

2.4 G. M. Sheldrick, SADABS: *Software for Empirical Absorption Correction*; University of Gottingen, Institute fur Anorganische Chemieder Universitat: Tammanstrasse 4, D-3400, Gottingen, Germany, 1999-2003.

2.5 G. M. Sheldrick, *Crystal structure refinement with SHELXL*, *Acta Crystallogr., Sect. C: Struct. Chem*., 2015, **71**, 3.

2.6 L. J. Farrugia, *J. Appl. Crystallogr*, 1997, **30**, 565.

2.7 Mercury 2.3 Supplied with Cambridge Structural Database, CCDC, Cambridge, U.K., 20011.

2.8 P. Van der Sluis and A. L. Spek, *Acta Crystallogr., Sect. A: Found. Crystallogr.,* 1990, **46**, 194.

Chapter 3

ortho-Phenylenediamine based isomeric neutral scaffolds: Evidence of [$(Cl)_3$-DMSO] dual guest encapsulation and cyclic [$(F)_2(H_2O)_2$] tetramer entrapment

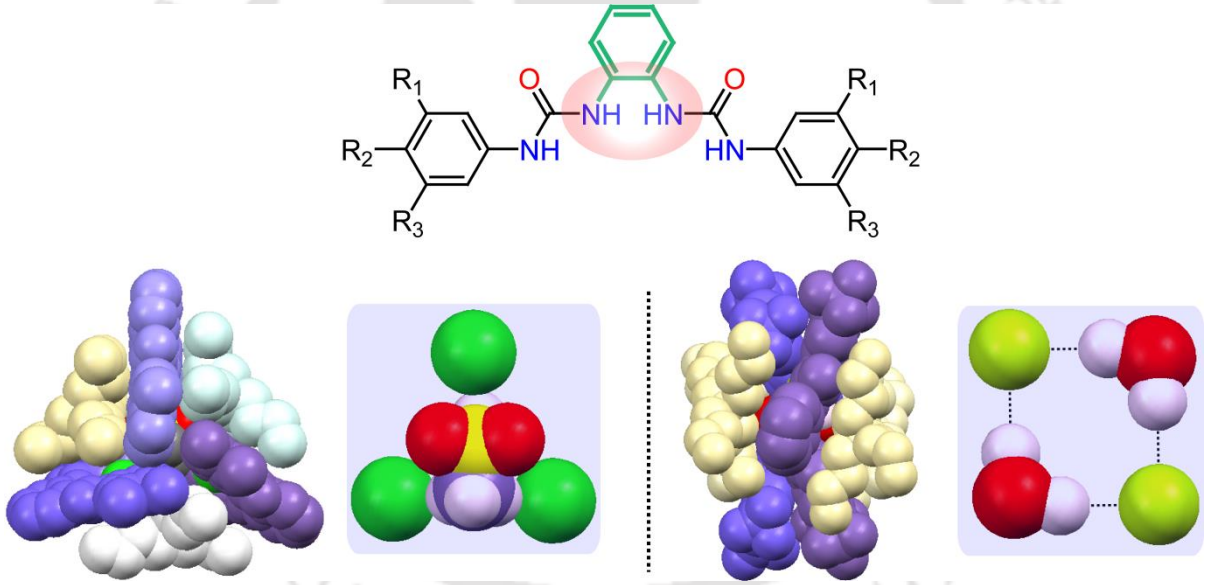

3.1 Background and Focus of the Chapter

As anions play critical and substantial roles in living organisms as well as in a range of biological, medical, industrial and environmental processes[3.1], the encapsulation or entrapment of anionic guests by a variety of non-covalent interactions within the multi-armed abiotic host receptor scaffolds have emerged as topics of principal importance in supramolecular chemistry.[3.2] Thus, the design of suitable receptors containing flexible and preorganized cavities with mostly tripodal scaffolds[3.3] have been designed and extensively studied from last two decades to inspect their coordination behavior with different dimensions of anions such as spherical (halides), planar (acetate, nitrate or carbonate), tetrahedral (sulfate or phosphate) in solid and solution states. Although proteins in natural systems can selectively and proficiently bind anions through precise non-covalent interactions, for the systematic and purposeful recognition from spherical halides to planar and tetrahedral oxyanions, the development of artificial neutral receptors other than the vastly explored tripodal receptors still remains a challenging area.[3.4] Among anions of various shapes, the recognition of hydrated/non-hydrated halides is an area of immense research interest because of their roles in chemistry, industry, food and toxicity.[3.5] The excess of fluoride in drinking water causes dental and skeletal fluorosis and beyond its toxic level in the human body fluoride can cause osteosarcoma. The larger chloride ion is crucial for its substantial role in biological processes like signal transduction or transport of organic solutes through the cell membrane. The spherical bromide anion also is an essential cofactor for the assembly of collagen IV scaffolds in tissue development, while the larger spherical iodide is one of the most important and overlooked components which is responsible for the correct function of thyroid hormones in the thyroid gland.[3.6] On the other hand among oxyanions, the tetrahedral sulfate anion is bound in proteins in a neutral environment inside the hydrophobic cavity in *Salmonella typhimurium* bacteria, and furthermore the harmful effect of sulfate has also been considered as a major hurdle to clean-up efforts in the remediation of nuclear waste; the planar carbonate works as a buffer in the blood as well as the major anions in biomineralized materials such as the exoskeletons of radiolarian, and acetate is utilized by organisms in the form of acetyl coenzyme A, etc.[3.7] Another major environmental matter

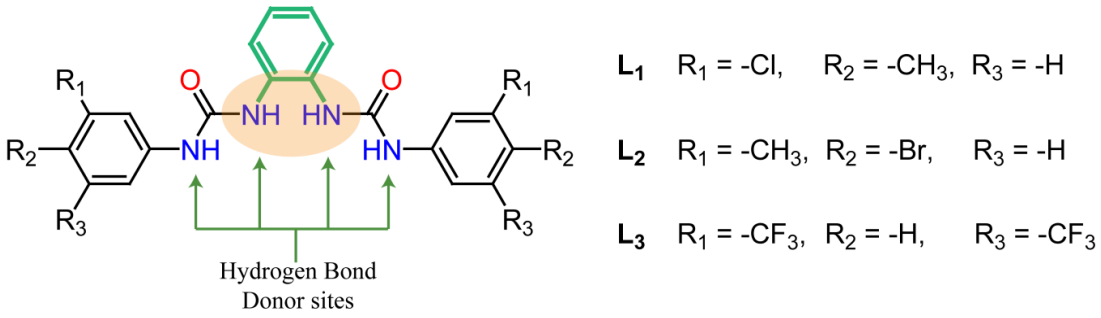

Scheme 3.1 A comprehensive representation of molecular receptor structures included in this chapter.

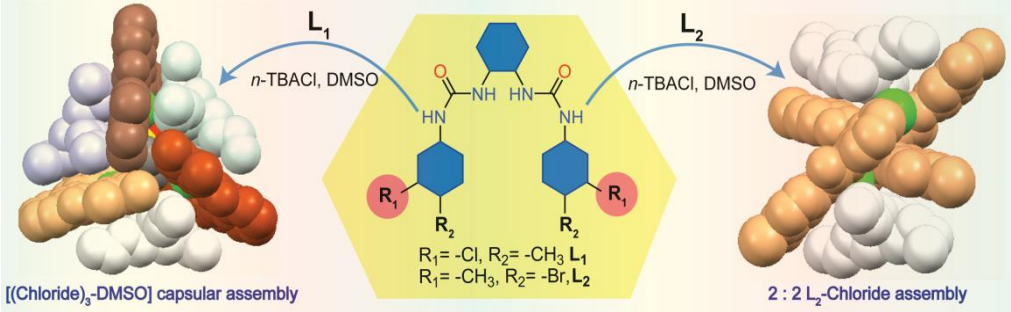

Fig 3.1 The comprehensive representation of one of the key outcomes of research work included in this chapter.

of utmost concern is the significant rise in the CO_2 concentration in the atmosphere caused by increased consumption of fossil fuels and the overgrowing number of automobiles, industries, etc., that eventually demands the efficient fixation and activation of atmospheric CO_2 into green chemical or as carbonate/bicarbonate within the self-assemblies of artificial receptors.[3.8] Alongside numerous flexible tripodal scaffolds, the strong and tuneable hydrogen bonding abilities and relatively easy syntheses of dipodal receptors synthesized from rigid *ortho* phenylenediamine containing urea/thiourea recognition sites are of particular interest, as it consists of most convergent diamine spacer compared to other rigid isomeric diamines.

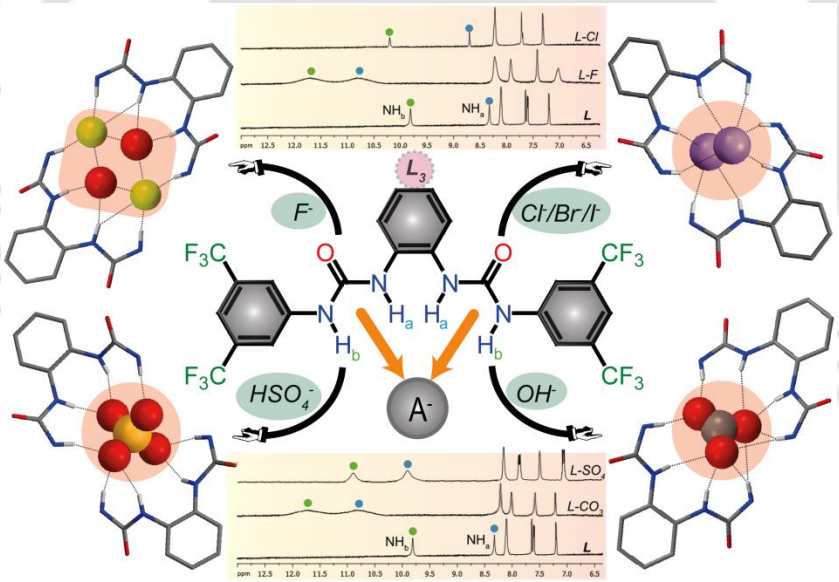

Fig 3.2 The comprehensive representation of one of the key outcomes of research work included in this chapter.

Some *ortho*-phenylenediamine based terminal mono-aryl substituted bis-urea receptors and their oxyanion binding studies have been reported by Wu *et. al.*, Light *et. al.*, and Gale *et. al.* in recent years.[3.9] However, the systematic investigation of electron withdrawing (chloro/bromo) and donating (methyl) or both electron-withdrawing functionalized terminal aryl di-substituted isomeric *ortho*-phenylene connected bis-urea scaffolds and their systematic, consistent as well as diverse anionic guest binding behaviour depending upon the substituents or anion dimension still remains as an inspiring research area to the supramolecular communities.

This chapter describes the design and syntheses of two 3,4-halo-methylphenyl (Fig. 3.1) functionalized (**L_1** and **L_2**) and one 3,5-trifluoromethyl-phenyl (Fig. 3.2) functionalized (**L_3**) *ortho*-phenylenediamine based isomeric dipodal bis-urea receptors for recognition of anions/hydrated anions or anion-solvent guest association within the neutral host assemblies.[3.10] The detailed X-ray analyses reveal that the three conformers of chloro-methylphenyl isomer **L_1** effectively encapsulate an unusual triangular [(chloride)$_3$-DMSO] anionic guest entirely sealed by three *n*-TBA^+ counteraction in complex **1a**, whereas the bromo-methylphenyl isomer **L_2** forms 2:2 noncooperative [(**L_2**)(Cl^-)]$_2$ complex **2a**. The **L_1** isomer further form noncapsular 2:2 neutral complex with acetate in **1b** and fully encapsulated 4:2 neutral complex with double carbonate anion in **1c**. In continuation with the diverse binding properties, the **L_2** isomer form 2:1 pseudo-capsular host-guest complexes **2b** and **2c** with tetrahedral sulfate and octahedral hexafluorosilicate anions respectively. The results of different halide and smaller oxyanion binding of the two receptors are witnessed due to the relative 3D orientations of the terminal aryl *meta*-substituents with respect to adjacent urea N−H moieties of particular receptor which play a vital role in the stabilization of the infrequent DMSO + host + salt co-crystals. In contrary, the SO_4^{2-} or SiF_6^{2-} bound complexes display different receptor binding modes because of the larger anion dimensions that overpowers the observation of aromatic *meta*-substituent driven anion binding. Secondly, another *ortho*-phenylene connected bis-(trifluoromethyl)-phenyl receptor **L_3** has been found to encapsulate *n*-TBA cation sealed cyclic fluoride-water [(F^-)$_2$(H_2O)$_2$] tetramer inside the dimeric complementary cavity in complex **3a** as well as unusual (Cl^-)$_2$, (Br^-)$_2$, and (I^-)$_2$ anionic guests in 2:2 neutral host–guest fashion in complexes **3b**, (**$3b^1$**, **$3b^2$**), **3c** and **3d** respectively. Interestingly, ligand **L_3** further form carbonate encapsulated complex **3e** by OH^- induced aerial CO_2 fixation and larger sulfate trapped complex **3f**, both inside the highly hydrophobic cation sealed neutral dimeric host capsules. The ^{1}H NMR titration and 2D NOESY experiments in solution-state heavily corroborate the binding and encapsulation of hydrated/non-hydrated anions in solid state. Scheme 3.1 shows the molecular receptor structures **L_1**-**L_3** and the representations of key findings of research work included in this chapter are shown Fig. 3.1-3.2.

3.2 Structural aspects of anion binding with L_1-L_3

A suitable receptor to bind with the anionic guests of different dimensions, should in principle, possess a particular supramolecular architecture containing directional hydrogen-bond donors tailored on a proper platform/framework. The *ortho*-phenylenediamine based, more than one terminal aryl substituent (either *meta-para* or *meta-meta*) containing dipodal receptors **L_1**, **L_2** and **L_3** each hold two urea functionalities, which can receive guests of different charges and sizes *via* formation of cooperative/non-cooperative host-guest assemblies depending upon either

positional aryl-substituent effect or size of the anionic guests. Structural information obtained from single crystal X-ray analyses of the isolated crystals provides insight into the proper binding topology of anions/hydrated-anions/solvated-anions with the neutral receptor molecules. Efforts were made to explore the solid-state binding properties of **L_1-L_3** with various anions in different crystallization conditions, by charging excess quaternary ammonium (*n*-TBA/TEA) anion salts to the individual solutions of receptors in aprotic solvents such as MeCN, DMF and DMSO. The purposeful inclusion of urea groups in highly organized 3,4-halo-methylphenyl/methyl-halophenyl or 3,5-bis(trifluoromethyl)phenyl terminal di-functionalized dipodal scaffolds become beneficial to determine the binding discrepancies of anionic guests *via* number of non-covalent interactions. In tradition, the crystallization followed by single crystal X-ray analysis of host-guest complexes has been the main focus in anion-recognition chemistry to understand the structural details of the complexes.

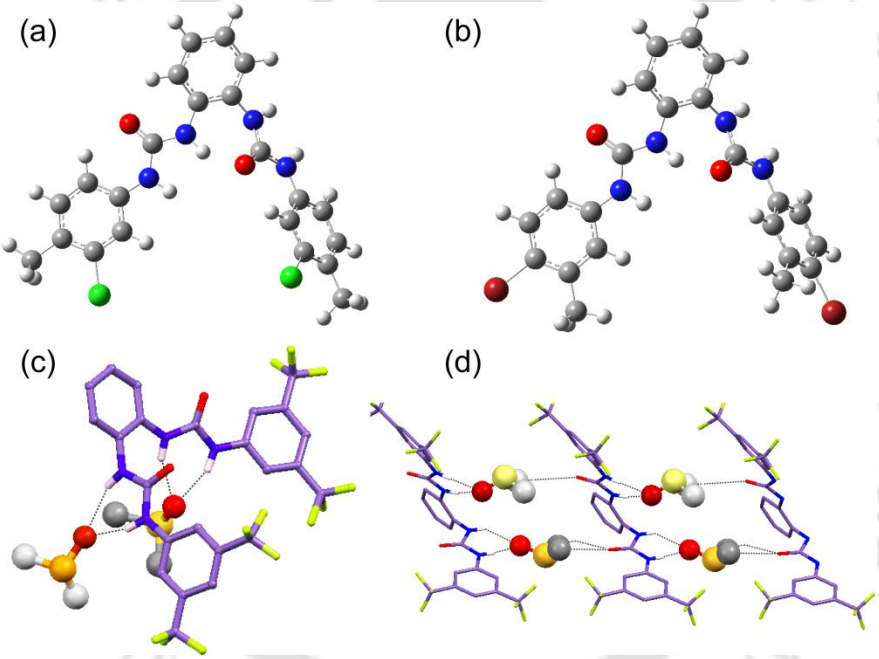

Figure 3.3 The optimized geometry of the free receptors (a) **L_1**, (b) **L_2** using B3LYP/6-31+G(d,p) basis set; Partial X-ray structures of the receptor **L_3** depicting (c) N–H···O hydrogen bonding contacts with DMSO, (d) DMSO-receptor linear polymeric aggregation through consecutive N–H···O and C–H···O interactions in free **L_3**.

It should be mentioned here that the crystal structures suitable for XRD analysis are obtained from the basic DMSO solutions of only trifluoromethylphenyl aryl di-substituted free receptor **L_3**, which is most acidic among the three receptors. Several attempts were made to crystallize the free receptors **L_1** and **L_2** also, from various solvents in different conditions, but most of the times the thick oily mass were found at the bottom of the crystallization vials. The DMSO solvated **L_3** receptor crystallizes in the triclinic space group *P*-1, where the two urea groups present at the two opposite sides of *ortho*-phenylene connector are non-cooperatively hydrogen-bonded in a typical six-membered N–H···O mode with two symmetry-independent DMSO

molecules (Fig. 3.3c). The X-ray analysis also reveals that each DMSO unit acts as a bridge between two adjacent ligand units *via* consecutive N–H···O and C–H···O interactions, constructing a 1D linear polymeric receptor-DMSO assembly (Fig. 3.3d). On the other hand, being unable to grow good quality crystals, density functional theory (DFT) studies are performed for structural exposition of isomeric receptors **L_1** (Fig. 3.3a) and **L_2** (Fig. 3.3b) which also reveals the *trans* orientation of the urea groups at the two opposite sides of *ortho*-phenylene connector showing non-cooperativity in both cases, as similar as in free **L_3** ligand.

3.2.1. Structural analysis of halide bound complexes of receptors L_1, L_2 and L_3

Single crystal XRD analyses of receptor-halide neutral complexes and consistent as well as discriminating binding behavior of receptors toward halide associations, hydrated-halides or solvated-halides anionic guests of varied shapes are heavily reliant on either the effect of terminal-aryl *meta*-substituents of di-functionalized isomeric receptors or the size of anionic associations.

3.2.1.1 [(Chloride)$_3$-DMSO] complex of receptor L_1 (1a):

Structural elucidation of complex **1a** [(**L_1**·TBACl)$_3$·DMSO], which crystallizes in triclinic *P*-1 space group from DMSO solution, revealed the construction of trimeric cooperative assemblies of **L_1** that fully encapsulate (chloride)$_3$-DMSO triangular guest assemblage *via* host-guest topological complementary (Fig. 3.4a), entirely sealed by three *n*-TBA counter-cations (Fig. 3.4c). Note that, the three **L_1** receptor conformers are not C_2-symmetric due to three symmetrically distinct conformations (syn/anti) of *meta*-chloro groups with respect to the adjacent N-H part of the urea moieties of each receptor. The two (Cl7 and Cl9) among three chlorides display six (four N−H···Cl receptor-anion, one C−H$_{DMSO}$···Cl solvent-anion and one C−H$_{n\text{-TBA}}$···Cl cation-anion) coordination, and Cl8 shows only four strong N−H···Cl receptor-anion interactions. Moreover, three C−H···O (two *n*-TBA-DMSO and a receptor-DMSO) and several intermolecular hydrogen-bonding C−H···Cl, halogen bonding Cl···Cl, anion-π (Cl···π) interactions are also helped to offer an appropriate binding pocket to engulf an unique (chloride)$_3$-DMSO solvated-anionic guest assembly (Fig. 3.4b). In the tris-chelate (Cl)$_3$-DMSO triangular guest (Fig. 3.4e), the average distance among three chlorides in the vertices are 6.823 Å, and the average distance among three *n*-TBA N atoms are 9.784 Å (Fig. 3.4d), whereas the average distances from central DMSO sulfur to three chlorides and three *n*-TBA Nitrogen atoms are 4.22 and 5.69 Å respectively (Fig. 3.4f).

3.2.1.2. Chloride complex of receptor L_2 (2a)

In presence of excess chloride ions in DMSO, the isomeric bromo-methyl receptor **L_2**

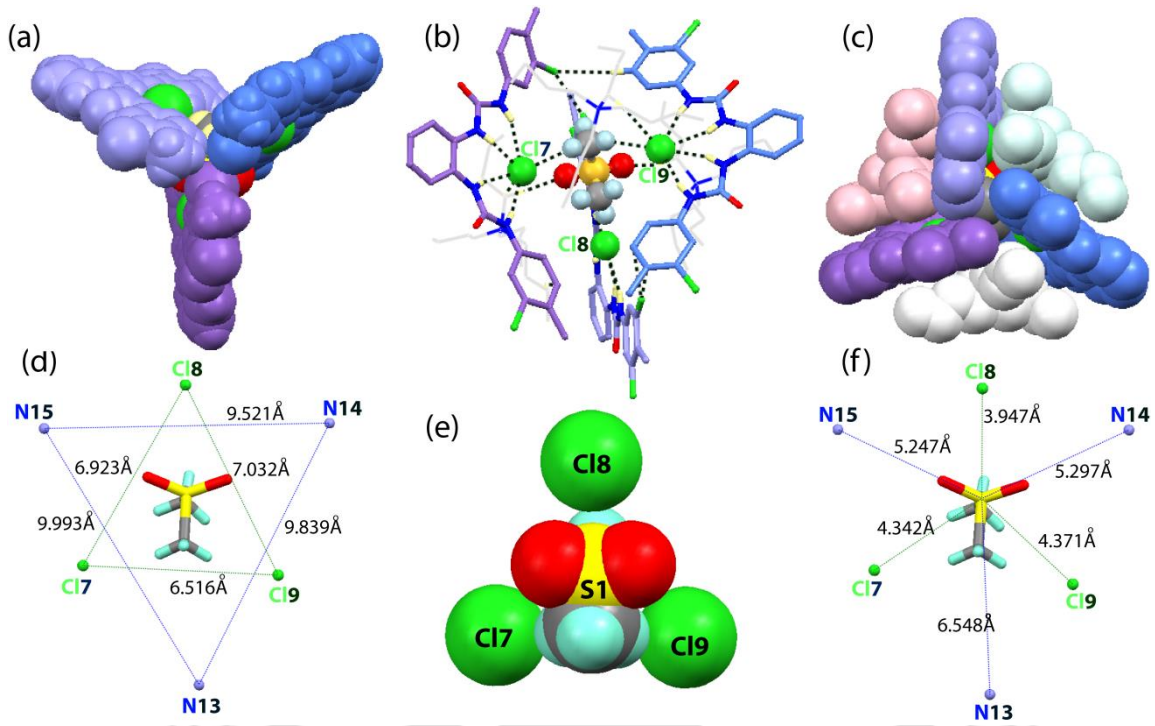

Figure 3.4 (a) Spacefill view of encapsulated [(chloride)$_3$-DMSO] inside three units of $\mathbf{L_1}$, (b) hydrogen-bonding contacts of dual guest with cation and receptors, (c) *n*-TBA cation sealed anion-solvent-receptor trimeric assembly, (d) distances among three guest chlorides and three *n*-TBA N atoms, (e) magnified view of triangular shaped [(Cl^-)$_3$-DMSO] guest assemblage, and (f) distances from central S atom of guest DMSO to guest chlorides and three *n*-TBA N atoms.

crystallizes in monoclinic space group *P*21/c and conforming 2:2 host-guest complex **2a** *via* an equal number of hydrogen-bond sharing of noncooperative urea groups of two symmetry-identical receptor units. The two symmetry identical chloride anions accept four strong N−H···Cl bonds each, among which two H-bonds are donated from one receptor unit and rest of two H-bonds are donated from the urea groups of other identical receptor unit of corresponding non-capsular 2:2 assembly (Fig. 3.5a). Furthermore, crystal packing shows consecutive $R_4^4(14)$ and $R_2^2(14)$ type cyclic architecture formation *via* four N−H···Cl and two C−H···O interactions respectively in complex **2a**. The stability of $\mathbf{L_2}$-chloride complex is further reinforced by four C−H···π and two C−H···O interactions among receptors and *n*-TBA counter-cations.

3.2.1.3 Cyclic [(fluoride)$_2$(water)$_2$] complex of receptor $\mathbf{L_3}$ (3a)

The hydrated fluoride complex **3a** of the highly acidic dipodal receptor $\mathbf{L_3}$ crystallizes in the monoclinic centrosymmetric space group *P*21/c. Structural elucidation reveals that two symmetry-identical $\mathbf{L_3}$ receptor units efficiently bind a H-bonded cyclic fluoride-water tetrameric cluster comprising two fluoride anions and two water molecules (Fig. 3.6a-e) inside the symmetric dipodal cleft *via* the ample cooperativity of four urea groups, constructing a *n*-TBA cation-sealed neutral dimeric host–guest capsular assembly (Fig. 3.6c). Each of the two symmetry-identical F13 fluoride anions in the cyclic cluster are coordinated by three strong urea

N–H···F interactions, one *ortho*-aryl C–H···F interaction and two intra-cluster interactions (O3–H3OA···F13 and O3– H3OB···F13) with adjacent water molecules and thus each fluoride anion in complex **3a** exhibits hexa-coordination. Subsequently, each of the two symmetry-identical water molecules is penta-coordinated *via* receiving two strong urea N–H···O interactions, one *n*-TBA C–H···O interaction followed by the donation of two intra-cluster O3–H3OA···F13 and O3–H3OB···F13 H-bonds (Fig. 3.6a). It is also clearly evident from the crystal lattice that two units of the monohydrated fluoride bound neutral receptor **L_3**, along with the *n*-TBA counter-cation, are held together by two very strong O–H···F hydrogen bonds, constructing a dimeric cation sealed assembly that entraps the $[F_2(H_2O)_2]$ cyclic cluster at its center *via* a total of 14 non-covalent host-guest interactions. The hydrated-fluoride cluster possesses almost a planar cyclic tetrameric arrangement, where the hydrogen bonding distances between each fluoride anion and the two water molecules are 2.653 Å and 2.626 Å; eventually close assessment of the distance and angle measurement values (84.04° and 95.96°) confirms that the tetrameric cluster is a perfect parallelogram (Fig. 3.6b). The weak π···π interactions (~4.735 Å) between the terminal aryl groups of the receptors also additionally stabilize the host-guest assembly.

3.2.1.4. Chloride, bromide, iodide complexes of receptor L_3 (3b^1, 3b^2, 3c, 3d)

The double anion entrapped non-hydrated neutral complexes **3b^1**, **3b^2**, **3c** and **3d** of receptor **L_3** with larger halides (Cl^-, Br^-, I^-) were obtained from individual basic DMF/DMSO solutions of receptors and *n*-TBACl, TEACl, *n*-TBABr and *n*-TBAI salts respectively. The halide complexes with *n*-TBA^+ salts crystallize in the monoclinic space group *P*21/c and the only chloride complex **3b^2** crystallizes in triclinic space group *P*-1. Structural elucidation of each halide complex reveal that, the urea -NH groups of two opposite side of the *ortho*-phenylene connector show good cooperativity to entrap the double anions, unlike the free receptor. In chloride complexes **3b^1** and **3b^2** the inversion-symmetric identical receptor units effectively capture two chloride ions *via* eight strong urea N–H···Cl interactions, equally shared between each symmetry-identical chloride anion, constructing 2:2 neutral host-guest assemblies. Each tetra-coordinated chloride anion accepts three N–H···Cl H-bonds from one receptor unit, while the fourth N–H···Cl bond is donated by the other receptor of host dimer in both the chloride complexes (Fig. 3.7b). The chloride complex **3b^1** is further stabilized by several weak C– H···O interactions among sealed *n*-TBA cations and receptor, whereas in complex **3b^2**, the two **L_3** receptors are assembled by two extra weak π···π interactions (3.874 Å) between the terminal aryl rings. The single crystals suitable for X-ray analysis of non-hydrated bromide complex **3c** and iodide complex **3d** are also obtained to acquire better understanding of the self-assembly processes with larger homologous spherical anions. Structural elucidation of two isostructural

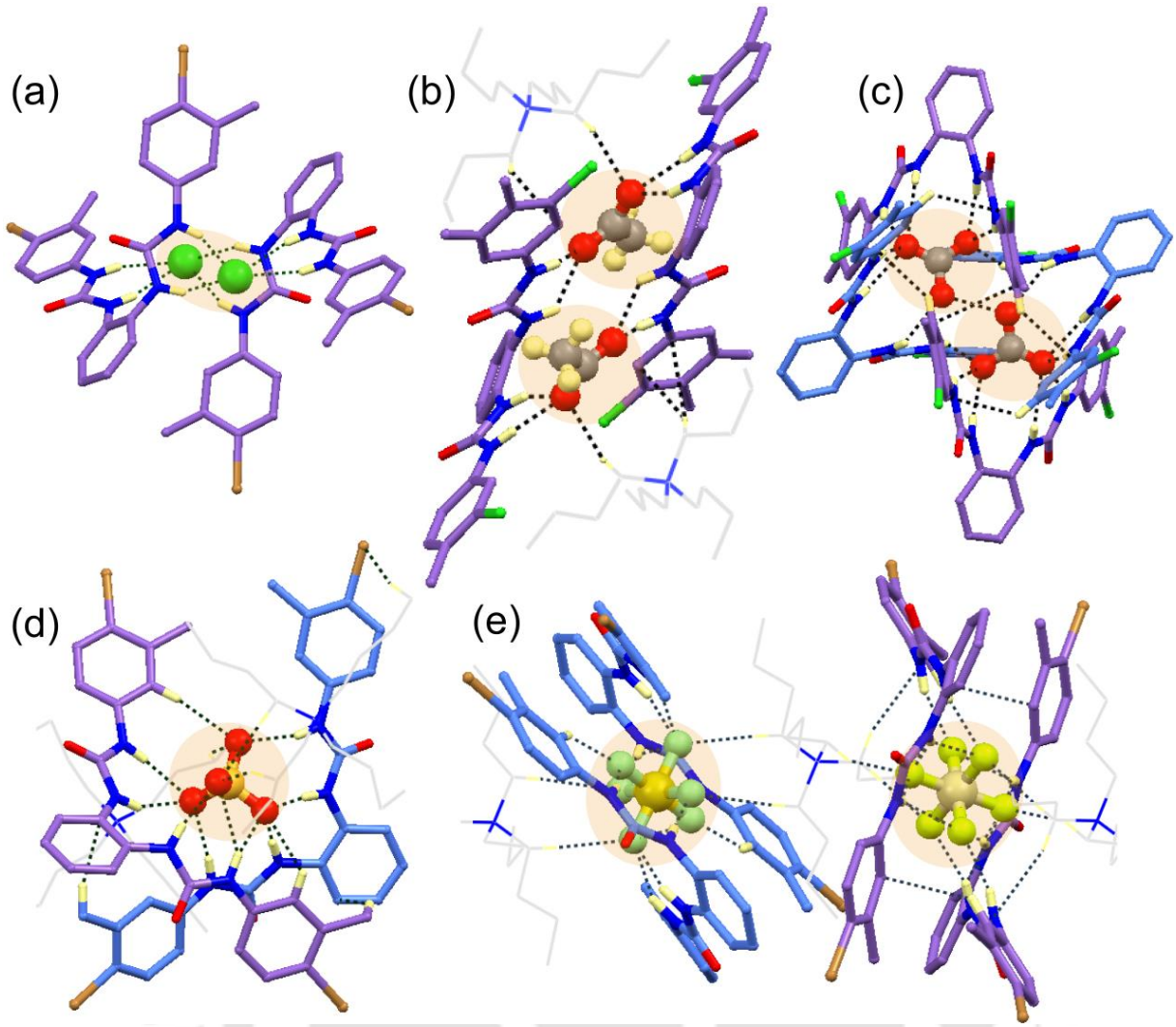

Figure 3.5 Partial X-ray structures depicting the non-covalent interactions in (a) chloride complex **2a** of $\mathbf{L_2}$, (b) acetate complex **1b** of $\mathbf{L_1}$, (c) carbonate complex **1c** of $\mathbf{L_1}$, (d) sulfate complex **2b** of $\mathbf{L_2}$, and (e) hexafluorosilicate complex **2c** of $\mathbf{L_2}$.

bromide (**3c**) or iodide (**3d**) complexes clearly demonstrate that the two symmetry-identical $\mathbf{L_3}$ receptor molecules effectively encapsulate the respective symmetry-identical double-bromide or double-iodide anionic guests into the dimeric receptor cavity through eight strong N–H···Br/I interactions (equally shared by each bromide/iodide anion), displaying complete cooperativity of four urea groups in respective complexes (Fig. 3.7c-d). Both the bromide and iodide complexes are further stabilized by two weak additional aryl C–H···Br/I interactions projected from two opposite sides, and on close inspection, both the structures with their semicircular ligands and C–H···Br/I bonds, looks like a bow and arrow. Note that, the cooperative neutral 2:2 dimeric assembly of complexes **3c** and **3d** are also found to be sealed by *n*-TBA counter-cations through several weak C–H···O and C–H···π cation-receptor interactions. The crystal motifs along the crystallographic *a*-axis of both complexes **3c** and **3d** display the near perpendicular orientation of each adjacent dimeric assembly and the *b*-axis packing exposes the linear double-bromide or double iodide entrapped arrangements with consecutive face-to-face receptor units.

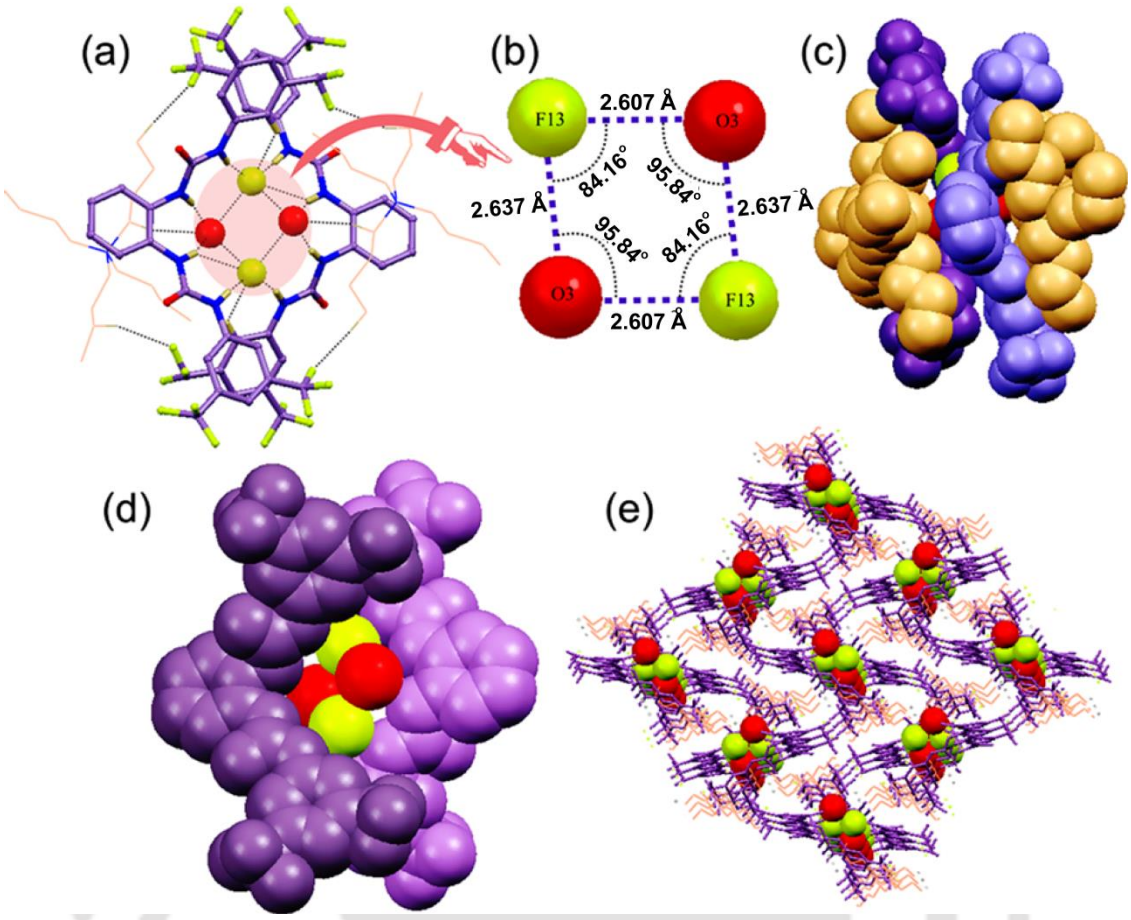

Fig. 3.6 X-ray structure of complex **3a** (partial) depicting (a) hydrogen bonding contacts in the cyclic fluoride-water cluster, (b) a magnified view of intra-hydrogen bonding in the tetrameric cluster, (c) encapsulation of hydrated-guestt in *n*-TBA cation-sealed environment, (d) entrapment of the guest inside the receptor dimer (spacefill representation) and (e) the crystal packing of complex **3a** as viewed down the crystallographic *a*-axis.

3.2.2. Structural analysis of oxyanion bound complexes of receptors L_1, L_2 and L_3

Single crystal XRD analyses of *ortho*-phenylenediamine based neutral receptors and oxyanions also demonstrate the consistent as well as discriminating binding conformations of receptors toward planar, tetrahedral or octahedral anionic guests of various dimensionalities depending upon either the effect of terminal-aryl *meta*-substituents of aryl di-functionalized isomeric receptors or mostly the size of larger oxyanions.

3.2.2.1 Acetate complex of receptor L_1 (1b)

The planar acetate anion bound complex **1b** of $\mathbf{L_1}$ crystallizes in monoclinic *P*21/c space group and X-ray analysis reveals the 2:2 host-guest assembly formations by non-cooperative hydrogen-bonding interactions of urea -NH groups and acetate anions (Fig. 3.5b) followed by construction of a $R_4^4(18)$ type cyclic architecture through four N−H···O interactions. The neutral host-guest assemblies of two symmetry-identical acetates and $\mathbf{L_1}$ receptors are further stabilized by two C−H···O and four weak C−H···π supportive interactions between the two peripheral *n*-TBA units with respective acetate and receptors (Fig. 3.5b).

3.2.2.2 Carbonate complex of receptor L_1 (1c)

DMSO solvated 4:2 host-guest complex **1c** crystallizes in monoclinic centrosymmetric space group *C*2/c. Structural elucidation reveals that two symmetry equivalent carbonate anions are fully encapsulated by two pairs of symmetry-independent $\mathbf{L_1}$ receptor conformers by a total of 16 strong N−H···O interactions, four interactions from each receptor unit (Fig. 3.5c). One pair of symmetry-identical receptor units bind single carbonate at a time, while another identical-symmetry receptor pair hydrogen-bonded triply with one CO_3^{2-} and singly with other CO_3^{2-} unit. The three oxygen atoms O5, O6, and O7 of identical C61-carbonate accept three, one, and four hydrogen-bonds respectively. The TEA^+ counter-cation units remain outside the cooperative host-guest capsular assemblies.

3.2.2.3 Sulfate complex of receptor L_2 (2b)

The sulfate complex **2b** of 4-bromo-3-methylphenyl substituted receptor $\mathbf{L_2}$ crystallizes in the monoclinic system with the space group *P* 21/c. Single crystal X-ray analysis illustrates that sulfate anion is coordinated by two symmetry-independent $\mathbf{L_2}$ conformers and two *n*-TBA cations by nine strong N−H···O and five C−H···O interactions constructing a pseudo-capsular cation-sealed 2:1 host-guest assemblies (Fig. 3.5d). Two urea groups from one ligand bind four edges of the tetrahedral anion (through eight-membered H-bonded rings), while the two urea groups of other ligand chelate two vertices of the sulfate ion (through six-membered H-bonded rings). The O5 and O7 atoms of sulfate anion form three hydrogen bonds each, and the O6 and O8 atoms receive four hydrogen bonds.

3.2.2.4 Hexafluorosilicate complex of receptor L_2 (2c)

DMSO solvated hexafluorosilicate complex **2c** was obtained from the mixture of excess *n*-TBAF salts and ligand $\mathbf{L_2}$ from a glass vial on reaction of fluoride with glass-silica and crystallizes in triclinic space group *P*-1. The crystal structure clearly shows that out of two symmetry-independent SiF_6^{2-} units from a unit cell in complex **2c**, $Si1F_6$ and $Si2F_6$ are coordinated *via* 18 and 16 H-bonds respectively conforming cation-sealed pseudo-capsular 2:1 host-guest assemblies (Fig. 3.5e), as similar as in complex **2b**. But, in complex **2c**, SiF_6^{2-} anion and *n*-TBA cation conform contact ion-pair type linear polymeric bridge assembly *via* $R_2^2(8)$ kind cyclic H-bonded network (Fig. 3.5e) with alternative Si1 and Si2, unlike complex **2b**. In addition, crystal packing of **2c** with cell axes displays a beautiful rectangular cubic architecture, where the entire eight vertexes contain eight $Si1F_6$ units, and four $Si2F_6$ units are present in the middle of axes between two $Si1F_6$ units.

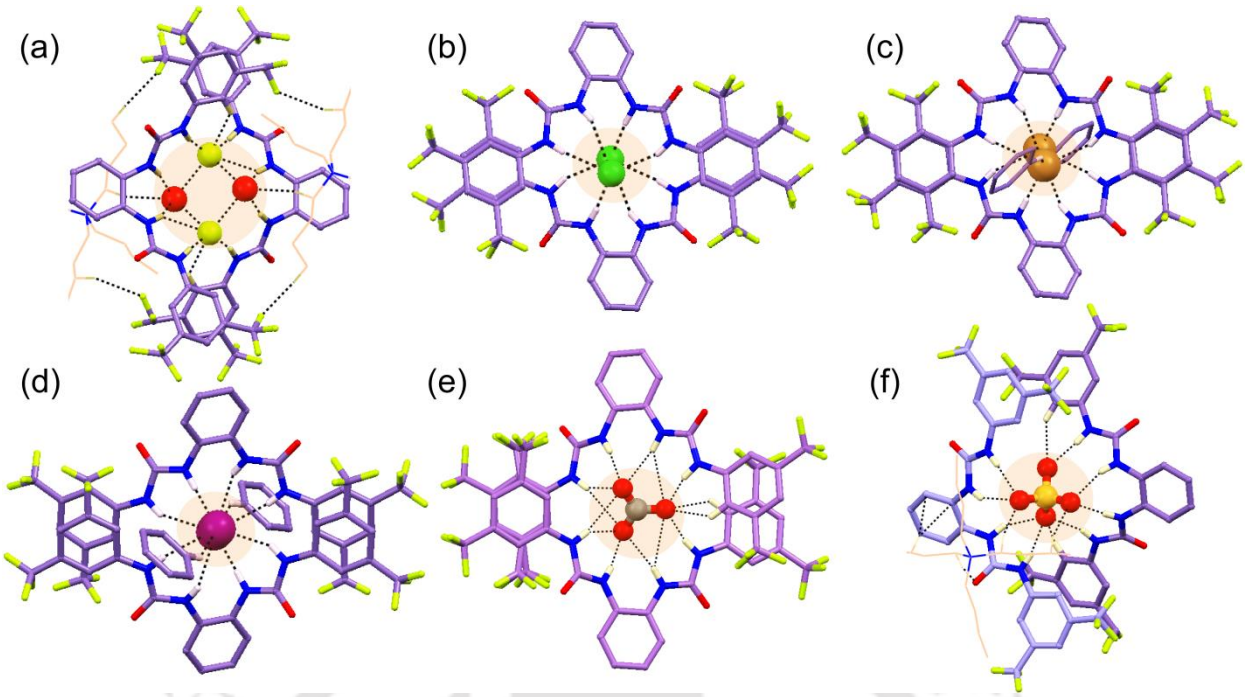

Figure 3.7 Partial X-ray structures depicting the non-covalent interactions in (a) hydrated-fluoride complex **3a**, (b) chloride complex **3b**[1], (c) bromide complex **3c**, (d) iodide complex **3d**, (e) carbonate complex **3e** and (f) sulfate complex **3f**.

3.2.2.5 Hydroxide induced carbonate complex of receptor L_3 (3e)

Suitable crystals of the $(n\text{-TBA})_2CO_3$ salt of the bis-(trifluoromethyl)-phenyl substituted neutral receptor $\mathbf{L_3}$ were attained from the reaction of $\mathbf{L_3}$ and excess *n*-TBAOH, and it crystallizes in the orthorhombic space group *Pccn*. Note that, the carbonate ion was not present in solution prior to crystallization and the entrance of carbonate into the system could be due to the transformation of aerial CO_2 to CO_3^{2-} due to the induction of hydroxide ions *in situ* in basic DMSO.

$$2F^- + H_2O \longrightarrow OH^- + HF_2^-$$

$$OH^- + CO_2 \longrightarrow HCO_3^-$$

Structural elucidation reveals that the two symmetry-independent conformers of $\mathbf{L_3}$ cooperatively encapsulate a single carbonate anion in a 2:1 host-guest fashion, by a total of fourteen intra-capsular urea N–H···O and *ortho*-aryl C–H···O interactions (Fig. 3.7e). The asymmetric unit of complex **3e** comprises half carbonate anion against one full unit of *n*-TBA counter-cation. It should also be noted that, due to crystal-imposed inversion symmetry, the O4 and O4′ atoms among the three oxygen atoms of the C41 containing carbonate are symmetry-identical and each of them being tetra-coordinated, accepts four urea N–H···O bonds. On the other hand, the O3 atom of carbonate accepts four urea N–H···O bonds and two *ortho*-aryl C–H···O bonds. The molecular packing along the crystallographic *c*-axis of **3e** displays the wave-like polymeric aggregation of two neighboring dimeric capsular units interconnected *via* inter-

receptor C–H···F interactions. Subsequently, the adjacent cation-sealed capsular assemblies generate hexagonal networks of carbonate captured dimeric cages around each capsular unit, which further construct a beautiful honey-comb type architecture as viewed down the crystallographic *a*-axis.

3.2.2.6 Sulfate complex of receptor L_3 (3f)

The sulfate complex **3f** was attained from the reaction of $\mathbf{L_3}$ and excess *n*-TBAHSO4, which crystallizes in the triclinic *P*-1 space group. The crystal structure clearly shows that two semi-circular receptor $\mathbf{L_3}$ conformers are projecting toward each other in a face-to-face fashion; effectively capture a deprotonated hydrogensulfate anion with the help of a partially sealed *n*-TBA counter-cation. The divalent sulfate anion is bound in a 2:1 host-guest fashion by a total of twelve N–H···O and C–H···O interactions (Fig. 3.7f) where the deprotonation of HSO_4^- can be ascribed to the hydrogen bonding activated proton transfer reaction between free and bound anions. Structural elucidation also reveals that the two receptors binding sulfate anion by cooperative interactions, are exhibiting two different coordination manners. Two urea groups from one ligand and two C–H groups from the only *n*-TBA unit bind four edges of the tetrahedral anion (through eight-membered H-bonded rings), while the two urea groups from the second ligand and two *ortho*-aryl C–H groups, with the aid of two respective adjacent urea N–H groups, chelate two vertices of the sulfate ion (six-membered H-bonded rings). Therefore, the O5 and O7 atoms of the sulfate accept three hydrogen bonds each, but the O6 atom receives four bonds and the O8 atom accepts only two hydrogen bonds; thus, the sulfate anion in complex **3f** exhibits the optimal coordination number twelve. Note that, the 2:1 pseudo-capsular $\mathbf{L_3}$-sulfate assemblies are interconnected through *n*-TBA counter-cation bridges, *via* consecutive weak aromatic C–H···O and C–H···π interactions from one side and two anion-cation C–H···O ion pair type interactions from other side, conforming a 1D polymeric chain of capsular assemblies along the crystallographic *b*-axis. Such 1D arrays are further interlinked with one another, generating hexagonal networks of sulfate trapped pseudo-capsular assemblies as viewed down the crystallographic *c*-axis.

3.3 Solution-state anion binding studies

Qualitative as well as quantitative ^{1}H NMR experiments are performed in DMSO-d_6 using quaternary ammonium (*n*-TBA/TEA) salts of all related common halides and oxyanions to investigate the solution state anion binding behavior of isomeric halo-methylphenyl based receptors $\mathbf{L_1}$, $\mathbf{L_2}$ and bis-(trifluoromethyl)-phenyl based receptor $\mathbf{L_3}$ to support the result obtained from the solid state. Not surprisingly, the most significant change is observed in the

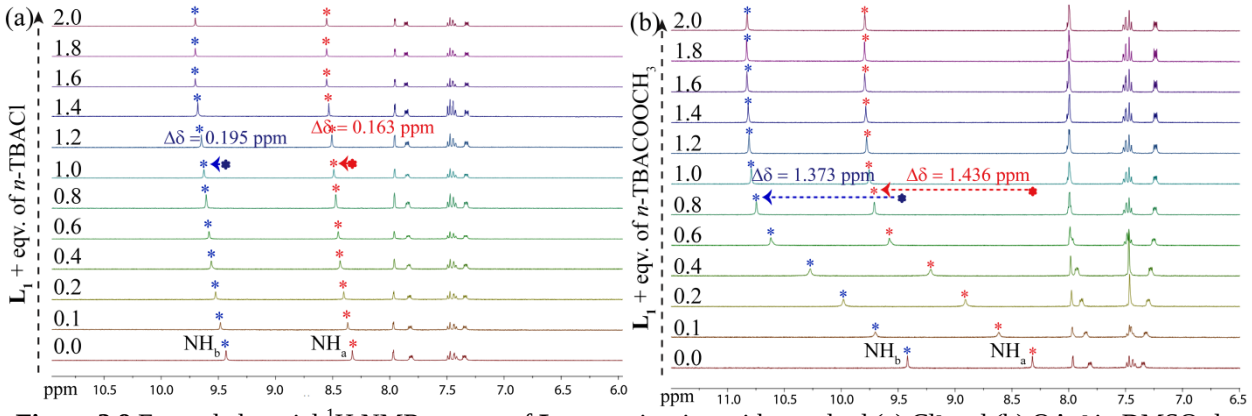

Figure 3.8 Expanded partial ^{1}H NMR spectra of $\mathbf{L_1}$ upon titration with standard (a) Cl^- and (b) OAc^- in DMSO-d_6.

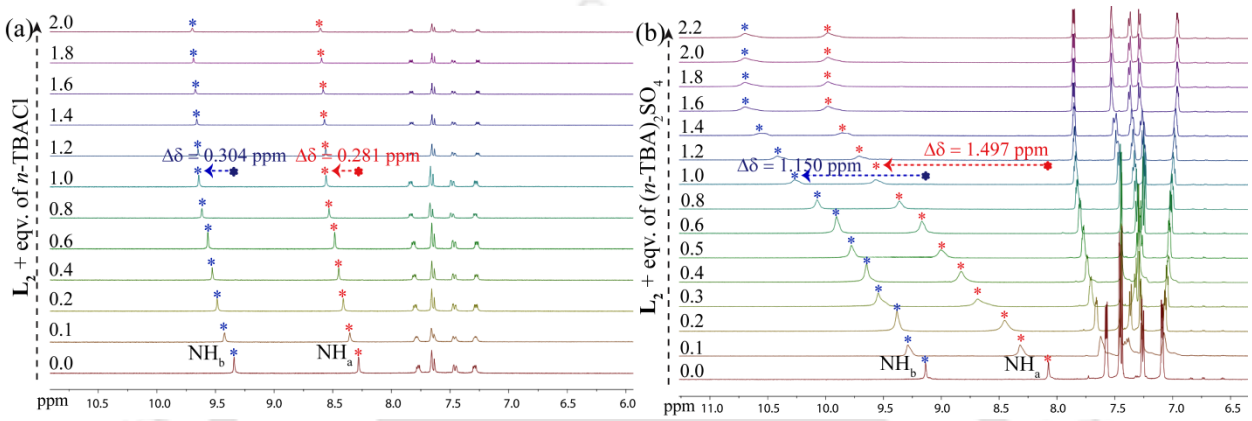

Figure 3.9 Expanded partial ^{1}H NMR spectra of $\mathbf{L_2}$ upon titration with standard (a) Cl^- and (b) SO_4^{2-} in DMSO-d_6.

urea -NH proton, as expected, indicating that the urea protons (-NH_a and -NH_b) act as the primary site for anion recognition. Addition of *n*-TBAF and $TEAHCO_3$ salts (0.1-0.3 eqv.) to the individual solutions of ligands $\mathbf{L_1}$ and $\mathbf{L_2}$ show instant color change of the solution due to proton abstraction and disappearance of both urea groups -NH signals in the ^{1}H NMR spectra immediately, whereas an average downfield shift of ~0.180 ppm (Fig. 3.8a, A3.1) and ~0.292 ppm (Fig 3.9a, A3.1) of urea -NH protons are observed upon gradual addition of important chloride salt to the individual solutions of respective $\mathbf{L_1}$ and $\mathbf{L_2}$. However, the chloride complexes **1a** and **2a** showed an average downfield shift of ~0.362 ppm and ~0.117 ppm respectively. Comparative partial ^{1}H NMR stack plots of $\mathbf{L_1}$ with an increasing concentration of *n*-TBACl and *n*-$TBAOCOCH_3$ show the relative chemical shift in ppm of NH_a and NH_b protons (Fig. 3.8) of $\mathbf{L_1}$ due to the anion-receptor complex formation in the solution state. Subsequently, the acetate complex (**1b**) and sulfate complex (**2b**) showed an average downfield shift of ~1.437 ppm and ~1.291 ppm of -NH protons respectively, while the ^{1}HNMR titration of $\mathbf{L_1}$ and $\mathbf{L_2}$ upon gradual addition of respective *n*-$TBAOCOCH_3$ and (*n*-TBA)$_2SO_4$, a huge average shift of ~1.404 ppm (Fig. 3.8b) and 1.323 ppm (Fig. 3.9b) of respective -NH protons are observed. Comparative partial ^{1}H NMR stack plots of $\mathbf{L_2}$ with increasing concentration of *n*-TBACl and (*n*-TBA)$_2SO_4$ show the relative chemical shift in ppm of NH_a and NH_b protons (Fig. 3.9) due to

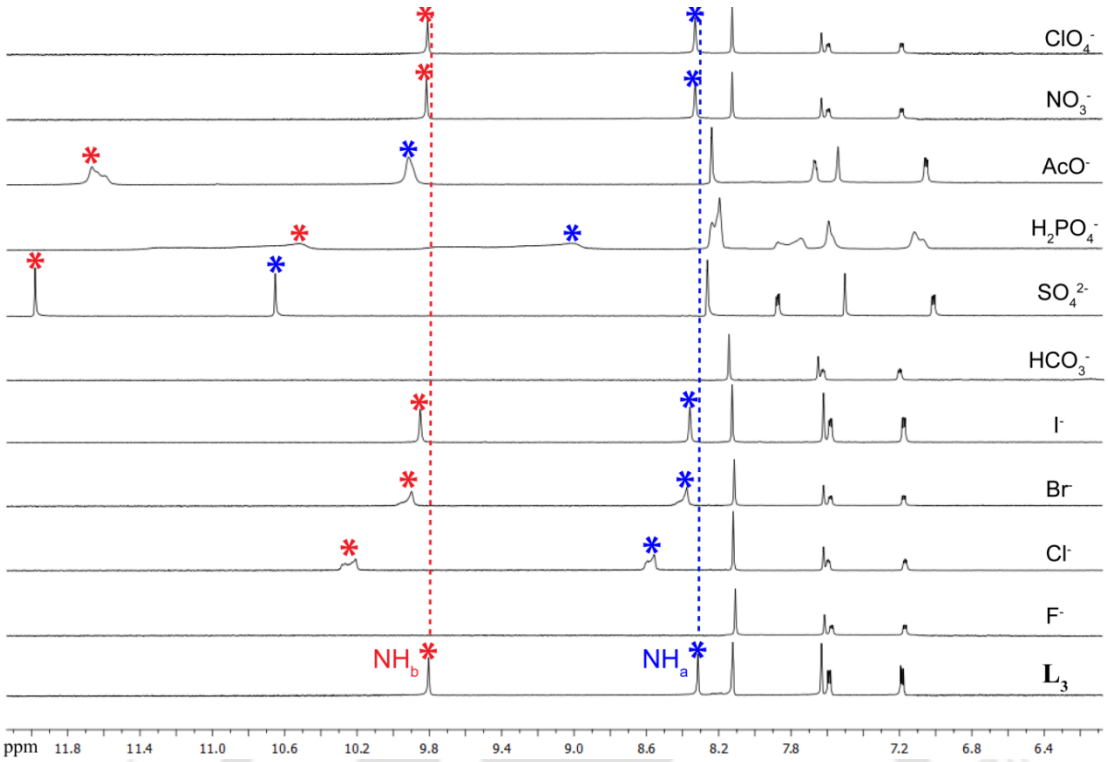

Fig. 3.10 Partial ^{1}H NMR spectra of $\mathbf{L_3}$ and the maximum observable shifts in urea-NH resonance upon the addition of excess F^-, Cl^-, Br^-, I^-, HCO_3^-, SO_4^{2-}, $H_2PO_4^-$, AcO^-, NO_3^-, ClO_4^-, OH^- in the form of their TEA/*n*-TBA salts in DMSO-d_6.

complex formation in solution. The Job's plot analysis of titration data gives a mixed equilibrium between 1:1 and 1:2 host-guest stoichiometries of both $\mathbf{L_1}$ and $\mathbf{L_2}$ with aliquots of standard *n*-TBACl solution. On the other hand, ^{1}H NMR titration data of $\mathbf{L_1}$ with aliquots of standard *n*-$TBAOCOCH_3$ solution give the best fit for 1:1 equilibrium between host and guest that supports 2:2 host-guest binding in the solid state. Besides, the titration data of $\mathbf{L_2}$ with aliquots of standard $(n\text{-TBA})_2SO_4$ resulted a mixed equilibrium between 1:1 and 1:2 host to guest as obtained from Job's plot. As the difference in binding of anions in solid and solution states is common in literature, the binding divergence of one or two chloride ions in the solution state against one chloride ion in the solid state probably attributed to the more organized and rigid receptor arrangement in solid compared to more floppy and loose orientations in solution. In the solid state, halo-methylphenyl substituted isomeric receptors $\mathbf{L_1}$ and $\mathbf{L_2}$ have shown diverse binding affinity toward the same chloride anion depending upon the geometrical conformation (syn/anti) of the terminal aryl *meta*-substituents with respect to the contiguous -NH part of the urea moiety, but they have shown similar kind of host-guest complexation in solution state. Then, Fig. 3.10 represents qualitative testing of the anions, displaying the chemical shift changes observed upon excess addition of different anions to individual DMSO-d_6 solutions of comparatively more acidic $\mathbf{L_3}$. In quantitative ^{1}H-NMR of $\mathbf{L_3}$ with standard fluoride and bicarbonate salts, the disappearance followed by the severe broadening of both urea

-NH signals were observed after the addition of ~0.6-1.0 equiv. of anions as similar in the cases of ligands **L_1** and **L_2**, which could be the consequences of proton abstraction. In fluoride titration experiment, a new characteristic signal from HF_2^- at 16.2 ppm is appeared upon further addition of *n*-TBAF to the ligand solution. However, ^{1}H NMR analysis of the cyclic fluoride-water entrapped complex **3a** and carbonate trapped complex **3e** show average downfield shifts of Δδ = 2.17 ppm and Δδ = 2.11 ppm respectively. Note that, the binding constants for fluoride and carbonate anions with **L_3** could not be determined because of the severe broadening and even vanishing of the -NH signals during the titration processes. Whereas, the double chloride entrapped complexes **$3b^1$** and **$3b^2$** show an average downfield shift of Δδ = 0.38 ppm and Δδ = 0.23 ppm respectively for the -NH protons and in titration, the gradual addition of *n*-TBACl salt to a solution of **L_3** also lead to an comparable average Δδ = 0.34 ppm downfield shift for the -NH protons, which give the best fit for a mixed equilibrium between 1:1 and 1:2 host-guest stoichiometry with an apparent value of log K = 3.83. Subsequently, from ^{1}H NMR titration of **L_3** with standard bromide and iodide solutions, the -NH resonances show much lower average downfield shifts of Δδ = 0.08 ppm and Δδ = 0.02 ppm respectively, compared to fluoride and chloride. The bromide complex **3c** and iodide complex **3d** also show respective average downfield shifts of Δδ = 0.08 ppm and Δδ = 0.11 ppm only for the -NH protons. Hence, due to very negligible shifts in the -NH signals from titration experiments, the association constants for bromide and iodide could not be calculated. Then the ^{1}H NMR titration data for **L_3** with aliquots of standard $(n\text{-TBA})_2SO_4$ solution display large chemical shifts in the -NH resonances, with an average Δδ value of 2.26 ppm (Fig. A3.3), which indeed supports the solid-state X-ray structure of the sulfate complex **3f**, where equal and strong participation from both the urea protons toward SO_4^{2-} binding within the dimeric cavity of **L_3** was observed. The 2:1 **L_3**-sulfate complex **3f** show an average downfield shift of Δδ = 1.20 ppm for the -NH protons in its ^{1}H NMR data; in contrast, the titration data for **L_3** with standard SO_4^{2-} give the best fit for 1:1 host-guest stoichiometry with apparent value of log K = 4.08. Note that, the variance in binding of anions in solid and solution states is common and is not unusual, because the receptor is much more organized in the solid state, which favors the binding of oxyanion within the dimeric **L_3** receptor cavity stabilized by a number of non-covalent interactions, whereas the binding of a single anion inside the receptor cavity has been observed in few cases of solution state, that may be due to much looser orientations. Finally, in the ^{1}H NMR titration of **L_3** with standard CH_3COO^- and $H_2PO_4^-$ solutions, the -NH resonance experiences downfield shifts with ultimate Δδ values of 1.58 and 1.79 ppm for CH3COO$^-$ (Fig. A3.4) and Δδ values of 0.85 and 0.89 ppm for $H_2PO_4^-$ respectively for the -NH_a and -NH_b signals, which is suggestive of the equal participation of the

-NH protons in the binding of the respective anions in 1:1 stoichiometry from the Job's plot with apparent log K values of 4.01 and 3.98 respectively. However, following the addition of other oxyanions like nitrate and perchlorate, no appreciable changes in the chemical shift values of the -NH signals are observed (Fig. 3.10), indicating almost no binding with ligand **L_3**. The 2D-NOESY NMR experiments of the **L_3** and the isolated anion complexes (Fig. A3.6) in DMSO-d_6 further confirm the solution state binding of halides and oxyanions. The free **L_3** shows strong NOE coupling between the urea NH_a and NH_b protons (Fig. A3.6a), but such through space interactions in hydrated-fluoride trapped 2:2 complex **3a** (Fig. A3.6b) and carbonate trapped 2:1 complex **3e** (Fig. A3.6c) are found to be absent, suggesting the trapping of respective anions within the dipodal platform, an observation which is also supported by the X-ray structures **3a** and **3e**. In contrast, three strong NOESY signals between the $NH_a\cdots NH_b$, $H_a\cdots H_b$ and $NH_b\cdots H_c$ protons are spotted in the 2:1 sulfate complex **3f** (Fig. A3.6d), which indeed indicates that in solution, the 2:1 host/guest mode is not prevalent for sulfate binding, although upon the excess addition of sulfate to a DMSO-d_6 solution of **3f**, the disappearance of those NOESY signals occurred (Fig. A3.6e), suggesting a conformational change in **L_3** due to the binding of a single sulfate anion in 1:1 host-guest ratio. No signals owing to through space interactions upon the addition of excess fluoride and bicarbonate to respective solutions of complexes **3a** and **3e** have also been observed, suggesting the binding of anions. Subsequently, the NOESY NMR spectra of chloride, bromide and iodide complexes (**$3b^1$**, **$3b^2$**, **3c** and **3d**) show similar types of off-diagonal $NH_a\cdots NH_b$ coupling as similar for the free receptor **L_3**, which is indicative of the poor binding of these anions in the solution state, an observation that is also supported by quantitative ^{1}H-NMR titration experiments from $Cl^-/Br^-/I^-$ and **L_3**.

3.4 Conclusion

The rational and purposeful design of terminal aryl di-substituted (either one electron-withdrawing and one electron donating or both electron-withdrawing) rigid *ortho*-phenylenediamine bridged three bis-urea receptors **L_1**, **L_2** and **L_3** are effective towards systematic and consistent binding of both halides and oxyanions depending upon either the terminal aryl *meta*-substituent effect of receptors or dimensions of anionic guests. In contrary to the some previously reported terminal aryl mono-substituted *ortho*-phenylene based bis-urea receptors, herein the rationally synthesized easy-to-make 3-chloro-4-methylpenyl aryl di-substituted organic bis-urea receptor **L_1** established the full encapsulation of an infrequent triangular $(chloride)_3$-DMSO anion-solvent dual guest assembly *via* formation of DMSO + host + salt co-crystals within the trimeric complementary cavity perfectly sealed by three *n*-TBA counter-cations in the solid state. Whereas the isomeric 4-bromo-3-methylphenyl aryl di-

substituted bis-urea receptor **L_2** formed noncapsular 2:2 host- guest assemblies with chloride ion *via* non-cooperative hydrogen-bonding interactions of the urea moieties. Moreover, **L_1** formed a non-cooperative cation sealed 2:2 assembly and fully encapsulated cooperative 4:2 assembly with acetate and double carbonate anions respectively. In continuation with the diverse binding properties, isomeric **L_2** formed a cation sealed 2:1 pseudo-capsular host-guest assemblies with bigger tetrahedral sulfate and octahedral hexafluorosilicate anions. Especially, receptor **L_1** in its neutral form has proven to be a decent and proficient organic scaffold for engulfing the large $(Cl)_3$-DMSO guest assemblage, while its alike isomeric receptor **L_2** was unable do the same. On the other hand, the bis-(trifluoromethyl)-phenyl aryl di-substituted another receptor **L_3** with its more acidic dipodal scaffold, demonstrated systematic and size mediated trapping of spherical halides to planar and tetrahedral oxyanions within dimeric complementary cooperative assemblies sealed by *n*-TBA cations. The anionic guests such as cyclic-hydrated $[(F)_2(H_2O)_2]^{2-}$, $(Cl^-)_2$, $(Br^-)_2$, $(I^-)_2$, planar CO_3^{2-} (*via* OH^- induced aerial CO_2 fixation) and tetrahedral SO_4^{2-} (*via* H-bonding activated proton transfer of HSO_4^-) are cooperatively entrapped within the neutral dimeric assemblies of **L_3**, sealed by *n*-TBA counter-cations in the solid state. The X-ray analyses clearly exposed that, the systematic size mediated capturing of bare-anions/hydrated-anions/solvated-anions by terminal aryl di-functionalized receptors **L_1**, **L_2** and **L_3** are deeply governed by the regular lengthening or shortening of the terminal aryl centroid distances in each host-guest complexes. Note that, except the *meta*-substituent driven non-cooperative acetate and chloride complexes of **L_1** and **L_2**, the average terminal aryl centroid distances of all other cooperative anion complexes become greater than 1 nm and the alteration of these centroid distances occur in an ordered way depending on the size of anionic guests. The solution-state ^{1}H-NMR titration experiments by and 2D-NOESY NMR experiments also corroborate the solid-state results simultaneously and the diverse as well as systematic halide and oxyanion binding of the three receptor systems are reliable to interpret the data and consistent to justify the variation. The relative 3D geometrical orientations of mainly *meta*-substituents with respect to adjacent N−H part of urea moiety of *meta-para* aryl di-substituted receptors **L_1** and **L_2** possibly played a vital role in the construction of smaller anion assembled cooperative/non-cooperative host assemblies, but the larger oxyanions or associations of halides/hydrated-halides or *meta-meta* aryl di-substitution in receptors (as in **L_3**) force to stretch the *ortho*-phenylenediamine bridged dipodal receptor arms to accommodate the larger guests through cooperative binding by overcoming any kinds of terminal aryl *meta*-substituent effect.

References

3.1 (a) B. J. Calnan, B. Tidor, S. Biancalana, D. Hudson and A. D. Frankel, *Science*, 1991, **252**, 1167; (b) P. Chakrabarti, *J. Mol. Biol.*, 1993, **234**, 463.; (c) M. Cametti and K. Rissanen, *Chem. Soc. Rev.*, 2013, **42**, 2016.

3.2 (a) M. Wenzel, J. R. Hiscock and P. A. Gale, *Chem. Soc. Rev*., 2012, **41**, 480; (b) B. P. Hay, *Chem. Soc. Rev*., 2010, **39**, 3700; (c) F. P. Schmidtchen, *Chem. Soc. Rev*., 2010, **39**, 3916; (d) C. Caltagirone and P. A. Gale, *Chem. Soc. Rev.*, 2009, **38**, 520.

3.3 (a) S. K. Dey, A. Basu, R. Chutia, and G. Das *RSC Adv.*, 2016, **6**, 26568; (b) R. Dutta and P. Ghosh *Chem. Commun.*, 2014, **50**, 10538.

3.4 (a) C. J. Avers, *Molecular Cell Biology*, Addison-Wesley, Reading, 1986; (b) Z. Wang, H. Luecke, N. Yao and F. A. Quiocho, *Nat. Struct. Biol.*, 1997, **4**, 519.

3.5 (a) M. Cametti and K. Rissanen, *Chem. Commun.*, 2009, 2809; (b) T. W. Hudnall, C.-W. Chiu and F. P. Gabbai, *Acc. Chem. Res.*, 2009, **42**, 388.

3.6 (a) S. Ayoob and A. K. Gupta, *Crit. Rev. Environ. Sci. Technol.*, 2006, **36**, 433; (b) *A systematic review of the efficacy and safety of fluoridation*, 2007, National Health and Medical Research Council, Australian Government, available at http://www. nhmrc.gov.au/; (c) A. S. McCall, C. F. Cummings, G. Bhave, R. Vanacore, A. Page-McCaw and B. G. Hudson, *Cell*, 2014, **15**, 1380.

3.7 (a) J. W. Pflugrath and F. A. Quiocho, *Nature* 1985, **314**, 257; (b) T. H. Milby and R. C. Baselt,. *Am. J. Ind. Med*. 1999, **35**, 192.

3.8 (a) *Climate Change, **2007**: Synthesis Report, International Panel on Climate Change;* Cambridge University Press: Cambridge, U.K., 2007. (b) D. S. Jenkinson, D. E. Adams and A. Wild, *Nature*, 1991, **351**, 304. (c) K. Caldeira, A. K. Jain and M. I. Hoffert, *Science*, 2003, **299**, 2052.

3.9 (a) R. Li, Y. Zhao, S. Li, P. Yang, X. Huang, X.-J. Yang and B. Wu, *Inorg. Chem*., 2013, **52**, 5851; (b) S. J. Brooks, P. R. Edwards, P. A. Gale and M. E. Light, *New J. Chem*., 2006, **30**, 65; (c) L. E. Karagiannidis, C. J. E. Haynes, K. J. Holder, I. L. Kirby, S. J. Moore, N. J. Wells and P. A. Gale, *Chem. Commun.*, 2014, **50**, 12050.

3.10 (a) U. Manna, B. Nayak, and G. Das *Cryst. Growth Des.* 2016, **16**, 7163; (b) U. Manna, S. Kayal, B. Nayak and G. Das *Dalton Trans.*, 2017, **46**, 11956.

Annexure 3

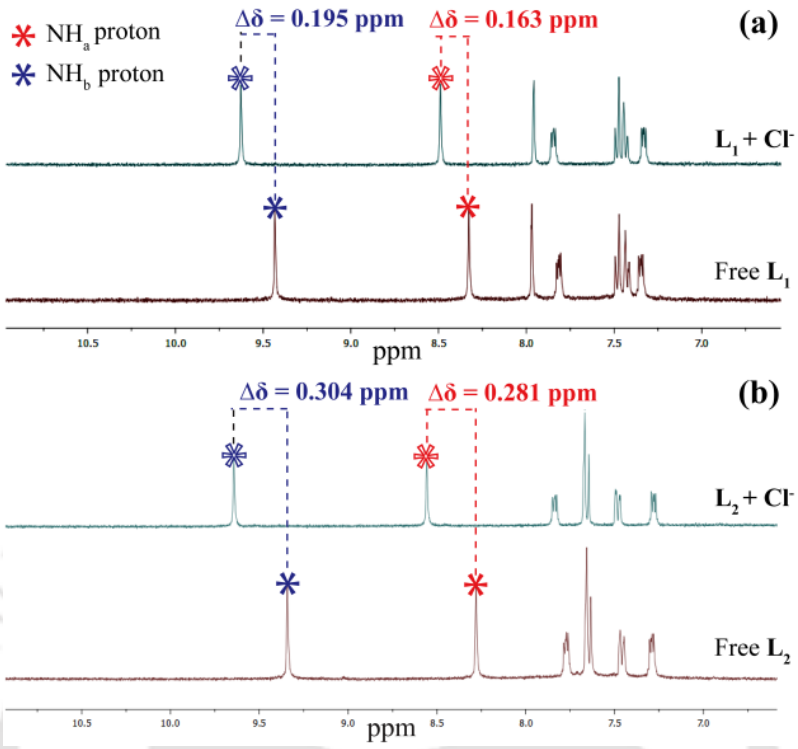

Fig A3.1 Partial ^{1}H NMR spectra (400 MHz, DMSO-d_6) of (a) $\mathbf{L_1}$ and (b) $\mathbf{L_2}$, with the observable shifts of urea -NH resonance upon the addition of 1.0 equivalent of *n*-TBACl

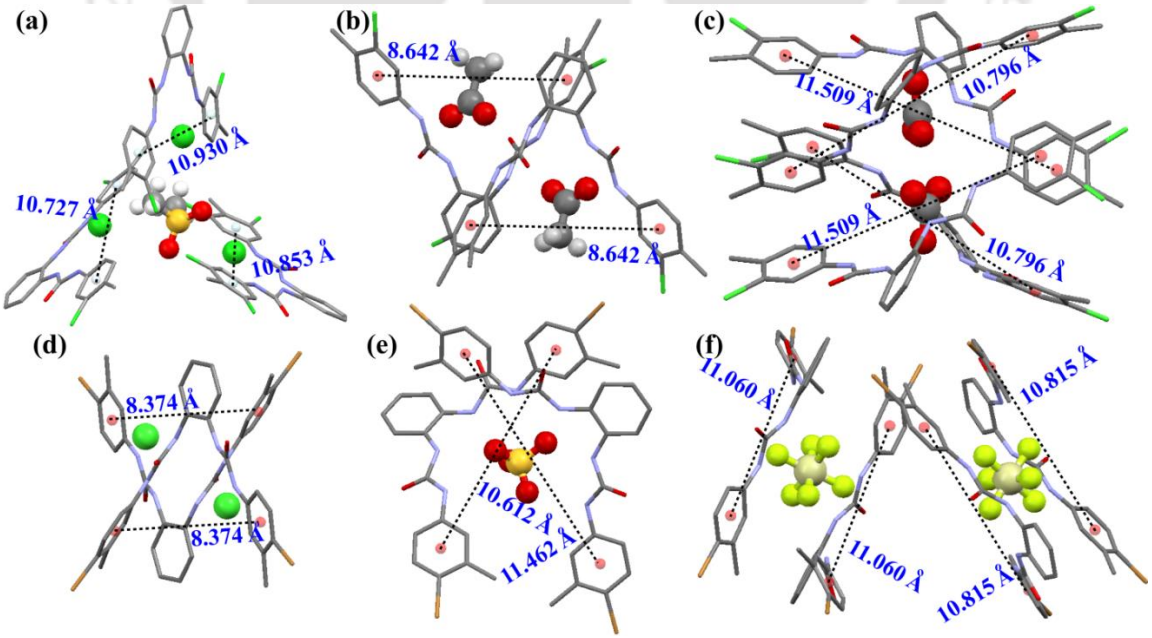

Fig A3.2 Partial X-ray structures of anion complexes depicting average terminal aryl centroid distances (a) ~10.836 Å in complex **1a**, (b) ~8.642 Å in complex **1b**, (c) ~11.152 Å in complex **1c**, (d) ~8.374 Å in complex **2a**, (e) ~11.037 Å in complex **2b**, and (f) ~10.937 Å in complex **2c**.

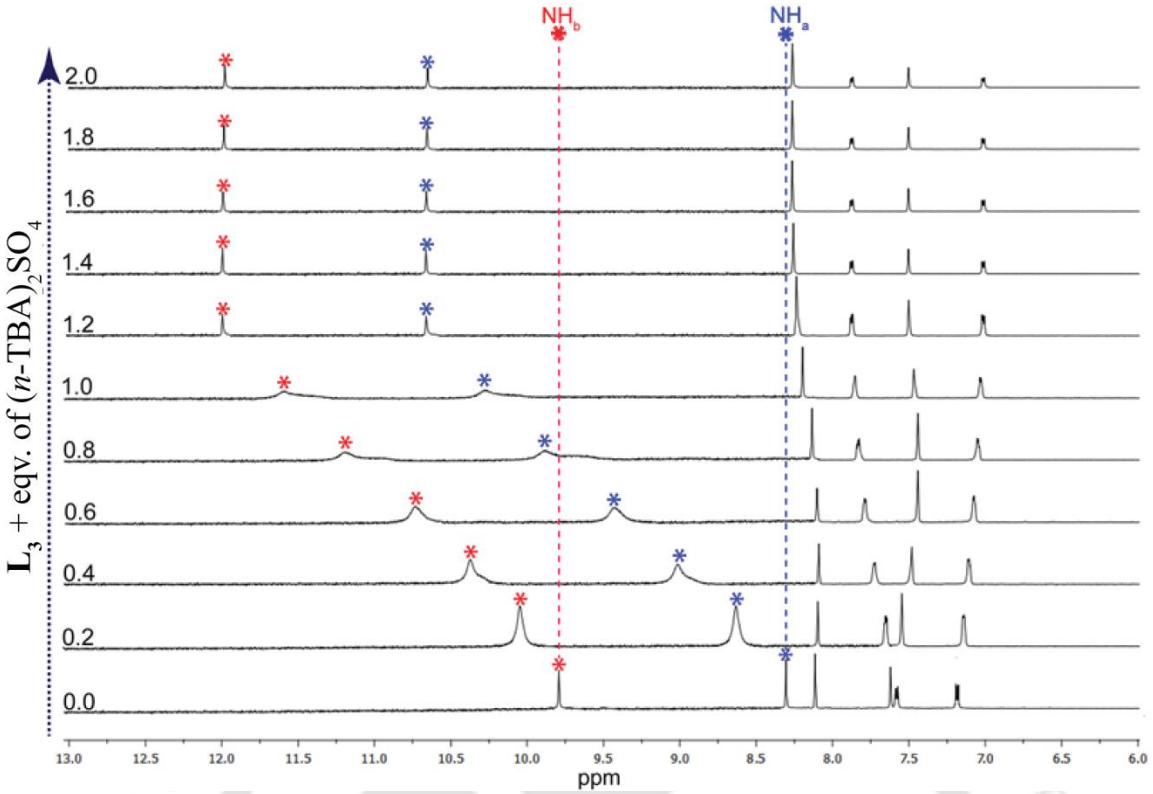

Fig A3.3. Expanded partial ^{1}H NMR spectra of $\mathbf{L_3}$ upon titration with $(n\text{-TBA})_2SO_4$ in DMSO-d_6.

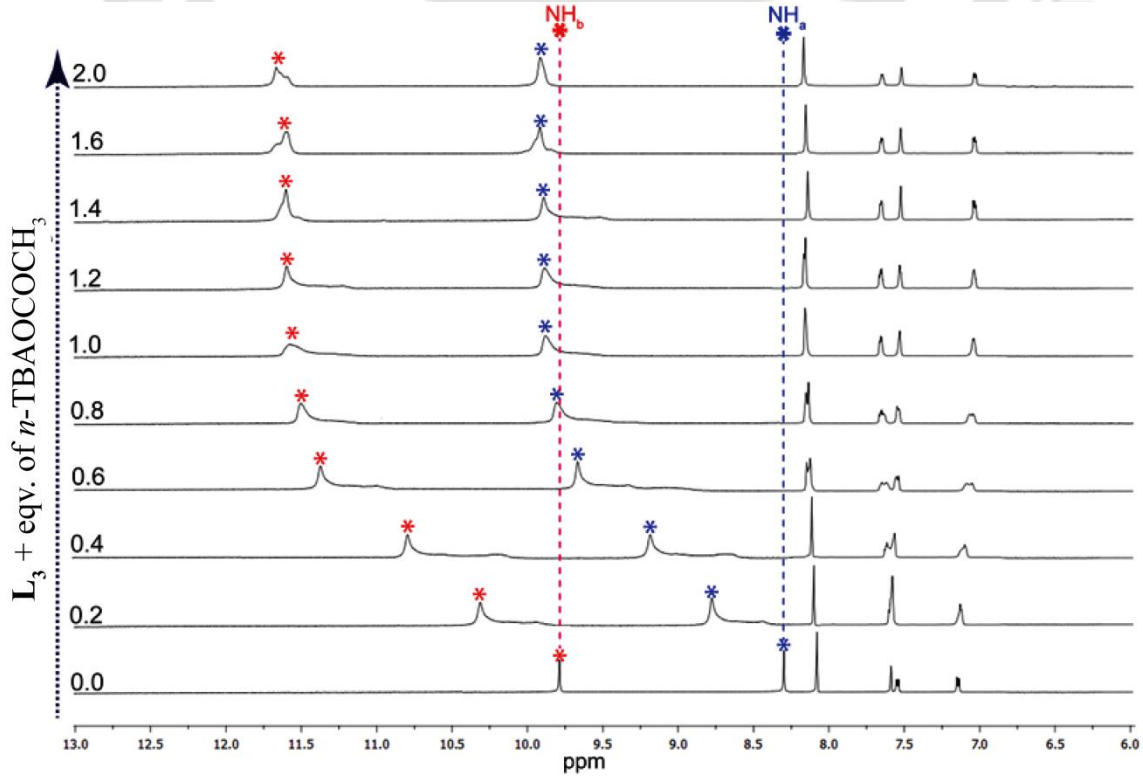

Fig A3.4 Expanded partial ^{1}H NMR spectra of $\mathbf{L_3}$ upon titration with n-$TBAOCOCH_3$ in DMSO-d_6.

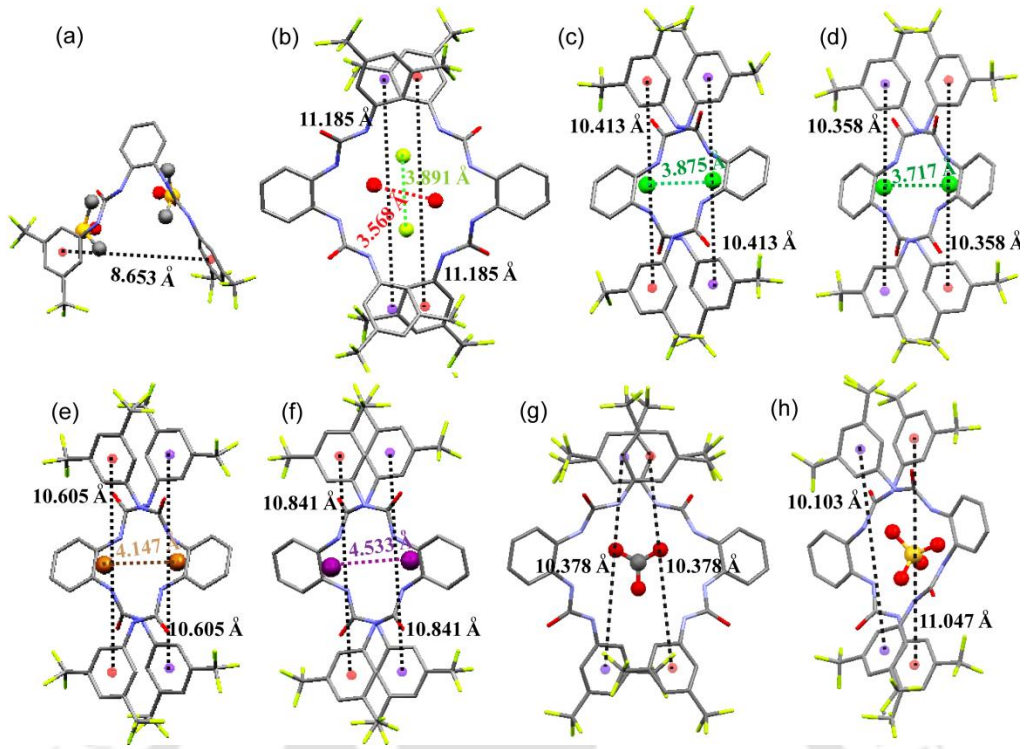

Fig A3.5 X-ray structure (partial) depicting average terminal aryl centroid distances and intra-guest distances (as applicable) in the (a) DMSO-solvated $\mathbf{L_3}$, (b) complex **3a**, (c) complex **3b**[1], (d) complex **3b**[2], (e) complex **3c**, (f) complex **3d**, (g) complex **3e** and (h) complex **3f**.

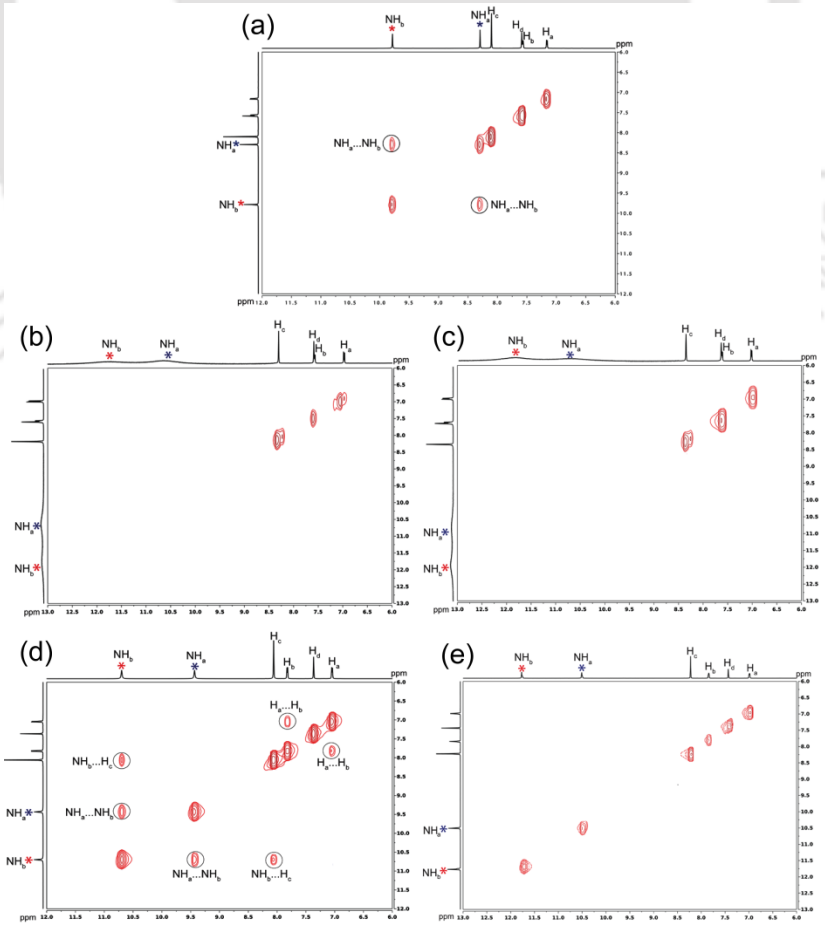

Fig. A3.6 2D-NOESY NMR spectra of (a) free $\mathbf{L_3}$, (b) fluoride-water complex **3a**, (c) carbonate complex **3e**, (d) sulfate complex **3f**, and (e) $\mathbf{L_3}$ in the presence of excess sulfate in DMSO-d_6.

Table A3.1 Crystallographic parameters and refinement details of anion complexes of receptors $\mathbf{L_1}$-$\mathbf{L_2}$

Parameters	1a	1b	1c	2a	2b	2c
Formula	$C_{116}H_{172}Cl_9N_{15}O_7S$	$C_{40}H_{58}Cl_2N_5O_4$	$C_{61}H_{80}Cl_4N_{10}O_7$	$C_{38}H_{56}Br_2ClN_5O_2$	$C_{76}H_{112}Br_4N_{10}O_8S$	$C_{76}H_{112}Br_4F_6N_{10}O_4Si$
Fw	2239.80	743.81	1207.15	810.13	1645.42	1691.45
Crystal system	triclinic	monoclinic	monoclinic	monoclinic	monoclinic	triclinic
Space group	P-1	P 21/c	C 2/c	P 21/c	P 21/c	P -1
a/Å	18.100(3)	11.462(6)	24.818(13)	11.886(11)	20.091(8)	14.393(15)
b/Å	19.280(3)	19.797(12)	18.488(13)	20.089(3)	17.917(8)	18.219(19)
c/Å	19.376(3)	18.614(9)	28.168(17)	17.645(3)	24.194(10)	18.926(19)
α/°	79.210(10)	90.00	90.00	90.00	90.00	116.87(10)
β/°	77.267(9)	93.946(5)	106.979(5)	93.257(11)	108.794(2)	97.800(8)
γ/°	83.013(10)	90.00	90.00	90.00	90.00	101.029(9)
V/Å^3	6455.7(18)	4214.0(4)	12361.7(14)	4206.6(10)	8245.3(6)	4203.1(9)
Z	2	4	8	4	4	2
D_c/g cm^{-3}	1.152	1.172	1.297	1.279	1.326	1.337
μ Mo $K_α$/mm^{-1}	0.266	0.197	0.252	2.027	2.034	1.993
F000	2396.0	1596.0	5120.0	1688.0	3432.0	1756.0
T/K	298(2)	298(2)	298(2)	298(2)	298(2)	298(2)
θ max.	17.08	22.88	16.88	21.35	21.43	17.76
Total no. of reflections	73277	19817	85636	21299	122796	40119
Independent reflections	28151	10643	14494	9709	18504	19195
Observed reflections	12607	6910	8599	6760	8218	4345
Parameters refined	1356	477	751	440	904	926
R_1, I > 2σ(I)	0.0979	0.0958	0.0879	0.0755	0.0634	0.1110
wR_2, I > 2σ(I)	0.2132	0.2013	0.2065	0.1660	0.1506	0.2221
GOF (F^2)	1.193	1.090	1.178	0.883	0.879	0.999
CCDC No.	1484815	1484816	1484817	1484818	1484819	1484820

Table A3.2 Crystallographic parameters and refinement details of free receptor $\mathbf{L_3}$ and its anion complexes

Parameters	$\mathbf{L_3}$	3a	3b[1]	3b[2]	3c	3d	3e	3f
Formula	$C_{28}H_{26}F_{12}N_4O_4S_2$	$C_{40}H_{52}F_{13}N_5O_3$	$C_{40}H_{50}ClF_{12}N_5O_2$	$C_{32}H_{34}ClF_{12}N_5O_2$	$C_{40}H_{50}BrF_{12}N_5O_2$	$C_{40}H_{50}F_{12}IN_5O_2$	$C_{81}H_{100}F_{24}N_{10}O_7$	$C_{80}H_{100}F_{24}N_{10}O_8S$
Fw	774.65	897.87	896.30	784.09	940.75	987.75	1781.71	1817.76
Crystal system	triclinic	monoclinic	monoclinic	triclinic	monoclinic	monoclinic	orthorhombic	triclinic
Space group	*P* -1	*P* 21/c	*P* 21/c	*P* -1	*P* 21/c	*P* 21/c	*P* c c n	*P* -1
a/Å	9.667(8)	14.902(10)	17.694(9)	10.055(9)	17.524(10)	17.644(6)	8.692(6)	14.849(8)
b/Å	13.217(11)	18.280(2)	14.522(10)	13.439(13)	14.788(8)	14.926(6)	24.936 (16)	17.800(11)
c/Å	13.911(12)	16.812(11)	18.033(11)	14.857(13)	17.980(9)	18.235(5)	40.194(3)	20.142(12)
α/°	104.440(7)	90.00	90.00	77.996(8)	90.00	90.00	90.00	113.187(6)
β/°	92.993(7)	91.476(6)	103.309(6)	87.728(7)	101.090(6)	100.787(3)	90.00	98.384(5)
γ/°	90.220(7)	90.00	90.00	70.382(8)	90.00	90.00	90.00	105.077(5)
V/Å^3	1718.6(3)	4578.3(7)	4509.2(5)	1848.9(3)	4572.7(4)	4717.6(3)	8711.7(10)	4536.6(6)
Z	2	4	2	2	4	4	4	2
D_c/g cm^{-3}	1.497	1.303	1.320	1.408	1.367	1.391	1.359	1.331
μ $K_α$/mm^{-1}	0.259	0.118	0.173	0.200	0.986	0.763	1.063	0.141
F000	788.0	1872.0	1864.0	804.0	1936.0	2008.0	3712.0	1892.0
T/K	298(2)	298(2)	298(2)	298(2)	298(2)	298(2)	150(2)	298(2)
θ max.	24.997	24.999	24.998	24.997	25.000	25.000	68.397	25.000
Total no. of reflections	11963	19533	19062	12746	22061	20609	135729	36260
Independent reflections	6060	8040	7932	6486	8034	8292	7901	15942
Observed reflections	3510	2939	4585	3800	4642	6099	4659	13480
Parameters refined	563	682	595	564	584	591	581	1197
R_1, I > 2σ(I)	0.0710	0.0976	0.0666	0.0871	0.0658	0.0443	0.0811	0.0994
wR_2, I > 2σ(I)	0.1703	0.1897	0.1671	0.2054	0.1609	0.1140	0.1716	0.1470
GOF (F^2)	1.068	1.128	1.007	1.049	1.037	1.035	1.027	1.097
CCDC No.	1525834	1525835	1525836	1525837	1525838	1525839	1525840	1525841

Table A3.3 Details of Hydrogen Bonding contacts in the anion complexes of receptors L_1-L_2

Complex	D−H···A	*d*(D···H)/Å	*d*(H···A)/Å	*d*(D···A)/Å	<D−H···A/°	Symmetry codes
1a	N1-H1N···Cl7	0.86	2.42	3.299(6)	160	x,y,z
	N2-H2N···Cl7	0.86	2.28	3.271(6)	152	x,y,z
	N3-H3N···Cl7	0.86	2.55	3.304(6)	147	x,y,z
	N4-H4N···Cl7	0.86	2.49	3.297(6)	158	x,y,z
	N5-H5N···Cl8	0.86	2.43	3.251(7)	160	x,y,z
	N6-H6N···Cl8	0.86	2.52	3.299(6)	152	x,y,z
	N7-H7N···Cl8	0.86	2.45	3.262(6)	158	x,y,z
	N8-H8N···Cl8	0.86	2.48	3.305(6)	161	x,y,z
	N9-H9N···Cl9	0.86	2.47	3.296(7)	162	x,y,z
	N10-H10N···Cl9	0.86	2.44	3.277(6)	164	x,y,z
	N11-H11N···Cl9	0.86	2.46	3.292(7)	163	x,y,z
	N12-H12N···Cl9	0.86	2.45	3.285(7)	162	x,y,z
	C107-H10B···O3	0.97	2.56	3.525(8)	175	1-x,1-y,1-z
1b	N1-H1N···O4	0.86	1.92	2.746(5)	160	1-x,1/2+y,1/2-z
	N2-H2N···O4	0.86	2.13	2.912(5)	151	1-x,1/2+y,1/2-z
	N4-H4N···O3	0.86	2.05	2.809(6)	147	-1+x,1/2-y,-1/2+z
	C7-H7···O1	0.93	2.51	3.385(6)	158	-x,1-y,1-z
	C23-H23A···O2	0.97	2.59	3.456(6)	149	1+x,y,z
	C31-H31B···O1	0.97	2.54	3.432(7)	152	1+x,y,z
	C35-H35A···O4	0.97	2.52	3.450(7)	161	x,y,z
1c	N1-H1N···O7	0.86	2.05	2.844(5)	153	x,y,z
	N2-H2N···O7	0.86	2.46	3.187(6)	143	x,y,z
	N3-H3N···O5	0.86	1.99	2.798(5)	156	x,y,z
	N4-H4N···O5	0.86	2.24	2.977(5)	144	x,y,z
	N5-H5N···O5	0.86	2.19	2.937(4)	145	x,y,z
	N6-H6N···O6	0.86	2.30	3.040(5)	144	-x,y,1/2-z
	N7-H7N···O7	0.86	2.23	3.013(6)	151	-x,y,1/2-z
	N8-H8N···O7	0.86	2.14	2.949(5)	157	-x,y,1/2-z
	C49-H49B···O1	0.97	2.57	3.369(9)	140	1/2-x,-1/2+y,1/2-z
	C54-H54A···O3	0.96	2.24	3.100(16)	148	x,y,z
	C54-H54C···O2	0.96	1.92	2.836(18)	158	1/2-x,1/2+y,1/2-z
2a	N1-H1N···Cl1	0.86	2.39	3.226(6)	163	1-x,-1/2+y,1/2-z
	N2-H2N···Cl1	0.86	2.49	3.312(5)	160	1-x,-1/2+y,1/2-z
	N4-H4N···Cl1	0.86	2.56	3.305(6)	145	x,1/2-y,1/2+z
	C4-H4···O1	0.93	2.52	3.423(9)	165	1-x,-y,-z
	C31-H31A···O2	0.97	2.46	3.349(8)	153	x,y,z
2b	N1-H1N···O5	0.86	2.11	2.923(6)	157	x,y,z
	N2-H2N···O5	0.86	2.23	3.018(6)	153	x,y,z
	N3-H3N···O8	0.86	2.00	2.844(6)	165	x,y,z
	N4-H4N···O8	0.86	2.47	3.204(6)	144	x,y,z
	N5-H5N···O7	0.86	2.05	2.875(6)	161	x,y,z
	N6-H6N···O6	0.86	2.02	2.865(7)	167	x,y,z
	N7-H7N···O6	0.86	2.05	2.867(7)	158	x,y,z
	N8-H8N···O5	0.86	2.21	3.064(6)	174	x,y,z
	C45-H45B···O1	0.97	2.57	3.512(8)	163	-x,1-y,-z
	C49-H49B···O8	0.97	2.44	3.412(8)	180	x,y,z
	C69-H69B···O3	0.97	2.35	3.294(7)	163	1-x,-1/2+y,1/2-z
2c	N1-H1N···F3	0.86	2.08	2.912(10)	164	x,-1+y,z
	N2-H2N···F2	0.86	2.10	2.921(10)	158	-x,1-y,-z
	N3-H3N···F1	0.86	2.22	3.019(12)	154	x,-1+y,z
	N3-H3N···F2	0.86	2.31	3.033(10)	142	-x,1-y,-z
	N4-H4N···F1	0.86	2.18	2.989(11)	156	x,-1+y,z
	N5-H5N···F6	0.86	2.07	2.857(10)	152	1-x,1-y,1-z
	N6-H6N···F6	0.86	2.16	2.929(12)	148	1-x,1-y,1-z
	N7-H7N···F4	0.86	2.00	2.849(13)	172	1+x,-1+y,z
	N8-H8N···F5	0.86	2.10	2.946(14)	170	1-x,1-y,1-z
	C39-H39···F5	0.93	2.50	3.299(14)	144	1-x,1-y,1-z
	C49-H49B···O2	0.97	2.47	3.420(2)	166	x,y,z
	C61-H61A···F6	0.97	2.35	3.187(11)	144	x,y,z
	C73-H73A···F1	0.97	2.34	3.239(16)	155	x,y,z

Table A3.4 Details of Hydrogen Bonding contacts in the free receptor $\mathbf{L_3}$ and its anion complexes

Complex	D−H···A	*d*(D···H)/Å	*d*(H···A)/Å	*d*(D···A)/Å	<D−H···A/°	Symmetry codes
$\mathbf{L_3}$	N1-H1N···O3	0.86	2.03	2.842(4)	157	1-x,1-y,1-z
	N2-H2N···O3	0.86	2.15	2.947(5)	154	1-x,1-y,1-z
	N3-H3N···O4	0.86	2.31	3.034(4)	143	1+x,y,z
	N4-H4N···O4	0.86	1.95	2.790(5)	164	1+x,y,z
	C25-H25B···O1	0.96	2.57	3.443(7)	152	x,-1+y,z
3a	N1-H1N···F13	0.86	1.91	2.760(6)	168	-x,1-y,1-z
	N2-H2N···O3	0.86	2.05	2.900(6)	168	-x,1-y,1-z
	N3-H3N···O3	0.86	2.53	3.290(7)	148	-x,1-y,1-z
	N4-H4NA···F13	0.86	1.85	2.665(8)	156	x,y,z
	N4-H4NB···F13	0.86	1.88	2.665(8)	152	x,y,z
	O3-H3OA···F13	0.85	1.89	2.652(6)	148	x,y,z
	C33-H33B···F11B	0.97	2.52	3.485 (15)	178	x,3/2-y,-1/2+z
	C35-H35A···O2	0.97	2.50	3.428(11)	145	-x,-1/2+y,1/2-z
	C37-H37B···O3	0.97	2.43	3.360(8)	161	x,y,z
3b[1]	N1-H1N···Cl1	0.86	2.63	3.268(3)	132	x,y,z
	N2-H2N···Cl1	0.86	2.40	3.208(3)	157	1-x,1-y,-z
	N3-H3N···Cl1	0.86	2.62	3.432(3)	157	x,y,z
	N4-H4N···Cl1	0.86	2.35	3.201(3)	170	x,y,z
	C25-H25A···O1	0.97	2.53	3.244(5)	130	x,1/2-y,1/2+z
	C29-H29B···O1	0.97	2.48	3.245(5)	136	x,1/2-y, 1/2+z
3b[2]	N1-H1N···Cl1	0.86	2.71	3.304(3)	127	x,y,z
	N2-H2N···Cl1	0.86	2.40	3.251(4)	169	-x,1-y,1-z
	N3-H3N···Cl1	0.86	2.71	3.288(4)	151	x,y,z
	N4-H4N···Cl1	0.86	2.38	3.233(4)	172	x,y,z
3c	N1-H1N···Br1	0.86	2.51	3.362(5)	171	x,y,z
	N2-H2N···Br1	0.86	2.77	3.588(5)	158	x,y,z
	N3-H3N···Br1	0.86	2.55	3.326(5)	150	-x,1-y,1-z
	N4-H4N···Br1	0.86	2.76	3.380(5)	131	x,y,z
	C29-H29A···O2	0.97	2.55	3.360(9)	141	x,1/2-y,-1/2+z
	C37-H37A···O2	0.97	2.53	3.339(9)	140	x,1/2-y,-1/2+z
3d	N1-H1N···I1	0.86	2.93	3.555(14)	131	x,y,z
	N2-H2N···I1	0.86	2.83	3.517(12)	138	-x,1-y,1-z
	N3-H3N···I1	0.86	3.02	3.830(12)	158	x,y,z
	N4-H4N···I1	0.86	2.76	3.607(13)	170	x,y,z
	C33-H33B···O1	0.97	2.57	3.40 (2)	143	x,3/2-y,-1/2+z
3e	N1-H1N···O3	0.86	1.87	2.686(4)	158	x,y,z
	N2-H2N···O4	0.86	2.27	3.051(5)	151	x,y,z
	N3-H3N···O4	0.86	1.87	2.689(5)	159	x,y,z
	N4-H4N···O4	0.86	2.21	2.943(6)	142	x,y,z
	N4-H4N···O4	0.86	2.53	3.357(5)	162	3/2-x,1/2-y,z
	C33-H61A···O1	0.97	2.48	3.387(5)	156	-1+x,y,z
	C35-H63B···O1	0.97	2.56	3.450(5)	152	-1+x,y,z
3f	N1-H1N···O6	0.86	2.01	2.84(9)	158	x,y,z
	N2-H2N···O6	0.86	2.18	2.96(8)	151	x,y,z
	N3-H3N···O5	0.86	2.18	2.95(8)	149	x,y,z
	N4-H4N···O5	0.86	2.07	2.87(9)	154	x,y,z
	N5-H5N···O6	0.87	1.99	2.83(10)	162	x,y,z
	N6-H6N···O7	0.86	1.97	2.83(10)	173	x,y,z
	N7-H7N···O7	0.86	2.12	2.94(9)	159	x,y,z
	N8-H8N···O8	0.86	1.91	2.76(9)	169	x,y,z
	C45-H45···F24	0.92	2.52	3.44(14)	174	1-x,-y,1-z
	C58-H58B···O3	0.98	2.55	3.47(12)	158	x,y,z
	C65-H65C···O4	0.97	2.50	3.43(16)	161	x,y,z
	C69-H69A···O5	1.10	2.20	3.22(14)	176	1+x,y,z

Chapter 4

meta-Phenylenediamine based isomeric neutral scaffolds: Evidence of $[SO_4^{2-}\text{-}(H_2O)_3\text{-}SO_4^{2-}]$, aerial CO_2 fixed $[CO_3^{2-}\text{-}(H_2O)_2\text{-}CO_3^{2-}]$ and asymmetric sulfate recognition

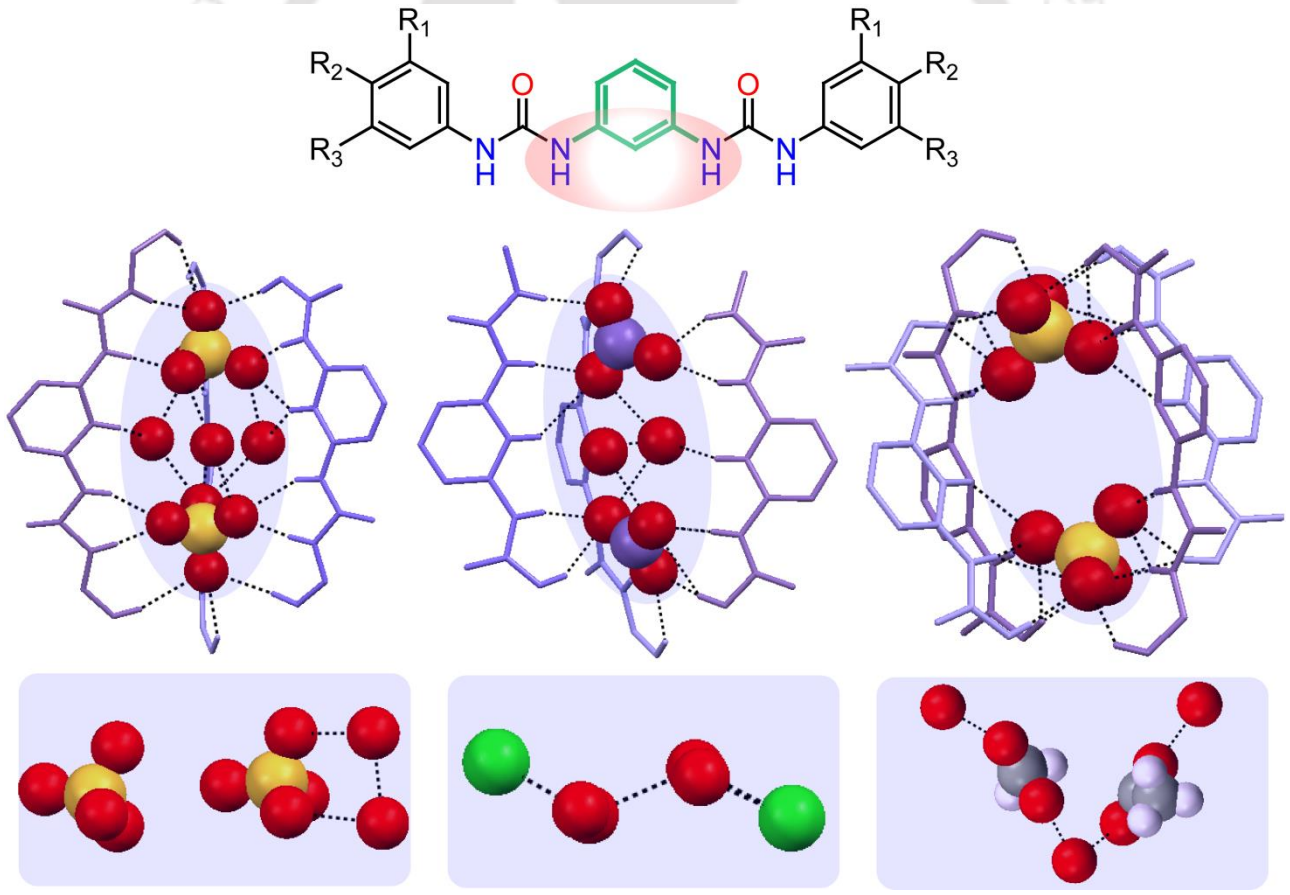

4.1 Background and Focus of the Chapter

Recognition of anions/hydrated anions *via* encapsulation or entrapment and their significant non-covalent interactions with neutral self-assembled host architectures are one of the contemporary sides in the field of supramolecular chemistry.[4.1] As most of the anions occur in their hydrated form in natural and biological environments such as marine water and several ecosystems, recognition of hydrated anions is of immense and ever-growing interest to researchers.[4.2] The hydrated architecture of anions is highly random in the case of discrete ordered anion-water clusters and they show a vast range of complicated interactions in aqueous environments due to the formation of strong and stable hydrogen bonds, whereas the ordered anion-water clusters arrangement within the receptor cavity delivers a unique opportunity to interpret the detailed molecular interactions in these restricted frameworks.[4.3] On account of their diverse functions in health, environmental, chemical, and biological interfaces,[4.4] enormous efforts have especially been paid by researchers to understand the water clusters in a hydrophobic receptor environment.[4.5] From the application point of view, the structural characterization of the anion-water cluster is a salient feature to appreciate the solvation mechanism, ion translocation in water-membrane interfaces, ion-mobility in the bulk and electrical phenomena.[4.6] Subsequently, the recognition of non-hydrated anionic guests has also been encouraged due to their key role in living organisms as well as direct influence on various environmental, biomedical, and industrial applications.[4.7] Because of the high abundance and existence of several hydrated halides in nature, the aqueous solvation of halides is a much more recognized area in supramolecular chemistry. In particular, the recognition or sensing of fluoride is important owing to its small size, high electronegativity, high hydration enthalpy as well as its function in industry, biology, food, and toxicity and the larger chloride is a major component of oceans, a dominant species in biological extra-cellular fluid followed by its crucial role in signal transduction or transport of organic solutes through the cell membrane.[4.8a-c] Among oxyanions, sulphate contamination in drinking water and its toxic effect has been acknowledged as a major hurdle to clean-up efforts in the remediation of nuclear waste, carbonate is one of the major components in biomineralized materials, works as a buffer in blood, and the acetate ion is utilized by organisms in the form of acetyl coenzyme A.[4.8d-e] Furthermore, the significant rise in aerial CO_2 concentration is another major ecological issue caused by increased consumption of fossil fuels of industries, automobiles, etc., that ultimately demands the efficient fixation and activation of atmospheric CO_2 into green chemicals or as carbonate/bicarbonate within the artificial receptors.[4.8f-g] Since the last decade, numerous tripodal scaffolds derived from aliphatic or aromatic amines with (thio)-urea functionalization containing structurally preorganized

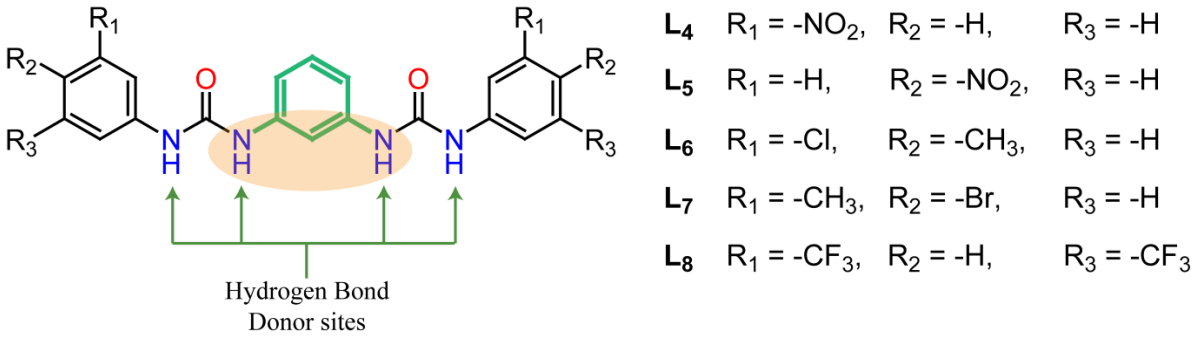

Scheme 4.1 A comprehensive representation of molecular receptor structures included in this chapter.

cavity,[4.9] and, some dipodal receptors derived from relatively better cooperative as well as most converging *ortho*-phenylenediamine[4.10] have been commonly used for anion recognition. However, the development of *meta*-phenylenediamine based dipodal (thio)-urea anion receptors containing one or more terminal aryl functionalization are very rare in literature may be due to the relatively less converging receptor conformations. Hence, the systematic investigation of terminal mono-aryl or di-aryl substituted isomeric *meta*-phenylene connected bis-urea scaffolds for recognition of anions/hydrated-anions depending upon the substituents or anion dimension is an exciting area of research to the supramolecular communities.

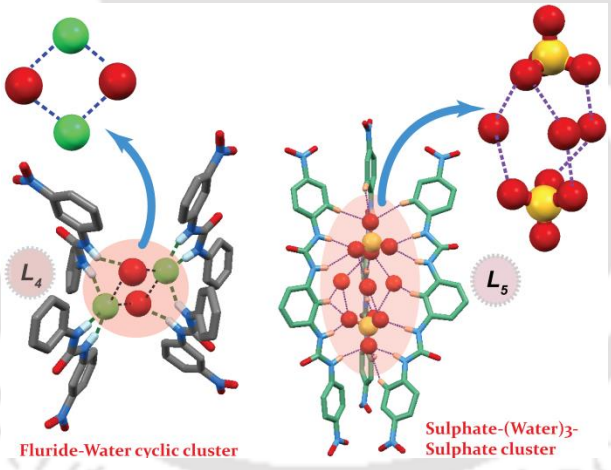

Fig 4.1 The comprehensive representation of one of the key outcomes of research work included in this chapter.

This chapter describes the design and synthesis of, two positional isomeric 3-nitro- and 4-nitro-phenyl functionalized (**L_4** and **L_5**), two 3,4-halo-methylphenyl functionalized (**L_6** and **L_7**) and one 3,5-trifluoromethyl-phenyl functionalized (**L_8**) *meta*-phenylenediamine based dipodal bis-urea receptors for recognition of anions/hydrated anions within the neutral host assemblies.[4.11] Firstly, the *meta*-nitrophenyl (**L_4**) and *para*-nitrophenyl (**L_5**) isomer have been found to entrap the cyclic fluoride-water $[(F^-)_2(H_2O)_2]$ tetrameric cluster (complex **4a**) within the tetrameric pillar of receptor **L_4** and sulfate-water-sulfate $[SO_4^{2-}\text{-}(H_2O)_3\text{-}SO_4^{2-}]$ rugby-ball shaped adduct (complex **5a**) within the trimeric long straight pillar of receptor **L_5**. In addition, receptor **L_4** has been authenticated structurally to entrap the divalent bare sulfate in complex **4b** and monovalent

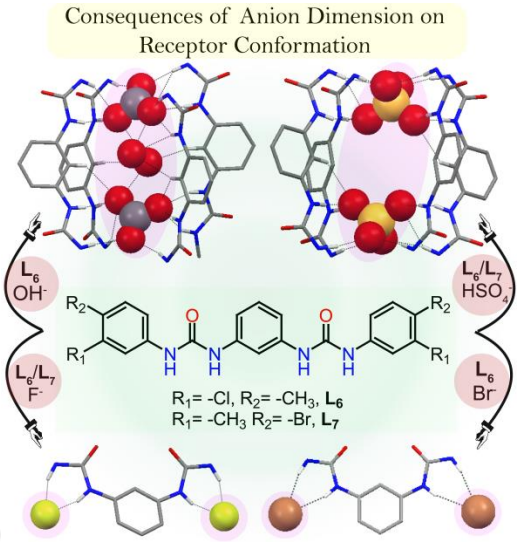

Fig 4.2 The comprehensive representation of one of the key outcomes of research work included in this chapter.

acetate anion in complex **4c** by non-cooperative interactions, while receptor $\mathbf{L_5}$ forms a cooperative host-guest assembly with the *n*-TBA and DMSO coordinated bromide ion in complex **5b**. The X-ray analysis clearly unveils the semi-circular ligand architecture of $\mathbf{L_4}$ and linear ligand architecture of $\mathbf{L_5}$ in the corresponding host-guest complexes that can be ascribed for the positional isomerism of *meta*-nitro and *para*-nitro functionality towards complex formation. Secondly, the two halo-methylphenyl terminal aryl-disubstituted receptors $\mathbf{L_6}$ (chloro-methyl isomer) and $\mathbf{L_7}$ (bromo-methyl isomer), have been found to capture an unique [CO_3^{2-}-$(H_2O)_2$-CO_3^{2-}] cluster (complex **6a**) within linear tetrameric barrel of receptor $\mathbf{L_6}$

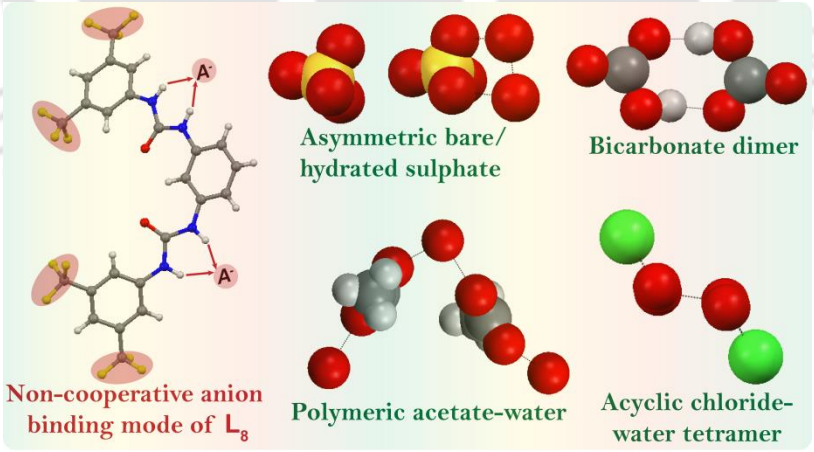

Fig 4.3 The comprehensive representation of one of the key outcomes of research work included in this chapter.

entirely sealed by *n*-TBA cations and water-free naked sulfate-sulfate double anion inside the similar linear tetrameric barrel of both receptors $\mathbf{L_6}$ (complex **6b**) and $\mathbf{L_7}$ (complex **7a**). Furthermore, receptor $\mathbf{L_6}$ self-assembles to form hexa-coordinated fluoride complex **6c** and tetra-coordinated bromide complex **6d** and receptor $\mathbf{L_7}$ self-assembles to form penta-coordinated fluoride complex **7b** in the solid state *via* semicircular receptor architectures and non-

cooperative interactions. Noticeably, here the anion recognition is much more governed by the size and dimension of the anions rather than the terminal aromatic substituent effect in the cases of **L_6** and **L_7**. Thirdly, the receptor **L_8** containing electron-withdrawing trifluoro-methylphenyl *meta*-disubstitution has also been recognized as a potential system for, unusual asymmetric entrapment of naked sulfate and cyclic hydrated-sulfate (complex **8a**) simultaneously, air-stable bicarbonate dimer capture (complex **8b**) by fluoride-induced atmospheric CO_2 fixation, entrapment of linear acetate-water polymeric assembly (complex **8c**) and also the trapping of chair-like $(chloride)_2$-$(water)_2$ hydrated-anionic assemblies (complex **8d**). Noticeably, here the recognition of hydrated-anion or anionic association within the semi-circular non-cooperative **L_8** receptor architecture are heavily governed by the steric effect of terminal aryl *meta*-di-functionalization. Scheme 4.1 shows the molecular receptor structures **L_4-L_8** and the representations of key findings of research work included in this chapter are shown Fig. 4.1-4.3.

4.2 Structural aspects of anion binding with L_4-L_8

In principle, a suitable synthetic receptor should have a particular rigid or flexible hydrogen-bond donating supramolecular architecture to bind with anions of different shapes and sizes. The *meta*-phenylenediamine based *meta*-nitrophenyl or *para*-nitrophenyl functionalized positional isomeric bis-urea receptors **L_4**, **L_5** (Fig. 4.1) and more than one terminal aryl substituent (either *meta-para* or *meta-meta*) containing dipodal receptors **L_6**, **L_7** (Fig. 4.2) and **L_8** (Fig. 4.3), each hold two urea functionalities, which can accept guests of different dimensions *via* formation of cooperative/non-cooperative host-guest assemblies depending upon either positional isomeric effect of substituents or size of anionic guests. Structural information obtained from single crystal X-ray analyses of the isolated crystals provides insight into the proper binding topology of anions/hydrated-anions with the neutral receptor molecules. Efforts were made to explore the solid-state binding properties of **L_4-L_8** with various anions in different crystallization conditions, by charging excess quaternary ammonium (*n*-TBA /TEA) anion salts to the individual solutions of receptors in aprotic solvents such as MeCN, DMF and DMSO. The purposeful attachment of urea groups in highly organized 3-/4-nitrophenyl or 3,4-halo-methylphenyl/methyl-halophenyl or 3,5-bis(trifluoromethyl)phenyl terminal mono- or di-functionalized dipodal scaffolds become helpful to determine the binding discrepancies of anionic guests *via* number of non-covalent interactions. Traditionally, crystallization has been the main focus in anion-recognition chemistry to understand the structural insight of the host-guest complexes.

It should be mentioned here that the crystals suitable for XRD analysis are obtained from the individual basic DMF solutions of either *meta*-nitro (**L_4**) or *para*-nitro (**L_5**) isomer, while, the bis-(trifluoromethyl)phenyl functionalized free receptor **L_8** is crystallized from both

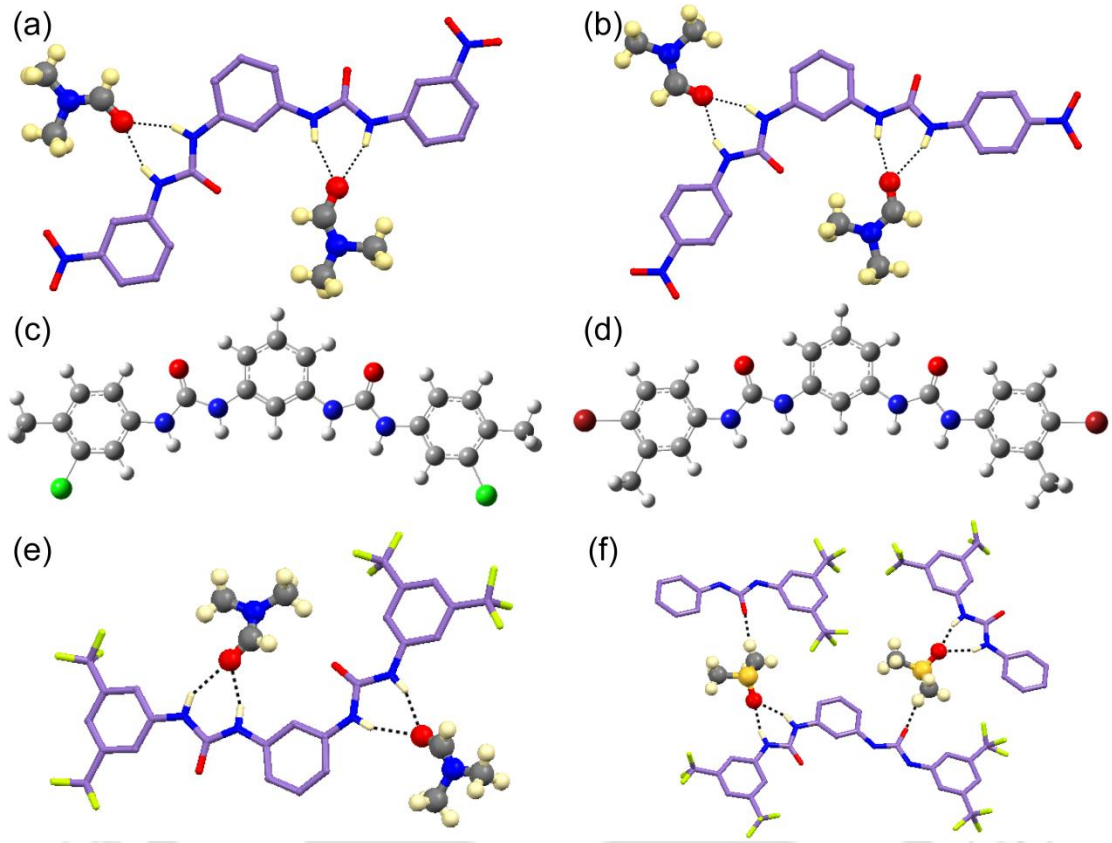

Figure 4.4 Partial X-ray structures depicting N–H···O contacts with solvent DMF in free receptors (a) $\mathbf{L_4}$, (b) $\mathbf{L_5}$; The optimized geometry of the free receptors (c) $\mathbf{L_6}$, (d) $\mathbf{L_7}$ using B3LYP/6-31+G(d,p) basis set; Partial X-ray structures depicting N–H···O contacts in free receptor (e) $\mathbf{L_8}$ with solvent DMF, (f) $\mathbf{L_8}$ with solvent DMSO.

DMF and DMSO solvents. The DMF solvated receptors $\mathbf{L_4}$ and $\mathbf{L_5}$ crystallize in the respective monoclinic space groups *C*2/c and *P*21/n and structural elucidation reveal that the two urea groups of each planar receptor are present in *anti*-fashion and N–H···O hydrogen-bonded to the solvent DMF molecule in similar non-cooperative ways (Fig. 4.4a-b). However, receptor $\mathbf{L_4}$ and $\mathbf{L_5}$ self-assemble with adjacent receptor conformer *via* formation of different kinds of cyclic H-bonded architectures that are ascribed for the positional distinction of the receptor nitro group. On the other hand, both DMF and DMSO solvated single crystals of free receptor $\mathbf{L_8}$ crystallize in the same monoclinic space group *P*21/c. Structural elucidation reveals that, in DMF-solvated $\mathbf{L_8}$ the two symmetry-independent ligands individually bind DMF molecule by two urea N–H···O interactions (Fig. 4.4e), whereas in DMSO-solvated $\mathbf{L_8}$, one receptor unit binds one DMSO molecule by two urea N–H···O interactions and another symmetry-identical DMSO unit is bound with the same receptor *via* single C–H···O interactions (Fig. 4.4f). In both X-ray structures, the orientations of the receptors are almost semicircular and interactions with solvent molecules occur in non-cooperative ways, as observed in the cases of free $\mathbf{L_4}$ and $\mathbf{L_5}$. Note that, being unable to grow good quality crystals from various solvents in different crystallization conditions, the density functional theory (DFT) studies are implemented for structural

elucidation of isomeric halo-mehtylphenyl di-functionalized receptors **L_6** (Fig. 4.4c) and **L_7** (Fig. 4.4d), which disclose the *cis*-conformations of urea groups around the two opposite flanks of *meta*-phenylene spacer and both receptors exhibit good cooperativity of urea –NH groups with almost linear and planar architecture unlike the other free receptor structures.

4.2.1. Structural analysis of halide bound complexes of receptors L_4-L_8

Single crystal XRD analyses of neutral host-halide complexes demonstrate that consistent as well as discriminating binding behavior of dipodal receptors toward hydrated or non-hydrated halides are heavily dependent on either the positional isomeric effect or terminal-aryl substituent effect of mono- or di-functionalized isomeric ligands or the size of anionic associations.

4.2.1.1 Cyclic [(fluoride)$_2$(water)$_2$] complex of receptor L_4 (4a):

The fluoride-water cluster complex **4a** crystallizes in the monoclinic space group *P*c and single crystal XRD analysis reveals that four urea arms of four different molecules of **L_4** assemble like a barrel entrapping a cyclic fluoride-water tetrameric cluster comprising of two fluoride anions and two water molecules. Though the two urea groups are present in *syn*-fashion unlike the free **L_4** structure, but they are hydrogen-bonded to two different cyclic fluoride-water clusters (Fig. 4.5a). From the hydrogen-bonding environment they can be identified: one is (FW Cluster 1) urea N–H and aryl C−H hydrogen-bonded, and the other one (FW Cluster 2) is only urea N–H hydrogen-bonded. Each pair of cyclic fluoride-water clusters (FW Cluster 1 and 2) is sharing only one receptor molecule and each fluoride ion in the cluster is being coordinated by three urea *via* strong N–H···F and two water O–H···F interactions (Fig. 4.5a), and thus fluoride is penta-coordinated (FW Cluster 2) with one weak extra aromatic C–H···O interaction (FW Cluster 1). Two among the four urea moieties are being shared between fluoride ion and water-O atom of the cyclic cluster where -NH_a and -NH_b respectively are hydrogen-bonded to the F^- and water O atom. The cyclic H-bonded O···F interaction is found to be very strong, being in the range d(O···F) ≤ 2.5-2.8 Å, indicating a strong entrapped discrete cyclic fluoride-water cluster in the solid state (Fig. 4.5a).

4.2.1.2. Bromide complex of receptor L_5 (5b):

DMSO solvated bromide complex **5b** crystallizes in the triclinic system with the space group *P*-1 and X-ray elucidation reveals that, unlike the hydrated fluoride complex **4a,** the nearly linear receptor **L_5** is coordinated to one bromide ion by one of the two urea groups through two urea N–H···Br hydrogen-bonds. The other urea moiety is coordinated to a DMSO solvent molecule *via* two urea N–H···O (DMSO) hydrogen-bonds (Fig. 4.6c). The bromide ion is also coordinated to the *n*-TBA cation and the DMSO molecule hydrogen-bonded to the other urea moiety

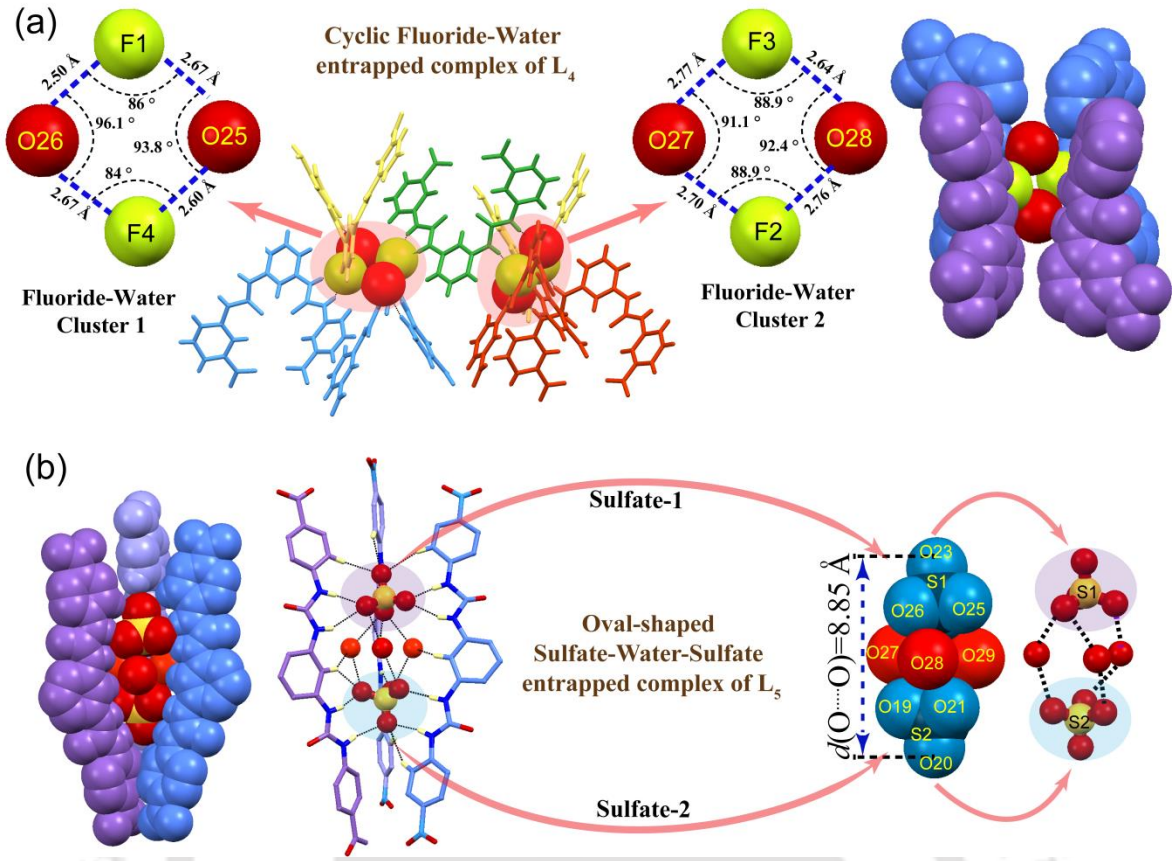

Figure 4.5 X-ray structure of complex **4a** (partial) depicting (a) two neighboring cyclic fluoride-water clusters with different environment and magnified view of intra-hydrogen bonding in FW-Cluster 1, FW-Cluster 2 and full entrapment of the guest in spacefill representation; X-ray structure of complex **5a** (partial) depicting (b) sulfate-(water)$_3$-sulfate entrapped host assembly in spacefill representation, non-covalent interactions involved in hydrated-sulfate trapping, magnified view of the oval-shaped adduct and intra-hydrogen bonding in sulfate-water cluster.

and thus overall having a coordination number of four. So, from XRD analysis it is evident that in halide complex **4a**, the two urea groups of semi-circular receptor **L$_4$** bind two different fluoride ions conforming two different fluoride-water tetrameric clusters, whereas in halide complex **5b** the two urea moieties of linear receptor **L$_5$** projecting in the same direction bind one bromide ion and one DMSO molecule separately (Fig. 4.6c), which could be the consequences of positional isomeric variation of receptors' nitro group.

4.2.1.3 Fluoride complexes of receptors L$_6$ (6c) and L$_7$ (7b)

The suitable crystals fluoride complexes **6c** of **L$_6$** and **7b** of **L$_7$** obtained from basic DMSO solutions crystallize in the monoclinic *P*21/n space group and orthorhombic *P*212121 space group respectively. In both complexes receptor **L$_6$** and **L$_7$** orients in semicircular fashion and entrap two symmetry-identical fluoride anions by non-cooperative hydrogen-bonding of urea N–H groups (Fig. 4.8e, g). The fluoride anions in complexes **6c** and **7b,** each exhibit hexa- and penta-coordination respectively. In both complexes, fluoride anions accept four strong N–H···F hydrogen bonds from two different ligands, whereas the fluoride ion receives two (Fig. 4.8e) and

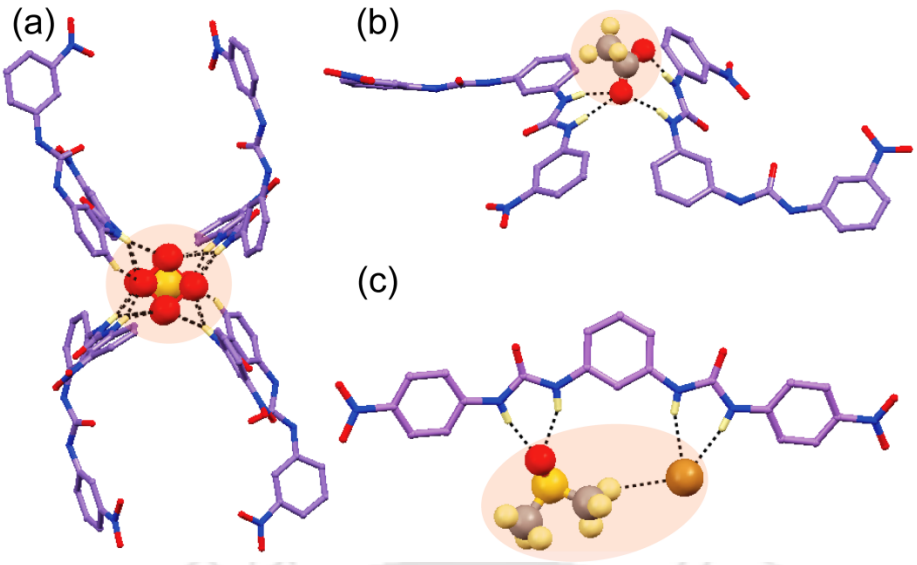

Figure 4.6 X-ray structures (partial) depicting (a) entrapment of SO_4^{2-} anion in **4b** by semi-circular receptor mode, (b) entrapment of SO_4^{2-} anion in complex **4c** by semi-circular receptor mode and (c) entrapment of DMSO coordinated bromide anion in complex **5b** by linear receptor mode.

one (Fig. 4.8g) C–H···F cation-anion hydrogen bonds in respective complexes **6c** and **7b**. Additionally, the urea carbonyl groups of receptor in each complex are projecting in the same direction stabilize the fluoride binding *via* weak C–H···O and two C–H···π contacts with *n*-TBA cations.

4.2.1.4. Bromide complex of receptor L_6 (6d):

The bromide complex **6d** crystallizes in orthorhombic *Pbca* space group and the asymmetric unit of the crystal contains a semicircular $\mathbf{L_6}$ receptor unit (Fig. 4.8f), as similar in fluoride complexes **6c** and **7b**. Structural elucidation reveals that in **6d**, one of the two symmetry-independent tetra-coordinated bromide anions, Br1 receives two N–H···Br, one aromatic C–H···Br and one *n*-TBA C–H···Br cation-anion hydrogen bond, whereas the other tetra-coordinated Br2 accepts two N–H···Br receptor–anion and two *n*-TBA C–H···Br cation-anion hydrogen bonds (Fig. 4.8f). The complex **6d** gains extra stability by additional weak C–H···O interactions among receptor carbonyl groups and *n*-TBA cations.

4.2.1.5 Acyclic [(chloride)$_2$(water)$_2$] complex of receptor L_8 (8d):

The chair-shaped hydrated-chloride [(Cl^-)-(H_2O)-(H_2O)-(Cl^-)] complex **8d** crystallizes in the monoclinic *I*2/c space group. Although some cyclic halide water tetrameric cluster [$(X)_2(H_2O)_2$] (X = F, Cl, Br) encapsulation or entrapmen by dipodal or tripodal synthetic receptors were reported in recent past by Ghosh *et al.* and our group,[4.4, 4.12] but the recognition of chair-like acyclic halide-water tetrameric guest by a synthetic receptor is very rare in literature. The asymmetric unit of the crystal contains one $\mathbf{L_8}$ receptor unit, one chloride anion, one (two half-occupied) water molecule and one *n*-TBA^+ counter-cation. Structural elucidation reveals that the

terminal aryl *meta*-disubstituted receptor **L_8** non-cooperatively binds the hydrated-chloride guest in complex **8d**, maintaining the *syn* orientations of urea N–H groups with respect to the central aromatic ring (Fig. 4.10d), unlike the DMF and DMSO-solvated free **L_8** receptor structures. The four urea arms of four symmetry-identical molecules of **L_8** assemble like a barrel entrapping a chair-shaped acyclic chloride-water-water-chloride cluster (Fig. 4.9d) comprising two symmetry-identical chloride ions Cl1 and two symmetry-identical water molecules. Two urea groups of a particular receptor unit are hydrogen-bonded to two symmetry-independent chloride-water clusters. Each chloride ion in the acyclic tetrameric cluster is hydrogen bonded by two strong urea N–H···Cl and one water O–H···Cl intra-cluster interactions, whereas each water oxygen atom is tetra-coordinated *via* two strong urea N– H···O, one O–H···O and one O–H···Cl contacts. It is also evident that four urea groups of four identical receptor units (N3–H3N & N4–H4N bind Cl1 and N1–H1N & N2–H2N bind half-occupied O3A & O3B) coordinate either the chloride anion or water molecule (through six-membered H-bonded rings) by either two strong N–H···Cl or two strong N–H···O interactions (Fig. 4.9d). The space-fill view along the crystallographic *a* axis display a dumbbell-shaped structural construction (Fig. 4.10e), whereas a ball-stick view along the crystallographic *c* axis demonstrates a beautiful bat shaped architecture (Fig. 4.10f) of tetrameric hydrated-chloride anionic guest with **L_8**.

4.2.2. Structural analysis of oxyanion bound complexes of receptors L_4-L_8

Single crystal XRD analyses of *meta*-phenylenediamine based terminal aryl mono- or di-functionalized neutral receptors with oxyanions/hydrated-oxyanions/oxyanion associations also demonstrate the consistent as well as discriminating binding behavior of neutral receptors toward planar, tetrahedral or octahedral anionic guests of various dimensionalities depending upon either the positional isomeric effect of terminal aryl receptor substituents or the size of oxyanion guests.

4.2.2.1 Sulfate complex of receptor L_4 (4b):

The sulfate complex **4b** of *meta*-nitrophenyl substituted receptor **L_4** crystallizes in the monoclinic space group *P*21/c and structural elucidation exposes that similar to the cyclic fluoride-water cluster complex **4a** of **L_4**, the four urea arms of four different molecules of **L_4** assemble like a barrel to entrap a sulfate anion (Fig. 4.6a). Each of the four O atoms of the sulfate anion is disordered in two positions showing a total of eight O atoms with half occupancy each. A total of 22 strong N–H···O interactions are stabilizing the disordered sulfate (Fig. 4.6a) anion and thus, a well-ordered sulfate anion can be viewed to have a coordination of 11 hydrogen-bonding interactions. Additionally, two weak *ortho*-aryl C–H···O interactions also helps to stabilize the sulfate anion entrapment.

4.2.2.2 Acetate complex of receptor L_4 (4c):

The acetate complex of **4c** crystallizes in the monoclinic space group *P*21/c and X-ray analysis exposes that the planar acetate anion is coordinated by two urea moieties of two different $\mathbf{L_4}$ receptor conformers through four N–H···O (acetate) interactions where one of the two acetate O atoms is being trifurcated (Fig. 4.6b) and note that, similar to the other complexes of $\mathbf{L_4}$, the carbonyl O atoms are pointing opposite side to the anion, conforming a semi-circular ligand architecture. The weak *n*-TBA C–H···O (carbonyl) interactions also provide extra stability towards complexation.

4.2.2.3 [(Sulfate)-(water)$_3$-(sulfate)] complex of receptor L_5 (5a):

The sulfate-water-sulfate complex **5a** of *para*-nitrophenyl substituted receptor $\mathbf{L_5}$ crystallizes in the triclinic the space group *P*-1 and structural elucidation discloses a beautiful receptor-anion architecture where three host molecules of $\mathbf{L_5}$ assemble like a linear barrel to fully entrap a [SO_4^{2-}-$(H_2O)_3$-SO_4^{2-}] oval shaped adduct (Fig. 4.6b). Interestingly, the *meta*-nitro derivative $\mathbf{L_4}$ orients in a *semi*-circular fashion, whereas the *para*-nitro derivative $\mathbf{L_5}$ orients in a linear fashion in the solid state upon anion complexation. In complex **5a**, the three $\mathbf{L_5}$ conformers form the edges of the barrel structure and the three upper urea functions entrap a sulfate anion (sulfate-1) in the axial mode with six N–H···O and four *ortho*-aryl C–H···O hydrogen-bonds (Fig. 4.6b). Two of the three O atoms of sulfate in the downward face further hydrogen-bonded to three water molecules through O–H···O interactions (O···O = 2.85-3.01 Å). These three water molecules are again further hydrogen-bonded to three O atoms of another upward facing sulfate anion (sulfate-2), which is entrapped by the lower three urea functions *via* six N–H···O and three *ortho*-aryl C–H···O hydrogen-bonds. Thus, the water molecules, which are getting extra stability from *meta*-phenylene C–H···O weak interactions, are the bridges between the two face-to-face oriented sulfate anions resulting in an oval-shaped rugby ball with axial length of *d*(O···O) = 8.85 Å (Fig. 4.6b). Overall the sulfate anions exhibit optimum coordination with 13 for sulfate-1 and 12 for sulfate-2 where all the N–H···O (sulfate) interactions are in strong H-bonding range *d*(H···O) ≤ 2.5 Å and *d*(D···O) ≤ 3.2 Å.

4.2.2.4 [Carbonate-(water)$_2$-carbonate] complex of receptor L_6 (6a):

Colorless needle-type good quality crystals of tetrabutylammonium carbonate salt unusually with water molecules are obtained from DMF/DMSO solution mixture of chloro-methylphenyl aryl di-substituted receptor $\mathbf{L_6}$ (complex **6a**) and excess tetrabutylammonium hydroxide (*n*-TBAOH). Carbonate anions were not present in the mixed solvent medium prior to crystallization and the incorporation of carbonate in the system could be due to the

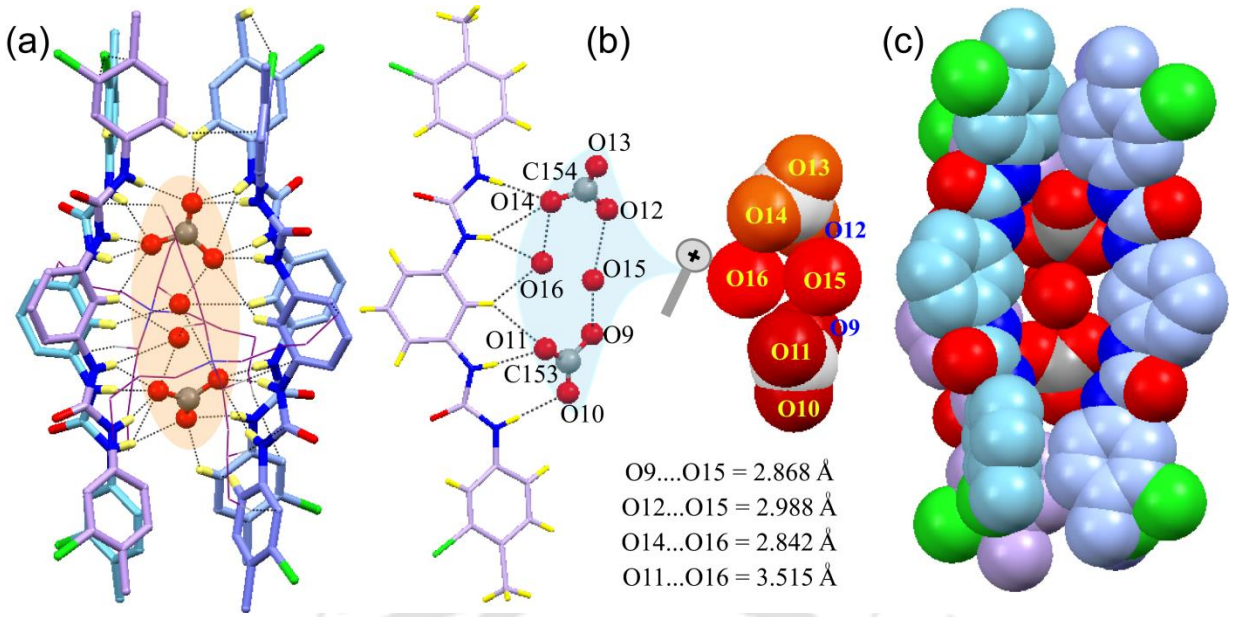

Fig 4.7 X-ray structure of complex **6a** (partial) depicting (a) hydrogen bonding contacts in hydrated-carbonate entrapment of $\mathbf{L_6}$, (b) magnified view showing *intra*-hydrogen bonding and distances in oval-shaped carbonate-$(water)_2$-carbonate cluster and (c) spacefill view of hydrated-guest entrapment inside tetrameric host barrel.

transformation of aerial CO_2 to CO_3^{2-} in basic DMF/DMSO solution. Hydroxide ions from *n*-TBAOH salt dissolve aerial CO_2 to CO_3^{2-} in the air-solvent interface resulting in the formation and crystallization of the $[CO_3^{2-}\text{-}(H_2O)_2\text{-}CO_3^{2-}]$ entrapped linear tetrameric barrel of $\mathbf{L_6}$ (Fig. 4.7a, c). Note that, crystallization of complex **6a** from the air/solvent interface is because of the higher CO_3^{2-} concentration in that area due to the consequence of aerial CO_2 contact with the solvent surface. Structural elucidation reveals that *in situ*-generated hydrated complex **6a** crystallizes in the monoclinic non-centrosymmetric space group *Cc* and four symmetry-independent $\mathbf{L_6}$ conformers beautifully preorganize themselves by displaying good cooperativity of urea N-H groups constructing long straight tetrameric pillars that fully entrap the unprecedented $[CO_3^{2-}\text{-}(H_2O)_2\text{-}CO_3^{2-}]$ cluster by eighteen strong N–H···O hydrogen bonds from eight urea groups and seven aryl-C–H···O hydrogen bonds from the receptors (Fig. 4.7). Note that, four $\mathbf{L_6}$ receptors construct the edges of the barrel architecture among which the upper four urea functions entrap the C154 carbonate ion in the axial mode with nine N–H···O hydrogen bonds and one *ortho*-aryl C–H···O hydrogen bond. Then, the two (O12 and O14) among the three C154 carbonate O atoms in the downward face are further O–H···O hydrogen-bonded to two water molecules O15 and O16 respectively, out of which the O15 water molecule is further O–H···O H-bonded directly and the O16 water molecule is C–H···O hydrogen-bonded consecutively *via* the *ortho*-aryl C–H group with two (O9 and O11 respectively) upward facing C153 carbonate O atoms, which are further trapped by the lower four urea functions *via* nine N–H···O and three *ortho*-aryl C–H···O hydrogen bonds (Fig. 4.7a, b). Thus, two independent water molecules, of penta-coordinated O15 and tetra-coordinated O16, which get extra stability from

the weak *meta*-phenylene C–H···O and *n*-TBA C–H···O interactions, act as the bridges between two face-to-face oriented carbonate ions, resulting in an oval-shaped unique carbonate-water-carbonate cluster (Fig. 4.7b). Some previous examples with evidence of CO_2 fixation using tetrabutylammonium fluoride/hydroxide salts within artificial receptors were reported by Gunlaugsson *et al.*, Gale *et al.*, Ghosh *et al.*, and also from our group.[4.13] However, herein we have demonstrated the entrapment of an innovative hydrated carbonate cluster within the tetrameric barrel receptor **L_6** *via* induction of hydroxide induced aerial CO_2 fixation.

4.2.2.5 Double sulphate complexes of receptors L_6 (6b) and L_7 (7a)

The non-hydrated sulfate complexes **6b** and **7a** of halo-methyl di-substituted receptors **L_6** and **L_7** respectively crystallize in the same triclinic *P*-1 space group and the asymmetric unit of the isostructural crystals contain two symmetry-independent **L_6**/**L_7** conformers and one (*n*-TBA)$_2SO_4$ unit in each case. Structural elucidation reveals that two pairs of symmetry-independent **L_6**/**L_7** ligand molecules construct the edges of the linear tetrameric pillar (Fig. 4.8b, d), which fully entrap the two symmetry-identical deprotonated hydrogensulfate anionic guests (entirely sealed with *n*-TBA cations) by a total of 22 (in **6b**) and 30 (in **7a**) N–H···O and C–H···O hydrogen-bonding interactions through all eight urea N–H groups, *ortho*-aryl C–H groups of the four receptors and *n*-TBA C–H groups directed towards the barrel cavity (Fig. 4.8a, c). In complex **6b** each sulfate exhibit coordination number of 11 (Fig. 4.8a), while in complex **7a** each sulfate exhibit coordination number of 15(Fig. 4.8c). Both the double sulfate entrapped complexes are additionally stabilized by weak intermolecular C–H$\cdots\pi$ and $\pi\cdots\pi$ interactions. The entrapment of divalent SO_4^{2-} anion by deprotonation of HSO_4^- in both complexes can be attributed to the hydrogen-bonding-activated proton transfer between the free and bound anions.

4.2.2.5 Naked and hydrated asymmetric sulfate complex of receptor L_8 (8a)

The unusual and asymmetric sulfate-coordinated complex **8a** of bis-(trifluoromethy)-phenyl substituted bis-urea receptor **L_8** is achieved from DMSO solution of ligand and excess *n*-TBAHSO$_4$ and it crystallizes in the monoclinic space group *P*21/c. The asymmetric unit contains three symmetry-independent **L_8** receptor molecules, which differ considerably in their dihedral angles of central *meta*-phenylene rings with respect to two terminal aromatic rings and the significant variation of coordination environments of each receptor. The X-ray structural elucidation reveals that, unusually, there are two types of symmetry-independent sulfate anions present in the unit cell of **8a**, out of which one is water-free naked divalent sulfate and another is $R_3^3(5)$-type cyclic [sulfate-(water)$_2$] cluster (Fig. 4.9a, b). One of the three symmetry-independent receptor units asymmetrically binds one naked sulfate and one hydrated-sulfate

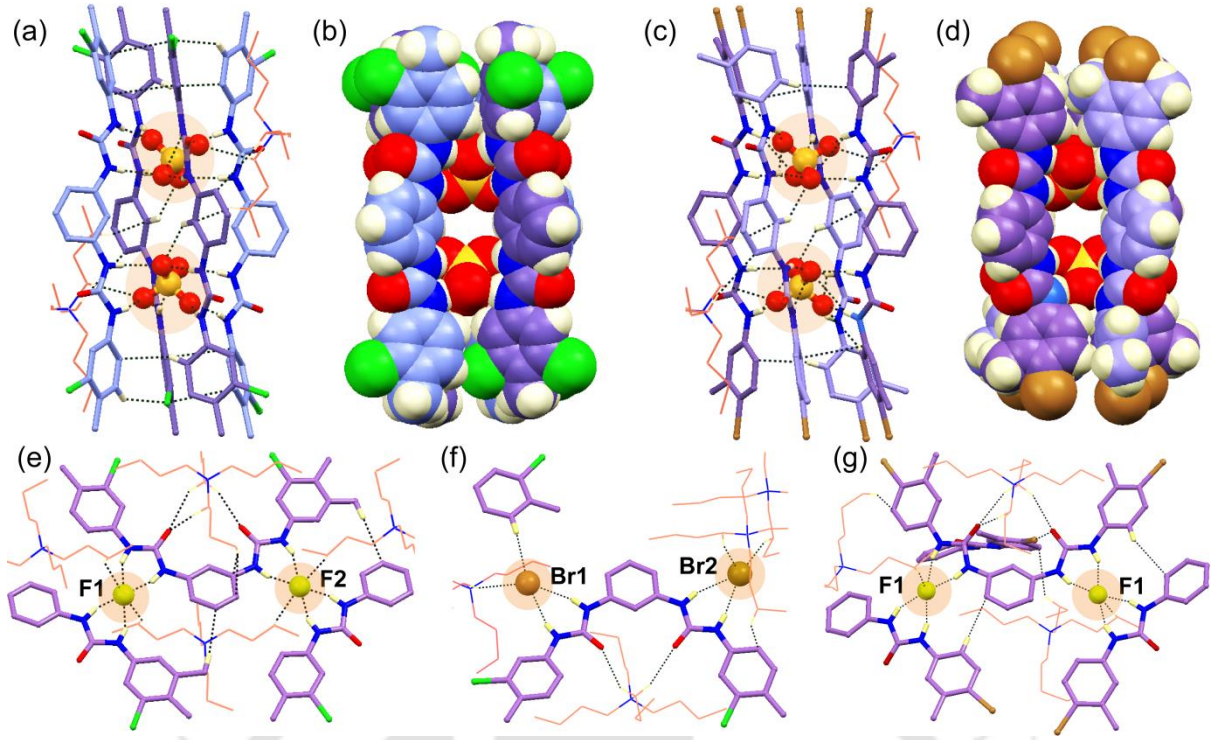

Fig 4.8 X-ray structure (partial) depicting (a) hydrogen bonding contacts involved in double-sulphate entrapment of $\mathbf{L_6}$ tetramer, (b) spacefill representation of host-guest assembly in complex **6b**, (c) hydrogen bonding contacts involved in double-sulphate entrapment of $\mathbf{L_7}$ tetramer, (b) spacefill representation of host-guest assembly in complex **7a**; The hydrogen bonding contacts of halides with *semi*-circular receptor $\mathbf{L_6}$/$\mathbf{L_7}$ and *n*-TBA cations in (e) complex **6c**, (f) complex **6d** and (g) complex **7b**.

separately, using two urea N–H groups (Fig. 4.9a, c). In contrast, the second receptor binds two naked sulfate ions separately and the third receptor unit binds two cyclic hydrated-sulfate ions separately, using their two urea N–H moieties (Fig. 4.9c) *via* strong urea N–H···O (sulfate) hydrogen-bonding interactions (Fig. 4.9a). Unlike the free DMF and DMSO solvated ligand $\mathbf{L_8}$, the orientations of each urea N-H moiety with respect to the central benzene ring of a particular receptor unit become *syn* in complex **8a** and the receptor architecture becomes more bent during non- cooperative anion binding. The tetrahedral divalent SO_4^{2-} bound in both hydrated as well as non-hydrated form, are actually generated from monovalent HSO_4^- anion by H-bonding activated proton transfer reaction. Each naked sulfate ion is coordinated by seven strong N–H···O and six C–H···O interactions, whereas each cyclic hydrated-sulfate cluster is coordinated by seven strong N–H···O, seven C– H···O and three intra-cluster O–H···O interactions (Fig. 4.9a). In the binding of both naked and hydrated sulfate, the two urea groups from two identical conformers bind two edges of the tetrahedral anion (through eight-membered H-bonded rings), while one urea group of a distinct conformer chelates one vertex of sulfate (through six membered H-bonded rings) and one edge of the tetrahedral anion (through eight-membered H-bonded rings). Although the O7, O8 and O9 atoms are trifurcated, the O10 atom receives four hydrogen bonds in non-hydrated sulfate, whereas in hydrated sulfate ion, O11 and O12 atoms

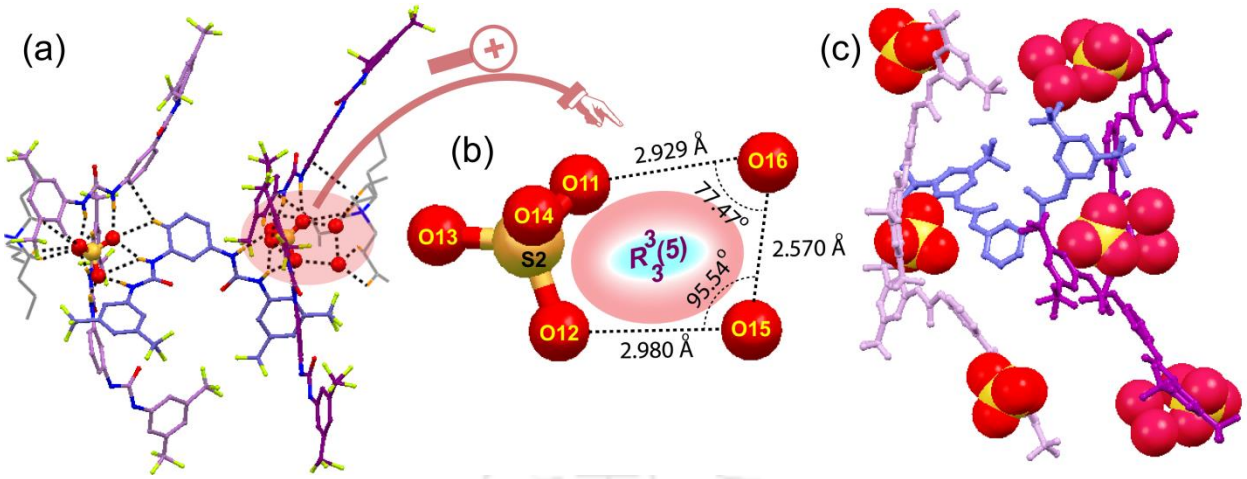

Fig. 4.9 X-ray structure (partial) depicting (a) coordination environment around naked and hydrated-sulphate in complex **8a**, (b) magnified view showing *intra*-cluster hydrogen bonding and distances in cyclic sulphate-$(water)_2$ cluster, (c) entrapment of asymmetric sulphate anions (spacefill) simultaneously by one (blue in ball-stick) of the three symmetry-identical receptors and symmetric sulphate coordination by other two ligands (pale blue and purple in ball-stick).

are trifurcated, but O13 and O14 receive four and two hydrogen bonds respectively. Thus, in asymmetric sulfate- coordinated complex **8a**, both naked and hydrated-sulfate exhibit optimum coordination numbers of 13 and 12 respectively (Fig. 4.9a).

4.2.2.6 Bicarbonate-dimer complex of receptor L_8 (8b)

Colorless crystals of bicarbonate dimer entrapped complex of receptor $\mathbf{L_8}$ are attained from the DMSO solution ligand and excess *n*-TBAF. Complex **8b** crystallizes in the monoclinic space group *P*21/c where the source bicarbonate is atmosphere and generated by fluoride ion induced aerial CO_2 fixation. The X-ray analysis reveals that two symmetry-identical $\mathbf{L_8}$ molecules with opposite orientation non-cooperatively bind two symmetry-independent bicarbonate by strong N–H···O interactions, and these two distinct bicarbonate anions conform a $R_2^2(8)$-type cyclic bicarbonate dimer *via* two strong O–H···O intra-dimer face-to-face interactions (Fig. 4.10a). Note that, one particular ligand unit binds two bicarbonate anions by using the two urea moieties in a non-cooperative manner. Unlike the free $\mathbf{L_8}$ receptor, the orientation of urea N-H groups becomes *syn* with respect to the central benzene ring (Fig. 4.10a) and the receptor architecture is even more bent in complex **8b** rather than sulfate complex **8a**, which may be ascribed to the relatively large bicarbonate dimer trapping sealed by four *n*-TBA cations. The X-ray structure clearly shows that C57-bicarbonate accepts two strong urea N–H···O, one *ortho*-aryl C–H···O and three *n*-TBA C–H···O hydrogen-bonds (where O3 is trifurcated and O4 and O5 receive two H-bonds each) and C58-bicarbonate coordinates by two strong urea N–H···O, one *ortho*-aryl C–H···O and two *n*-TBA C–H···O H-bonds (where O6 is trifurcated and O7 and O8 accept two and one H-bonds respectively). In each $(HCO_3)_2$ trapping, the two different urea groups from two

identical conformers (N1–H1N & N2–H2N bind O3 & O4 and N3–H3N & N4–H4N bind O6 & O7, respectively) bind two edges of symmetry-independent planar bicarbonate (through eight-membered H-bonded rings). Overall, the C57 and C58 bicarbonates exhibit coordination numbers of 8 and 7 respectively (Fig. 4.10a).

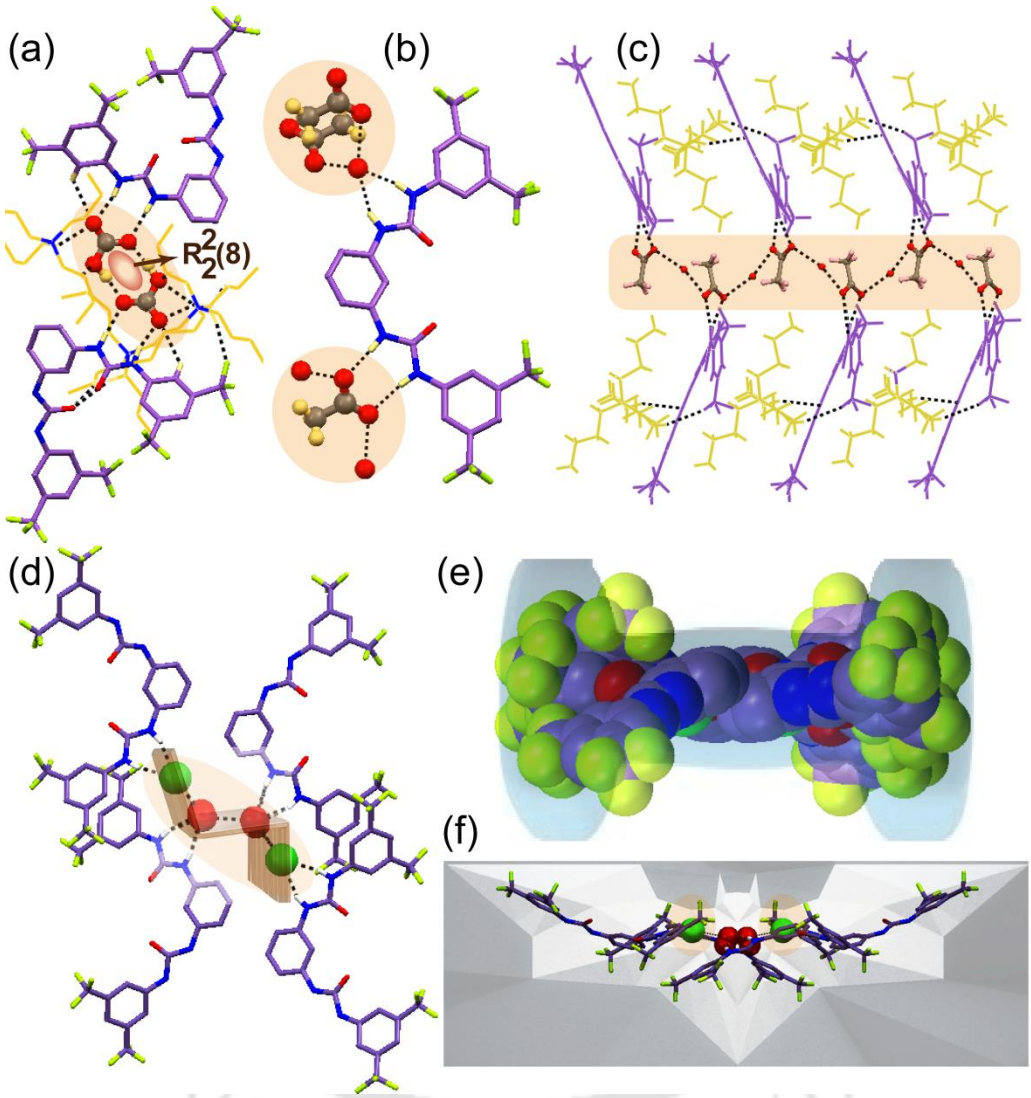

Fig. 4.10. X-ray structures (partial) depicting (a) hydrogen bonding contacts involved in cyclic bicarbonate dimer entrapment in complex **8b**, (b) N–H···O (acetate) and N–H···O (water) contacts involved in $[(acetate)(water)]_n$ cluster trapping in complex **8c**, (c) packing motif of acetate-water polymeric aggregated host-guest assemblies along crystallographic *a* axis (d) hydrogen bonding contacts involved in chair-shaped acyclic hydrated-chloride cluster entrapment in complex **8d**, (e) dumbbell shaped construction of complex **8d** (spacefill view) along crystallographic *b* axis, (f) bat-shaped architecture of tetrameric hydrated-chloride (ball-stick view) trapping by $\mathbf{L_8}$.

4.2.2.7 Polymeric hydrated acetate complex of receptor L_8 (8c)

The hydrated acetate complex **8c** crystallizes in the monoclinic space group *P*21 and the asymmetric unit contains one $\mathbf{L_8}$ receptor unit, one acetate anion, one water molecule and one *n*-TBA^+ counter-cation. Note that unlike the free $\mathbf{L_8}$ receptor, the urea N–H groups of a particular receptor unit in complex **8c** orient in a non-cooperative *syn* fashion (Fig. 4.10b), similar like the

complexes **8a** and **8b**. The crystal structure clearly shows that one urea group of a particular receptor unit (N1–H1N and N2–H2N bind with O3 and O4, respectively) coordinates one edge of a planar acetate anion (through eight-membered H-bonded rings) by two strong urea N–H···O (acetate) interactions, while the second urea N-H group of that receptor unit (N3–H3N and N4–H4N bind with O5) coordinates with a single water molecule (through six-membered H-bonded rings) by two strong urea N–H···O (water) interactions. The O3 and O4 oxygen atoms of the first urea-coordinated acetate are further O–H···O hydrogen-bonded with two symmetry-identical water O5 oxygen atoms separately, whereas the second urea coordinated water O5 atom is further O–H···O H-bonded separately with O3 and O4 acetate oxygen atoms of two symmetry-identical acetate anions (Fig. 4.10b). In hydrated-acetate $[(OCOCH_3)(H_2O)]_n$ cluster, both the guest acetate and water molecule exhibit tetra-coordination. The crystal packing along the crystallographic *a* axis clearly displays the formation of a linear polymeric aggregated $[(acetate)\text{-}(water)]_n$ cluster assembly of receptor $\mathbf{L_8}$ coordinated by *n*-TBA counter cations (Fig. 4.10c).

4.3 Solution-state anion binding studies

The solution-state anion binding properties of *meta*-phenylenediamine based dipodal bis-urea receptors $\mathbf{L_4}$-$\mathbf{L_8}$ are investigated by qualitative as well as quantitative ^{1}H NMR experiments in DMSO-d_6 using the quaternary ammonium (*n*-TBA/TEA) salts of different anions as evidenced from the solid state studies. The most significant change has been observed for the urea –NH proton, as expected, indicating that the -NH function acts as the primary site for anion recognition. Fig. 4.11a,b and Fig. 4.12a,b show the chemical shift changes observed upon gradual addition of F^- and SO_4^{2-} (DMSO-d_6) solution as their *n*-TBA salts to the individual solutions of $\mathbf{L_4}$ and $\mathbf{L_5}$, respectively. The ^{1}H NMR analysis of the cyclic fluoride-water complex **4a** showed an average downfield shift of $\Delta\delta$ = 1.75 ppm for the -NH protons in its ^{1}H NMR data, whereas the titration data of $\mathbf{L_4}$ with aliquots of standard *n*-TBAF solution give the best fit for mixed equilibrium between 1:1 and 1:2 host-guest stoichiometry with an apparent log K value of 4.02. After the addition of 1.0 eqv. of F^-, the urea -NH protons of $\mathbf{L_4}$ are shifted by $\Delta\delta$ = 1.77 ppm (Figure 4.11a), indicating more proficient participation of $-NH_a$ than $-NH_b$ in the host-guest assembly, supported by the solid-state evidence (Fig. 4.5a). But in the case of $\mathbf{L_5}$, F^- causes less shift to the urea -NH protons with an average of $\Delta\delta$ = 0.85 ppm ($-NH_a$) (Fig. 4.11b), which give the best fit for close to 1:2 host-guest stoichiometry with an apparent log K value of 3.82, indicating it to be a relatively much less efficient host for fluoride. Sulfate anion entrapped complex **4b** show an average downfield shift of $\Delta\delta \sim 1.20$ ppm for the -NH protons in its ^{1}H-

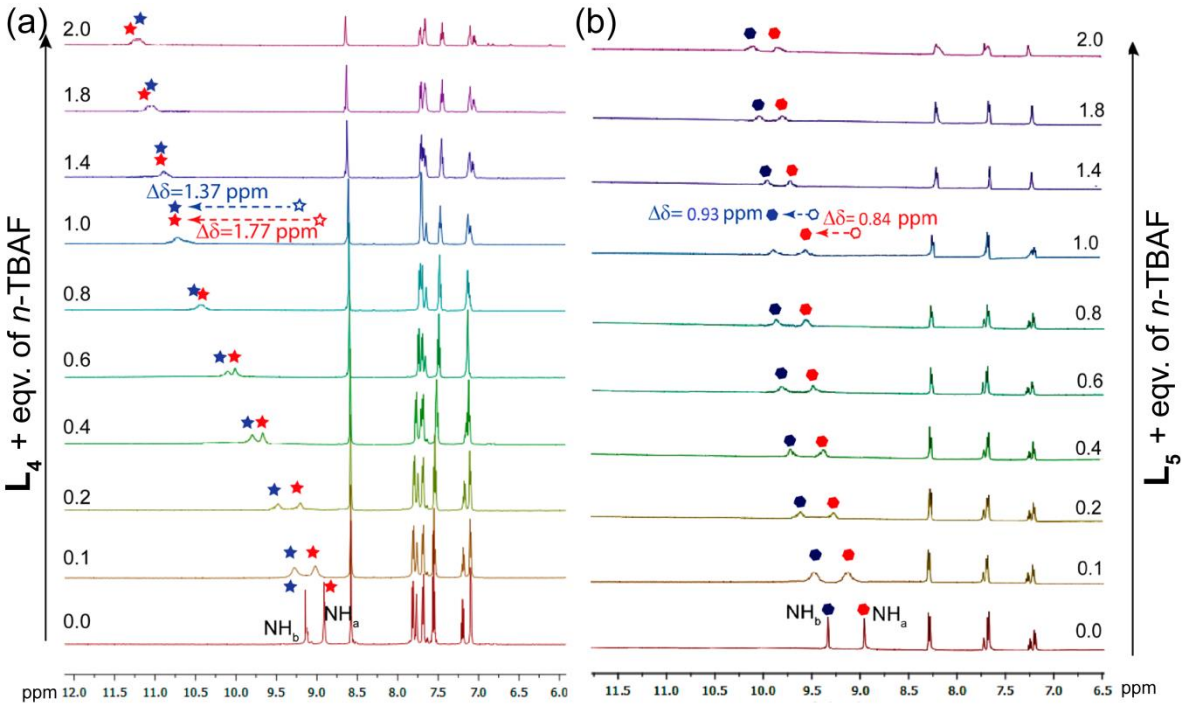

Figure 4.11 Expanded partial ^{1}H NMR spectra of (a) **L$_4$** and (b) **L$_5$**, upon titration with *n*-TBAF in DMSO-d_6.

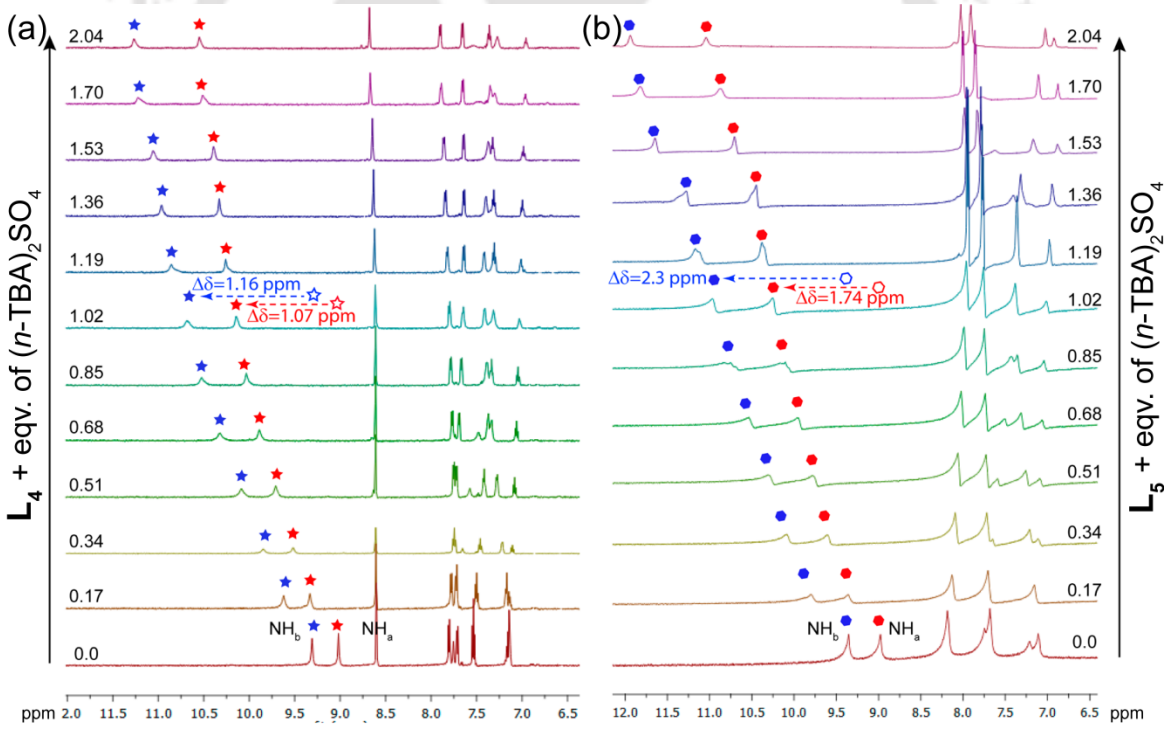

Figure 4.12 Expanded partial ^{1}H NMR spectra of (a) **L$_4$** and (b) **L$_5$**, upon titration with *n*-TBA$(SO_4)_2$ in DMSO-d_6.

NMR data and titration data of **L$_4$** with aliquots of standard $(n\text{-TBA})_2SO_4$ solution give the best fit for mixed equilibrium between 1:1 and 1:2 host-guest stoichiometry with an apparent log K value of 3.93. The sulfate-water-sulfate complex **5a** has shown an almost similar shift of the urea -NH protons like **4b** with an average of $\Delta\delta \sim 1.25$ ppm. However, the ^{1}H NMR titration of **L$_5$** with standard sulfate solution has shown that after 1.0 eqv. anion addition , both the **L$_5$** urea -NH protons experience a huge shift by $\Delta\delta = 1.7$ ppm (-NH$_a$) and $\Delta\delta = 2.3$ ppm (-NH$_b$) (Fig.

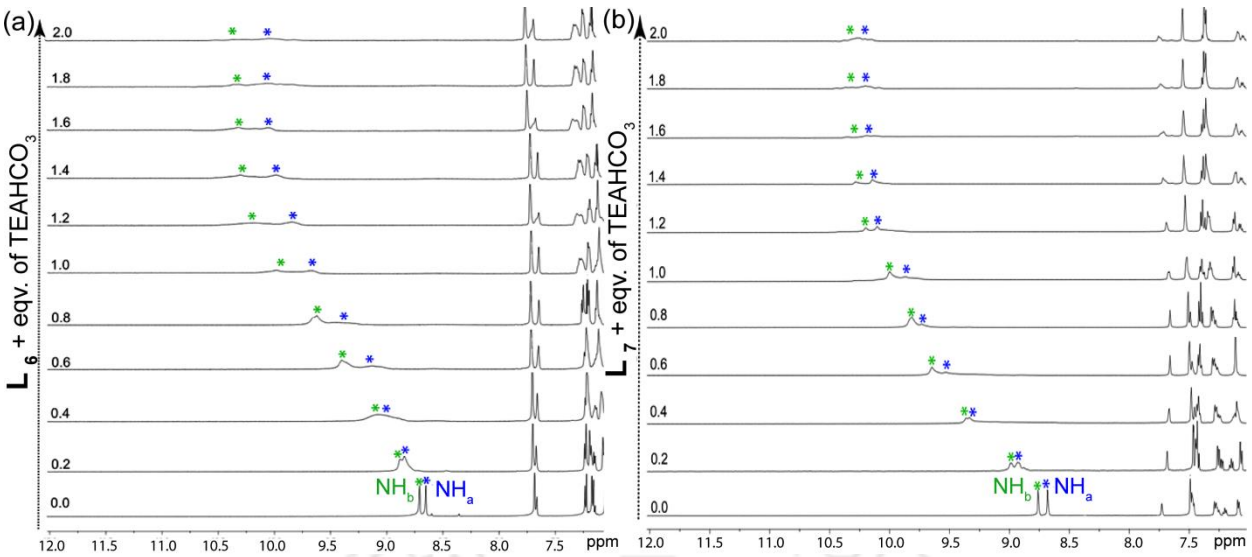

Figure 4.13 Expanded partial ^{1}H NMR spectra of (a) **L$_6$** and (b) **L$_7$**, upon titration with $TEAHCO_3$ in DMSO-d_6.

4.12b). Thus, ^{1}H NMR quantitative solution study signifies receptor **L$_4$** to be more proficient host for fluoride, while **L$_5$** to be more proficient host for sulfate, an indication from solid-state evidence also confirms the same. Job's plot of **L$_5$**-SO_4^{2-} titration has given the best fit for mixed equilibrium between 1:1 and 1:2 host-guest stoichiometries with an apparent log K value of 4.06. ^{1}H NMR analysis of the acetate complex **4c** and bromide complex **5b** showed an average downfield shift of $\Delta\delta$ = 1.55 ppm and 0.10 ppm respectively. On the other hand, the chemical shift changes observed upon quantitative gradual addition of $TEAHCO_3$ to the individual DMSO-d_6 solutions of **L$_6$** and **L$_7$** show a similar average downfield shift of $\Delta\delta$ = 1.50 ppm (Fig. 4.13a) and $\Delta\delta$ = 1.49 ppm (Fig. 4.13b) respectively followed by severe broadening of the -NH signals. Although the carbonate-water entrapped complex **6a** of chloro-methyl substituted ligand **L$_6$** shows an average -NH downfield shift of only $\Delta\delta$ = 0.71 ppm, which indeed is supported from the solution state results where similar strong participation from both the urea protons occur. The ^{1}H NMR titration data of **L$_6$** and **L$_7$** with aliquots of standard $TEAHCO_3$ solution show the best fit for a mixed equilibrium between the 1:1 and 1:2 host-guest stoichiometries. Then in the quantitative ^{1}H NMR titration of both receptors with standard sulfate solutions, the -NH resonances experience an average downfield shift of $\Delta\delta$ = 1.14 ppm and $\Delta\delta$ = 1.13 ppm respectively, which also provide the best fit for a mixed equilibrium. Subsequently, the sulfate complexes **6b** and **7a** show average downfield shift of $\Delta\delta$ = 1.14 ppm and $\Delta\delta$ = 1.05 ppm, respectively for the -NH protons in the ^{1}H NMR which is strongly supported by the solution state study because of the equal and strong participation of both the urea protons toward SO_4^{2-} binding with both receptors. Moreover, the fluoride complexes **6c** and **7b** respectively exhibit an average downfield shift of $\Delta\delta$ = 0.56 ppm and $\Delta\delta$ = 0.34 ppm in their ^{1}H NMR data, while in

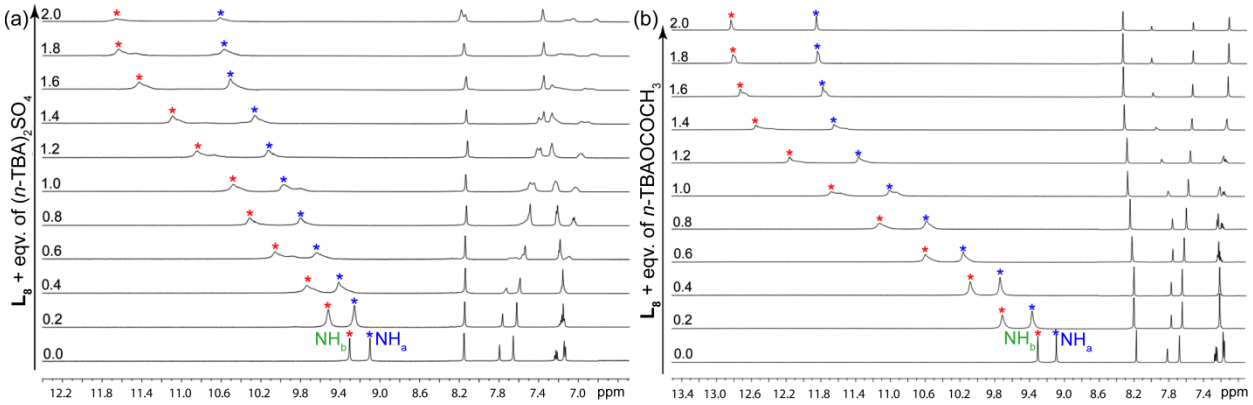

Figure 4.14 Expanded partial ^{1}H NMR spectra of $\mathbf{L_8}$ on titration with standard (a) SO_4^{2-} and (b) OAc^-, in DMSO-d_6.

the quantitative ^{1}H NMR titration with standard fluoride solutions, the -NH resonances experience a huge average downfield shift of $\Delta\delta$ = 2.78 ppm and $\Delta\delta$ = 2.27 ppm respectively followed by massive broadening. However, on addition of other anions like chloride, bromide, iodide, nitrate, and perchlorate, no appreciable changes in the chemical shift values of the -NH signals are observed, indicative of almost no binding with ligands. The NOESY spectra of the novel hydrated carbonate complex **6a** display significantly strong NOE couplings of urea -NH protons and highly acidic *ortho*-aryl protons with water (H-O-H) (Fig. A4.1b), while no such types (N-H···H-O-H) of interactions are observed in the case of the free receptor $\mathbf{L_6}$, instead some through-space interactions between the urea NH_a and *ortho*-aryl proton (Fig. A4.1a) are detected and these results also suggest the efficient trapping of the unique hydrated carbonate guest within the linear barrel assembly of $\mathbf{L_6}$ fully supported by the X-ray structures of **6a**. Furthermore, the solution-state anion binding of receptor $\mathbf{L_8}$ are studied with the standard *n*-TBA salts of individual sulfate (Fig. 4.14a) and acetate (Fig. 4.14b), which demonstrate the considerable chemical shift changes in their ^{1}H-NMR titration spectra. The asymmetric sulfate coordinated complex **8a** shows an average downfield shift of $\Delta\delta$ = 1.58 ppm for the -NH protons in its ^{1}H NMR data, whereas quantitative titration data of $\mathbf{L_8}$ with aliquots of standard (*n*-TBA)$_2SO_4$ solution show downfield average shift of $\Delta\delta$ = 2.04 ppm followed by little -NH peak broadening (Fig. 4.14a), which gives the best fit for mixed equilibrium between 1:1 and 1:2 host-guest stoichiometry in Job's plot. The association constant of $\mathbf{L_8}$ with sulfate anion results the log K11 and log K12 values of 2.44 and 5.04 respectively. Similarly, the hydrated acetate complex **8c** shows an average downfield shift of $\Delta\delta$ = 3.40 ppm for the -NH protons in its ^{1}H-NMR data (Fig. 4.14b), while titration experiments of $\mathbf{L_8}$ with aliquots of standard acetate solution exhibit a huge average downfield and sharp -NH shift of $\Delta\delta$ = 3.15 ppm, that gives the best fit for 1:1 host–guest stoichiometry in Job's plot. The overall log K11 of $\mathbf{L_8}$ with acetate is found to be 2.31. The -NH_a and -NH_b shifts in qualitative as well as quantitative ^{1}H-NMR experiments indicate more proficient participation of -NH_b than -NH_a in the host-guest

assembly, which is also supported from the solid-state evidence. Furthermore, the bicarbonate dimer complex **8b** shows average chemical shift of $\Delta\delta$ = 2.50 ppm as relatively broad -NH signals in its ^{1}H-NMR data, but the gradual quantitative addition up to 2.0 equiv. of $TEAHCO_3^-$ solution results in severe and huge broadening of downfield shifted urea -NH protons. Subsequently, the disappearance followed by severe broadening of both urea -NH signals of $\mathbf{L_8}$ upon titration with *n*-TBAF salts is observed due to proton abstraction. The binding constant for bicarbonate and fluoride with $\mathbf{L_8}$ could not be determined due to massive broadening and even vanishing of -NH signals during the titration process. The hydrated chloride complex **8d** shows negligible average downfield shift ($\Delta\delta$ = 0.014 ppm for the -NH protons in its ^{1}H NMR data) compared to oxyanions, indicating relatively less binding of chloride in the solution state. Overall, the binding of a particular anion with respective receptor and the discrepancies of the binding mode in the solid and solution states are common in the literature. As in the solid state, the anion binding within the receptor cavity is stabilized by a number of non-covalent interactions; hence receptors exhibit well-organized and compact conformation with the respective anions. Meanwhile, due to the very loose orientations of the receptor and anion in solution, a different host-guest binding stoichiometry is observed in most of the cases, which is mainly governed by the weaker non-covalent interactions.

4.4 Conclusion

In conclusion, the rational design of terminal aryl mono- as well as di-substituted rigid *meta*-phenylenediamine bridged bis-urea receptors $\mathbf{L_4}$-$\mathbf{L_8}$ are effective towards systematic and consistent recognition of both anions and hydrated anions despite the less preorganized receptor architecture, depending upon either the positional isomeric effect of terminal aryl receptor substituent or size of the anionic guests. Firstly, two positional isomeric nitrophenyl functionalized bis-urea receptors $\mathbf{L_4}$ and $\mathbf{L_5}$ unveil them as the efficient hosts toward fluoride-water cluster and sulfate-water adducts respectively as evidenced from the solid state as well as the solution state. Receptor $\mathbf{L_4}$ is also authenticated structurally to entrap non-hydrated sulfate anion and to be a good receptor for acetate anion *via* semicircular receptor orientations, while $\mathbf{L_5}$ forms host-guest assembly with the cation and DMSO coordinated bromide anion *via* linear receptor structure. Furthermore, among the halo-methylphenyl aryl di-functionalized bis-urea receptors $\mathbf{L_6}$ and $\mathbf{L_7}$, the 3-chloro-4-methyl substituted receptor $\mathbf{L_6}$ has efficiently entrapped the OH^- ion fixed air-stable unique $[CO_3^{2-}\text{-}(H_2O)_2\text{-}CO_3^{2-}]$ oval-shaped cluster within the linear tetrameric receptor barrel, consistently corroborated by the quantitative ^{1}H NMR titration and 2D-NOESY NMR studies in the solution state. However, the formation of water-free double sulfate entrapped almost isostructural 4:2 host-guest complexes has been found within the linear

tetrameric cooperative barrel of both the isomeric receptors **L_6** and **L_7**. Moreover, both halo-methylphenyl functionalized receptors form either fluoride or bromide trapped non-cooperative host-guest self-assembly *via* construction of semicircular ligand architecture. On the other hand, the bis-(trifluoromethyl)-phenyl aryl di-substituted bis-urea receptor **L_8** has been proved to be a decent receptor for recognition of hydrated anions in solid as well as in solution state. Receptor **L_8** in its neutral form and with its very highly acidic urea -NH groups effectively entrap, the asymmetrically coordinated (hydrated and naked) divalent sulfate anions, fluoride ion-induced $(HCO_3)_2$ dimer by aerial CO_2 fixation, polymeric acetate-water cluster and acyclic chair-shaped unique acyclic chloride-water tetrameric guest. Hence, the results obtained from host-guest self-assemblies and calculating the terminal aryl centroid distances in each anion complex of *meta*-phenylenediamine based bis-urea receptors **L_4-L_8**, it is clearly concluded that the architecture and anion binding modes of particular receptor in respective anion complexes are heavily governed by either the positional isomeric variation of terminal aryl substituents or anion dimensions in case of receptors **L_4-L_7**, but the terminal aryl *meta*-disubstitutionin **L_8** become regularly accountable for the non-cooperative anion binding mode and the semi-circular architecture of receptor in its anion complexes irrespective of the guest dimensions. Overall, the report of substituent-driven systematic anion/hydrated anion binding of the potential bis-urea receptors is reliable to interpret the data and consistent to justify the variation, which would be useful to develop new categories of uncommon host-guest assemblies.

References

4.1 (a) P. A. Gale, *Acc. Chem. Res.*, 2006, **39**, 465; (b) D. A. Jose, D. K. Kumar, B. Ganguly and A. Das, *Org. Lett.*, 2004, **6**, 3445.

4.2 (a) C. A. Ilioudis, D. A. Tocher and J. W. Steed, *J. Am. Chem. Soc.*, 2004, **126**, 12395; (b) G. W. Bates, P. A. Gale and M. E. Light, *Chem. Commun.*, 2007, 2121; (c) *Anion Coordination Chemistry*, *ed.* K. Bowman-James, A. Bianchi and E. Garcia-España, Wiley-VCH, New York, 2012.

4.3 (a) M. Arunachalam and P. Ghosh, *Chem. Commun.* 2009, 5389; (b) T. W. Hudnall, C.-W. Chiu, F. P. Gabbai, *Acc. Chem. Res.* 2009, **42,** 388; (c) M. Arunachalam and P. Ghosh, *Inorg. Chem*. 2010, **49**, 943.

4.4 (a) P. D. Beer, P. A. Gale and D. K. Smith, *Supramolecular Chemistry; Oxford University Press*: Oxford, U.K., 1999; (b) J. L. Sessler, P. A. Gale and W. S. Cho, *Anion Receptor Chemistry: Monographs in Supramolecular Chemistry;* RSC Publishing: Cambridge, UK, 2006.

4.5 (a) M. Zuhayra, W. U. Kampen, E. Henze, Z. Soti, L. Zsolnai, G. Huttner and F. Oberdorfer, *J. Am. Chem.* Soc. 2006, **128**, 424; (b) B.-Q. Ma, H.-L. Sun and S. Gao, *Chem. Commun*. 2004, 2220; (c) M. Mascal, L. Infantes, J. Chisholm, *Angew. Chem., Int. Ed.* 2006, **45**, 32; (d) S. O. Kang, D. Powell, V. W. Day and K. Bowman-James, *Cryst. Growth Des.* 2007, **7**, 606; (e) M. Yoshizawa, T. Kusukawa, M. Kawano, T. Ohhara, I. Tanaka, K. Kurihara, N. Niimura and M. Fujita, *J. Am. Chem. Soc.* 2005, **127**, 2798.

4.6 (a) H. Ohtaki, T. Radnai, *Chem. Rev.* 1993, **93**, 1157; (b) D. T. Richens, *The Chemistry of Aqua Ions;* Wiley: Chichester, 1987.

4.7 (a) P. A. Gale, S. E. Garcıa-Garrido and J. Garric, *Chem. Soc. Rev*., 2008, **37**, 151; (b) C. Caltagirone and P. A. Gale, *Chem. Soc. Rev*., 2009, **38**, 520.

4.8 (a) Cametti, M.; Rissanen, K. *Chem. Commun*. 2009, 2809; (b) Kang, S. O.; VanderVelde, D.; Powell, D.; Bowman-James, K. *J. Am. Chem. Soc.* 2004, **126**, 12272 (c) *A systematic review of the efficacy and safety of fluoridation*, National Health and Medical Research Council, Australian Government, 2007, available at: http://www.nhmrc.gov.au/. (d) J. W. Pflugrath and F. A. Quiocho, *Nature*, 1985, **314**, 257; (e) T. H. Milby and R. C. Baselt, *Am. J. Ind. Med.*, 1999, **35**, 192; (f) K. Caldeira, A. K. Jain and M. I. Hoffert, *Science*, 2003, **299**, 2052; (g) *Climate Change, 2007: Synthesis Report, International Panel on Climate Change*; Cambridge University Press: Cambridge, U.K., 2007

4.9 (a) S. K. Dey, A. Basu, R. Chutia, and G. Das *RSC Adv.*, 2016, **6**, 26568; (b) R. Dutta and P. Ghosh *Chem. Commun.*, 2014, **50**, 10538.

4.10 (a) R. Li, Y. Zhao, S. Li, P. Yang, X. Huang, X.-J. Yang and B. Wu, *Inorg. Chem*., 2013, **52**, 5851; (b) S. J. Brooks, P. R. Edwards, P. A. Gale and M. E. Light, *New J. Chem*., 2006, **30**, 65; (c) L. E. Karagiannidis, C. J. E. Haynes, K. J. Holder, I. L. Kirby, S. J. Moore, N. J. Wells and P. A. Gale, *Chem. Commun.*, 2014, **50**, 12050.

4.11(a) U. Manna, R. Chutia, and G. Das *Cryst. Growth Des.* 2016, **16**, 2893; (b) U. Manna, S. Kayal, S. Samanta and G. Das *Dalton Trans*., 2017, **46**, 10374; (c) U. Manna and G. Das *CrystEngComm*, 2017, **19**, 5622.

4.12 (a) A. Basu and G. Das, *Chem. Commun.*, 2013, **49**, 3997; (b) S. Chakraborty, R. Dutta, M. Arunachalam and P. Ghosh, *Dalton Trans.*, 2014, **43**, 2061; (c) U. Manna, S. Kayal, B. Nayak and G. Das *Dalton Trans.*, 2017, **46**, 11956

4.13(a) T. Gunnlaugsson, P. E. Kruger, P. Jensen, F. M. Pfeffer and G. M. Hussey, *Tetrahedron Lett.*, 2003, **44**, 8909; (b) S. J. Brooks, P. A. Gale and M. E. Light, *Chem. Commun*., 2006, 4344; (c) I. Ravikumar and P. Ghosh, *Chem. Commun*., 2010, **46**, 1082; (d) S. K. Dey, R. Chutia and G. Das, *Inorg. Chem*., 2012, **51**, 1727.

Annexure 4

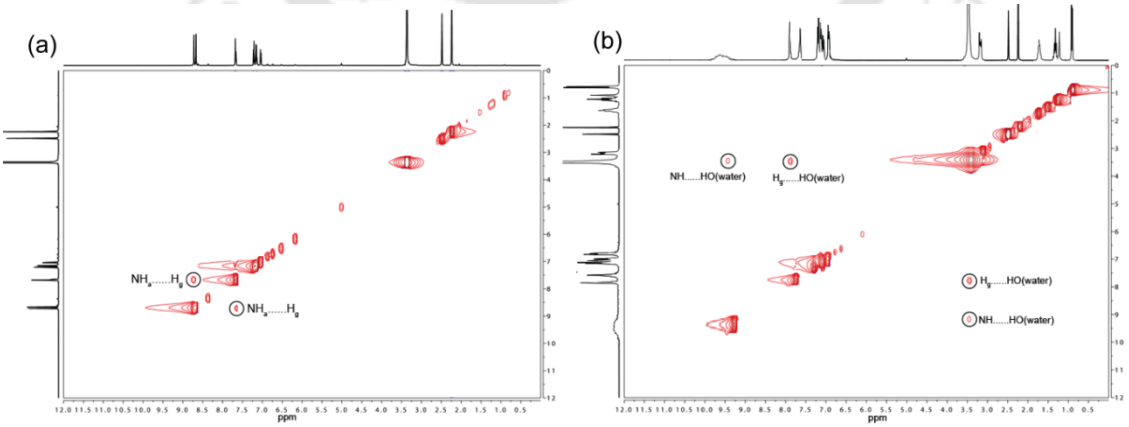

Fig A4.1 2D-NOESY NMR spectra of (a) free $\mathbf{L_6}$ receptor and (b) isolated carbonate-(water)$_2$-carbonate complex **6a** in DMSO-d$_6$.

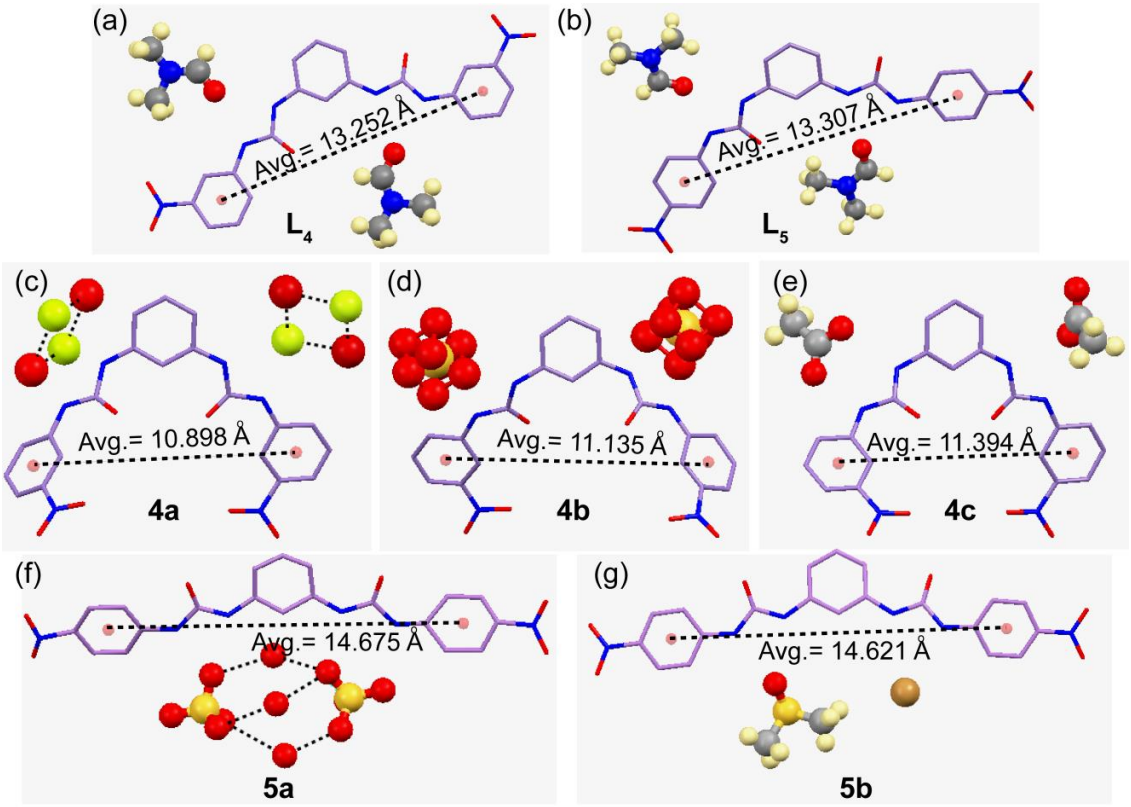

Figure A4.2 X-ray structures (partial) depicting average terminal aryl centroid distances in (a) DMF-solvated free receptor $\mathbf{L_4}$, (b) DMF-solvated free receptor $\mathbf{L_5}$, (c) hydrated-fluoride complex **4a**, (d) sulfate complex **4b**, (e) acetate complex **4c**, (f) hydrated-sulfate complex **5a** and (g) DMSO-coordinated bromide complex **5b**.

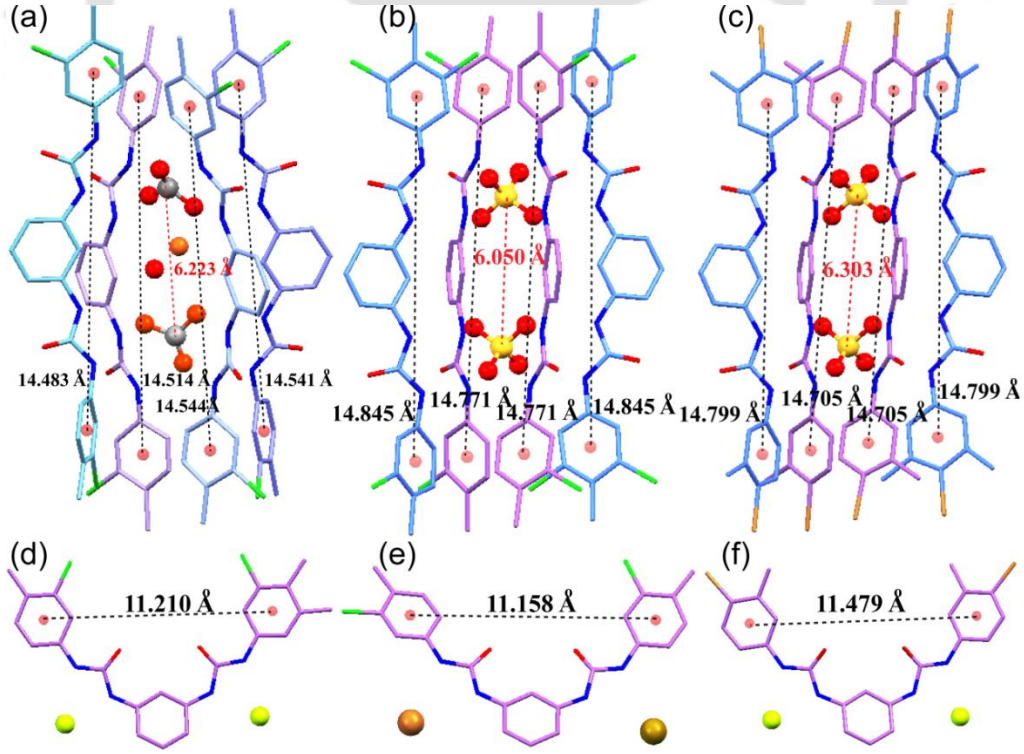

Fig A4.3 X-ray structures (partial) depicting average terminal aryl centroid distances and intra-guest distances inside tetrameric barrel (as applicable) in (a) hydrated-carbonate complex **6a**, (b) double sulfate trapped complex **6b**, (c) double sulfate trapped complex **7a**, (d) fluoride complex **6c**, (e) bromide complex **6d** and (f) fluoride complex **7b**.

Table A4.1 Crystallographic parameters and refinement details of receptors L_4-L_5 and their anion complexes

Parameters	L_4	4a	4b	4c	L_5	5a	5b
Formula	$C_{26}H_{30}N_8O_8$	$C_{36}H_{52}FN_7O_7$	$C_{72}H_{104}N_{14}O_{20}S$	$C_{38}H_{55}N_7O_8$	$C_{26}H_{30}N_8O_8$	$C_{60}H_{48}N_{18}O_{29}S_2$	$C_{38}H_{62}BrN_7O_7S$
Fw	582.58	713.85	1473.75	737.89	582.58	1549.28	840.91
Crystal system	Monoclinic	Monoclinic	Monoclinic	Monoclinic	Monoclinic	Triclinic	Triclinic
Space group	*C 2/c*	*P C*	*P2 1/c*	*P2 1/c*	*P* 21/*n*	*P -1*	*P -1*
a/Å	27.673(3)	16.7790(13)	16.8011(7)	16.8967(11)	17.2678(11)	17.903(2)	10.8105(7)
b/Å	14.7494(15)	32.2701(19)	16.5666(8)	17.0645(12)	13.2242(8)	20.595(4)	11.8310(9)
c/Å	15.122(3)	15.5234(14)	15.4398(6)	15.4683(11)	25.5435(15)	23.597(3)	18.7901(17)
α/°	90.00	90.00	90.00	90.00	90.00	110.030(9)	99.875(6)
β/°	106.169(13)	105.795(9)	108.543(3)	110.564(4)	100.374(3)	111.747(7)	95.166(6)
γ/°	90.00	90.00	90.00	90.00	90.00	93.136(9)	111.252(4)
V/Å^3	5928.1(15)	8087.9(11)	4074.4(3)	4175.8(5)	5737.6(6)	7426.0(2)	2176.1(3)
Z	8	8	2	4	8	2	2
D_c/g cm^{-3}	1.306	1.173	1.185	1.174	1.349	0.693	1.283
μ Mo K_α/mm^{-1}	0.099	0.085	0.109	0.083	0.102	0.083	1.045
T/K	298(2)	298(2)	298(2)	298(2)	298(2)	298(2)	298(2)
θ max.	19.25	12.82	23.18	21.84	20.44	15.47	24.46
Total no. of reflections	28691	42094	61251	19254	31799	75492	26172
Independent reflections	5224	41635	10223	7415	10860	25679	5773
Observed reflections	2741	29062	4870	4916	7632	14969	4529
Parameters refined	383	1854	488	483	766	970	504
R_1, I > 2σ(I)	0.0854	0.1024	0.1051	0.0530	0.0655	0.1002	0.0540
wR_2 (all data)	0.3099	0.3184	0.3098	0.1845	0.2058	0.1396	0.1548
GOF (F^2)	1.102	1.180	1.161	1.073	1.007	0.988	1.020
CCDC No.	1450225	1450226	1450227	1450229	1450230	1450231	1450232

Table A4.2 Crystallographic parameters and refinement details of anion complexes of receptors L_6-L_7

Parameters	6a	6b	6c	6d	7a	7b
Formula	$C_{154}H_{226}Cl_8N_{20}O_{16}$	$C_{76}H_{112}Cl_4N_{10}O_8S$	$C_{38}H_{55}Cl_2FN_5O_2$	$C_{54}H_{92}Br_2Cl_2N_6O_2$	$C_{76}H_{111}Br_4N_{10}O_8S$	$C_{38}H_{56}Br_2FN_5O_2$
Fw	2893.11	1467.62	703.77	1088.04	1644.41	793.68
Crystal system	monoclinic	triclinic	monoclinic	orthorhombic	triclinic	orthorhombic
Space group	*C* c	*P* -1	*P* 21/n	*P* b c a	*P* -1	*P* 21 21 21
a/Å	28.888 (14)	12.812(6)	9.612(6)	15.301(5)	12.800(8)	9.595(10)
b/Å	23.264(9)	16.220(7)	19.079(19)	25.296(8)	16.278(7)	18.924(12)
c/Å	24.761(11)	21.053(9)	21.675(17)	31.713(11)	20.793(9)	22.044(17)
α/°	90.00	73.309(3)	90.00	90.00	74.842(4)	90.00
β/°	97.383(4)	83.915(3)	91.739(6)	90.00	84.573(4)	90.00
γ/°	90.00	84.668(3)	90.00	90.00	84.538(4)	90.00
V/Å^3	16502.5(13)	4158.2(3)	3973.1(6)	12275.0(7)	4151.6(4)	4002.4(6)
Z	4	2	4	8	2	4
D_c/g cm^{-3}	1.164	1.172	1.177	1.178	1.316	1.317
μ Mo K_α/mm^{-1}	0.200	0.223	0.206	1.448	2.020	2.067
F000	6208.0	1572.0	1508.0	4624.0	1714.0	1656.0
T/K	298(2)	298(2)	298(2)	298(2)	298(2)	298(2)
θ max.	28.770	28.453	28.901	25.321	28.849	28.676
Total no. of reflections	42484	63157	19914	96099	37580	12928
Independent reflections	39853	19182	9752	10728	20041	9727
Observed reflections	12984	12020	3673	5199	9516	6225
Parameters refined	1748	958	457	615	915	439
R_1, I > 2σ(I)	0.1042	0.0754	0.0821	0.0593	0.0930	0.0808
wR_2, I > 2σ(I)	0.2619	0.1890	0.1925	0.1537	0.1699	0.1491
GOF (F^2)	0.939	0.976	1.115	1.029	1.088	0.964
CCDC No.	1536469	1536470	1536471	1536472	1536473	1536474

Table A4.3 Crystallographic parameters and refinement details of anion complexes of receptors $\mathbf{L_8}$

Parameters	$\mathbf{L_8}$.DMF	$\mathbf{L_8}$.DMSO	**8a**	**8b**	**8c**	**8d**
Formula	$C_{57}H_{49}F_{24}N_{11}O_7$	$C_{28}H_{26}F_{12}N_4O_4S_2$	$C_{136}H_{186}F_{36}N_{16}O_{16}S_2$	$C_{58}H_{88}F_{12}N_6O_8$	$C_{42}H_{53}F_{12}N_5O_5$	$C_{40}H_{50}ClF_{12}N_5O_3$
Fw	1456.07	774.65	3049.13	1225.34	935.89	912.30
Crystal system	monoclinic	monoclinic	monoclinic	monoclinic	monoclinic	monoclinic
Space group	*P 21/c*	*P 21/c*	*P 21/c*	*P 21/c*	*P 21*	*I 2/c*
a/Å	16.624(8)	17.969(15)	22.490 (8)	19.591 (19)	13.450(11)	25.970 (11)
b/Å	21.501(8)	20.983(14)	22.667(7)	22.197 (14)	8.627(15)	8.754(5)
c/Å	20.832(9)	9.532 (10)	31.102(13)	16.033(14)	20.472(2)	45.267(3)
α/°	90.00	90.00	90.00	90.00	90.00	90.00
β/°	111.63(5)	104.71(9)	96.970(3)	102.823(9)	94.730(8)	104.053(5)
γ/°	90.00	90.00	90.00	90.00	90.00	90.00
V/Å^3	6922.1(6)	3476.3(5)	15738.0(10)	6798.4(10)	2367.4(5)	9983.0(10)
Z	4	4	4	4	2	8
D_c/g cm^{-3}	1.397	1.480	1.287	1.197	1.313	1.214
μ Mo K_α/mm^{-1}	0.137	0.256	0.138	0.101	0.118	0.159
F000	2960.0	1576.0	6392.0	2600.0	976.0	3792.0
T/K	298(2)	298(2)	298(2)	298(2)	298(2)	298(2)
θ max.	28.957	28.827	28.876	28.816	28.732	28.867
Total no. of reflections	36632	17317	71348	39758	12485	22919
Independent reflections	17117	8651	38839	16771	11419	12349
Observed reflections	5729	3326	29512	9160	7479	4724
Parameters refined	934	519	1890	764	592	654
R_1, I > 2σ(I)	0.1122	0.0957	0.1072	0.1262	0.1119	0.0969
wR_2, I > 2σ(I)	0.3241	0.2466	0.2547	0.2939	0.2513	0.2723
GOF (F^2)	1.171	1.171	1.152	1.171	1.177	1.186
CCDC No.	1551278	1551279	1551280	1551281	1551282	1551283

Table A4.4 Details of Hydrogen Bonding contacts in receptors $\mathbf{L_4}$-$\mathbf{L_5}$ and their anion complexes

Complex	D−H···A	*d*(H···A)/Å	*d*(D···A)/Å	<D−H···A/°
$\mathbf{L_4}$	N2H···O8	2.061(3)	2.88(4)	158.6(2)
	N3H···O8	2.086(3)	2.90(4)	157.1(2)
	N4H···O7	2.130(3)	2.95(4)	157.8(2)
	N5H···O7	2.090(3)	2.90(4)	156.9(2)
4a	N2H···F1	1.881(8)	2.67(1)	152.2(7)
	N3H···F1	1.878(7)	2.68(1)	155.6(7)
	N21H···F1	1.989(9)	2.79(1)	154.6(7)
	N16H···F4	1.916(7)	2.70(1)	150.9(7)
	N17H···F4	1.856(8)	2.66(1)	155.8(7)
	N4H···F4	1.943(9)	2.75(2)	156.0(8)
	N10H···F2	2.052(7)	2.86(1)	156.2(7)
	N22H···F2	1.909(6)	2.69(1)	150.3(6)
	N23H···F2	1.878(6)	2.67(9)	153.1(6)
	N8H···F3	1.847(6)	2.65(1)	153.9(6)
	N9H···F3	1.899(6)	2.68(9)	150.3(6)
	N15H···F3	1.989(7)	2.83(1)	164.7(7)
4b	N2H···O7	2.08(1)	2.89(1)	157.3(4)
	N2H···O8	2.106(7)	2.90(9)	152.4(4)
	N3H···O7	2.308(9)	3.34(8)	151.1(4)
	N3H···O9	2.388(8)	3.11(1)	141.8(4)
	N3H···O10	1.999(8)	2.83(1)	163.4(4)
	N4H···O7	2.155(8)	2.90(9)	144.5(4)
	N4H···O9	2.137(7)	2.98 (8)	168.6(4)
	N5H···O8	2.069(6)	2.90(7)	161.7(4)
	N5H···O10	2.085(7)	2.86(8)	148.7(4)
4c	N2H···O9	1.966(6)	2.821(9)	173.9(4)
	N3H···O8	1.983(4)	2.820(8)	163.6(4)
	N4H···O8	2.015(3)	2.836(7)	159.4(4)
	N5H···O8	2.066(3)	2.863(5)	153.6(4)
$\mathbf{L_5}$	N2H···O16	2.066(3)	2.878(4)	157.0(2)
	N3H···O16	2.003(2)	2.828(3)	160.5(2)
	N4H···O17	2.117(3)	2.927(4)	156.9(2)
	N5H···O17	2.082(2)	2.901(3)	158.9(2)
	N8H···O19	2.134(2)	2.937(4)	155.4(2)
	N9H···O19	2.076(3)	2.901(4)	160.4(2)
	N10H···O13	2.030(2)	2.854(4)	159.9(2)

	N11H···O13	2.064(3)	2.869(4)	155.7(2)
5a	N2H···O20	2.244(4)	3.082(6)	164.7(4)
	N3H···O19	1.931(6)	2.746(9)	157.8(5)
	N4H···O26	2.499(4)	3.284(8)	152.0(5)
	N5H···O26	1.986(3)	2.839(6)	170.8(5)
	N8H···O25	2.031(3)	2.876(6)	167.7(5)
	N9H···O25	2.237(4)	3.053(6)	158.4(5)
	N10H···O21	2.011(4)	2.868(7)	174.2(5)
	N11H···O20	2.303(6)	3.143(9)	165.5(5)
	N14H···O23	2.211(5)	3.02(1)	155.7(5)
	N15H···O24	2.003(8)	2.86(1)	170.6(4)
	N16H···O22	2.346(6)	3.101(1)	147.2(5)
	N17H···O22	1.872(6)	2.724(1)	170.3(5)
5b	N2H···O7	1.992(3)	2.813(5)	159.6(3)
	N3H···O7	2.151(3)	2.952(5)	154.8(3)
	N4H···Br1	2.658(6)	3.480(4)	160.3(3)
	N5H···Br1	2.435(6)	3.288(4)	171.4(3)

Table A4.5 Details of Hydrogen Bonding contacts in anion complexes of receptors $\mathbf{L_6}$-$\mathbf{L_7}$

Complex	D−H···A	*d*(D···H)/Å	*d*(H···A)/Å	*d*(D···A)/Å	<D−H···A/°	Symmetry codes
6a	N1-H1N···O10	0.86	2.09	2.905(15)	158	x,y,z
	N2-H2N···O11	0.86	1.93	2.781(15)	174	x,y,z
	N4-H4N···O14	0.86	2.06	2.894(17)	164	x,y,z
	N5-H5N···O10	0.86	2.09	2.915(15)	160	x,y,z
	N6-H6N···O9	0.86	2.08	2.932(15)	171	x,y,z
	N7-H7N···O12	0.86	2.07	2.900(16)	163	x,y,z
	N8-H8N···O12	0.86	2.21	2.981(17)	149	x,y,z
	N9-H9N···O13	0.86	2.10	2.878(18)	150	x,y,z
	N10-H10N···O14	0.86	1.93	2.790(17)	177	x,y,z
	N11-H11N···O11	0.86	2.13	2.932(15)	155	x,y,z
	N12-H12N···O11	0.86	2.06	2.860(15)	154	x,y,z
	N13-H13N···O13	0.86	2.01	2.846(18)	165	x,y,z
	N14-H13P···O12	0.86	1.95	2.806(16)	174	x,y,z
	N15-H15N···O9	0.86	2.08	2.939(15)	172	x,y,z
	N16-H16N···O10	0.86	2.23	3.048(16)	158	x,y,z
6b	N1-H1N···O7	0.83	1.99	2.803(9)	167	1-x,1-y,1-z
	N2-H2N···O9	0.87	2.11	2.972(8)	176	1-x,1-y,1-z
	N3-H3N···O5	0.91	2.03	2.893(8)	157	1+x,y,z
	N4-H4N···O5	0.86	2.51	3.217(7)	140	1+x,y,z
	N4-H4N···O8	0.86	2.24	3.057(8)	158	1+x,y,z
	N5-H5N···O8	0.86	2.13	2.923(8)	154	-x,1-y,1-z
	N6-H6N···O9	0.90	2.01	2.887(8)	166	-x,1-y,1-z
	N7-H7N···O5	0.83	2.09	2.922(8)	172	x,y,z
	N8-H8N···O7	0.84	2.02	2.851(8)	172	x,y,z
6c	N1-H1N···F1	0.86	2.04	2.825(4)	152	3/2-x,-1/2+y,1/2-z
	N2-H2N···F1	0.86	1.81	2.639(4)	162	3/2-x,-1/2+y,1/2-z
	N3-H3N···F1	0.86	1.79	2.624(4)	163	1+x,y,z
	N4-H4N···F1	0.86	2.06	2.831(4)	149	1+x,y,z
6d	N4-H1···Br1	0.86	2.49	3.318(7)	162	x,y,z
	N3-H2···Br1	0.86	2.52	3.354(6)	164	x,y,z
	N2-H3A···Br2	0.86	2.63	3.460(5)	163	-1/2+x,1/2-y,-z
	N1-H4A···Br2	0.86	2.56	3.403(5)	166	-1/2+x,1/2-y,-z
7a	N1-H1N···O8	0.86	2.19	2.986(8)	154	1-x,1-y,-z
	N2-H2N···O6	0.86	2.09	2.911(7)	160	1-x,1-y,-z
	N3-H3N···O5	0.86	2.11	2.958(8)	171	x,-1+y,z
	N4-H4N···O7	0.86	2.06	2.864(8)	156	x,-1+y,z
	N5-H5N···O7	0.86	2.04	2.819(7)	151	1-x,1-y,-z
	N6-H6N···O6	0.86	2.15	2.989(7)	165	1-x,1-y,-z
	N7-H7N···O5	0.86	2.08	2.906(7)	160	x,-1+y,z
	N8-H8N···O5	0.86	2.37	3.105(8)	144	x,-1+y,z
	N8-H8N···O8	0.86	2.36	3.151(8)	153	x,-1+y,z
7b	N1-H1N···F1	0.86	1.91	2.722(8)	156	x,y,z
	N2-H2N···F1	0.86	1.86	2.681(8)	159	x,y,z
	N3-H3N···F1	0.86	1.84	2.644(9)	156	-x,1/2+y,1/2-z
	N4-H4N···F1	0.86	2.00	2.793(9)	152	-x,1/2+y,1/2-z

Table A4.6 Details of Hydrogen Bonding contacts in receptors $\mathbf{L_8}$ and its anion complexes

Complex	D−H···A	*d*(D···H)/Å	*d*(H···A)/Å	*d*(D···A)/Å	<D−H···A/°	Symmetry codes
$\mathbf{L_8}$.DMF	N1-H1N···O5	0.86	2.14	2.940(5)	156	1-x,-1/2+y,1/2-z
	N2-H2N···O5	0.86	2.03	2.843(5)	157	1-x,-1/2+y,1/2-z
	N5-H5N···O6	0.86	2.05	2.863(6)	158	1-x,1-y,1-z
	N6-H6N···O6	0.86	2.13	2.932(6)	156	1-x,1-y,1-z
	N7-H7N···O7	0.86	2.00	2.821(6)	161	x,y,z
	N8-H8N···O8	0.86	2.12	2.880(6)	146	x,y,z
$\mathbf{L_8}$.DMSO	N1-H1N···O4	0.86	2.07	2.883(6)	158	1-x,-y,1-z
	N2-H2N···O4	0.86	2.10	2.908(5)	157	1-x,-y,1-z
8a	N1-H1N···O10	0.86	1.97	2.817(7)	168	-1+x,y,z
	N2-H2N···O9	0.86	1.99	2.805(6)	157	-1+x,y,z
	N3-H3N···O8	0.86	2.01	2.843(6)	162	1-x,1/2+y,1/2-z
	N4-H4N···O7	0.86	1.93	2.750(6)	159	1-x,1/2+y,1/2-z
	N5-H5N···O12	0.86	2.26	3.082(8)	160	x,y,z
	N5-H5N···O13	0.86	2.57	3.277(6)	140	x,y,z
	N6-H6N···O13	0.86	2.00	2.831(6)	163	x,y,z
	N7-H7N···O8	0.86	2.05	2.842(6)	153	-1+x,y,z
	N8-H8N···O9	0.86	1.87	2.729(6)	175	-1+x,y,z
	N9-H9N···O14	0.86	1.93	2.769(7)	167	1-x,-1/2+y,1/2-z
	N10-H10N···O12	0.86	2.27	3.113(8)	166	1-x,-1/2+y,1/2-z
	N11-H11N···O11	0.86	1.99	2.845(6)	171	x,y,z
	N12-H12N···O13	0.86	2.01	2.841(6)	162	x,y,z
8b	N1-H1N···O3	0.86	1.89	2.724(5)	165	x,y,z
	N2-H2N···O4	0.86	1.95	2.802(5)	172	x,y,z
	N3-H3N···O7	0.86	1.92	2.777(5)	173	x,y,z
	N4-H4N···O6	0.86	1.92	2.767(5)	167	x,y,z
	O5-H5O···O7	0.99	1.63	2.614(7)	174	-x,1/2+y,1/2-z
	O8-H8O···O4	1.00	1.70	2.611(5)	149	-x,-1/2+y,1/2-z
8c	N1-H1N···O3	0.86	2.01	2.859(8)	169	1-x,-1/2+y,-z
	N2-H2N···O4	0.86	1.94	2.784(8)	168	1-x,-1/2+y,-z
	N3-H3N···O5	0.86	2.17	2.981(7)	157	-1+x,y,z
	N4-H4N···O5	0.86	2.00	2.832(8)	162	-1+x,y,z
8d	N1-H1N···O3A	0.86	2.24	3.059(9)	158	-x,y,1/2-z
	N1-H1N···O3B	0.86	2.37	3.173(14)	155	-x,y,1/2-z
	N2-H2N···O3A	0.86	2.45	3.231(9)	152	-x,y,1/2-z
	N2-H2N···O3B	0.86	2.18	3.023(14)	165	-x,y,1/2-z
	N3-H3N···Cl1	0.86	2.40	3.210(3)	158	x,y,z
	N4-H4N···Cl1	0.86	2.31	3.119(3)	157	x,y,z

Chapter 5

para-Phenylenediamine based isomeric neutral scaffolds: Evidence of cyclic $(HCO_3)_2$-dimer and $(H_2PO_4)_n$-polymer entrapment

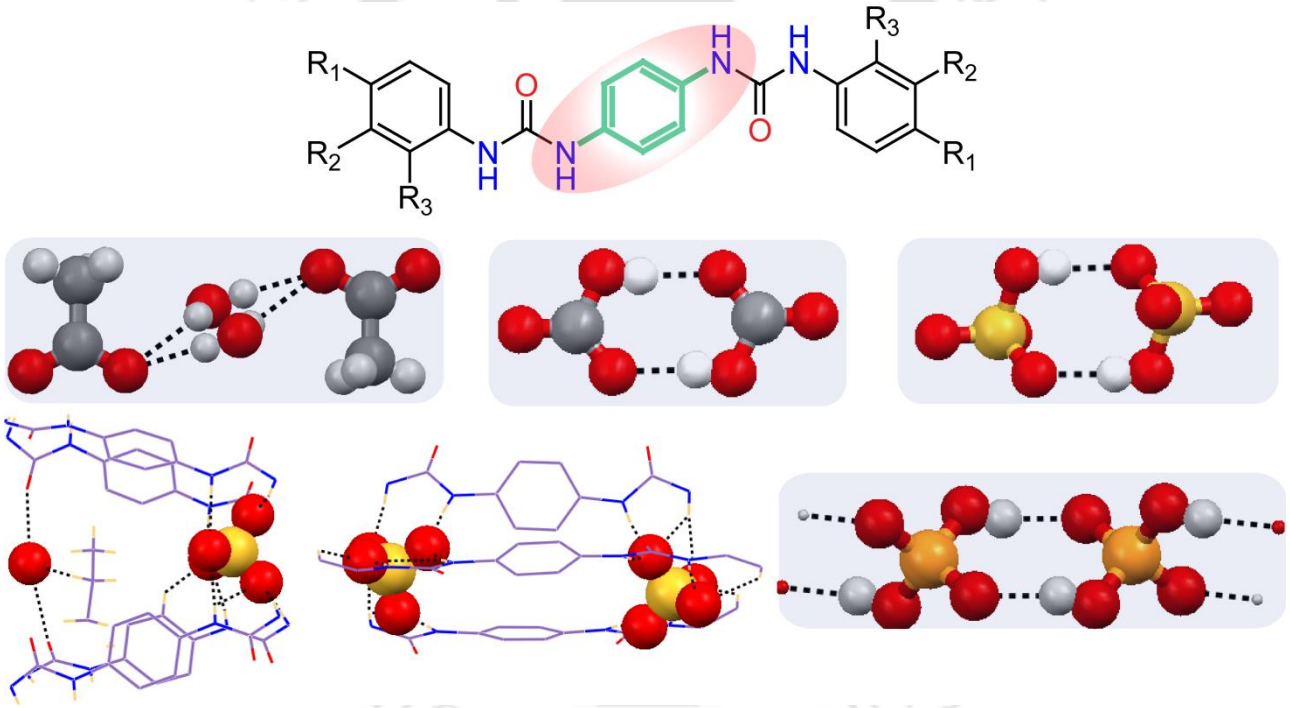

5.1 Background and Focus of the Chapter

Anion-receptor neutral self-assemblies formed by non-covalent interactions is one of the essential and contemporary aspects of supramolecular host-guest chemistry owing to the critical relevance of anions in a range of environmental, biological, medical and chemical routes.[5.1] In natural system, the hydrogen-bonding environment of sulfate binding proteins in *Salmonella typhimurium* bacteria[5.2a] or phosphate binding proteins in *Escherichia Coli* bacteria[5.2b] have also encouraged the researchers to develop various synthetic abiotic receptors containing hydrogen-bond accessible functionalities for recognition of these anions. One of the major environmental issues is the increasing concentration of CO_2 in the atmosphere due to consumption of fossil fuels, the growing number of automobiles, industries, etc. and these demands efficient fixation[5.3] and activation of aerial CO_2 as carbonate/bicarbonate by artificial receptors. Among the spherical halides, the smallest fluoride causes dental, skeletal fluorosis and osteosarcoma, the chloride ion is crucial for biological signal transduction processes and organic solute transportation through the cell membrane and the bromide is one of the essential cofactor for the assembly of collagen IV scaffolds in tissue development.[5.4] On the other hand among oxyanions, carbonate works as buffer in the blood and acetate is used by organisms in the form of acetyl coenzyme A, the harmful effect of sulfate has been recognized as one of the key obstacle to cleanup processes of hard water as well as nuclear waste and high phosphate concentration in aquatic ecosystems is accountable for eutrophication.[5.2,5.5] Thus far, alongside the wide range of tripodal scaffolds derived from aliphatic or aromatic amines mostly containing thio-(urea) functionalities, some dipodal scaffolds with most convergent *ortho*-phenylenediamine spacer among rigid aromatic diamines were reported since the last decade, as they offer structurally preorganized architecture in most of the cases with topological complementarity.[5.6-5.7] Very recently, comparatively less preorganized *meta*-phenynenediamine based rigid dipodal bis-urea anion receptors were also reported by our group and Gunnlaugsson's group.[5.8] However, the dipodal bis-urea receptors derived from linear and least convergent rigid *para*-phenynenediamine spacer for anionic guests of different dimensions is an underexplored research area in supramolecular host-guest chemistry, owing to the less preorganized and less cooperative receptor conformations.

Hence, in continuing our group's interest in the field of substituent directed host-guest self-assemblies, in this chapter we demonstrate the entrapment of anions/hydrated-anions or anionic associations[5.9] within the neutral self-assemblies of seven newly designed and synthesized *para*-phenylediamine based terminal aryl mono- and di-functionalized bis-urea receptors **L_9-L_{15}.** Firstly, a set of positional isomeric nitro-phenyl functionalized three dipodal bis-urea scaffolds

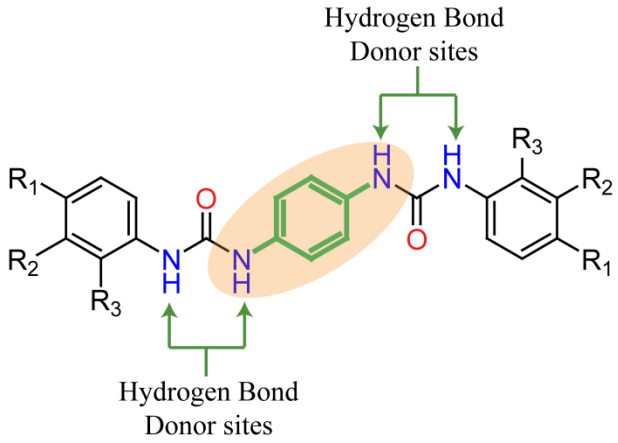

L_9	R_1 = -NO_2,	R_2 = -H,	R_3 = -H
L_{10}	R_1 = -H,	R_2 = -NO_2,	R_3 = -H
L_{11}	R_1 = -H,	R_2 = -H,	R_3 = -NO_2
L_{12}	R_1 = -CH_3,	R_2 = -Cl,	R_3 = -H
L_{13}	R_1 = -Br,	R_2 = -CH_3,	R_3 = -H
L_{14}	R_1 = -Cl,	R_2 = -H,	R_3 = -H
L_{15}	R_1 = -Br,	R_2 = -H,	R_3 = -H

Scheme 5.1 A comprehensive representation of molecular receptor structures included in this chapter.

(**L_9**-**L_{11}**) have been synthesized, where *para*-nitro isomer (**L_9**) and *meta*-nitro-isomer (**L_{10}**) both readily form $(HCO_3)_2$ dimer entrapped non-cooperative self-assemblies **9a**, **10a**, **10b** by either fluoride or hydroxide induced atmospheric CO_2 fixation. The acetate anions in bare and hydrated form are also trapped by hydrogen-bonding interactions in complexes **9b** of **L_9** and **10c** of **L_{10}** respectively. Furthermore, receptor **L_9** entraps $(HSO_4)_2$-dimeric associations (complex **9c**), whereas the receptor **L_{10}** has been found to self-assemble with divalent SO_4^{2-} and linear polymeric associations of $(H_2PO_4)_n$ by non-cooperative hydrogen-bonding interactions in complexes **10d** and **10e** respectively. In contrast, the *ortho*-nitro isomer **L_{11}** become unable to form any anion complexes, instead the structures free **L_{11}** from DMF or DMSO solvent medium are obtained in most of the cases, which occurs due to the steric hindrance provided by the nitro group at the *ortho*-position and existence of strong intramolecular H···O interactions in free **L_{11}** structures. Then, the two halo-methylphenyl terminal aryl di-substituted receptors **L_{12}** (chloro-methyl isomer) and **L_{13}** (bromo-methyl isomer) have been synthesized, which readily form similar kinds of non-cooperative anion entrapped neutral host-guest complexes **12a**, **13a**, **13b**

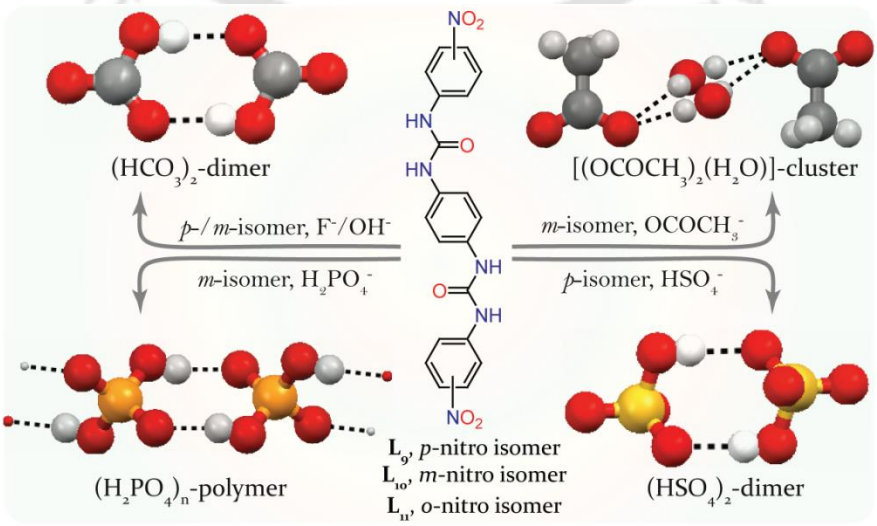

Fig. 5.1 The comprehensive representation of one of the key outcomes of research work included in this chapter.

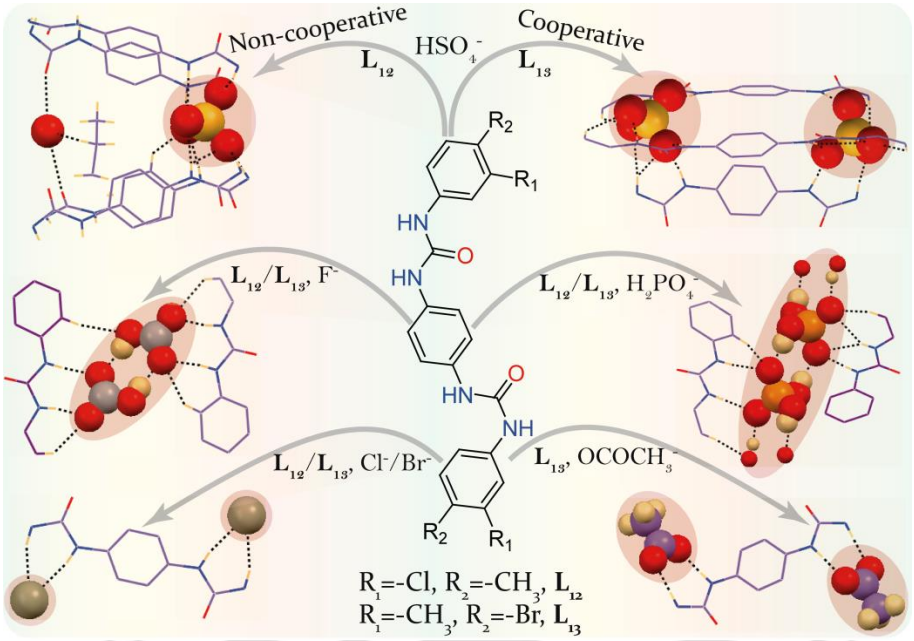

Fig.. 5.2 The comprehensive representation of one of the key outcomes of research work included in this chapter.

with homologous chloride or bromide anions and smaller planar acetate anions in complex **13d**. Similarly, like receptors **L_9** and **L_{10}**, in presence of *n*-TBAF or *n*-$TBAH_2PO_4$ salts, both isomers **L_{12}** and **L_{13}** entrap cyclic $(HCO_3)_2$ dimeric associations *via* aerial CO_2 fixation (complexes **12b** and **13c**) and polymeric associations of $(H_2PO_4)_n$ within non-cooperative host assemblies (complexes **12d** and **13f**). In contrast, receptor **L_{12}** forms non-cooperative self-assemblies with divalent sulfate anion and water molecule in complex **12c**; whereas receptor **L_{13}** forms divalent sulfate entrapped only cooperative barrel-shaped neutral assemblies in complex **13e**.

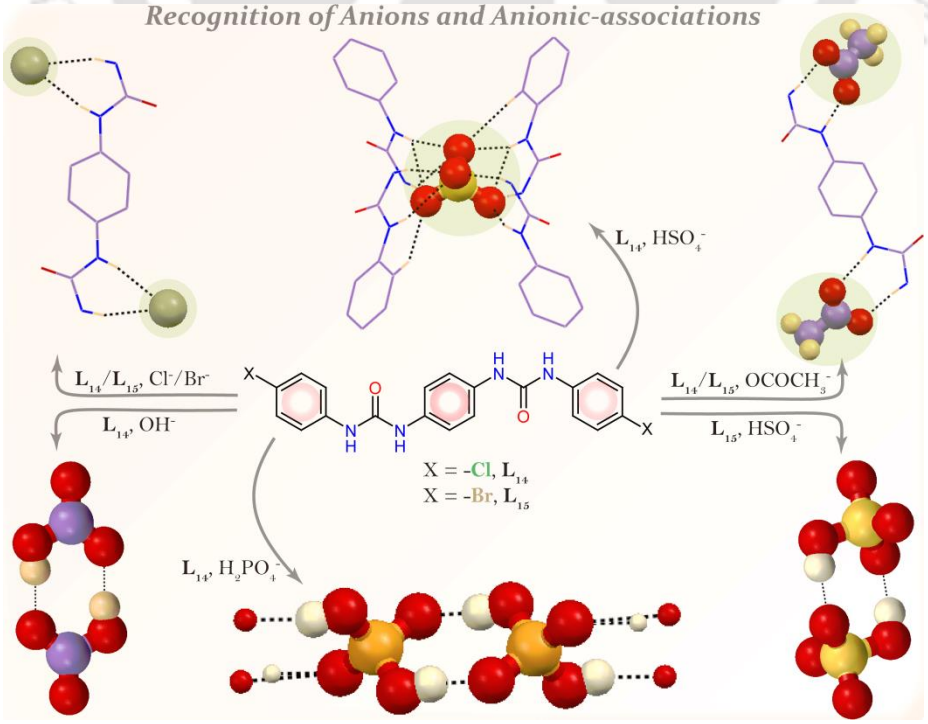

Fig. 5.3 The comprehensive representation of one of the key outcomes of research work included in this chapter.

Furthermore, another two *para*-halophenyl substituted linear bis-urea receptors **L_{14}** (*para*-chloro) and **L_{15}** (*para*-bromo) can readily form non-cooperative neutral complexes with chloride or bromide anions (complexes **14a**, **15a**, **15b**) as well as with planar acetate anions (complexes **14c**, **15c**) just similar as receptors **L_{12}** and **L_{13}**. Receptor **L_{14}** has also been structurally authenticated to form cyclic $(HCO_3)_2$ anionic dimer by OH^- induced atmospheric CO_2 fixation (complex **14b**) and linear polymeric $(H_2PO_4)_n$ entrapped neutral self-assemblies (complex **14e**), like the other above described *para*-phenylendiamine based receptors. Furthermore, in presence of *n*-$TBAHSO_4$ salts, receptor **L_{14}** show non-cooperative capture of divalent SO_4^{2-} anion in complex **14d**, but receptor **L_{15}** forms cyclic $(HSO_4)_2$ dimer trapped non-cooperative self-assemblies in complex **15d**. Scheme 5.1 shows the molecular receptor structures **L_9-L_{15}** and the representations of key findings of research work included in this chapter are shown Fig. 5.1-5.3.

5.2 Structural aspects of anion binding with L_9-L_{15}

In principle an appropriate artificial receptor must require a particular rigid or flexible hydrogen-bond donating supramolecular architecture to bind with anionic guests of different shapes and sizes. The *para*-phenylenediamine based mono-nitrophenyl functionalized (*para*-, *meta*- and *ortho*-) isomeric bis-urea receptors **L_9**, **L_{10}** and **L_{11}** (Fig. 5.1) as well as more than one terminal aryl substituent (*meta*-*para*) containing dipodal receptors **L_{12}**, **L_{13}** (Fig. 5.2) and mono-halophenyl functionalized (*para*-Cl, *para*-Br) bis-urea receptors **L_{14}**, **L_{15}** (Fig. 5.3) each hold two urea functionalities, which can receive guests of different dimensions *via* formation of non-cooperative host–guest assemblies in most of the cases due to the less preorganized and least converging host architectures, irrespective of any terminal substituent effect or size of anionic guests. Structural evidence obtained from single crystal X-ray studies of the isolated crystals provides insight into the proper binding topology of anions/hydrated-anions or anionic associations with the neutral receptor molecules. Efforts were made to explore the solid-state binding properties of **L_9-L_{15}** with various quaternary ammonium (*n*-TBA /TEA) anion salts in aprotic solvents such as MeCN, DMF and DMSO. The purposeful attachment of urea groups in highly organized 4-/3-/2-nitrophenyl or 3,4-halo-methylphenyl/methyl-halophenyl or 4-chloro/bromo-phenyl mono- or di-functionalized dipodal scaffolds become helpful to determine the binding discrepancies of anionic guests *via* number of non-covalent interactions. Conventionally, crystallization has been the main focus in anion-recognition chemistry to comprehend the structural insight of the host-guest complexes.

It should be mentioned here that, the crystal structures suitable for XRD analysis are obtained from the basic DMF or DMSO solutions of all the three nitro-phenyl functionalized free receptors **L_9-L_{11}** and halo-methylphenyl functionalized free receptors **L_{12}-L_{13}**, whereas several

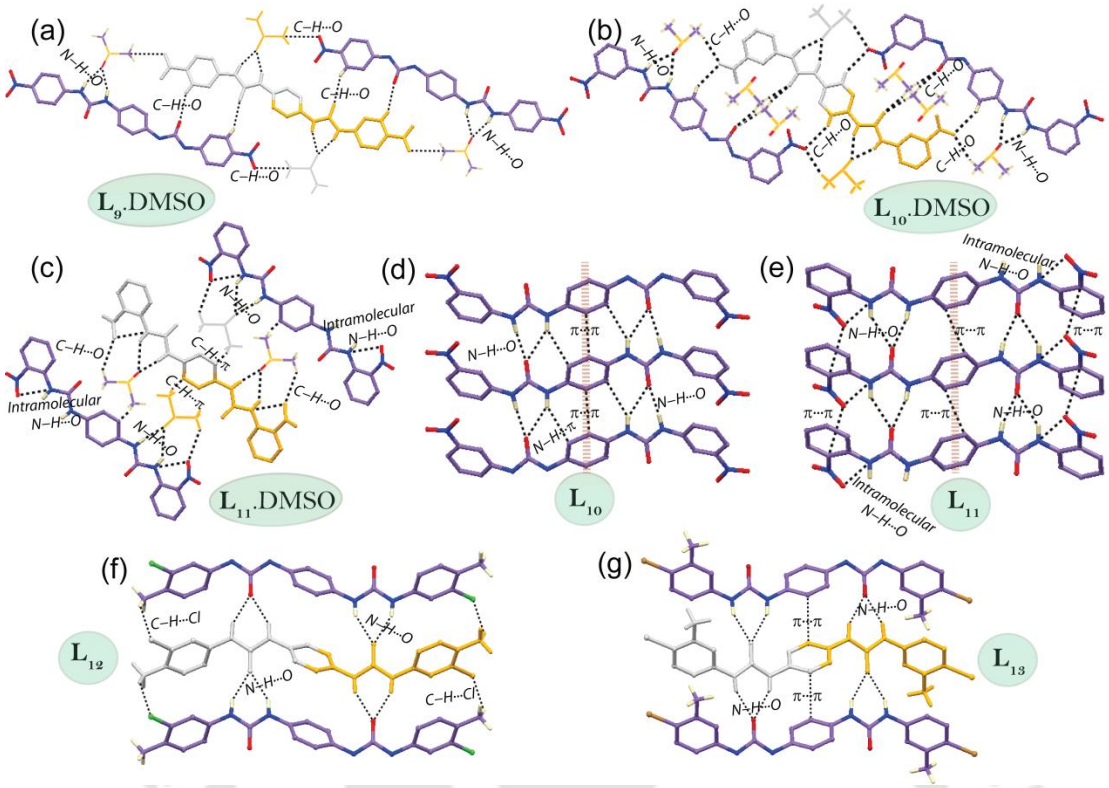

Fig. 5.4 X-ray structures (partial) of the free ligands obtained from DMF/DMSO solvents depicting non-covalent interactions within the array of (a) **L9**.DMSO, (b) **L10**.DMSO, (c) **L11**.DMSO (d) **L10**, (e) **L11**, (f) **L12** and (g) **L13**; Solvent free (d) **L10**, (e) **L11**, (f) **L12** and (g) **L13** structures obtained from DMF solvents depicting parallel β-sheet type architecture through non-covalent interactions.

attempts in various solvents and different crystallization conditions were failed to recrystallize the *para*-halophenyl functionalized free receptors **L14** and **L15**, as in most of the times the off-white precipitate or thick oily mass were found at the bottom of crystallization vials.

The structural elucidation of single crystals of free **L9**-**L11** obtained from either DMF or DMSO solutions clearly reveal that the existence of half-unit of C_{2v}-symmetric **L9**/**L10**/**L11** ligand unit either in presence or absence of solvent molecule in the asymmetric unit. In each nitro-functionalized isomeric free bisurea receptors, the orientation of receptor are almost planar and the adjacent urea groups at the two opposite side of *para*-phenylene spacer are present in *anti*-orientation (Fig. 5.4a-e). In the structures of **L9**·DMSO, **L10**.DMSO and **L11**.DMSO, each urea group is H-bonded to one solvent DMSO molecule, although each self-assemblies form different kinds of cyclic H-bonded network by number of weak C–H···O or C–H···π interactions (Fig. 5.4a, b, c). But the free ligand structures of *meta*-isomer **L10** and *ortho*-isomer **L11** achieved from DMF solution mixture reveals the construction of parallel β-sheet type architectures with the help of few cyclic H-bonded networks formed by strong N–H···O and weak N–H···π or $\pi_{aryl}\cdots\pi_{aryl}$ interactions among the adjacent receptor moieties (Fig. 5.4d, e). The free *ortho*-isomer **L11** obtained from DMF and DMSO solvent, both are additionally stabilized by strong intra-molecular N–H···O interactions, that typically resist complexation of **L11** with any anion

(Fig. 5.4c, e). On the other hand, the suitable crystals obtained from individual DMF solutions of free $\mathbf{L_{12}}$ and $\mathbf{L_{13}}$ ligands, also contain the half-molecule of C_{2v}-symmetric $\mathbf{L_{12}}$ or $\mathbf{L_{13}}$ units in the asymmetric units, like the free receptors $\mathbf{L_9}$, $\mathbf{L_{10}}$ and $\mathbf{L_{11}}$. Note that, despite the linear shaped architecture with exactly opposite directed urea -NH groups in $\mathbf{L_{12}}$ and $\mathbf{L_{13}}$, the orientations of central aromatic ring with terminal aryl rings are almost perpendicular in both ligands. The X-ray analyses clearly reveal that the two anti-oriented urea -NH groups of both linear receptors are engaged in strong N–H···O interactions with carbonyl oxygen atoms of adjacent symmetry-identical receptor units *via* construction of parallel β-sheet type architectures (Fig. 5.4f, g), like the free $\mathbf{L_{10}}$ and $\mathbf{L_{11}}$ structures obtained from DMF solutions.

5.2.1. Structural analysis of halide bound complexes of receptors L_9-L_{15}

Single crystal XRD analyses of receptor-halide neutral complexes and the consistent non-cooperative binding behavior toward halides are probably ascribed for the linear less preorganized ligands' architecture as well as least converging nature of *para*-phenylenediamine spacer compared to other isomeric aromatic diamines. Note that, in presence of *n*-TBAF salt, most of the receptors among $\mathbf{L_9}$-$\mathbf{L_{15}}$, conform bicarbonate dimer entrapped complex *via* aerial CO_2 fixation. In addition, other than the nitrophenyl substituted receptors $\mathbf{L_9}$-$\mathbf{L_{11}}$, the halo-methylphenyl and halophenyl functionalized receptors $\mathbf{L_{12}}$-$\mathbf{L_{15}}$ construct either chloride or bromide entrapped neutral host-guest complexes in presence of respective *n*-TBACl or *n*-TBABr salts.

5.2.1.1 Bromide complex (12a) of L_{12} and chloride (13a), bromide (13b) complexes of L_{13}

Structural elucidation reveals that the halide bound non-cooperative assemblies of halo-methylphenyl substituted receptors such as, bromide complex **12a** of $\mathbf{L_{12}}$, chloride complex **13a** of $\mathbf{L_{13}}$ and bromide complex **13b** of $\mathbf{L_{13}}$ crystallize in the monoclinic space group *P*n, *C*2/c and *P*21/n respectively. The X-ray analyses clearly reveal that, despite the presence of anionic guests, the urea -NH groups of a particular $\mathbf{L_{12}}$ or $\mathbf{L_{13}}$ receptor moiety are still present in opposite direction like the free receptors, although each receptor architecture in halide trapped complexes exhibit more linearity compared to free ligand structures. A particular receptor (either $\mathbf{L_{12}}$ or $\mathbf{L_{13}}$) in each halide complex is non-cooperatively hydrogen-bonded with two symmetry-independent (complex **12a**) or two symmetry-identical (complexes **13a**, **13b**) anions. In bromide complex **12a**, the coordination numbers of two symmetry-independent bromide anions are 5 (for Br1) and 4 (for Br2) which consist of strong N−H···Br, weak C−$H_{n\text{-TBA}}$···Br and C−H_{aryl}···Br interactions (Fig. 5.5a). Subsequently, in chloride complex **13a**, each symmetry-identical chloride ion is coordinated by four strong N−H···Cl interactions (Fig. 5.5b) and in bromide

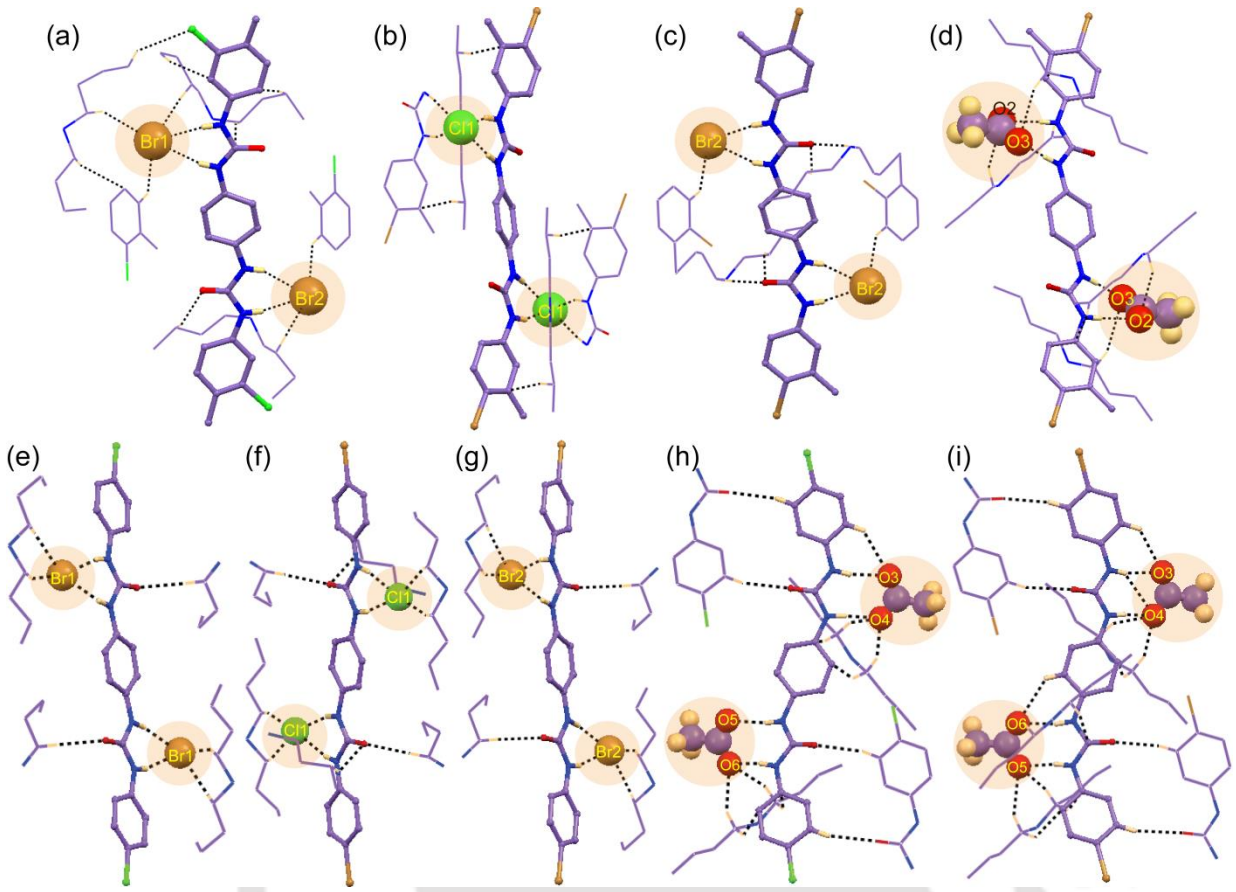

Fig. 5.5 Partial X-ray structures depicting the non-covalent interactions involved in non-cooperative self-assemblies of (a) bromide complex **12a**, (b) chloride complex **13a**, (c) bromide complex **13b**, (d) acetate complex **13d**, (e) bromide complex **14a**, (f) chloride complex **15a**, (g) bromide complex **15b**, (h) acetate complex **14c** and (i) acetate complex **15c**.

complex **13b**, each symmetry-identical bromide ion is coordinated by two strong N−H···Br along with one C−H_{aryl}···Br interactions (Fig. 5.5c). Note that, complexes **12a**, **13a** and **13b** are stabilized by additional weak C−H_{TBA}··· π_{aryl} or C−H_{TBA}··· O interactions (Fig. 5.5a-c).

5.2.1.2 Bromide complex (14a) of L_{14} and chloride (15a), bromide (15b) complexes of L_{15}

The isolated single crystals of halide entrapped non-cooperative complexes of *para*-halophenyl functionalized receptors $\mathbf{L_{14}}$ and $\mathbf{L_{15}}$ are also attained, like the bis-urea receptors $\mathbf{L_{12}}$ and $\mathbf{L_{13}}$. The X-ray analyses clearly reveal that the halide complexes **14a** of $\mathbf{L_{14}}$, **15a** of $\mathbf{L_{15}}$ and **15b** of $\mathbf{L_{15}}$ are almost isostructural and they also crystallize from the same monoclinic space group *P*21/n. Similarly, the asymmetric unit of each halide complex (**14a** or **15a** or **15b**) contains a C_{2v}-inversion symmetric half-receptor unit, a halide (Cl^- or Br^-) anion and its corresponding *n*-TBA^+ counteraction. Structural elucidation reveals that the adjacent urea groups of a particular $\mathbf{L_{14}}$ or $\mathbf{L_{15}}$ receptor moiety are oriented in *anti*-fashion in each halide complex and the less coordinating chloride or bromide anions are bound within the individual non-cooperative host assemblies by four hydrogen-bonding (two strong N−H···Cl/Br and two weak C−H_{n}-

$_{TBA}$···Cl/Br) interactions (Fig. 5.5e, f, g). Note that, all the non-cooperative halide trapped host-assemblies get additional stability by several weak C−H$_{n\text{-TBA}}$···O interactions (Fig. 5.5e-g).

5.2.2. Structural analysis of oxyanion bound complexes of receptors L_9-L_{15}

Single crystal XRD analyses of *para*-phenylenediamine based terminal aryl mono- or di-functionalized receptors with oxyanions/hydrated-oxyanions/oxyanion associations also demonstrate the consistent as well as discriminating binding behavior of neutral receptors toward planar, tetrahedral or octahedral anionic guests irrespective of anion size, heavily depending upon the linear less preorganized ligands' architecture as well as least converging nature of *para*-phenylene spacer.

5.2.2.1 F^-/OH^- induced bicarbonate complexes 9a of L_9, 10a of L_{10}, and 10b of L_{10}

The isolated single crystals of cyclic $R^2_2(8)$ type $(HCO_3)_2$ dimer entrapped neutral complexes **9a**, **10a** and **10b** of either *para*-isomer (**L_9**) or *meta*-isomer (**L_{10}**) reveal that fluoride and hydroxide induced complexes (**9a** and **10b** respectively) crystallize in the triclinic *P*-1 space group, whereas the DMF solvated fluoride induced complex **10a** crystallize in the monoclinic space group *P*21/c. Note that in each complex the bicarbonate anions were not present in the individual solution mixtures of receptors prior to crystallization and the source of bicarbonate is atmospheric CO_2, where the *in situ* generated hydroxide anions from basic ligand/F^- or ligand/OH^- solution dissolves aerial CO_2 to HCO_3^- at the air solvent interface.

$$2F^- + H_2O \longrightarrow OH^- + HF_2^-$$

$$OH^- + CO_2 \longrightarrow HCO_3^-$$

The X-ray analyses clearly show that in each complex, the two molecules of **L_9**/**L_{10}** bis-urea derivatives are responsible for one bicarbonate dimer binding i.e. two molecules of monovalent bicarbonate anions. The O−H···O hydrogen-bonded anionic dimer $(HCO_3)_2$ is bound within the self-assemblies of either **L_9** or **L_{10}** with an array of nine, eleven and nine hydrogen bonding interactions (N−H···O, C−H$_{o\text{-aryl}}$···O and C−H$_{TBA}$···O) respectively in complexes **9a** (Fig. 5.6a), **10a** (Fig. 5.6b) and **10b** (Fig. 5.6c). The asymmetric unit of each complex contains C_{2v}-inversion-symmetric half unit of **L_9**/**L_{10}** receptor, one monovalent bicarbonate anion with its corresponding *n*-TBA counter-cation and it is also evident that the adjacent urea-NH groups of a particular receptor are projected in *anti*-fashion in all complexes despite the presence of anionic guests. Note that, one extra DMF solvent molecule is also crystallized with fluoride induced bicarbonate complex of **L_{10}** that contributes additional stability to complex **10a** *via* several hydrogen-bonding interactions (Fig. 5.6b). Interestingly, despite the absence of any receptor cooperativities or more coordinating sites, herein the linear *para*-phenylenediamine based

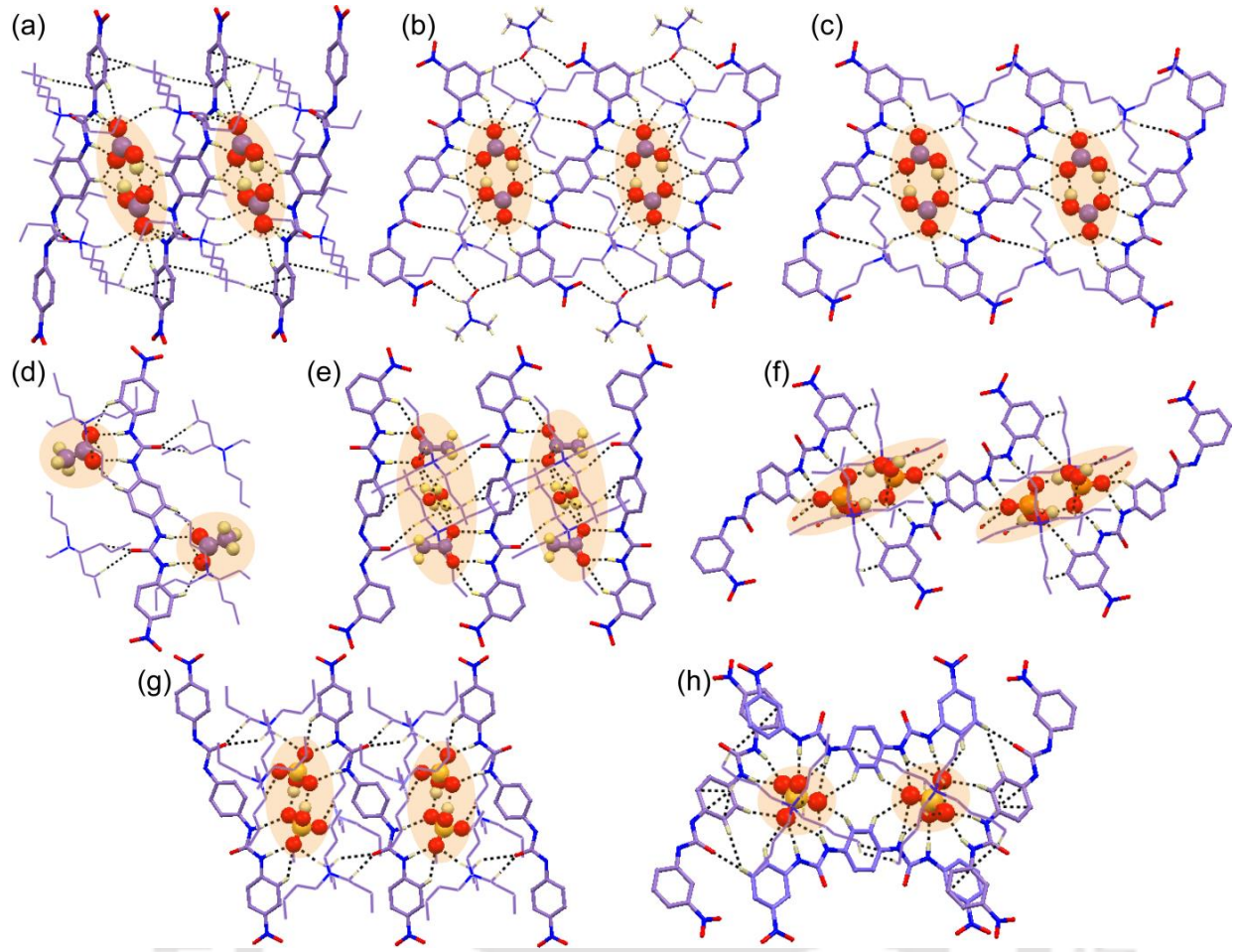

Fig. 5.6 X-ray structures (partial) of anion complexes depicting array of hydrogen bonding interactions in (a) $(HCO_3)_2$ entrapped complex **9a**, (b) DMF solvated $(HCO_3)_2$ entrapped complex **10a**, (c) $(HCO_3)_2$ entrapped complex **10b**, (d) bare acetate trapped complex **9b**, (e) hydrated-acetate trapped complex **10c**, (f) $(H_2PO_4)_n$ entrapped complex **10e**, (g) $(HSO_4)_2$ entrapped complex **9c** and (h) divalent sulfate captured complex **10d**.

isomeric *para*- and *meta*-bisurea neutral receptors are still capable to capture dimeric association of bicarbonate created by donor-acceptor H-bonding interactions.

5.2.2.2 Acetate complex of L_9 (9b) and hydrated-acetate complex of L_{10} (10c)

The bare and hydrated acetate complexes **9b** and **10c** of *meta*-isomer $\mathbf{L_9}$ and *para*-isomer $\mathbf{L_{10}}$ crystallize in the same triclinic space group *P*-1 and each of their asymmetric units contain inversion-symmetric half $\mathbf{L_9}$/$\mathbf{L_{10}}$ ligand molecule, one monovalent acetate anion and corresponding *n*-TBA counter-cation, although complex **10c** contains an additional half-occupied water molecule of crystallization. In complex **9b**, the acetate anions are trapped through the non-cooperative assembly of $\mathbf{L_9}$ and each monovalent OAc^- anion is coordinated by a total of eight (two N−H···O, two C−$H_{o\text{-aryl}}$···O and four C−H_{TBA}···O) hydrogen-bonding interactions (Fig. 5.6d). On the other hand, an uncommon type of H-bonded acyclic hydrogen-bonded acetate-water assembly is entrapped within the self-assemblies of symmetry-identical *meta*-isomers $\mathbf{L_{10}}$ in complex **10c** with an array of total four N−H···O, two C−$H_{o\text{-aryl}}$···O and six C−H_{TBA}···$O_{acetate/water}$ interactions, where each symmetry-identical monovalent acetate anion and

water molecule exhibit hexa-coordination and tetra-coordination respectively (Fig. 5.6e). Note that, alike the bicarbonate complexes **9a**, **10a** and **10b**, the adjacent urea -NH groups of a particular receptor moiety are projected in *anti*-fashion despite the presence of hydrated/non-hydrated anionic guests.

5.2.2.3 Bisulfate complex 9c of L_9, sulfate complex 10d of L_{10} and biphosphate complex 10e of L_{10}

The larger tetrahedral monovalent or divalent oxyanion or oxyanion association trapped neutral self-assembled complexes **9c**, **10d** and **10e** of either isomeric receptors $\mathbf{L_9}$ or $\mathbf{L_{10}}$ crystallize in the same triclinic space group *P*-1. The asymmetric unit cyclic $(HSO_4)_2$-dimer entrapped complex **9c** and $(H_2PO_4)_n$ polymer entrapped complex **10e** consist of inversion-symmetric half $\mathbf{L_9}$/$\mathbf{L_{10}}$ receptor unit, one monovalent HSO_4^-/$H_2PO_4^-$ anion and their corresponding *n*-TBA counter-cation unit respectively. Structural elucidation reveals that the $(HSO_4^-)_2$ anionic dimer formed by two O−H···O donor-acceptor interactions in complex **9c** is bound within the self-assemblies of $\mathbf{L_9}$ with an array of total twelve hydrogen bonding interactions (N−H···O, C−$H_{o\text{-}aryl}$···O and C−H_{TBA}···O), where each HSO_4^- anion exhibit octa-coordination (Fig. 5.6g). Subsequently in complex **10e**, a linear chain of $(H_2PO_4)_n$ polymer constructed by four O−H···O donor-acceptor interactions around single monovalent $H_2PO_4^-$ anion is also trapped within the self-assemblies $\mathbf{L_{10}}$ by N−H···O, C−$H_{o\text{-}aryl}$···O and C−H_{TBA}···O interactions, where each $H_2PO_4^-$ anion exhibit coordination number of ten (Fig. 5.6f). On the other hand, the divalent single sulfate bound complex **10d** of $\mathbf{L_{10}}$ contain an inversion-symmetric half $\mathbf{L_2}$ receptor unit, another symmetry-independent full $\mathbf{L_2}$ conformer, one divalent SO_4^{2-} anion generated *via* H-bonding activated proton transfer from HSO_4^- anion and its corresponding two *n*-TBA counter-cations. Structural elucidation reveals that one divalent sulfate in complex **10d** is entrapped within the self-assemblies of conformational isomorphs of $\mathbf{L_{10}}$ with an array of total fifteen (N−H···O, C−$H_{o\text{-}aryl}$···O and C−H_{TBA}···O) hydrogen- bonding interactions (Fig. 5.6h). Note that in complex **10d**, the adjacent urea -NH groups of one $\mathbf{L_2}$ conformer are present in cooperative *syn*-fashion, while they are in non-cooperative *anti*-fashion in other symmetry-independent conformer (Fig. 5.6h). These kinds of existence of more than one molecular conformer in the same crystal is known by the term '*conformational isomorphism*' in supramolecular chemistry caused may be due the interrupted crystallization and their occurrence clarifies the kinetic and thermodynamic crystal stability concepts, as exemplified by Desiraju *et. al.*[5.10] Note that, six urea -NH groups are involved in close entrapment of divalent SO_4^{2-} anion in complex **10d**, whereas comparatively open self-assemblies of only four urea -NH groups are enough to capture dimeric associations

of monovalent HSO_4^- or $H_2PO_4^-$ anions in complexes **9c** and **10e** respectively.

5.2.2.4 F^- induced bicarbonate complexes 12b of L_{12} and 13c of L_{13}

The neutral self-assemblies of cyclic $R^2_2(8)$ type $(HCO_3)_2$ dimer entrapped complexes **12b** and **13c** of halo-methylphenyl aryl di-functionalized receptors $\mathbf{L_{12}}$ and $\mathbf{L_{13}}$ respectively crystallize in the orthorhombic space group *P*bc21 and *P*21ca respectively. Note that, the bicarbonate anionic species were not present inside the individual solution mixtures of either $\mathbf{L_{12}}$ or $\mathbf{L_{13}}$ prior to crystallization and in both complexes **12b** and **13c**, the source of the HCO_3^- anion is atmosphere where the hydroxide ions generated *in situ* from the basic receptor-fluoride solution, that dissolves aerial CO_2 into HCO_3^- at the edge of air and solvent, as was observed in the cases of complexes **9a**, **10a**, **10b** of nitrophenyl substituted isomeric receptors $\mathbf{L_9}$ or $\mathbf{L_{10}}$.

$$2F^- + H_2O \longrightarrow OH^- + HF_2^-$$
$$OH^- + CO_2 \longrightarrow HCO_3^-$$

The X-ray analyses clearly reveal that the asymmetric unit of both complexes **12b** and **13c** contain single $\mathbf{L_{12}}$ or $\mathbf{L_{13}}$ linear receptor unit, two symmetry-independent HCO_3^- anions and their corresponding two symmetry-independent *n*-TBA^+ counter-cations. It is also evident that like free receptor structures the adjacent urea-NH groups of a particular ligand unit are projected in *anti*-fashion in both complexes that may be ascribed for the divergent nature of *para*-phenylene moieties. Two O−H···O hydrogen-bonded cyclic $(HCO_3)_2$-dimer are effectively bound within the non-cooperative self-assemblies of either linear receptors $\mathbf{L_{12}}$ or $\mathbf{L_{13}}$ by eleven or twelve hydrogen bonding interactions (N−H···O, C−$H_{o\text{-aryl}}$···O and C−H_{TBA}···O) respectively in complexes **12b** (Fig. 5.7a) and **13c** (Fig. 5.7b).

5.2.2.5 Acetate complex 13d of receptor L_{13}

The acetate complex of bromo-methylphenyl substituted receptor $\mathbf{L_{13}}$ crystallizes in the triclinic space group *P*-1 and despite the presence of anionic guests the urea -NH groups of particular receptor $\mathbf{L_{13}}$ are still present in anti-fashion like the free receptor structures. However, the receptor architecture of acetate complex exhibit more linearity than free ligand structures, like the halide complexes of ligands $\mathbf{L_{12}}$ or $\mathbf{L_{13}}$. In complex **13d**, the urea groups of receptor $\mathbf{L_{13}}$ are non-cooperatively hydrogen-bonded with two symmetry-identical acetate anions (Fig. 5.5d), where each anion exhibit tetra-coordination (two strong N−H···O and two weak C−H_{aryl}··· O) and each acetate oxygen atom (either O2 or O3) accepts two hydrogen bonds. Note that, the non-cooperative anion-receptor complex **13d** gains additional stability by weak C−H_{TBA}··· π or C−H_{TBA}···O interactions (Fig. 5.5d).

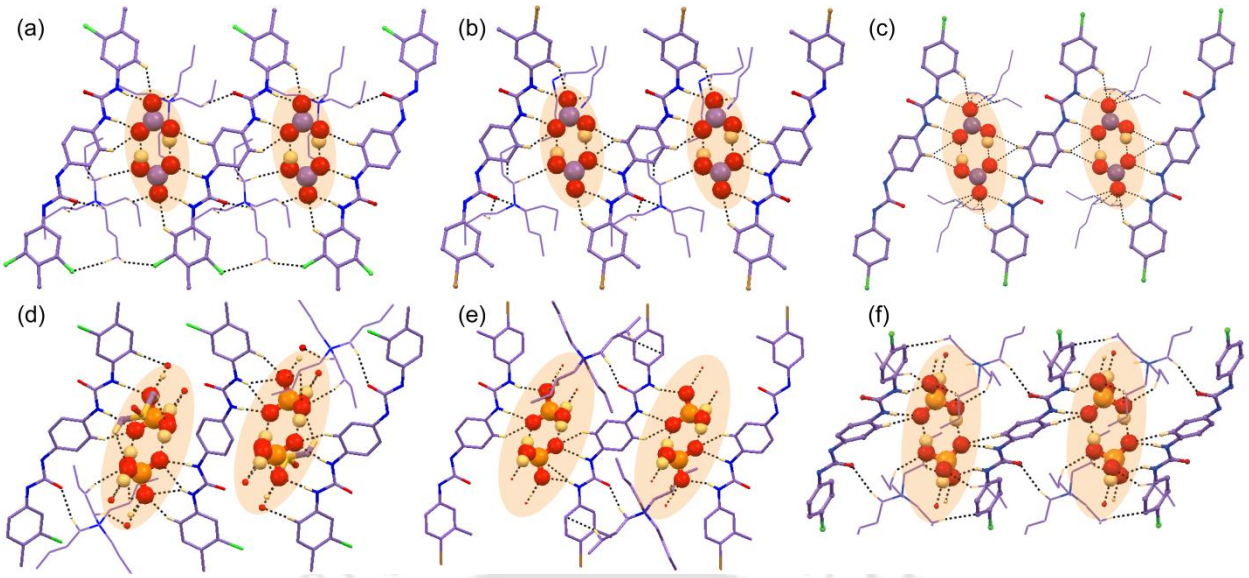

Fig. 5.7 X-ray structures (partial) of anion complexes depicting array of hydrogen bonding interactions in (a) $(HCO_3)_2$ entrapped complex **12b**, (b) $(HCO_3)_2$ entrapped complex **13c**, (c) $(HCO_3)_2$ entrapped complex **14b**, (d) $(H_2PO_4)_n$ entrapped complex **12d**, (e) $(H_2PO_4)_n$ entrapped complex **13f** and (f) $(H_2PO_4)_n$ entrapped complex **14e**.

5.2.2.6 Sulfate complexes 12c of L_{12} and 13e of L_{13}

The isolated crystals of divalent sulfate entrapped complexes **12c** and **13e** of receptors $\mathbf{L_{12}}$ and $\mathbf{L_{13}}$ respectively were attained by hydrogen bonding activated proton transfer reactions from monovalent HSO_4^- anion and the complexes **12c** and **13e** crystallize in the monoclinic system with space groups *P*21/n and *P*21/c respectively. The asymmetric unit of complex **12c** contains two symmetry-independent $\mathbf{L_{12}}$ receptor units, one divalent sulfate anion with its corresponding two *n*-TBA^+ counter-cations along with one water molecule of crystallization. But, complex **13e** contains three conformational isomorph of receptor $\mathbf{L_{13}}$, two divalent symmetry-independent sulfate anions and their corresponding four *n*-TBA^+ counter-cations in the asymmetric unit. Note that, in complex **12c** the urea -NH groups of a particular linear $\mathbf{L_{12}}$ receptor are oriented in *anti*-fashion (Fig. 5.8a) as observed in other complexes of *para*-phenylene connected bis-urea receptors, but in complex **13e** the urea -NH groups of a particular $\mathbf{L_{13}}$ receptor exhibit bow shaped architecture are projected in *syn*-fashion (Fig. 5.8c) unlike the free receptor structures or other anion complexes. Structural elucidation reveals that a SO_4^{2-} anion is entrapped by eleven hydrogen bonding (ten strong N−H···O and one C−$H_{o\text{-aryl}}$···O) interactions within the tetrameric non-cooperative barrel of receptors in complex **12c** (Fig. 5.8a). Furthermore, the lower part of non-cooperative tetrameric barrel is bridged by a trifurcated water (two O−H···O and one C−H_{TBA}···O_{water}) molecule and the lower eight urea -NH groups of four linear receptors are engaged in coordination of four different symmetry-identical sulfate anions in complex **12c** (Fig. 5.8a). In contrast, in complex **13e**, the three bow-shaped conformational isomorphs of receptor $\mathbf{L_{13}}$ construct *n*-TBA cation-assisted trimeric barrel, that cooperatively entraps one SO_4^{2-} anion

by ten hydrogen-bonding (eight strong N−H···O, one C−$H_{o\text{-aryl}}$···O and one C−H_{TBA}···O) interactions in one part (Fig. 5.8c) and another symmetry-independent SO_4^{2-} anion by ten hydrogen-bonding (seven strong N−H···O, two C−$H_{o\text{-aryl}}$···O and one C−H_{TBA}···O) interactions in another part (Fig. 5.8c) of the barrel. It is quite clear from the X-ray structures of non-cooperative *vs* cooperative receptor self-assemblies that, upon efficient entrapment of sulfate ion through non-cooperative assemblies, each **L_{12}** receptor exhibit linear conformation (average terminal centroid distance ~15.19 Å) in complex **12c** (Fig. 5.8a) like other complexes, whereas each **L_{13}** receptor deviates from linearity and exhibits bow-shaped architecture (average terminal centroid distance ~14.69 Å) in complex **13e** (Fig. 5.8c) which efficiently entrap two tetrahedral sulfate anion through cooperative self-assemblies, unlike the other complexes.

5.2.2.7 Biphosphate complexes 12d of L_{12} and 13f of L_{13}

The linear polymeric aggregated $(H_2PO_4^-)_n$ trapped complexes **12d** and **13f** of halo-methylphenyl functionalized receptors crystallize in the triclinic space group *P*-1 and monoclinic space group *P*21/c respectively owing to the presence of different numbers of ligand or anion salts in the asymmetric units. However, structural elucidation demonstrates that in both complexes the similar kinds of linear $(H_2PO_4^-)_n$ polymeric chains built by four O−H···O donor-acceptor interactions around single $H_2PO_4^-$ ion are efficiently captured within the linear non-cooperative self-assemblies of either **L_{12}** (complex **12d**) (Fig. 5.7d) or **L_{13}** (complex **13f**) (Fig. 5.7e). Note that, in complex **12d** each $H_2PO_4^-$ ion is bound by N−H···O, C−$H_{o\text{-aryl}}$···O, C−H_{TBA}···O and C−H_{DMSO}···O interactions, where the adjacent symmetry-independent $H_2PO_4^-$ anions exhibit coordination number of twelve and nine (Fig. 5.7d). On the other hand, each symmetry-identical $H_2PO_4^-$ ion in polymeric aggregation of complex **13f** is bound by N−H···O, C−$H_{o\text{-aryl}}$···O and C−H_{TBA}···O interactions, where each $H_2PO_4^-$ ion exhibit hepta-coordination (Fig. 5.7e). It is also evident that, in both complexes the adjacent urea -NH groups of a particular **L_{12}** or **L_{13}** receptor unit are projected in *anti*-fashion, like other anion complexes except the sulfate complex **13e**. The urea groups of a particular ligand moiety in complexes **12d** (Fig. A5.1b) or **13f** (Fig. A5.1c) are engaged in entrapment of two different polymeric aggregated chains made by $H_2PO_4^-$ anions.

5.2.2.8 OH^- induced bicarbonate complex 14b of receptor L_{14}

The single crystals of cyclic $(HCO_3)_2$-dimer captured neutral complex **14b** of *p*-halophenyl functionalized receptor **L_{14}** crystallize in the triclinic space group *P*-1. The asymmetric unit of hydroxide anion induced cyclic $R^2_2(8)$ type $(HCO_3)_2$-dimer trapped complex and **14b** contains one C_{2v}-inversion symmetric half **L_{14}** receptor unit, one planar HCO_3^- anion and its corresponding *n*-TBA^+ counter-cation. Structural elucidation reveals that the strong O−H···O

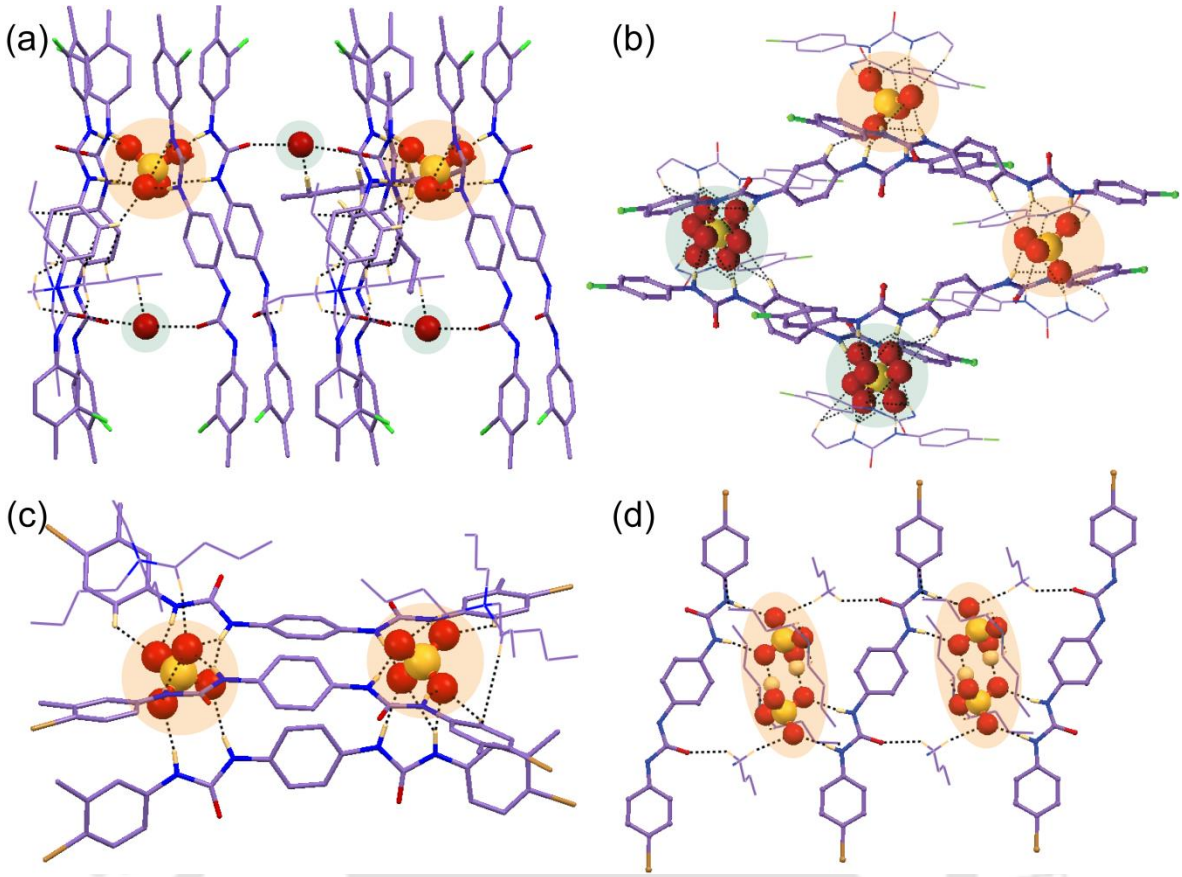

Fig. 5.8 X-ray structures (partial) of anion complexes depicting array of hydrogen bonding interactions in (a) sulfate and water trapped non-cooperative complex **12c**, (b) sulfate trapped non-cooperative complex **14d**, (c) sulfate trapped cooperative complex **13e** and (d) $(HSO_4)_2$ trapped non-cooperative complex **15d**.

hydrogen-bonded cyclic dimeric anion association built by two symmetry-identical monovalent HCO_3^- ion (Fig. 5.7c) is efficiently entrapped within the arrays of linear non-cooperative neutral self-assemblies of *para*-chloro isomer $\mathbf{L_{14}}$ by a total of sixteen hydrogen bonding interactions (four strong N−H···O, six C−$H_{o\text{-aryl}}$···O and six weak C−H_{TBA}···O) in complex **14b** (Fig. 5.7c). Note that, each HCO_3^- anion of cyclic dimer exhibit coordination number of ten which is the combination of two strong N−H···O, two strong O−H···O, three C−$H_{o\text{-aryl}}$···O and three weak C−H_{TBA}···O interactions. It is also worth mentioning that, the planar HCO_3^- anion was absent in the basic solvent mixtures prior to crystallization and the bicarbonate anion is produced from the atmospheric CO_2, where the hydroxide anions generated *in situ* from basic ligand/OH^- solution at the air solvent interface dissolves aerial CO_2 to HCO_3^-, and this is similar like the other *para*-phenylenediamine based complexes **9a**, **10a**, **10b, 12b** and **13c**.

$$2F^- + H_2O \longrightarrow OH^- + HF_2^-$$

$$OH^- + CO_2 \longrightarrow HCO_3^-$$

5.2.2.9 Acetate complexes 14c of L_{14} and 15c of L_{15}

The single crystals of monovalent acetate entrapped complexes **14c** and **15c** are almost isostructural and they crystallize in the same monoclinic space group *P*21/c. Subsequently, the

asymmetric unit of each complex contains a single **L_{14}** or **L_{15}** receptor unit, two symmetry-independent acetate anions and two corresponding *n*-TBA^+ counter-cations. The X-ray analyses clearly reveal that the urea groups of particular **L_{14}** or **L_{15}** linear receptor unit are oriented in *anti*-fashion which efficiently entraps the symmetry-independent acetate anions by non-cooperative hydrogen-bonding interactions (Fig. 5.5h, i). In complex **14c**, the symmetry-independent acetate anions exhibit coordination number of four (two strong N−H···O and two weak C−H_{TBA}···O) and five (two strong N−H···O, one C−$H_{o\text{-aryl}}$···O and two weak C−H_{TBA}···O) (Fig. 5.5h). On the other and, in complex **15c** the each symmetry-independent acetate anions show coordination number of six, among which one acetate is bound by the combination of three strong N−H···O, one C−$H_{o\text{-aryl}}$···O and two weak C−H_{TBA}···O interactions and other independent acetate ion is entrapped by the combination of two strong N−H···O, one C−$H_{o\text{-aryl}}$···O and three weak C−H_{TBA}···O interactions (Fig. 5.5i). Furthermore both the neutral non-cooperative acetate trapped assemblies of **L_{14}** and **L_{15}** are additionally stabilized by several weak C−$H_{o\text{-aryl}}$···O interactions among the adjacent linear receptors (Fig. 5.5h, i).

5.2.2.10 Sulfate complex 14d of L_{14} and bisulfate complex 15d of L_{15}

The isolated single crystals of tetrahedral divalent sulfate complex **14d** of *para*-chloro isomer **L_{14}** and cyclic $(HSO_4^-)_2$ dimer complex **15d** of *para*-bromo isomer **L_{15}**, both produced from the solution of *n*-$TBAHSO_4$ salts, crystallize in the monoclinic space group *P*21/c triclinic space group *P*-1 respectively. The asymmetric unit of complex **14d** contains one **L_{14}** receptor, one divalent SO_4^{2-} (four oxygen atoms are disordered over eight positions with 0.5 occupancies each) anion produced by H-bonding activated proton transfer and two corresponding *n*-TBA counter-cations. Whereas, the asymmetric unit of complex **15d** comprises of one C_{2v}-inversion symmetric half **L_{15}** receptor, one monovalent HSO_4^- anion, its corresponding one *n*-TBA counter-cation and one solvent DMF molecule of crystallization. The X-ray analysis reveals that higher coordinating divalent sulfate is efficiently captured with the aid of eight urea -NH groups from four non-cooperative linear **L_{14}** conformers in complex **14d** and the coordination number of tetrahedral divalent sulfate anion becomes fourteen which is the combination of twelve strong N−H···O and two weak C−$H_{o\text{-aryl}}$···O interactions (Fig. 5.8b). Structural study of complex **14d** also unveils the formation of a cyclic tetrameric host-guest assemblies through consecutive $(\mathbf{L_{14}}\text{-}SO_4^{2-})_4$ non-cooperative interactions (Fig. 5.8b). Subsequently, in complex **15d**, the cyclic $(HSO_4^-)_2$ dimeric association (formed by strong O−H···O donor-acceptor interactions between monovalent HSO_4^-) is entrapped within the non-cooperative assemblies of **L_{15}** (Fig. 5.8d) with an array of total ten (four strong N−H···O and six weak C−H_{TBA}···O) hydrogen bonding interactions, where each HSO_4^- anion exhibit hepta-coordination (Fig. 5.8d). Additionally, both

the complexes get extra stability by several weak C−H_{TBA}···O interactions between receptor and counter-cations.

5.2.2.11 Biphosphate complex 14e of receptor L_{14}

The colorless single crystals of tetrahedral monovalent polymeric $(H_2PO_4^-)_n$ confined neutral complex **14e** of *para*-chloro isomer $\mathbf{L_{14}}$ crystallize in the triclinic space group *P*-1. Structural elucidation reveals that one C_{2v} inversion-symmetric $\mathbf{L_{14}}$ receptor, one tetrahedral $H_2PO_4^-$ anion and its corresponding *n*-TBA^+ counter-cation is present in the asymmetric unit of complex **14e**. A linear polymeric $(H_2PO_4^-)_n$ anionic association, aggregated by four O−H···O donor-acceptor interactions around single monovalent $H_2PO_4^-$ anion is efficiently captured within the arrays of non-cooperative $\mathbf{L_{14}}$ host assemblies (Fig. 5.7f) with the aid of strong N−H···O, C−$H_{o\text{-aryl}}$···O and weak C−H_{TBA}···O interactions, where each $H_2PO_4^-$ exhibit coordination number of eleven in neutral complex **14e** (Fig. 5.7f), similar like the *para*-phenylenediamine based complexes **10e**, **12d** and **13f**.

Overall, It should be noted that, depending on the size, shape and coordination number anion or anionic association, the orientation of non-cooperative host-assemblies and participation of urea groups has been systematically altered in most of the complexes of *para*-phenylenediamine based receptors $\mathbf{L_9}$-$\mathbf{L_{15}}$. As a consequence, only one urea group of a particular *para*-phenylene bis-urea receptor was involved in the coordination of spherical chloride, bromide or planar single acetate anion. Whereas, for entrapment of dimeric or polymeric anionic associations such as $(HCO_3^-)_2$, $(HSO_4^-)_2$ or $(H_2PO_4^-)_n$, at least two urea groups of different receptor conformers were involved in coordination and furthermore, four urea groups from four different receptor conformers were engaged in entrapping larger coordinating tetrahedral divalent sulfate anion to form non-cooperative neutral host-guest self-assemblies.

5.3 Solution-state anion binding studies

The ^{1}H NMR analyses (DMSO-d_6) of the free receptors $\mathbf{L_9}$-$\mathbf{L_{15}}$, their isolated anion complexes in presence of equivalent amounts of different dimension of anions further demonstrate the solution-state anion-receptor binding as evidenced from the solid state results. The qualitative as well as quantitative ^{1}H NMR experiments using the quaternary ammonium (*n*-TBA/TEA) salts of halides as well as oxyanions in DMSO-d_6 show the most significant changes of the urea -NH protons, which are expected to be the primary site for anion recognition. Fig. 5.9a, b show the chemical shift changes observed upon quantitative gradual addition of *n*-TBAOAc salts to the individual solutions of $\mathbf{L_9}$ and $\mathbf{L_{10}}$, whereas Fig. 5.10a, b display the quantitative ^{1}H-NMR titration of standard SO_4^{2-} and $H_2PO_4^-$ salts to the individual solutions of $\mathbf{L_{10}}$, following the result of maximum chemical shift changes in solid state complexes. The ^{1}H NMR analysis of the free

isomeric receptors reveals that *ortho*-isomer **L_{11}** exhibit the chemical shift values of δ -NH_a = 9.58 ppm; δ - NH_b = 9.78 ppm, that exist in far downfield region compared to the *para*-isomer **L_9** (δ -NH_a = 8.85 ppm; δ - NH_b = 9.40 ppm) and *meta*-isomer **L_{10}** (δ -NH_a = 8.75 ppm; δ - NH_b = 9.17 ppm), which is the consequences of strong intramolecular N−H···O interactions in solution state also between *ortho*-nitro group and adjacent urea -NH protons of receptor **L_3**, as observed in the solid state. ^{1}H NMR analysis of the bicarbonate complexes of receptors **L_9** and **L_{10}** obtained from either F^- or OH^- induced aerial CO_2 fixation showed average downfield shift of $\Delta\delta$ = 1.20 ppm, $\Delta\delta$ = 2.74 ppm and $\Delta\delta$ = 0.73 ppm relative to the corresponding free receptors through severe broadening of urea -NH signals, which suggests the decent anion binding capabilities of the receptors in solution states. Subsequently, the ^{1}H NMR data of the acetate complexes **9b** and **10c** respectively showed huge average downfield shift of $\Delta\delta$ = 3.31 ppm and $\Delta\delta$ = 2.91 ppm for the -NH (Figure S20 Supporting Information). Whereas, ^{1}H NMR titration data of **L_9** and **L_{10}** separately with aliquots of 2.0 eqv. standard OAc^- salt shows the urea -NH protons' shift of **L_9** by $\Delta\delta$ = 3.17 ppm (-NH_a) and $\Delta\delta$ = 3.42 ppm (-NH_b) (Fig. 5.9a) and urea -NH protons' shift of **L_{10}** by $\Delta\delta$ = 3.10 ppm (-NH_a) and $\Delta\delta$ = 3.38 ppm (-NH_b) (Fig. 5.9b), which are very closely resemble with the solid state results and also indicating more proficient participation of -NH_a than -NH_b in the host-guest assembly. Note that, due to huge broadening followed by the splitting of both ureas -NH resonances upon acetate addition, the binding stoichiometries could not be determined in solution state. The significant broadening and splitting of urea -NH signals in ^{1}H-NMR spectra have been appeared due to the consequences of rapid hydrogen bonding interactions between anion and receptor. Similarly, divalent sulfate and polymeric $(H_2PO_4)_n$ entrapped complexes **10d** and **10e** showed moderate average downfield shift of $\Delta\delta$ = 1.27 ppm and $\Delta\delta$ = 2.14 ppm respectively for the -NH protons; however the ^{1}H NMR titration data of **L_{10}** with aliquots of standard (*n*-TBA)$_2SO_4$ solution experience urea -NH shift of $\Delta\delta$ = 2.12 ppm (-NH_a) and $\Delta\delta$ = 2.61 ppm (-NH_b) (Fig. 5.10a), while **L_{10}** with aliquots of standard (*n*-TBA)$_2H_2PO_4$ solution show urea -NH shift of $\Delta\delta$ = 1.15 ppm (-NH_a) and $\Delta\delta$ = 1.31 ppm (-NH_b) (Fig. 5.10b), also indicating more proficient -NH_a participation than -NH_b in anion binding supported from the solid-state evidence. The titration data of **L_{10}** with standard (*n*-TBA)$_2SO_4$ and (*n*-TBA)$_2H_2PO_4$ give the best fit for mixed equilibrium between 1:1 and 1:2 host-guest stoichiometry with apparent binding constant (log K) value of 3.31 and 2.34 respectively. The cyclic $(HSO_4)_2$-dimer entrapped complex **10c** showed average downfield shift of $\Delta\delta$ = 0.14 ppm only for urea -NH protons and because of very negligible shift, the titration experiments of **L_1**with standard bisulfate salt could not

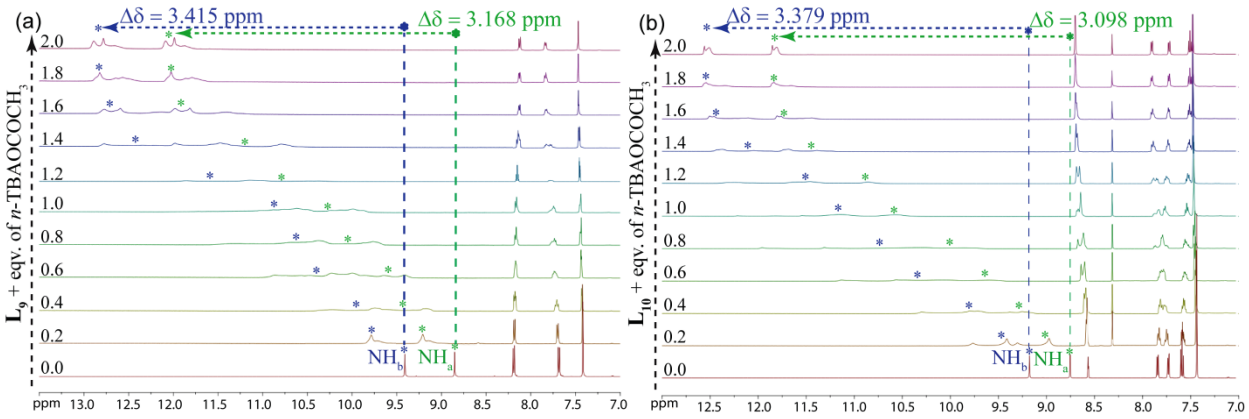

Fig. 5.9 Expanded partial ^{1}H NMR titration spectra of (a) **L$_9$** and (b) **L$_{10}$**, with standard OAc^- anion in DMSO-d_6.

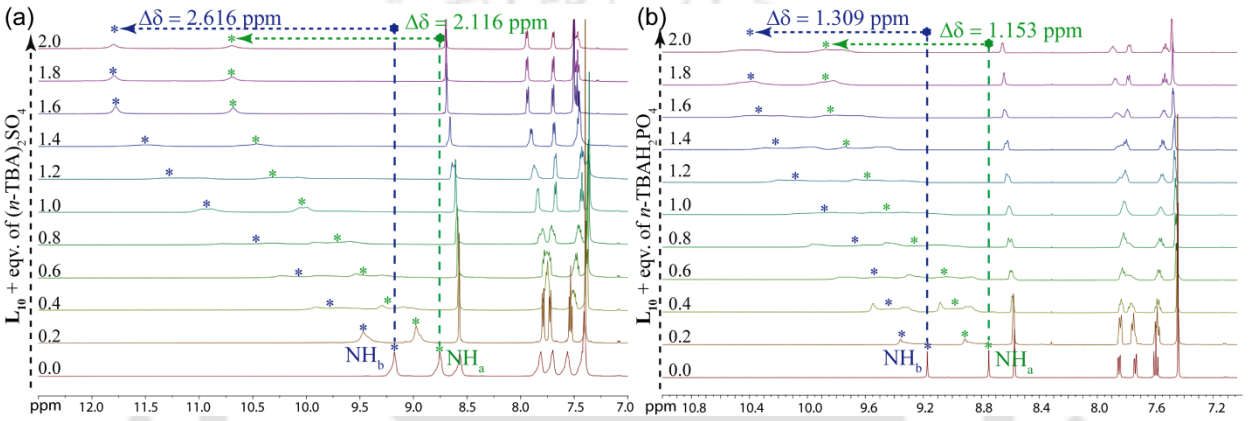

Fig. 5.10 Expanded partial ^{1}H NMR spectra of **L$_{10}$** upon titration with standard (a) SO_4^{2-} and (b) $H_2PO_4^-$ anions in DMSO-d_6.

performed. Subsequently, the anion binding studies of halo-methylphenyl substituted receptors **L$_{12}$** and **L$_{13}$** in presence of different anion salts in solution phase have also been performed to correlate with the solid state results. Fig. 5.11b, c represent the maximum amount of chemical shift changes observed in presence of halide or oxyanion individually to the respective solutions of **L$_{12}$** and **L$_{13}$**. The ^{1}H NMR analysis of the free receptors reveal that both ligands exhibit the comparable chemical shift (δ) values for urea -NH protons such as, -NH_a = 8.702 ppm and NH_b = 8.576 ppm for **L$_{12}$**, and -NH_a = 8.672 ppm and NH_b = 8.570 ppm for **L$_{13}$**. As evidenced from the solid state results, the addition of *n*-TBABr salts to the DMSO-d_6 solutions of either of the **L$_{12}$** or **L$_{13}$** receptors show very negligible average downfield shifts of urea -NH protons of both receptors (avg. $\Delta\delta$ = 0.065 ppm for **L$_{12}$** and avg. $\Delta\delta$ = 0.135 ppm for **L$_{13}$**). Similarly, to compare with solid state chloride complex of **L$_{13}$**, the chloride salt addition to the DMSO-d_6 solution of ligand **L$_{13}$** also show small average downfield shifts $\Delta\delta$ = 0.23 ppm for urea -NH protons in its ^{1}H-NMR data. But, in case of acetate complex of **L$_{13}$**, despite its similar kind of non-cooperative binding like the halides in solid state, it shows large average downfield shifts $\Delta\delta$ = 1.34 ppm for urea -NH protons in the ^{1}H-NMR data, which may be ascribed for the presence of stronger N–H···O interactions in acetate complex compared to N-H···Cl/Br interactions of

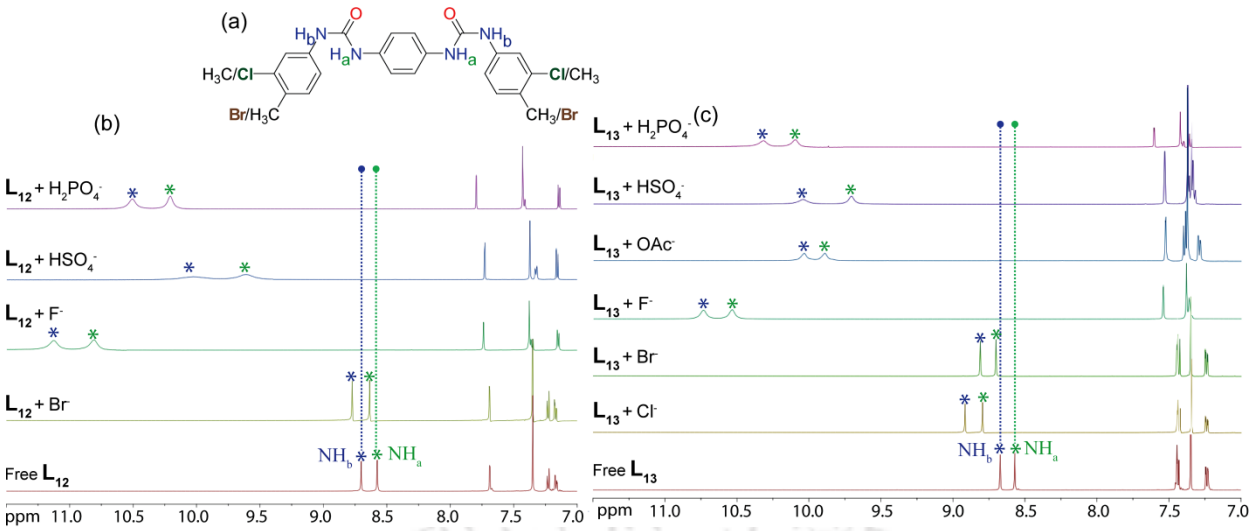

Fig. 5.11 (a) Representation of urea -NH_a and -NH_b of receptors $\mathbf{L_{12}}$/$\mathbf{L_{13}}$; Expanded partial ^{1}H NMR comparative stacked spectra (b) of receptor $\mathbf{L_{12}}$ and (c) of receptor $\mathbf{L_{13}}$, with different anions in solution phase as evidenced from the solid state results.

halide complexes in solution state. As we go from acetate to bicarbonate complexes, the ^{1}H-NMR solution data of $(HCO_3)_2$-dimer entrapped complexes show huge average downfield shifts of urea -NH protons for both receptors such as, $\Delta\delta$ = 2.33 ppm for $\mathbf{L_{12}}$ and $\Delta\delta$ = 2.02 ppm for $\mathbf{L_{13}}$. Subsequently, the non-cooperative $(H_2PO_4)_n$-polymer of both receptors exhibit large average downfield shifts of urea -NH protons in solution phase i.e. $\Delta\delta$ = 1.73 ppm for $\mathbf{L_{12}}$ and $\Delta\delta$ = 1.59 ppm for $\mathbf{L_{13}}$. Then, the sulfate entrapped non-cooperative and cooperative complexes of respective ligands $\mathbf{L_{12}}$ and $\mathbf{L_{13}}$ show average downfield shifts of urea -NH protons in solution phase such as $\Delta\delta$ = 1.18 ppm for $\mathbf{L_{12}}$ and $\Delta\delta$ = 1.26 ppm for $\mathbf{L_{13}}$. Interestingly, it is quite significant that the average downfield shifts of urea -NH protons for single acetate or single sulfate complexes are comparatively less than the average downfield shifts of $(HCO_3)_2$-dimer or $(H_2PO_4)_n$-polymer entrapped complexes in solution states, which may be ascribed for the more number of hydrogen-bonding interactions involved in dimeric or polymeric $(HCO_3)_2$ or $(H_2PO_4)_n$ association trapping compared to the monomeric anions OAc^- or SO_4^{2-}, as was also evidenced from solid state. Furthermore, the solution phase anion binding studies of *para*-halophenyl substituted receptors $\mathbf{L_{14}}$ and $\mathbf{L_{15}}$ have also been thoroughly carried out by ^{1}H NMR experiments (DMSO-d_6) in presence of halide and oxyanion salts as evidenced from the solid state results (Fig. 5.12a, b). The ^{1}H NMR analyses of the free receptors reveal that both $\mathbf{L_{14}}$ and $\mathbf{L_{15}}$ respectively exhibit very closely resemble chemical shift (δ) values for urea -NH protons i.e. , -NH_a = 8.58 ppm and NH_b = 8.76 ppm for $\mathbf{L_{14}}$ and -NH_a = 8.59 ppm and NH_b = 8.76 ppm for $\mathbf{L_{15}}$. The addition of *n*-TBABr salts to the individual DMSO-d_6 solutions of the receptors $\mathbf{L_{14}}$ and $\mathbf{L_{15}}$ exhibit very negligible and exactly similar average downfield shifts $\Delta\delta$ = 0.06 ppm and $\Delta\delta$ = 0.06 ppm respectively for the urea -NH protons. Whereas, the chloride salt addition to the

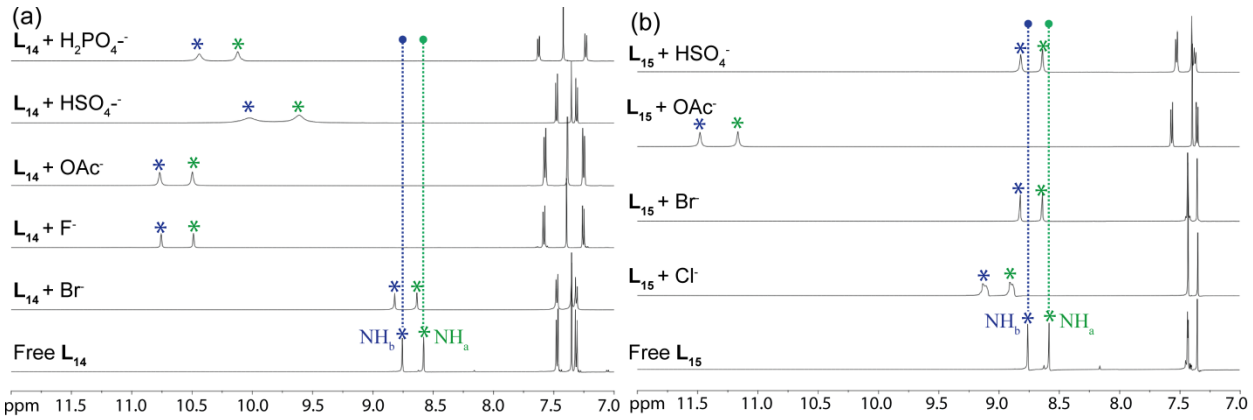

Fig. 5.12 Expanded partial ^{1}H NMR comparative stacked spectra of (a) receptor **L_{14}** and (b) receptor **L_{15}**, in solution phase with different anions as evidenced from the solid state results.

solution of **L_{15}** results average downfield shift of $\Delta\delta$ = 0.35 ppm for urea -NH protons, thus explains the better binding efficiency of chloride with receptor than bromide anion in solution state. But, despite the similar kinds of non-cooperative binding like halides in solid state, the acetate complexes of each ligand display large average downfield shifts of $\Delta\delta$ = 1.97 ppm and $\Delta\delta$ = 2.65 ppm for the urea -NH protons and these indicates the efficient binding of acetate anions with receptors in solution state as evidenced from solid state studies. Then, entrapment of oxyanion associations in solid state are fully supported from the ^{1}H-NMR solution state studies, such as the hydroxide induced $(HCO_3)_2$-dimer and $(H_2PO_4)_n$-polymer entrapped complexes of receptor **L_{14}** show huge average downfield shifts of $\Delta\delta$ = 1.96 ppm and $\Delta\delta$ = 1.56 ppm respectively for the urea -NH protons in their ^{1}H-NMR data. Therefore, the greater binding efficiency of oxyanions relative to halides with either of the bis-urea receptors **L_{12}**-**L_{15}** can be ascribed for the presence of stronger N−H···O interactions in oxyanion complexes compared to the weaker N−H···Cl/Br interactions in halide complexes in solution phase. However, the higher coordinating divalent sulfate complex of **L_{14}** exhibit moderate average downfield shifts of $\Delta\delta$ = 1.16 ppm for urea -NH protons in solution phase, but the dimeric $(HSO_4^-)_2$ complex of **L_{15}** show tiny average downfield shifts of $\Delta\delta$ = 0.04 ppm for urea -NH protons, that can be attributed to the stronger coordinating power of divalent sulfate with more number of ligand urea -NH groups compared to the monovalent bisulfate anion in solution state, as also evidenced from the solid state analyses. Finally, it should be noted that, the anion binding dissimilarities with any receptor molecule in solid and solution states are common phenomena in literature that can happen because of the rigid as well as more organized receptor arrangement in solid state compared with the floppy and looser orientations in solution state.

5.4 Conclusion

In summary, the rational design and synthesis of terminal aryl mono- as well as di-substituted

rigid *para*-phenylenediamine bridged bis-urea receptors **L_9-L_{15}** are effective towards systematic and consistent recognition of anions/hydrated anions or anionic associations despite the less preorganized and least convergent receptor architecture among the other rigid isomeric aromatic diamine based bis-urea receptors. Firstly, the effect of positional isomerism in a new class of nitrophenyl functionalized rigid and planar aromatic bis-urea receptors **L_9-L_{11}** have been extensively established toward the solid-state anion binding, further validated by solution state studies. Secondly, the halo-methylphenyl terminal aryl di-substituted bis-urea receptors **L_{12}-L_{13}** and thirdly the *para*-halophenyl functionalized bis-urea receptors **L_{14}-L_{15}** derived from rigid and linear *para*-phenylenediamine have also been established as the potential halide as well as oxyanion binding scaffolds thorough the formation of neutral host-guest self-assemblies despite the linear less preorganized receptor architectures. Evidence of atmospheric CO_2 fixation from strongly basic fluoride or hydroxide ion induction in the form of air-stable crystals of cyclic bicarbonate dimeric association has been found to be entrapped within the hydrogen-bonded self-assemblies of nitro-functionalized receptors **L_9-L_{10}**, halo-methylphenyl functionalized receptors **L_{12}-L_{13}** and *para*-chlorophenyl functionalized receptors **L_{14}**. The halo-methylphenyl as well as halo-phenyl functionalized receptors **L_{12}-L_{15}** form similar kinds of non-cooperative host-guest complexes with spherical chloride or bromide anions. The monovalent planar acetate anions are also bound either in their bare or hydrated form within the non-cooperative self-assemblies of *para*-phenylene connected bis-urea receptors **L_9**, **L_{10}**, **L_{13}**, **L_{14}** and **L_{15}**. However, in presence of *n*-$TBAHSO_4^-$ salt, **L_9**, **L_{15}** capture cyclic $(HSO_4)_2$ dimer within the non-cooperative hydrogen-bonded array, **L_{10}** arrests divalent sulfate anion inside the mixed (cooperative and non-cooperative) self-assemblies *via* hydrogen-bonded activated proton transfer, **L_{12}** entraps divalent sulfate anion and a water molecule through non-cooperative self-assembly and **L_{13}** captures two divalent sulfate anions inside the cation-assisted trimeric barrel through the construction of only cooperative self-assemblies. Subsequently, the bis-urea receptors **L_{10}**, **L_{12}**, **L_{13}** and **L_{14}** have also proved to be the decent dipodal scaffolds for capturing $(H_2PO_4)_n$ linear polymeric aggregated anionic association by non-cooperative hydrogen-bonding interactions. Conversely, no structural evidence of anion binding with *ortho*-isomer **L_{11}** could be demonstrated, owing to the presence of strong intramolecular N−H···O interactions in receptor structure that resists the facile inclusion of anions within the dipodal scaffold. The solution-state ^{1}H-NMR anion binding studies also heavily corroborate the solid-state results. Therefore, the set of least convergent aromatic diamie (*para*-phenylenediamine) based less preorganized linear rigid dipodal bis-urea scaffolds can still offer an appropriate understanding for construction of neutral host-guest self-assemblies mainly independent of any aryl-substituent incorporation as

peripheral groups or anion dimensions and these self-assembly processes are reliable to interpret the data and consistent to explain the variation.

References

5.1 (a) J. W. Steed and J. L. Atwood, *Supramolecular Chemistry. John Wiley & Sons, Ltd.:* New York, 2009; (b) R. Martinez-Manez and F. Sancenon, *Chem. Rev.* 2003, **103**, 4419; (c) P. R. Edwards, J. R. Hiscock, P. A. Gale and M. E. Light, *Org. Biomol. Chem*. 2010, **8**, 100; (d) E. A. Katayev, Y. A. Ustynyuk and J. L. Sessler, *Coord. Chem. Rev.* 2006, **250**, 3004.

5.2 (a) J. W. Pflugrath and F. A. Quiocho, *Nature*, 1985, **314**, 257; (b) Z. Wang, H. Luecke, N. Yao and F. A. Quiocho, *Nat. Struct. Biol.*, 1997, **4**, 519.

5.3 *Climate Change 2007: Synthesis Report, International Panel on Climate Change*; Cambridge University Press: Cambridge, U.K., 2007.

5.4 (a) S. Ayoob and A. K. Gupta, *Crit. Rev. Environ. Sci. Technol.*, 2006, **36**, 433; (b) *A systematic review of the efficacy and safety of fluoridation, 2007,* National Health and Medical Research Council, Australian Government, available at http://www. nhmrc.gov.au/.; (c) A. S. McCall, C. F. Cummings, G. Bhave, R. Vanacore, A. Page-McCaw and B. G. Hudson, *Cell*, 2014, **157**, 1380.

5.5 (a) M. C. Barth and A. T. Church, *J. Geophys. Res.*, 1999, **104**, 30231; (b) W. D. Heizer, R. S. Sandler, E. Seal, S. C. Murrai, M. G. Busby, B. G. Schliebe and S. N. Pusek, *Dig. Dis. Sci.*, 1997, **42**, 1055; (c) T. H. Milby and R. C. Baselt, *Am. J. Ind. Med.* 1999, **35**, 192.

5.6 (a) S. K. Dey, A. Basu, R. Chutia and G. Das, *RSC Adv.*, 2016, **6**, 26568; (b). R. Dutta and P. Ghosh, *Chem. Commun*., 2014, **50**, 10538; (c) M. Arunachalam and P. Ghosh, *Chem. Commun*., 2011, **47**, 8477.

5.7 (a) S. J. Brooks, P. A. Gale and M. E. Light, *Chem. Commun.*, 2005, 4696; (b) S. J. Brooks, P. A. Gale and M. E. Light, *CrystEngComm*, 2005, **7**, 586; (c) D. A. Jose, D. K. Kumar, B. Ganguly and A. Das, *Org. Lett.*, 2004, **6**, 3445; (d) R. Li, Y. Zhao, S. Li, P. Yang, X. Huang, X-J. Yang and B. Wu *Inorg. Chem.* 2013, **52**, 5851; (d) G. Xu and M. A. Tarr, *Chem. Commun*., 2004, 1050; (e) F. Otón, A. Tárraga, M. D. Velasco, A. Espinosa and P. Molina, *Chem. Commun.*, 2004, 1658; (f) U. Manna, B. Nayak, and G. Das *Cryst. Growth Des.* 2016, **16**, 7163; (g) U. Manna, S Kayal, B. Nayak and G. Das *Dalton Trans.*, 2017, **46**, 11956.

5.8 (a) U. Manna, R. Chutia and G. Das Cryst. Growth Des. 2016, **16**, 2893; (b) U. Manna, S. Kayal, S. Samanta and G. Das *Dalton Trans*., 2017, **46**, 10374; (c) U. Manna and G. Das *CrystEngComm*, 2017, **19**, 5622; (d) D. M. Gillen, C. S. Hawes and T. Gunnlaugsson *J. Org. Chem.* 83, **17**, 10398.

5.9 (a) U. Manna, A. Das, and G. Das *Cryst. Growth Des.*, 2018, **18**, 6801; (b) U. Manna, and G. Das *CrystEngComm*, 2017, DOI: 10.1039/C8CE01558A.

5.10 G. R. Desiraju, *Angew. Chem, Int. Ed.* 2007, **46**, 8342.

Annexure 5

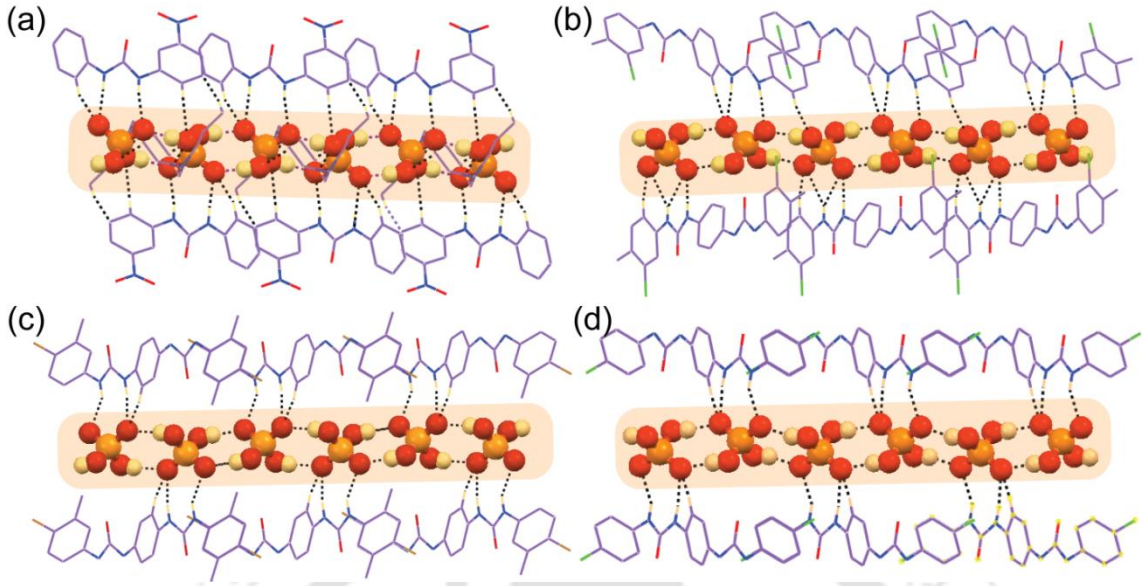

Fig.A5.1 X-ray structures (partial) depicting the hydrogen bonded array of linear *para*-phenylenediamine based bis-urea receptors on entrapment of linear $(H_2PO_4)_n$ polymeric aggregated anionic associations in (a) complex **10e**, (b) complex **12d**, (c) complex **13f** and (d) complex **14e**.

Table A5.1 Crystallographic parameters and refinement details of free receptors $\mathbf{L_9}$-$\mathbf{L_{11}}$ and complexes of $\mathbf{L_9}$

Parameters	$\mathbf{L_9}$.DMSO	$\mathbf{L_{10}}$.DMSO	$\mathbf{L_{11}}$.DMSO	$\mathbf{L_{10}}$	$\mathbf{L_{11}}$	**9a**	**9b**	**9c**
Formula	$C_{24}H_{28}N_6O_8S_2$	$C_{24}H_{28}N_6O_8S_2$	$C_{24}H_{28}N_6O_8S_2$	$C_{20}H_{16}N_6O_6$	$C_{20}H_{16}N_6O_6$	$C_{54}H_{90}N_8O_{12}$	$C_{56}H_{94}N_8O_{10}$	$C_{52}H_{90}N_8O_{14}S_2$
Fw	592.64	592.64	592.64	436.39	436.39	1043.34	1039.39	1115.44
Crystal system	triclinic	triclinic	monoclinic	monoclinic	triclinic	triclinic	triclinic	triclinic
Space group	*P* -1	*P* -1	*P* 21/c	*P* 21/n	*P* -1	*P* -1	*P* -1	*P* -1
a/Å	7.027(7)	7.417(12)	8.885(7)	6.770(3)	4.672(4)	8.140(7)	8.612(8)	8.308(5)
b/Å	8.092(7)	9.607(14)	5.495(4)	4.770(3)	5.936(7))	10.766(6)	10.217(9)	10.844(8)
c/Å	13.279(12)	10.828(17)	28.494(2)	29.712(16)	17.365(13)	18.409(11)	17.768(16)	17.490(13)
α/°	101.936(8)	106.215(13)	90.00	90.00	82.729(4)	88.114(5)	94.155(7)	93.273(6)
β/°	94.021(8)	96.982(13)	92.154(7)	95.749(3)	86.665(6)	77.750(6)	91.983(7)	94.126(6)
γ/°	100.656(8)	103.563(13)	90.00	90.00	84.947(6)	69.833(7)	106.768(8)	98.275(6)
V/Å^3	721.3(12)	705.6(2)	1390.2(18)	954.7(9)	475.25(8)	1478.3(19)	1490.5(2)	1551.7(19)
Z	1	1	2	2	1	1	1	1
D_c/g cm^{-3}	1.364	1.395	1.416	1.518	1.525	1.172	1.158	1.194
μ Mo K_α/mm^{-1}	0.241	0.246	0.250	0.116	0.116	0.083	0.079	0.150
F000	310.0	310.0	620.0	452.0	226.0	566.0	566.0	602.0
T/K	298(2)	298(2)	298(2)	298(2)	298(2)	298(2)	298(2)	298(2)
θ max.	24.996	24.999	25.000	28.590	25.000	24.998	24.999	24.999
Total no. of reflections	4706	4395	4692	14138	6593	9363	10126	10629
Independent reflections	2547	2482	2457	2408	1649	5195	5233	5433
Observed reflections	1667	1472	1762	2081	1379	2912	3318	3274
Parameters refined	193	183	202	145	145	339	339	348
R_1, I > 2σ(I)	0.0687	0.0593	0.0662	0.0471	0.0589	0.0888	0.0692	0.0703
wR_2, I > 2σ(I)	0.1417	0.1582	0.1872	0.1790	0.1476	0.1984	0.1687	0.1873
GOF (F^2)	1.016	0.999	1.175	1.148	0.973	1.034	1.101	1.016
CCDC No.	1847547	1847548	1847549	1847550	1847551	1847552	1847553	1847554

Table A5.2 Crystallographic parameters and refinement details of complexes of $\mathbf{L_{10}}$

Parameters	**10a**	**10b**	**10c**	**10d**	**10e**
Formula	$C_{60}H_{104}N_{10}O_{14}$	$C_{54}H_{90}N_8O_{12}$	$C_{56}H_{96}N_8O_{11}$	$C_{124}H_{192}N_{22}O_{26}S_2$	$C_{52}H_{92}N_8O_{14}P_2$
Fw	1189.53	1043.34	1057.41	2471.12	1115.28
Crystal system	monoclinic	triclinic	triclinic	triclinic	triclinic
Space group	*P* 21/c	*P* -1	*P* -1	*P* -1	*P* -1
a/Å	8.154(3)	7.921(16)	9.0578(3)	9.7001(8)	8.482(7)
b/Å	11.276(4)	11.255(2)	9.7515(4)	18.1688(13)	11.632(9)
c/Å	36.355(13)	16.684(3)	18.6766(7)	21.5764(17)	16.188(13)
α/°	90.00	79.358(12)	91.447(2)	111.391(7)	85.317(6)
β/°	94.733(2)	85.246(13)	99.350(2)	95.955(7)	79.343(7)
γ/°	90.00	88.625(13)	108.564(2)	92.633(7)	87.979(7)
V/Å^3	3331.0(2)	1456.7(5)	1537.81(10)	3507.1(5)	1564.0(2)
Z	2	1	1	1	1
D_c/g cm^{-3}	1.186	1.189	1.142	1.170	1.184
μ Mo K_α/mm^{-1}	0.084	0.084	0.079	0.111	0.133
F000	1292.0	566.0	576.0	1330.0	602.0
T/K	298(2)	298(2)	298(2)	298(2)	298(2)
θ max.	28.450	24.991	25.000	24.998	24.995
Total no. of reflections	50536	15038	11136	24276	10627
Independent reflections	8338	5004	5353	12340	5488
Observed reflections	6867	2737	3034	9131	3356
Parameters refined	386	340	359	793	363
R_1, I > 2σ(I)	0.0806	0.1132	0.0525	0.0976	0.0672
wR_2, I > 2σ(I)	0.1464	0.2158	0.1178	0.1847	0.1762
GOF (F^2)	1.049	1.159	1.041	1.071	1.105
CCDC No.	1847555	1847556	1847557	1847558	1847559

Table A5.3 Crystallographic parameters and refinement details of free receptors $\mathbf{L_{12}}$-$\mathbf{L_{13}}$ and their complexes

Parameters	$\mathbf{L_{12}}$	$\mathbf{L_{13}}$	**12a**	**12b**	**12c**	**12d**
Formula	$C_{22}H_{20}N_4O_2Cl_2$	$C_{22}H_{20}N_4O_2Br_2$	$C_{54}H_{91}N_6O_2Cl_2Br_2$	$C_{56}H_{93}N_6O_8Cl_2$	$C_{76}H_{108}N_{10}O_9Cl_4S$	$C_{56}H_{102}N_6O_{11}Cl_2P_2S$
Fw	443.32	532.22	1087.03	1049.26	1479.58	1200.34
Crystal system	monoclinic	triclinic	monoclinic	orthorhombic	monoclinic	triclinic
Space group	*P* 21/c	*P* -1	*P* n	*P* b c 21	*P* 21/n	*P* -1
a/Å	20.831(19)	4.647(13)	9.074(7)	11.148(6)	12.992(13)	8.5711(3)
b/Å	4.589(7)	7.068(2)	16.049(13)	14.998(12)	15.068(17)	20.396(9)
c/Å	10.521(13)	16.825(5)	21.293(14)	35.745(3)	43.128(3)	21.285(9)
α/°	90.00	95.97(2)	90.00	90.00	90.00	66.060(4)
β/°	90.751(11)	93.20(2)	99.970(7)	90.00	97.169(9)	82.359(3)
γ/°	90.00	108.52(3)	90.00	90.00	90.00	83.330(3)
V/Å^3	1005.6(2)	518.8(3)	3054.0(4)	5976.8(8)	8376.8(14)	3362.7(2)
Z	2	1	2	4	4	2
D_c/g cm^{-3}	1.464	1.704	1.182	1.166	1.173	1.186
μ Mo K_α/mm^{-1}	0.351	3.934	1.455	0.163	0.223	0.231
F000	460.0	266.0	1154.0	2276.0	3160.0	1296.0
T/K	298(2)	298(2)	298(2)	298(2)	298(2)	298(2)
θ max.	24.993	24.988	24.998	25.000	24.999	24.999
Total no. of reflections	3384	3173	11958	22846	37152	25136
Independent reflections	1778	1838	9963	9884	14726	11821
Observed reflections	1178	1023	6636	6939	8662	8104
Parameters refined	137	137	593	671	913	756
R_1, I > 2σ(I)	0.0697	0.0693	0.0714	0.1134	0.0873	0.0600
wR_2, I > 2σ(I)	0.1718	0.1478	0.1400	0.2164	0.1883	0.1882
GOF (F^2)	1.098	0.997	1.038	1.186	1.137	1.032
CCDC No.	1860313	1860314	1860315	1860316	1860317	1860318

Table A5.4 Crystallographic parameters and refinement details of anion complexes of receptor $\mathbf{L_{13}}$

Parameters	**13a**	**13b**	**13c**	**13d**	**13e**	**13f**
Formula	$C_{38}H_{56}N_5O_2Br_2Cl$	$C_{54}H_{92}N_6O_2Br_4$	$C_{56}H_{94}N_6O_8Br_2$	$C_{58}H_{94}N_6O_6Br_2$	$C_{130}H_{204}N_{16}O_{14}Br_6S_2$	$C_{54}H_{96}N_6O_{10}P_2Br_2$
Fw	810.13	1176.94	1139.17	1131.19	2758.61	1211.11
Crystal system	monoclinic	monoclinic	orthorhombic	triclinic	monoclinic	monoclinic
Space group	*C* 2/c	*P* 21/n	*P* 21 c a	*P* -1	*P* 21/c	*P* 21/c
a/Å	21.091(3)	8.983(5)	35.909(19)	8.464(10)	42.595(3)	11.519(8)
b/Å	11.449(8)	16.352(13)	11.206(9)	12.828(2)	12.806(11)	8.528(6)
c/Å	19.789(3)	21.105(12)	15.059(15)	14.890(19)	26.623(3)	32.260(19)
α/°	90.00	90.00	90.00	95.227(12)	90.00	90.00
β/°	121.336(17)	97.569(5)	90.00	93.285(10)	92.827(9)	96.752(6)
γ/°	90.00	90.00	90.00	99.204(12)	90.00	90.00
V/Å^3	4081.7(10)	3073.2(3)	6059.7(8)	1584.9(4)	14504(2)	3147.2(4)
Z	4	2	4	1	4	2
D_c/g cm^{-3}	1.318	1.272	1.249	1.185	1.263	1.278
μ Mo K_α/mm^{-1}	2.089	2.659	1.392	1.327	1.750	1.394
F000	1688.0	1228.0	2424.0	602.0	5800.0	1284.0
T/K	298(2)	298(2)	298(2)	298(2)	298(2)	298(2)
θ max.	24.999	24.999	24.999	24.999	25.000	24.999
Total no. of reflections	5737	13138	16296	10313	114464	12133
Independent reflections	3525	5405	9967	5554	25500	5532
Observed reflections	2042	3928	5666	3766	15025	3098
Parameters refined	221	303	661	331	1511	347
R_1, I > 2σ(I)	0.0490	0.0773	0.0844	.0903	0.1126	0.0580
wR_2, I > 2σ(I)	0.1284	0.1405	0.1728	0.1781	0.1908	0.1579
GOF (F^2)	0.884	1.076	1.112	1.051	1.182	0.853
CCDC No.	1860319	1860320	1860321	1860322	1860323	1860324

Table A5.5 Crystallographic parameters and refinement details of anion complexes of receptor $\mathbf{L_{14}}$

Parameters	**14a**	**14b**	**14c**	**14d**	**14e**
Formula	$C_{52}H_{88}N_6O_2\ Cl_2Br_2$	$C_{54}H_{90}N_6O_8Cl_2$	$C_{56}H_{94}N_6O_6Cl_2$	$C_{72}H_{104}N_{10}O_8Cl_4S$	$C_{52}H_{92}N_6O_{10}Cl_2P_2$
Fw	1059.98	1022.22	1018.27	1411.51	1094.16
Crystal system	monoclinic	triclinic	monoclinic	monoclinic	triclinic
Space group	*P* 21/n'	*P* -1	*P* 21/c	*P* 21/c	*P* -1
a/Å	8.9461(6)	8.4539(7)	13.2862(6)	18.1061(11)	8.4459(5)
b/Å	16.1753(10)	10.2145(8)	16.5740(8)	13.5141(7)	11.6202(10)
c/Å	20.8774(17)	18.1488(15)	28.0803(13)	17.5192(9)	15.6367(11)
α/°	90.00	92.095(7)	90.00	90.00	82.597(7)
β/°	100.396(8)	99.967(7)	93.874(5)	111.113(6)	83.548(5)
γ/°	90.00	107.977(7)	90.00	90.00	86.964(6)
V/Å^3	2971.5(4)	1461.4(2)	6169.3(5)	3999.0(4)	1511.05(19)
Z	2	1	4	2	1
D_c/g cm^{-3}	1.185	1.165	1.096	1.172	1.202
μ Mo K_α/mm^{-1}	1.494	0.165	0.154	0.230	0.217
F000	1124.0	554.0	2216.0	1508.0	590.0
T/K	298(2)	298(2)	298(2)	298(2)	298(2)
θ max.	25.000	24.999	24.999	25.000	24.999
Total no. of reflections	11706	9820	25218	17306	10428
Independent reflections	5232	5119	10858	7031	5307
Observed reflections	2896	2468	5267	4069	3542
Parameters refined	293	338	642	453	331
R_1, I > 2σ(I)	0.0655	0.0853	0.0797	0.0683	0.0640
wR_2, I > 2σ(I)	0.1767	0.2052	0.1791	0.1422	0.1684
GOF (F^2)	1.119	0.998	1.179	1.083	0.871
CCDC No.	1860326	1860327	1860328	1860329	1860330

Table A5.6 Crystallographic parameters and refinement details of anion complexes of receptor $\mathbf{L_{15}}$

Parameters	**15a**	**15b**	**15c**	**15d**
Formula	$C_{52}H_{88}N_6O_2Cl_2Br_2$	$C_{52}H_{88}N_6O_8Br_4$	$C_{56}H_{94}N_6O_6Br_2$	$C_{58}H_{104}N_6O_{12}Br_2S_2$
Fw	1059.98	1148.88	1107.17	1329.41
Crystal system	monoclinic	monoclinic	monoclinic	triclinic
Space group	*P* 21/n	*P* 21/n	*P* 21/c	*P* -1
a/Å	9.0143(6)	8.9473(16)	13.2635(9)	8.2364(9)
b/Å	15.6469(17)	16.101(4)	16.5661(12)	10.9069(14)
c/Å	21.0997(15)	21.153(4)	28.231(3)	20.0064(17)
α/°	90.00	90.00	90.00	85.053(8)
β/°	98.821(7)	100.90(2)	93.852(7)	79.089(8)
γ/°	90.00	90.00	90.00	81.371(10)
V/Å^3	2940.8(4)	2992.3(10)	6189.1(8)	1741.7(3)
Z	2	2	4	1
D_c/g cm^{-3}	1.197	1.275	1.188	1.268
μ Mo $K_α$/mm^{-1}	1.509	2.729	1.358	1.283
F000	1124.0	1196.0	2360.0	706.0
T/K	298(2)	298(2)	298(2)	298(2)
θ max.	24.998	24.998	24.999	24.998
Total no. of reflections	12250	11098	25495	12265
Independent reflections	5174	5147	10864	6100
Observed reflections	3780	2196	7625	4133
Parameters refined	294	293	642	378
R_1, I > 2σ(I)	0.0818	0.0777	0.0743	0.0922
wR_2, I > 2σ(I)	0.1850	0.1773	0.1560	0.1801
GOF (F^2)	1.154	1.183	1.001	1.147
CCDC No.	1860331	1860332	1860333	1860334

Table 5.7 Details of Hydrogen Bonding contacts in free receptors $\mathbf{L_9}$-$\mathbf{L_{11}}$ and their anion complexes

Ligand/Complex	D−H···A	*d*(D···H)/Å	*d*(H···A)/Å	*d*(D···A)/Å	<D−H···A/°	Symmetry codes
L_9-DMSO	N2-H2N···O10	0.86	1.97	2.808(5)	164	x,y,z
	N3-H3N···O10	0.86	2.12	2.928(5)	156	x,y,z
L_{10}-DMSO	N2-H2N···O7	0.86	2.08	2.893(4)	157	x,-1+y,z
	N3-H3N···O7	0.86	2.08	2.888(4)	157	x,-1+y,z
L_{11}-DMSO	N3-H3N···O4A	0.86	1.91	2.730(3)	158	x,1+y,z
	N3-H3N···O4B	0.86	2.03	2.871(18)	165	x,1+y,z
L_{10}	N2-H2N···O3	0.86	2.08	2.895(17)	159	x,1+y,z
	N3-H3N···O3	0.86	2.43	3.198(17)	149	x,1+y,z
L_{11}	N2-H2N···O3	0.86	2.30	3.053(3)	146	-1+x,y,z
	N3-H3N···O3	0.86	1.99	2.826(3)	164	-1+x,y,z
9a	N2-H2N···O5	0.86	1.91	2.765(4)	171	x,y,z
	N3-H3N···O4	0.86	1.96	2.811(5)	170	x,y,z
	O6-H6O···O4	0.82	1.82	2.640(4)	173	1-x,1-y,-z
9b	N2-H2N···O5	0.86	1.92	2.755(3)	164	1+x,y,z
	N3-H3N···O4	0.86	1.97	2.815(3)	168	1+x,y,z
9c	N2-H2N···O6	0.86	2.04	2.879(5)	164	1-x,-y,1-z
	N3-H3N··· O5	0.86	2.15	3.002(5)	169	1-x,-y,1-z
	O4-H4···O5	0.82	1.84	2.657(4)	175	1-x,-y,1-z
10a	N2-H2N···O5	0.86	1.96	2.800(3)	164	x,y,z
	N3-H3N···O4	0.86	2.00	2.845(3)	167	x,y,z
	O6-H6O···O4	0.82	1.80	2.615(3)	171	1-x,1-y,-z
10b	N2-H2N···O4	0.86	1.93	2.783(7)	169	x,y,z
	N3-H3N··· O6	0.86	1.99	2.835(6)	169	x,y,z
	O5-H5A··· O6	0.82	1.81	2.615(7)	167	1-x,1-y,1-z
10c	N2-H3···O4	0.97	1.83	2.782(3)	168	x,-1+y,z
	N3-H3···O5	0.85	1.97	2.814(3)	175	x,-1+y,z
	O6-H6A···O5	0.85	1.93	2.775(7)	173	x,-1+y,z
	O6-H6B···O5	0.85	2.39	3.101(6)	142	1-x,1-y,-z
10d	N4-H4N···O12	0.86	1.91	2.763(5)	172	x,y,z
	N5-H5N···O12	0.86	2.52	3.260(6)	145	x,y,z
	N6-H6N···O15	0.86	2.17	3.004(6)	162	1-x,1-y,-z
	N7-H7N···O14	0.86	1.91	2.765(5)	176	1-x,1-y,-z
	N10-H10N···O13	0.86	2.01	2.836(5)	160	1-x,1-y,1-z
	N11-H11N···O13	0.86	2.09	2.904(6)	158	1-x,1-y,1-z
10e	N2-H2N···O5	0.80	2.09	2.884(4)	169	x,y,z
	N3-H3N···O4	0.86	1.99	2.842(4)	174	x,y,z
	O6-H6O···O4	0.81	1.77	2.563(3)	167	-x,1-y,1-z
	O7-H7O···O5	0.86	1.69	2.544(3)	169	1-x,1-y,1-z

Table 5.8 Details of Hydrogen Bonding contacts in free receptors $\mathbf{L_{12}}$-$\mathbf{L_{13}}$ and their anion complexes

Ligand/Complex	D−H···A	*d*(D···H)/Å	*d*(H···A)/Å	*d*(D···A)/Å	<D−H···A/°	Symmetry codes
L_{12}	N1-H1N···O1	0.86	2.06	2.856(4)	153	x,1+y,z
	N2-H2N···O1	0.86	2.10	2.881(4)	151	x,1+y,z
L_{13}	N1-H1N···O1	0.86	2.08	2.883(8)	154	-1+x,y,z
	N2-H2N···O1	0.86	2.13	2.923(8)	153	-1+x,y,z
12a	N1-H1N···Br2	0.86	2.47	3.298(19)	161	x,y,z
	N2-H2N···Br2	0.86	2.55	3.350(2)	155	x,y,z
	N3-H3N···Br1	0.86	2.54	3.379(19)	166	-1/2+x,1-y,-1/2+z
	N4-H4N··· Br1	0.86	2.62	3.437(17)	159	-1/2+x,1-y,-1/2+z
12b	N1-H1N···O4	0.86	1.86	2.691(13)	162	x,y,z
	N2-H2N···O3	0.86	1.97	2.826(12)	172	x,y,z
	N3-H3N···O6	0.86	1.97	2.817(12)	167	-x,1-y,1/2+z
	N4-H4N···O7	0.86	1.87	2.718(13)	168	-x,1-y,1/2+z
	O5-H5···O6	0.82	1.83	2.640(2)	172	1-x,1-y,1/2+z
	O8-H8···O3	0.82	1.83	2.640(2)	171	1-x,1-y,-1/2+z
12c	N1-H1N···O7	0.86	1.96	2.814(7)	171	3/2-x,-1/2+y,1/2-z
	N2-H2N···O8	0.86	2.08	2.901(7)	159	3/2-x,-1/2+y,1/2-z
	N3-H3N···O6	0.86	2.14	2.971(6)	161	x,y,z
	N4-H4N···O7	0.86	1.95	2.794(7)	168	x,y,z
	N5-H5N···O5	0.86	2.03	2.844(7)	158	x,y,z
	N6-H6N···O6	0.86	2.14	2.972(7)	164	x,y,z
	N7-H7N···O8	0.86	2.03	2.884(7)	174	1/2-x,-1/2+y,1/2-z
	N8-H8N···O5	0.86	2.18	2.948(8)	149	1/2-x,-1/2+y,1/2-z
	N8-H8N···O8	0.86	2.58	3.317(7)	144	1/2-x,-1/2+y,1/2-z
12d	N1-H1N···O3	0.80	2.49	3.203(5)	151	1-x,-y,1-z
	N1-H1N···O6	0.80	2.50	3.207(5)	149	1-x,-y,1-z
	N2-H2N···O6	0.75	2.04	2.784(4)	173	1-x,-y,1-z
	N3-H3N···O7	0.87	2.00	2.862(4)	178	x,y,z
	N4-H4N···O8	0.86	2.04	2.886(4)	167	x,y,z
	O4-H4O···O7	0.78	1.80	2.571(3)	169	x,y,z
	O5-H5O···O8	0.96	1.65	2.590(3)	169	-1+x,y,z
	O9-H9O···O3	0.80	1.83	2.574(4)	154	x,y,z
	O10-H10O···O6	0.82	1.76	2.566(4)	172	1+x,y,z
13a	N1-H1N···Cl1	0.86	2.49	3.301(4)	157	1/2+x,-1/2+y,z
	N2-H2N···Cl1	0.86	2.37	3.219(4)	167	1/2+x,-1/2+y,z
13b	N1-H1N···Br2	0.86	2.55	3.367(8)	160	1/2-x,1/2+y,1/2-z
	N2-H2N···Br2	0.86	2.51	3.347(6)	163	1/2-x,1/2+y,1/2-z
13c	N1-H1N···O8	0.86	1.94	2.795(13)	172	x,1-y,-1/2+z
	N2-H2N··· O6	0.86	1.99	2.831(12)	166	x,1-y,-1/2+z
	N3-H3N··· O5	0.86	2.00	2.855(12)	171	x,1-y,-1/2+z
	N4-H4N··· O3	0.86	1.99	2.797(13)	156	x,1-y,-1/2+z
	O4-H4O···O6	0.82	1.84	2.647(17)	166	x,y,z
	O7-H7O···O5	0.82	1.82	2.608(18)	162	x,y,z
13d	N1-H1N···O2	0.86	1.97	2.824(9)	170	x,y,z
	N2-H2N···O3	0.86	1.94	2.787(9)	169	x,y,z
13e	N1-H2N···O7	0.86	2.01	2.858(11)	166	x,1+y,z
	N2-H3N··· O10	0.86	1.95	2.805(10)	171	x,1+y,z
	N3-H4N··· O11	0.86	2.23	3.066(11)	162	x,1+y,z
	N4-H5N··· O13	0.86	1.91	2.769(9)	174	x,1+y,z
	N5-H6N···O14	0.86	2.26	3.054(8)	153	x,3/2-y,-1/2+z
	N6-H7N··· O12	0.86	1.94	2.792(9)	171	x,3/2-y,-1/2+z
	N7-H8N···O9	0.86	1.97	2.822(11)	169	x,3/2-y,-1/2+z
	N8-H9N···O8	0.86	2.01	2.845(11)	162	x,3/2-y,-1/2+z
	N9-H10N···O14	0.86	1.99	2.841(11)	168	x,1/2-y,-1/2+z
	N10-H11N···O11	0.86	2.18	3.009(11)	162	x,1/2-y,-1/2+z
	N11-H12N···O10	0.86	2.00	2.820(10)	161	x,1/2-y,-1/2+z
	N12-H13N···O8	0.86	2.36	3.158(11)	155	x,1/2-y,-1/2+z
	N12-H13N···O10	0.86	2.48	3.196(11)	142	x,1/2-y,-1/2+z
13f	N1-H1N···O2	0.86	2.12	2.905(5)	151	1-x,1-y,-z
	N2-H2N···O5	0.86	1.99	2.826(5)	163	1-x,1-y,-z
	O3-H3O···O5	0.74	1.86	2.568(5)	161	1-x,2-y,-z
	O4-H4O···O2	0.78	1.79	2.565(4)	175	1-x,2-y,-z

Table 5.9 Details of Hydrogen Bonding contacts in anion complexes of receptors L_{14}-L_{15}

Ligand/Complex	D−H···A	*d*(D···H)/Å	*d*(H···A)/Å	*d*(D···A)/Å	<D−H···A/°	Symmetry codes
14a	N1-H1N···Br1	0.86	2.52	3.351(5)	162	1/2-x,-1/2+y,1/2-z
	N2-H2N···Br1	0.86	2.50	3.332(4)	163	1/2-x,-1/2+y,1/2-z
14b	N1-H1N···O2	0.86	1.93	2.76(13)	164	x,y,z
	N2-H2N···O3	0.86	2.00	2.83(13)	165	x,y,z
	O4-H4O···O3	0.82	1.83	2.64(13)	169	1-x,1-y,-z
14c	N1-H1N···O3	0.86	2.00	2.834(4)	163	x,y,z
	N2-H2N···O4	0.86	1.93	2.776(4)	166	x,y,z
	N3-H3N···O5	0.86	1.97	2.785(4)	158	1-x,-1/2+y,1/2-z
	N4-H4N···O6	0.86	1.96	2.809(4)	167	1-x,-1/2+y,1/2-z
14d	N1-H1N···O4	0.86	2.00	2.833(7)	162	x,y,z
	N1-H1N···O6	0.86	2.06	2.854(7)	154	x,y,z
	N2-H2N···O4	0.86	2.58	3.248(6)	135	x,y,z
	N2-H2N···O5	0.86	2.17	2.927(6)	147	x,y,z
	N2-H2N···O3	0.86	1.95	2.765(5)	159	1-x,-y,1-z
	N3-H3N···O6	0.86	2.54	3.299(6)	148	1-x,1/2+y,1/2-z
	N3-H3N···O3	0.86	2.00	2.798(5)	154	x,1/2-y,-1/2+z
	N3-H3N···O4	0.86	2.29	3.051(6)	148	x,1/2-y,-1/2+z
	N3-H3N···O5	0.86	2.51	3.233(6)	142	x,1/2-y,-1/2+z
	N4-H4N···O6	0.86	2.03	2.828(6)	153	1-x,1/2+y,1/2-z
	N4-H4N···O5	0.86	2.00	2.835(6)	163	x,1/2-y,-1/2+z
14e	N1-H1N···O5	0.86	2.13	2.923(4)	153	x,y,z
	N2-H2N···O4	0.86	2.01	2.833(4)	161	x,y,z
	O2-H2O···O5	0.82	1.75	2.549(4)	164	1-x,-y,1-z
	O3-H3O···O4	0.82	1.76	2.558(4)	166	-x,-y,1-z
15a	N1-H1N···Cl1	0.86	2.35	3.181(6)	161	3/2-x,1/2+y,1/2-z
	N2-H2N···Cl1	0.86	2.35	3.181(6)	162	3/2-x,1/2+y,1/2-z
15b	N1-H1N···Br2	0.86	2.52	3.352(6)	163	1/2-x,-1/2+y,1/2-z
	N2-H2N···Br2	0.86	2.49	3.319(6)	163	1/2-x,-1/2+y,1/2-z
15c	N1-H1N···O3	0.86	1.97	2.809(7)	164	x,y,z
	N2-H2N··· O4	0.86	1.92	2.766(7)	166	x,y,z
	N3-H3N··· O6	0.86	1.96	2.778(7)	158	1+x,y,z
	N4-H4N··· O5	0.86	1.97	2.812(7)	166	1+x,y,z
15d	N1-H1N···O10	0.86	2.04	2.902(7)	175	x,y,z
	N2-H2N··· O11	0.86	2.15	2.992(7)	166	x,y,z
	O8-H8··· O11	0.82	1.83	2.646(6)	172	1-x,1-y,1-z

Chapter 6

Tren-based positional and electronic isomeric receptors for encapsulation of anions/hydrated anions

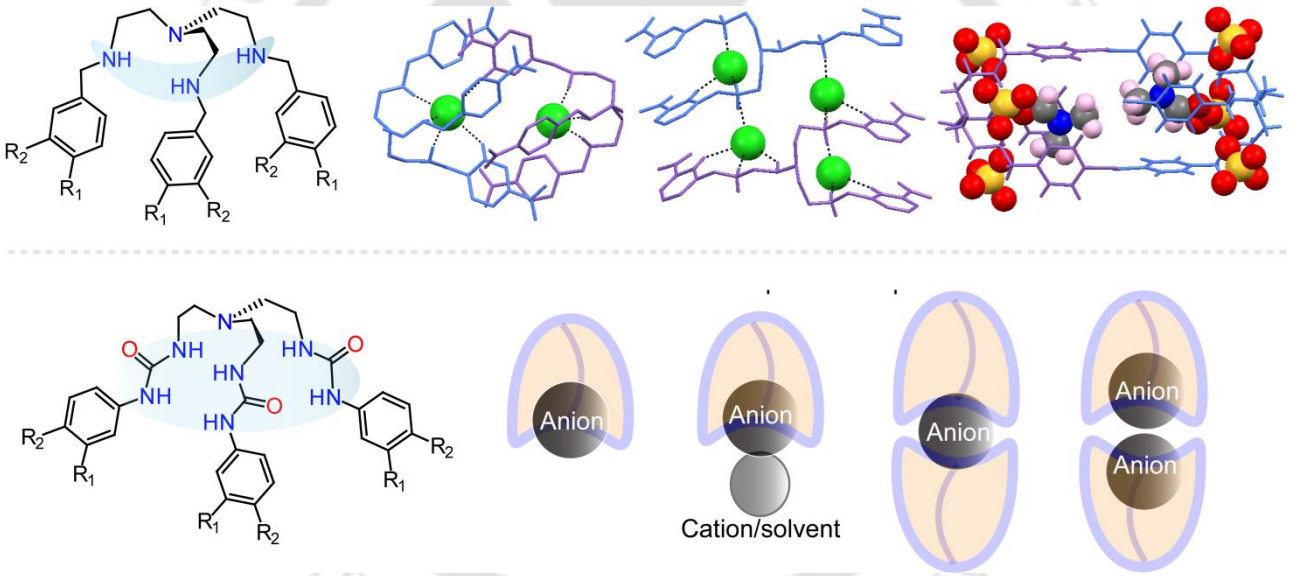

6.1 Background and Focus of the Chapter

As anions are ubiquitous in nature, the development of abiotic receptors for recognition and sensing of anions have become an active area of research interests not only in supramolecular chemistry but also have immense implication in biological, environmental and clinical applications.[6.1] The tris(2-aminoethyl)-amine, tren, is a characteristic tripodal building block for anions in coordination chemistry that has been studied by different research groups over the past decades and motivated by the observations in natural anion binding systems, several hydrogen bonding functionalities such as amines, amides, urea/thiourea have been frequently employed for coordinating size and shape-selective targeted anionic guest species *via* the formation of monomeric and dimeric capsular assemblies.[6.2] Mainly, a self-assembly process results from simple to complex molecular/supramolecular systems and the most attractive features of molecular capsule is their ability to sequester a guest molecule by creating specific microcavity from the competitive bulk media by encapsulation *via* topological complementarity. In this consequence, the formation of halide and oxyanion-induced capsular assemblies represents one of the key approaches in the area of supramolecular self-assembly as well as molecular recognition.[6.3] The encapsulation of halides by synthetic receptors are of huge significance, because the excess of fluoride ion in drinking water may cause skeletal and dental fluorosis and it can also cause osteosarcoma in human body beyond its toxic levels. The larger chloride ions are essential owing to their crucial roles in biological routes like signal transduction, the transport of organic solutes through cell membranes and the heavier bromide ions are belonging to an essential cofactor for the assembly of collagen IV scaffolds in tissue growth.[6.4] The encapsulation of higher coordinating oxyanions (planar, tetrahedral or octahedral) within the molecular receptor cage becomes also a challenging job, as the planar carbonate work as buffer in the blood and the larger tetrahedral sulfate exist as a contaminant in drinking water because of its high charge density and they also act as pollutant in nuclear and radioactive waste

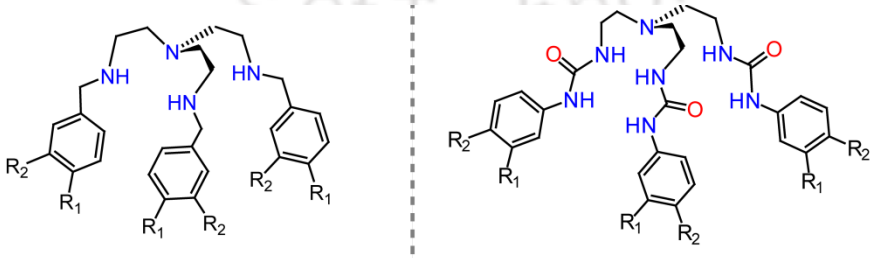

L_{16} $R_1 = -NO_2$, $R_2 = -H$
L_{17} $R_1 = -Br$, $R_2 = -H$
L_{18} $R_1 = -H$, $R_2 = -NO_2$

L_{19} $R_1 = -Cl$, $R_2 = -CH_3$
L_{20} $R_1 = -CH_3$, $R_2 = -Br$
L_{21} $R_1 = -Cl$, $R_2 = -H$
L_{22} $R_1 = -Br$, $R_2 = -H$
L_{23} $R_1 = -I$, $R_2 = -H$

Scheme 6.1 A comprehensive representation of molecular receptor structures included in this chapter.

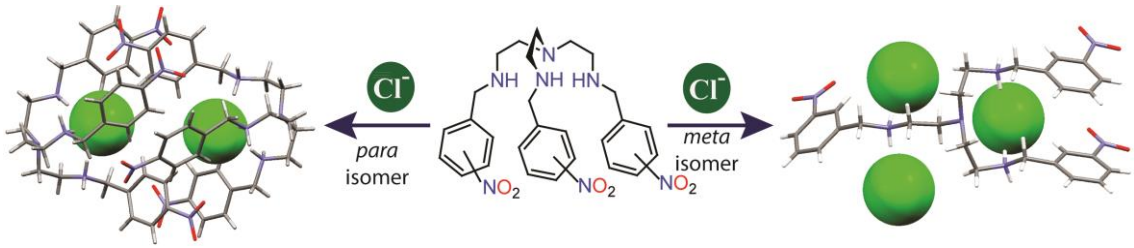

Fig. 6.1 The comprehensive representation of one of the key outcomes of research work included in this chapter.

that can destruct the vitrification process.[6.5] Thus far, among the numerous neutral or charged tren-based tripodal podands containing various -NH functionalization reported from late nineteenth century, comprise of either electron-withdrawing or electron-donating terminal aryl substituents or some positional isomeric terminal substituents attached with tris-urea moiety.[6.2] However, tripodal isomeric receptors containing less coordinating polyamine moieties or some tripodal tris-(thio)-urea receptors with more than one simultaneous EWG and EDG containing aryl terminals are still an unfamiliar area among the wide-spread tren-based anion-receptor chemistry.

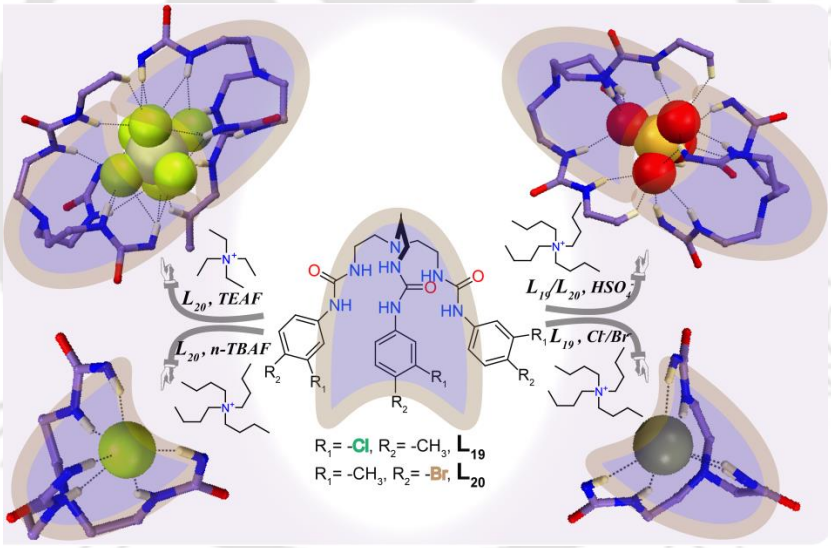

Fig. 6.2 The comprehensive representation of one of the key outcomes of research work included in this chapter.

Hence, in continuing our group's special interest on investigating substituent driven host-guest self-assemblies as well as cavity-induced encapsulation of anionic guests of different shapes, in this chapter we describe the rationally designed and newly synthesized three N-bridged flexible isomeric polyammonium[6.6a] receptors (**L_{16}**-**L_{18}**) among which the *para*- nitrophenyl (**L_{16}**) and *para*-bromophenyl (**L_{17}**) functionalized tris-polyamine receptors form protonated capsular assemblies with halide ions (complexes **16a**, **17a**), whereas the *meta*-nitrophenyl functionalized tripodal polyamine receptor **L_{18}** (a positional isomer of receptor **L_{16}**) shows entrapment of chloride anion within the protonated non-capsular Y-shaped host-assemblies (complexes **18a**), which is the consequences of steric effect provided by the *meta*-nitro group towards the smaller

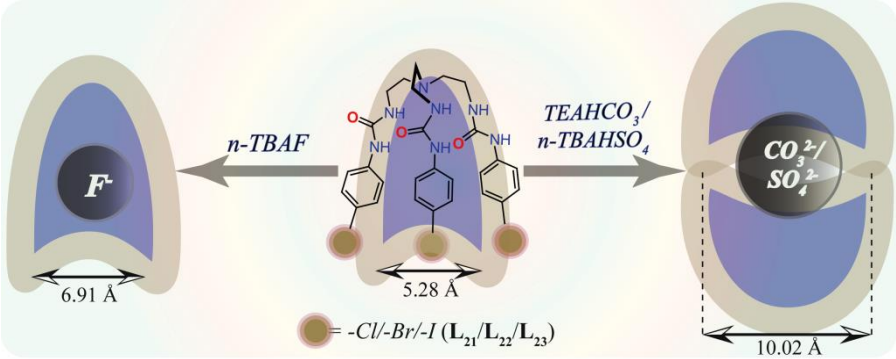

Fig. 6.3 The comprehensive representation of one of the key outcomes of research work included in this chapter.

tripodal receptor cavity. Furthermore, the presence of relatively smaller cavity in these polyamine based receptors hinders the binding of larger oxyanions such as divalent sulfate. As a result, the protonated tripodal scaffolds of receptors **L_{16}** and **L_{17}** both encapsulate small DMF solvent molecule inside the receptor cavity (complexes **16b**, **17b**) due to size mismatch with larger sulfate anion and these help in side-cleft binding of the larger sulfate anion outside the receptor cavities *via* construction of discrete sulfate-water clusters. On the other hand, the two halo-methylphenyl terminal aryl-disubstituted tris-urea receptors **L_{19}** (chloro-methyl isomer) and **L_{20}** (bromo-methyl isomer) derived from flexible [tris(2-aminoethyl)-amine] skeleton,[6.6b] efficiently capture spherical chloride or bromide anions (complexes **19a**, **19b**) within the cation-sealed neutral unicapsular assemblies of **L_{19}** and encapsulate the smallest halide anion *via* formation of unimolecular polymeric host-guest assemblies (complexes **20a**) of receptor **L_{20}** and fluoride. The X-ray analyses also expose that the planar carbonate, tetrahedral sulfate and octahedral hexafluorosilicate divalent anions of varied dimensionalities are fully engulfed inside the dimeric capsular cages of either of the isomeric neutral receptors **L_{19}** or **L_{20}** in 2:1 host-guest fashion (complexes **19c**, **19d**, **20b**, **20c**), irrespective of the size of counter-cations. Subsequently, another three *para*-halophenyl functionalized tren-based tripodal urea receptors **L_{21}** (*para*-chloro), **L_{22}** (*para*-bromo) and **L_{23}** (*para*-iodo) [6.6c] showcase a constant proof of fluoride encapsulation with 1:1 host-guest stoichiometry (complexes **21a**, **22a**, **23a**). Moreover, each isomer have been structurally authenticated to self-assemble into a 2:1 neutral dimeric molecular cage in the presence of either planar carbonate or larger tetrahedral sulfate anions (complexes **21b**, **22b**, **23b**, **23c**) irrespective of the size of counter-cations, just similar as in oxyanion complexes of receptors **L_{19}** or **L_{20}**. Scheme 6.1 shows the molecular receptor structures **L_{16}-L_{23}** and the representations of key findings of research work included in this chapter are shown Fig. 6.1-6.3.

6.2 Structural aspects of anion binding with L_{16}-L_{23}

In general, a particular synthetic receptor molecule should possess preorganized directional

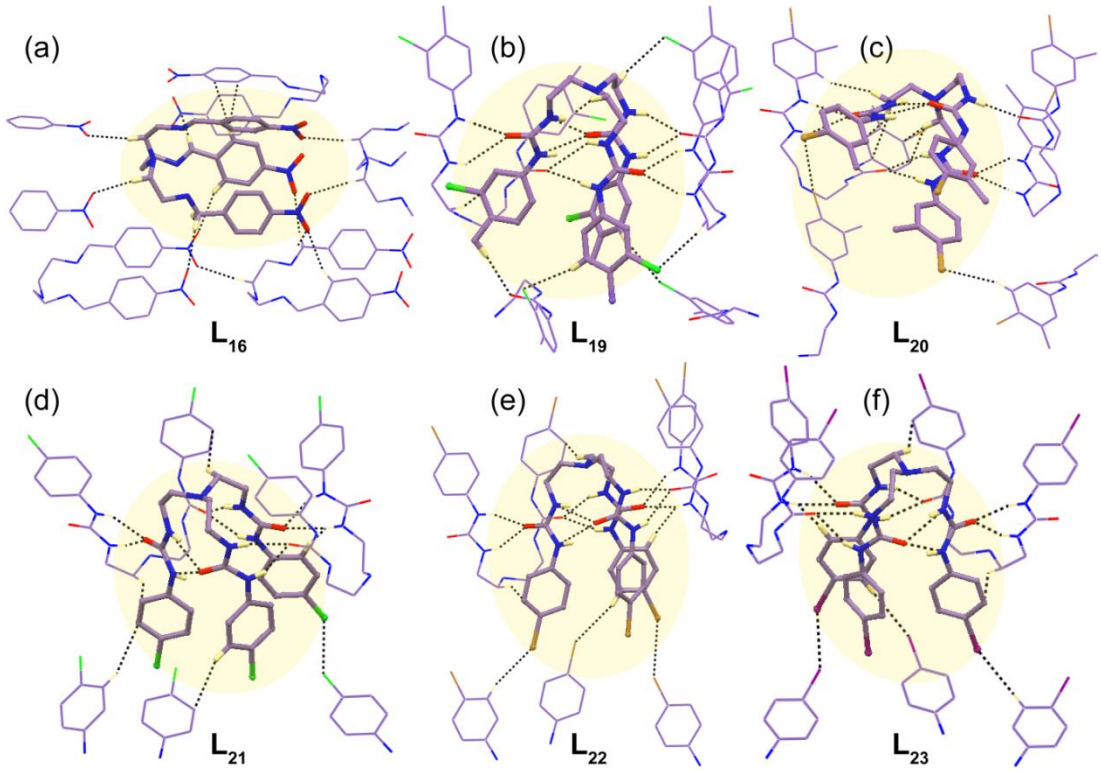

Fig. 6.4 Partial X-ray structures depicting non-covalent interactions of a particular receptor unit (ball and stick) with adjacent ligand conformers (wireframe) in individual free receptor structure of (a) $\mathbf{L_{16}}$, (b) $\mathbf{L_{19}}$, (c) $\mathbf{L_{20}}$, (d) $\mathbf{L_{21}}$, (e) $\mathbf{L_{22}}$ and (f) $\mathbf{L_{23}}$.

hydrogen-bond donating suitable platform to encapsulate the size and shape dependent anionic guest by topological complementarity. Noticeably, the tris(2-aminoethyl)-amine based, three tris-polyammonium receptors $\mathbf{L_{16}}$-$\mathbf{L_{18}}$ (Fig. 6.1) with positional and functional distinction as well as the 3,4-halo-methylphenyl (Fig. 6.2) and 4-halophenyl (Fig. 6.3) substituted five tris-urea receptors $\mathbf{L_{19}}$-$\mathbf{L_{23}}$ each hold appropriate organized tripodal scaffold with amine or urea functions, that can non-covalently bind anionic guests of various dimensions, consistently influenced by the receptor cavity size or terminal aryl substituent effect. Structural evidences obtained from single crystal X-ray studies of the isolated crystals provide insight into the proper binding topology of anions/hydrated-anions with the neutral or protonated receptor molecules. Efforts were made to explore the solid-state binding properties of $\mathbf{L_{16}}$-$\mathbf{L_{23}}$ with various anions in different crystallization conditions. The purposeful attachment of amine groups in 4-nitro/4-bromo/3-nitro-phenyl functionalized tripodal scaffolds and urea groups in highly organized 3,4-halo-methylphenyl/methyl-halophenyl or 4-chloro/bromo/iodo-phenyl functionalized tripodal scaffolds become helpful to determine the binding discrepancies of anionic guests *via* number of non-covalent interactions. Basically, the crystallization is a conventional route comprehending the structural insights of the anion complexes from the perspective of anion coordination chemistry, primarily by single-crystal XRD analysis, which is then associated to the observed selectivity in solution.

It should be mentioned here that, the crystal structures suitable for XRD analysis are obtained from the basic DMF/DMSO solutions of *para*-nitrophenyl functionalized free tris-amine receptor **L_{16}** and each halo-methylphenyl or halo-phenyl functionalized tris-urea receptors **L_{19}-L_{23}**, whereas several crystallization attempts for free tris-amine receptors **L_{17}** and **L_{18}** from various solvents and different crystallization conditions were failed may be due to the semi-solid nature of the respective ligands. The free tris-amine receptor **L_{16}** crystallize in the orthorhombic space groups $P2_12_12_1$ and structural elucidation reveals that all the three arms of the receptor orient towards cavity constructing a molecular cup capsular assembly (Fig. 6.4a) with almost no free space or no tripodal cavity. Each **L_{16}** receptor in the asymmetric unit are attached with adjacent conformers by intermolecular C−H···π and C−H···O interactions (Fig. 6.4a). On the other hand, the halo-methylphenyl substituted tris-urea free receptors **L_{19}-L_{20}** both crystallize in the monoclinic space group *P*21/c and the halo-phenyl substituted tris-urea free receptors **L_{21}-L_{23}** each exhibiting almost isostructural nature crystallizes in the same triclinic space group *P*-1. In each free tris-urea ligands **L_{19}-L_{23}**, the urea -NH atoms flanked from the bridgehead N-atom are projected towards three different directions, not towards the inner tripodal capsular cavity (Fig. 6.4b-f). Note that, in absence of any guest, the architecture of free receptors **L_{19}-L_{23}** are still capsular and resist the opening of the tripodal side arms with C_3 symmetry, which are ascribed for the combined effect of intramolecular as well as intermolecular non-covalent interactions. The rest of the two urea -NH moieties are involved in strong intermolecular N−H···O interactions with either of adjacent receptors' arms in **L_{19}-L_{23}** (Fig. 6.4b-f). All the free tris-urea ligands **L_{19}-L_{23}** also form linear 1D-polymeric aggregated assemblies *via* intramolecular as well as intermolecular N−H···O interactions, which are then further interconnected with adjacent linear polymeric layers by several weak interactions other than strong N−H···O contacts.

6.2.1. Structural analysis of halide bound complexes of receptors L_{16}-L_{23}

Single crystal XRD analyses of neutral or protonated receptor-halide complexes and the consistent as well as discriminating binding behavior of receptors in cooperative or non-cooperative mode toward halides are severely dependent upon the isomeric effect of terminal aryl receptor substituents or influence of the receptor cavity or size of the halide guests.

6.2.1.1 Chloride complex 16a of receptor L_{16}

The chloride salt complex of protonated tris-amine receptor **L_{16}** crystallize in orthorhombic space group $P2_12_12_1$ where all the three secondary amine groups of tripodal receptor are protonated. Structural elucidation reveals that, the tripodal receptor in complex **16a** opens up its

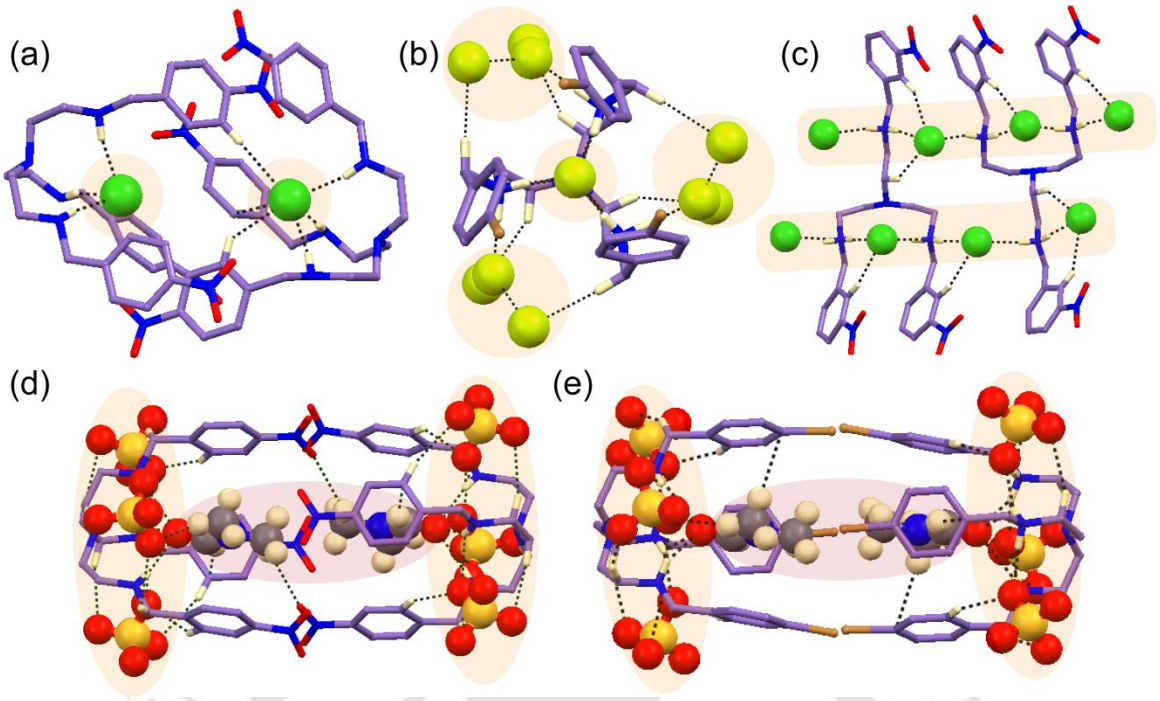

Fig. 6.5 Partial X-ray structures depicting the non-covalent interactions involved in (a) chloride encapsulated salt-complex **16a**, (b) fluoride encapsulated salt-complex **17a**, (c) chloride entrapped non-capsular salt-complex **18a**, (d) side cleft sulfate bound DMF encapsulated salt-complex **16b** and (e) side cleft sulfate bound DMF encapsulated salt-complex **17b**.

arms by maintaining the capsular orientation and encapsulates the chloride ion (Fig. 6.5a). Among the six ammonium hydrogen atoms (NH_2^+) in three arms of the polyamine receptor **L_{16}**, half of them are pointed towards the receptor cavity and remaining three hydrogen atoms are pointed in outward direction of the cavity. There are six chloride ions present in the near vicinity of the protonated receptor to balance the charge and it is evident that out of six chloride ions in complex **6a**, Cl1 and Cl3 are fully encapsulated into the molecular cup of the receptor **L_{16}**, among which Cl1 is stabilized only by three strong N−H···Cl interactions and Cl3 is stabilized by three N−H···Cl, two C−H···Cl and one Cl···π interactions (Fig. 6.5a). The other four chloride anions (Cl2, Cl4, Cl5, Cl6), which are free from encapsulation into the molecular cup of tripodal host, gain stability *via* several non-covalent interactions with adjacent conformers. The chloride ions Cl2, Cl4 are stabilized *via* four C−H···Cl and two N−H···Cl interactions and Cl5, Cl6 are stabilized *via* three C−H···Cl and one N−H···Cl interactions through the H-bond donor sites of receptors, pointed outward direction of the receptor cavity.

6.2.1.2 Fluoride complex 17a of receptor L_{17}

The fluoride salt complex of *para*-bromophenyl substituted tris-amine receptor **L_{17}** crystallizes in trigonal space group *R*3 and complex **17a** contains three-fold symmetry where the C_3-axis passes through the apical N1 atom and encapsulated F1 ion. The asymmetric unit of **17a** carries one-third part of the protonated receptor $[\mathbf{L_{17}}H_3]^{3+}$ and three fluoride anions, where the tripodal

cavity size is close enough to the free **L_{16}** receptor. Structural elucidation of **17a** reveals that the fluoride ion F1 is fully encapsulated into the cavity of the receptor stabilized by three strong N−H···F interactions *via* three polyamine -NH hydrogen bond donor groups pointed towards the host cavity (Fig. 6.5b). The remaining three exo-oriented -NH atoms are bound to three symmetry-identical fluoride ions (F2) separately *via* N−H···F interactions (Fig. 6.5b). In addition, there are C−H···F H-bonding interactions also exist outside the cavity between the protonated receptor **L_{17}** and fluoride anion F3 (Fig. 6.5b). Among F2 and F3 anions present outside the tripodal host cavity, F2 is tri-coordinated (two with F3 and one with receptor *exo*-N-H group) and F3 is tetra-coordinated (two with F3 and two with receptor C-H groups).

6.2.1.3 Chloride complex 18a of receptor L_{18}

The chloride salt complex of **L_{18}** crystallizes in triclinic space group *P*1 and structural interpretation of complex **18a** shows that all the three amine groups of a particular receptor are protonated like the salt complexes of **L_{16}** and **L_{17},** but due to the positional dissimilarity of terminal aryl functional group**,** receptor **L_{18}** orients in a non-capsular fashion. Eventually, these non-capsular assemblies of **L_{18}** exhibits a Y-shaped architecture and *meta*-nitro terminal aryl functionalization into tris-amine scaffold prevent to bind any guest molecule in capsular fashion (Fig. 6.5c). In **18a**, the three (Cl2, Cl4, Cl5) out of six chloride ions in the asymmetric unit are stabilized by four hydrogen-bonding interactions, two (Cl1, Cl3) are stabilized by five hydrogen-bonding and the sixth one gets stability *via* six hydrogen-bonding interactions through N−H···Cl and C−H···Cl modes with one or more adjacent protonated **L_{18}** conformers (Fig. 6.5c). The chloride ions consecutively hydrogen-bonded *via* polyamine NH_2^+ groups of receptor, self-assemble to conform a linear network, where the binding and sustainability of each chloride ion is supported by C−H···Cl interaction/s through the adjacent receptor C-H group/s.

6.2.1.4 Chloride (19a), bromide (19b) complexes of L_{19} and fluoride complex 20a of L_{20}

The appropriate single crystals of only chloride (**19a**), bromide (**19b**) and fluoride (**20a**) complexes are obtained from either of the halo-methylphenyl di-functionalized bis-urea receptors **L_{19}** or **L_{20}**. Structural elucidation reveals that, chloride complex **19a** and bromide complex **19b** are almost isostructural and both crystallize in the same orthorhombic space group *Pna*21, while the smallest halide encapsulated complex **20a** crystallizes in the monoclinic space group *P*21/c. The halide anion ($Cl^-/Br^-/F^-$) in respective complexes is encapsulated first within the tripodal unicapsular cavity of either of the receptors **L_{19}/L_{20}** by six strong N−H···F interactions to all six urea protons of a particular receptor. In addition, the chloride and bromide anions further accept one C_{TBA}−H···Cl/Br hydrogen-bond in complexes **19a** and **19b** (Fig. 6.6a, b), whereas the fluoride anion receives one C_{aryl}−H···F hydrogen-bond from adjacent receptor

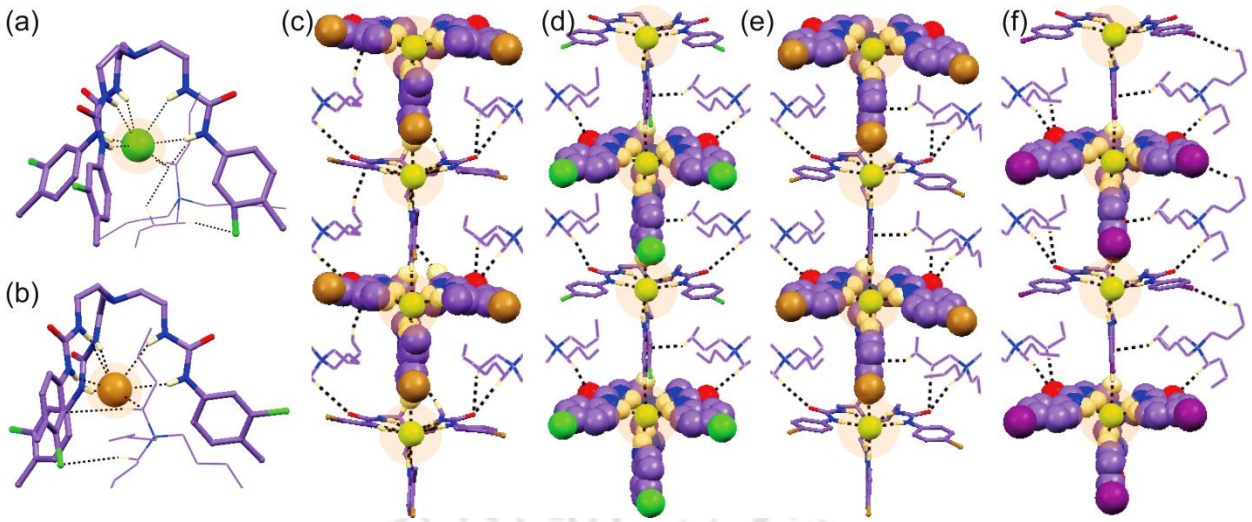

Fig. 6.6 Partial X-ray structures depicting the non-covalent interactions involved in (a) chloride complex **19a**, (b) bromide complex **19b**; The linear polymeric aggregated fluoride encapsulated host-guest assemblies in (c) complex **20a**, (d) complex **21a**, (e) complex **22a** and (f) complex **23a**.

moiety in complex **20a** (Fig. 6.6c). Therefore, each halide anion ($F^-/Cl^-/Br^-$) in the complexes of receptors $\mathbf{L_{19}}$ and $\mathbf{L_{20}}$ exhibit hepta-coordination. However, receptor $\mathbf{L_{19}}$ forms cation sealed chloride and bromide encapsulated 1:1 host-guest complexes (Fig. 6.6a, b), while receptor $\mathbf{L_{20}}$ produces fluoride encapsulated 1:1 complex *via* polymeric aggregation unimolecular host-guest capsular assemblies (Fig. 6.6c). Additionally, each halide encapsulated neutral complexes are stabilized by several weak C_{TBA}–H···Cl/Br, C_{TBA}–H···O, C_{aryl}–H···O and C_{TBA}–H···π interactions.

6.2.1.5 Fluoride complexes 21a of L_{21}, 22a of L_{22} and 23a of L_{23}

Good quality single crystals of neutral complexes **21a**, **22a** and **23a** are obtained by slow evaporation of basic DMF solution of homologous *para*-halophenyl substituted tripodal tris-urea receptors $\mathbf{L_{21}}$, $\mathbf{L_{22}}$ and $\mathbf{L_{23}}$ respectively in the presence of excess *n*-TBAF salts. Structural elucidation reveals that complexes **21a** and **22a** crystallize in the monoclinic space group *P*2/c and *P*21/c respectively, while complex 2**3a** crystallize in the triclinic space group *P*-1. The crystal structures clearly show that the smallest halide anion is encapsulated inside the tripodal cavity with strong hydrogen bonds to all six urea protons of a particular receptor unit ($\mathbf{L_{21}}/\mathbf{L_{22}}/\mathbf{L_{23}}$) in each complex (Fig. 6.6d, e, f). The fluoride anion in each complex also exhibits hepta-coordination despite its smallest size in anion family, which comprises of six strong N–H···F interactions and one extra C–H···F interactions with adjacent fluoride encapsulated receptor moiety. Two adjacent symmetry-independent fluoride ion encapsulated unicapsular units are further interlinked by C_{aryl}–H···F interactions in all the three almost isostructural complexes of *p*-chlorophenyl, *p*-bromophenyl and *p*-iodophenyl substituted neutral receptors $\mathbf{L_{21}}$, $\mathbf{L_{22}}$ and $\mathbf{L_{23}}$ respectively (Fig. 6.6d, e, f). These interconnected capsular units in complexes

21a, **22a** or **23a** further develop a linear aggregated polymeric assemblies stabilized by number of weak C_{TBA}−H···O interactions (Fig. 6.6d, e, f).

6.2.2. Structural analysis of oxyanion bound complexes of receptors L_{16}-L_{23}

Single crystal XRD analyses of neutral or protonated receptor-oxyanion complexes and the consistent as well as discriminating binding behavior of tris-amine and tris-urea receptors toward planar, tetrahedral or octahedral oxyanions in variable host-guest ratios are heavily dependent upon the influence of the receptor cavity or dimension of anionic guests.

6.2.2.1 Sulfate complexes 16b of L_{16} and 17b of L_{17}

The DMF solvated hydrated-sulfate salt complexes **16b** and **17b** of *para*-nitrophenyl and *para*-bromophenyl substituted protonated tris-amine receptors $\mathbf{L_{16}}$ and $\mathbf{L_{17}}$ respectively crystalize in the same triclinic space group *P*-1. Structural elucidation of both complexes reveal that, single DMF molecule is encapsulated within the complementary cavity of receptor $\mathbf{L_{16}}$ or $\mathbf{L_{17}}$ instead tetrahedral anionic guest sulfate, when they open up their three arms along same direction. Each DMF guest is stabilized by strong three strong N−H···O and C−H···O interactions between the carbonyl oxygen atom of DMF and three polyammonium -NH groups pointed towards the cavity of the receptor in both complexes **16b** (Fig. 6.5d) and **17b** (Fig. 6.5e). The capsular size i.e. the distances between the apical N-atoms of these 2:2 receptor-DMF capsular assemblies become ~16.88 (9) Å and ~17.22 (1) Å in complexes **16b** and **17b** respectively. Note that, the bigger size of sulfate oxyanion prevents it to bind inside the tripodal cavity of either of the tris-amine hosts $\mathbf{L_{16}}$ or $\mathbf{L_{17}}$ due to the size mismatch of host and guest; as a consequence the solvent DMF acts as guest binds strongly inside the complementary cavity of both the receptors (Fig. 6.5d, e). Eventually, the bigger sulfate anions in the asymmetric units of both complexes **16b** or **17b** have surrounded themselves through side-cleft binding at the exterior environment of DMF encapsulated receptors $\mathbf{L_{16}}$ (Fig. 6.5d) or $\mathbf{L_{17}}$ (Fig. 6.5e). The sulfate anions present outside the protonated receptor cavity in both complexes are stabilized by strong N−H···O and C−H···O interactions through the receptors and water molecules exist in the periphery of the receptor capsular cavities (Fig. 6.5d, e). The C−H···O and C−H···π weak interactions also help the DMF guests to stay inside the tripodal capsular cavities of the hosts $\mathbf{L_{16}}$ or $\mathbf{L_{17}}$ in both complexes.

6.2.2.2 Carbonate Complex 19c of receptor L_{19}

The good quality colorless crystals of divalent carbonate encapsulated complex **19c** of halo-methylphenyl substituted neutral tripodal receptor $\mathbf{L_{19}}$ crystallizes in the monoclinic space group *P*2/n and the asymmetric unit contains two symmetry-independent $\mathbf{L_{19}}$ tris-urea receptor molecules, two half-occupied divalent carbonate anions and two symmetry-distinct TEA

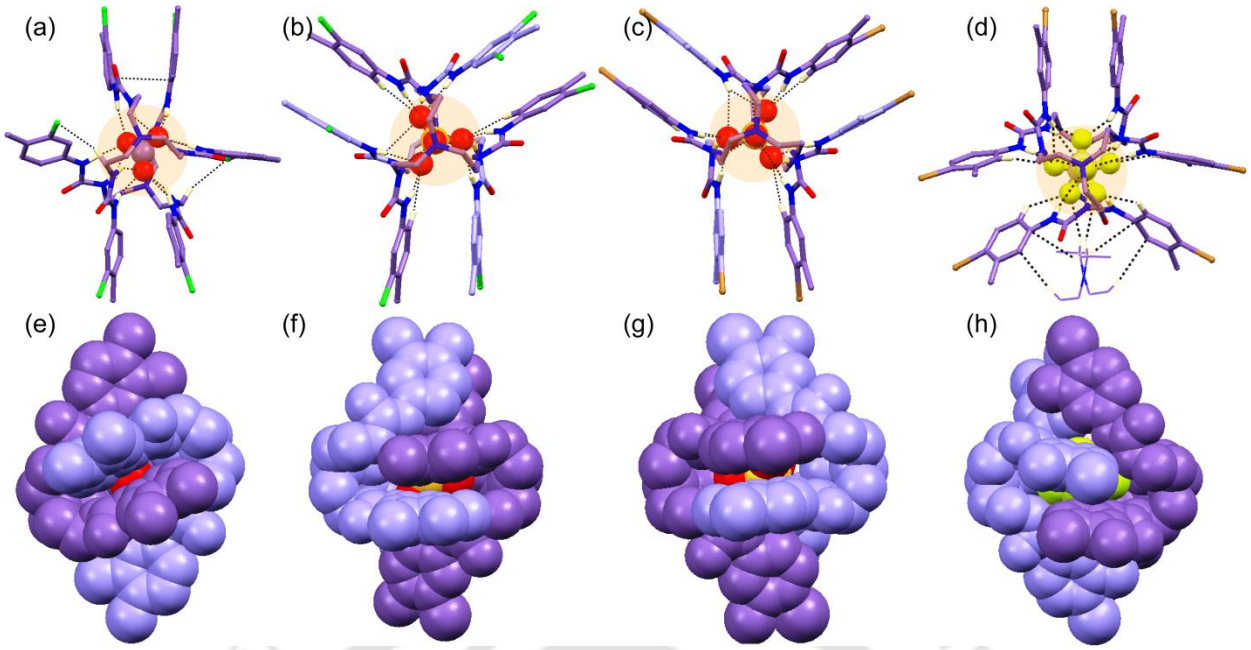

Fig. 6.7 Partial X-ray structures depicting the non-covalent interactions involved in (a) CO_3^{2-} encapsulated complex **19c**, (b) SO_4^{2-} encapsulated complex **19d**, (c) SO_4^{2-} encapsulated complex **20b**, (d) SiF_6^{2-} encapsulated complex **20c**; Spacefill view of oxyanion engulfment within the dimeric receptor cages in (e) carbonate complex **19c**, (f) sulfate complex **19d**, (g) sulfate complex **20b** and (h) hexafluorosilicate complex **20c**.

counter-cations. The X-ray analysis clearly specifies that a particular divalent carbonate anion become fully encapsulated inside the micro-cavity (Avg. $d_{N1/N8\cdots N1/N8}$ = 9.181 Å in **19c**) of two symmetry-identical $\mathbf{L_{19}}$ molecules flipped inward toward each other in a face-to-face fashion (Fig. 6.7a, e). Each half-occupied C61 and C62 containing carbonate anions in the asymmetric unit consist of two oxygen atoms (one with 0.5 occupancy and other with full occupancy), among which the two carbonate oxygen atoms are distributed over three positions in one case and in other case two oxygen atoms are distributed over four positions. Structural elucidation reveals that C62 carbonate are fully encapsulated by six receptor urea groups by a total of 12 strong N−H···O bonds (Fig. 6.7a) (each O atoms accept four hydrogen-bonds), whereas the C61 carbonate are fully engulfed inside the dimeric capsular cavity of $\mathbf{L_{19}}$ receptors by a total of 22 hydrogen-bonding interactions (twenty strong N−H···O and two weak C_{aryl}−H···O) *via* four carbonate oxygen atoms. The divalent carbonate anions were not present in the solution mixture prior to crystallization and note that, the HCO_3^- anion has deprotonated in CO_3^{2-} *via* hydrogen-bonding activated proton transfer reaction in complex **19c**. The divalent carbonate engulfed 2:1 dimeric receptor capsular cage (Fig. 6.7e) gets extra stability by weak C−H···Cl and π···π interactions.

6.2.2.3 Sulfate Complexes 19d of L_{19} and 20b of L_{20}

The appropriate block-shaped crystals of divalent sulfate encapsulated dimeric cage complexes **19d** (Fig. 6.7b) and **20b** (Fig. 6.7c) of halo-methylphenyl based tripodal receptors $\mathbf{L_{19}}$ and $\mathbf{L_{20}}$

respectively, crystallize in the same triclinic space group *P*-1. The X-ray analysis clearly reveals the almost isostructural complexes of isomeric receptors **L_{19}** and **L_{20}** each contain two symmetry-independent neutral receptor units, one divalent sulfate anion and its corresponding two *n*-TBA counter-cations. Two symmetry-independent **L_{19}/L_{20}** receptor molecules of asymmetric unit in complexes **19d/20b**, flip inward toward each other in a face-to-face fashion producing a nano-cavity ($d_{N1\cdots N8}$ = 10.054 Å in **19d**/10.230 Å in **20b**) that engulf divalent sulfate anion in its center (Fig. 6.7f, g) with the aid of six urea groups *via* a total of 16 hydrogen bonding (13 N−H···O and 3 $C_{o\text{-aryl}}$−H···O bonds) interactions in complex **19d** (Fig. 6.7b) and 17 hydrogen bonding (14 N−H···O and 3 $C_{o\text{-aryl}}$−H···O bonds) interactions in complex **20b** (Fig. 6.7c). Note that in both complexes **19d** and **20b**, the three urea groups from one tripodal ligand bind three edges of the tetrahedral anion (through eight-membered H-bonded rings), while the three urea groups from other symmetry-independent **L_{19}/L_{20}** ligand chelate three vertices of the sulfate ion (through six-membered H-bonded rings). Thus, the O7 atom of sulfate accepts three, the O8 and O10 form four hydrogen bonds each, but the O9 receives five hydrogen bonds in complex **19d**, while in complex **20b**, O7 atom of sulfate accepts five hydrogen-bonds but O8, O9 and 10 atoms receive four hydrogen bonds each. Hence, each sulfate oxygen atom behaves as at least trifurcatated hydrogen-bond acceptor in both complexes **19d** or **20b** and this is reliable with the electronic structure calculations reported by Hay and coworkers[6.7] proposing that each oxyanion oxygen atom could be engaged in a maximum of three hydrogen bonds. Note that, the divalent sulfate anion is encapsulated within the dimeric receptor cage (Fig. 6.7f, g) by hydrogen-bonding activated proton transfer reaction from monovalent HSO_4^- anion. Similar kinds of solution-state deprotonation of the protonated state of an anion, *viz.*, $H_2PO_4^-$, HCO_3^- and HSO_4^- are common in literature and this occurs due to the formation of multiple H-bonding interactions with ligand, assisting in lowering the *pKa* of the bound guest to the range that it is deprotonated by the free guest species in solution. Such deprotonation of HSO_4^- anion has previously been detected by Ghosh *et al.* as well as from our group[6.8] and we presume the identical process to occur here confirmed by Gale and coworkers.[6.9]

6.2.2.4 Hexafluorosilicate complex 20c of receptor L_{20}

The needle shaped colorless crystals of hexafluorosilicate encapsulated complex **20c** of neutral bromo-methylphenyl substituted tripodal tris-urea receptor **L_{20}** crystallizes in the monoclinic centerosymmetric space group *C*2/c. It is important to mention here that the silicon hexafluoride anion (SiF_6^{2-}) was not present in the reaction mixture prior to crystallization and the complex **20c** is attained by the reaction of the tripodal ligand and TEAF with glass-silica in DMSO, presumably as a result of glass corrosion. Structural elucidation reveals that two units of

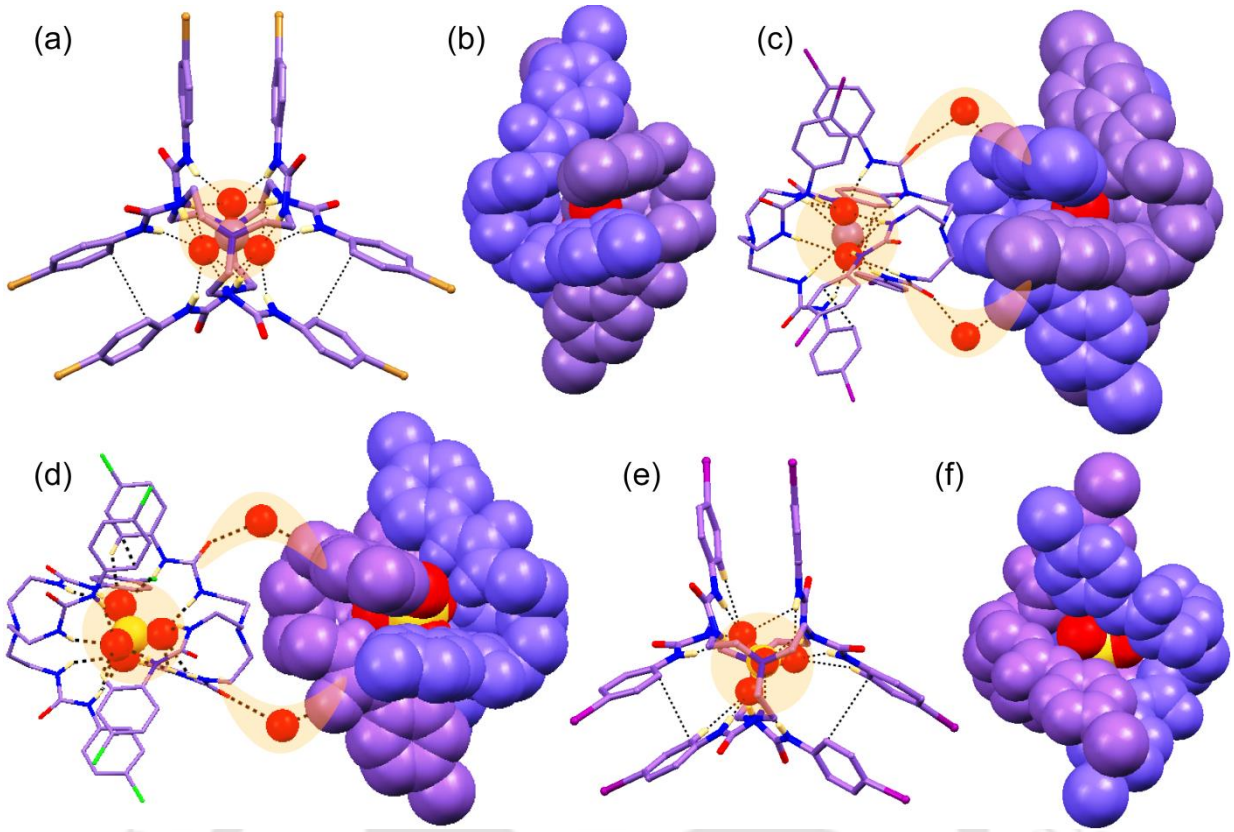

Fig. 6.8 Partial X-ray structures depicting (a) the hydrogen-bonding interactions involved in CO_3^{2-} encapsulated complex **22b**, (b) spacefill view of carbonate engulfment within dimeric cage of receptor $\mathbf{L_{22}}$, (c) two adjacent carbonate encapsulated dimeric cages of receptor $\mathbf{L_{23}}$ (capped-stick followed by spacefill view) bridged by two O_{water}–H···$O_{carbonyl}$ interactions in complex **23b**, (d) two adjacent sulfate encapsulated dimeric cages of receptor $\mathbf{L_{21}}$ (capped-stick followed by spacefill view) bridged by two O_{water}–H···$O_{carbonyl}$ interactions in complex **21b**, (e) the hydrogen-bonding interactions involved in SO_4^{2-} encapsulated complex **23c**, (f) spacefill view of sulfate engulfment within dimeric cage of receptor $\mathbf{L_{23}}$.

symmetry-identical conformer of $\mathbf{L_{20}}$ are flipped inward toward each other in a face-to-face fashion produce a nano-cavity (distance N1···N1 = 10.579 Å) with the aid of a TEA^+ cation, that efficiently engulfs (Fig. 6.7h) a large divalent silicon hexafluoride anion (SiF_6^{2-}) by a total of 26 hydrogen-bonding interactions (twenty strong N–H···F, four $C_{o\text{-}aryl}$–H···F and two C_{TEA}–H···F connections) (Fig. 6.7d). Note that, one of inversion symmetric atoms F2 from silicon hexafluoride anion becomes distributed over two positions and each F2 atom accepts three hydrogen bonds from ligands and TEA^+ cation. The larger coordinating octahedral hexafluorosilicate anion encapsulated 2:1 host-guest complex **20c** (Fig. 6.7h) gains additional stability *via* several C_{TEA}–H···π, C–H···O, Br···Br weak interactions (Fig. 6.7d).

6.2.2.5 Carbonate complexes 22b of L_{22} and 23b of L_{23}

The good quality crystals of divalent carbonate encapsulated complexes **22b** and **23b** of *para*-halophenyl substituted tripodal tris-urea receptors $\mathbf{L_{22}}$ and $\mathbf{L_{23}}$ respectively crystallize in the monoclinic centrosymmetric space group *C*2/c. The asymmetric unit of complex **23b** contains a

water molecule of crystallization that is additional compared to complex **22b**. The X-ray analysis clearly shows that two symmetry-identical conformers of either $\mathbf{L_{22}}$ or $\mathbf{L_{23}}$ flipped inward toward each other in a face-to-face fashion ($d_{N1\cdots N1}$ = 8.929 Å in **22b** and $d_{N1\cdots N1}$ = 8.987 Å in **23b**) produce a micro-cavity that encapsulate a divalent carbonate anion (Fig. 6.8a, b, c) in their centre *via* 16 (Fig. 6.8a) and 14 (Fig. 6.8c) strong N−H···O interactions respectively. Note that, the monovalent HCO_3^- anion has deprotonated and is bound in the form of divalent CO_3^{2-} *via* hydrogen-bonding activated proton transfer reaction in both complexes as observed from X-ray structures. Subsequently, the asymmetric unit of each complex contains divalent carbonate anion of half-occupancy and as a result the O5 atom of carbonate becomes inversion-symmetric and distributed over two positions in **22b** as well as in **23b**. Note that, unlike complex **22b**, the two adjacent carbonate encapsulated dimeric capsular cages in complex **23b**, are interlinked by four O−H···O connections, where the two symmetry-identical water molecules separately act as the bridges between two adjacent dimeric host-guest capsules (Fig. 6.8c). In complex **22b**, two identical O5 oxygen atoms of carbonate accept six and O4 oxygen accepts four N−H···O bonds, resulting in a total of 16 hydrogen-bonding contacts. Whereas, identical O5 atoms of carbonate accept five and O4 atom receives four N−H···O bonds, exhibiting a total carbonate coordination number of 14 in complex **23b**. Hence, the structures reported in **22b** and **23b** exhibit optimal coordination number for the carbonate anion, as it is reliable with the electronic structure calculations by Hay *et. al.*[6.7] describing each oxyanion oxygen atom could be involved in a maximum of three hydrogen bonds. Note that, the 2:1 host-guest dimeric cages (Fig. 6.8b, c) of both complexes get additional stability by several intermolecular weak π···π interactions among respective receptors.

6.2.2.6 Sulfate complexes 21b of L_{21} and 23c of L_{23}

The suitable crystals of neutral sulfate complexes **21b** and **23c** (obtained by hydrogen-bonding activated proton transfer from monovalent HSO_4^- anion) of respective neutral *para*-halophenyl substituted tripodal receptors $\mathbf{L_{21}}$ and $\mathbf{L_{23}}$ crystallize in the monoclinic space group *P*21/n and *P*21 respectively. Structural elucidation reveals that two symmetry-independent $\mathbf{L_{21}}$ receptor molecules of asymmetric unit in complex **21b**, flipped inward toward each other in a face-to-face fashion form a nano-cavity ($d_{N1\cdots N8}$ = 10.073 Å) that encapsulates a divalent sulfate anion (Fig. 6.8d) in its centre *via* a total of 17 hydrogen bonding (14 N−H···O and 3 C_{aryl}−H···O bonds) interactions to the six urea groups (Fig. 6.8d). In contrary, the two symmetry-independent divalent SO_4^{2-} anions in asymmetric unit of **23c** become separately encapsulated inside two distinct dimeric capsular cages (average $d_{N\cdots N}$ distance = 9.932 Å) of four independent $\mathbf{L_{23}}$ receptors by a total of 16 hydrogen bonding (13 N−H···O and 3 C_{aryl}−H···O

bonds) interactions (Fig. 6.8e, f) in both symmetry-independent capsules. Note that two adjacent symmetry-identical sulfate encapsulated dimeric cages are interconnected by four O−H···O interactions through two symmetry-identical water molecules (Fig. 6.8d) in the asymmetric unit of complex **21b**, just similar as carbonate encapsulated complex **23b** (Fig. 6.8c). Although, no such hydrogen bond donating water molecules are available in the unit cell of complex **23c** (Fig. 6.8e, f), which exhibits similar properties with carbonate encapsulated neutral complex **22b** (Fig. 6.8a, b).The X-ray analysis also reveals that each oxygen atom of sulfate anions in complexes **21b** and **23c** accept three or more hydrogen-bonds, hence each sulfate anion exhibit optimum coordination in both complexes. Alike carbonate complex **22b** and **23b**, several weak intermolecular π···π interactions among the receptors also provide additional stability to the 2:1 sulfate bound neutral complexes **21b** (Fig. 6.8d) and **23c** (Fig. 6.8f).

Hence, overall, it should be noted that, depending on the size and shape of the tripodal cavity of tris-amine or tris-urea receptors or effect of terminal aryl receptor substituent and subsequently on anion coordination number, the orientation of host-guest assemblies regularly and consistently alters in the cases of tripodal receptor platforms **L_{16}-L_{23}**.

6.3 Solution-state anion binding studies

The behavior of ligands/receptors in dilute or very dilute solution may be dissimilar from their behavior in neutral molecular capsules in the solid state. Therefore, to find out the receptor-anion binding modes in solution, qualitative as well as quantitative ^{1}H NMR titration experiments of tris-urea receptors **L_{19}-L_{23}** with different anion salts have been carried out in DMSO-d_6 as evidenced from the solid state. The most substantial shifts have been observed for the urea -NH protons (-NH_a and -NH_b) as expected, indicating the most suitable sites of interaction between the receptor and anions. The ^{1}H NMR analysis of fluoride bound complexes of halo-methylphenyl functionalized tris-urea receptors **L_{19}** or **L_{20}** demonstrate the large downfield shifts of urea -NH protons for fluoride or silicon hexafluoride encapsulation in complexes **20a** or **20c** compared to chloride or bromide encapsulation in complexes **19a** or **19b** in solution state. Complexes **20a** and **20c** show average downfield shift of $\Delta\delta$ = 1.52 ppm and $\Delta\delta$ = 2.24 ppm respectively for the -NH protons in their ^{1}H NMR data. Whereas, the complexes **19a** and **19b** display considerably less -NH average downfield shifts of $\Delta\delta$ = 0.46 ppm and $\Delta\delta$ = 0.11 ppm respectively. This observation in the chemical shift values clearly indicates that there is an obvious discrepancy in binding of halides in solution, which were almost similar solid state. On the other hand, the average chemical shift changes of $\Delta\delta$ = 1.48 ppm for the –NH protons are observed upon gradual addition of *n*-TBAF to the solutions of **L_{20}** in DMSO-d_6,

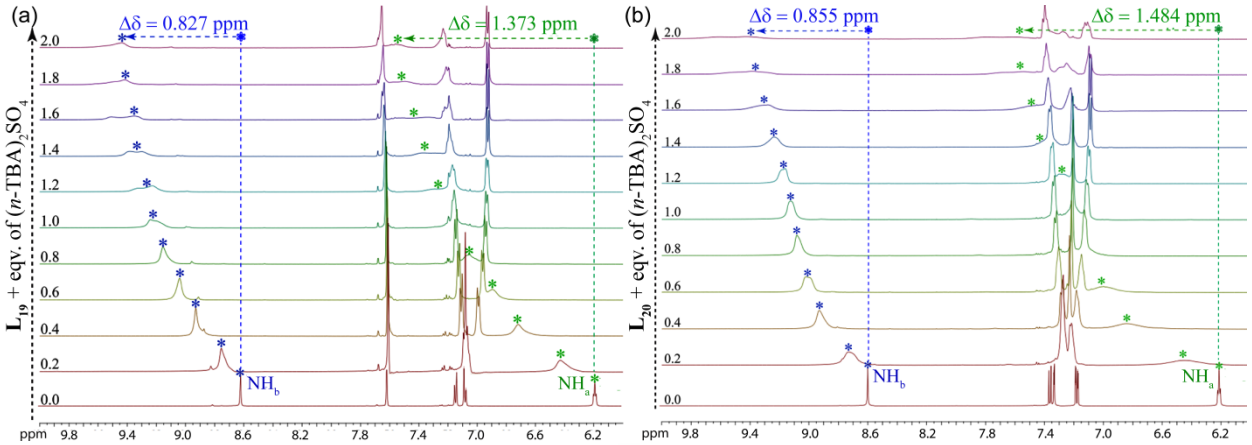

Fig. 6.9 Partial ^{1}H NMR titration stack plot of ligands (a) **L_{19}** and (b) **L_{20}**, with standard SO_4^{2-} anion in DMSO-d_6.

which is closely resemble with the average ($\Delta\delta$ = 1.52 ppm) -NH_a and -NH_b shift of fluoride complex. The carbonate encapsulated complex **19c** exhibits average downfield shift of $\Delta\delta$ = 1.68 ppm *via* huge broadening of both the peaks of urea -NH protons, which supports the host-guest complexation phenomena *via* rapid formation of hydrogen-bonding interactions in solution. Furthermore, the ^{1}H NMR titration experiments of both **L_{19}** and **L_{20}** with gradual addition standard (*n*-TBA)$_2SO_4$ salt solution exhibit average downfield shift of urea -NH resonances $\Delta\delta$ = 1.10 ppm (Fig. 6.9a) and $\Delta\delta$ = 1.17 ppm ((Fig. 6.9b), whereas the divalent sulfate encapsulated dimeric complexes **19d** and **20b** show average downfield shift of $\Delta\delta$ = 1.29 ppm and $\Delta\delta$ = 0.88 ppm in their ^{1}H-NMR data and hence these results also suggest that the divalent sulfate anion is bound more strongly to -NH_a rather than -NH_b protons in both urea receptors in solution state. The titration data of **L_{19}** and **L_{20}** with aliquots of standard sulfate give the best fit close to 1:1 host-guest stoichiometry in Job's plot with apparent log K values of 2.72 and 2.47 respectively. Furthermore, the anion binding properties of *p*-halophenyl functionalized tris-urea receptors **L_{21}**, **L_{22}** and **L_{23}** are also examined by qualitative as well as quantitative ^{1}H NMR experiments in solution-state using the different anion salts, as evidenced from the solid state. Fig. 6.10a, 6.11a and 6.12a show the average chemical shift changes of $\Delta\delta$ = 1.42 ppm, $\Delta\delta$ = 1.49 ppm and $\Delta\delta$ = 1.47 ppm for the -NH protons observed upon gradual addition of *n*-TBAF to the individual solutions of **L_{21}**, **L_{22}** and **L_{23}** respectively in DMSO-d_6. Interestingly, the ^{1}H NMR analysis the fluoride encapsulated complexes **21a, 22a** and **23a** display the average downfield shift sof $\Delta\delta$ = 1.47 ppm, $\Delta\delta$ = 1.48 ppm and $\Delta\delta$ = 1.51 ppm respectively for the -NH protons in their ^{1}H NMR data and these very closely resembled average chemical shift values of isolated crystals and quantitative titration analyses clearly indicate the similar binding tendency of individual urea -NH protons in the solid as well as in solution state. However, the binding constants for fluoride encapsulation could not be determined because the ^{1}H-NMR titration analysis of respective receptors show the instant large downfield shift of urea -NH

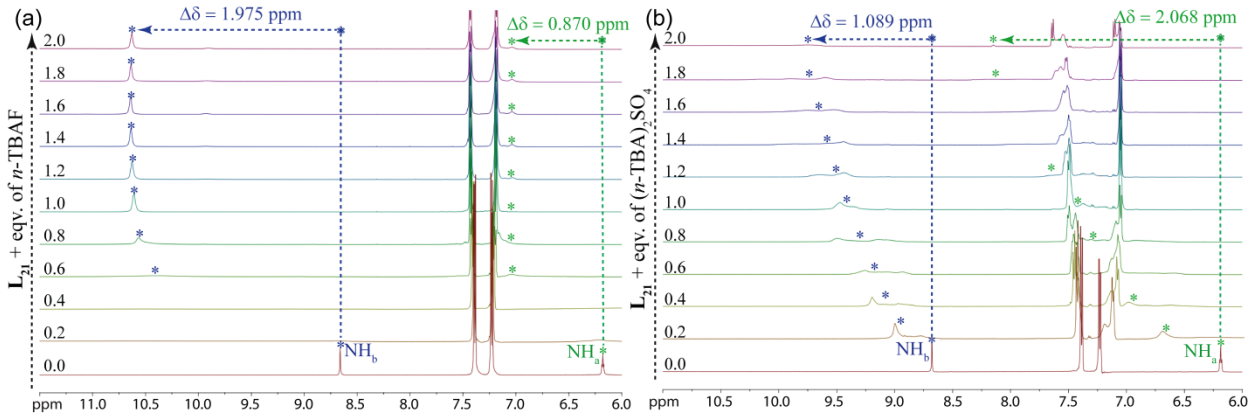

Fig. 6.10 Partial ^{1}H NMR stack plots of $\mathbf{L_{21}}$ upon titration with standard (a) F^- and (b) SO_4^{2-} in DMSO-d_6.

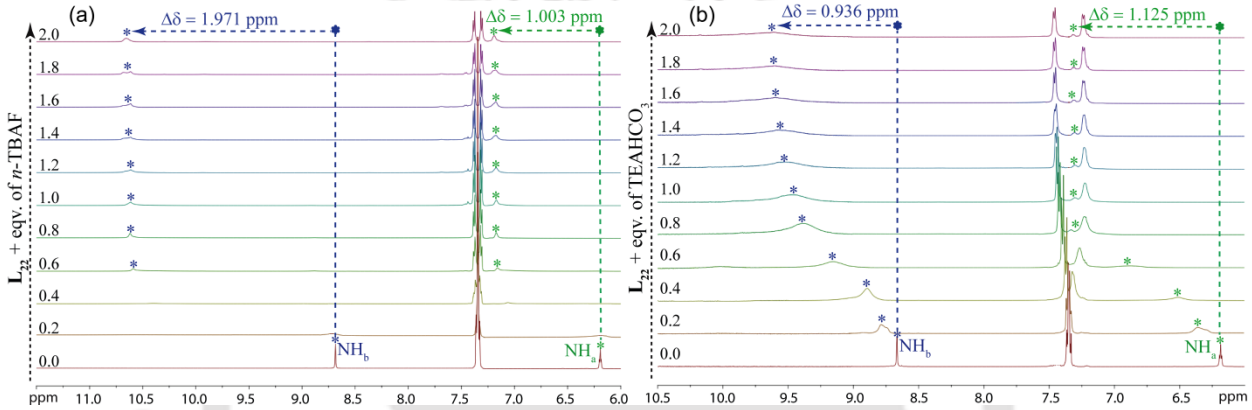

Fig. 6.11 Partial ^{1}H NMR stack plots of $\mathbf{L_{22}}$ upon titration with standard (a) F^- and (b) HCO_3^- in DMSO-d_6.

signals after 0.1-0.6 eqv. addition of F^- salt to the individual ligand solutions. Then, Fig. 6.10b, 6.11b and 6.12b show the average chemical shift changes of $\Delta\delta$ = 1.58 ppm, $\Delta\delta$ = 1.03 ppm and $\Delta\delta$ = 1.50 ppm respectively for the -NH protons observed upon gradual addition of (*n*-TBA)$_2$SO$_4$, TEAHCO$_3$ and (*n*-TBA)$_2$SO$_4$ to the individual solutions of $\mathbf{L_{21}}$, $\mathbf{L_{22}}$ and $\mathbf{L_{23}}$ respectively, whereas, the ^{1}H NMR analysis the sulfate complex **21b**, carbonate complex **22b** and sulfate complex **23c** exhibit the average downfield shift of $\Delta\delta$ = 0.87 ppm, $\Delta\delta$ = 1.63 ppm and $\Delta\delta$ =0.86 ppm respectively for the -NH protons in their ^{1}H NMR data, that supports the similar kinds of proficient participation of -NH$_a$ protons upon anion complexation in solid as well as in solution state. The titration data for $\mathbf{L_{22}}$ and $\mathbf{L_{23}}$ with standard carbonate and sulfate give the best fit for mixed equilibrium close to 1:1 host-guest stoichiometry with log K_{11} = 4.19 and log K_{11} = 3.01 respectively. It is worth mentioning that, the association constants for the sulfate titration with receptor $\mathbf{L_{21}}$ could not be determined due to huge broadening and splitting of both urea -NH resonances upon sulfate addition (Fig. 6.10b), that may be the consequences of rapid hydrogen-bonding interactions between anion and receptor. Note that, such kind of binding discrepancy in host-guest-guest stoichiometry in the solid and solution states is not uncommon in literature. As the receptors are much more organized in the solid state, hence they favor the binding of the anions *via* entrapment or encapsulation by several non-covalent

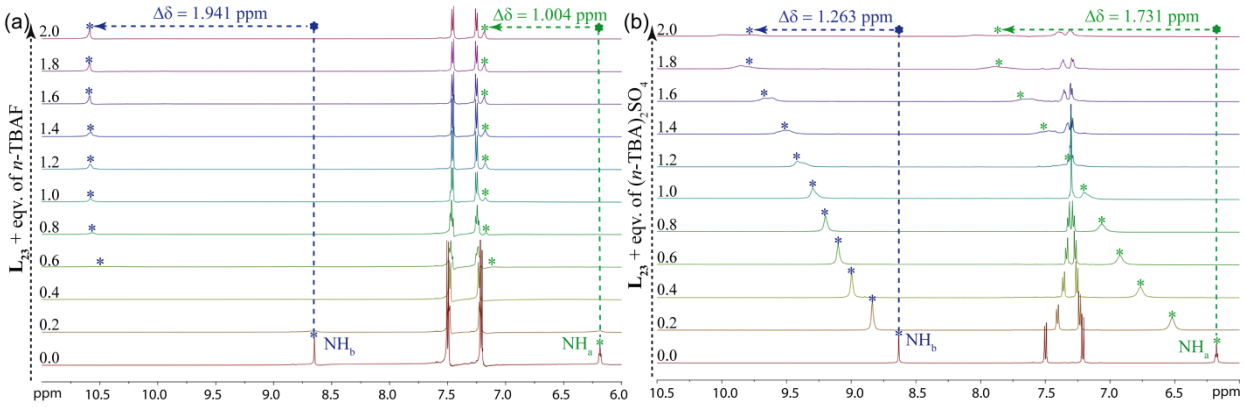

Fig. 6.12 Partial ^{1}H NMR titration stack plot of ligand **L_{23}** with standard (a) F^- ion and (b) SO_4^{2-} ion in DMSO-d_6.

interactions inside the dimeric cage assemblies, while in solution state, binding of a single anion inside the receptor cavity has been seen to be observed in most of the cases. Moreover, the titration experiments of tris-amine receptors **L_{16}-L_{18}** in presence different inorganic anions in $CDCl_3$ or DMSO-d_6 have also been carried out to find out the anion binding processes of protonated receptors, as evidenced from the solid state. But there are very negligible changes of the protonated amine group resonances have been seen to be observed in ^{1}H-NMR spectra upon anion addition to the respective nitro-phenyl or bromo-phenyl substituted tris-amine receptors. Hence, binding stoichiometry as well as association constant of anions with respective protonated receptors in solution phase could not be determined.

6.4 Conclusion

In summary, we have developed a set of tren-based tris-amine (**L_{16}-L_{18}**) and tris-urea (**L_{19}-L_{23}**) receptors bearing dissimilar tripodal cavity size and containing either mono or di-substituted terminal aryl functionalization, which can bind anionic guests of variable dimensions in protonated or neutral forms *via* formation of capsular or non-capsular or pseudo-capsular host-guest assemblies. The polyammonium based three tripodal receptors **L_{16}-L_{18}** with positional and functional terminal aryl variation demonstrate effective binding abilities towards halides and sulfate anion in solid state. Especially, receptor **L_{16}** and **L_{17}** has proved to be a decent receptor for capsular recognition of chloride and fluoride anions due to positional similarity of terminal aryl substitution. However, both **L_{16}** and **L_{17}** have failed to encapsulate larger sulfate oxyanion as it is too big to fit into the molecular capsular cavity of protonated tris-amine receptors, instead the DMF solvent molecules are encapsulated in 2:2 fashions inside the both receptors in similar ways. The receptor **L_{18}** is not efficient for capsular binding of anions due to the positional dissimilarity of functional group compared to **L_{16}** and **L_{17}.** However, **L_{18}** self assembles with chloride ion *via* linear consecutive hydrogen-bonded network with open arm conformation. On the other hand, the emergence of chloro-methylphenyl substituted tris-urea receptors **L_{19}**

containing ethylene chain-induced cavity demonstrates the construction of *n*-TBA cation-sealed pseudo-capsular assemblies of chloride and bromide anions followed by the engulfment of divalent planar carbonate and tetrahedral sulfate inside the neutral dimeric capsular cages. Subsequently, the isomeric bromo-methylphenyl functionalized tris-urea receptor **L_{20}** also produces 2:1 dimeric host-guest capsule with sulfate anion. But interestingly in presence of *n*-TBAF, unimolecular fluoride encapsulated polymeric aggregated assemblies of **L_{20}** has been formed, however excess TEAF salt addition in the basic **L_{20}** solution yields octahedral SiF_6^{2-} bound dimeric receptor capsule, possibly as a result of glass corrosion. Note that, these kinds of host-guest assemblies by neutral halo-methylphenyl based tripodal scaffolds turn out to be the prime crystallographic proof of molecular capsules consisting of both electron-withdrawing and electron-donating terminal aryl-substituents simultaneously. Furthermore, homologous series of neutral tris(4-halophenylurea) receptor systems **L_{21}-L_{23}** have also been widely established as potential receptors for fluoride anion in solid as well as in solution phase. Moreover, the engulfment of planar carbonate as well as tetrahedral sulfate within the dimeric capsular cages of either of three receptors **L_{21}-L_{23}** in 2:1 host-guest mode have been observed and to the best our knowledge, hydrogen-bonding activated oxyanion complexation by any tren-based tris(4-halophenylurea) scaffolds in this present study is one of the prime results, especially in the solid state. Overall, the nature and dimensionality of the anionic guests play the crucial role on the self-alignment, orientation and flexibility of the ligand units in host-guest complexes. As a consequence, a class of protonated and neutral tripodal receptor systems has been rationally developed for recognition of biologically and environmentally related anions/hydrated-anions.

References

6.1 (a) F. P. Schmidtchen and M. Berger, *Chem. Rev.*, 1997, **97**, 1609; (b) C. Caltagirone and P. A. Gale, *Chem. Soc. Rev.*, 2009, **38**, 520; (c) K. Bowman-James, A. Bianchi and E. Garcia-Espana, *Anion Coordination Chemistry, Wiley-VCH*, New York, 2011; (d) P. D. Beer and P. A. Gale, *Angew. Chem., Int. Ed.*, 2001, **40**, 486; (e) J. Svec, M. Necas and V. Sindelar, *Angew. Chem., Int. Ed.*, 2010, **49**, 2378.

6.2 (a) S. K. Dey, A. Basu, R. Chutia and G. Das, *RSC Adv.*, 2016, **6**, 26568; (b). R. Dutta and P. Ghosh, *Chem. Commun*., 2014, **50**, 10538; (c) M. N. Hoque, U. Manna and G. Das *Supamol. Chem.* 2016, **28**, 284.

6.3 (a) P. Ballester, *Chem. Soc. Rev*. 2010, **39**, 3810; (b) M. Arunachalam and P. Ghosh *Chem. Commun*. 2011, **47**, 8477.

6.4 (a) S. Ayoob and A. K. Gupta, *Crit. Rev. Environ. Sci. Technol.*, 2006, **36**, 433; (b) F. Hofmeister, *Arch. Exp. Pathol. Pharmakol.*, 1888, **24**, 247; (c) Y. J. Marcus, *J. Chem. Soc., Faraday Trans.*, 1991, **87**, 2995; (d) A. S. McCall, C. F. Cummings, G. Bhave, R. Vanacore, A. Page-McCaw and B. G. Hudson, *Cell*, 2014, **15**, 1380.

6.5 (a) C. J. Fowler, T. J. Haverlock, B. A. Moyer, J. A. Shriver, D. E. Gross, M. Marquez, J. L. Sessler, M. A. Hossain and K. Bowman-James *J. Am. Chem. Soc.* 2008, **130**, 14386; (b) D. A. Jose, D. K. Kumar, B. Ganguly

and A. Das, *Inorg. Chem.* 2007, **46**, 5817; (c) L. R. Eller, M. Stepien, C. J. Fowler, J. T. Lee, J. L. Sessler and B. A. Moyer, *J. Am. Chem. Soc.*, 2007, **129**, 11020.

6.6 (a) U. Manna, B. Nayak, M. N. Hoque and G. Das *CrystEngComm*, 2016, **18**, 5036; (b) U. Manna and G. Das *CrystEngComm*, 2018, **20**, 4406; (c) U. Manna and G. Das *New J. Chem.*, 2018, **42**, 19164.

6.7 B. P. Hay, T. K. Firman, B. A. Moyer, *J. Am. Chem. Soc.* 2005, **127**, 1810.

6.8 (a) I. Ravikumar, P. S. Lakshminarayanan, M. Arunachalam, E. Suresh and P. Ghosh, *Dalton Trans.*, 2009, 4160; (b) S. K. Dey, R. Chutia and G. Das, *Inorg. Chem.*, 2012, **51**, 1727; (c) U. Manna, B. Nayak, and G. Das, *Cryst. Growth Des.* 2016, **16**, 7163; (d) U. Manna and G. Das, *CrystEngComm*, 2017, **19**, 5622.

6.9 (a) P. A. Gale, J. R. Hiscock, S. J. Moore, C. Caltagirone, M. B. Hursthouse and M. E. Light, *Chem. Asian J* 2010, **5**, 555; (b) C. Caltagirone, J. R. Hiscock, M. B. Hursthouse, M. E. Light, P. A. Gale, *Chem. Eur. J* 2008, **14**, 10236.

Annexure 6

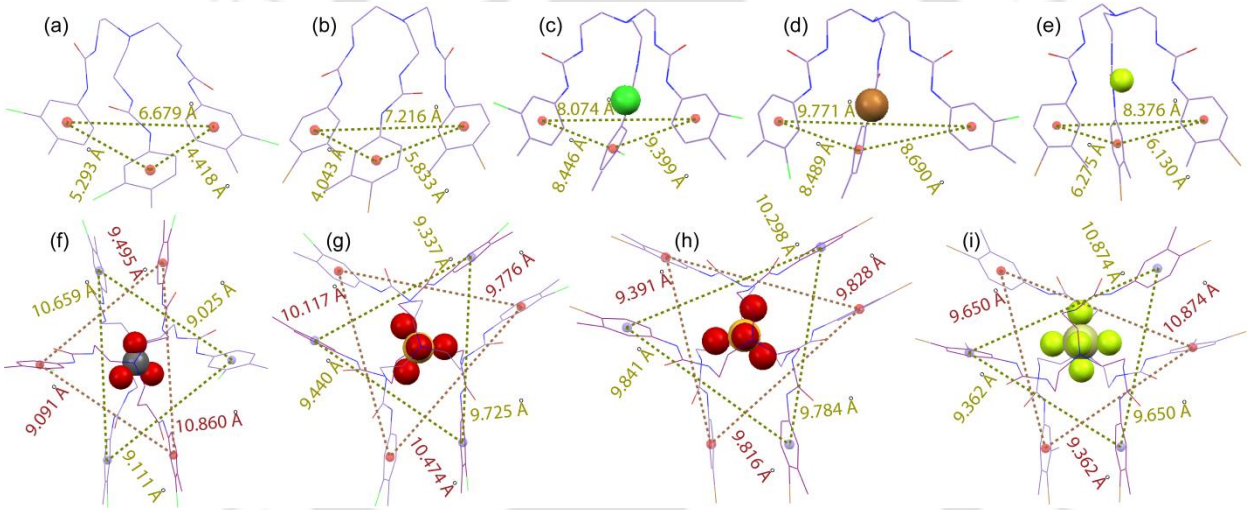

Fig. A6.1 Pictorial depiction from X-ray structures (partial) representing the centroid to centroid distances among the terminal aryl rings in (a) free $\mathbf{L_{19}}$, (b) free $\mathbf{L_{20}}$, (c) chloride complex **19a**, (d) bromide complex **19b**, (e) fluoride complex **20a**, (f) carbonate complex **19c**, (g) sulfate complex **19d**, (h) sulfate complex **20b** and (i) hexafluorosilicate complex **20c**.

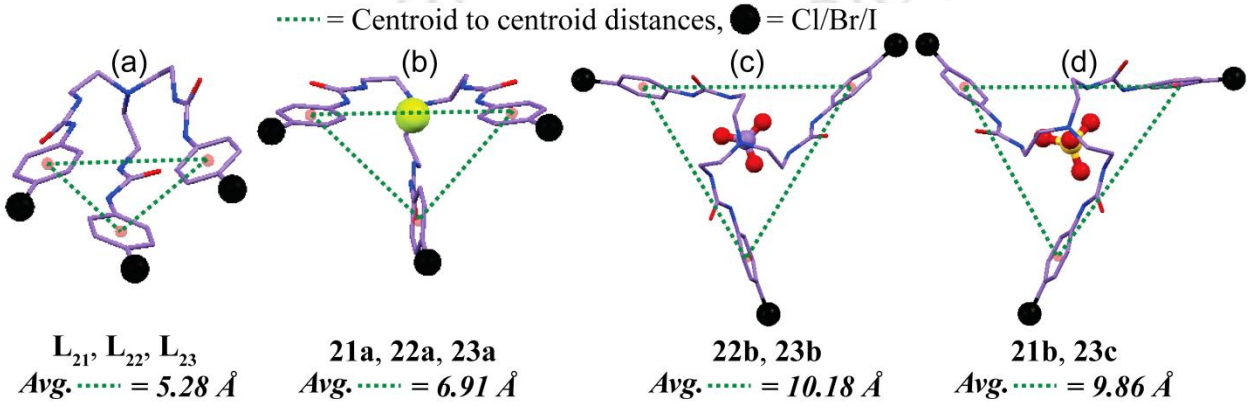

Fig. A6.2 Pictorial depiction from X-ray structures (partial) representing the average centroid to centroid distances among the terminal aryl rings of in (a) free receptors $\mathbf{L_{21}}$, $\mathbf{L_{22}}$, $\mathbf{L_{23}}$, (b) fluoride complexes **21a**, **22a**, **23a**, (c) carbonate complexes **22b**, **23b** and (d) sulfate complexes **21b**, **23c**.

Table A6.1 Crystallographic parameters and refinement details of receptor $\mathbf{L_{16}}$ and anion complexes of $\mathbf{L_{16}}$-$\mathbf{L_{18}}$

Parameters	$\mathbf{L_{16}}$	**16a**	**16b**	**17a**	**17b**	**18a**
Formula	$C_{27}H_{33}N_7O_6$	$C_{27}H_{36}Cl_3N_7O_6$	$C_{63}H_{103}N_{17}O_{35}S_3$	$C_{27}H_{36}Br_3F_7N_4$	$C_{66}H_{116}Br_6N_{12}O_{24}S_3$	$C_{27}H_{36}Cl_3N_7O_6$
Fw	551.60	660.98	1754.79	789.30	2030.92	660.98
Crystal system	Orthorhombic	Orthorhombic	Triclinic	Trigonal	Triclinic	Triclinic
Space group	*P 2₁ 2₁ 2₁*	*P 2₁ 2₁ 2₁*	*P-1*	*R3*	*P-1*	*P1*
a/Å	11.8182(14)	14.3519(9)	15.3493(11)	15.1064(3)	15.3545(17)	7.8600(6)
b/Å	12.3712(13)	21.1721(13)	15.4384(13)	15.1064(3)	15.5993(18)	11.1738(10)
c/Å	18.764(2)	21.6903(12)	21.0130(16)	12.4344(5)	21.362(2)	19.0870(17)
α/°	90.00	90.00	84.839(6)	90.00	83.354(6)	77.214(6)
β/°	90.00	90.00	75.566(5)	90.00	72.763(6)	85.475(5)
γ/°	90.00	90.00	61.549(5)	120.00	62.704(6)	75.105(6)
V/Å^3	2743.4(5)	6590.8(7)	4237.4(6)	2457.4(16)	4341.4(9)	1579.4(2)
Z	4	8	2	3	2	2
D_c/g cm^{-3}	1.336	1.332	1.369	1.600	1.503	1.390
μ Mo K_α/mm^{-1}	0.097	0.328	0.177	3.757	2.910	0.342
F000	1168.0	2768.0	1832.0	1182.0	1996.0	692.0
T/K	298(2)	298(2)	298(2)	298(2)	298(2)	298(2)
θ max.	24.003	17.60	20.56	23.00	13.17	18.55
Total no. of reflections	8071	45425	25922	13573	38150	11560
Independent reflections	5742	6776	6719	2681	14721	7427
Observed reflections	1802	5479	4731	1648	4507	3934
Parameters refined	362	770	1013	124	803	771
R_1, I > 2σ(I)	0.1122	0.0505	0.0749	0.0514	0.0843	0.0825
wR_2, I > 2σ(I)	0.2715	0.1481	0.2137	0.1164	0.2171	0.1866
GOF (F^2)	1.194	0.993	0.894	0.891	0.837	0.988
CCDC No.	1449438	1449439	1449440	1449441	1449442	1449443

Table A6.2 Crystallographic parameters and refinement details of receptor $\mathbf{L_{19}}$ and its anion complexes

Parameters	$\mathbf{L_{19}}$	**19a**	**19b**	**19c**	**19d**
Formula	$C_{30}H_{36}Cl_3N_7O_3$	$C_{46}H_{71}Cl_4N_8O_3$	$C_{46}H_{72}BrCl_3N_8O_3$	$C_{77}H_{110}Cl_6N_{16}O_9$	$C_{92}H_{143}Cl_6N_{16}O_{10}S$
Fw	649.01	925.91	971.37	1616.51	1877.98
Crystal system	monoclinic	orthorhombic	orthorhombic	monoclinic	triclinic
Space group	*P 21/c*	*P n a 21*	*P n a 21*	*P 2/n*	*P -1*
a/Å	13.436(3)	16.686(13)	16.793(12)	19.372(13)	13.620(7)
b/Å	19.819(3)	21.503(18)	21.300(13)	22.564(14)	16.462(6)
c/Å	13.591(3)	14.740(13)	14.835(6)	19.522(10)	25.0998(13)
α/°	90.00	90.00	90.00	90.00	108.871(4)
β/°	118.29(2)	90.00	90.00	92.140(6)	95.521(4)
γ/°	90.00	90.00	90.00	90.00	91.523(4)
V/Å^3	3186.9(13)	5288.4(8)	5306.1(5)	8527.1(9)	5290.6(5)
Z	4	4	4	4	2
D_c/g cm^{-3}	1.353	1.163	1.216	1.259	1.179
μ Mo K_α/mm^{-1}	0.331	0.268	0.970	0.264	0.241
F000	1360.0	1980.0	2056.0	3432.0	2010.0
T/K	298(2)	298(2)	298(2)	298(2)	298(2)
θ max.	28.670	25.000	24.998	25.000	28.752
Total no. of reflections	10707	16340	13759	20037	51128
Independent reflections	7465	8911	8597	14622	26177
Observed reflections	3539	6419	3437	8683	9388
Parameters refined	391	554	538	1012	1150
R_1, I > 2σ(I)	0.1065	0.0956	0.0901	0.0973	0.0964
wR_2, I > 2σ(I)	0.1065	0.1837	0.1589	0.1486	0.2502
GOF (F^2)	1. 106	1.192	1.158	1.161	1.173
CCDC No.	1840353	1840355	1840356	1840357	1840358

Table A6.3 Crystallographic parameters and refinement details of receptor $\mathbf{L_{20}}$ and its anion complexes

Parameters	$\mathbf{L_{20}}$	**20a**	**20b**	**20c**
Formula	$C_{30}H_{36}Br_3N_7O_3$	$C_{46}H_{72}Br_3FN_8O_3$	$C_{92}H_{144}Br_6N_{16}O_{10}S$	$C_{60}H_{70}Br_6F_6N_{14}O_6Si$
Fw	782.36	1043.82	2145.69	1704.79
Crystal system	monoclinic	monoclinic	triclinic	monoclinic
Space group	*P 21/c*	*P 21/c*	*P -1*	*C 2/c*
a/Å	13.564(8)	8.949(5)	13.738(2)	15.372(6)
b/Å	29.320(14)	22.503(14)	16.583(3)	21.983(6)
c/Å	17.585(14)	25.721(2)	25.631(4)	26.797(9)
α/°	90.00	90.00	108.151(15)	90.00
β/°	109.811(8)	90.732(6)	97.637(12)	92.632(10)
γ/°	90.00	90.00	93.047(14)	90.00
V/Å^3	6579.9(8)	5179.4(6)	5471.6(16)	9046(5)
Z	8	4	2	4
D_c/g cm^{-3}	1.579	1.339	1.302	1.252
μ Mo K_α/mm^{-1}	3.721	2.385	2.278	2.734
F000	3152.0	2168.0	2228.0	3416.0
T/K	298(2)	298(2)	298(2)	298(2)
θ max.	28.827	24.999	24.253	24.999
Total no. of reflections	30744	21566	19808	22832
Independent reflections	15020	9120	16564	7890
Observed reflections	11692	4053	10364	5341
Parameters refined	781	557	1140	380
R_1, I > 2σ(I)	0.0703	0.0677	0.0990	0.0927
wR_2, I > 2σ(I)	0.1410	0.1564	0.2657	0.2090
GOF (F^2)	0.884	1.150	1.192	1.103
CCDC No.	1840354	1840359	1840360	1840361

Table A6.4 Crystallographic parameters and refinement details of free receptors $\mathbf{L_{21}}$-$\mathbf{L_{23}}$ and fluoride complexes

Parameters	$\mathbf{L_{21}}$	$\mathbf{L_{22}}$	$\mathbf{L_{23}}$	**21a**	**22a**	**23a**
Formula	$C_{27}H_{30}Cl_3N_7O_3$	$C_{27}H_{30}Br_3N_7O_3$	$C_{27}H_{30}I_3N_7O_3$	$C_{43}H_{66}Cl_3FN_8O_3$	$C_{43}H_{66}Br_3FN_8O_3$	$C_{43}H_{66}I_3FN_8O_3$
Fw	606.93	740.28	881.28	868.39	1001.74	1142.74
Crystal system	triclinic	triclinic	triclinic	monoclinic	monoclinic	triclinic
Space group	*P -1*	*P -1*	*P -1*	*P 2/c*	*P 21/c*	*P -1*
a/Å	9.422(10)	9.464(2)	9.618(5)	23.756(16)	9.124(5)	9.206(17)
b/Å	12.988(12)	13.104(3)	13.244(6)	9.124(3)	20.617(11)	23.534(4)
c/Å	13.680(13)	13.846(3)	13.946(7)	25.244(16)	26.103(14)	25.684(5)
α/°	83.836(8)	83.330(14)	84.13(3)	90.00	90.00	113.443(6)
β/°	70.603(9)	70.953(14)	72.77(3)	116.950(8)	90.927(7)	90.877(7)
γ/°	70.406(9)	70.070(14)	69.73(3)	90.00	90.00	94.305(6)
V/Å^3	1487.6(3)	1525.9(6)	1591.7(14)	4877.3(6)	4910(5)	5084.8(16)
Z	2	2	2	4	4	4
D_c/g cm^{-3}	1.355	1.611	1.839	1.183	1.355	1.493
μ Mo K_α/mm^{-1}	0.349	4.006	2.985	0.236	2.513	1.890
F000	632.0	740.0	848.0	1856.0	2072.0	2288.0
T/K	298(2)	298(2)	298(2)	298(2)	298(2)	298(2)
θ max.	24.997	25.000	24.996	24.999	25.000	24.999
Total no. of reflections	5638	12314	16333	22106	57289	59081
Independent reflections	4968	4883	5591	8573	8576	17523
Observed reflections	3513	2281	4066	4515	6152	8399
Parameters refined	361	361	361	528	527	1063
R_1, I > 2σ(I)	0.0513	0.0665	0.0652	0.0744	0.0564	0.0763
wR_2, I > 2σ(I)	0.1265	0.1690	0.1687	0.1854	0.1375	0.1973
GOF (F^2)	1.039	1.129	1.069	1.056	0.937	1.173
CCDC No.	1832718	1832719	1832720	1832721	1832723	1832725

Table A6.5 Crystallographic parameters and refinement details of oxyanion complexes of receptors L_{21}-L_{23}

Parameters	**21b**	**22b**	**23b**	**23c**
Formula	$C_{86}H_{132}Cl_6N_{16}O_{11}S$	$C_{71}H_{100}Br_6N_{16}O_9$	$C_{55}H_{60}I_6N_{14}O_{11}$	$C_{86}H_{132}I_6N_{16}O_{10}S$
Fw	1810.84	1801.07	1854.57	2343.54
Crystal system	monoclinic	monoclinic	monoclinic	monoclinic
Space group	*P 21/n*	*C 2/c*	*C 2/c*	*P 21*
a/Å	17.951(8)	17.362(9)	17.736(5)	18.049(6)
b/Å	21.384(9)	20.718(15)	20.899(9)	21.726(6)
c/Å	26.265(9)	23.564(15)	23.853(9)	28.435(10)
α/°	90.00	90.00	90.00	90.00
β/°	97.717(4)	98.846(5)	99.333(3)	107.237(3)
γ/°	90.00	90.00	90.00	90.00
V/Å^3	9991.2(7)	8375.1(9)	8724.1(5)	10649.5(6)
Z	4	4	4	4
D_c/g cm^{-3}	1.204	1.428	1.412	1.462
μ Mo K_α/mm^{-1}	0.254	2.937	2.186	1.826
F000	3864.0	3680.0	3576.0	4696.0
T/K	298(2)	298(2)	298(2)	298(2)
θ max.	25.000	25.000	25.000	24.998
Total no. of reflections	41701	19078	17797	44541
Independent reflections	17572	7329	7674	36998
Observed reflections	7559	6079	3938	15433
Parameters refined	1089	467	389	2231
R_1, I > 2σ(I)	0.0771	0.0921	0.0582	0.0620
wR_2, I > 2σ(I)	0.1770	0.1787	0.1853	0.1552
GOF (F^2)	0.974	1.111	1.039	0.906
CCDC No.	1832722	1832724	1832726	1832727

Table A6.6 Details of Hydrogen Bonding contacts in the protonated complexes of receptors L_{16}-L_{18}

Complex	D−H···A	*d*(D···H)/Å	*d*(H···A)/Å	*d*(D···A)/Å	<D−H···A/°	Symmetry codes
16a	N2-H2C···Cl6	0.90	2.22	3.092(5)	164	x,y,z
	N2-H2D···Cl3	0.90	2.28	3.155(4)	163	x,y,z
	N4-H4C···Cl3	0.90	2.21	3.077(5)	162	x,y,z
	N4-H4D···Cl2	0.90	2.21	3.098(5)	170	-x, y-1/2, -z+3/2
	N6-H6C···Cl3	0.90	2.31	3.177(4)	163	x,y,z
	N6-H6D···Cl2	0.90	2.28	3.140(5)	161	-x+1/2, -y+1, z-1/2
	N9-H9C···Cl1	0.90	2.35	3.237(4)	167	x,y,z
	N9-H9D···Cl5	0.90	2.18	3.073(5)	171	x,y,z
	N11-H11C···Cl1	0.90	2.31	3.184(5)	164	x,y,z
	N11-H11D···Cl4	0.90	2.25	3.094(5)	157	-1/2+x,1/2-y,-z
	N13-H13C···Cl1	0.90	2.25	3.129(5)	167	x,y,z
	N13-H13D···Cl4	0.90	2.21	3.085(5)	162	-1+x,y,z
16b	N2-H2N···O13	0.86	2.14	2.951(9)	158	x,y,z
	N4-H4N···O13	0.86	2.30	3.063(8)	148	x,y,z
	N9-H9N···O14	0.86	2.21	2.919(9)	140	x,y,z
	N11-H11N···O14	0.86	2.30	3.108(9)	156	x,y,z
	N13-H13N···O14	0.86	2.37	3.134(8)	148	x,y,z
17a	N2-H2C···F1	0.90	1.72	2.614(6)	173	2/3+x,1/3+y,-2/3+z
	N2-H2D···F2	0.90	1.76	2.663(10)	178	1-x+y,1-x,z
17b	N4-H4BD···O21	0.90	2.13	2.898(16)	143	x,1+y,z
	N2-H2A···O4A	0.97	1.77	2.738(18)	173	x,1+y,z
	N2-H2A···O4B	0.97	1.78	2.715(13)	162	x,1+y,z
	N3-H3B···O12	0.97	1.75	2.710(10)	168	x,y,z
	N6-H6A···O3	0.90	1.86	2.758(9)	173	x+1, y, z
	N6-H6B···O5	0.90	2.09	2.871(8)	145	x,y,z
	N7-H7A···O3	0.97	2.18	2.932(9)	134	x+1,y,z
	N7-H7B···O9	0.97	1.85	2.806(9)	167	x+1,y,z
	N8-H8C···O9	0.97	2.07	2.910(9)	144	x+1,y,z
	N8-H8D···O5	0.97	1.88	2.841(9)	172	x,y,z
18a	N2-H2C···Cl2	0.90	2.24	3.075(10)	153	x,y,z
	N2-H2D···Cl1	0.90	2.28	3.152(10)	164	1+x,1+y,z
	N4-H4C···Cl2	0.90	2.40	3.285(12)	167	x,y,z
	N4-H4D···Cl6	0.90	2.21	3.078(11)	163	x,y,z
	N6-H6C···Cl5	0.90	2.25	3.137(11)	166	1+x,1+y,z
	N6-H6D···Cl3	0.90	2.25	3.110(11)	159	x,y,z
	N9-H9C···Cl6	0.90	2.27	3.143(11)	163	x,y,z
	N9-H9D···Cl1	0.90	2.21	3.078(10)	162	x,y,z
	N11-H11C···Cl4	0.90	2.42	3.312(12)	172	x,y,z
	N11-H11D···Cl5	0.90	2.18	3.051(11)	162	x,-1+y,z
	N13-H13C···Cl3	0.90	2.28	3.160(10)	167	x,y,z
	N13-H13D···Cl4	0.90	2.24	3.080(10)	156	x,y,z

Table A6.7 Details of Hydrogen Bonding contacts of anion complexes of receptors $\mathbf{L_{19}}$-$\mathbf{L_{20}}$

Complex	D−H···A	*d*(D···H)/Å	*d*(H···A)/Å	*d*(D···A)/Å	<D−H···A/°	Symmetry codes
$\mathbf{L_{19}}$	N3-H3N···O2	0.86	1.99	2.847(10)	178	-x,-y,-z
	N4-H4N···O3	0.86	2.07	2.877(10)	157	x,y,z
	N5-H5N···O3	0.86	2.08	2.881(9)	155	x,y,z
	N6-H6N···O1	0.86	2.16	2.956(10)	154	1-x,-y,1-z
	N7-H7N···O1	0.86	2.13	2.921(9)	152	1-x,-y,1-z
$\mathbf{L_{20}}$	N2-H2N···O3	0.86	2.13	2.927(9)	153	x,y,z
	N3-H3N···O3	0.86	2.12	2.907(9)	152	x,y,z
	N4-H4N···O4	0.86	2.19	2.971(9)	151	1+x,1/2-y,1/2+z
	N5-H5N···O4	0.86	2.11	2.899(8)	152	1+x,1/2-y,1/2+z
	N6-H6N···O6	0.86	2.01	2.869(9)	177	x,1/2-y,1/2+z
	N9-H9N···O5	0.86	2.12	2.919(8)	154	x,y,z
	N10-H10N···O5	0.86	2.20	2.991(8)	153	x,y,z
	N11-H11N···O2	0.86	2.01	2.870(9)	175	x,1/2-y,-1/2+z
	N13-H13N···O1	0.86	2.31	3.062(9)	147	x,1/2-y,-1/2+z
	N14-H14N···O1	0.86	2.01	2.827(9)	158	x,1/2-y,-1/2+z
19a	N2-H2N···Cl4	0.86	2.66	3.449(12)	154	-1/2+x,1/2-y,z
	N3-H3N···Cl4	0.86	2.49	3.301(11)	158	-1/2+x,1/2-y,z
	N4-H4N···Cl4	0.86	2.65	3.443(12)	153	-1/2+x,1/2-y,z
	N5-H5N···Cl4	0.86	2.43	3.274(8)	166	-1/2+x,1/2-y,z
	N6-H6N···Cl4	0.86	2.74	3.527(9)	153	-1/2+x,1/2-y,z
	N7-H7N···Cl4	0.86	2.39	3.220(13)	162	-1/2+x,1/2-y,z
19b	N2-H2N···Br1	0.86	2.77	3.5595	153	-1/2+x,1/2-y,z
	N3-H3N···Br1	0.86	2.50	3.3416	166	-1/2+x,1/2-y,z
	N4-H4N···Br1	0.86	2.85	3.6309	152	-1/2+x,1/2-y,z
	N5-H5N···Br1	0.86	2.52	3.3233	156	-1/2+x,1/2-y,z
	N6-H6N···Br1	0.86	2.77	3.5670	154	-1/2+x,1/2-y,z
	N7-H7N···Br1	0.86	2.61	3.4295	159	-1/2+x,1/2-y,z
19c	N2-H2N···O8	0.86	2.19	2.975(10)	151	x,y,z
	N3-H3N··· O8	0.86	2.13	2.920(10)	153	x,y,z
	N4-H4N···O7	0.86	2.17	2.884(12)	141	1/2-x,y,3/2-z
	N5-H5N···O7	0.86	2.41	3.075(13)	134	1/2-x,y,3/2-z
	N5-H5N···O8	0.86	2.36	3.201(10)	166	1/2-x,y,3/2-z
	N6-H6N···O8	0.86	2.31	3.152(10)	167	x,y,z
	N7-H7N···O7	0.86	1.89	2.748(13)	173	x,y,z
	N7-H7N···O7	0.86	2.35	3.094(14)	144	1/2-x,y,3/2-z
	N9-H9N···O10	0.86	2.50	3.239(8)	144	x,y,z
	N10-H10N···O10	0.86	2.08	2.868(12)	153	x,y,z
	N11-H11N···O9	0.86	2.44	3.160(10)	141	x,y,z
	N12-H12N···O9	0.86	2.14	2.984(12)	167	1/2-x,y,1/2-z
	N13-H13N···O9	0.86	2.52	3.253(10)	144	x,y,z
	N14-H14N···O9	0.86	1.93	2.792(10)	175	x,y,z
19d	N2-H2N···O7	0.86	2.12	2.937(5)	160	x,y,z
	N3-H3N···O9	0.86	2.19	3.018(5)	161	x,y,z
	N4-H4N···O7	0.86	2.12	2.904(6)	152	x,y,z
	N5-H5N···O8	0.86	2.12	2.941(5)	158	x,y,z
	N6-H6N···O7	0.86	2.08	2.908(5)	160	x,y,z
	N7-H7N···O10	0.86	2.13	2.951(5)	159	x,y,z
	N9-H9N···O9	0.86	2.24	3.025(5)	152	x,y,z
	N10-H10N···O9	0.86	2.08	2.915(6)	164	x,y,z
	N11-H11N···O8	0.86	2.24	3.028(5)	152	x,y,z
	N12-H12N···O8	0.86	2.10	2.932(5)	161	x,y,z
	N13-H13N···O10	0.86	2.30	3.077(5)	150	x,y,z
	N14-H14N···O10	0.86	2.10	2.931(5)	163	x,y,z
20a	N2-H2N···F1	0.86	2.03	2.826(6)	154	x,y,z
	N3-H3N··· F1	0.86	2.01	2.816(6)	156	x,y,z
	N4-H4N··· F1	0.86	2.29	3.033(5)	144	x,y,z
	N5-H5N··· F1	0.86	1.88	2.721(6)	164	x,y,z
	N6-H6N··· F1	0.86	2.24	2.982(5)	144	x,y,z
	N7-H7N··· F1	0.86	1.90	2.720(6)	160	x,y,z
20b	N2-H2N···O7	0.86	2.36	3.134(14)	150	x,y,z
	N3-H3N···O7	0.86	2.06	2.908(17)	167	x,y,z
	N4-H4N···O9	0.86	2.33	3.109(16)	151	x,y,z
	N5-H5N···O9	0.86	2.11	2.947(16)	165	x,y,z
	N6-H6N···O10	0.86	2.21	3.006(14)	154	x,y,z
	N7-H7N···O10	0.86	2.30	3.054(14)	146	x,y,z
	N9-H9N···O8	0.86	2.14	2.897(15)	146	x,y,z
	N10-H10N···O7	0.86	2.11	2.945(16)	165	x,y,z
	N11-H11N···O8	0.86	2.14	2.910(13)	148	x,y,z
	N12-H12N···O9	0.86	2.26	3.077(16)	159	x,y,z
	N13-H13N···O8	0.86	2.19	2.957(16)	149	x,y,z
	N14-H14N···O10	0.86	2.11	2.943(15)	163	x,y,z

20c	N2-H2N···F1	0.86	1.97	2.800(3)	161	x,y,z
	N3-H3N··· F4	0.86	2.46	3.220(2)	148	x,y,z
	N4-H4N··· F1	0.86	2.41	3.155(18)	145	x,y,z
	N5-H5N··· F3	0.86	2.27	3.100(2)	161	x,y,z
	N6-H6N··· F1	0.86	2.16	2.933(19)	150	x,y,z
	N7-H7N··· F2	0.86	2.17	3.000(2)	164	1-x,y,1/2-z

Table A6.8 Details of Hydrogen Bonding contacts of free receptors $\mathbf{L_{21}}$-$\mathbf{L_{23}}$ and their anion complexes

Complex	D−H···A	*d*(D···H)/Å	*d*(H···A)/Å	*d*(D···A)/Å	<D−H···A/°	Symmetry codes
L_{21}	N2-H2N···O2	0.86	2.15	2.950(3)	156	x,y,z
	N3-H3N···O2	0.86	2.13	2.931(3)	155	x,y,z
	N4-H4N···O3	0.86	2.04	2.876(3)	162	1-x,-y,1-z
	N5-H5N···O3	0.86	2.34	3.102(3)	149	1-x,-y,1-z
	N6-H6N···O1	0.86	2.25	2.997(3)	145	-x,1-y,1-z
	N7-H7N···O1	0.86	2.05	2.878(3)	155	-x,1-y,1-z
L_{22}	N2-H1N···O2	0.86	2.04	2.872(7)	163	-x,1-y,2-z
	N3-H2N···O2	0.86	2.35	3.111(8)	148	-x,1-y,2-z
	N4-H3N···O3	0.86	2.29	3.039(9)	146	1-x,-y,2-z
	N5-H4N···O3	0.86	2.02	2.838(7)	159	1-x,-y,2-z
	N6-H5N···O1	0.86	2.14	2.946(8)	155	x,y,z
	N7-H6N···O1	0.86	2.12	2.923(9)	155	x,y,z
L_{23}	N2-H2N···O2	0.86	2.14	2.944(9)	156	x,y,z
	N3-H3N···O2	0.86	2.16	2.960(9)	154	x,y,z
	N4-H4N···O3	0.86	2.08	2.901(8)	160	1-x,-y,1-z
	N5-H5N···O3	0.86	2.30	3.083(8)	151	1-x,-y,1-z
	N6-H6N···O1	0.86	2.44	3.164(9)	143	-x,1-y,1-z
	N7-H7N···O1	0.86	2.01	2.843(8)	164	-x,1-y,1-z
21a	N2-H2N···F1	0.86	2.17	2.928(4)	147	x,y,z
	N3-H3N···F1	0.86	1.93	2.740(3)	156	x,y,z
	N4-H4N···F1	0.86	2.09	2.880(4)	152	x,y,z
	N5-H5N···F1	0.86	1.95	2.779(4)	161	x,y,z
	N6-H6N···F1	0.86	2.26	2.998(4)	143	x,y,z
	N7-H7N···F1	0.86	1.88	2.719(4)	167	x,y,z
21b	N2-H2N···O10	0.86	2.38	3.144(6)	149	x,y,z
	N3-H3N··· O10	0.86	2.13	2.965(6)	165	x,y,z
	N4-H4N···O9	0.86	2.28	3.053(5)	149	x,y,z
	N5-H5N···O9	0.86	2.01	2.834(5)	160	x,y,z
	N6-H6N···O7	0.86	2.19	2.985(5)	155	x,y,z
	N7-H7N···O7	0.86	2.19	3.000(6)	157	x,y,z
	N9-H9N···O8	0.86	2.09	2.887(5)	154	x,y,z
	N10-H10N···O9	0.86	2.10	2.939(5)	165	x,y,z
	N11-H11N···O8	0.86	2.23	2.909(6)	136	x,y,z
	N12-H12N···O10	0.86	2.30	3.142(6)	168	x,y,z
	N13-H13N···O8	0.86	2.13	2.926(6)	155	x,y,z
	N14-H14N···O7	0.86	2.07	2.911(5)	164	x,y,z
22a	N2-H2N···F1	0.86	2.19	2.935(7)	145	x,y,z
	N3-H3N···F1	0.86	1.92	2.751(6)	163	x,y,z
	N4-H4N···F1	0.86	2.09	2.883(6)	152	x,y,z
	N5-H5N···F1	0.86	2.03	2.837(6)	155	x,y,z
	N6-H6N···F1	0.86	2.28	3.005(7)	143	x,y,z
	N7-H7N···F1	0.86	1.92	2.761(6)	166	x,y,z
	C8-H8···F1	0.93	2.40	3.315(8)	167	1+x,y,z
	C19-H19B···O1	0.97	2.50	3.423(8)	160	-1+x,y,z
22b	N2-H2N···O5	0.86	2.49	3.347(14)	177	1-x,y,1/2-z
	N3-H3N··· O4	0.86	1.98	2.801(17)	159	x,y,z
	N4-H4N··· O5	0.86	2.30	3.157(14)	178	x,y,z
	N5-H5N··· O5	0.86	2.01	2.804(14)	153	1-x,y,1/2-z
	N6-H6N··· O4	0.86	2.40	3.253(11)	172	x,y,z
	N7-H7N··· O5	0.86	2.03	2.844(13)	159	x,y,z
23a	N2-H2N···F1	0.86	2.08	2.867(9)	152	x,y,z
	N3-H3N···F1	0.86	1.96	2.779(9)	159	x,y,z
	N4-H4N···F1	0.86	2.25	2.988(9)	145	x,y,z
	N5-H5N···F1	0.86	1.90	2.725(8)	162	x,y,z
	N6-H6N···F1	0.86	2.20	2.952(10)	147	x,y,z
	N7-H7N···F1	0.86	1.92	2.738(9)	159	x,y,z
	N9-H9N···F2	0.86	2.05	2.849(8)	155	x,y,z
	N10-H10N···F2	0.86	2.05	2.854(10)	156	x,y,z
	N11-H11N···F2	0.86	2.20	2.942(9)	144	x,y,z
	N12-H12N···F2	0.86	1.99	2.756(8)	148	x,y,z
	N13-H13N···F2	0.86	2.22	2.984(9)	149	x,y,z
	N14-H14N···F2	0.86	1.93	2.762(8)	161	x,y,z
23b	N2-H2N···O4	0.86	2.45	3.301(5)	170	x,y,z

	N3-H3N···O5	0.86	2.06	2.869(8)	156	x,y,z
	N4-H4N···O5	0.86	2.27	3.125(9)	177	x,y,z
	N5-H5N···O5	0.86	2.01	2.791(9)	150	-x,y,1/2-z
	N6-H6N···O5	0.86	2.60	3.455(9)	174	x,y,z
	N7-H7N···O4	0.86	1.99	2.810(8)	159	x,y,z
23c	N2-H2N···O17B	0.86	2.27	3.050(3)	151	1-x,1/2+y,1-z
	N2-H2N···O19A	0.86	2.11	2.920(18)	157	1-x,1/2+y,1-z
	N3-H3N···O19A	0.86	2.23	3.019(17)	153	1-x,1/2+y,1-z
	N3-H3N···O20B	0.86	2.03	2.807(3)	165	1-x,1/2+y,1-z
	N4-H4N···O17B	0.86	2.35	3.120(3)	149	1-x,1/2+y,1-z
	N4-H4N···O18A	0.86	2.21	2.990(2)	151	1-x,1/2+y,1-z
	N5-H5N···O18A	0.86	2.12	2.933(19)	159	1-x,1/2+y,1-z
	N5-H5N···O19B	0.86	2.21	3.040(2)	162	1-x,1/2+y,1-z
	N6-H6N···O17B	0.86	2.25	3.000(3)	147	1-x,1/2+y,1-z
	N6-H6N···O20A	0.86	2.19	3.000(2)	157	1-x,1/2+y,1-z
	N7-H7N···O18B	0.86	2.06	2.890(3)	161	1-x,1/2+y,1-z
	N7-H7N···O20A	0.86	2.21	3.031(19)	159	1-x,1/2+y,1-z
	N9-H9N···O13B	0.86	2.43	3.190(3)	148	1-x,-1/2+y,-z
	N9-H9N···O14A	0.86	2.16	2.877(17)	141	1-x,-1/2+y,-z
	N10-H10N···O13B	0.86	2.07	2.920(2)	169	1-x,-1/2+y,-z
	N10-H10N···O15A	0.86	2.29	3.112(19)	159	1-x,-1/2+y,-z
	N11-H11N···O14A	0.86	2.11	2.932(16)	158	1-x,-1/2+y,-z
	N11-H11N···O15B	0.86	2.20	2.940(3)	144	1-x,-1/2+y,-z
	N12-H12N···O15B	0.86	2.00	2.810(4)	156	1-x,-1/2+y,-z
	N12-H12N···O16A	0.86	2.14	2.988(17)	170	1-x,-1/2+y,-z
	N13-H13N···O14A	0.86	2.18	2.940(18)	147	1-x,-1/2+y,-z
	N13-H13N···O16B	0.86	2.10	2.910(3)	156	1-x,-1/2+y,-z
	N14-H14N···O13A	0.86	2.18	3.018(17)	166	1-x,-1/2+y,-z
	N14-H14N···O16B	0.86	2.15	2.960(3)	156	1-x,-1/2+y,-z
	N16-H16N···O17A	0.86	2.17	2.899(18)	143	x,y,z
	N16-H16N···O19B	0.86	2.28	3.070(2)	152	x,y,z
	N17-H17N···O18A	0.86	2.27	3.068(19)	155	x,y,z
	N17-H17N···O19B	0.86	2.07	2.910(3)	164	x,y,z
	N18-H18N···O17A	0.86	2.21	3.010(18)	154	x,y,z
	N18-H18N···O20B	0.86	2.00	2.810(2)	155	x,y,z
	N19-H19N···O19A	0.86	2.06	2.901(16)	166	x,y,z
	N19-H19N···O20B	0.86	2.26	3.010(2)	145	x,y,z
	N20-H20N···O17A	0.86	2.22	2.948(18)	142	x,y,z
	N20-H20N···O18B	0.86	2.13	2.920(3)	152	x,y,z
	N21-H21N···O18B	0.86	2.13	2.930(3)	155	x,y,z
	N21-H21N···O20A	0.86	2.33	3.064(17)	162	x,y,z
	N23-H23N···O14B	0.86	2.35	3.110(3)	147	x,y,z
	N23-H23N···O16A	0.86	2.14	2.935(17)	153	x,y,z
	N24-H24N···O15B	0.86	2.04	2.900(3)	176	x,y,z
	N24-H24N···O16A	0.86	2.24	3.040(17)	155	x,y,z
	N25-H25N···O13A	0.86	2.23	3.011(18)	150	x,y,z
	N25-H25N···O14B	0.86	2.18	2.960(4)	149	x,y,z
	N26-H26N···O13A	0.86	2.04	2.868(17)	160	x,y,z
	N26-H26N···O16B	0.86	2.31	3.130(3)	161	x,y,z
	N27-H27N···O14B	0.86	2.38	3.130(4)	146	x,y,z
	N27-H27N···O15A	0.86	2.23	3.053(19)	159	x,y,z
	N28-H28N···O13B	0.86	2.01	2.870(3)	174	x,y,z
	N28-H28N···O15A	0.86	2.31	3.120(2)	156	x,y,z

Chapter 7

Phenyl and naphthyl substituted electron-rich tris-(thio)urea neutral receptors: Ice like cyclic $(H_2O)_6$ trapping within hexameric halide-receptor core

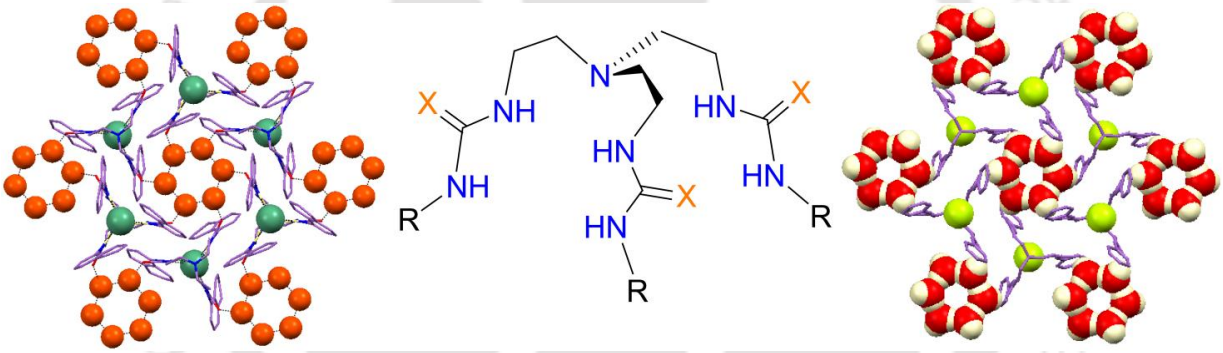

7.1 Background and Focus of the Chapter

Encouraged by the observations in natural anion binding proteins, which are potential specific binding pocket containing receptors for active transport systems in cells,[7.1] the researchers in the field of supramolecular chemistry develop several neutral artificial receptors. Over the past decades, the tren, [tris(2-aminoethyl)amine] skeleton consisting of three pendant primary amine groups with a tertiary amine center has materialized as one of the supreme archetypal anion binding building block demonstrating strong interplay among topology, complementarity, cooperativity and coordination. Besides, number of biologically and environmentally important anionic guests, water has also acknowledged as scientific and technological interest despite its most abundance in earth than any other substance. Primarily, it is a major chemical constituent of our planet's surface as well as its necessity for the genesis of life and secondly, it unveils an interesting array of uncommon properties in pure form and as a solvent.[7.2] Although the stereochemical role of water in proteins is well recognized, however the comprehensive positional evidence for nature of the water molecules such as their ability to form clusters of various size and shape is still preliminary.[7.3] Hence, the study of water clusters, stabilized by hydrogen bonding interactions, their fluctuations and their rearrangement dynamics is significant to understand the structures and characteristics of liquid water and ice.[7.4] Now the recognition of these water molecules with anions such as anion-water cluster or water assisted anionic guests within-the self-assemblies of size and shape-selective preorganized neutral organic frameworks have also attracted a lot of attention due to the critical roles of anions in living organisms as well as in a range of environmental, biological and medical purposes.[7.5] Among halides, the recognition of smallest fluoride ion has of special interest owing to its small size, high electronegativity, high hydration enthalpy as well as its functions in biological processes and also in drinking water purification process. The chloride ion is one of the major component of ocean and essential for its critical biological roles like signal transduction or carriage of organic solutes through cell membrane.[7.6] The carbonate oxyanion works as a buffer in the blood and the significant rise of atmospheric CO_2 in environment caused by increased consumption of fossil fuels, automobiles, industries, etc. which finally demands the fixation and activation of aerial CO_2 as carbonate.[7.7]

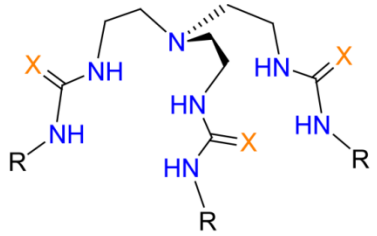

L_{24} X = O, R= -Naphthyl
L_{25} X = O, R= -Phenyl
L_{26} X = S, R= -Naphthyl
L_{27} X = S, R= -Phenyl

Scheme 7.1 A comprehensive representation of molecular receptor structures included in this chapter

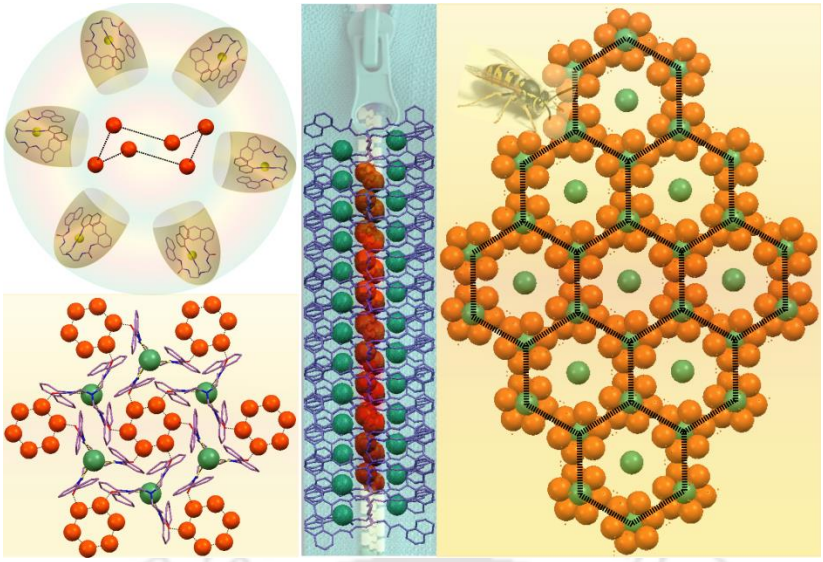

Fig. 7.1 The comprehensive pictorial depiction of one of the key outcomes of research works of this chapter.

Encapsulation of SO_4^{2-} and $H_2PO_4^-$ are also required for biological and environmental issues, as the harmful effects of sulfate have been measured as a key hurdle to cleanup efforts in the remediation of nuclear waste and $H_2PO_4^-$ anion due to its donor-acceptor property acts similar as the water molecule and becomes the most abundant among the three forms of inorganic phosphate[7.8] i.e. $H_2PO_4^-$, HPO_4^{2-} and PO_4^{3-}. Thus far, a large set of reported tren-based tripodal (thio)-urea receptors[7.9] mostly with electron withdrawing aryl terminals have been developed for the recognition and separation of anionic guests, which mainly focus on the structural aspects of anion binding followed by related selectivity in solution state. However, anion recognition by modest tren-based phenyl or naphthyl substituted (thio)-urea receptors with no terminal aryl functionalization have been underexplored in most traditional solid state, mainly due to the deficiency of π-acidic or electron-withdrawing aryl terminals.

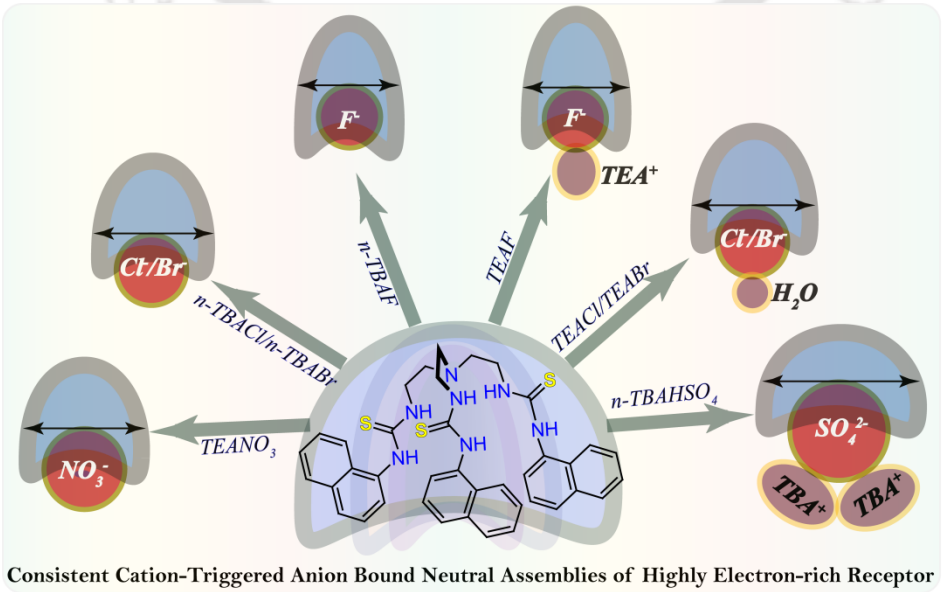

Fig. 7.2 The comprehensive representation of one of the key outcomes of research work included in this chapter.

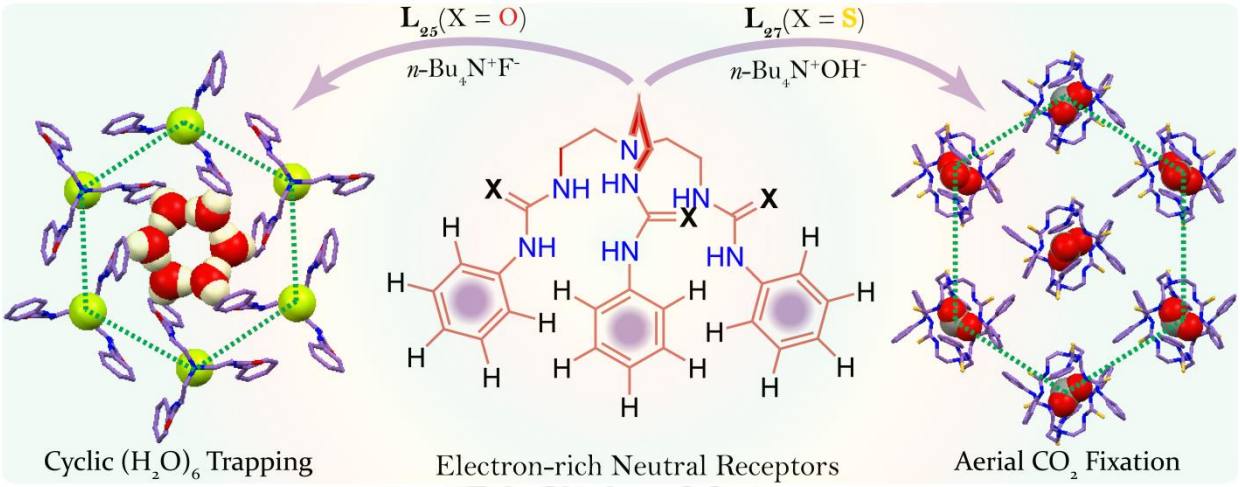

Fig. 7.3 The comprehensive representation of one of the key outcomes of research work included in this chapter.

Hence, in continuing our group's effort in the field of substituent driven host-guest assemblies, in this chapter we demonstrate the solid state anion-coordination abilities of two modest naphthyl and phenyl substituted tris-urea (**L_{24}** and **L_{25}**) receptors and their tris-thiourea analogues (**L_{26}** and **L_{27}**) derived from [tris(2-aminoethyl)-amine] skeleton,[7.10] which was considered as an underexplored area of solid-state tren-based anion-receptor chemistry over the last two decades. Note that, the tripodal receptors **L_{24}**-**L_{27}** (denoted as compounds 56, 57, 72, 73 in introduction chapter 1), previously synthesized by Moran and S. Wu's groups,[7.11] where they reported sulfate and phosphate anion binding with these receptors in solution phase only, however no structural data were available to support those host-guest binding in literature. This chapter establishes the formation of unique hexameric receptor-anion-water neutral molecular self-assemblies as evidenced single crystal X-ray analyses, where the conformationally flexible C_{3v}-symmetric halide (F^-/Cl^-) encapsulated electron-rich naphthyl based tripodal urea receptor **L_{24}** effectively entrap the chair-shaped ice-like neutral cyclic water hexamer (complexes **24a**, **24b**) within the exceptional hexameric cavity of receptor-halide bound host-guest association. On the other hand, the naphthyl based electron-rich thio-urea analog **L_{26}** even in the absence of any π-acidic or electron-withdrawing aryl terminals effectively entraps spherical fluoride (complexes **26a**^{1}, **26a**^{2}), relatively larger spherical chloride (complexes **26b**^{1}, **26b**^{2}) and bromide (complexes **26c**^{1}, **26c**^{2}), planar nitrate (complex **26d**), and tetrahedral divalent sulfate (complex **26e**) anions inside the relatively smaller inner tripodal cleft (compared to many previously reported tren-based thiourea receptors) *via* 1:1 host-guest complexation mode, regularly assisted by *n*-TBA/TEA counter-cations. Subsequently, the phenyl substituted simple tris-urea receptor **L_{25}** and its thio-urea analogue **L_{27}**, despite their electron-rich tripodal cavities, are still capable of capturing chair-shaped cyclic water hexamer within the infrequent fluoride (complex **25a**) encapsulated hexameric **L_{25}** core (similar as complexes **24a**, **24b**) as well as encapsulating

divalent carbonate anion (complex **27c**) inside the dimeric capsular cage of receptor $\mathbf{L_{27}}$ *via* hydroxide ion induced aerial CO_2 fixation. Moreover, structural analyses also elucidate the capturing of large dihydrogen phosphate $[(H_2PO_4^-)_2]$ dimeric association (complex **25b**) within the neutral dimeric pseudo-capsular assembly of receptor $\mathbf{L_{25}}$, whereas the thiourea analogue $\mathbf{L_{27}}$ exhibits chloride (complex **27a**) and acetate (complex **27b**) bound 1:1 unimolecular capsular assembly and divalent sulfate (complex **27d**) bound dimeric cage *via* hydrogen-bonding activated proton transfer reaction from monovalent HSO_4^- anion. Scheme 7.1 shows the molecular receptor structures $\mathbf{L_{24}}$-$\mathbf{L_{27}}$ and the representations of key findings of research work included in this chapter are shown Fig. 7.1-7.3.

7.2 Structural aspects of anion binding with $\mathbf{L_{24}}$-$\mathbf{L_{27}}$

In principle, for a particular receptor molecule to bind with the anionic guests of particular size and geometry, it should hold preorganized directional hydrogen-bond donors especially, tailored on a proper platform/framework. Noticeably, the Tren based, highly electron-rich naphthyl and phenyl-substituted tris-(thio)-urea receptors $\mathbf{L_{24}}$-$\mathbf{L_{27}}$ (Fig. 7.1-7.3) also possess highly organized hydrogen-bonding urea/thiourea functions suitable for anion encapsulation in spite of the absence of any π-acidic moieties as aryl terminals. Structural data obtained from X-ray analyses can offer insight into the binding differences of halides and oxyanions with particular neutral receptor. Traditionally from the viewpoint of anion-receptor chemistry, crystallization has been a key route to realize the structural visions of the anion complexes, which are then related to the observed selectivity in solution.

It should be mentioned here that good quality single crystals of only phenyl-substituted free (thio)-urea ligands $\mathbf{L_{25}}$ and $\mathbf{L_{27}}$ are attained from DMF solutions and they crystallize from the triclinic space group *P*-1 and orthorhombic space group *Pca*21 respectively. However, several attempts to grow single crystals of naphthyl-substituted free (thio)-urea receptors $\mathbf{L_{24}}$ and $\mathbf{L_{26}}$ in different crystallization conditions were not fruitful, instead most of the cases thick oily mass were found at the bottom of crystallization vials. Structural analysis reveals that each urea -NH moieties of receptor arms of tris-urea ligand $\mathbf{L_{25}}$ are projected toward three different directions, among which two intramolecular N−H···O interactions exist between two arms (Fig 7.4c). The free $\mathbf{L_{25}}$ molecule is further connected with adjacent symmetry-identical conformers *via* intermolecular N−H···O interactions also and two adjacent ligand units are also linked by four weak C−H···π connections (Fig 7.4c). The combined effect of intramolecular as well as intermolecular H-bonds resists the opening of the tripodal side arms of $\mathbf{L_{25}}$. On the other hand, the asymmetric unit of free tris-thiourea ligand $\mathbf{L_{27}}$ contains two almost similar symmetry-independent receptor units connected by one weak intermolecular C−H···π contact (Fig 7.4d).

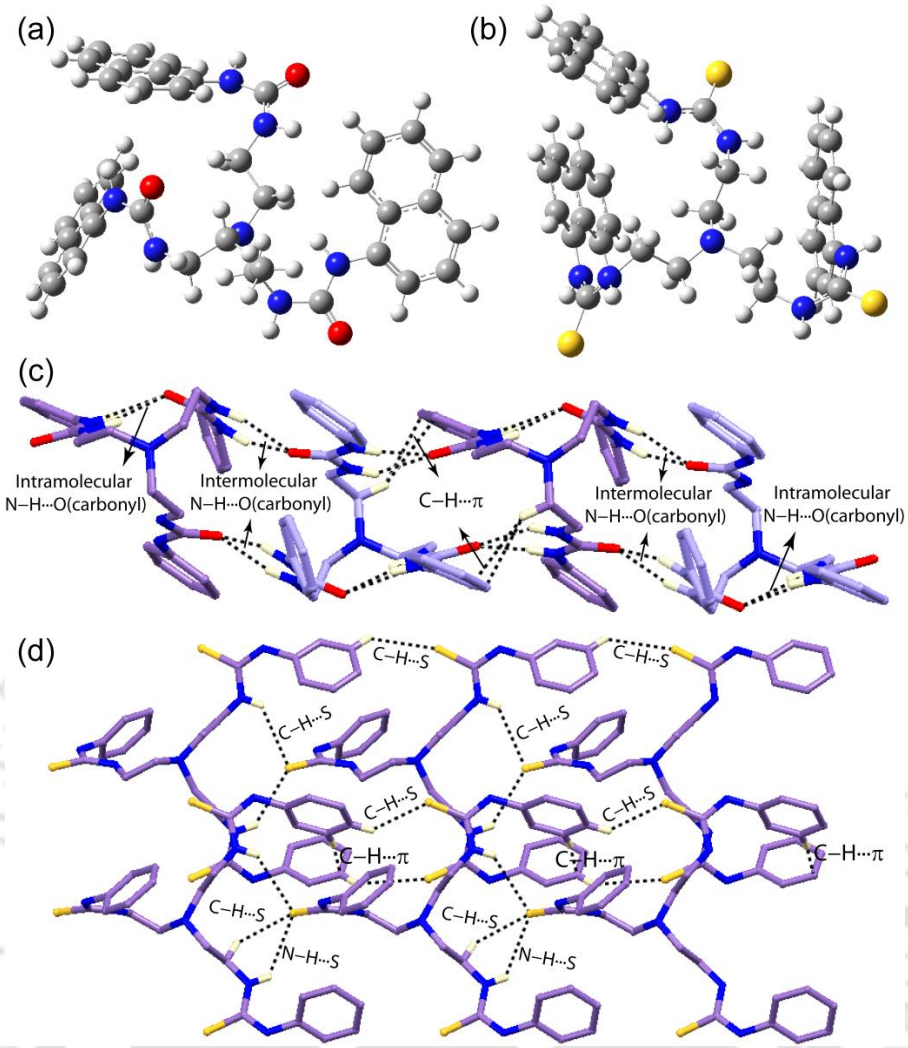

Fig. 7.4 The optimized structures of (a) free tris-urea receptor $\mathbf{L_{24}}$, (b) free tris-thiourea receptor $\mathbf{L_{26}}$, using B3LYP/6-31+ G(d) (5D, 7F) basis set; Partial X-ray structures depicting non-covalent interactions among adjacent conformers in (c) tris-urea receptor $\mathbf{L_{25}}$ and (d) tris-thiourea receptor $\mathbf{L_{27}}$.

Unlike free $\mathbf{L_{25}}$ receptor, the three thiourea receptor arms in $\mathbf{L_{27}}$ are projected towards three different directions with no intramolecular interactions, exhibiting more open conformation compared to $\mathbf{L_{25}}$ with larger average terminal aryl centroid distance. Each symmetry-independent conformer of $\mathbf{L_{27}}$ are linearly connected with adjacent symmetry-identical conformer by four intermolecular C−H···S interactions (Fig 7.4d). Note that, being unable to grow good quality crystals from various solvents in different crystallization conditions, the density functional theory (DFT) studies are implemented for structural elucidation of napthyl substituted tris-urea receptor $\mathbf{L_{24}}$ (Fig. 7.4a) and tris-tiourea receptor $\mathbf{L_{26}}$ (Fig. 7.4b), which disclose the non-capsular scattered receptor conformations and reveals the complete non-cooperativity of thio(urea) -NH protons exhibiting no tripodal cavity at all in both cases.

7.2.1. Structural analysis of halide bound complexes of receptors L_{24}-L_{27}

Single crystal XRD analyses of neutral receptor-halide or water-assisted encapsulated receptor-

halide complexes are severely dependent upon the electronic effect as well as the size of the highly electron-rich terminal naphthyl or phenyl groups and dimensions of the anionic guests.

7.2.1.1 Ice-like cyclic water trapped fluoride (24a) and chloride (24b) complexes of L_{24}

The X-ray analysis reveals almost isostructural cyclic water-hexamer trapping induced by encapsulated fluoride (complex **24a**) or chloride (complex **24b**) anions in trigonal system, although **24a** crystallizes in *P*31c space group and complex **24b** crystallizes in *R*-3 space group. Theoretical study of free neutral ligand $\mathbf{L_{24}}$ predicts almost no cavity of N-bridged tripodal scaffold, where the orientation of six urea N-H protons is not unidirectional (Fig. 7.4a). Interestingly, in presence of anionic guests (F^-/Cl^-), receptor $\mathbf{L_{24}}$ encapsulates the guest halide inside its C_{3v}-symmetric tripodal cleft by projecting all six urea -NH towards the cavity, as revealed from X-ray analysis of **24a** (Fig. 7.5a-d) and **24b** (Fig. 7.5e-h), which is known as the term 'complementary' and 'cooperativity' in supramolecular chemistry. The asymmetric unit of halide complexes contain two (in **24a**) and one (in **24b**) symmetry-independent one-third parts of the neutral $\mathbf{L_{24}}$ receptor/s, F^-/Cl^- anion/s and *n*-TBA cation/s along with two/one fully occupied water-oxygen atoms respectively. Each neutral $\mathbf{L_{24}}$ unit employing its six H-bond donating -NH groups engulf one fluoride/chloride anion by six strong N–H···F/Cl interactions *via* unicapsular assembly formation, where C_3-symmetry axis passes through apical N-atom and F^-/Cl^- ion respectively in **24a** and **24b** (Fig. 7.5). Then, the H-bond accepting three carbonyl oxygen atoms of a ligand unit projecting outside the receptor cavity are independently connected by strong O–H···O interactions with three different symmetry-identical Ow atoms in both complexes (Fig. 7.5). Interestingly, each Ow atom being trifurcated becomes further H-bonded with either adjacent symmetry-independent (in **24a**) or symmetry-identical (in **24b**) water molecules, constructing an ice-like chair-shaped cyclic water hexamer (Fig. 7.5b, f). The X-ray analysis also reveals that one hexameric water cluster which is a simplest supramolecular analogue of cyclohexane, completely stabilized by six O–H···O interactions with six different fluoride (in **24a**)/chloride (in **24b**) encapsulated ligand moieties. Note that, in cyclic centerosymmetric water hexamer, the average O···O distances are 2.773 and 2.732 Å in complexes **24a** and **24b** respectively, which are very similar with the average O···O distances in ice I_c (2.75 Å) and I_h (2.759 Å).[7.12] The average O···O···O angles are 105.6° for **24a** and 104.5° for **24b**, which are closely comparable to the value of 109.3° in the hexagonal ice. It is also evident that in both the complexes each Ow atoms donate two H-bonds and accept one H-bond i.e. each of them exhibit three coordination with adjacent water molecules and carbonyl oxygen of receptor (Fig. 7.5b, f). Such hydrogen-bond deficient water molecules exist at the surface of ice although X-ray absorption spectroscopy and Raman scattering studies of liquid water

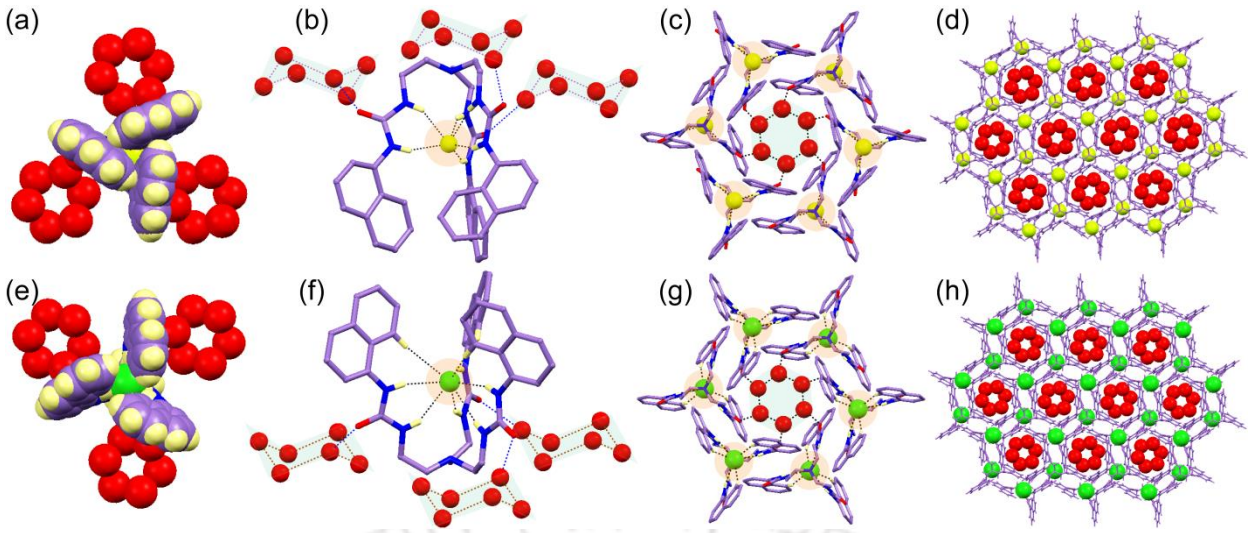

Figure 7.5 Partial X-ray structures depicting, spacefill view of (a) fluoride/ (e) chloride, engulfment inside receptor $\mathbf{L_{24}}$ and position of cyclic water-hexamer around each three receptor arms; Hydrogen-bonding contacts of encapsulated (b) fluoride/ (f) chloride surrounded by chair-shaped water hexamer; Cyclic water hexamer trapping inside the (c) fluoride/ (g) chloride encapsulated hexameric cavity of $\mathbf{L_{24}}$; Crystal packing of, (d) complex **24a/** (h) complex **24b** displaying honeycomb shaped architecture as viewed down along the crystallographic *c* axis.

recently also revealed that significant numbers of O atoms show less than four-coordination in liquid water.[7.13] The most fascinating feature of complexes **24a** and **24b** describes the cyclic hexameric water-cluster grabbing inside the unprecedented anionic guest (F^-/Cl^-) induced supramolecular self-assembled hexameric core of electron rich tripodal hosts (Fig. 7.5c, g), that is very different from the examples of a hexameric cluster coordinated by metal in organic or inorganic host systems. The average centroid distances (if centroids are the vertices of a triangle) among three hexameric water clusters where a halide ion is present inside the center of a triangle become 12.936 and 13.165 Å in complexes **24a** and **24b** respectively that are ascribed for the larger ionic radii of chloride compare to fluoride anion (Fig. A7.1). Several weak C_{TBA}–H···π interactions between receptors and counter-cations become also supportive to gain extra stability of water hexamer trapped honey-comb shaped hexameric host-guest assemblies (Fig. 7.5d, h).

7.2.1.2 Fluoride complexes 26a^1 and 26a^2 of receptor L_{26}

The fluoride encapsulated complexes **26a^1** and **26a^2** of naphthyl substituted tris-thiourea receptor $\mathbf{L_{26}}$ obtained from respective *n*-TBAF and TEAF salts, crystallize in monoclinic space group *P*21/c and trigonal space group *R*3c respectively. The asymmetric unit of complex **26a^1** contains two symmetry independent capsular receptor units which individually encapsulate two smallest spherical halides inside their tripodal cavities with hydrogen bonds to all six thiourea -NH protons (Fig. 7.6a). The two adjacent fluoride bound monomeric ligand capsular units, are interconnected by one *n*-TBA unit *via* one weak C–H···O and three weak C–H···π contacts. Moreover, two symmetry-identical adjacent capsular units conform a $R^2_2(14)$ type cyclic H-

bonding network *via* two C–H···S interactions. On the other hand, the asymmetric unit of complex **26a^2** contains one-third part of a neutral receptor **L$_{26}$**, single fluoride anion and its corresponding TEA counteraction. The X-ray analysis reveals the cation-sealed unicapsular assembly of naphthyl thiourea ligand **L$_{26}$**, where fluoride anion is encapsulated inside the C_{3v}-symmetric tripodal cavity by six strong thiourea N–H···F and one relatively weaker C_{TEA}–H···F interactions, exhibiting hepta-coordination (Fig. 7.6e), unlike complex **26a^1**. The cation-sealed 1:1 fluoride-receptor assembly **26a^2** gets extra stability by three weak C–H···π interactions.

7.2.1.3 Chloride complexes 26b^1 and 26b^2 of receptor L$_{26}$

The pseudo-encapsulated chloride complexes **26b^1** and **26b^2** of thiourea receptor **L$_{26}$** obtained from respective *n*-TBACl and TEACl salts and crystallize in the same triclinic space group *P*-1. The asymmetric unit of complex **26b^1** contains one **L$_{26}$** unit, one Cl^- anion and its corresponding *n*-TBA counter-cation whereas complex **26b^2** contains ligand **L$_{26}$**, Cl^- anion, TEA counter-cation and one additional water molecule of crystallization. Structural elucidation reveals that unlike the fluoride complexes of **L$_{26}$** and even the very small tripodal cavity (relative to the many reported first generation tren-based thiourea receptors) of **L$_{26}$** readily opens up its three arms, creating a pseudo-capsular cavity to encapsulate larger chloride ion (Fig. 7.6b,f). In complex **26b^1** the pseudo-capsular receptor first encapsulates a single chloride *via* six thiourea N–H···Cl interactions and the same Cl^- is again additionally C–H···Cl hydrogen bonded with another adjacent face-to-face oriented identical-symmetry chloride encapsulated pseudo-capsular receptor unit (Fig. 7.6b). Overall, the hepta-coordinated chloride bound 2:2 pseudo-capsular neutral assemblies get extra stability by three weak C–H···S and three C–H···π interactions in **26b^1** (Fig. 7.6b). On the other hand, in complex **26b^2** the pseudo-capsular **L$_{26}$** unit traps one chloride anion *via* hydrogen bonding to the six thiourea groups and the vacant space of 1:1 pseudo-capsular host-guest assembly is occupied by a water molecule which becomes O–H···S hydrogen bonded with adjacent receptor unit (Fig. 7.6f). Noticeably, unlike complex **26b^1**, two adjacent chloride encapsulated host assemblies are oppositely oriented in the crystal system of **26b^2**, which gains extra stability by weak C–H···S and C–H···π interactions.

7.2.1.4 Bromide complexes 26c^1 and 26c^2 of receptor L$_{26}$

The pseudo-encapsulated bromide complexes **26c^1** and **26c^2** of thiourea receptor **L$_{26}$** obtained from respective *n*-TBABr and TEABr salts crystallize in the same triclinic space group *P*-1, alike the chloride complexes **26b^1** and **26b^2**. Structural elucidation of both complexes would be helpful to understand the assembly progression with larger homologous spherical anions. Interestingly, the X-ray analysis also confirms the isostructural nature of complexes **26b^1** and

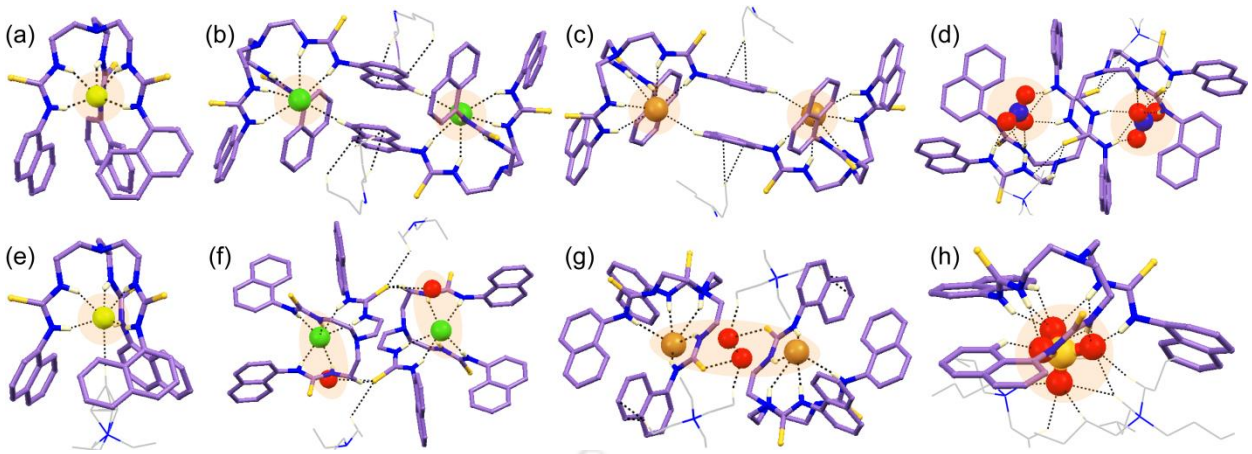

Fig. 7.6 X-ray structures (partial) depicting hydrogen bonding coordination environment in (a) fluoride complex **26a**^{1}, (b) chloride complex **26b**^{1}, (c) bromide complex **26c**^{1}, (d) nitrate complex **26d**, (e) fluoride complex **26a**^{2}, (f) hydrated-chloride complex **26b**^{2}, (g) hydrated-bromide complex **26c**^{2} and (h) sulfate complex **26e**.

26c^{1} as well as complexes **26b**^{2} and **26c**^{2}, which clearly indicates the substantial role of corresponding counteraction (either *n*-TBA^{+} or TEA^{+}) in host-guest assembly formation. In complex **26c**^{1}, the tris-thiourea receptor $\mathbf{L_{26}}$ in the asymmetric unit first encapsulates a bromide anion by six N–H···Br interactions within its pseudo-capsular cavity and then it becomes connected with exactly similar symmetry-identical bromide-bound assembly in face-to-face fashion by two identical C–H···Br interactions (Fig. 7.6c). Overall, the hepta-coordinated bromide-trapped 2:2 host-guest assemblage of **26c**^{1} is further stabilized by six C–H···S and four C–H···π weak interactions (Fig. 7.6c). In contrary, in complex **26c**^{2}, the two adjacent symmetry-identical hexa-coordinated bromide encapsulated 1:1 assemblies are not present in face-to-face fashion, but they are interconnected by C–H···S and C–H···π interactions (Fig. 7.6g). Note that, the vacant space of each tripodal pseudo-cavity in complex **26c**^{2} is occupied by water molecule in the crystal lattice and two intermolecular hydrogen-bonded water molecules along with few C–H···O_{water} interactions helps to gain stability of the self-assembled complex (Fig. 7.6g).

7.2.1.5 Cyclic $(H_2O)_6$ trapped fluoride complex 25a of receptor L_{25}

The chair-shaped cyclic $(H_2O)_6$ entrapped fluoride encapsulated hexameric complex **25a** of elctron-rich phenyl group substituted tris-urea receptor $\mathbf{L_{25}}$ crystallizes in symmetric trigonal space group *R*-3. The asymmetric unit contains one-third part of a neutral $\mathbf{L_{25}}$ receptor, a fluoride anion and its corresponding *n*-TBA counter-cation along with a fully occupied water molecule. Structural elucidation reveals the formation of 1:1 unimolecular $\mathbf{L_1}$-F^{-} capsule primarily (Fig. 7.7a), followed by the building of beautiful receptor-anion hexameric host-guest architecture, which then efficiently entraps the ice-like cyclic water hexamer by topological complementarity *via* symmetric number of non-covalent interactions (Fig. 7.7b) and finally the construction of unique honeycomb architecture have been observed from crystallographic *a*-axis

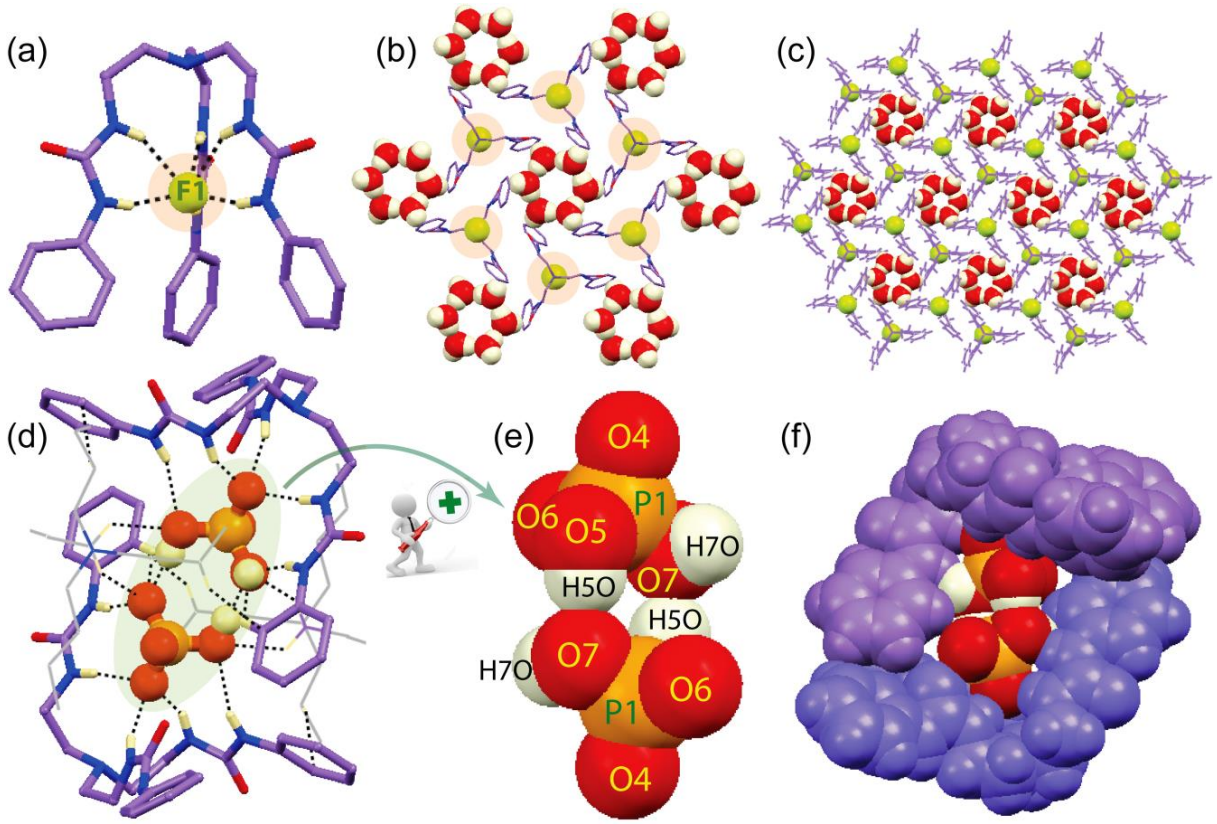

Fig. 7.7 Partial X-ray structures depicting (a) hydrogen bonding interactions of encapsulated fluoride in complex **25a**, (b) cyclic water hexamer entrapment around F^- encapsulated hexameric host-guest assemblies, (c) the packing motif of **25a** displaying construction of honeycomb architecture from *a* axis, (d) hydrogen-bonding interactions of pseudo-encapsulated cation-sealed $(H_2PO_4)_2$ dimer in complex **25b**, (e) magnified view of large anionic $H_2PO_4^-$ dimer and (f) spacefill view of pseudo-encapsulated $H_2PO_4^-$ dimer inside the $\mathbf{L_{25}}$ receptor dimer of complex **25b**..

view (Fig. 7.7c). In the presence of fluoride anion, all six H-bond donating urea -NH protons of a particular neutral $\mathbf{L_{25}}$ unit, orient them towards the C_{3v}-symmetric cavity, unlike the free $\mathbf{L_1}$ receptor, encapsulating one fluoride by six strong N–H···F contacts (Fig. 7.7a) and the C_3-symmetry axis passes through apical N-atom of receptor. Note that, the hydrogen-bond accepting three carbonyl oxygen atoms of a ligand unit projecting outside the receptor cavity are independently connected by strong O–H···O interactions with three different symmetry-identical water-oxygen (O_w) atoms in complex **25a** (Fig. 7.7b), which is completely an unusual phenomena in contrast to the large number of tren-based urea/thiorea anion-receptors reported[7.9] in past decades. Note that each Ow atom being tetra-coordinated (accepts one O–H···O, one C–H···O and donates two O–H···O) becomes further hydrogen-bonded with adjacent symmetry-independent water molecules, constructing an ice-like chair-shaped cyclic water hexamer. The X-ray analysis also reveals that, one hexameric water cluster which is a simplest supramolecular analogue of cyclohexane, like the complexes **24a** and **24b**, completely stabilized by six O–H···O interactions with six different $\mathbf{L_{25}}$-F^- unimolecular capsule. The cyclic centerosymmetric water hexamer exhibits the average O···O distance of 2.704 Å, closely resembles with the average

O···O distances in ice I_c (2.75 Å) and I_h (2.759 Å). The average O···O···O angle is 115.1° incomplex **25a** becomes also comparable to the value of 109.3° in the hexagonal ice.

7.2.1.6 Chloride complex 27a of receptor L_{27}

The relatively more acidic phenyl substituted tris-thiourea ligand $\mathbf{L_{27}}$ forms 1:1 chloride encapsulated complex **27a** that crystallizes in the monoclinic space group *P*21/c. Structural elucidation reveals that one Cl^- ion is bound inside the unimolecular receptor cavity by six strong cooperative thiourea N–H···Cl^- interactions (Fig. 7.8a). Note that, this kind of halide encapsulation inside the tripodal cavity of highly electron-rich modest tren-based thiourea receptors is still in its infancy because of the presence of very less acidic -NH protons in receptors. Fortunately, in complex **27a**, all the six low acidic thiourea -NH protons of $\mathbf{L_{27}}$ projecting towards the cavity, efficiently encapsulates the spherical chloride by hexa-coordination *via* topological complementarity (Fig. 7.8b). The X-ray analysis also shows that, two adjacent Cl^- encapsulated neutral assemblies are connected and stabilized by two weak intermolecular C–H···π interactions and one π···π interaction (Fig. 7.8a) through the construction of 2:2 neutral host-guest assemblies.

7.2.2. Structural analysis of oxyanion bound complexes of receptors L_{24}-L_{27}

Single crystal XRD analyses of encapsulated/pseudo-encapsulated neutral receptor-oxyanion complexes and the consistent as well as discriminating binding behavior of tris-(thio)-urea receptors toward oxyanions of various shapes in different host-guest ratios are heavily dependent upon the electronic effect as well as the size of the highly electron-rich terminal naphthyl or phenyl groups and dimensions of the anionic guests.

7.2.2.1 Nitrate complex 26d of receptor L_{26}

The pseudo-encapsulated nitrate complex **26d** of naphthyl substituted neutral tris-thiourea receptor $\mathbf{L_{26}}$ crystallizes in the triclinic space group *P*-1. Structural elucidation reveals that one nitrate-bound neutral receptor $\mathbf{L_{26}}$ in the asymmetric unit assembles with another adjacent identical-symmetry 1:1 receptor-nitrate pseudo-capsular unit by intermolecular C–H···S receptor-receptor interactions. The nitrate anion is coordinated by nine hydrogen bonds from three thiourea groups of the receptor (Fig. 7.6d) and notably, the receptor around the nitrate ion is not C_{3v}-symmetric, exhibiting two different coordination behaviors. Two thiourea groups from the ligand unit bind three edges of the planar anion (through eight-membered H-bonded rings), while all of the three thiourea groups from same ligand chelate two of the three vertices of the nitrate ion (six-membered H-bonded rings). Thus, the O1 atom of nitrate form six hydrogen bonds, but O2 atom accepts two and O3 accepts only one hydrogen bond. Additionally, the

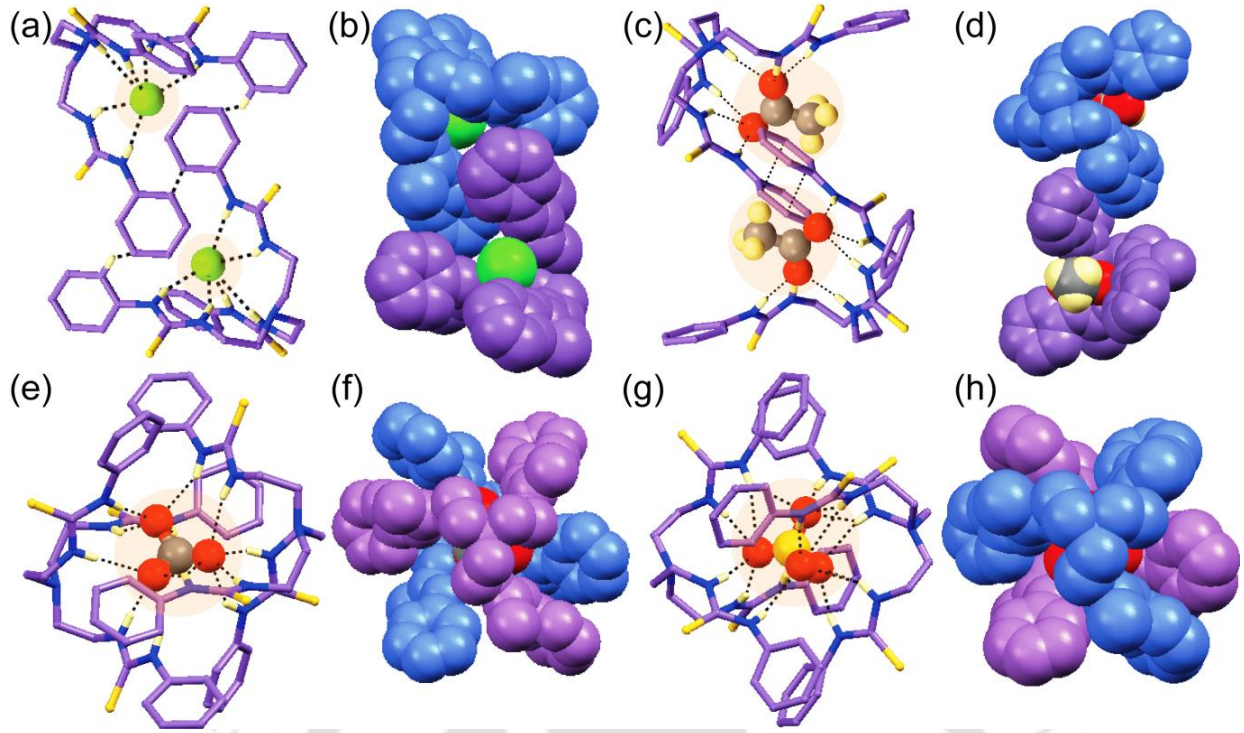

Fig. 7.8 X-ray structures (partial) depicting intermolecular host-guest hydrogen bonding interactions (a) in chloride complex **27a**, (c) in acetate complex **27b**, (e) in carbonate engulfed complex **27c**, (g) in sulfate engulfed complex **27d**; Spacefill view showing (b) 2:2 pseudo-encapsulation of chloride by $\mathbf{L_{27}}$ in **27a**, (d) 2:2 pseudo-encapsulation of acetate by $\mathbf{L_{27}}$ in **27b**, (f) full encapsulation of carbonate in 2:1 host-guest fashion by $\mathbf{L_{27}}$ in **27c** and (h) full encapsulation of sulfate in 2:1 host-guest fashion by $\mathbf{L_{27}}$ in **27d**.

nitrate anion trapped pseudo-capsular host assembly gets extra stability by several C–H···S and C–H···π interactions (Fig. 7.6d).

7.2.2.2 Sulfate complex 26e of receptor L_{26}

The *n*-TBA cation-sealed pseudo-encapsulated sulfate complex **26e** suitable for crystallographic analysis of naphthyl substituted tris-thiourea receptor $\mathbf{L_{26}}$ crystallizes in the monoclinic space group *Cc* and the asymmetric unit contains one neutral $\mathbf{L_{26}}$ unit, one divalent sulfate anion and its corresponding two *n*-TBA^+ counteraction. Interestingly, unlike the numerous reported 2:1divalent sulfate encapsulated tripodal (thio)-urea receptors in literature, herein the relatively smaller cavity and less acidic thio-urea -NH group containing tripodal scaffold $\mathbf{L_{26}}$ expands its three arms in such a way that it encapsulates a large tetrahedral sulfate anion in 1:1 host-guest fashion, inside the receptor pseudo-cavity completely sealed by two *n*-TBA counter-cations (Fig. 7.6h). The divalent sulfate anion generated by hydrogen-bonding activated proton transfer reaction, is coordinated by a total of 18 hydrogen bonding interactions among which nine hydrogen-bonds are donated from three thiourea -NH groups, two are donated from *o*-aryl -CH of receptor and the rest seven are donated from two *n*-TBA^+ counter-cations *via* ion-pair type interactions(Fig. 7.6h). The O1 and O4 oxygen atoms of sulfate anion accept four hydrogen

bonds each, while the O2 and O3 each receive five hydrogen bonds exhibiting optimum coordination for sulfate anion.

7.2.2.3 Biphosphate complex 25b of receptor L_{25}

The dimeric $[(H_2PO_4)_2]$ anionic guest encapsulated complex **25b** of electron-rich phenyl group substituted tris-urea receptor $\mathbf{L_{25}}$ crystallises in the monoclinic space group *P*21/c. Structural elucidation reveals the encapsulation of dimeric $H_2PO_4^-$ anions (constructed *via* two intermolecular O–H···O interactions between two monovalent biphosphate units) inside the pseudo-capsular cavity of two inversion-symmetric $\mathbf{L_{25}}$ host molecules (Fig. 7.7d), entirely sealed by two identical-symmetry *n*-TBA cations. Note that, same receptor showed 1:1 binding with $H_2PO_4^-$ *via* six hydrogen-bonds inside the tripodal cleft from the ^{1}H-NMR solution state studies only, was first shown by Morán *et al*. in 1995.[7.11a] However, from then, no X-ray structures of anion/phosphate bound complex of modest tris-urea receptor $\mathbf{L_{25}}$ were reported in literature. Noticeably, despite the absence of any electron-withdrawing aryl terminals, two inversion-symmetric $\mathbf{L_{25}}$ receptor units with the aid of two *n*-TBA cations efficiently bound a large cyclic $(H_2PO_4)_2$ dimer in 2:2 host-guest fashion (Fig. 7.7f), by a total of eighteen noncovalent hydrogen-bonding interactions (Fig. 7.7d). X-ray analysis reveals that one $H_2PO_4^-$ unit is first trapped by five strong N–H···O (urea), one *o*-aryl C–H···O and two *n*-TBA C–H···O interactions. Then, two (O5 and O7) of the three O atoms in the downward face of phosphate further O–H···O H-bonded to two (O7 and O5 respectively) of the another three O atoms in the upward face of symmetry-identical phosphate which is again entrapped by same number of H-bonds (eight) from inversion-symmetric receptor and *n*-TBA cations. Note that, the five out of six urea -NH protons of a particular $\mathbf{L_{25}}$ receptor unit orients towards the pseudo-capsular cavity (Fig. 7.7d) in course of encapsulating $(H_2PO_4^-)_2$ anionic dimer (Fig. 7.7e), while the remaining urea -NH proton is connected with urea carbonyl O-atom of adjacent symmetry-identical oppositely oriented receptor conformer *via* strong N–H···O connections. Such interlinked arrays of pseudo-capsular assemblies are further connected with one another by intermolecular strong N–H···O and weak aliphatic C−H···O interactions, constructing hexagonal networks of dimeric cages around each pseudo-capsular unit.

7.2.2.4 Acetate complex 27b of receptor L_{27}

The pseudo-encapsulated acetate complex **27b** of phenyl substituted tris-thiourea receptor $\mathbf{L_{27}}$ crystallizes in the triclinic space group *P*-1 and structural elucidation reveals that the neutral tripodal ligand $\mathbf{L_{27}}$ opens up its three thiourea arms little bit more compared to chloride encapsulated complex **27a** of $\mathbf{L_{27}}$, on encapsulating the relatively larger planar acetate ion. The

thiourea -NH groups of a particular receptor unit projecting towards the tripodal cavity are involved in six strong cooperative N–H···O interactions with two carboxylate oxygen atoms of an acetate ion *via* 1:1 host-guest complexation. Each carboxylate oxygen atom is trifurcated, exhibiting hexa-coordination of single acetate anion (Fig. 7.8c). Note that, two symmetry-identical face-to-face oriented acetate encapsulated assemblies get additional stability by weak intermolecular π···π interactions between receptors and few C–H···S interactions (Fig. 7.8c). The spacefill representation reveals the 2:2 cation-sealed encapsulation of acetate inside the receptor cavities (Fig. 7.8d) and to the best of our knowledge this kind of acetate anion encapsulated self-assembly by tren-based neutral receptor is very rare in literature.

7.2.2.5 OH^- induced carbonate complex 27c of receptor L_{27}

The divalent carbonate encapsulated complex **27c** of tris-thiourea receptor **L_{27}** is achieved from the basic DMF/DMSO mixtures of **L_{27}** and excess *n*-TBAOH salts and this *in situ* generated complex **27c** crystallizes in the orthorhombic space group *Pna*21. The CO_3^{2-} anion was not present in the mixed solution prior to crystallization and the carbonate incorporation occurs due to the transformation of atmospheric CO_2 to CO_3^{2-} from basic DMF/DMSO solution. The strongly basic hydroxide ion (OH^-) present in the solution dissolves aerial CO_2 from the air-solvent interface *in situ*, generating CO_3^{2-} anion, which then trapped by dimeric capsule of **L_{27}** *via* crystallization. The X-ray analysis reveals that, two symmetry-independent **L_{27}** receptor from the asymmetric unit of complex **27c** produce a capsular cavity (9.33 Å) with opposite orientation, that efficiently encapsulates a carbonate anion in its center *via* thirteen N–H···O (thiourea) hydrogen bonds by employing the six thiourea -NH functions (Fig. 7.8e). The two of the three carbonate oxygen atoms O1A and O2A accept four N–H···O bonds each, while the third oxygen atom O3A accepts five N–H···O bonds resulting in total of 13 hydrogen-bonding contacts. The packing motif from crystallographic *b* axis shows that, the carbonate encapsulated dimeric cages of two conformational isomers of **L_{27}** are further interlinked with one another by intermolecular *n*-TBA C−H···S (thiourea) interactions, fabricating hexagonal network of dimeric cages around each capsular unit. To the best of our knowledge, complex **27c** becomes one of the prime dimeric molecular capsules (Fig. 7.8f) of tren-based thiourea receptor, where carbonate anion is trapped by fixation of atmospheric CO_2. These kinds of aerial CO_2 fixation as a trapped CO_3^{2-} within in the molecular capsule of thiourea conformers (complex **27c**) become one of the significant aspects in anion recognition chemistry, because the tendency of deprotonation is much higher in more acidic thiourea scaffolds compared to less acidic urea scaffolds in presence of strong basic anion like hydroxide.

7.2.2.6 Sulfate complex 27d of receptor L_{27}

The divalent sulfate encapsulated complex **27d** of phenyl substituted neutral tris-thiourea receptor $\mathbf{L_{27}}$ crystallizes in the orthorhombic space group *Pna*21, which consists of similar kind of host-guest assemblies like the carbonate complex **27c.** The asymmetric unit of the crystal consists of two symmetry-independent tris-thiourea receptor units $\mathbf{L_{27}}$, two symmetry-independent *n*-TBA counter-cations and single divalent sulfate anion where each of the four O atoms of sulfate is disordered over eight half occupied O atoms. The X-ray analysis of complex **27d** clearly reveals that, in presence of monovalent hydrogen sulfate anion, the two symmetry-independent tris thiourea $\mathbf{L_{27}}$ conformers orients in face-to-face fashion conforming a dimeric cavity of capsular size 9.40 Å, that well engulfs a divalent tetrahedral sulfate in its center *via* sixteen N–H···O (thiourea) hydrogen bonds by employing the six thiourea -NH functions (Fig. 7.8g). The sulfate oxygen atoms accept four N–H···O hydrogen bonds each, resulting in 16 hydrogen-bonds to the six thiourea functions (Fig. 7.8g) exhibiting optimum coordination number of sulfate in complex **27d**. Note that, the HSO_4^- anion in solution prior to crystallization has deprotonated and is bound in the form of divalent SO_4^{2-} inside the dimeric receptor capsule, which is not uncommon in literature. It is also fascinating to note that, despite the absence of any π-acidic aryl terminals, the simple tris-thiourea receptor $\mathbf{L_{27}}$ efficiently encapsulates tetrahedral sulfate oxyanion in 2:1 host-guest fashion (Fig. 7.8h).

7.3 Solution-state anion binding studies

The qualitative as well as quantitative solution state binding properties of highly electron-rich neutral receptors $\mathbf{L_{24}}$-$\mathbf{L_{27}}$ with anionic guests are thoroughly investigated by performing ^{1}H NMR experiments in DMSO-d_6 by using different anion salts, as evidenced from the solid state results. Upon gradual addition of standard fluoride to the solution of receptor $\mathbf{L_{24}}$ in titration experiment, a large instant downfield shift of both urea -NH signals Δδ -NH_a = 1.68 ppm and -NH_b = 2.02 ppm (Fig. 7.9a) have been observed, which is closely resemble with the ^{1}H-NMR data of isolated crystals of **24a** (Δδ -NH_a = 1.61 ppm and -NH_b = 1.93 ppm) and this observation strongly backed the equal participation of -NH protons toward fluoride encapsulation in solid state. Successively, the ^{1}H-NMR titration of $\mathbf{L_{24}}$ with standard *n*-TBACl salt displays appreciable downfield shift of urea -NH resonances with an average Δδ value of 0.54 ppm (Fig. 7.9b) attributable for the strong and equal involvement of urea -NH signals as observed from the ^{1}H-NMR data of complex **24b** (average Δδ value of 0.50 ppm). Additionally, the aliphatic -NCH_2 (Δδ = 0.13 and 0.12 ppm in respective F^-/Cl^- titration) and few naphthyl aromatic protons of the receptor experience a perceptible upfield shift (Fig. 7.9b), indicative for structural alteration of $\mathbf{L_{24}}$ in solution that could influence the urea functions from each receptor side arm

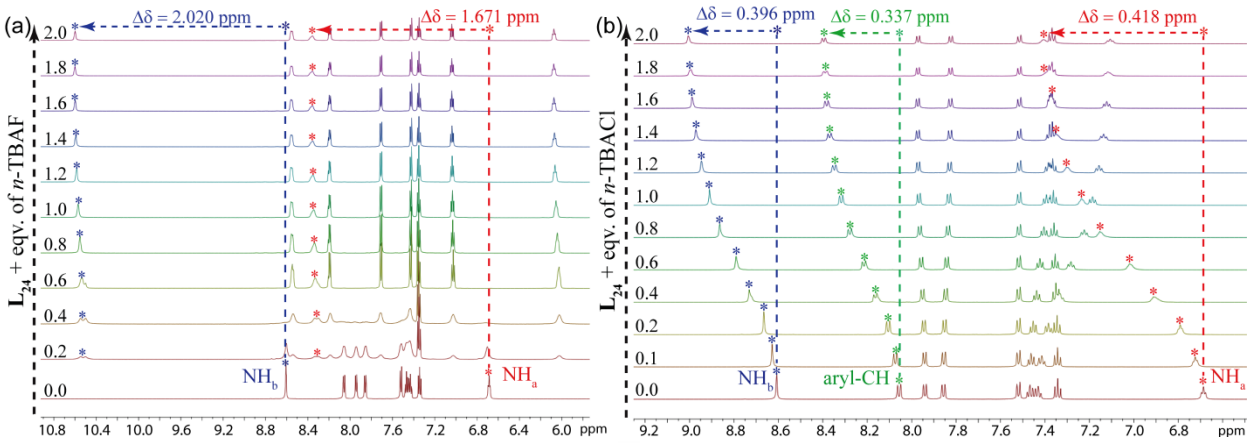

Fig. 7.9 Expanded partial ^{1}H NMR titration spectra of $\mathbf{L_{24}}$ with standard (a) F^- and (b) Cl^-, ions in DMSO-d_6.

to encapsulate the halide within the tripodal cavity by multiple N–H···X hydrogen bonds. The competitive halide binding studies of $\mathbf{L_{24}}$ have also been carried out from qualitative ^{1}H NMR experiments to investigate the relative binding selectivity, which rationalizes the better binding affinity of receptor $\mathbf{L_{24}}$ toward fluoride ion compared to other halides. Furthermore, ^{1}H-NMR studies of all anion complexes as well as titration experiments with more acidic naphthyl substituted tris-thiourea receptor $\mathbf{L_{26}}$ have also been carried out in DMSO-d_6 in qualitative as well as in quantitative way (Fig. 7.10). The ^{1}H-NMR spectra of fluoride complex **26a**[1] (-NH peaks at 9.38 and 11.36 ppm) and sulfate complex **26e** (-NH peaks at 10.38 and 11.24 ppm) individually shows large downfield shift of thiourea hydrogen atoms relative to the -NH peaks free receptor $\mathbf{L_{26}}$ (-NH peaks at 7.35 and 9.67 ppm) indicating the rapid formation of hydrogen bonds with fluoride and sulfate anions in solution. On the other hand, the chloride (**26b**[1]), bromide (**26c**[2]) and nitrate (**26d**) complexes show negligible downfield shift of thiourea -NH protons, suggesting that the interaction of these anions are energetically unfavorable in solution state, which is not very uncommon case in literature. Subsequently, following the qualitative studies., we have performed ^{1}H-NMR titration analysis of free ligand with aliquots of standard *n*-TBAF salt, which shows instant large downfield shift of both thiourea -NH signals ($\Delta\delta$ -NH_a = 2.05 ppm and -NH_b = 1.72 ppm) after 0.1 eqv F^- ion addition, which is closely resemble with ^{1}H-NMR data of isolated crystals of fluoride complex of $\mathbf{L_{26}}$. Similarly, the gradual addition of $(n\text{-TBA})_2SO_4$ salts to the solutions of free thiourea ligand $\mathbf{L_{26}}$ in titration experiments, lead to the massive downfield shift of thiourea -NH protons ($\Delta\delta$ -NH_a = 2.99 ppm and -NH_b = 1.50 ppm) followed by huge broadening, which also becomes closely resemble with the ^{1}H-NMR data of isolated crystals of sulfate complex **26e**. Note that, the considerably larger shift of -NH_a ($\Delta\delta$ = 2.99 ppm) relative to -NH_b signals ($\Delta\delta$ = 1.50 ppm) in sulfate titration suggests that the divalent sulfate anion is bound more strongly to -NH_a rather than -NH_b protons of thiourea receptor $\mathbf{L_{26}}$ in solution, that becomes reliably supported from solid state sulfate binding of

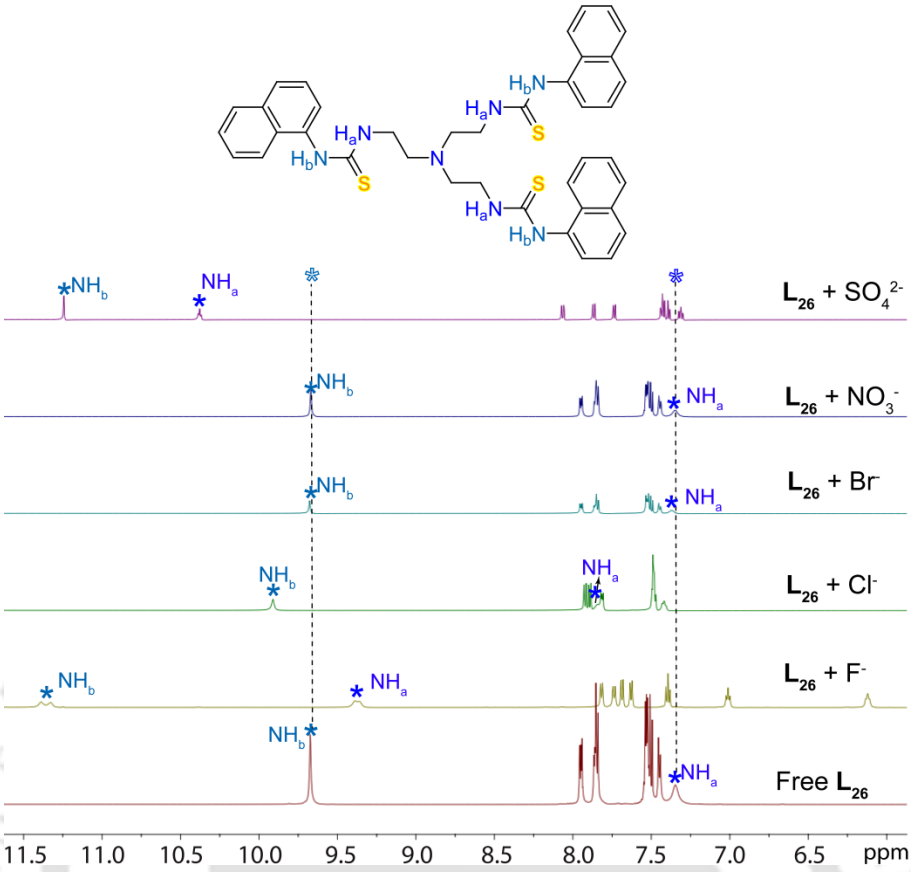

Fig. 7.10 Expanded partial ^{1}H NMR comparative stacked spectra in solution phase of tris-thiourea receptor $\mathbf{L_{26}}$ with halides and oxyanions as evidenced from the solid state results.

receptor, where three -NH_a thiourea protons are involved in six hydrogen-bond donation and three -NH_b protons donates only three hydrogen-bonds as observed from structural analysis of complex **26e**. Then, the solution-state anion binding studies of phenyl substituted oxyurea receptor $\mathbf{L_{25}}$ and thiourea receptor $\mathbf{L_{25}}$ are also investigated by qualitative as well as quantitative ^{1}H NMR experiments in DMSO-d_6 using the related anion salts as evidenced from the solid state results. The ^{1}H NMR titration analysis of $\mathbf{L_{25}}$ with aliquots of standard *n*-TBAF shows instant large downfield shift of both urea -NH signals ($\Delta\delta$ -NH_a = 1.16 ppm and -NH_b = 1.99 ppm) after 0.1 eqv. F^- addition, which is very closely resemble with ^{1}H NMR data of isolated crystals of hexameric water trapped fluoride complex **25a** ($\Delta\delta$ -NH_a = 1.14 ppm and-NH_b = 2.01 ppm) and this observation learly indicates the similar binding aptitude of individual urea -NH protons in complex as well as in solution. In contrary, the qualitative ^{1}H-NMR studies of thiourea receptor $\mathbf{L_{27}}$ with excess of fluoride and bicarbonate salts, result the disappearance of both thiourea -NH signals which is ascribed for the abstraction of more acidic thiourea protons compared to urea protons and in addition, a new characteristic signal of HF_2^- also appears at around 15.5 ppm in the ^{1}H-NMR spectrum $\mathbf{L_{27}}$-F^-. The ^{1}H-NMR titration data of $\mathbf{L_{25}}$ with aliquots of standard *n*-$TBAH_2PO_4$ solution shows average downfield shift of $\Delta\delta$ = 1.20 ppm

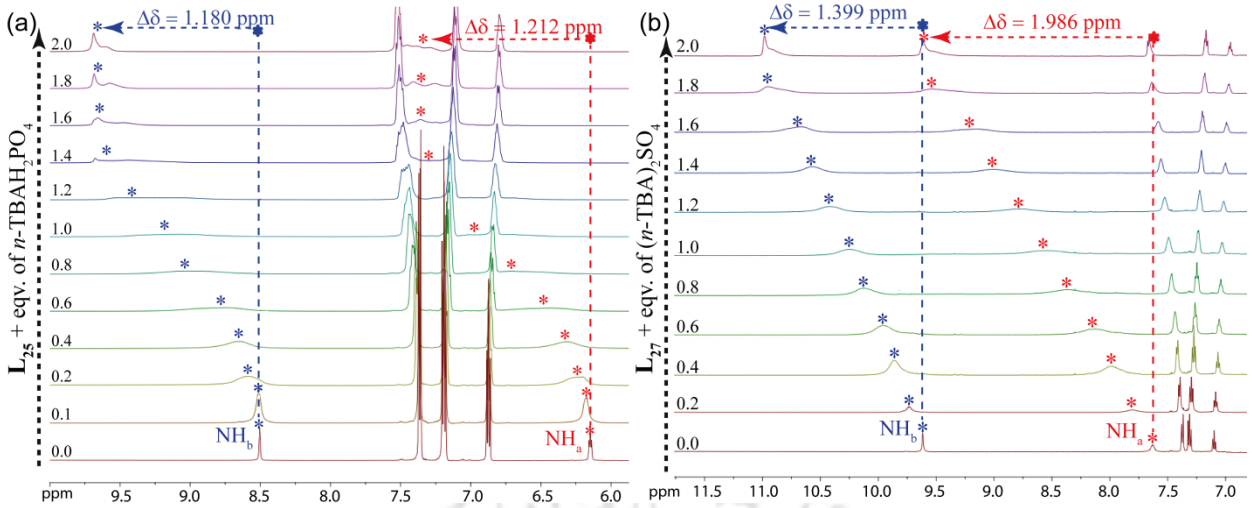

Fig. 7.11 Expanded partial ^{1}H NMR titration spectra of (a) **L$_{25}$** with $H_2PO_4^-$ and (b) **L$_{27}$** with SO_4^{2-} in DMSO-d_6.

(Fig. 7.11a) and interestingly, the isolated $[(H_2PO_4)_2]$ encapsulated complex **25b** exhibited exactly equal average downfield shift of $\Delta\delta$ =1.20 ppm which indicates the strong and equal participation of urea -NH protons in solution and solid state. Moreover, the ^{1}H NMR analysis of chloride complex **27a** and sulfate complex **27d** showed average downfield shifts of $\Delta\delta$ = 0.49 ppm and $\Delta\delta$ = 1.26 ppm respectively, whereas the gradual addition of respective *n*-TBACl and $(n\text{-TBA})_2SO_4$ salts to the solutions of thiourea ligand **L$_{27}$** in titration experiments, lead to the average downfield shift of $\Delta\delta$ = 0.31 ppm and $\Delta\delta$ = 1.70 ppm (Fig. 7.11b) respectively for the thiourea -NH protons, which give the best fit for a mixed equilibrium between 1:1 and 1:2 host-guest stoichiometry from Job's plot in both cases. The association constants (log K) become 2.78 for chloride and 3.01 for sulfate with thiourea receptor **L$_{27}$**, calculated by following the shift of the most deshielded thiourea proton (-NH_a or -NH_b) of ligand in the ^{1}H NMR titration. Note that, the isolated carbonate complex **27c** also shows average thiourea -NH downfield shift of $\Delta\delta$ = 1.05 ppm, which is in between the average shifts of complex **27a** ($\Delta\delta$ = 0.49 ppm) and **27d** $\Delta\delta$ = (1.26 ppm) and this may be ascribed for the higher and lower coordination number of planar carbonate compared to spherical chloride and tetrahedral sulfate respectively with receptor **L$_{27}$**. However, the binding stoichiometry and association constant of carbonate with **L$_{27}$** could not be calculated because of the disappearance of both thiourea -NH signals upon anion addition in ^{1}H-NMR titration spectra. Whereas, the acetate complex **27b** of **L$_{27}$** shows average downfield shift of $\Delta\delta$ = 1.15 ppm and in quantitative titration, upon gradual addition of *n*-$TBAOCOCH_3$ salts to the solutions of **L$_{27}$** lead to the average downfield shift of $\Delta\delta$ = 1.27 ppm for the thiourea -NH protons and give the best fit for a mixed equilibrium with apparent log K value of 3.04. Overall, it is worth mentioning that, such binding discrepancy between host to guest in solid and solution states is common in literature, because the organizations of receptors

are much more compact in the solid state, which favors the binding of the halides and oxyanion within respective unimolecular and dimeric receptor capsule stabilized by a number of non-covalent interactions, whereas the binding of a single anion inside the receptor cavity or mixed anion-receptor stoichiometry have been observed, due to much looser orientation of receptors in solution phase.

7.4 Conclusion

In summary, we have especially developed and structurally demonstrated the anion coordination properties of highly electron-rich naphthyl urea receptors (**L_{24}**/**L_{25}**). These kinds of cooperative association among the organic receptor and the water molecule play a critical role in the formation of the water cluster and stabilizing its multidimensional supramolecular architecture without suffering any defects and hopefully these brands of studies would be helpful in investigating the H-bonding motifs accountable for the anomalous character of water in natural and biological systems, as well as valuable in theoretical and computational studies of synthetic models. Furthermore, the tripodal thioura scaffold **L_{26}** can also effectively entraps anions of different dimensions *via* conformational change of receptor framework, despite consisting of unfavorable highly electron-rich naphthyl functionalization and in the absence of any electron withdrawing π-acidic aryl terminals. Receptor **L_{26}** fully encapsulates the smallest halide within its C_3-symmetric tripodal cavity, but it little bit opens up its three arms to catch relatively larger spherical chloride, bromide and planar nitrate *via* pseudo-encapsulation. Moreover, to grab the bigger tetrahedral sulfate, ligand **L_{26}** stretches its three arms *via* formation of a more open bowl-shaped cavity in a cation-sealed environment. Successively, the three dimensional flexible molecular structure of **L_{26}** permits the shape as well as preorganization of the receptor to monitor the recognition process and adds directionality to the whole system. Furthermore, the comprehensive development of solid state halide as well as oxyanion binding by electron-rich phenyl substituted tris-(thio)-urea receptors **L_{25}** and **L_{27}** have also been successfully authenticated, which was underexplored area in anion receptor chemistry from last two decades. Interestingly, despite the absence of any π-acidic, electronegative and positive cloud effect containing terminal aryl functionalization, both the (thio)-urea receptors **L_{25}** and **L_{27}** have been capable to form host-guest complexes with different dimensions of anions. Single crystal X-ray study confirms the fluoride encapsulation by **L_{25}** *via* infrequent trapping of cyclic $(H_2O)_6$ and chloride, acetate encapsulation by **L_{27}** in 1:1 receptor-anion mode. Subsequently, **L_{25}** encapsulates $[(H_2PO_4)_2]$ dimer inside cation sealed dimeric pseudo-capsular assembly *via* 2:2 host-guest fashion, while **L_{27}** completely engulfs carbonate *via* aerial CO_2 fixation and divalent sulfate inside the dimeric capsular cage through 2:1 complexation mode. Overall, the results of

this chapter represents the primary structural report on encapsulation of halides and oxyanions by modest tren-based electron-rich (thio)-urea receptors, which would be helpful for the researchers to understand the underexplored space of tren-based anion-receptor chemistry.

References

7.1 (a) H. Luecke and F. A. Quiocho, *Nature*, 1990, **347**, 402; (b) J. J. He and F. A. Quiocho, *Science*, 1991, **251**, 1479; (c) E. V. Anslyn, J. Smith, D. M. Kneeland, K. Ariga and F. Chu, *Supramol. Chem.*, 1993, **1**, 201.

7.2 R. Ludwig. *Angew. Chem. Int. Ed.* 2001, **40**, 1808.

7.3 U. Mukhopadhyay and I. Bernal *Cryst. Growth Des* 2005, **5**, 1687.

7.4 (a) L. Infantes and S. Motherwell, *CrystEngComm* 2002, **4**, 454; (b) A. L. Gillon, N. Feeder, R. J. Davey and R. Storey, *Cryst. Growth Des.* 2003, **3**, 663; (c) S. W. Benson and E. D. Siebert, *J. Am. Chem. Soc.* 1992, **114**, 4269; (d) K. A. Udachin and J. A. Ripmeester, *Nature* 1999, **397**, 420; (e) B.-Q. Ma, H.-L. Sun and S. Gao, *Angew. Chem., Int. Ed.* 2004, **43**, 1374.

7.5 (a) F. P. Schmidtchen and M. Berger, *Chem. Rev.*, 1997, **97**, 1609; (b) C. Caltagirone and P. A. Gale, *Chem. Soc. Rev.*, 2009, **38**, 520; (c) K. Bowman-James, A. Bianchi and E. Garcia-Espana, *Anion Coordination Chemistry*, Wiley-VCH, New York, 2011.

7.6 (a) *Biochemistry of Halogens and Inorganic Halides*, ed. Krik, K. L. Plenum Press, New York, 1991; (b) *A systematic review of the efficacy and safety of fluoridation*, 2007, National Health and Medical Research Council, Australian Government, available at http://www. nhmrc.gov.au/.

7.7 (a) *Climate Change 2007: Synthesis Report, International Panel on Climate Change*; Cambridge University Press: Cambridge, U.K., 2007; (b) D. S. Jenkinson, D. E. Adams and A. Wild, *Nature* 1991, **351**, 304; (c) K. Caldeira, A. K. Jain and M. I. Hoffert, *Science* 2003, **299**, 2052.

7.8 (a) J. W. Pflugrath and F. A. Quiocho, *Nature*, 1985, **314**, 257; (b) T. H. Milby and R. C. Baselt, *Am. J. Ind. Med.*, 1999, **35**, 192; (c) A. K. H. Hirsch, F. R. Fischer and F. Diederich, *Angew. Chem, Int. Ed.*, 2007, **46**, 338.

7.9 (a) S. K. Dey, A. Basu, R. Chutia and G. Das, *RSC Adv.*, 2016, **6**, 26568; (b). R. Dutta and P. Ghosh, *Chem. Commun*., 2014, **50**, 10538; (c) M. N. Hoque, U. Manna and G. Das *Supamol. Chem.* 2016, **28**, 284.

7.10 (a) U. Manna, S. Halder and G. Das *Cryst. Growth Des.* 2018, **18**, 1818; (b) U. Manna and G. Das *Cryst. Growth Des.* 2018, **18**, 3138; (c) U. Manna and G. Das *CrystEngComm*, 2018,**20**, 3741.

7.11(a) C. Raposo, M. Almaraz, M. Martin, V. Weinrich, M. L. Mussons, V. Alcazar, M. C. Caballero and J. R. Morán, *Chem. Lett*., 1995, **37**, 2795; (b) H. Xie, S. Yi, X. Yang and S. Wu, *New. J. Chem*. 1999, **23**, 1105; (c) H. Xie, S. Yi and S. Wu, *J. Chem. Soc. Perkin Trans. 2*, 1999, 2751.

7.12 (a) H. König, *Kristallogr.* 1944, **105,** 279; (b) D. Eisenberg and W. Kauzmann, *The Structure and Properties of Water*; Oxford University Press: Oxford, U.K., 1969.

7.13 Ph. Warnet, D. Nordlund, U. Bergmann, M. Cavalleri, M. Odelius, H. Ogasawara, L. A. Näslund, T. K. Hirsch, L. Ojamäe, P. Glatzel, L. G. M. Pettersson and A. Nilsson, *Science* 2004, **304**, 995.

Annexure 7

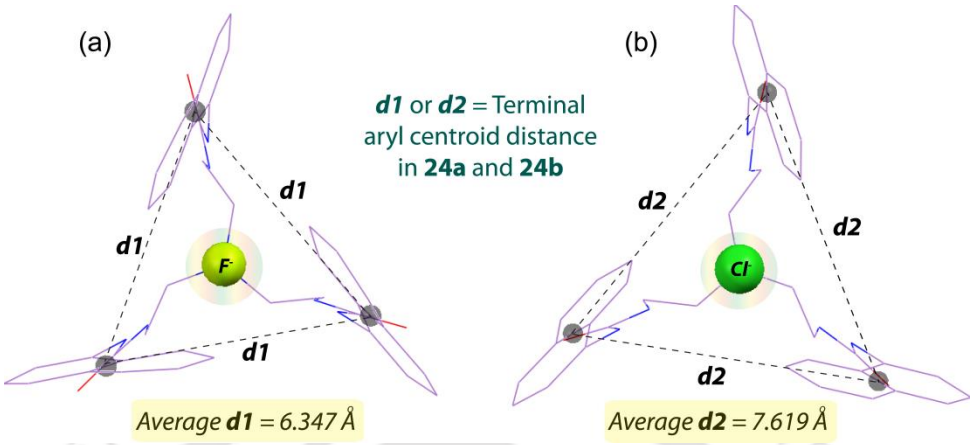

Fig. A7.1 X-ray structures (partial) depicting the average terminal naphthyl centroid distances of receptor $\mathbf{L_{24}}$ in (a) fluoride complex **24a** and (b) chloride complex **24b.**

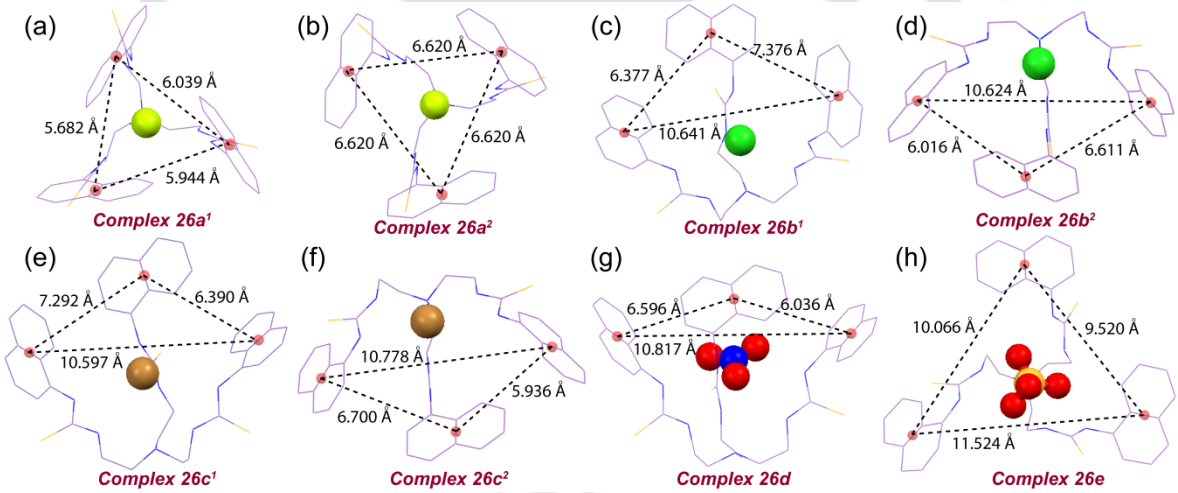

Fig. A7.2 X-ray structures (partial) depicting the average terminal naphthyl distances of receptor $\mathbf{L_{26}}$ in the neutral anion complexes (a) **26a**$^{\mathbf{1}}$, (b) **26a**$^{\mathbf{2}}$, (c) **26b**$^{\mathbf{1}}$, (d) **26b**$^{\mathbf{2}}$, (e) **26c**$^{\mathbf{1}}$, (f) **26c**$^{\mathbf{2}}$, (g) **26d** and (h) **26e**.

Table A7.1 Crystallographic parameters and refinement details of complexes **24a** and **24b** of receptor $\mathbf{L_{24}}$

Parameters	Complex **24a**	Complex **24b**
Formula	C39 H45 F N7 O6	C55 H69 Cl N8 O6
Fw	720.78	973.51
Crystal system	trigonal	Rhombohedral
Space group	P 3 1 c	R-3
a/Å	12.936(6)	13.165(8)
b/Å	12.936(6)	13.165(8)
c/Å	39.022(3)	57.807(4)
α/o	90.00	90.00
β/o	90.00	90.00
γ/o	120.00	120.00
V/Å3	5654.9(8)	8676.4(12)
Z	4	6
Dc/g cm-3	0.847	1.118
μ Mo Kα/mm-1	0.061	0.118
F000	1516.0	3119.6
T/K	298(2)	298(2)
θ max.	24.993	28.325
Total no. of reflections	10603	33422
Independent reflections	6439	4764
Observed reflections	2508	1681
Parameters refined	319	217
R1, I > 2σ(I)	0.0887	0.0944
wR2, I > 2σ(I)	0.2235	0.2529
GOF (F2)	1.115	1.178
CCDC No.	1574568	1574569

Table A7.2 Crystallographic parameters and refinement details of free receptors $\mathbf{L_{25}}$ and its complexes

Parameters	**L_{25}**	**25a**	**25b**
Formula	$C_{27}H_{33}N_7O_3$	$C_{43}H_{66}FN_8O_6$	$C_{43}H_{71}N_8O_7P$
Fw	503.60	810.02	843.05
Crystal system	triclinic	trigonal	monoclinic
Space group	*P -1*	*R -3*	*P 21/c*
a/Å	9.463(10)	13.850(10)	15.470(14)
b/Å	12.248(14)	13.850(10)	25.496(2)
c/Å	12.785(13)	43.014(4)	12.347(17)
α/°	84.367(9)	90.00	90.00
β/°	71.200(9)	90.00	94.928(10)
γ/°	74.329(10)	120.00	90.00
V/Å^3	1350.5(3)	7145.6(12)	4851.8(9)
Z	2	6	4
D_c/g cm^{-3}	1.238	1.129	1.154
μ Mo K_α/mm^{-1}	0.084	0.079	0.110
F000	536.0	2621.9	1824.0
T/K	298(2)	298(2)	298(2)
θ max.	24.999	25.000	25.000
Total no. of reflections	8182	6282	20006
Independent reflections	4757	2816	8535
Observed reflections	2399	1785	3362
Parameters refined	334	214	538
R_1, I > 2σ(I)	0.0772	0.0821	0.0862
wR_2, I > 2σ(I)	0.1809	0.2513	0.1711
GOF (F^2)	1.130	1.178	0.996
CCDC No.	1576489	1576490	1576491

Table A7.3 Crystallographic parameters and refinement details of fluoride and chloride complexes of receptor $\mathbf{L_{26}}$

Parameters	**26a[1]**	**26a[2]**	**26b[1]**	**26b[2]**
Formula	$C_{55}H_{75}FN_8S_3$	$C_{47}H_{55}FN_8S_3$	$C_{55}H_{75}ClN_8S_3$	$C_{47}H_{59}ClN_8OS_3$
Fw	963.41	847.05	979.86	883.65
Crystal system	monoclinic	trigonal	triclinic	triclinic
Space group	*P 21/c*	*R 3 c*	*P -1*	*P -1*
a/Å	24.648(12)	16.017(15)	10.601(9)	12.186(7)
b/Å	21.278(6)	16.017(15)	16.312(8)	12.926(7)
c/Å	22.391(8)	30.658(3)	16.915(9)	16.403(9)
α/°	90.00	90.00	93.425(4)	90.00
β/°	105.744(4)	90.00	95.816(5)	85.660(3)
γ/°	90.00	120.00	106.427(6)	81.205(3)
V/Å^3	11302.1(8)	6811.4(17)	2779.3(3)	2399.6(2)
Z	8	6	2	2
D_c/g cm^{-3}	1.132	1.239	1.171	1.223
μ Mo $K_α$/mm^{-1}	0.176	0.210	0.224	0.253
F000	4144.0	2699.6	1052.0	1265.0
T/K	298(2)	298(2)	298(2)	298(2)
θ max.	25.000	24.999	25.000	27.485
Total no. of reflections	47878	8584	20218	23312
Independent reflections	19882	2555	9761	10850
Observed reflections	7489	1398	4841	3667
Parameters refined	1215	185	628	545
R_1, I > 2σ(I)	0.0900	0.0692	0.1010	0.0801
wR_2, I > 2σ(I)	0.1586	0.1771	0.1687	0.2351
GOF (F^2)	1.084	1.100	0.853	1.118
CCDC No.	1818837	1818838	1818839	1818840

Table A7.4 Crystallographic parameters and refinement details of bromide, nitrate and sulfate complexes of $\mathbf{L_{26}}$

Parameters	**26c[1]**	**26c[2]**	**26d**	**26e**
Formula	$C_{55}H_{75}BrN_8S_3$	$C_{47}H_{61}BrN_8OS_3$	$C_{47}H_{59}N_9O_3S_3$	$C_{71}H_{111}N_9O_4S_4$
Fw	1024.31	930.12	894.21	1282.93
Crystal system	triclinic	triclinic	triclinic	monoclinic
Space group	*P -1*	*P -1*	*P -1*	*C c*
a/Å	10.660(7)	12.344(10)	12.283(7)	21.512(3)
b/Å	16.306(11)	12.778(11)	12.922(6)	16.070(13)
c/Å	17.030(10)	16.416(13)	16.155(8)	22.399(2)
α/°	93.451(5)	84.883(5)	85.459(4)	90.00
β/°	96.068(5)	70.394(5)	70.109(5)	91.554(9)
γ/°	106.259(6)	80.731(5)	80.961(4)	90.00
V/Å^3	2813.3(3)	2405.6(4)	2380.3(2)	7740.4(14)
Z	2	2	2	4
D_c/g cm^{-3}	1.209	1.281	1.248	1.101
μ Mo $K_α$/mm^{-1}	0.884	1.028	0.206	0.172
F000	1024.31	976.0	952.0	2784.0
T/K	298(2)	298(2)	298(2)	298(2)
θ max.	24.999	28.370	24.999	24.999
Total no. of reflections	15628	39366	16221	14499
Independent reflections	9644	11558	8378	12916
Observed reflections	5486	4403	6068	8532
Parameters refined	661	545	590	783
R_1, I > 2σ(I)	0.0757	0.0644	0.0783	0.0759
wR_2, I > 2σ(I)	0.1832	0.1708	0.1955	0.1875
GOF (F^2)	1.026	1.068	0.947	1.090
CCDC No.	1818841	1818842	1818843	1818844

Table A7.5 Crystallographic parameters and refinement details of free receptors $\mathbf{L_{27}}$ and its complexes

Parameters	$\mathbf{L_{27}}$	**27a**	**27b**	**27c**	**27d**
Formula	$C_{54}H_{65}N_{14}S_6$	$C_{43}H_{69}ClN_8S_3$	$C_{45}H_{72}N_8O_2S_3$	$C_{87}H_{138}N_{16}O_3S_6$	$C_{86}H_{138}N_{16}O_4S_7$
Fw	1102.56	829.69	853.29	1648.49	1684.54
Crystal system	orthorhombic	monoclinic	triclinic	orthorhombic	orthorhombic
Space group	*P c a 21*	*P 21/c*	*P -1*	*P n a 21*	*P n a 21*
a/Å	25.988(8)	10.343 (9)	12.475(15)	30.643(4)	30.977(6)
b/Å	9.851(3)	22.987(4)	12.498(9)	13.478(16)	13.483(3)
c/Å	26.893(11)	20.053(2)	16.629(16)	23.218(3)	23.390(5)
α/°	90.00	90.00	102.863(7)	90.00	90.00
β/°	90.00	100.231(10)	96.291(9)	90.00	90.00
γ/°	90.00)	90.00	97.109(8)	90.00	90.00
V/Å^3	6884.6(4)	4691.9(10)	2482.9(4)	9589.0(2)	9769.0(4)
Z	4	4	2	4	4
D_c/g cm^{-3}	1.064	1.175	1.141	1.142	1.145
μ Mo $K_α$/mm^{-1}	0.240	0.253	0.192	0.196	0.215
F000	2332.0	1792.0	924.0	3568.0	3640.0
T/K	298(2)	298(2)	298(2)	298(2)	298(2)
θ max.	24.999	25.000	25.000	24.998	25.000
Total no. of reflections	18835	17433	16084	68006	78900
Independent reflections	10986	8245	8626	15901	17114
Observed reflections	7701	6156	4090	5463	7514
Parameters refined	631	557	528	1044	1062
R_1, I > 2σ(I)	0.0715	0.0986	0.0815	0.0704	0.0662
wR_2, I > 2σ(I)	0.1910	0.1306	0.1752	0.1383	0.1530
GOF (F^2)	1.100	0.997	0.966	0.933	0.902
CCDC No.	1589919	1576492	1589920	1576493	1576494

Table A7.6 Details of Hydrogen Bonding contacts in the complexes **24a** and **24b** of receptor $\mathbf{L_{24}}$

Complex	D−H···A	d(D···H)/Å	d(H···A)/Å	d(D···A)/Å	<D−H···A/°
24a	N2-H2N···F1	0.86	2.16	2.900(7)	144
	N3-H3N···F1	0.86	2.05	2.852(8)	155
	N5-H5N···F2	0.86	2.15	2.920(6)	150
	N6-H6N···F2	0.86	2.03	2.839(6)	157
24b	N2-H2N···Cl1	0.86	2.54	3.330(4)	153
	N3-H3N···Cl1	0.86	2.48	3.301(4)	160

Table A7.7 Details of Hydrogen Bonding contacts in the anion complexes of receptor $\mathbf{L_{26}}$

Complex	D−H···A	*d*(D···H)/Å	*d*(H···A)/Å	*d*(D···A)/Å	<D−H···A/°	Symmetry codes
26a[1]	N2-H2N···F1	0.86	2.03	2.826(7)	153	x,y,z
	N3-H3N···F1	0.86	1.93	2.756(6)	160	x,y,z
	N4-H4N···F1	0.86	2.11	2.870(5)	148	x,y,z
	N5-H5N···F1	0.86	1.97	2.790(5)	159	x,y,z
	N6-H6N···F1	0.86	2.10	2.901(6)	154	x,y,z
	N7-H7N···F1	0.86	1.99	2.808(5)	159	x,y,z
	N9-H9N···F2	0.86	2.07	2.829(4)	147	x,y,z
	N10-H10N···F2	0.86	1.98	2.797(4)	157	x,y,z
	N11-H11N···F2	0.86	2.04	2.826(5)	152	x,y,z
	N12-H12N···F2	0.86	1.94	2.747(5)	156	x,y,z
	N13-H13N···F2	0.86	2.09	2.868(5)	151	x,y,z
	N14-H14N···F2	0.86	1.95	2.776(5)	161	x,y,z
26a[2]	N2-H2N···F1	0.86	2.08	2.867(12)	151	x,y,z
	N3-H3N···F1	0.86	1.92	2.741(6)	160	x,y,z
26b[1]	N2-H2N···Cl1	0.86	2.53	3.321(5)	153	x,y,z
	N3-H3N···Cl1	0.86	2.67	2.445(5)	151	x,y,z
	N4-H4N···Cl1	0.91	2.49	2.337(6)	156	x,y,z
	N5-H5N···Cl1	0.86	2.48	3.290(6)	157	x,y,z
	N6-H6N···Cl1	0.86	2.76	3.545(6)	152	x,y,z
	N7-H7N···Cl1	0.86	2.41	3.259(5)	169	x,y,z
26b[2]	N2-H2N···Cl1	0.86	2.63	3.363(4)	144	x,y,z
	N3-H3N···Cl1	0.86	2.48	3.269(4)	153	x,y,z
	N4-H4N···Cl1	0.86	2.80	3.596(5)	154	x,y,z
	N5-H5N···Cl1	0.86	2.46	3.311(5)	171	x,y,z
	N6-H6N···Cl1	0.86	2.61	3.401(4)	154	x,y,z
	N7-H7N···Cl1	0.86	2.39	3.213(5)	161	x,y,z
26c[1]	N2-H2N···Br1	0.86	2.91	3.691(5)	152	x,y,z
	N3-H3N··· Br1	0.86	2.50	3.358(5)	174	x,y,z
	N4-H4N··· Br1	0.86	2.70	3.497(6)	155	x,y,z
	N5-H5N··· Br1	0.86	2.58	3.400(7)	159	x,y,z
	N6-H6N··· Br1	0.86	2.65	3.449(6)	154	x,y,z
	N7-H7N··· Br1	0.86	2.73	3.512(5)	152	x,y,z
26c[2]	N2-H2N···Br1	0.86	2.78	3.569(4)	154	1-x,1-y,1-z
	N3-H3N···Br1	0.86	2.54	3.354(5)	158	1-x,1-y,1-z
	N4-H4N···Br1	0.86	2.74	3.503(5)	148	1-x,1-y,1-z
	N5-H5N···Br1	0.86	2.63	3.420(5)	153	1-x,1-y,1-z
	N7-H7N···Br1	0.86	2.63	3.491(5)	176	1-x,1-y,1-z
26d	N2-H2N···O2	0.86	2.23	3.056(5)	161	x,y,z
	N3-H3N···O2	0.86	2.39	3.186(5)	154	x,y,z
	N2-H3N···O3	0.86	2.39	3.061(5)	136	x,y,z
	N4-H4N···O2	0.86	2.43	3.229(5)	155	x,y,z
	N5-H5N···O2	0.86	2.26	3.095(4)	164	x,y,z
	N6-H6N···O2	0.86	2.46	3.168(5)	140	x,y,z
	N7-H7N···O1	0.86	2.12	2.958(5)	140	x,y,z
26e	N2-H2N···O1	0.86	2.57	3.233(10)	135	x,y,z
	N2-H2N···O2	0.86	2.12	2.949(10)	162	x,y,z
	N3-H3N···O1	0.86	2.06	2.863(8)	154	x,y,z
	N4-H4N···O2	0.86	2.51	3.168(11)	134	x,y,z
	N4-H4N···O4	0.86	2.23	3.060(12)	163	x,y,z
	N5-H5N···O2	0.86	2.23	2.787(11)	123	x,y,z
	N6-H6N···O1	0.86	2.10	2.946(12)	166	x,y,z
	N7-H7N···O4	0.86	2.02	2.835(12)	158	x,y,z

Table A7.8 Details of Hydrogen Bonding contacts in the anion complexes of receptors $\mathbf{L_{25}}$ and $\mathbf{L_{27}}$

Complex	D−H···A	*d*(D···H)/Å	*d*(H···A)/Å	*d*(D···A)/Å	<D−H···A/°	Symmetry codes
$\mathbf{L_{25}}$	N2-H2N···O3	0.86	2.15	2.953(4)	155	x,y,z
	N3-H3N···O3	0.86	2.17	2.965(5)	153	x,y,z
	N4-H4N···O1	0.86	2.18	2.935(4)	147	2-x,1-y,-z
	N5-H5N···O1	0.86	2.12	2.921(4)	154	2-x,1-y,-z
	N6-H6N···O2	0.86	2.04	2.863(3)	161	1-x,1-y,1-z
	N7-H7N···O2	0.86	2.30	3.074(4)	150	1-x,1-y,1-z
$\mathbf{L_{27}}$	N3-H3N···S2	0.86	2.59	3.439(4)	168	-1/2+x,1-y,z
	N7-H6N···S1	0.86	2.49	3.331(5)	166	1/2+x,1-y,z
	N12-H12N···S5	0.86	2.59	3.411(5)	160	-1/2+x,1-y,z
	N14-H14N···S6	0.86	2.63	3.463(4)	162	1/2+x,1-y,z
25a	O2-H1O···O2	0.85	1.86	2.704(9)	177	-1/3+y,1/3-x+y,1/3-z
	O2-H2O···O1	0.85	1.94	2.781(6)	171	x,y,z
	N2-H2N···F1	0.86	2.14	2.916(5)	150	x,y,z
	N3-H3N···F1	0.86	1.88	2.717(3)	163	x,y,z
25b	N2-H2N···O4	0.86	2.10	2.935(6)	164	x,y,z
	N3-H3N···O2	0.86	2.06	2.884(6)	160	-x,-y,1-z
	N4-H4N···O4	0.86	2.06	2.823(6)	147	x,y,z
	N5-H5N···O5	0.86	2.32	3.134(6)	159	x,y,z
	N6-H6N···O4	0.86	2.05	2.896(6)	168	x,y,z
	N7-H7N···O7	0.86	2.07	2.924(6)	169	x,y,z
	O5-H5O···O7	0.82	1.74	2.557(4)	177	1-x,-y,1-z
27a	N2-H2N···Cl1	0.86	2.57	3.374(7)	155	-1+x,y,z
	N3-H3N···Cl1	0.86	2.38	3.212(7)	164	-1+x,y,z
	N4-H4N···Cl1	0.86	2.66	3.451 (7)	153	-1+x,y,z
	N5-H5N···Cl1	0.86	2.37	3.226(7)	172	-1+x,y,z
	N6-H6N···Cl1	0.86	2.59	3.400(7)	157	-1+x,y,z
	N7-H7N···Cl1	0.86	2.40	3.249(8)	168	-1+x,y,z
27b	N2-H2N···O1	0.86	1.97	2.824(6))	173	x,y,z
	N3-H3N···O2	0.86	2.12	2.980(6)	173	x,y,z
	N4-H4N···O2	0.86	2.56	3.321(6)	148	x,y,z
	N5-H5N···O2	0.86	2.09	2.923(6)	162	x,y,z
	N6-H6N···O1	0.86	2.24	2.960(6)	141	x,y,z
	N7-H7N···O1	0.86	1.94	2.779(6)	166	x,y,z
27c	N2-H2N···O2B	0.86	2.04	2.890(12)	169	x,y,z
	N3-H3N···O1B	0.86	2.11	2.946(13)	164	x,y,z
	N4-H4N···O1B	0.86	2.13	2.928(11)	154	x,y,z
	N6-H6N···O2B	0.86	2.12	2.910(13)	153	x,y,z
	N7-H7N···O2B	0.86	2.09	2.907(12)	158	x,y,z
	N9-H9N···O3B	0.86	2.15	2.996(16)	170	x,-1+y,z
	N10-H10N···O2B	0.86	2.19	2.981(14)	154	x,-1+y,z
	N11-H11N···O3B	0.86	2.03	2.859(18)	160	x,-1+y,z
	N12-H12N···O3B	0.86	2.34	3.104(14)	149	x,-1+y,z
	N13-H13N···O3B	0.86	2.31	3.155(15)	166	x,-1+y,z
	N14-H14N···O3B	0.86	2.13	2.916(12)	151	x,-1+y,z
27d	N2-H2N···O1A	0.86	2.40	3.131(13)	144	1/2-x,-1/2+y,-1/2+z
	N2-H2N···O3A	0.86	2.32	3.104(13)	152	1/2-x,-1/2+y,-1/2+z
	N2-H2N···O4B	0.86	2.13	2.964(9)	162	1/2-x,-1/2+y,-1/2+z
	N3-H3N···O1A	0.86	2.16	2.961(12)	155	1/2-x,-1/2+y,-1/2+z
	N3-H3N···O2B	0.86	2.22	2.999(9)	151	1/2-x,-1/2+y,-1/2+z
	N4-H4N···O2A	0.86	2.44	3.175(11)	144	1/2-x,-1/2+y,-1/2+z
	N4-H4N···O4B	0.86	2.06	2.917(9)	173	1/2-x,-1/2+y,-1/2+z
	N5-H5N···O1B	0.86	2.22	2.949(8)	143	1/2-x,-1/2+y,-1/2+z
	N5-H5N···O3A	0.86	2.04	2.881(13)	166	1/2-x,-1/2+y,-1/2+z
	N6-H6N···O1A	0.86	2.15	2.960(13)	156	1/2-x,-1/2+y,-1/2+z
	N6-H6N···O4B	0.86	2.11	2.942(9)	163	1/2-x,-1/2+y,-1/2+z
	N7-H7N···O2A	0.86	2.08	2.923(11)	166	1/2-x,-1/2+y,-1/2+z
	N9-H9N···O2B	0.86	2.30	3.076(8)	150	x,y,z
	N9-H9N···O4A	0.86	2.07	2.912(11)	167	x,y,z
	N10-H10N···O3B	0.86	2.02	2.883(8)	177	x,y,z
	N11-H11N···O3B	0.86	2.35	3.104(8)	146	x,y,z
	N11-H11N···O4A	0.86	2.11	2.959(13)	167	x,y,z
	N12-H12N···O1B	0.86	2.09	2.935(8)	165	x,y,z
	N13-H13N···O1B	0.86	2.07	2.901(9)	161	x,y,z
	N13-H13N···O4B	0.86	2.12	2.919(13)	155	x,y,z
	N14-H14N···O2B	0.86	2.13	2.939(9)	157	x,y,z
	N14-H14N···O3A	0.86	2.22	3.007(11)	151	x,y,z

In summary, this thesis provides some substantial outcomes in the domain of 'supramolecular anion recognition chemistry' where the anions/hydrated anions or anionic associations are captured by some series of isomeric dipodal or tripodal artificial acyclic receptors driven by positional or electronic effect of terminal aryl substituents or anion size or molecular host architectures in solid state, which are then heavily corroborated by solution state anion binding studies as well as Hirshfeld surface or FT-IR analyses of host-guest complexes. In general, the present findings from the experimental studies deliver the anionic guest induced capsular, pseudo-capsular, paddle-wheel shaped, linear barrel shaped or polymeric aggregated assembly formation *via* neutral host-guest associations in most of the cases. The individual receptor or each set of isomeric receptor have unveiled an interesting feature/s in presence of a specific anion/hydrated anions or anionic associations.

The *ortho*-phenylenediamine based three units of receptor $\mathbf{L_1}$ has been shown to encapsulate the unique triangular [(chloride)$_3$-DMSO] dual guest association, while its isomeric receptor isomer $\mathbf{L_2}$ forms 2:2 noncooperative [($\mathbf{L_2}$)(Cl^-)]$_2$ complex. Another *ortho*-phenylenediamine based receptor $\mathbf{L_3}$ has been found to encapsulate cyclic [(F^-)$_2$(H_2O)$_2$] tetramer as well as unusual (Cl^-)$_2$, (Br^-)$_2$ and (I^-)$_2$ anionic assemblies and divalent carbonate by hydroxide ion induced atmospheric CO_2 fixation. The cyclic [(F^-)$_2$(H_2O)$_2$] tetramer, rugby-ball shaped [SO_4^{2-}-(H_2O)$_3$-SO_4^{2-}] adduct, unprecedented [CO_3^{2-}-(H_2O)$_2$-CO_3^{2}] cluster, double divalent sulfate anions as well as unusual asymmetric sulfate anions (naked and cyclic hydrated), linear [($OCOCH_3$)(H_2O)]$_n$ polymeric assembly and acyclic (Cl^-)$_2$-(H_2O)$_2$ assemblies have been found to be captured within the neutral self-assemblies of isomeric *meta*-phenylenediamine based receptors $\mathbf{L_4}$-$\mathbf{L_8}$. Furthermore, the *para*-phenylenediamine based linear isomeric receptors $\mathbf{L_9}$-$\mathbf{L_{15}}$ have been found to entrap cyclic (HCO_3^-)$_2$ dimer by F^-/OH^- induced aerial CO_2 fixation and linear polymeric aggregation of ($H_2PO_4^-$)$_n$ in most of the cases within the non-cooperative receptor assemblies. On the other hand, the terminal-aryl substituted multi-armed isomeric tripodal tris-amine ($\mathbf{L_{16}}$-$\mathbf{L_{18}}$)/ tris-urea ($\mathbf{L_{19}}$-$\mathbf{L_{23}}$) receptors demonstrated the cavity induced encapsulation of halide and oxyanions in either protonated or neutral host-guest assemblies. Furthermore, the highly electron-rich isomeric tripodal tris–urea receptors $\mathbf{L_{24}}$-$\mathbf{L_{25}}$ showed ice-like cyclic (H_2O)$_6$ entrapment inside the unique hexameric core of receptor-halide neutral capsular assemblies and among their thiourea analogues $\mathbf{L_{26}}$-$\mathbf{L_{27}}$, receptor $\mathbf{L_{26}}$ form unimolecular pseudo-capsular assemblies with all anionic guests and the receptor $\mathbf{L_{27}}$ form dimeric receptor capsular cages with anions in either 2:2 or 2:1 host-guest fashions. Overall, the whole thesis establishes the substituent-driven or anion-size dependent systematic binding

behavior of the potential dipodal/tripodal receptor systems (**L_1-L_{27}**) towards bare as well as hydrated anionic guests or anionic associations, which is reliable to interpret the data, reliable to justify the variation and would be beneficial to develop new categories of uncommon host-guest assemblies.

Hence, some of the fundamental and erratic concepts of supramolecular chemistry and versatility of the acyclic receptors as efficient building block through systematic advancement have been successfully demonstrated in the thesis for the generation of neutral molecular barrel or molecular capsules. The recognition of anions, hydrated-anions or anionic association within molecular assembly or molecular cavity is definitely a field which can expand significantly and bring immense advances in specialized applications such as drug delivery, transmembrane anion transport, salt solubilization, extraction, catalysis, stabilizing the anionic reactive intermediates inside the molecular assembly *etc*. However, for these applications to reach their prospective, basic work in tuning the binding of anions/hydrated-anions inside the molecular assembly such as capsules or barrel is highly appreciated. Although the results included in this thesis are extremely convenient from a fundamental viewpoint, there is other challenging aspects in supramolecular chemistry that need to be developed, basically from an applicative approach. Research in these areas with an emphasis on environmental, technological and biomedical applications, based upon the extraordinary anion/hydrated-anion binding molecular barrels or molecular capsules appear to be forthcoming.

Utsab Manna

Date of Birth: 22-11-1991

Place of Birth: Howrah, West Bengal, India.

Nationality: Indian

Email: utsab.manna@iitg.ac.in, utsabmanna1991@gmail.com

Contact no: +917002423076, +918721871438

Academic Summary

2014-present: Ph.D. student at Indian Institute of Technology Guwahati, India.
(Thesis has been submitted)
Thesis title: "**Recognition of Anionic Guests by Dipodal/Tripodal Receptors: Positional Isomeric and Electronic Effect**".

2012-2014: Master of Science in Chemistry (CPI-8.61) from Indian Institute of Technology Guwahati, Assam, India.

2009-2012: Bachelor of Science (Hons.) in Chemistry (60.63%) from R.K.M.V.C. College, Rahara (West Bengal State University), WB, India.

2007-2009: Higher Secondary (10+2) in Science (83%) from W.B.C.H.S.E.

2007: Secondary Education (10) (82.86%) from W.B.B.S.E.

Research Interests

- **Supramolecular chemistry of biologically and environmentally relevant anions:** Solid and solution-state studies of biologically and environmentally relevant anions in highly electron-rich system, π–acidic systems and anion templated synthesis of supramolecular architectures such as, catenanes, rotaxanes and molecular boxes.

- **Isomeric neutral receptor systems:** Rational design and development of isomeric neutral hosts and their ability of binding with the anionic guests depending upon the electronic and positional isomeric effect of terminal aromatic substituents.

- **Supramolecular capsules based on hydrogen bonds or metal-ligand coordination bonds:** The rational design and synthesis of supramolecular capsules with controllable encapsulation and release of a guest molecule remains an important subject from the viewpoint of molecular recognition, stabilization of reactive intermediates, catalysis of chemical reactions, and as microvesicles for drug delivery application.

Publications

1. Entrapment of cyclic fluoride-water and sulfate-water-sulfate cluster within the self-assembled structure of linear *meta*-Phenylenediamine based bis-urea receptors: Positional isomeric effect
   Utsab Manna, Romen Chutia and Gopal Das ***Cryst. Growth Des.*** 2016, **16**, 2893.
2. Influence of the cavity dimension on encapsulation of halide within the capsular assembly and side-cleft recognition of sulphate-water cluster assisted by polyammonium tripodal receptor
   Utsab Manna, Biswajit Nayak, Md. Najbul Hoque and Gopal Das ***CrystEngComm***, 2016, **18**, 5036.
3. Dual guest [(Chloride)$_3$-DMSO] encapsulated cation-sealed neutral trimeric capsular assembly: *meta*-substituent directed halide and oxyanion binding discrepancy of isomeric neutral di-substituted bis-urea receptors
   Utsab Manna, Biswajit Nayak and Gopal Das ***Cryst. Growth Des.*** 2016, **16**, 7163.
4. Fixation of atmospheric CO_2 as novel carbonate-(water)$_2$-carbonate cluster and entrapment of double sulphate within a linear tetrameric barrel of a neutral bis-urea scaffold
   Utsab Manna, Santanu Kayal, Soham Samanta and Gopal Das ***Dalton Trans.***, 2017, **46**, 10374.
5. Systematic size mediated trapping of anions of varied dimensionality within a dimeric capsular assembly of a flexible neutral bis-urea platform
   Utsab Manna, Santanu Kayal, Biswajit Nayak and Gopal Das ***Dalton Trans.***, 2017, **46**, 11956.
6. Anion binding consistency by influence of aromatic meta-disubstitution of a simple urea receptor: regular entrapment of hydrated halide and oxyanion clusters
   Utsab Manna and Gopal Das ***CrystEngComm***, 2017, **19**, 5622.
7. Ice-like cyclic water hexamer trapped within a halide encapsulated hexameric neutral receptor core: First crystallographic evidence of a water cluster confined within a receptor-anion capsular assembly
   Utsab Manna, Senjuti Halder and Gopal Das ***Cryst. Growth Des.*** 2018, **18**, 1818.
8. Progressive cation triggered anion binding by electron-rich scaffold: Case study of a neutral tripodal naphthyl thiourea receptor
   Utsab Manna and Gopal Das ***Cryst. Growth Des.*** 2018, **18**, 3138.
9. Cyclic $(H_2O)_6$ confined hexameric host-guest assemblies and aerial CO_2 fixation by electron-rich neutral urea/thiourea scaffolds
   Utsab Manna and Gopal Das ***CrystEngComm***, 2018, **20**, 3741.
10. Halo-methylphenyl substituted neutral tripodal receptors for cation-assisted encapsulation of anionic guests of varied dimensionality
    Utsab Manna and Gopal Das ***CrystEngComm***, 2018, **20**, 4406.
11. Self-assemblies of positional isomeric linear bis-urea ligands with qxyanions/hydrated Oxyanions: Evidence of F^- and OH^- induced atmospheric CO_2 fixation
    Utsab Manna, Asesh Das and Gopal Das ***Cryst. Growth Des.*** 2018, **18**, 6801.
12. Neutral host-guest capsular associations by homologous halophenyl substituted organic tris-urea receptor series: Solid and solution state studies
    Utsab Manna and Gopal Das ***New J. Chem.,*** 2018, **42**, 19164.
13. Halo-phenyl based linear dipodal receptors for entrapment of anions/anionic associations within neutral non-cooperative self-assemblies

Utsab Manna and Gopal Das ***CrystEngComm,*** 2019, **21**, 65.

14. Aggregation-Induced Emission (AIE) active probe for multiple targets: Fluorescent sensor for Zn^{2+} and Al^{3+} & colorimetric sensor for Cu^{2+} and F^-
    Soham Samanta, **Utsab Manna**, Turjya Ray and Gopal Das ***Dalton Trans.***, 2015, **44**, 18902.
15. Encapsulation of fluoride and hydrogen sulfate dimer by polyammonium functionalized first and second generation tripodal: Cavity induced anion encapsulation
    Md. Najbul Hoque, **Utsab Manna** and Gopal Das ***Supramol. Chem.*** 2016, **28**, 284.
16. Discrepancy in anion coordination directed by isomeric pyridine-urea receptors: solid state recognition of hydrated anions
    Md. Najbul Hoque, **Utsab Manna** and Gopal Das ***Polyhedron***, 2016, **119**, 307.
17. White light emission from simple AIE-ESIPT-Excimer tripled single molecular system
    Soham Samanta, **Utsab Manna** and Gopal Das ***New J. Chem.***, 2017, **41**, 1064.
18. Ratiometric fluorogenic probe for real-time detection of SO_3^{2-} in aqueous medium: Application in cellulose paper based device and potential to sense SO_3^{2-} in mitochondria
    Soham Samanta, Senjuti Halder, Poulomi Dey, **Utsab Manna**, Aiyagari Ramesh and Gopal Das ***Analyst***, 2018, **143**, 250.
19. A Cytocompatible Zinc Oxide Nanocomposite Loaded with an Amphiphilic Arsenal for Alleviation of Staphylococcus Biofilm
    Preeti Chauhan, Poulomi Dey, Sandipan Mukherjee, **Utsab Manna**, Gopal Das and Aiyagari Ramesh ***ChemistrySelect*** 2018, **3**, 2492.
20. Consistent binding aptitude of halides and oxyanions via cooperative *vs.* non-cooperative binding modes by neutral naphthyl bis-urea receptors
    Biswajit Nayak, **Utsab Manna** and Gopal Das ***ChemistrySelect***, 2018, **3**, 3548.
21. Steric influence of adamantane substitution in tris-urea receptor: Encapsulation of sulphate and fluoride-water cluster
    Santanu Kayal, **Utsab Manna** and Gopal Das ***J. Chem. Sci.***, 2018, **130**, 1.
22. Fixation of atmospheric CO_2 and recognition of anions/hydrated anions: Differential binding mode in protonated vs. neutral tripodal urea/thiourea receptors
    Santanu Kayal, **Utsab Manna** and Gopal Das ***Inorg. Chim. Acta*** 2019, **486**, 576.
23. *para*-Phenylenediamine based halo-methylphenyl substituted neutral bis-urea receptors: Evidences of cooperative/non-cooperative sulphate binding and aerial CO_2 fixation
    Utsab Manna and Gopal Das, Manuscript submitted.

Conference attended

- Oral presentation in '***Frontiers in Chemical Science 2016'***, Indian Institute of Technology Guwahati, Guwahati.
- Oral presentation in '***Regional Conference on Science for Sustainable Development (SSD-2019)'***, Department of Chemistry, B. Borooah College, Guwahati.
- Poster presented in '***20th CRSI National Symposiums in Chemistry 2017'***, Gauhati University, Guwahati.
- Poster presented in '***Research Conclave 2017'***, Indian Institute of Technology Guwahati, Guwahati.

- Poster presented in '***International Conference on Sophisticated Instruments in Modern Research ICSIMR 2017***', Indian Institute of Technology Guwahati, Guwahati.
- Poster presented in '***Modern Trends in Inorganic Chemistry (MTIC-XVII) 2017***', CSIR-NCL Pune and IISER Pune, Pune.
- Poster presented in '***Chemconvene 2017'***, Indian Institute of Technology Guwahati, Guwahati.
- Poster presented in '***Frontiers in Chemical Science 2018'***, Indian Institute of Technology Guwahati, Guwahati.

Workshop attended

- ***'Workshop on Procedures & Applications of XRD, XRF & Single Crystal XRD'*** Gauhati University, Guwahati. (27th July to 1st August, 2018).